VOL. 459 DECEMBER 28, 1988
COMPLETE IN ONE ISSUE

12th International Symposium on Column Liquid Chromatography Washington, DC, June 19–24, 1988 Part II

JOURNAL OF
CHROMATOGRAPHY
INTERNATIONAL JOURNAL ON CHROMATOGRAPHY, ELECTROPHORESIS AND RELATED METHODS

SYMPOSIUM VOLUMES

ELSEVIER

JOURNAL OF CHROMATOGRAPHY

Scope. The *Journal of Chromatography* publishes papers on all aspects of chromatography, electrophoresis and related methods. Contributions consist mainly of research papers dealing with chromatographic theory, instrumental development and their applications. The section *Biomedical Applications*, which is under separate editorship, deals with the following aspects: developments in and applications of chromatographic and electrophoretic techniques related to clinical diagnosis or alterations during medical treatment; screening and profiling of body fluids or tissues with special reference to metabolic disorders; results from basic medical research with direct consequences in clinical practice; drug level monitoring and pharmacokinetic studies; clinical toxicology; analytical studies in occupational medicine.

Submission of Papers. Papers in English, French and German may be submitted, in three copies. Manuscripts should be submitted to: The Editor of *Journal of Chromatography*, P.O. Box 681, 1000 AR Amsterdam, The Netherlands, or to: The Editor of *Journal of Chromatography, Biomedical Applications*, P.O. Box 681, 1000 AR Amsterdam, The Netherlands. Review articles are invited or proposed by letter to the Editors. An outline of the proposed review should first be forwarded to the Editors for preliminary discussion prior to preparation. Submission of an article is understood to imply that the article is original and unpublished and is not being considered for publication elsewhere. For copyright regulations, see below.

Subscription Orders. Subscription orders should be sent to: Elsevier Science Publishers B.V., P.O. Box 211, 1000 AE Amsterdam, The Netherlands, Tel. 5803 911, Telex 18582 ESPA NL. The *Journal of Chromatography* and the *Biomedical Applications* section can be subscribed to separately.

Publication. The *Journal of Chromatography* (incl. *Biomedical Applications* and *Cumulative Author and Subject Indexes, Vols. 401–450*) has 37 volumes in 1988. The subscription prices for 1988 are:

J. Chromatogr. (incl. *Cum. Indexes, Vols. 401–450*) + *Biomed. Appl.* (Vols. 424–460):
Dfl. 6290.00 plus Dfl. 962.00 (p.p.h.) (total *ca.* US$ 3537.50)

J. Chromatogr. (incl. *Cum. Indexes, Vols. 401–450*) only (Vols. 435–460):
Dfl. 5070.00 plus Dfl. 676.00 (p.p.h.) (total *ca.* US$ 2803.00)

Biomed. Appl. only (Vols. 424–434):
Dfl. 2145.00 plus Dfl. 286.00 (p.p.h.) (total *ca.* US$ 1185.75).

Our p.p.h. (postage, package and handling) charge includes surface delivery of all issues, except to subscribers in Argentina, Australia, Brasil, Canada, China, Hong Kong, India, Israel, Malaysia, Mexico, New Zealand, Pakistan, Singapore, South Africa, South Korea, Taiwan, Thailand and the U.S.A. who receive all issues by air delivery (S.A.L. — Surface Air Lifted) at no extra cost. For Japan, air delivery requires 50% additional charge; for all other countries airmail and S.A.L. charges are available upon request. Back volumes of the *Journal of Chromatography* (Vols. 1 through 423) are available at Dfl. 230.00 (plus postage). Claims for missing issues will be honoured, free of charge, within three months after publication of the issue. Customers in the U.S.A. and Canada wishing information on this and other Elsevier journals, please contact Journal Information Center, Elsevier Science Publishing Co. Inc., 655 Avenue of the Americas, New York, NY 10010. Tel. (212) 989-5800.

Abstracts/Contents Lists published in Analytical Abstracts, ASCA, Biochemical Abstracts, Biological Abstracts, Chemical Abstracts, Chemical Titles, Chromatography Abstracts, Current Contents/Physical, Chemical & Earth Sciences, Current Contents/Life Sciences, Deep-Sea Research/Part B: Oceanographic Literature Review, Excerpta Medica, Index Medicus, Mass Spectrometry Bulletin, PASCAL-CNRS, Referativnyi Zhurnal and Science Citation Index.

See inside back cover for Publication Schedule, Information for Authors and information on Advertisements.

0021-9673/88/$03.50

Printed in The Netherlands

For contents see p. VII

JOURNAL OF CHROMATOGRAPHY

VOL. 459 (1988)

JOURNAL
of
CHROMATOGRAPHY

INTERNATIONAL JOURNAL ON CHROMATOGRAPHY,
ELECTROPHORESIS AND RELATED METHODS

SYMPOSIUM VOLUMES

ELSEVIER
AMSTERDAM — OXFORD — NEW YORK — TOKYO

J. Chromatogr., Vol. 459 (1988)

James G. Blaine House, Washington, DC, U.S.A.;
wood engraving, 1884

0021-9673/88/$03.50

Printed in The Netherlands

SYMPOSIUM VOLUME

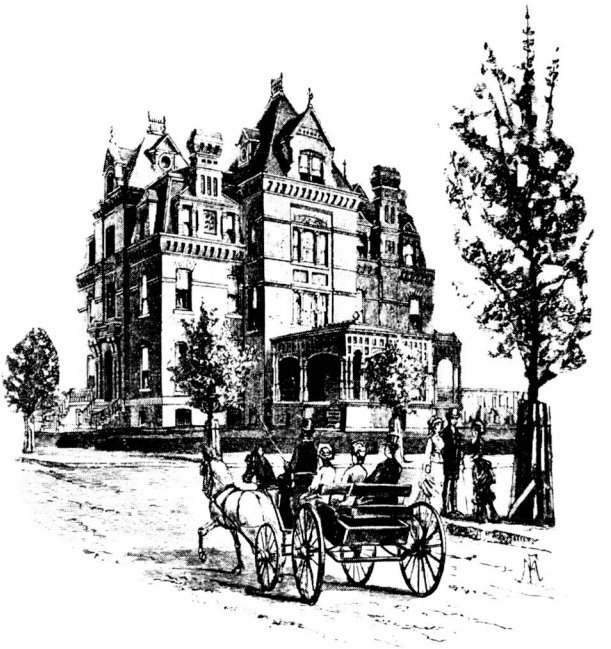

TWELFTH INTERNATIONAL SYMPOSIUM ON COLUMN LIQUID CHROMATOGRAPHY

PART II

Washington, DC (U.S.A.), June 19–24, 1988

Guest Editor

G. GUIOCHON

(Knoxville and Oak Ridge, TN)

The proceedings of the *Twelfth International Symposium on Column Liquid Chromatography, Washington, DC, June 19–24, 1988*, are published in three volumes of the *Journal of Chromatography*: Vols. 458 and 459 (1988) and 461 (1989). The Foreword to the proceedings, and information on the Sponsoring Scientific Organizations and the Scientific and Organization Committees only appear in Vol. 458. Vol. 459 is dedicated to the memory of **Dr. István Halász**, and opens with an obituary.

CONTENTS

12th INTERNATIONAL SYMPOSIUM ON COLUMN LIQUID CHROMATOGRAPHY, WASHINGTON, DC, JUNE 19–24, 1988, PART II

In articles with more than one author, the name of the author to whom correspondence should be addressed is indicated in the article heading by a 6-pointed asterisk (*)

This volume of the proceedings of HPLC '88 is dedicated to the memory of

Dr. ISTVÁN HALÁSZ

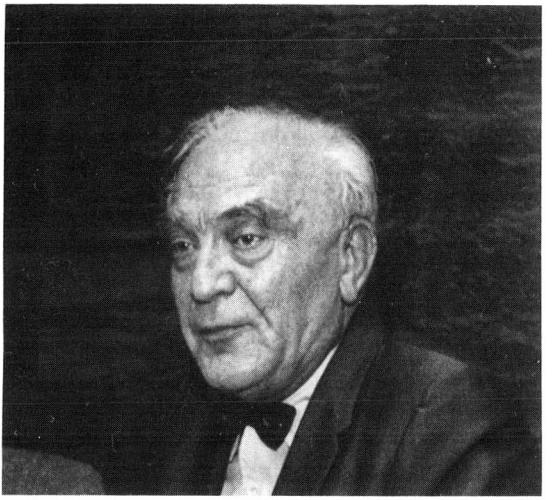

1922–1988

GEORGES GUIOCHON
Chairman HPLC '88

Journal of Chromatography, 459 (1988) XIII
Elsevier Science Publishers B.V., Amsterdam — Printed in The Netherlands

Obituary

István Halász, 1922–1988

Professor Dr. István Halász died on August 18, 1988, a few weeks after returning home from HPLC '88 in Washington, DC. This was the first international chromatography symposium he attended following his retirement some years back. His forceful lecture full of wit reflecting 40 years of experience in chromatography was one of the highlights of the scientific programme. Remembering his leading role at so many chromatography meetings in the past, many of us hoped that his participation would be a new beginning. Now we know that it was a finale, the last performance at the end of a highly successful scientific carreer. One of the architects of modern chromatography left us for the Elysian Fields.

István Halász was born and educated in Budapest, Hungary, and received his Ph.D. from the University of Szeged, Hungary, in 1949. In the ensuing seven years he was on the faculty of the Institute of Physical Chemistry at the Technical University in Budapest, working closely with Professor Géza Schay. The main thrust of his research was aimed at studies on gas adsorption, a preliminary to the emerging gas chromatography. He obtained "habilitation" in 1954 with his thesis entitled "Investigation of the structure of catalysts and adsorbents by vapor adsorption." In the same year he was among the founders of the Central Research Institute for Chemistry of the Hungarian Academy of Sciences and became the head of the Department of Gas Adsorption and Catalysis.

The tumultuous events in Hungary made Dr. Halász move to Frankfurt am Main in the Federal Republic of Germany at the end of 1956. He became a research associate of Professor H. Hartmann, the head of the Institute of Physical Chemistry at the Johann Wolfgang Goethe University. At the beginning of 1958 he received the *venia legendi* to physical chemistry and became a "Privatdozent" at the university. His deep involvement with chromatography commenced in these years when he clearly recognized that gas chromatography was on the way to becoming a widely used analytical tool at a time when many educated people had difficulty in pronouncing the word chromatography. In the years from 1958 to 1961 Dr. Halász held two positions simultaneously: he taught and set up a research laboratory at the University in Frankfurt and he was the head of the gas laboratory at Scholven Chemie AG in Gelsenkirchen-Buer. It was a *tour de force* that gave him a unique perspective of chromatography from the viewpoint of both industry and academia. However, these were difficult years for him personally since his wife Ágnes and daughter Vera were in Budapest and the family was not reunited until 1962. Dr. Halász was appointed fulltime "Dozent" at the University in Frankfurt in 1961 and received the title of professor in 1964. His laboratory in Frankfurt became one of the most prominent research establishments and a leading school in the field of gas chromatography.

In the years 1970–1971 he was a visiting professor at Northeastern University in Boston, MA, U.S.A. and at the University of Nice, France. From 1971 until his retirement in 1987, he held the chair of Applied Physical Chemistry at the University of Saarland in Saarbrücken, F.R.G.

István Halász lived in an era that had seen an obscure separation technique,

chromatography, grow into the most important analytical tool; when, by virtue of instrumentation, gas chromatography and high-performance liquid chromatography were born and underwent a meteoric growth. He made his mark in both of these techniques after a felicitous beginning of his professional life as a disciple of Géza Schay, one of the most respected names in research on adsorption. In the field of gas chromatography Halász and co-workers made very important contributions to the development of open-tubular (capillary) columns and of bonded stationary phases for gas chromatography in the late 1950s and during the 1960s. At the end of the 1960s Halász had become a pioneer of modern liquid chromatography and made his laboratory in Saarbrücken a leading place for research in various aspects of high-performance liquid chromatography. The wide-ranging accomplishments from this laboratory included in-depth investigations of column dynamics and some of the most profound studies on reversed-phase chromatography. In recognition of his achievements Dr. Halász was awarded the Chromatography Commemorative Medal of the U.S.S.R. Academy of Sciences in 1978 and the M.S. Tswett Chromatography Award in 1980.

Above all, he will be remembered as a teacher who established the internationally recognized Halászian school. His disciples have not only greatly benefited from his scientific guidance but were also enlightened by his sagacity. He was a man who for his whole professional life stood for clear thinking and honesty in science and who instilled these in his students. In his lecture at HPLC '88 we had the last opportunity to be reminded by him of the importance of logical thinking and common sense in the interpretation of experimental and theoretical results in chromatography. As so many times before, he cut through some fallacious theories with his acute logic and was applauded by a thankful audience. With Professor Halász's departure the expanding world of chromatography has lost a leader and many of us have lost a wise teacher, mentor and a dear personal friend.

CSABA HORVÁTH

Journal of Chromatography, 459 (1988) 1–23
Elsevier Science Publishers B.V., Amsterdam — Printed in The Netherlands

CHROMSYMP. 1451

DESIGN OF OPTIMIZED HIGH-PERFORMANCE LIQUID CHROMATOGRAPHIC GRADIENTS FOR THE SEPARATION OF EITHER SMALL OR LARGE MOLECULES

I. MINIMIZING ERRORS IN COMPUTER SIMULATIONS

B. F. D. GHRIST*
Medical Products Department, E. I. Du Pont de Nemours & Co., Concord Plaza, Wilmington, DE 19898 (U.S.A.)
B. S. COOPERMAN
Department of Chemistry, University of Pennsylvania, Philadelphia, PA 19104 (U.S.A.)
and
L. R. SNYDER*
LC Resources Inc., 26 Silverwood Court, Orinda, CA 94563 (U.S.A.)

SUMMARY

Computer simulations can be used to develop high-performance liquid chromatographic gradient elution methods. However, the usefulness of this approach depends on the accuracy of the resulting predictions. Possible sources of error in computer simulation for the prediction of separation based on gradient elution have been investigated. This has in turn led to recommendations for minimizing such errors. With suitable precautions it appears possible to make adequately reliable predictions of separation by gradient elution. Several examples with protein mixtures as samples are reported.

INTRODUCTION

Many samples are relatively complex and difficult to separate by means of high-performance liquid chromatography (HPLC), *e.g.*, mixtures containing a large number (20–30 or more) of major components of similar chemical structure. Such mixtures often require gradient elution. Separations of this type are usually carried out with simple linear gradients, but some samples benefit from the use of more complex gradient shapes. Thus the distribution of bands within the chromatogram may be uneven, suggesting steeper gradients in regions that are relatively empty of bands. Bands within the chromatogram may show increasing bunching for later-eluted compounds, and this favors the use of a curved (convex) gradient[1]. Finally, many samples exhibit pronounced changes in band spacing as the gradient steepness is

* Present address: Eli Lilly Co., Indianapolis, IN 46285, U.S.A.

0021-9673/88/$03.50

varied[2–5]; such samples may be better separated using segmented (non-linear) gradients.

Gradients of optimal shape are in many instances not obvious, which means that a number of trial-and-error runs are usually necessary before an adequate separation can be achieved. Complex samples of the kind under discussion also often require relatively long run-times for adequate separation (*e.g.*, 1 h or more), which then means a substantial method-development effort. Previous work has shown that this process can be considerably accelerated (and better gradient methods developed) by the use of computer simulation[2–5]. Only two experimental runs are required (linear gradients in which only the gradient time is varied), and then a small computer (*e.g.*, IBM PC) can be used to explore the effects of different gradient conditions on the separation. The initial and final mobile phase compositions can be varied, the gradient time can be changed and gradients of any shape can be studied. Each simulated run requires only *ca.* 1 min or so to carry out and evaluate.

There are two limitations to this approach, however. First, accurate simulations (leading to optimal final conditions) depend on the HPLC equipment used and the choice of conditions for the two initial experimental runs. Significant errors in simulated chromatograms can result when inappropriate equipment or conditions are employed. Second, trial-and-error changes in the gradient can be an inefficient way to approach optimal final conditions. The success of this procedure (whether carried out experimentally or via computer simulation) depends markedly on the experience and insight of the chromatographer. Clearly, it would be helpful to have some rules or generalizations to more guide effectively the empirical optimization of gradient conditions. Finally, the need for (a) sufficiently accurate computer predictions in combination with (b) an effective strategy for optimizing the gradient appears to be greater for the case of higher-molecular-weight samples such as peptides and proteins, for reasons illustrated in the examples of refs. 5, 6 and 28.

In this paper, we explore the causes and effects of errors in computer-simulated predictions of gradient-elution separation. Experimental data relating to this issue will also be presented. The following two papers[5,6] examine the theory of how to design optimal gradients for different situations. Because the problems and opportunities associated with computer simulation are enhanced with macromolecular samples, we shall emphasize the use of gradient elution with this class of samples, particularly biological macromolecules such as peptides, proteins and oligonucleotides.

THEORY AND BACKGROUND

Errors in computer simulation

Retention in gradient elution can be related in a rigorous fashion to certain characteristics of the sample and to the experimental conditions[7–9]. This in turn allows the use of a small number of experimental runs to (a) measure these sample characteristics (parameters) and (b) predict retention as a function of any gradient conditions. However, these relationships apply for "ideal" systems, where all parameters are precisely measurable, the HPLC equipment functions in an ideal manner and certain complicating processes can be ignored (*e.g.*, changes in column performance with time).

In addition, it is convenient to make certain simplifying assumptions concerning

retention in the HPLC system under study. For reversed-phase HPLC (the subject of this paper), computer simulation as described here (DryLab G software) assumes that isocratic retention is given by

$$\log k' = \log k_w - S\,\varphi \qquad (1)$$

where k' is the capacity factor for a given compound when the volume fraction of organic component in the mobile phase (%B) is φ, k_w is the value of k' for water as mobile phase ($\varphi = 0$) and S is a constant for that compound (for fixed experimental conditions other than φ).

In the real world, we need to be concerned about various "non-ideal" effects and approximations such as eqn. 1, and to limit their impact so that resulting computer simulations are as reliable as possible. Previous papers have discussed various non-ideal conditions[10,11] and the failure of eqn. 1[12,13] as these relate to accuracy in computer predictions of retention. However, most of this earlier work has been concerned with isocratic–gradient relationships; *i.e.*, the simulation of gradient retention from starting isocratic runs, or *vice versa*. Here, we desire to simulate gradient retention on the basis of initial (experimental) gradient runs.

Table I summarizes several factors that can limit the accuracy of computer simulations for the prediction of gradient retention (assumes two experimental gradient runs to start). Several of these factors (and other questions that we shall address) can be conveniently studied through the use of computer simulations. As computer simulations (DryLab G) are based on "ideal" conditions, errors caused by variability in different experimental parameters can be assessed by repeating such simulations with different (erroneous) values of each parameter.

TABLE I

ERRORS IN COMPUTER-SIMULATED RETENTION TIMES AS A RESULT OF VARIOUS FACTORS

Factor	*Comment*
(1) Dwell volume, V_D	Error in V_D of $\pm$ 10–20% not important, except for bands eluted at the beginning of the chromatogram
(2) Mixing volume, V_M	Large V_M causes errors in predicted separation for segmented gradients
(3) Flow-rate, F	Error in F seldom has a significant effect on predicted separations
(4) Column dead volume, V_m	Error in V_m has little effect on predicted separations
(5) Change in retention due to change in column, temperature, etc.	The main problem is the change in column retention characteristics due to loss of bonded phase; accurate predictions of separation require that initial experimental runs be carried out within a 48-h period, and the column must be "broken in"
(6) Solvent demixing	Normally has a negligible effect on separation, particularly for large molecules
(7) Failure of eqn. 1	Can lead to errors in extrapolative predictions of separation; DryLab G guards against this possibility
(8) Error in t_g due to band overlap	Can cause appreciable errors in predicted separations
(9) Misassigned bands for initial experimental runs	Can cause major errors in predicted separation; a third run can be used to eliminate these errors
(10) Conformational change in protein molecules	Make sure that sample is fully denatured prior to separation

Dwell volume, V_D. The gradient retention time t_g depends on the volume (V_D) of the HPLC system between the inlet gradient mixer and the column (measured as described in ref. 9). We examined the effect of errors in V_D on computer simulation by using experimental data (two runs with a fifteen component herbicide sample; gradient times, t_G, of 30 and 90 min) plus DryLab G to predict the retention for both intermediate (t_G = 60 min) and extrapolated (t_G = 150 min) gradient times. The numerous band-spacing changes in this sample as a function of t_G (ref. 4) should make this computer simulation sensitive to errors in V_D.

Initial predictions were based on the correct (*i.e.*, "best") dwell volume for our HPLC system, equal to 5.5 ml. Then DryLab simulations were repeated assuming an (erroneous) V_D value of 6.5 ml. These results are compared in Table II. The effect of this +18% error in V_D on the predicted values of the retention time t_g (min) is an average error of −0.2% for the 60-min run and 0.5% for the 150-min run. Fig. 1a and b compare the resulting (simulated) chromatograms for correct *vs.* incorrect values of V_D for the 60-min run. The simulations in Table II also show a constant error of +8% in R_s for all band pairs (both 60- and 150-min runs) as a result of this +18% error in

TABLE II

ERRORS IN SIMULATED RETENTION AS A RESULT OF ERRORS IN DWELL VOLUME

Data for the fifteen-component herbicide sample described in ref. 4; 25 × 0.46 cm I.D. C_8 column; flow-rate, 2 ml/min; correct V_D value is 5.5 ml.

Band No.	*Retention time (min)*						
	5–80%B gradient				*40–80%B gradient*		
	t_G = *60 min*		t_G = *150 min*		t_G = *32 min*		
	V_D = *5.5*	V_D = *6.5**	V_D = *5.5*	V_D = *6.5**	V_D = *5.5*	V_D = *6.5**	*Error*
1	11.99	11.96	14.76	14.85	1.61	1.43	−0.2
2	13.91	13.88	17.87	17.98	1.85	1.60	−0.3
3	14.26	14.23	18.30	18.40	1.91	1.65	−0.3
4	15.50	15.45	21.01	21.16	1.97	1.69	−0.3
5	22.38	22.32	35.78	36.07	2.93	2.44	−0.5
6	24.59	24.53	39.42	39.70	3.35	2.74	−0.6
7	26.02	25.95	46.11	46.48	3.90	3.19	−0.7
8	27.13	27.06	47.49	47.85	4.21	3.55	−0.7
9	27.17	27.10	48.65	49.04	4.32	3.58	−0.7
10	27.94	27.87	49.66	50.03	4.61	3.83	−0.8
11	28.64	38.57	51.81	52.20	4.78	3.98	−0.8
12	30.49	30.42	53.42	53.77	6.88	6.22	−0.7
13	32.96	32.88	59.70	60.08	8.25	7.64	−0.6
14	36.29	36.21	67.65	68.04	10.61	10.1	−0.5
15	49.37	49.29	99.92	100.35	21.86	21.64	−0.2
Average error		−0.2%		−0.5%		−9.5%	

* Erroneous value of V_D.

V_D. As values of V_D will not normally be in error by this much, actual errors in the predicted values of t_g and R_s for every band pair should be adequately small. Similar results were obtained for an assumed (erroneous) value of V_D = 4.5 ml, rather than 6.5 ml.

For isocratic predictions from gradient data, it was shown previously that errors in values of V_D lead to generally larger errors in predicted values of retention time t_R[13] and resolution R_s[14]. Early bands in a gradient run can exhibit "pre-elution"[10], *i.e.*, isocratic migration under the influence of the volume V_D of the starting mobile phase when the starting %B in the gradient is sufficiently large. The predicted separation of such bands should therefore be more sensitive to errors in V_D. This is indeed so, as illustrated for the same herbicide sample in Fig. 1c and d. Here, a higher %B is used initially (40% *vs.* 5% in Fig. 1a and 5), and simulated chromatograms are compared for correct (5.5 ml) and incorrect (6.5 ml) values of V_D.

As seen in Table II, use of the incorrect value of V_D (6.5 ml) causes an average error in predicted retention times of 9.5%. The largest errors occur for bands that are eluted near $t_0 + t_D$, equal to about 4.0 min for the examples in Table II. The effect on the relative separation, however, is less significant, as can be seen by comparing Fig. 1c and d; the overall appearances of these two chromatograms are similar.

Mixing volume, V_M. The mixing volume, V_M, of a gradient HPLC system measures the tendency of the system to round the ends of the gradient as a result of mobile-phase dispersion during its passage between the mixer and column inlet. This is illustrated in Fig. 2a. As discussed in ref. 10, this rounding of the gradient is greater for

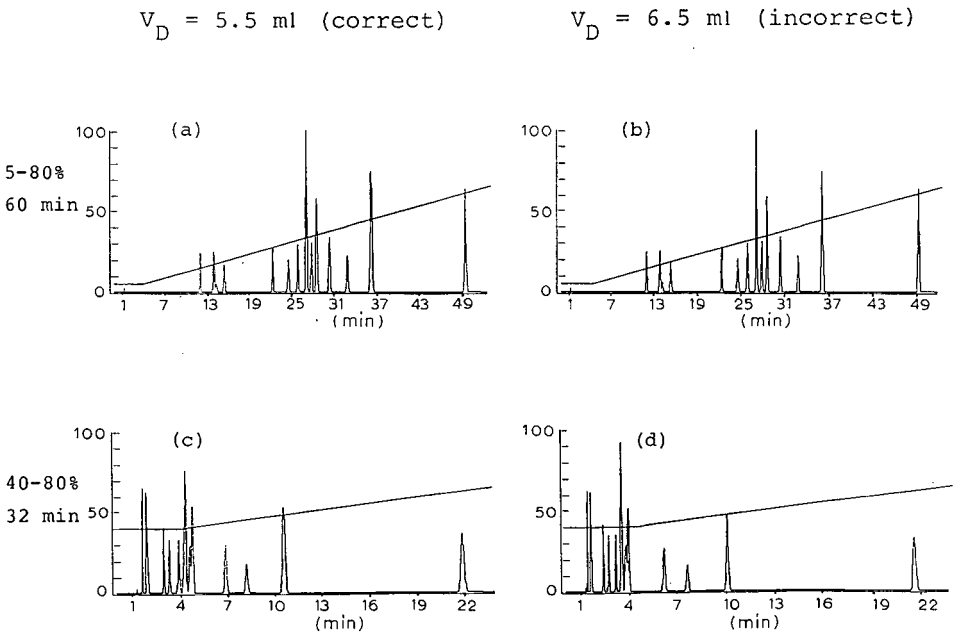

Fig. 1. Effect of error in the value of V_D on prediction of gradient elution separation. Sample, fifteen-component mixture of herbicides[4]; column, 25 × 0.46 cm I.D. Zorbax C_8; 5–80% acetonitrile–water gradients; flow-rate, 2 ml/min; gradient times t_G are indicated.

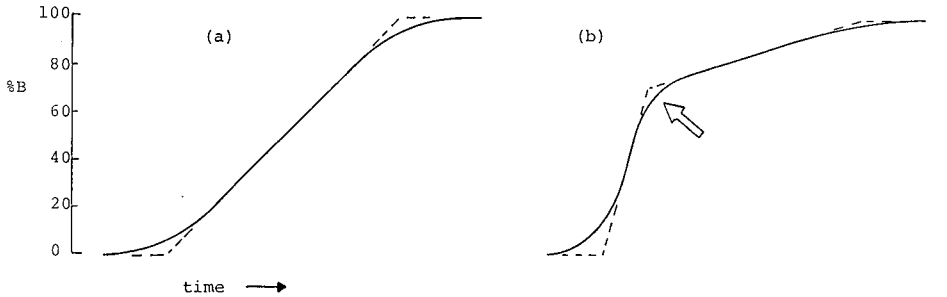

Fig. 2. Rounding of gradient due to a large mixing volume, V_M. (a) Linear (unsegmented) gradient; (b) segmented gradient.

larger values of V_M, and is smaller for larger values of $t_G F$, where F is the flow-rate. As rounding of the gradient primarily affects the retention of bands at the beginning and end of the gradient, mixing-volume effects can be minimized by starting the gradient earlier and ending it later (smaller values of φ at the beginning of the gradient and larger values of φ at the end). For linear gradients and modern HPLC equipment (with values of $V_M < 2$ ml), in most instances gradient rounding is not a serious contribution to errors in predicted values of t_g. This is discussed more fully elsewhere[15]. One conclusion that emerges from the above discussion, however, is that the computer simulations of gradient runs will generally be less accurate for early bands in the chromatogram.

Rounding of the gradient as in Fig. 2a can also affect the retention of bands that are eluted in the middle of the chromatogram when segmented gradients are used (Fig. 2b). This can in turn lead to errors in computer-simulated separations. As discussed in the following paper[5], however, the resulting errors in the prediction of retention time should be smaller than for initial rounding of the gradient.

Mobile phase flow-rate, F. The effect of errors in flow-rate, F, on gradient retention was discussed in ref. 10. Errors in F can arise from faulty pumping or from inadequately compensated mobile phase compression effects, and also from errors in selecting the correct flow-rate. The separation of biological samples such as peptides and proteins often involves lower flow-rates and lower operating pressures, and for these conditions errors in flow-rate will usually be much less than 1%.

We can derive an equation relating errors in t_g (δt_g) to errors in flow-rate. The gradient retention time t_g is given approximately by[7–9]

$$t_g = (t_0/b)\,[\log(2.3k_0 b)] + t_0 + t_D \tag{2}$$

where

$$b = V_m \Delta\varphi\, S/t_G\, F \tag{3}$$

(see below and the Glossary of Symbols for the definitions of these commonly used terms). Combining eqns. 2 and 3 yields

$$t_g = (t_G/\Delta\varphi S)\,[\log(2.3k_0) + \log(V_m\, \Delta\varphi S/t_G F)] + (V_m + V_D)/F \tag{4}$$

Differentiating eqn. 4 with respect to F gives the error in t_g (δt_g) as a function of error in F (δF):

$$\delta t_g = -\{[t_G/(2.3\ \Delta\varphi\ S\ F)] + [(V_m + V_D)/F^2]\}\ \delta F \quad (5)$$

For a typical example involving a protein separation, we might have the following conditions (corresponding to the 60-min 30S ribosomal-protein runs in this study): gradient time t_G = 60 min, gradient range $\Delta\varphi$ = 0.2, S = 30, F = 0.7 ml/min, column dead-volume V_m = 2.5 and V_D = 5.5 ml. A 1% error in F (δF = 0.007) would then result in an error in t_g of 0.2 min, or about 0.4% for the average band. However, this error will be about the same for all bands in the sample (assuming the S values are roughly constant), meaning that little change in relative retention will result. Typical errors in flow-rate (see ref. 10) should therefore have little impact on predicted t_g values from computer simulation, and a negligible effect on predicted values of R_s.

Column dead volume, V_m. Our computer-simulation software (DryLab G) assumes that V_m equals a constant fraction of the total column volume (62%). This fraction can actually vary by ±10–20% for different columns, leading to potential errors in simulated t_g values. Simulations as in Table II were therefore repeated for a change in V_m of +20%. The effect on predicted values of retention and resolution (for t_G = 60 and 150 min, as in Table II) was negligible: a 0.1–0.3% decrease in retention time and a 1–3% increase in resolution. It can be concluded that errors in our assumed value of V_m (based on a 62% void volume) can be ignored. Similar conclusions have been drawn for the effect of error in V_m on the prediction of isocratic retention from gradient data[13]. This suggests that errors in V_m will have little effect on t_g values for early bands (unlike the errors in V_D; see above).

Change in sample retention. For a given separation (fixed conditions), sample retention can vary as a result of unintended changes between replicate runs: uncontrolled temperature, changes in the column with continued use, errors in assigning various parameters (flow-rate, gradient conditions, etc.). In a previous study[10,11] most of these effects have been analysed in detail; it was shown that such errors are not usually significant insofar as separation is concerned. However, that study was based on neutral sample molecules (dialkylphthalate) and unmodified organic–water mixtures as the mobile phase.

In reversed-phase separations of peptide and protein samples, low-pH mobile phases containing buffers or ion-pairing agents are often used. These mobile phases typically degrade the column by removing the alkyl-bonded phase[16,17], so that sample retention tends to change during use; usually the retention of all compounds decreases with time. Changes in sample retention can lead to errors in computer simulations. If the retention changes between the two initial experimental runs used in computer simulation, the derived sample parameters (S, k_w) will be in error, as will subsequent predictions of retention. If the retention changes after the two initial runs, predictions from computer simulation will not match the corresponding experimental runs.

Solvent demixing. This refers to uptake by the column of organic solvent during the gradient[11]. Errors due to this effect are greater for high-surface-area columns and for steep gradients. Neither of these conditions is likely in typical protein separations*

* Separations of proteins generally employ wide-pore packings that have low surface areas; similarly, the large S values found for proteins require relatively flat gradients for acceptable values of b (eqn. 3).

and this effect can therefore be considered unimportant. Even for small-molecule samples and steep gradients, errors due to solvent demixing are unlikely to have much effect on predictions of separation via computer simulation, because these errors cancel for adjacent bands.

Failure of eqn. 1. In several studies it has been observed that larger peptides and proteins obey eqn. 1 within experimental error[18–20], whereas other studies have

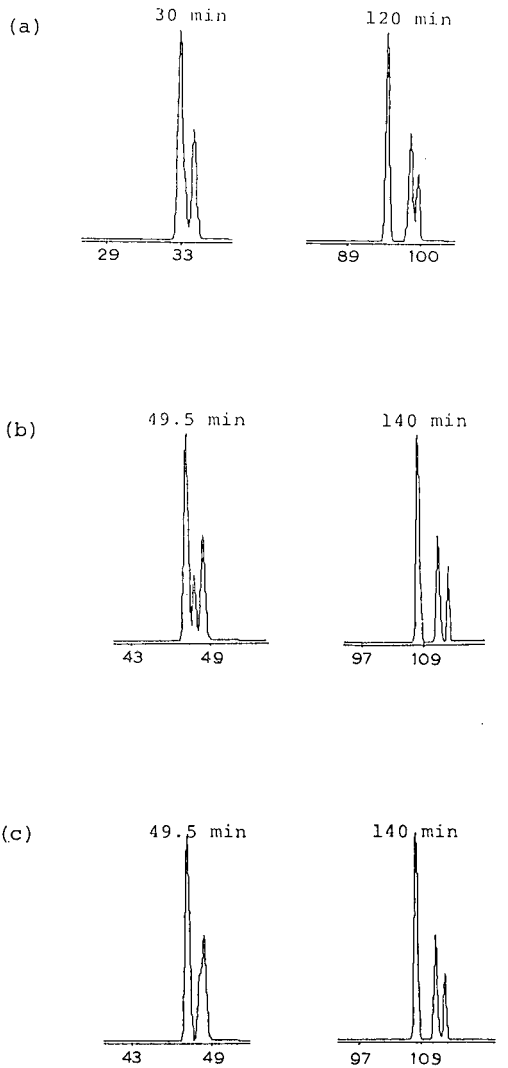

Fig. 3. Effect of error in input t_g values on accuracy of predicted chromatograms; hypothetical example of Table III (see text). (a) Input data; (b) simulated chromatograms for optimal gradient times (49.5 and 140 min) predicted from incorrect t_g value for band 2 (32.91 min in 30-min run); (c) simulated chromatograms as in (b), except correct value of t_g (33.19 min) used as input.

reported modes curvature in plots of log k' *vs.* φ for peptide and protein samples[21,22]. The general effect of log k'–φ curvature on computer simulation by DryLab G software has been examined for small-molecule samples[4,12,13], with the conclusion that significant errors are not introduced in interpolative predictions of t_g. Extrapolative predictions must be treated with greater caution, however.

Error in retention times due to band overlap. This problem is illustrated in Fig. 3 and Table III. Two experimental runs are shown (simulations) for t_G equal to 30 and 120 min. Two bands overlap in the 30-min run (t_g = 32.91 and 33.19 min), whereas all three bands are resolved in the 120-min run. The usual procedure in this instance is to use the observed ("average") retention time (32.91 min) for each of the two overlapping bands, as the correct retention times for each of the two bands are not known. The use of this procedure, followed by trial-and-error computer simulations, led to the prediction that acceptable separations could be obtained either with t_G = 49.5 or 140 min ("optimized simulations" in Fig. 3). However, repeating these simulations with correct values of t_g for all bands (Table III) gave the "experimental" runs in Fig. 3 (corresponding to what would have been observed if actual experiments had been carried out).

It is clear from Fig. 3 and Table III that significant errors in the computer simulations have resulted because of the initial errors in t_g (bands 1 and 2, 30-min run). This particular example represents an extreme case, corresponding to significant resolution in the overlapped band pair, but just short of the resolution required to measure t_g for the second band. The actual resolution is R_s = 0.6 for bands 1 and 2 in the 30-min run, with a 4:1 ratio for the band areas of the two compounds. The relative error in the predicted resolution of band 2 is greatest for small changes in retention as a result of changing t_G, *e.g.*, 49.5-min run (simulated) *vs.* 30-min run (experimental). Means for dealing with this kind of error in computer simulation are discussed under Results and Discussion.

Misassigned bands. Computer simulation requires that the bands in the second

TABLE III

EFFECT OF RETENTION ERRORS DUE TO BAND OVERLAP ON COMPUTER SIMULATIONS

Examples are simulated by DryLab G. Conditions: dwell volume, 5.5 ml; 25 × 0.46 cm I.D. column; flow-rate, 1 ml/min; 5–100%B gradient; three bands.

t_G (min)	Retention time, t_g (min)			Resolution, R_s	
	Band 1	Band 2	Band 3	Bands 1 and 2	Bands 2 and 3
30	32.91	33.19	33.71		
120	95.13	99.70	98.60		
49.5*	47.23	47.91	48.59	1.2	1.2
49.5**	47.23	48.20	48.59	1.7	0.7
140*	108.0	114.0	112.1	3.1	1.6
140**	108.0	113.8	112.1	3.1	1.4

* Simulation based on incorrect value of t_g (32.91 min) for band 2 in 30-min run.

** Simulation based on correct value of t_g (33.19 min) for band 2 in 30-min run.

experimental run be matched with those in the first run, *i.e.*, if compound A is responsible for band 1 in run 1, it is necessary to identify the band in run 2 that contains compound A (and so on for all other bands). In some instances this presents no difficulty, because band size and relative retention make these assignments obvious. When this is not so, it may be necessary to run a third experiment (of intermediate gradient time) and compare this chromatogram with that predicted by computer simulation from the first two runs. Errors in band assignment will usually be obvious from such a comparison[3–5].

Changes in protein conformation during separation. Several studies have shown that the tertiary structure of a protein molecule can change during reversed-phase HPLC[23,24]. In principle, such changes in conformation could lead to errors in predicted separations based on computer simulation. Changes in conformation during HPLC can be minimized by experimental conditions that favor denaturation of the sample, and such conditions also favor the improved separation of most protein samples[23,24].

EXPERIMENTAL

Equipment and software

The HPLC system was a DuPont 8800 liquid chromatograph, consisting of an 8800 gradient controller, an 870 pump, and two 862 variable-wavelength detectors connected in series for detection at both 214 and 280 nm (DuPont, Wilmington, DE, U.S.A.). The column compartment was equipped with a manual Rheodyne injection valve fitted with a 50-μl loop. A 5.0 × 0.46 cm I.D. precolumn was positioned between the pump and injector, and an in-line 2-μm filter was placed between the injector and analytical column. The dwell volume of the system was equal to 6.8 ml for detection by the second detector (at 214 nm; all chromatograms shown here were monitored at 214 nm). Analog data were digitized and archived by a Nelson Analytical Series interface (Nelson Analytical, Cupertino, CA, U.S.A.). Computer simulations were carried out using DryLab G software (LC Resources, Lafayette, CA, U.S.A.).

Materials

Reagents and solvents. Acetonitrile was of HPLC grade (Fisher Scientific, Fair Lawn, NJ, U.S.A.). Water was deionized and further purified with a Milli-Q system (Millipore, Bedford, MA, U.S.A.). Trifluoroacetic acid (TFA) was of Sequanal grade (Pierce, Rockford, IL, U.S.A.). Triethylamine (TEA) was Gold Label grade (Aldrich Chemical, Milwaukee, WI, U.S.A.).

Columns. Most of the separations for the ribosomal proteins were carried out on 25 × 0.46 cm I.D. Zorbax BioSeries Protein PLUS columns (DuPont). In earlier studies (Table V), columns from other suppliers (Synchrome, West Lafayette, IN, U.S.A.; Separations Group, Hesperia, CA, U.S.A.) were also used (see ref. 6 for details).

Samples. Ribosomal protein samples were prepared from *E. coli* bacteria as described by Kerlavage *et al.*[25]; see ref. 28 for further details.

Procedures. All gradients were formed from water plus acetonitrile [containing 0.085% (v/v) TFA and 0.1% (v/v) TEA, pH 2.8] plus acetonitrile. Columns were re-equilibrated by running a 10-min reversed gradient, followed by at least 20 min of the starting mobile phase. The flow-rate was 0.7 ml/min in all instances.

RESULTS AND DISCUSSION

Comparison of experimental and predicted retention for several protein samples

30S ribosomal protein sample. This sample contains a total of 21 proteins having molecular weights between 8000 and 28 000 Da. In the following two papers[5,6] and elsewhere[28] we have presented examples of computer simulation for the 30S ribosomal proteins; the predicted separations closely match experimental runs based on the same (reversed-phase) gradient conditions. These examples[5,6,28] illustrate our current ability to use computer simulation for protein samples in place of trial-and-error experimental runs.

It is instructive to review a number of other (earlier and unreported) comparisons that were made in our laboratory, before we fully appreciated what steps are necessary to achieve accurate computer simulations (see the following section for recommendations). Over a period of several months, we carried out separations of the 30S ribosomal proteins on several different columns, but with generally similar gradient conditions (26–46% acetonitrile–water gradients, 0.7 ml/min; see Experimental). In each instance gradient runs were repeated for gradient times of 60, 120 and 240 min. It was therefore possible to compare the ability of computer simulation (based on two of these runs) to predict the results of the third run. Previous studies[4,13] suggest that interpolative predictions will generally be more reliable than extrapolative simulations, *i.e.*, prediction of the 120-min run from the 60- and 240-min runs will be more accurate than prediction of the 240-min run from the 60- and 120-min runs. Likewise, the use of two initial runs differing in gradient time by a larger factor (*e.g.*, four-fold for 60- and 240-min runs) will also allow more accurate simulations[12]. The gradient equipment was also checked[10] to ensure satisfactory operation.

Table IV illustrates the kind of accuracy that we have observed for simulated runs when appropriate precautions are taken. In this series of runs, we were able to recognize 17 distinct bands. The 60- and 240-min experimental runs were used to predict retention times for the 120-min run. Table IV lists experimental (expt.) and predicted (calc.) retention times (t_g); retention-time differences for adjacent bands ($t_j - t_i$ for bands i and j) are also listed. Values of $t_j - t_i$ are proportional to resolution; predicted values of this quantity must therefore be reliable within $\pm$10–20% if computer simulation is to be useful for method development.

We see from the example in Table IV that retention times are predicted with acceptable accuracy ($\pm$0.2 min or $\pm$0.5%). This is better (by a factor of about 5) than the average accuracy of similar predictions in the case of small-molecule sample[4]. One reason is that gradient retention times for large molecules (having large S values) vary much less with changes in the experimental conditions. Other factors being equal (similar gradient-slope values b), a change in k' (or k_0) during gradient elution (due to a change in experimental conditions) causes a change in t_g (δt_g) that is proportional to $1/S$.

Retention time differences ($t_j - t_i$) are also accurately predicted in Table IV ($\pm$0.2 min or $\pm$5%). When two bands are close together (barely resolved), as with bands 15 and 16 or 16 and 17, the relative error in $t_j - t_i$ is generally larger.

Table V summarizes similar comparisons as in Table IV for eleven different sets of runs. These experiments were carried out over a period of about 1 year and involved six different columns. During most of this time we ignored the potential problems

caused by change in column retention characteristics with time. In some instances, these data for computer simulation were carried out on new columns, prior to conditioning the column (by injecting protein samples until constant retention and recoveries were observed for a given sample). In other instances, the three runs for computer simulation were not completed within a period of 48 h. It is instructive to compare the accuracy of computer simulation as a function of these variables; this information is provided in Table V.

The format of Table V requires comment. Consider run series G (which is detailed in Table IV) as an example. The designations "NO"–"NO" indicate that the column was conditioned before use, and all three runs for comparison were carried out within a period of 2 days. The error in predicted values of t_g is 0.2 ± 0.3 min, meaning that the average error was +0.2 min, and the random scatter around this value was 0.3 min (1 S.D.). The relative standard deviation of all t_g values *vs.* experimental values was 0.5%. The relative standard deviation of predicted values of $t_j - t_i$ was 5%. These values may be compared with the results in Table IV.

If we group the results in Table V according to whether the three runs were carried out within a 2-day period and/or a new column was used, we obtain the results

TABLE IV

COMPARISON OF PREDICTED *VS.* ACTUAL RETENTION TIMES FOR 30S RIBOSOMAL PROTEIN SAMPLE (DRYLAB SIMULATION)

Run series G of Table V; 60- and 240-min runs used to predict 120-min run. Column, 25 × 0.46 cm I.D. BioSeries Protein PLUS; flow-rate, 0.7 ml/min; 26–46% acetonitrile–water gradients.

Band No.	t_g *(min)*		*Error (min)*		*Error (%)*	
	Expt.	*Calc.*	t_g	$t_j - t_i$	t_g	$t_j - t_i$
1	22.0	22.9	0.9	−0.6	4.0	5
2	33.7	34.0	0.3	0.0	0.9	0
3	47.0	47.3	0.3	−0.2	0.6	3
4	53.4	53.5	0.1	−0.1	0.2	2
5	58.5	58.5	0.0	0.0	0.0	0
6	60.1	60.1	0.0	0.1	0.0	8
7	61.0	61.1	0.1	−0.1	0.2	5
8	63.3	63.3	0.0	0.0	0.0	0
9	67.1	67.1	0.0	0.1	0.0	1
10	80.7	80.8	0.1	−0.3	0.1	12
11	83.2	83.0	−0.2	0.6	0.2	–
12	83.2	83.6	0.4	0.2	0.5	7
13	86.5	86.5	0.0	−0.2	0.0	2
14	100.2	100.0	−0.2	0.4	0.2	–
15	100.2	100.6	0.4	−0.5	0.4	36
16	101.6	101.5	−0.1	0.3	0.1	18
17	103.3	103.5	0.2	–	0.2	–
Average absolute error			±0.2	±0.2	±0.5	±5

TABLE V

COMPARISON OF PREDICTED *VS.* ACTUAL RETENTION TIMES FOR 30S RIBOSOMAL PROTEIN SAMPLES (DRYLAB SIMULATION)

Summary of several run series as in Table IV (60- and 240-min runs used to predict 120-min run). Conditions similar to those in Table IV, except for the use of different columns. See text for further details.

*Column**	*New column?***	*Runs in >2 days?****	*Errors in retention (min, ±1 S.D.)*	
			t_g	$t_j - t_i$
A	NO	YES	0.6 ± 0.5 (±1.4%)	±7
B	NO	NO	−0.1 ± 0.2 (±0.4%)	±3
C	YES	NO	0.8 ± 0.3 (±1.6%)	±10
D	YES	YES	0.8 ± 0.4 (±1.7%)	±8
E	NO	YES	0.8 ± 0.4 (±1.6%)	±8
F	NO	YES	0.7 ± 0.6 (±1.9%)	±6
G	NO	NO	0.2 ± 0.3 (±0.5%)	±5
H	NO	YES	0.9 ± 0.6 (±2.1%)	±6
I	NO	YES	0.4 ± 0.3 (±0.8%)	±8
J	YES	YES	4.0 ± 1.6 (±8.4%)	±12
K	NO	NO	−0.1 ± 0.2 (±0.4%)	±5

Summary:

Run conditions	*Error in predicted data (%)*	
	t_g	$t_j - t_i$
Conditioned column; all runs completed within 2 days	±0.4	±4
Unconditioned column, or completion of all runs required >2 days	±1.3	±7
Unconditioned column and completion of all runs required >2 days	±5	±11

* See Experimental section for columns.
** "NO" indicates that the column was conditioned before use for these runs.
*** "NO" indicates that the three runs for this comparison were carried out within a 48-h period.

summarized at the bottom of Table V. These summary results clearly demonstrate the need to condition the column prior to computer-simulation experiments, and to complete these runs within a 2-day period. However, the data in Table V also depend on the stability of the HPLC column under the conditions of separation. In later studies, using a newly developed, more stable column for reversed-phase protein HPLC (BioSeries Protein PLUS; DuPont), we experienced fewer problems with time-dependent changes in column retention.

Table V also shows that good comparisons between predicted and experimental gradient separations are possible when the above precautions are taken. However, it is expected that once a gradient method has been developed, it will be applied (with the same or equivalent column) over a period of weeks or months. The data in Table V suggest that during this time sample retention will change. The obvious question is

then the effect that this will have on separation. If the separation changes enough over a period of about 1 week to require redevelopment of the method, this could be a serious problem.

The data in Table V show a tendency toward shifts in retention that are larger than random variations in retention. This suggests that whereas shifts in retention do occur with continued use of the column, changes in relative retention (and resolution) will be smaller. This is borne out by the variation in values of $t_j - t_i$, which change more slowly with continued use of the column than do values of t_g, *e.g.*, for "NO–NO" *vs.* "YES–YES" cases in Table V (summary at the bottom of the table), variation in t_g increases 12-fold (5% *vs.* 0.4%), but the $t_j - t_i$ values show only a 3-fold increase in variability (11% *vs.* 4%).

If loss in resolution is experienced with continued use of a given column, it is possible to use computer simulation to modify the method. In the simplest case, the original input runs for computer simulation can be used to predict how the gradient should be modified to pull two overlapping bands apart. If a significant loss of resolution is experienced for several band pairs, two new runs (*e.g.*, with $t_G = 60$ and 240 min) can be carried out and the method redeveloped from the beginning*.

Runs B and G in Table V were carried out under conditions that should insure reliable predictions by computer simulation. It was of interest to examine the accuracy obtained when predicting retention for the 240-min run by using the 60- and 120-min runs as inputs for DryLab G (extrapolative prediction). When this was done, the same accuracy in the predicted values of t_g ($\pm 0.45\%$) and $t_j - t_i$ ($\pm 4\%$) was observed. In this instance, it is seen that comparable accuracy in computer predictions is obtained in either the 120-min or 240-min run (suggesting that curvature in the plots of log k' *vs.* φ in this system is minimal).

The accuracy of computer simulation for early eluted bands was also studied by starting the gradient at a higher acetonitrile concentration (as in Fig. 1c). Two runs with 26–46% actonitrile and gradient times of 60 and 240 min were used as inputs for computer simulation. Under these conditions, no bands showed significant pre-elution. Gradient steepness was next maintained constant (0.33%B/min), while the starting %B was varied from 21 to 41%. These experiments are summarized in Fig. 4, together with corresponding predicted separations from computer simulation. Experimental and predicted retention times are also summarized in Table VI. It is seen in Table VI that the overall precision of computer simulation for these examples (all bands) is about ± 0.4 min in retention time. However, bands pre-eluting near $t_0 + t_D = 13.4$ min ($8 < t_g < 20$ min; indicated by triple asterisks in Table VI) show about a 3-fold poorer agreement (± 1.4 min). This is not surprising, for the reasons discussed above. However, the effects of these errors on the predicted separations in Fig. 4 are seen to be of minor significance.

50S ribosomal protein sample. This sample contains a total of 32 proteins with molecular weights between 5000 and 30 000 Da. Several runs were carried out initially, varying only the gradient time. These data (summarized in Table VII) allow further comparisons of the accuracy of computer simulation for protein samples. Two runs with gradient times of 192 and 768 min (21–69% acetonitrile–water gradients) were

* This assumes that excess band broadening is not observed. If it does occur, the column may have to be replaced.

TABLE VI

EXPERIMENTAL *VS.* COMPUTER-SIMULATED RETENTION TIMES FOR GRADIENT RUNS WITH VARYING INITIAL %B (DRYLAB SIMULATION)

Data for 30S ribosomal protein sample. Conditions as in Table IV, except for gradient time and range.

*Band No.**	*Retention time (min)***							
	21–51%		*31–51%*		*36–56%*		*41–61%*	
	Expt.	*Calc.*	*Expt.*	*Calc.*	*Expt.*	*Calc.*	*Expt.*	*Calc.*
1	40.5	40.0	5.6	5.5		3.7		3.7
2	46.9	46.4	10.8	12.7***		4.1		3.7
3	51.9	51.5	20.2	20.7***		4.3		3.7
4	54.6	54.3	23.9	23.9		4.9		3.7
5	56.5	56.2	26.1	26.0		5.5		3.7
6	57.0	56.7	26.6	26.5		5.9		3.7
7	57.0	57.7	26.6	26.6	6.3	6.4		3.7
8	58.7	58.4	28.3	28.3	7.0	7.4		3.7
9	61.0	60.8	30.7	30.7	9.4	11.0***		3.8
10	68.2	67.8	37.9	37.8	21.1	22.1		4.1
11	68.8	68.4	38.7	38.4	23.2	23.0		4.6
12	68.8	68.4	38.7	38.4	23.2	23.3	5.6	5.2
13	70.1	69.7	39.9	39.7	25.0	24.3	5.6	5.2
14	70.7	70.3	40.6	40.3	25.0	25.1	5.6	5.5
15	71.6	71.1	41.1	41.1	25.8	25.9	6.1	5.8
16	78.7	78.1	48.4	48.1	33.1	33.0	14.4	15.8***
17	78.7	78.1	48.4	48.1	33.1	33.1	14.4	15.8***
18	80.1	79.4	49.7	49.4	34.4	34.4	17.1	18.1***
19	85.4	85.1	55.2	55.1	40.0	40.1	25.0	25.0
Average error:								
All bands	±0.4 min		±0.3 min		±0.3 min		±0.6 min	
Bands marked with	±0.6%		±0.9%		±1.3%		±4.1%	
triple asterisks			±1.2 min		±1.6 min		±1.3 min	
			±8%		±17%		±9%	

* Bands numbered in order of retention; band 1 is the second band in the chromatogram (the first band is omitted).

** 21–51% run has t_G = 90 min; other runs have t_G = 60 min.

*** Bands eluted within 8–20 min, *i.e.*, close to $t_0 + t_D$ = 13 min.

used as input data for computer simulation. The experimental retention-time data for several runs of intermediate t_G value are compared with computer-simulated values in Table VII, with generally good agreement (±0.8%). Predictions of average resolution are seen to be adequate (±4% overall).

In the following paper[5], a four-segment gradient for the optimized separation of this sample is described. Experimental and predicted retention times for this run agreed within ±0.5% (±0.8 min) and the average resolution agreed within ±8%.

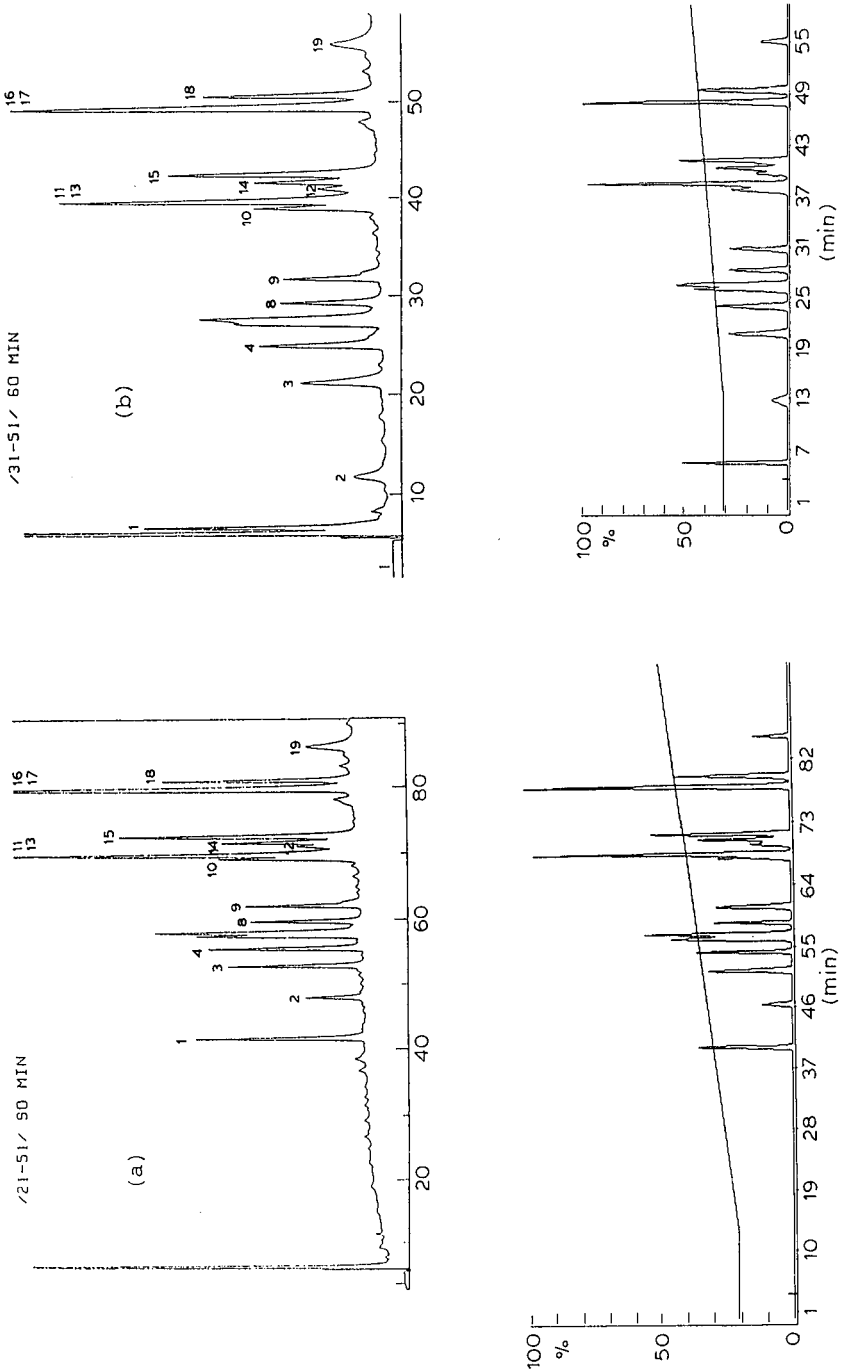
/21-51/ 90 MIN
(a)
/31-51/ 60 MIN
(b)
100
%
50
0
(min)

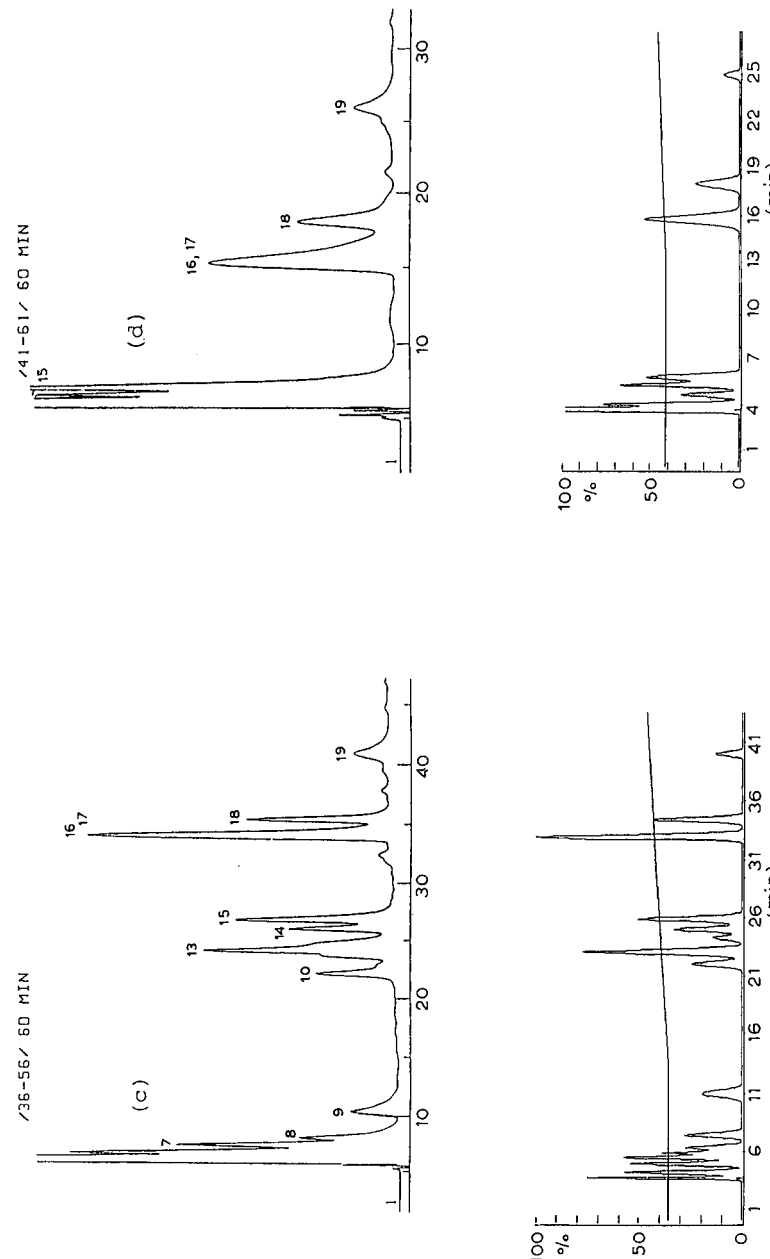

Fig. 4. Comparison of experimental and simulated chromatograms for 30S ribosomal sample (initial %B varying). Gradient steepness held constant (3 min/%); flow-rate, 0.7 ml/min. Input data for 26–46% B gradients; t_G = 60 and 240 min.

TABLE VII

COMPARISON OF PREDICTED *VS.* ACTUAL RETENTION TIMES FOR THE 50S RIBOSOMAL PROTEIN SAMPLE (DRYLAB SIMULATION)

Conditions as in Table IV, except for gradient range and time; 21–69% acetonitrile–water gradients. Experimental data for runs with t_G = 192 and 768 min (0.7 ml/min) were input into DryLab G.

*Band No.**	*Retention time (min)***							
	240 min		*288 min*		*480 min*		*576 min*	
	Expt.	*Calc.*	*Expt.*	*Calc.*	*Expt.*	*Calc.*	*Expt.*	*Calc.*
1	30.4	30.1	31.8	32.2	37.8	38.9	41.3	41.6
2	44.5	44.5	48.6	49.5	65.7	68.2	73.8	76.8
3	66.0	66.0	74.8	75.5	109.0	111.9	126.1	129.5
4	70.6	70.4	79.9	80.6	117.3	120.2	135.8	139.3
5	81.1	81.1	92.8	93.4	138.5	141.2	161.6	164.5
6	82.1	82.3	94.1	94.8	140.4	143.3	164.0	166.8
7	87.4	87.4	99.7	100.6	148.5	151.5	173.2	176.0
8	90.3	90.4	104.1	104.6	156.4	159.4	184.4	186.0
9	90.3	90.7	104.1	105.0	157.9	161.1	186.3	188.5
10	93.1	93.4	107.6	108.5	164.2	167.5	194.5	196.4
11	94.7	95.3	109.6	110.4	166.3	169.5	196.4	198.3
12	95.6	95.5	110.3	111.0	168.9	171.8	200.0	201.6
13	98.7	98.7	114.5	114.3	172.3	174.9	203.5	204.4
14	97.7	97.9	113.1	113.9	173.9	176.8	206.4	207.7
15	98.7	99.2	114.5	115.4	175.9	178.8	208.8	209.9
16	100.6	101.1	116.3	117.3	178.1	181.0	210.4	212.1
17	105.6	106.0	122.6	123.3	188.4	190.9	223.6	224.0
18	107.8	108.2	125.1	126.0	192.9	195.4	228.8	229.4
19	113.4	113.3	132.3	132.1	204.0	205.3	242.4	241.1
20	113.4	113.5	132.3	132.4	204.0	206.0	243.6	243.0
21	114.5	114.9	132.3	134.2	207.1	210.1	246.8	247.4
22	121.7	121.8	141.0	142.2	219.4	221.8	261.0	260.8
23	121.6	122.2	141.0	142.9	221.7	224.6	265.0	264.8
24	127.8	128.2	149.2	150.5	235.9	238.8	283.3	282.5
25	135.8	136.7	158.3	159.9	247.5	250.5	295.4	294.9
26	141.3	142.3	165.1	167.0	260.6	264.5	313.1	312.7
27	145.2	146.3	169.8	171.6	267.7	271.4	321.0	320.5
28	173.3	174.7	203.3	204.7	319.5	321.6	380.3	378.6
29	178.7	180.2	209.7	211.1	329.7	331.4	391.9	390.1
Average error, all bands:								
t_g	±0.4 min		±1.0 min		±2.6 min		±1.5 min	
	±0.4%		±0.8%		±1.4%		±0.7%	
R_s***	±5%		±4%		±3%		±5%	

* Bands numbered in order for 768-min run; one band pair overlaps in all gradients; two other bands omitted.

** Gradient times indicated for each run.

*** Average absolute error in $t_j - t_i$ divided by average value of $t_j - t_i$.

TABLE VIII

COMPARISON OF PREDICTED *VS.* ACTUAL RETENTION TIMES FOR IL-2 MUTEINS AND OXIDIZED DERIVATIVES (DRYLAB G SIMULATIONS)

Column, 25 × 0.46 cm I.D. C_8; 35–60% acetonitrile–water gradients (0.1% TFA); flow-rate, 2 ml/min. Data from ref. 26.

*Compound**	*Retention times, t_g (min), for indicated gradient times*				
	Experimental values			*Calculated values*	
	20	*40*	*80*	*40***	*80****
Ala^{1}Cys^{125}:					
M/S	20.02	33.18	57.43	33.28	57.02
O/S	21.04	35.03	61.06	35.21	60.34
M/O	22.18	36.30	62.50	36.71	60.87
O/O	23.56	38.99	67.78	39.41	66.11
Ala^{1}Ser^{125}:					
M/S	18.08	29.60	50.87	29.70	50.46
O/S	18.98	31.41	53.90	31.36	54.10
M/O	19.59	31.94	54.75	32.18	53.78
O/O	20.98	34.61	59.74	34.82	58.90
Error (1 S.D.):					
t_g				±0.25 (0.7%)	±1.02 (1.8%)
$t_j - t_i$				±0.17 (9%)	±0.64 (20%)

* M refers to an oxidized methionine, S to an oxidized sulfide bridge; thus M/S is the methione-oxidized disulfide form of the molecule; in ref. 19, M/S is referred to as A-ox, O/S as B-ox, M/O as A-red and O/O as B-red.

** Calculated from 20- and 60-min runs.

*** Calculated from 20- and 40-min runs.

Other examples from the literature

IL-2 muteins. Kunitani *et al.*[26] reported gradient retention data for 30 muteins* and/or oxidized derivatives of interleukin-2 (IL-2, molecular weight 14000 Da), including runs for each compound at three different gradient times (20, 40 and 80 min). These data can further test the accuracy of computer simulation in the same way as the preceding example for the ribosomal proteins. Two gradient runs can be used to predict retention for the third run (only t_G varying). Table VIII illustrates this for two different muteins and their various oxidized derivatives.

The predicted (calculated) t_g values for the 40-min run are in good agreement with experimental values (±0.7%), as are the retention time differences ($t_j - t_i$, ±9%). For the entire set of 30 compounds from ref. 25, retention times for the 40-min run agree within ±0.9% (1 S.D.).

* "Muteins" refer to related proteins which differ only in the substitution of one or a few amino acids (by other amino acids) in the polypeptide chain.

The comparisons for the 80-min run in Table VIII are much poorer, and the retention order of two bands is predicted incorrectly ($Ala^{1}Ser^{125}$ O/S and M/O). For the entire 30 compounds, the error in t_g was $\pm 2.3\%$. The poor results found for the 80-min runs may reflect (a) the use of initial t_G values (20 and 40 min) that are too similar, and/or (b) the use of extrapolative prediction for the 80-min runs *vs.* interpolative prediction for the 40-min runs. However, these factors did not limit the accuracy of extrapolative predictions for the 30S ribosomal proteins (above), suggesting that column variability may have been less well controlled in the IL-2 study in ref. 26 (*cf.*, discussion of Table V). DryLab G software tests for both (a) initial t_G values (experimental inputs) that are too similar and (b) computer predictions that involve excessive extrapolation. The user is alerted to possible errors in computer-simulated results when either of the latter tests fails. In either instance, more accurate computer simulations can be obtained by carrying out an additional experimental run (new value of t_G) and inputting the new data into the computer.

Nuclease muteins. Ford and Smith[27] reported gradient retention times for thirteen muteins of nuclease. Each compound was run with three different gradient times, 10, 20 and 60 min. Values of t_g for the 20-min runs agreed with computer simulated values (using 10- and 60-min runs) within ± 0.15 min (1 S.D.), corresponding to $\pm 1.2\%$. Retention time differences ($t_j - t_i$) were in much closer agreement (± 0.04 min).

These various studies (30S and 50S ribosomal proteins, IL-2 and nuclease muteins) suggest that computer simulation can be useful for purposes of method development when care is taken in the choice of conditions for the initial experimental runs.

Recommendations for the use of computer simulation with protein samples

The preceding discussion provides guidelines for maximizing the accuracy of computer-simulated separations by gradient elution, as summarized in Table I. Problems 5 and 7–9 are seen to be potentially the most serious. The impact of these sources of error in computer simulation can be minimized by the following procedures.

(1) Use HPLC systems with low mixing volumes, V_M, especially when using segmented gradients.

(2) When carrying out the initial two experimental runs, collect data in sequential runs within a 48-h period and use columns that have been previously conditioned by running several protein samples.

(3) Select initial gradient times that differ by a factor of at least 3–4 (*e.g.*, t_G values of 30 and 120 min); samples having higher molecular weights require longer gradient times.

(4) When entering data for two bands that overlap excessively in one of the initial (experimental) runs, be aware that the predicted resolution for these two bands can be in error. See further discussion below.

(5) Make sure that bands for the two initial runs are properly assigned for entry into DryLab G; this can be checked by comparing a simulated chromatogram for one run, based on band areas for the other. Alternatively, carry out a third experimental run with an intermediate gradient time and compare this chromatogram with one predicted by computer simulation. Errors in initial band assignment will result in major errors in the predicted retention of only a few bands, with most bands showing

much better agreement between experimental and computer-simulated runs. For further discussion, see ref. 3.

So far, we have said little about the problem of inaccurate t_g values from the initial experimental runs (illustrated in Fig. 3). Errors of this type are less common, inasmuch as special circumstances are required to create discrepancies as large as those of Fig. 3. One approach to dealing with this problem is as follows. First, be aware that errors of this type are possible when two bands overlap in one of the initial runs so as to yield only one value of t_g for the two bands. Second, when a simulated (optimized) chromatogram exhibits discrepancies as in Fig. 3 which seems attributable to band overlap, try to adjust the t_g values for the initially overlapped bands in a reasonable manner, so as to achieve better prediction of the final optimized run. With this new set of computer-simulation input values, it should be possible to largely correct for errors of the type illustrated in Fig. 3 (see also the further discussion of Fig. 5 in the following paper[6]). Note finally that the use of columns with large plate numbers minimizes the problem of inaccurate t_g values in the input data.

CONCLUSIONS

Computer simulation can be used to greatly reduce trial-and-error experiments in the laboratory during the development of HPLC methods based on gradient elution. However, the effective use of computer simulation requires sufficient accuracy in the predicted results. A number of experimental factors can lead to errors in predictions of separation via computer simulation. We have examined these various factors from both a theoretical and an empirical standpoint; practical recommendations are presented so as to ensure accurate predictions by computer simulation.

Experimental parameters or conditions that can play a significant role in affecting predictions of separation by computer simulation include: (a) the mixing volume, V_M, of the HPLC system, (b) changes in retention due to alteration of the column during use, (c) non-linearity of plots of log k' *vs.* percentage of organic compound for sample components, (d) errors in the measurement of experimental retention times t_g and (e) failure to recognize band reversals in the two experimental runs required for computer simulation. Each of these (and other) factors were examined in detail.

When experimental conditions were chosen to minimize these errors in computer simulation, good agreement was found between experimental and predicted separations for several protein samples. This in turn allows the use of computer simulation to facilitate the design of optimal gradients for the separation of protein samples.

GLOSSARY OF SYMBOLS

These apply to both this and the following two papers[5,6]. Reference to the following paper[5] is noted by use of "II" (*e.g.*, eqn. II-3 is eqn. 3 in ref. 5; Fig. II-2 is Fig. 2 in ref. 5); III refers to ref. 6

A, B, C.. bands or compounds in sample
b gradient steepness parameter, defined by eqn. 3
F mobile phase flow-rate (ml/min)

k' solute capacity factor (isocratic separation)
$\bar{k}$ average or effective value of k' for a band during gradient elution; equal to $1/1.15b$
k_f value of k' for band in gradient elution at the time the band leaves the column (eqn. II-2)
k_0 value of k' for a mobile phase having the same composition as at the start of the gradient (φ_0)
k_w value of k' for water as mobile phase ($\varphi = 0$)
n gradient shape parameter (eqn. III-4)
N column plate number
RRM relative resolution map, *e.g.*, Fig. II-12
R_s resolution of two adjacent bands; equal to the difference in retention times divided by the average baseline bandwidth
S defined by eqn. 1; equal to $d(\log k')/d\varphi$
S.D. standard deviation
t time after injection of sample and start of gradient (min)
t_D dwell time of gradient equipment (min); equal to V_D/F
t_g solute retention time in gradient elution (min)
$(t_g)_{10\%}$ time at which a band has migrated 10% of the distance through the column (min); eqn. II-5
t_i, t_j retention times t_g for adjacent solute bands i and j
t_G gradient time (min)
t_0 column dead-time (min)
V_D dwell volume of gradient elution equipment (ml); volume between (and including) mixer and column inlet
V_m dead volume of column (ml)
V_M mixing volume of gradient elution equipment (ml); usually equal to volume of gradient mixer
δF error in assumed value of F (eqn. 8)
δt_g error in a measured value of t_g (eqn. 8)
$\Delta\varphi$ change in mobile-phase composition (φ) during the gradient
φ mobile-phase composition (volume fraction of organic solvent in a water–organic solvent mixture)
φ_e mobile-phase composition (value of φ) in which a band is eluted from the column
φ_0 value of φ at the beginning of the gradient
φ^* value of φ which two adjacent gradient segments share; corresponds to the φ value at the end of the preceding segment and the φ value at the beginning of the following segment; φ^* equals φ_0 when the first segment is due to V_D and the second segment is the first gradient segment.

REFERENCES

1 L. R. Snyder and J. J. Kirkland, *Introduction to Modern Liquid Chromatogrphy*, Wiley-Interscience, New York, 2nd ed., 1979, p. 680.
2 J. L. Glajch, M. A. Quarry, J. F. Vasta and L. R. Snyder, *Anal. Chem.*, 58 (1986) 280.
3 J. W. Dolan and L. R. Snyder, *LC · GC, Mag. Liq. Gas Chromatogr.*, 5 (1987) 971.
4 J. W. Dolan, L. R. Snyder and M. A. Quarry, *Chromatographia*, 24 (1988) 261.

5 B. F. D. Ghrist and L. R. Snyder, *J. Chromatogr.*, 459 (1988) 25.
6 B. F. D. Ghrist and L. R. Snyder, *J. Chromatogr.*, 459 (1988) 43.
7 L. R. Snyder, in Cs. Horváth (Editor), *High-Performance Liquid Chromatography. Advances and Perspectives*, Vol. 1, Academic Press, New York, 1980, p. 207.
8 P. Jandera and J. Churacek, *Gradient Elution in Column Liquid Chromatography—Theory and Practice*, (*Journal of Chromatography Library*, Vol. 31), Elsevier, Amsterdam, 1985.
9 M. A. Stadalius and L. R. Snyder, in Cs. Horváth (Editor), *High-Performance Liquid Chromatography. Advances and Perspectives*, Vol. 4, Academic Press, New York, 1986, p. 195.
10 M. A. Quarry, R. L. Grob and L. R. Snyder, *J. Chromatogr.*, 285 (1984) 1.
11 M. A. Quarry, R. L. Grob and L. R. Snyder, *J. Chromatogr.*, 285 (1984) 19.
12 M. A. Quarry, R. L. Grob and L. R. Snyder, *Anal. Chem.*, 58 (1986) 907.
13 L. R. Snyder and M. A. Quarry, *J. Liq. Chromatogr.*, 10 (1987) 1789.
14 M. A. Quarry, R. L. Grob, L. R. Snyder, J. W. Dolan and M. P. Rigney, *J. Chromatogr.*, 384 (1987) 163.
15 L. R. Snyder and E. L. Inman, to be submitted.
16 C. T. Mant and R. S. Hodges, *LC · GC, Mag. Liq. Gas Chromatogr.*, 4 (1986) 250.
17 J. L. Glajch, J. J. Kirkland and J. Köhler, *J. Chromatogr.*, 384 (1987) 81.
18 M. A. Stadalius, H. A. Gold and L. R. Snyder, *J. Chromatogr.*, 296 (1984) 31.
19 M.-I. Aguilar, A. N. Hodder and M. T. W. Hearn, *J. Chromatogr.*, 327 (1985) 115.
20 S. Terabe, H. Nishi and T. Ando, *J. Chromatogr.*, 212 (1981) 295.
21 M. T. W. Hearn, in Cs. Horváth (Editor), *High-Performance Liquid Chromatography. Advances and Perspectives*, Vol. 3, Academic Press, New York, 1983, p. 88.
22 G. Jilge, R. Janzen, H. Giesche, K. K. Unger, J. N. Kinkel and M. T. W. Hearn, *J. Chromatogr.*, 397 (1987) 71.
23 W. G. Burton, K. D. Nugent, T. K. Slattery, B. R. Summers and L. R. Snyder, *J. Chromatogr.*, 443 (1988) 263.
24 K. D. Nugent, W. G. Burton, T. K. Slattery, B. F. Johnson and L. R. Snyder, *J. Chromatogr.*, 443 (1988) 381.
25 A. R. Kerlavage, T. Hasan and B. S. Cooperman, *J. Biol. Chem.*, 258 (1983) 6313.
26 M. Kunitani, D. Johnson and L. R. Snyder, *J. Chromatogr.*, 371 (1986) 313.
27 J. C. Ford and J. A. Smith, *J. Chromatogr.*, 390 (1987) 307.
28 B. F. D. Ghrist, B. S. Cooperman and L. R. Snyder, in F. E. Regnier and K. M. Gooding (Editors), *HPLC of Biological Macromolecules: Methods and Applications*, Marcel Dekker, New York, 1989.

Journal of Chromatography, 459 (1988) 25–41
Elsevier Science Publishers B.V., Amsterdam — Printed in The Netherlands

CHROMSYMP. 1452

DESIGN OF OPTIMIZED HIGH-PERFORMANCE LIQUID CHROMATOGRAPHIC GRADIENTS FOR THE SEPARATION OF EITHER SMALL OR LARGE MOLECULES

II.* BACKGROUND AND THEORY

B. F. D. GHRIST**
Medical Products Department, E.I. Du Pont de Nemours & Co., Concord Plaza, Wilmington, DE 19898 (U.S.A.)
and
L. R. SNYDER*
LC Resources Inc., 26 Silverwood Court, Orinda, CA 94563 (U.S.A.)

SUMMARY

The effect of the gradient on high-performance liquid chromatographic separations has been examined from a theoretical standpoint, using computer simulations to visualize the effects of different variables. Samples to be separated by gradient elution can be classified according to their separation characteristics into three groups (referred to here as cases I, II and III). Each of these sample types responds differently to a change in gradient conditions.

Case III samples exhibit changes in band spacing when the gradient conditions are varied, and gradients composed of multiple linear segments are especially useful for controlling band spacing and resolution for such samples. The effect of different gradient conditions (starting %B, gradient steepness and gradient shape) on the separation of case III samples is examined in detail.

INTRODUCTION

In some respects, the design of an appropriate gradient for a given sample in high-performance liquid chromatography (HPLC) is not a difficult task. Conventional wisdom[1–3] suggests that gradient steepness can be decreased for adequate resolution, then the gradient range (change in %B during the gradient) can be narrowed to save time. This procedure is illustrated in Figs. 1 and 2 for the simulated separation by gradient elution of a ten-component sample. Fig 1 shows that a 100-min gradient provides adequate resolution (Fig. 1d), which is not improved by longer gradients. In Fig. 2, a similar separation as in Fig. 1d results by trimming the gradient from 5–100% B to 40–85% B (Fig. 2f) while holding the gradient steepness constant.

* For Part I, see ref. 7.

** Present address: Eli Lilly Co., Indianapolis, IN 46285, U.S.A.

0021-9673/88/$03.50

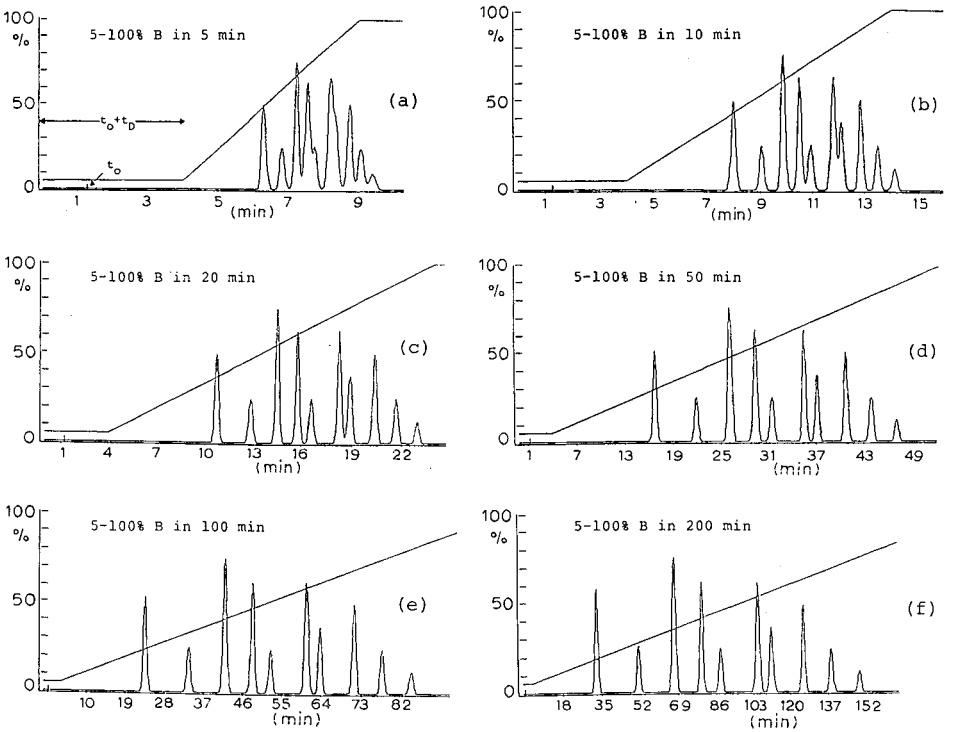

Fig. 1. Computer simulations (DryLab G) of the effect of gradient time on separation. Input conditions: V_D = 5.5 ml; 25 × 0.46 cm I.D. column; flow-rate, 2 ml/min; 5–100% B; t_G = 20 and 60 min; S = 5 for all compounds; log k_w = 2.0, 2.5, 2.9, 3.2, 3.4, 3.8, 3.95, 4.3, 4.6 and 4.9.

However, the latter separation requires only half as much time (47 min in Fig. 2f *vs.* 100 min in Fig. 1d).

Gradient shape is less often manipulated, although for some samples it is obvious that step gradients or gradient holds will be beneficial. As the sample complexity increases, however, there are greater rewards to be reaped from optimizing the gradient shape, *i.e.*, precisely tailoring the gradient to meet the needs of a given sample. Samples also often differ with respect to how relative retention changes with the gradient conditions; such differences can further favor the use of gradients having special shapes

The relationship between changes in gradient conditions and resulting changes in the chromatogram are widely, if somewhat vaguely, understood. These rough perceptions are often inadequate when dealing with very complex samples (such as many mixtures of peptides or proteins). This immediately becomes clear when using computer simulation as a means of developing a gradient method[4]. With this approach, many different gradients can be tried within a few minutes, and any limitations on the accuracy of our intuitional predictions quickly become apparent.

In this paper, we have tried to develop a better understanding of how chromatographic separation responds to various changes in gradient shape. Our

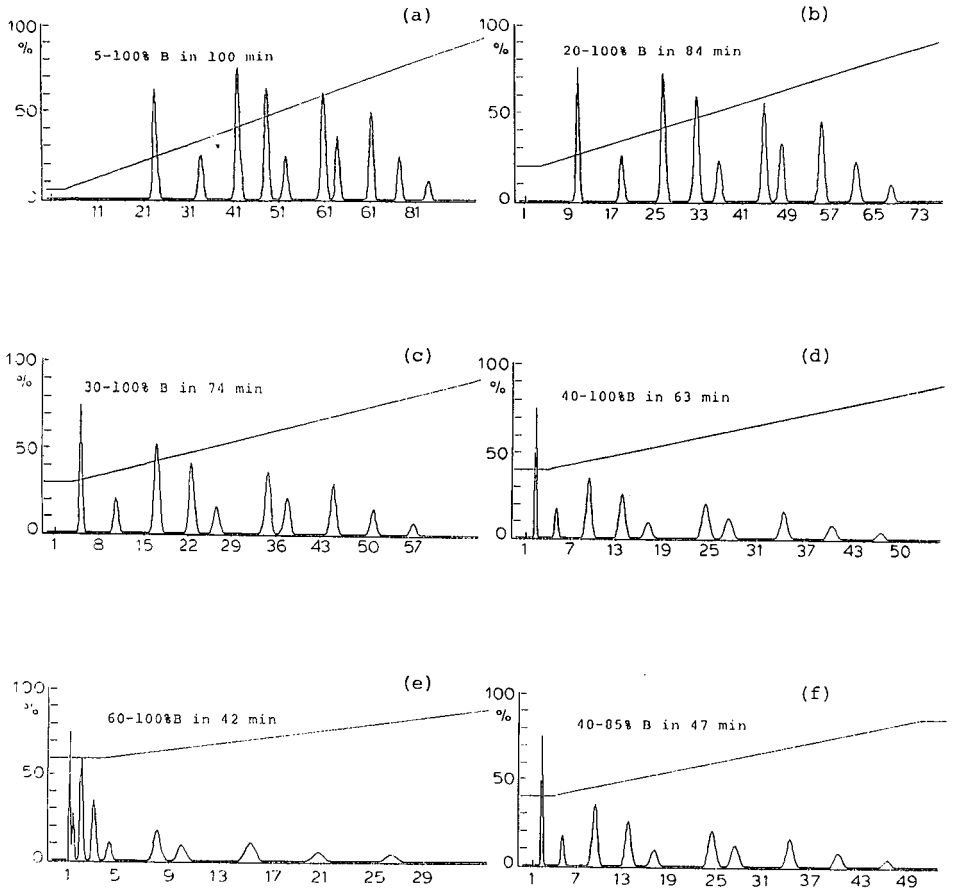

Fig. 2. Computer simulations (DryLab G) of the effect of gradient range on separation. Gradient steepness held constant. Conditions as in Fig. 1, unless indicated otherwise.

approach has been to use computer simulations (DryLab G software), where the results of change in the gradient are modeled according to theory without any of the (many) complications that can occur in experimental gradient separations. We have shown elsewhere[4–8] that (with suitable precautions) gradient simulation accurately predicts the results obtained from actual experimental runs, thus validating the approach that follows.

In the following paper[8], we apply the principles presented here for the design of optimized gradients for various samples.

THEORY

As discussed in the preceding paper[7], isocratic retention in reversed-phase systems can be approximated by

$$\log k' = \log k_w - S\,\varphi \qquad (1)$$

For the definition of these symbols and others introduced in Part I[7], see the Glossary of Symbols in that paper. There is generally some relationship between values of S and k_w for the components of a given sample, and this relationship determines how the gradient conditions will affect separation.

It is useful to recognize three possible relationships between S and k_w (or sample retention):

Case I: S values are approximately constant for all sample bands (independent of k_w).

Case II: S values tend to increase with increasing values of k_w (and increasing solute retention).

Case III: S values vary randomly with k_w and band retention.

Other cases (of limited practical interest) can also be imagined.

Cases I and II (no band-spacing changes)

For many samples comprising mixtures of closely related compounds, values of S for each compound are approximately equal, leading to parallel plots of isocratic retention *vs.* mobile-phase composition φ as in Fig. 3a. The dashed horizontal line in Fig. 3a corresponds to conditions of constant k' for every compound in the sample, or to values of k' at elution (k_f) in gradient elution (which are also constant for all bands). If a linear gradient is used, the quantity k_f is given by

$$k_f = 0.42\, t_G\, F/V_m\, \Delta\varphi\, S \qquad (2)$$

In a given separation, values of t_G, F, V_m and $\Delta\varphi$ are constant. This means that if the values of S are equal for all sample components, the values of k_f will also be equal; this is equivalent to values of k_f falling on the dashed horizontal line in Fig. 3a for a given run.

Retention in gradient elution (linear gradients) will parallel the intersection of these (solid) plots with horizontal (dashed) lines, as in Fig. 3a. Hence, values of k_f determine corresponding values of φ at elution (φ_e), and values of φ are proportional to time t during the gradient (the scale for the chromatogram at the bottom of Fig. 3a).

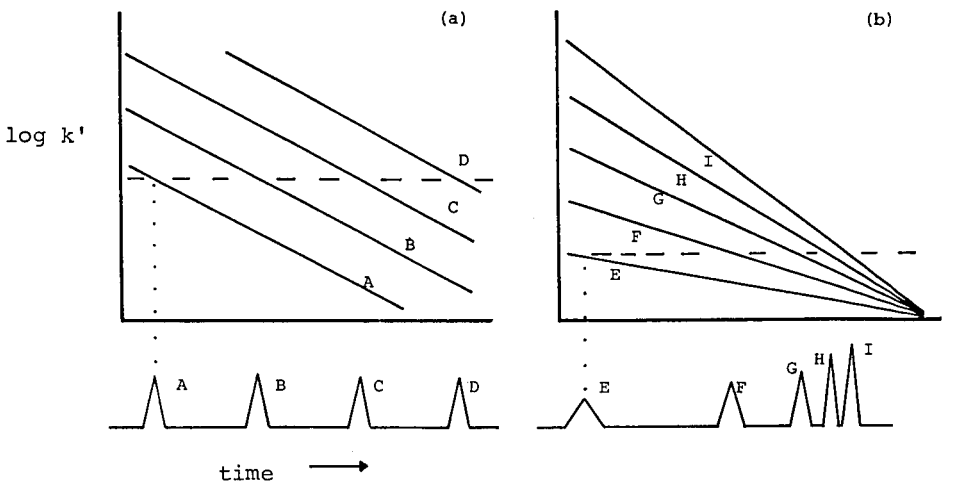

Fig. 3. Illustration of samples having a regular dependence of S on k_w. (a) Case I; (b) case II.

For constant S values (Fig. 3a) it is seen that the spacing of bands within the chromatogram tends to be regular and does not change with the gradient conditions (a change in t_G, F, V_m or $\Delta\varphi$ results in a change in k_f and a vertical shifting of the dashed line in Fig. 3a to higher or lower k_f values).

For many samples, there is a general tendency for values of S and log k_w to be linearly related[9,10]; in these cases S and sample retention usually increase continuously with increasing k_w. This gives rise to plots of log k' *vs.* φ as in Fig. 3b. It is seen that this results in a tendency for later bands to bunch together, with a resulting decrease in resolution; that is, a more or less regular spacing of bands is observed for Fig. 3a, but not for Fig. 3b* (linear gradients in each instance). However, the band sequence does not change with change in gradient conditions (just as for case I in Fig. 3a).

It is possible to make the spacing of bands as in Fig. 3b more even by using a convex gradient (*e.g.*, Fig. 16.9 in ref. 1 and Fig. 21 in ref. 2). However, such curved gradients come in a variety of forms, and the optimization of gradient curvature for a given sample is not straightforward. In the following paper[8], it will be seen that curved gradients are seldom required for samples as in Fig. 3b.

Case III (band-spacing changes)

The general pattern of Fig. 3b is often observed for samples such as homologues, benzologues, oligonucleotides and other oligomers[11–13]. For most samples containing peptides or proteins, however, the dependence of S on k_w is weak, leading to plots of log k' *vs.* φ as in Fig. 4a. Here, it is seen that the retention plots for each compound (A–G) are not parallel or congruent as in Fig. 3, but instead frequently intersect as φ is varied. For this example, four different gradient runs are indicated (dashed lines, t_G = 20, 40, 80 and 160 min). Note that gradient steepness can be defined as[1,2]

$$b = V_m \Delta\varphi \, S/t_G \, F = 1/(2.3 \, k_t) \tag{3}$$

If values of S for the sample are similar (as is often the case for non-oligomeric samples), then the value of k_f for each compound in a given gradient run (with V_m, $\Delta\varphi$, t_G and F fixed) will be roughly constant, corresponding to the horizontal dashed lines in Fig. 4a (as in Fig. 3a for case I samples).

The corresponding chromatograms for the 20-, 40- 80- and 160-min runs in Fig. 4a are shown in Fig. 4b. Because of the intersection of the different log k' *vs.* φ plots in Fig. 4 as φ is varied, the band spacing in these four runs varies:

20 min: A < B < E < D = C < F < G
40 min: A < B < C < D = E < F < G
80 min: A < B = C < D < E < F < G
160 min: A < B = C < D < E < F < G

If we compare Fig. 4a with the chromatograms in Fig. 4b, it is seen that the retention

---

* Note also that values of S increase with increasing solute retention, leading to smaller values of k_f and band narrowing (eqn. 2). This decrease in k_f also means that the dashed line in Fig. 3b (corresponding to band retention with a linear gradient) should be tilted (slightly) downward to the left.

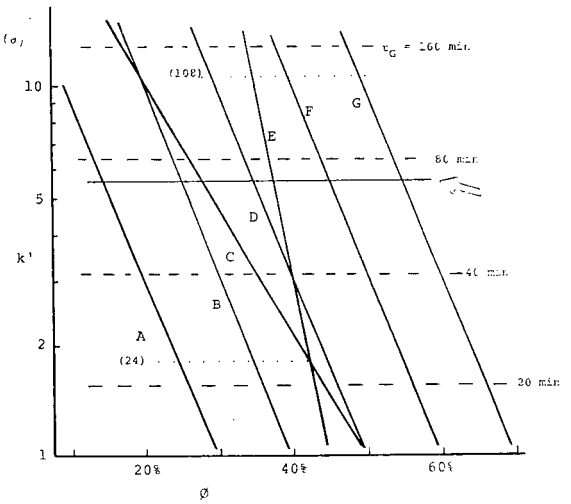

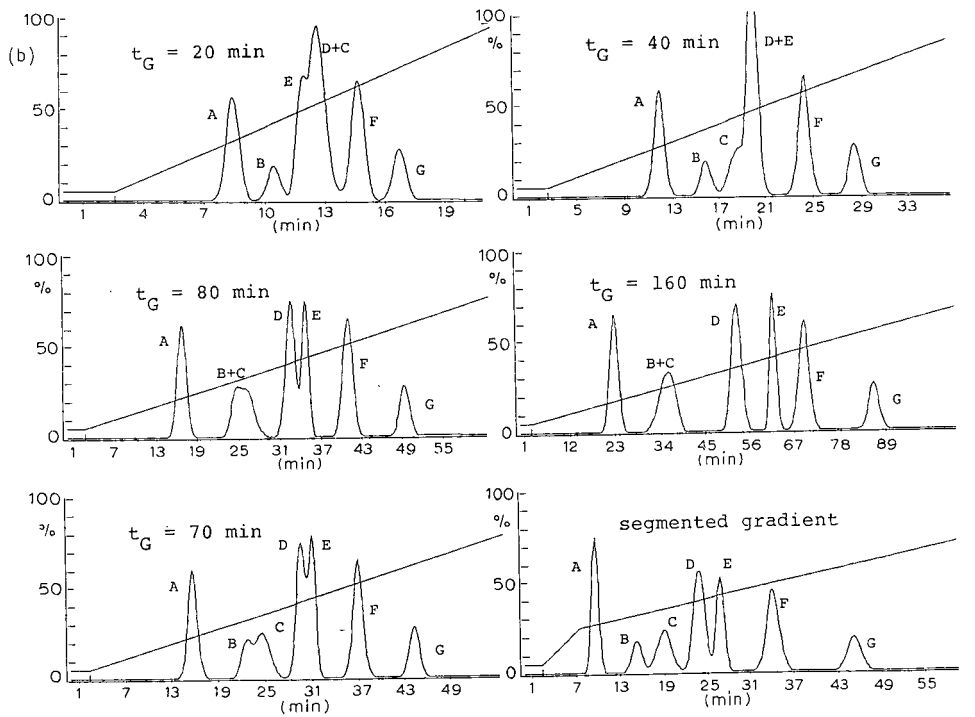

Fig. 4. Illustration of a sample having an irregular dependence of S on k_w (case III). (a) isocratic plots of log k' *vs.* φ (heavy diagonal lines); (b) gradient runs with t_G varying (5–100%B gradients). DryLab G simulations; arrow in (a) indicates the gradient time for an optimum overall band spacing (and resolution).

order for different gradient times is accurately predicted by the isocratic plots in Fig. 4a*.

For this particular sample, no single gradient time (20–160 min) provides a good spacing of the bands within the chromatogram, although the optimal time [t_G = 70 min; see Fig. 4a (arrow) and b] give a marginal resolution of all bands. However, we see that t_G = 20 min provides a good separation of bands A–C, and gradient times of 80–160 min provide good resolution for bands C–G. This suggests beginning with a steep gradient (similar to the 20-min gradient) for the elution and good resolution of bands A–C, followed by a decrease in gradient steepness (80 < t_G < 160 min) for the successful resolution of the remainder of the sample. This separation is shown in Fig. 4b (last chromatogram, "segmented gradient"). Now all seven bands are much better resolved.

The design of the optimal segmented gradient in Fig. 4b can be inferred from the log k' *vs.* φ plots in Fig. 4a. Thus in Fig. 4a it is seen that a gradient time of 24 min (4.8%/min) provides an optimal spacing of bands A–C (lower dotted horizontal line), whereas a gradient time of 108 min (0.9%/min) provides an optimal spacing of bands C–G (upper dotted horizontal line). The segmented gradient in Fig. 4b begins with a gradient steepness of 4.8% B/min, then changes to 0.9% B/min just prior to elution of band A. However, choosing the point in the gradient (φ*) for a change in gradient steepness is not so obvious, as discussed below.

Segmented gradients: effects of slope changes on retention

Segmented gradients (as in the foregoing example) have been successfully used for the improved resolution of complex samples[5,6]. However, this approach is less simple than suggested by the above discussion. The reason is that retention and band spacing depend not only on the steepness of the gradient during the time two bands are eluted, but also on the steepness (and duration) of the preceding gradient segment.

Consider first the migration of a band through the column during gradient elution, as pictured in Fig. 5. During the beginning of gradient elution (time < 10 min), the k' value of the band is usually large and the band remains at the column inlet. At some time during the gradient, the value of φ becomes large enough to decrease k' for the band to *ca.* 20, and the band begins to move through the column (at about 12 min in Fig. 5). Eventually the band leaves the column (at 24.5 min in the example in Fig. 5). Changes in the gradient prior to the time when $k' \approx 20$ will have little effect on the separation of a band from adjacent bands in the sample, because during this time ($k' > 20$) there has been little movement (< 10%) of the band(s) from the column inlet; that is, the history of the separation up to the point where $k' < 20$ is irrelevant to the subsequent migration and separation of these sample bands.

On the other hand, a change in gradient steepness after significant band migration has occurred (segmented gradient as in Fig. 4b) means that the band *will* have

---

* The horizontal lines in Fig. 4a correspond to k' values for each solute when that solute has migrated 40% of the way through the column, corresponding to $k' = 1.25\,\bar{k}$. This reflects the fact that separation is influenced more by initial elution ($k' > \bar{k}$) than by later elution, because resolution is greater for larger values of k', other factors being equal.

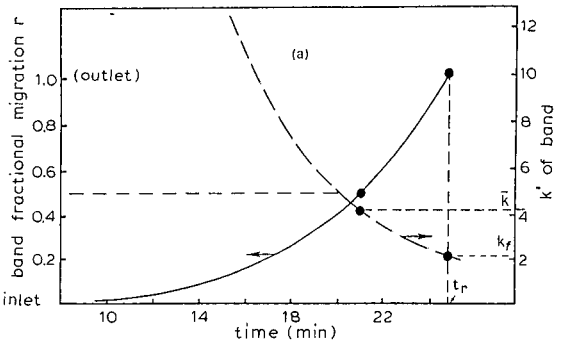

Fig. 5. Illustration of migration of a sample band along the column during gradient elution (solid curve); corresponding dependence of solute k' value on time is indicated by the dashed line. See text for details.

been influenced by both gradient segments. In this instance, we cannot assume that the separation will be independent of the preceding gradient segment. In the use of segmented gradients, it is conceptually convenient to assume that the final separation is determined by the segment during which bands of interest are eluted. This then raises the question of how much time must have elapsed since a change in gradient steepness in order for this to be true; or, if the change in gradient steepness occurs at some value of $\varphi(\varphi^*)$, what value of $\varphi_e - \varphi^*$ is required for there to be no effect on separation by the preceding gradient segment.

The condition for 10% (or less) migration of a band during gradient elution is readily derived. The retention time of a band during gradient elution is given by eqn. 2 in ref. 7 (assumes that k_0 is large):

$$t_g = (t_0/b)\,[\log(2.3\,k_0\,b)] + t_0 + t_D \tag{4}$$

Similarly, the time required for migration of the band 10% along the column (from the inlet) is[2]

$$(t_g)_{10\%} = (t_0/b)\,[\log(0.23\,k_0\,b)] + 0.1\,t_0 + t_D \tag{5}$$

The last two terms in eqns. 4 and 5 can be ignored as far as band spacing is concerned, as they comprise a constant term for each of two adjacent bands. The difference in retention times (corresponding to band migration from 10 to 100% of the column length) is then

$$t_g - (t_g)_{10\%} = (t_0/b)[\log(10)] \tag{6}$$

which (with eqn. 3) gives

$$t_g - (t_g)_{10\%} = t_G/(\Delta\varphi\,S) \tag{7}$$

or

$$t_g(\Delta\varphi/t_G) - (t_g)_{10\%}\,(\Delta\varphi/t_G) = 1/S \tag{7a}$$

The two left-hand-side terms correspond to values of φ at elution (φ_e) and after 10% migration through the column (φ^*), so that

$$\varphi_e - \varphi^* = 1/S \tag{8}$$

Eqn. 8 indicates the condition for a prior gradient segment *not* affecting separation in a following segment. For example, if a band is eluted at $\varphi_e = 0.6$, and $S = 20$ for the compound, then a change in gradient steepness (new gradient segment) should start at $\varphi^* = 0.60 - (1/20) = 0.55$ or earlier, if the separation of the band from adjacent bands is not to be influenced by the preceding gradient segment (however, smaller values of $\varphi_e - \varphi^*$ may still yield acceptable resolution for a given sample, despite a significant change in resolution as a function of φ^*).

APPLICATION

Case III: principles of separation

Samples corresponding to case III are the most amenable to gradient optimization; that is, fine tuning the gradient can make a more significant difference in the final separation than for case I or II samples. Mixtures of peptides and proteins generally fall into case III, as do many other samples of both high and low molecular weight. Case III samples usually show an average improvement in resolution as gradient time is increased, similarly to the case I example in Fig. 1. For samples corresponding to case III, however, one or more band pairs will show maximum resolution for intermediate values of t_G. This is clearly different from the examples in Fig. 1 (case I) and Fig. 1 of the following paper[8] (case II).

Fig. 4 shows the advantage of using either an intermediate gradient time (70 min) or a multi-segment gradient for case III samples. Examples of this for both low- and high-molecular-weight samples have been reported[5,6]. Often the overall problem of designing an optimal gradient can be broken down into a series of "critical" band groups (*e.g.*, B/C and D/E in Fig. 4). By varying the gradient steepness for a critical group of adjacent bands, we can position the bands so as to achieve equal resolution for each band pair in the group (and thereby maximize the resolution of the poorest resolved band pair in the sample). In order to design an optimal gradient for case III samples, we need to understand how various changes in the gradient affect band spacing and resolution. The following discussion will attempt to provide this understanding, by using model three-component samples as examples.

Effects of gradient time and starting %B. Fig. 6 describes the isocratic retention of a hypothetical three-component sample as a function of mobile-phase composition (%B or φ). In this example, compound 2 has a much smaller value of S (3) than the other two compounds ($S = 5$). This will magnify the effects of gradient time and starting %B on band spacing. The separation of this sample with a 5–100% B gradient and different gradient times t_G is shown in Fig. 7a–c ("real" samples will normally exhibit less extreme changes in band spacing for similar changes in gradient conditions, because of smaller differences in S for adjacent bands). Band 2 is seen to change its position in the chromatogram as t_G (and gradient steepness) changes. Similarly, if the gradient steepness is held constant (runs in Fig. 7c–f), a change in the starting %B also

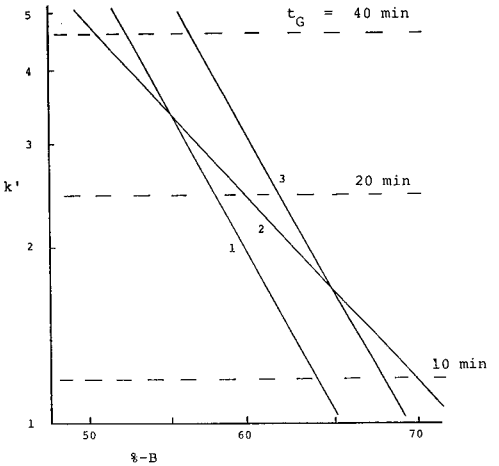

Fig. 6. Isocratic retention of a hypothetical three-component sample, showing band reversals with change in φ (isocratic) or t_G (gradient). Values of S: (1) 5.11; (2) 3.04; (3) 5.11. Values of log k_w: (1) 3.337; (2) 2.204; (3) 3.542.

leads to changes in band spacing. These variations in band spacing can be understood in terms of the retention diagram in Fig. 6. Thus, an increase in gradient time (10–40 min) corresponds to an increase in $k' = \bar{k}$ (dashed lines in Fig. 6), leading to the same change in band spacing as seen in Fig. 7a–c (relative retention of band 2 decreases). Likewise, an increase in %B (isocratic) leads to an increase in the relative retention of band 2 (Fig. 6); a similar increase in the relative retention of band 2 is seen in Fig. 7c–f for gradient elution when φ_0 is increased (as a result of the isocratic pre-elution of the sample by the starting mobile phase).

We have carried out simulations for other hypothetical samples, where both S and k_w for the bands were varied over wide limits. These results are plotted in Fig. 8 (circles) as values of $\varphi_e - \varphi_0$ *vs.* S for a 10% change in resolution. Also included (squares) are values for several critical band pairs found in the 30S ribosomal protein sample described in ref. 6. These data lie reasonably close to the solid curve in Fig. 8; the dashed curve is that predicted by eqn. 7. Differences between the two curves reflect (a) our arbitrary definition of a "sigificant" change in resolution (5% change in R_s), (b) a minor dependence of experimental values of $\varphi_e - \varphi_0$ on the differences in S values for the bands within the triplet and (c) other factors.

The main significance of Fig 8 is that it provides an approximate measure of when φ_0 (or φ^*) is likely to affect the separation of a band triplet. Note in Fig. 8 (top scale) that an estimate of $\varphi_e - \varphi_0$ (or $\varphi_e - \varphi^*$) can be obtained from the molecular weight of the sample; a value of S need not be known. Values of $\varphi_e - \varphi_0$ or $\varphi_e - \varphi^*$ estimated from Fig. 8 are conservative. Often larger values of φ_0 or φ^* can be used before an unacceptable loss of resolution occurs.

Segmented gradients: pre-elution. The simplest segmented gradient results from the use of a linear (unsegmented) gradient under normal conditions. When there is an appreciable dwell volume V_D in the system (as in all the present examples, *e.g.*, Fig. 7a), the initial elution of the sample is effected by a mobile phase with $\varphi = \varphi_0$ (isocratic

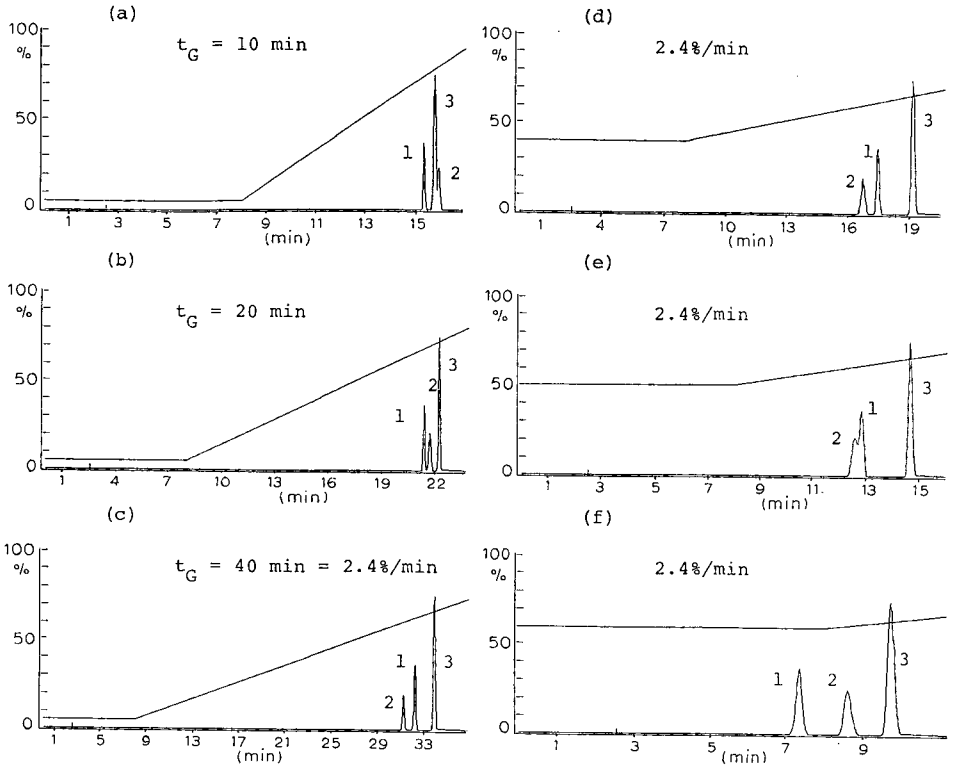

Fig. 7. Changes in band spacing for the sample in Fig. 6 when the gradient time t_G or the initial mobile-phase composition φ_0 is changed. Conditions: V_m = 2.5 ml; V_D = 5.5 ml; flow-rate, 1.0 ml/min; 5–100% B unless indicated otherwise.

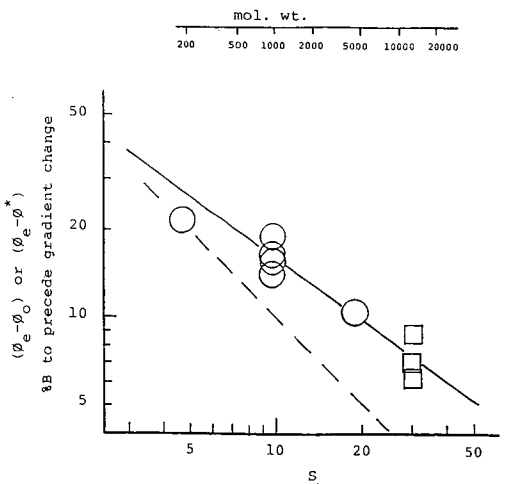

Fig. 8. Necessary length of gradient segment prior to elution of a critical band pair without loss of resolution. See text.

elution). Hence an initial segment equivalent to a very flat gradient precedes the gradient that is entered into the gradient controller. This particular case is of interest in its own right; it also provides a basis for understanding what happens when multi-segment gradients are intentionally used.

Fig. 9 shows further simulations for another hypothetical sample (involving smaller, more realistic, differences in S). Because the initial elution of the sample occurs under isocratic conditions (during passage through the column of a volume V_D of mobile phase having $\varphi = \varphi_0$), it is helpful to examine band elution under isocratic conditions. Fig. 9a shows the effect of a change in φ (isocratic elution) on the relative

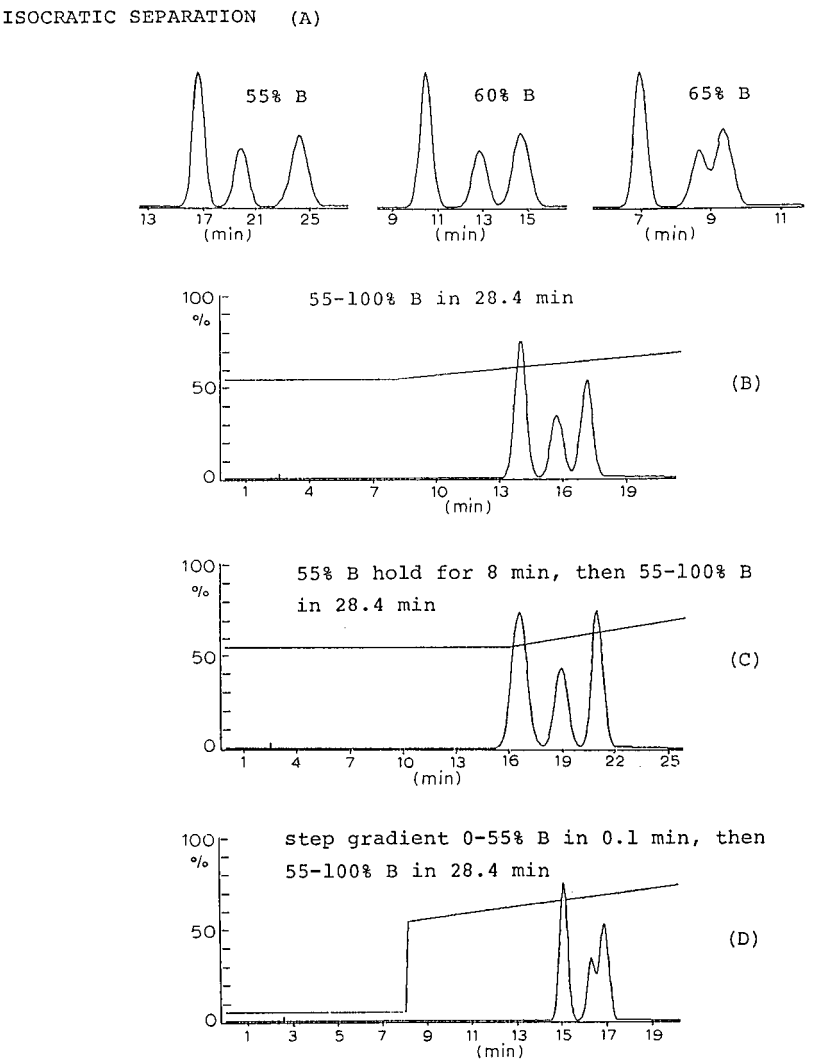

Fig. 9. Effect of isocratic elution in a preceding segment on separation in a following gradient segment. Conditions and sample as in Fig. 6, unless indicated otherwise. Values of S for these three compounds are 5, 5 and 4.5.

spacing and resolution of the three bands. As φ is increased, the middle band (smaller S value) moves toward the late-eluted band.

Now consider the effect of the dwell volume on the corresponding gradient separation (Fig. 9). The initial gradient separation (Fig. 9b, φ_0 = 55% B and V_D = 5.5 ml) shows the middle band slightly closer to the later eluted band, whereas the isocratic separation (Fig. 9a) with φ = 55% B places the middle band closer to the early eluted band. Increasing the value of V_D or incorporating a gradient hold at the

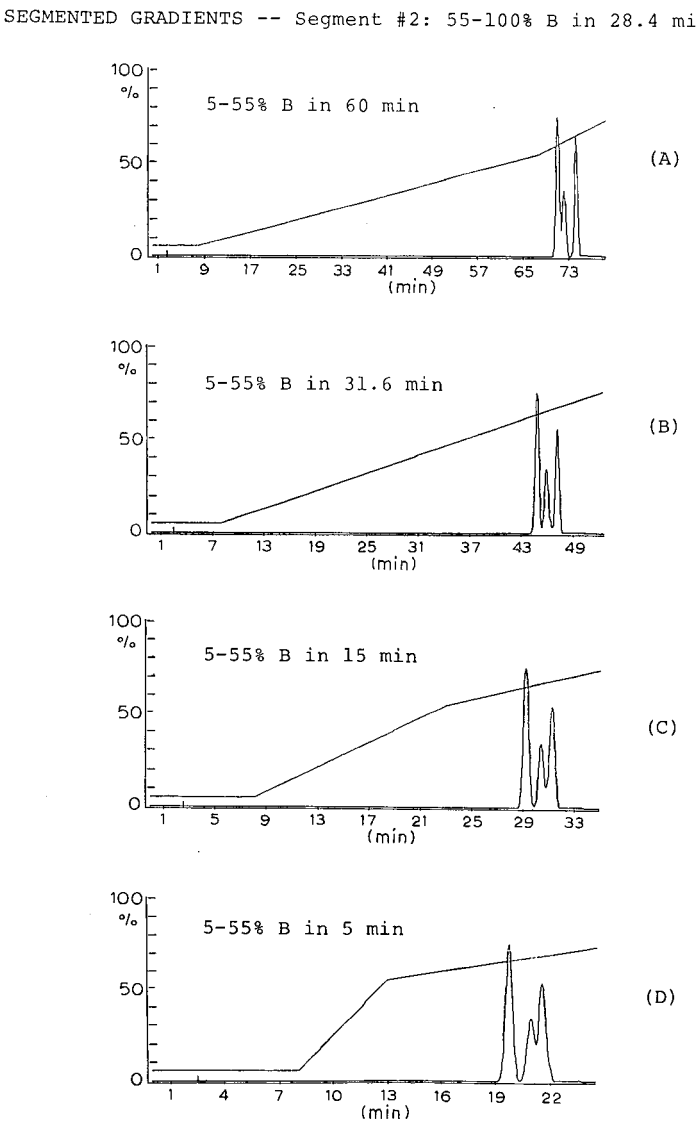

Fig. 10. Effect of prior gradient segment on separation of a critical band pair eluted in a subsequent segment. Conditions and sample as in Fig. 6, unless indicated otherwise.

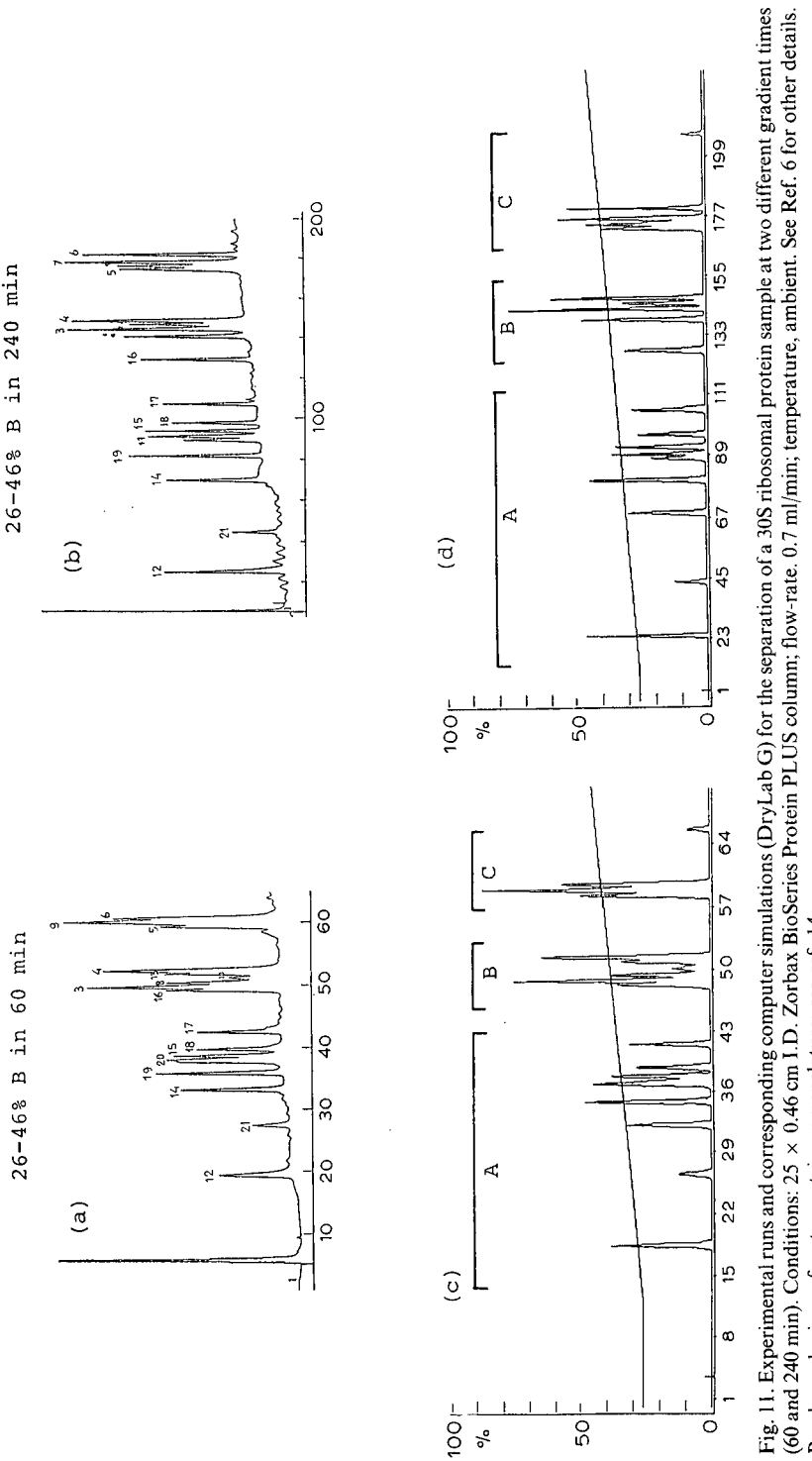

Fig. 11. Experimental runs and corresponding computer simulations (DryLab G) for the separation of a 30S ribosomal protein sample at two different gradient times (60 and 240 min). Conditions: 25 × 0.46 cm I.D. Zorbax BioSeries Protein PLUS column; flow-rate. 0.7 ml/min; temperature, ambient. See Ref. 6 for other details. Band numbering refers to protein nomenclature; see ref. 14.

beginning of the separation should lead to a separation more like that for isocratic elution with 55% B, and this is seen to be the case in Fig. 9c.

Conversely, the use of an initial step gradient freezes the sample at the column inlet until the actual start of the gradient. This should be equivalent to eliminating the dwell volume, giving the separation shown in Fig. 9d (movement of middle band toward later eluted band).

Segmented gradients: effect of prior segment. The effect of a prior gradient segment on separation by multi-segmented gradients is illustrated in Fig. 10. In each of these examples the second gradient segment (during which the sample bands are eluted) is held fixed at 55–100% B in 28.4 min. The preceding gradient segment varies from shallower (Fig. 10a) to equal (Fig. 10b) to steeper (Fig. 10c and d). These results (same sample as for Fig. 9) can be understood in terms of the similar examples in Fig. 9. The use of a shallower preceding segment will give rise to effects similar to those produced by more extensive pre-elution (larger value of V_D). Likewise, the use of a steeper preceding segment yields results like those obtained with a step gradient (Fig. 9d).

The examples in Figs. 6–10 plus the above discussion suggest that the effect of a previous gradient segment on the separation of bands eluted in a following segment can be complicated. From a practical standpoint, however, this is relatively unimportant. Changes in relative peak position (and resolution) as a result of the preceding segment can to a considerable extent be offset by changing the slope of the segment in which the bands of interest are eluted (as in Fig. 7). This is next illustrated by the separation of the 30S ribosomal proteins (Fig. 11).

The separation of the 30S ribosomal proteins by reversed-phase gradient elution yields chromatograms which can be subdivided into three distinct groups of bands: A, B and C in Fig. 11 [experimental (a and b) and simulated (c and d) chromatograms]. Bands 10–15 are eluted as a marginally resolved cluster (B), over a φ_e range of 38–39%. The closest preceding bands which are difficult to resolve (bands 5–7 in group A) are eluted before 35% B. We shall see that it is profitable to use different gradient slopes for the separation of bands 1–7 (A) and 10–15 (B); this means a change in slope will be required at about 35% B. As the value of $\varphi_e - \varphi^*$ for this sample (see Fig. 11) is about 7%, this suggests that the initial gradient segment (to elute bands 1–7) may have a significant effect on the resolution of bands 10–15 in the following segment. The question is whether we can still obtain the same resolution (regardless of the first segment) by varying the slope of the second segment, that is, whether slope adjustments can compensate for changes due to the preceding segment.

We can answer this question for the sample in question by constructing resolution maps for just the six bands of interest (bands 10–15) as a function of gradient range. The results for different values of φ_0 are shown in Fig. 12. It can be seen that there is no significant change in these maps until φ_0 exceeds 34%. Interestingly, the adjustment of gradient time for larger values of φ_0 leads to the same minimum resolution ($R_s = 0.8$) for $0 < \varphi_0 < 37\%$. Only when φ_0 exceeds 37% (Fig. 12g) and the sample is eluted isocratically does the minimum resolution drop below a value of $R_s = 0.8$. This example confirms that adjustments in the slope of a gradient segment can be used to largely overcome the effect of a preceding segment, even for $\varphi_e - \varphi^*$ values much smaller than predicted by Fig. 8. Hence $\varphi_e - \varphi_0 > 1\%$ is acceptable in the present case.

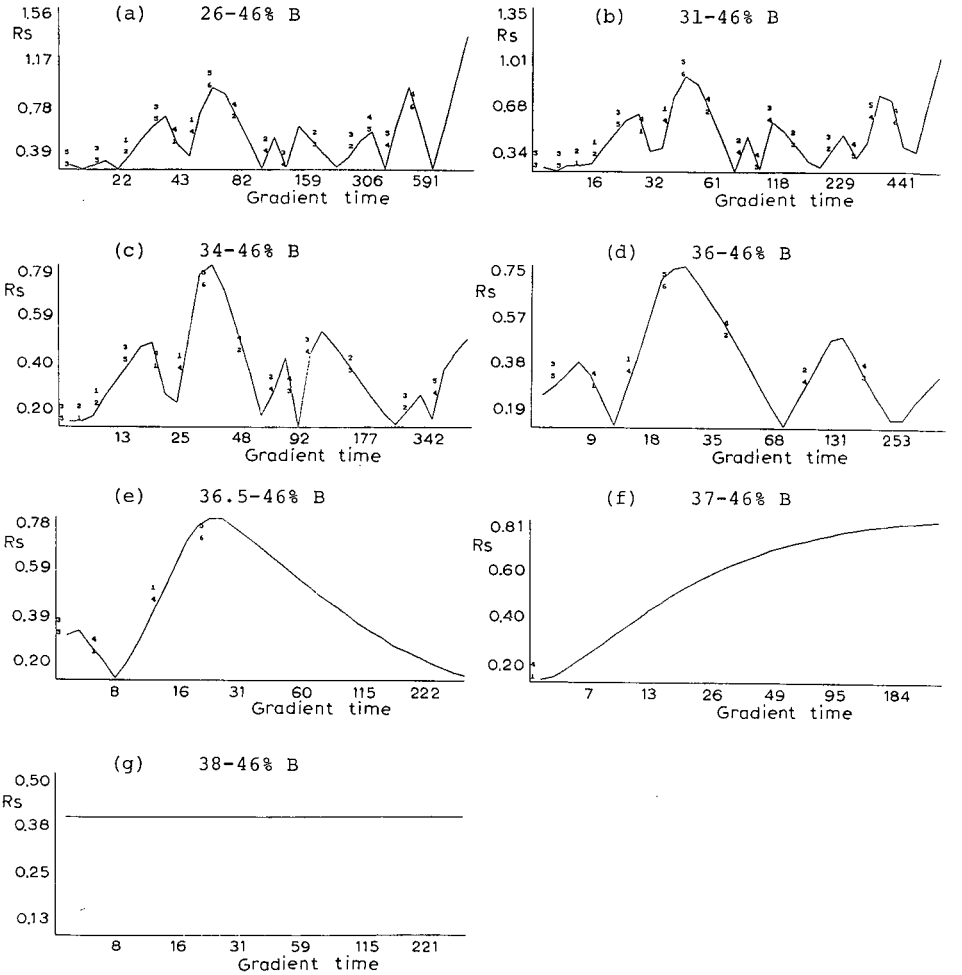

Fig. 12. Separation of bands 10–15 of a ribosomal protein sample as a function of initial %B (φ_0). Relative resolution maps ($N = 2500$) as a function of gradient time. DryLab G simulations. For conditions, see Fig. 11.

CONCLUSIONS

The various factors that contribute to maximizing resolution in a gradient elution separation have been examined in detail. Various samples can be categorized according to the appearance of two initial (linear gradient) chromatograms with different t_G values for the two runs, *e.g.*, see Figs. 3 and 4. Some samples exhibit minimum changes in band position as the gradient time is changed. The selection of optimized gradient conditions for these samples is relatively straightforward (see the following paper[8]).

Other samples (these include many peptide and protein mixtures) exhibit

pronounced changes in band spacing as the gradient steepness (or time) is varied. Typically, the resolution of such samples can be optimized by choosing gradients of different steepness for different parts of the chromatogram (multi-segmented gradients). However, the separation in any one region of the chromatogram will be dependent on some fraction of the (multi-segmented) gradient that precedes the elution of that part of the sample. Criteria for evaluating the magnitude of this effect are given and illustrated with various examples.

REFERENCES

1 L. R. Snyder and J J. Kirkland, *Introduction to Modern Liquid Chromatography*, Wiley-Interscience, New York, 2nd ed., 1979, Ch. 16.
2 L. R. Snyder, in Cs. Horváth (Editor), *High-Performance Liquid Chromatography. Advances and Perspectives*, Vol. 1, Academic Press, New York, 1980, p. 207.
3 L. R. Snyder, M. A. Stadalius and M. A. Quarry, *Anal. Chem.*, 55 (1983) 1412A.
4 J. W. Dolan and L. R. Snyder, *LC · GC Mag. Liq. Gas Chromatogr.*, 5 (1987) 91.
5 J. W. Dolan, L. R. Snyder and M. A. Quarry, *Chromatographia*, 24 (1988) 261.
6 B. F. D. Ghrist, B. S. Cooperman and L. R. Snyder, in F. E. Regnier and K. M. Gooding (Editors), *HPLC of Biological Macromolecules: Methods and Applications*, Marcel Dekker, New York, 1989.
7 B. F. D. Ghrist, B. S. Cooperman and L. R. Snyder, *J. Chromatogr.*, 459 (1988) 1.
8 B. F. D. Ghrist and L. R. Snyder, *J. Chromatogr.*, 459 (1988) 43.
9 P. J. Schoenmakers, H. A. H. Biliet and L. de Galan, *J. Chromatogr.*, 185 (1980) 179.
10 L. R. Snyder, M. A. Quarry and J. L. Glajch, *Chromatographia*, 24 (1987) 33.
11 N. Tanaka and E. R. Thornton, *J. Am. Chem Soc.*, 99 (1977) 7300.
12 J. P. Larmann, J. J. DeStefano, A. P. Goldberg, R. W. Stout, L. R. Snyder and M. A. Stadalius, *J. Chromatogr.*, 255 (1983) 163.
13 J. D. Pearson and F E. Regnier, *J. Chromatogr.*, 255 (1983) 137.
14 A. R. Kerlerage, T. Hasan and B. S. Cooperman, *J. Biol. Chem.*, 258 (1983) 6313.

Journal of Chromatography, 459 (1988) 43–63
Elsevier Science Publishers B.V., Amsterdam — Printed in The Netherlands

CHROMSYMP. 1453

DESIGN OF OPTIMIZED HIGH-PERFORMANCE LIQUID CHROMATOGRAPHIC GRADIENTS FOR THE SEPARATION OF EITHER SMALL OR LARGE MOLECULES

III*. AN OVERALL STRATEGY AND ITS APPLICATION TO SEVERAL EXAMPLES

B. F. D. GHRIST**
Medical Products Department, E. I. Du Pont de Nemours & Co., Concord Plaza, Wilmington, DE 19898 (U.S.A.)
and
L. R. SNYDER*
LC Resources Inc., 26 Silverwood Court, Orinda, CA 94563 (U.S.A.)

SUMMARY

Recommendations are presented for an efficient approach to the design of optimized gradients for complex samples using computer simulation. Examples based on the separation of polyaromatic hydrocarbon and ribosomal protein mixtures are shown.

INTRODUCTION

The preceding paper[1] described how different sample types (cases I–III) respond to various changes in gradient conditions. Based on that discussion, this paper outlines a general approach to the design of gradients for maximum resolution and/or minimum run time for each sample type, especially case III samples (where the band spacing varies with the gradient conditions).

DESIGN OF OPTIMAL GRADIENTS

Case I samples

This is illustrated in Figs. 1 and 2 in ref. 1, assuming a sample with a molecular weight of about 200. Increasing the gradient time (with other conditions fixed) leads to a progressive increase in resolution, until the average k' value for sample bands ($\overline{k} = 1/1.15b$) equals about 10. A further increase in t_G beyond this point leads to minimal additional improvement in resolution. At the same time, bands broaden in approxi-

* For Parts I and II, see refs. 4 and 1.
** Present address: Eli Lilly Co., Indianapolis, IN 46285, U.S.A.

0021-9673/88/$03.50

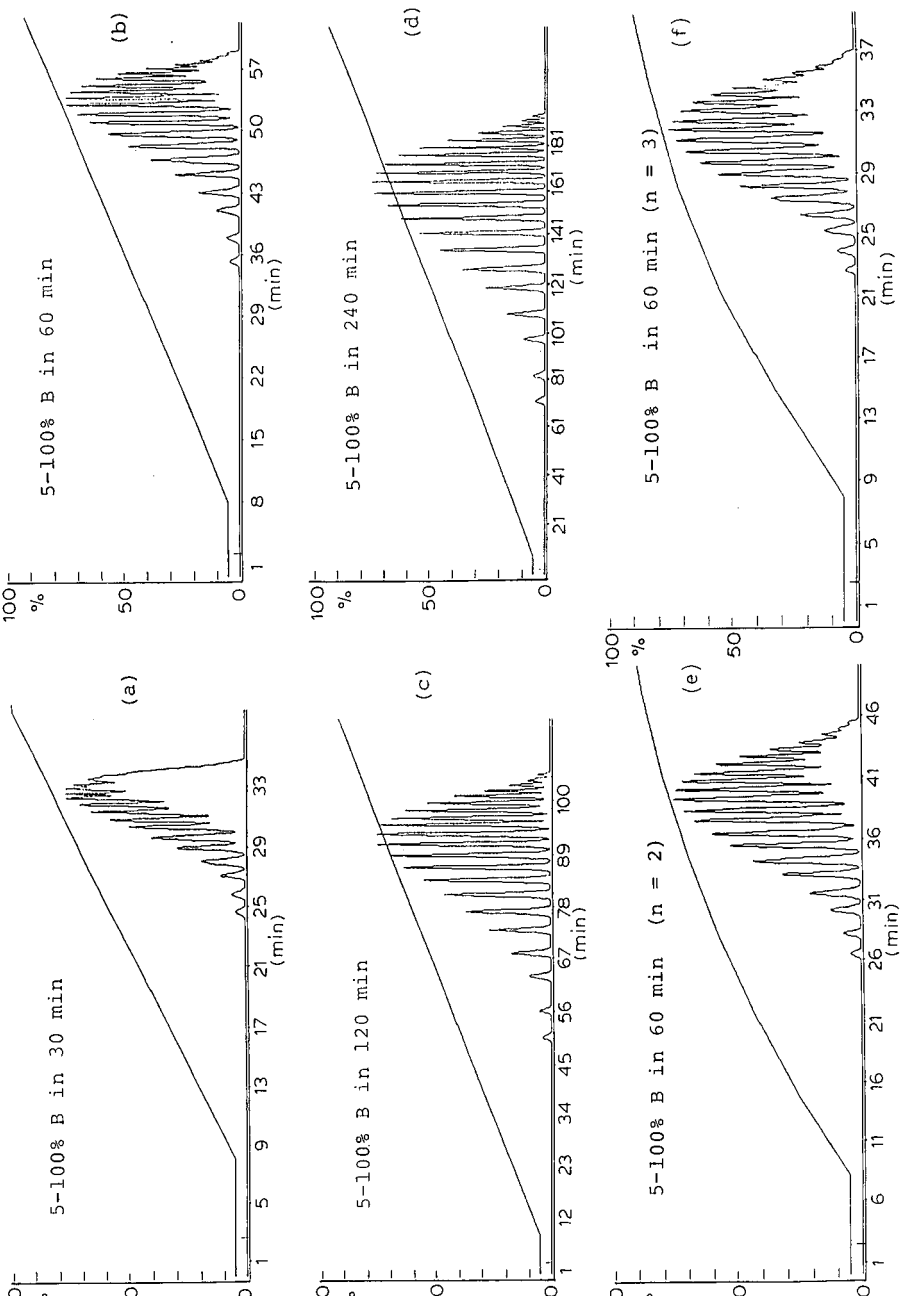

Fig. 1. Effect of gradient time and shape on the separation of a sample described by case II; computer simulations using DryLab G. Conditions: V_D = 5.5 ml; 25 × 0.46 cm I.D. column; flow-rate, 1 ml/min; solute characteristics described by eqn. 3.

mate proportions to t_G, meaning that there will be a significant loss in detection sensitivity for longer gradient times (not shown in Fig. 1 in ref. 1; all peak heights there are normalized to a fixed maximum value). This means that there is an optimal intermediate gradient time, equal to 50–100 min for this example ($\bar{k}$ = 7–14).

For samples that can be classified as case I, there are no reversals of peak position as the gradient time is changed. The effect of changing the starting value of φ (φ_0) while holding the gradient steepness (b) constant is shown in Fig. 2 in ref. 1. If the flow-rate and column dimensions are unchanged, the gradient time t_G must be reduced in proportion to $\Delta\varphi$ for b to remain constant, because

$$b = (V_m S/F)(\Delta\varphi/t_G) \tag{1}$$

Fig. 2 in ref. 1 can be better understood in terms of eqn. 8 in ref. 1:

$$\varphi_e - \varphi_0 = 1/S \tag{2}$$

The value of φ_0 (equal to φ^* for a linear, single-segmented gradient) must be sufficiently different from φ at elution (φ_e) to prevent initial elution of the sample by the starting mobile phase if the separation is to be unaffected by the choice of φ_0. In this instance S = 5, so that $\varphi_e - \varphi_0$ should be greater than 0.20 (20% B).

As an example, consider the resolution of the first two bands of the chromatograms in Fig. 2 in ref. 1. The average value of φ_e for these two bands is about 35% B (see gradient overlay, which represents φ at the column outlet). This means that when φ_0 exceeds 35 − 20 = 15% B, the resolution of the first two bands will be decreased.For values of $\varphi_0 < 0.15$, the relative retention and resolution of the two bands should be unaffected. The resolution R_s of these two bands as a function of φ_0 is as follows: when φ_0 = 0.05, 0.20, 0.30, 0.40 and 0.50, R_s = 5.8, 5.7, 5.5, 4.8 and 2.7, respectively. A significant decrease in resolution is seen to occur for $\varphi_0 > 0.30$. That is, eqn. 8 appears to be conservative for estimating the maximum value of φ_0 for samples of this type (case I). The final value of φ in the gradient has no effect on the appearance of the chromatogram, as long as all bands are eluted before the end of the gradient. This is illustrated by Fig. 2f and d in ref. 1.

Segmented gradients are not usually advantageous for improving the resolution of case I samples. However, segmented gradients can be used to reduce the run time whenever later portions of the chromatogram have much higher resolution (lower density of bands), by using steeper segments for the elution of these bands.

Case II samples

Homologous or oligomeric samples often correspond to case II and show plots of log k' *vs.* φ that extrapolate to about −1.0 for φ = 1. We have therefore carried out computer simulations with DryLab G for a series of hypothetical compounds where

$$S = \log k_w + 1 \tag{3}$$

and values of log k_w change by equal increments (as in Fig. 3b in ref. 1). The effect of gradient time on the separation of the latter sample is shown in Fig. 1a–d. Sample resolution increases regularly with increase in t_G, as in the simulations in Fig. 1 in ref. 1 for a case I sample. However, the chromatograms in Fig. 1a–d show initial bands that

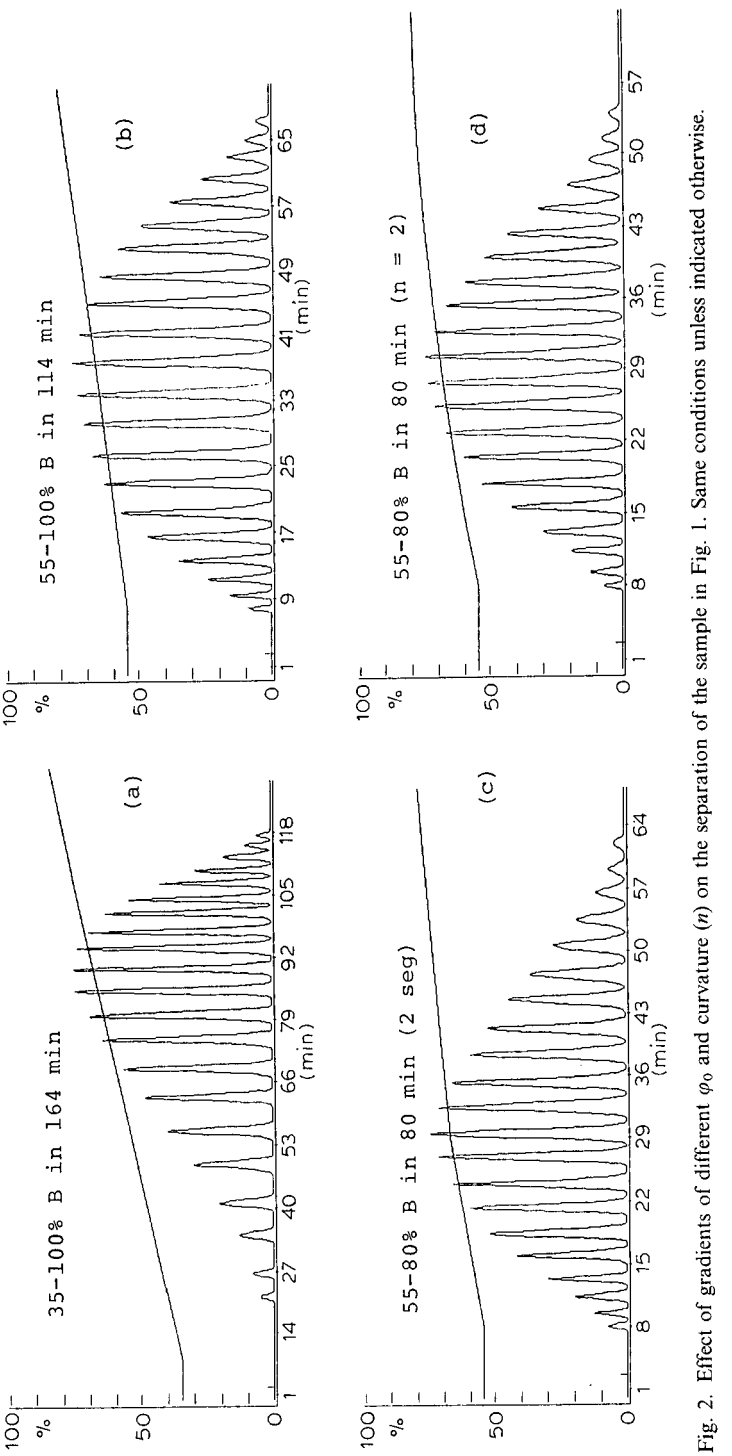

Fig. 2. Effect of gradients of different φ_0 and curvature (n) on the separation of the sample in Fig. 1. Same conditions unless indicated otherwise.

are overresolved, even for fairly short gradient times, whereas later bands are only marginally resolved even for very long gradients (240 min, Fig. 1d).

For examples of this type it is generally recommended to try a convex gradient. Such gradients are usually described by equations of the form

$$\varphi = 1 - [1 - (t/t_G)]^n \quad (4)$$

However, it is seen in Fig. 1e and f that the use of convex gradients (of varying convexity; $n = 2$ and 3) with a gradient time of 60 min does *not* improve the separation obtained by a linear gradient in the same time (Fig. 1b). The reason is that the initial steep portion of these convex gradients rises to a high value of φ before the sample can be eluted from the column. The resolution of the sample is in turn determined by the values of φ_e (or k_f) for each band pair.

Fig. 2a and b show further separations of the sample in Fig. 1, where the value of φ_0 is varied while the gradient steepness (value of b) is maintained the same as in the separation in Fig. 1d ($t_G = 240$ min). The use of $\varphi_0 = 55\%$ B (Fig. 2b) yields similar resolution at the two ends of the chromatogram, so as to equalize the resolution considerably over the entire chromatogram.

Now we can test the effects of a convex gradient for a similar gradient range and steepness. In Fig. 2c a two-step convex gradient is used, with a modest improvement in resolution for the end of the chromatogram and further equalization of overall resolution. The separation based on this two-step gradient is little different from that obtained with a corresponding continuous convex gradient as defined by eqn. 1 (Fig. 2d).

We can draw the following conclusions from the simulations in Figs. 1 and 2:

(1) Samples corresponding to case II show a continuous improvement in resolution as the gradient time is increased, especially for later eluted bands; however, the gradient time required for adequate resolution of the final bands in the sample may be prohibitive, if a linear gradient from 5 to 100% B is used.

(2) The most effective strategy is to increase φ_0 to the point where the resolution of initially eluted bands is no greater than that of bands eluted near the end of the chromatogram; this can be combined with an increase in t_G so as to increase the resolution of both early and later eluted bands to an acceptable level.

If the gradient time is excessive at this point, or resolution is still inadequate, either a two-segment gradient or a convex gradient (eqn. 1 with $n = 2$) can be used to advantage; however, the resulting improvement in separation may be minor.

Although it is also of interest to consider gradients of increasing curvature (increased n values in eqn. 1), it appears that increasing n is really equivalent to decreasing t_G, with little other effect on the separation. Thus a gradient for $n = 3$ has virtually the same shape as a gradient for $n = 2$, if t_G for the $n = 3$ gradient is increased 1.3-fold. Therefore, the separation resulting from a gradient with $n = 3$ should be similar to that obtained with a gradient where $n = 2$ and the gradient time is 1.3-fold shorter. This is shown in Fig. 3 for the same sample as in Figs. 1 and 2. The resulting retention times and resolution are essentially the same in the two instances (each gradient could be terminated at 46 min, when all bands have left the column).

It appears from the preceding examples and discussion that (a) the use of convex gradients is generally of little advantage compared with two-segment gradients of

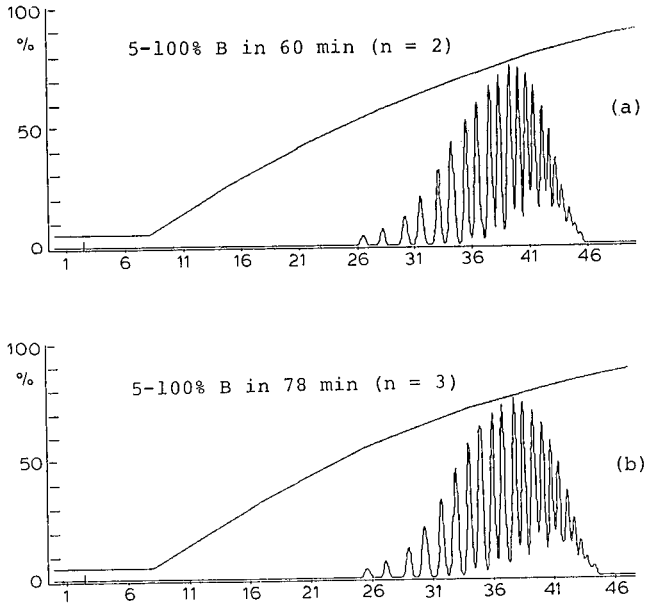

Fig. 3. Effect of starting %B and gradient shape on the separation of the sample in Fig. 1. Same conditions unless indicated otherwise.

similar gradient range and time* and (b) there is no advantage in changing the curvature of convex gradients (*i.e.*, using different values of n in eqn. 1). This considerably simplifies our study of gradient shape as it relates to separation, particularly for case II samples. Our further discussions can therefore focus on segmented gradients, as opposed to the continuously curved gradients described by eqn. 1.

Case III samples: example of sixteen polyaromatic hydrocarbons

We shall now apply some of the principles discussed above to the design of optimal gradients for two different samples that have been described previously: (a) a sixteen-component sample of polyaromatic hydrocarbons (PAHs) and (b) a twenty-component sample of 30S ribosomal proteins. Because of the practical differences that result for samples of differing molecular weight, it will prove useful to compare and contrast these two examples.

The PAH sample was described in ref. 2, but with little discussion of how an optimal gradient was obtained. The two initial runs used as experimental inputs for computer simulation are shown in Fig. 4a and b (computer simulations; original chromatograms shown in ref. 2). Preliminary examination of these two chromato-

* The latter conclusion concerning curved gradients (*i.e.*, they are not very useful) should be qualified for oligomeric mixtures having a wide range of molecular weight. The sample used in Figs. 1–3 corresponds to a mixture with a maximum molecular weight of less than 1000. As the sample molecular weight (and corresponding values of S) become larger, the advantage of segmented or curved gradients may increase.

grams shows that there are three critical band pairs: 3–4, 9–10 and 14–15. Values of R_s (for a 10 000-plate column) are superimposed on the critical band pairs in each chromatogram. Usually the best first step in computer simulation is to examine a relative resolution map (RRM) as a function of gradient time t_G. This is shown in Fig. 4c, and it appears that a gradient time of *ca.* 20 min is optimal.

The next step is to adjust the gradient range for maximal resolution in the minimal time. This can be done by trial-and-error, using computer simulation. Fig. 4e–g illustrate this process, with the conclusion that a 45–90% gradient in 9.5 min is probably near optimal. Alternatively, DryLab G will recommend an appropriate gradient range: 42–94% B in this instance, with the same gradient steepness (t_G = 11 min). At this point (Fig. 4f) it is seen that a minimum resolution of R_s = 1.2 can be achieved, in a time of 9.5 min per sample (the total analysis time is closer to 19 min if column re-equilibration is taken into account[4]).

Returning to Fig. 4a and b, it is seen that bands 3 and 4 are better resolved at higher values of t_G (60 min), whereas bands 14 and 15 are better resolved at low values of t_G. This suggests that a shallow gradient to elute bands 1–4, followed by a steeper gradient to elute the remainder of the sample, might prove better than a simple linear (unsegmented) gradient in this instance. A further example of these trends in resolution with gradient time is shown in Fig. 4d for t_G = 10 min.

It is usually instructive at this point to examine the resolution of critical band pairs as a function of gradient time, using computer simulations. Table I summarizes data for the PAH sample obtained in this way. The resolution of band pair 3–4 continues to increase with increasing t_G, the resolution of band pair 9–10 is more or less independent of t_G and the resolution of band pair 14–15 is a maximum for a gradient time of about 10 min (9.5%/min).

A good strategy for designing an optimal gradient is to first optimize the gradient steepness for maximal resolution of the front end of the chromatogram. This would suggest an initial gradient steepness that is as low as possible (Table I). However, this turns out to be wrong for two reasons. First, a very shallow gradient for the elution of bands 3 and 4 will adversely affect the resolution of bands 9 and 10 and 14 and 15, even though a steeper (second) segment is used to elute these compounds. This can be seen as follows. Fig. 8 in ref. 1 suggests that the second segment must begin about 25% before the elution of bands 9 and 10 or 14 and 15 if their separation is not to be affected by the first (shallow) segment. However, bands 3 and 4 elute only 15% earlier than bands 9 and 10.

A second reason not to make the initial gradient so shallow is that there is usually little point in increasing the resolution of band pair 3 and 4 beyond the maximal resolution that can be obtained for bands 9 and 10 and 14 and 15 (R_s = 1.6). This suggests a starting gradient (first segment) with a steepness of about 3%/min and a second segment with a steepness of about 10%/min. As bands 3 and 4 are eluted in the initial gradient with φ_e = 50%, this suggests a gradient of 5–52% B in 15 min and 52–100% B in 5 min. Fine tuning of this gradient (by trial and error) then resulted in the chromatogram shown in Fig. 4h. Finally, this gradient was shortened by starting at a higher value of φ_0 (trial-and-error simulations), giving the final separation of Fig. 4i. Further trial-and-error modification of the gradient was attempted without a significant further increase in resolution. A separation similar to that in Fig. 4i was confirmed

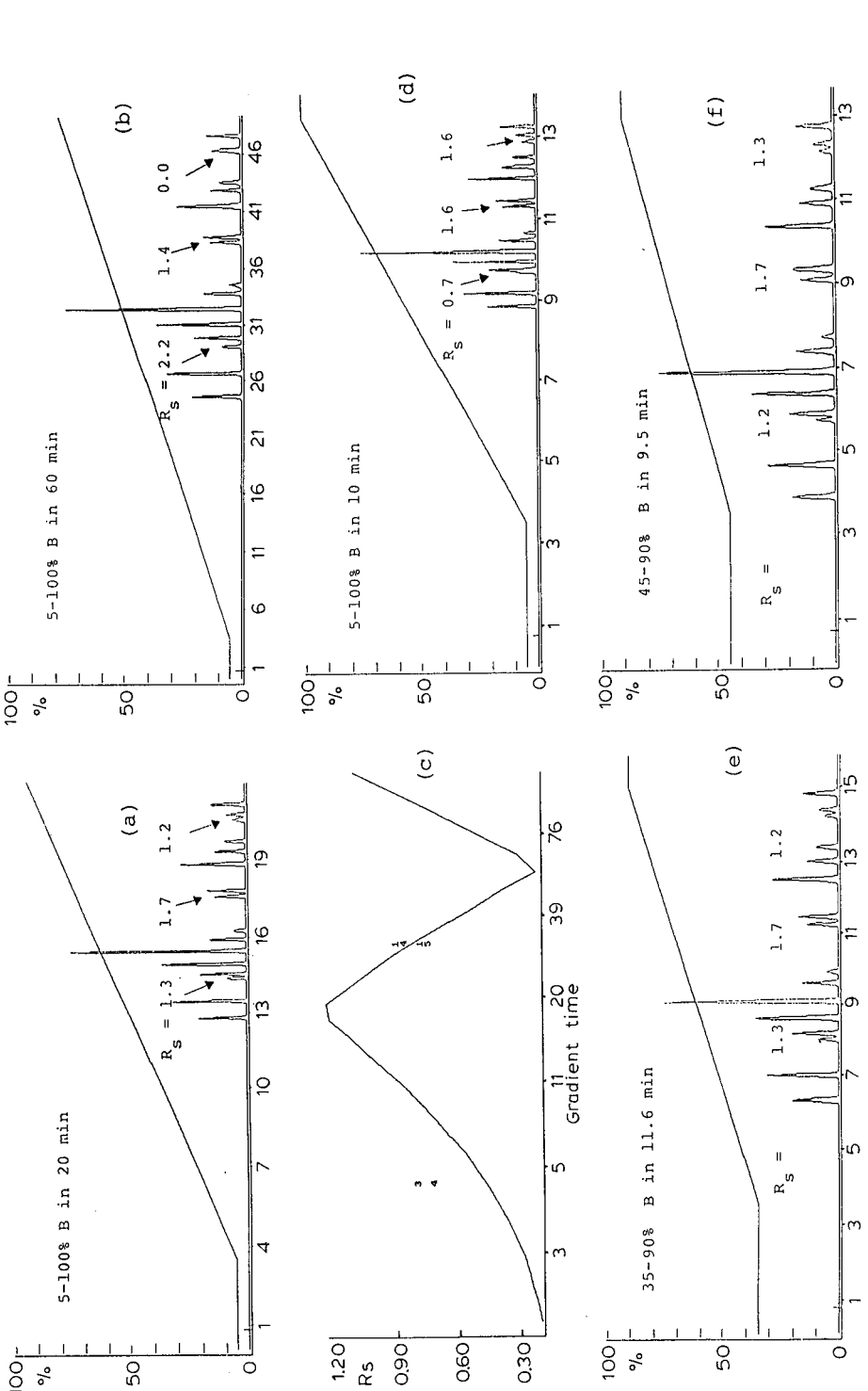
(a)
5-100% B in 20 min
R_s = 1.3
1.7
1.2
(b)
5-100% B in 60 min
R_s = 2.2
1.4
0.0
(c)
Rs
Gradient time
(d)
5-100% B in 10 min
R_s = 0.7
1.6
1.6
(e)
35-90% B in 11.6 min
R_s =
1.3
1.7
1.2
(f)
45-90% B in 9.5 min
R_s =
1.2
1.7
1.3
%

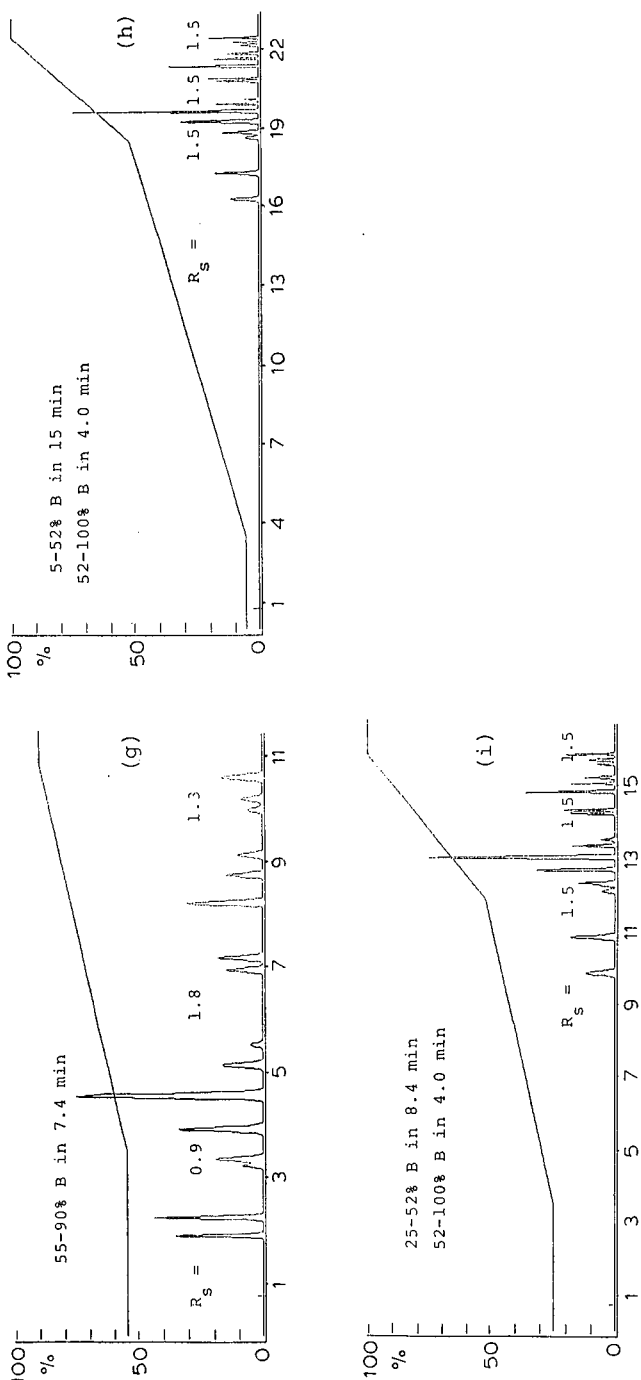

Fig. 4. Separation of a sixteen-component PAH sample as a function of gradient conditions. Computer simulations (DryLab G) based on experimental data in ref. 2.

TABLE I

RESOLUTION OF CRITICAL BAND PAIRS FOR A PAH SAMPLE AS A FUNCTION OF GRADIENT TIME

Other conditions given in ref. 2.

t_G (min)	R_s (N = 10 000) for indicated band pair (%/min)*			
	3–4	9–10	14–15	% B/min
5	0.3	1.4	1.4	19
10	0.7	1.6	1.6	9.5
20	1.3	1.7	1.2	4.7
40	1.8	1.6	0.5	2.4
60	2.2	1.4	0.0	1.6

* Change in %B per minute (gradient steepness).

experimentally in ref. 2. The separation in Fig. 4i exhibits a 25% increase in minimal resolution (R_s = 1.5) compared with the run of Fig. 4f (R_s = 1.2)*.

Case III samples: example of twenty 30S ribosomal proteins

Editing initial experimental runs. Two experimental runs were carried out initially, as shown in Fig. 11a and b in ref. 1. Individual bands were matched between the two runs as described in refs. 2–4. Comparison of a simulated run as in Fig. 14d in ref. 1 with the corresponding experimental run (Fig. 14b in ref. 1) can be used to confirm that bands in run 2 have been matched to those in run 1, prior to inputting final retention times into the computer**. For this example, there is a close similarity between the experimental and simulated chromatograms (Fig. 5b and d), confirming the accuracy of peak matching.

A similar comparison for run 1 may also be useful for picking up any errors in retention time (it is assumed that band areas from run 1 were entered into DryLab G). This is illustrated in Fig. 5 for the same chromatograms as in Fig. 11a and c in ref. 1. The initial computer simulation (Fig. 5b) differs in minor respects from the experimental chromatogram (Fig. 5a). Minor adjustments in the retention times of three bands (by 0.1–0.2 min) results in a better match (Fig. 5c) with Fig. 5a.

The further correction of the input data for run 1 (as in Fig. 5c *vs.* 5b) is not essential to accurate computer simulation, but it can have a favorable impact. The errors in Fig. 5a arise from band overlap (see discussion in ref. 4), and in such instances it is advisable to correct the value of t_g for the overlapped band (*i.e.*, so as to improve the accuracy of the predicted resolution of run 1).

The correction of minor errors in retention time (as described above) becomes more important as the sample complexity increases. As will be seen, samples such as the 30S ribosomal proteins can be difficult to resolve completely, and this places additional emphasis on the accuracy of computer simulation.

* The run time is greater in Fig. 4i (12.4 min) than in Fig. 4f (9.5 min), but the separation in Fig. 4i is still superior; adjustment of the column plate number (flow-rate, column length) can be used to normalize the run time, which then provides greater resolution for the conditions in Fig. 4i than those in Fig. 4f.

** A useful first step in computer simulation is to adjust the resolution of predicted chromatograms so as to match one of the starting experimental runs. This was done in this instance by using the 240-min run (Fig. 5b and d). The resulting value of N for the experimental column corresponded to 2500 plates.

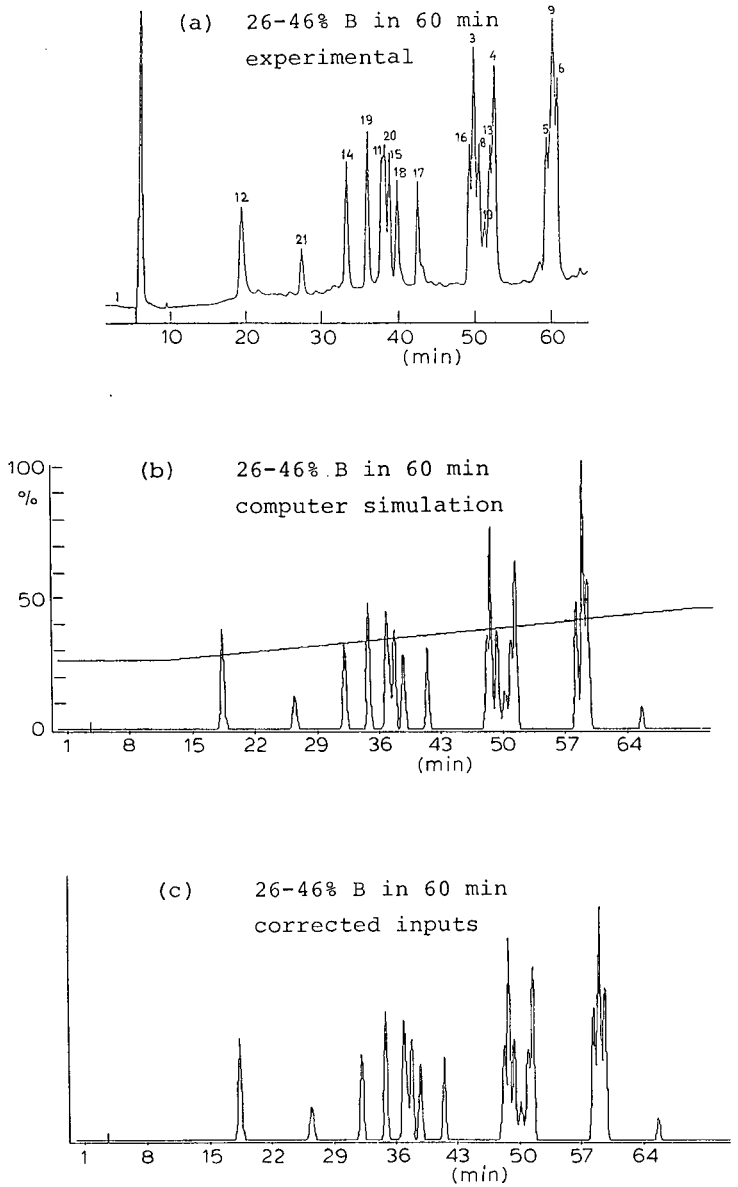

Fig. 5. Use of corrected ribosomal protein retention times for a 60-min run to improve computer simulations. (a) Experimental run; (b) simulation based on retention time data from (a); (c) simulation based on empirically corrected retention times. Conditions as in Fig. 14 in ref. 1 except where indicated otherwise.

Subdividing the chromatogram. A good initial step for any sample is to examine a relative resolution map as in Fig. 4c for the PAH sample. Fig. 6a shows such a map (RRM) for the ribosomal protein sample (all 20 bands, $N = 2500$). A maximum resolution of $R_s = 0.7$ is possible, but only for a long gradient time ($t_G \approx 8$ h). This suggests that a segmented gradient may be preferable.

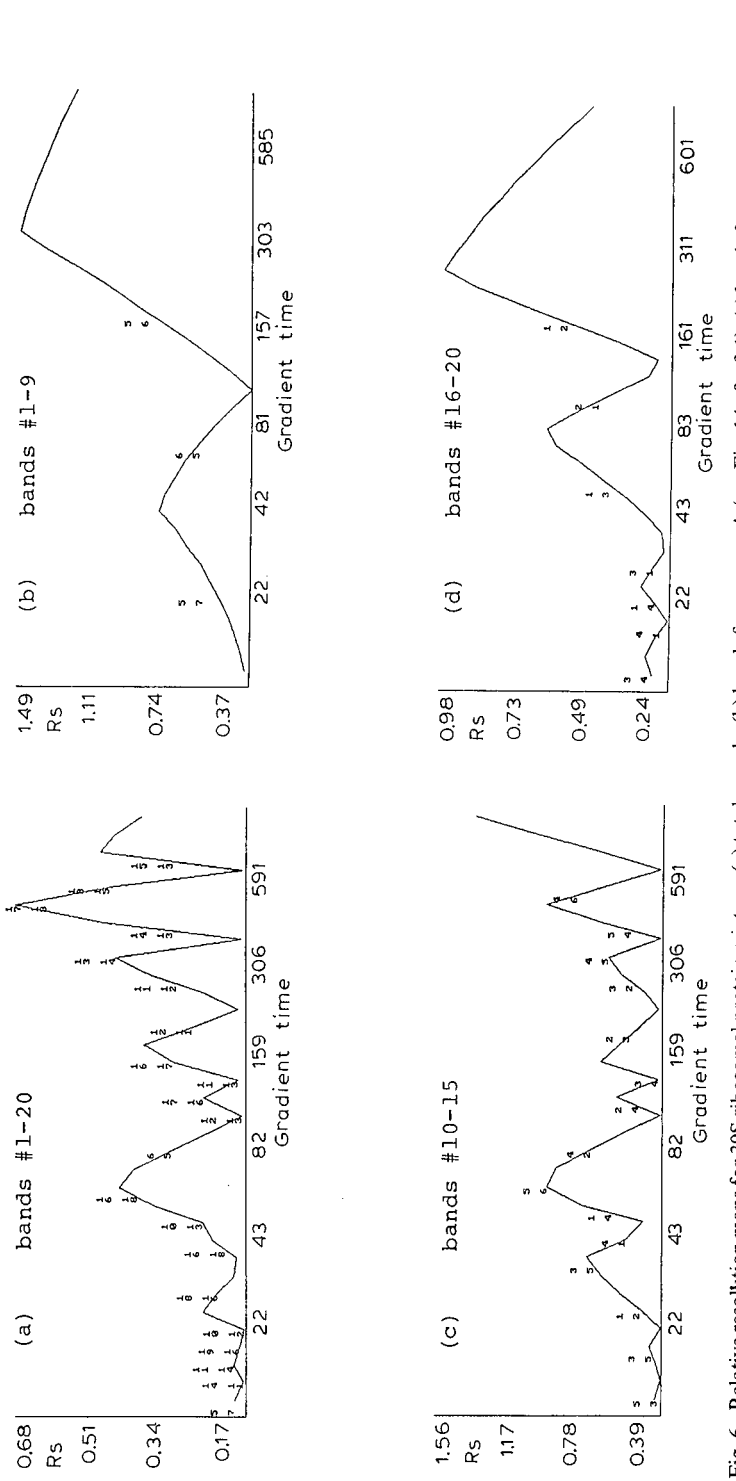

Fig. 6. Relative resolution maps for 30S ribosomal protein mixture. (a) total sample; (b) bands from group A (see Fig. 14 of ref. 1); (c) bands from group B; (d) bands from group C. Conditions as in Fig. 5 except where indicated otherwise.

For complex samples such as this, we should attempt (if possible) to divide the chromatogram into groups of adjacent bands. As seen in Fig. 11b and d in ref. 1 (t_G = 240 min), there are three such groups of bands, A, B and C, consisting of bands 1–9, 10–15 and 16–20, respectively. There are no crossovers of bands between these three groups; as a first step, we can therefore treat each group separately. Having grouped the sample bands in this way, the next step is to look at RRMs for each band set.

Fig. 6b–d show the RRMs for groups A–C. A minimum resolution is predicted of R_s = 1.5 for group A, 1.5 for group B and 1.0 for group C. This suggests that we should be able to achieve a minimum resolution of R_s = 1.0 for the entire sample by optimizing the gradient segments for each group. We shall see that this is possible. The (predicted) optimal separation of each group is shown in Fig. 7a, c and d. Fig. 7b shows a sub-optimum for group B (shorter gradient) that we shall examine later. The very long gradient time suggested for group B (1200 min, Fig. 7c) need not be a problem, inasmuch as the actual gradient segment can be very much shorter than for the full 26–46% B range (about 150 min, as seen in Fig. 7c).

Designing the gradient. The best strategy is usually to optimize each gradient segment sequentially, beginning with the first group of compounds (bands 1–9 in this instance). Reference to Fig. 7a suggests a gradient of 20% per 350 min or 0.057%/min for this segment, with the segment ending at about φ^* = 33% (the φ_e value of band 9). Values of φ_e can be determined from the retention time t_g of the band. For a linear gradient

$$\varphi_e = \varphi_0 + \Delta\varphi[(t_g - t_D - t_0)/t_G] \tag{5}$$

For band 9, t_g = 141 min and $t_D + t_0$ = 11.5, so that φ_e = 26% + [(129.5/350) · 20] = 33%.

Similar calculations can be used to determine φ_e for segmented gradients, or values of φ_e can be read (approximately) from chromatograms such as that in Fig. 7, which have a gradient overlay that is corrected for t_D and t_0. The first segment is therefore calculated as 26–32.6% B in 115 min (φ^* = 32.6% was fine-tuned during the addition of an additional segment to the gradient; see below). The resulting separation will be the same as in Fig. 7a, as neither φ_0 nor the gradient steepness (b) have been changed.

The next step is to optimize the second gradient segment for group B compounds. The optimal gradient in Fig. 7c for this group of bands suggests a gradient steepness of 20% per 1200 min = 0.0167% B/min, *e.g.*, 32.6–46% B in 800 min. Use of this second gradient segment (in combination with the first segment above) gave a separation that is inferior to that observed in Fig. 7c, because of the influence of the first segment on the separation of bands eluted by the second segment. As discussed earlier, this can generally be corrected for by varying the slope of the second segment.

Trial-and-error adjustments yielded an optimal slope of 0.0136% B/min for the second segment, and this two-segment gradient gave a resolution of bands 1–15 that was equivalent to that provided in Fig. 7a and c. Band 13 (the last eluted band of group B under these conditions) is eluted with a retention time of 310 min and a φ_e value of 36% B. Correcting for the effects of t_D and t_0 on the gradient at the outlet of the column, this suggests a second gradient segment of 32.6–35% B in 177 min. The

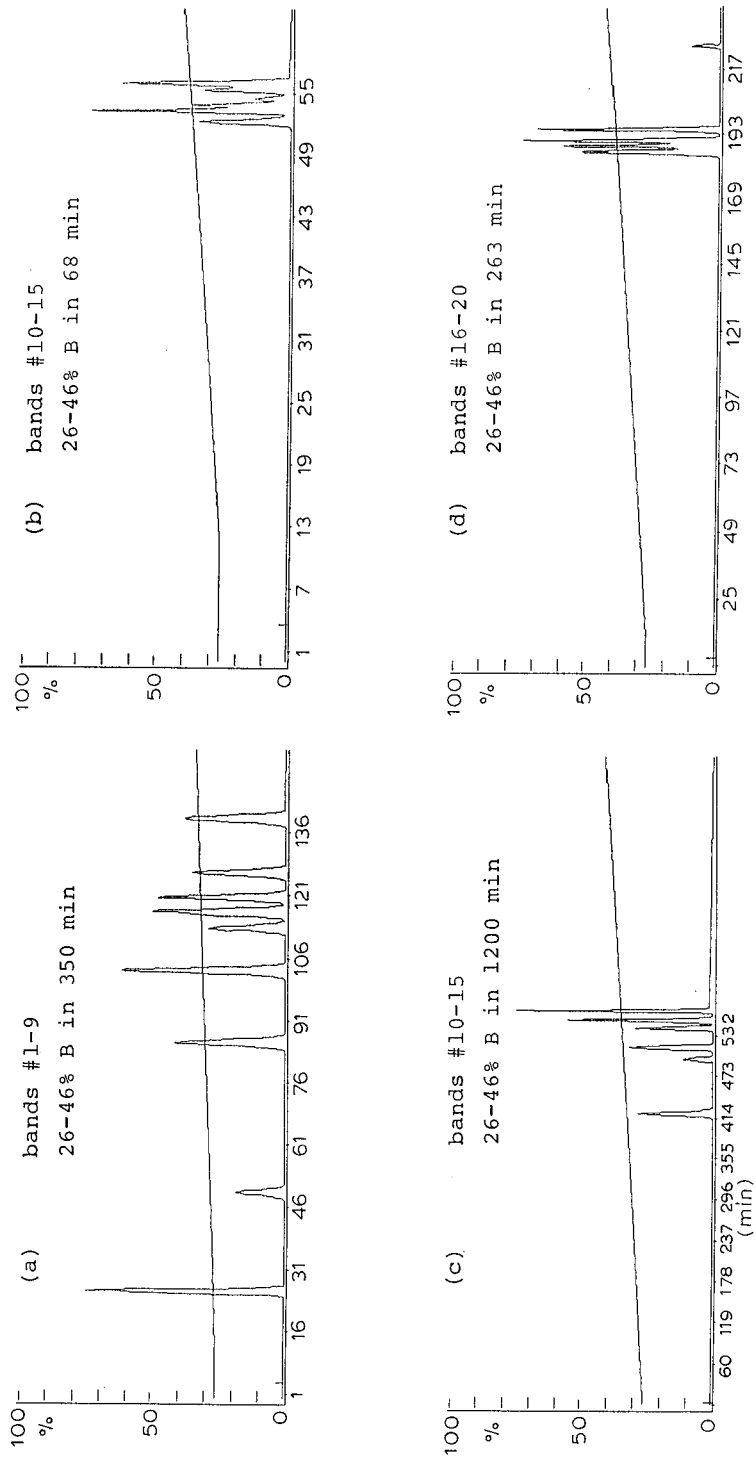

Fig. 7. Separation of various ribosomal protein band groups using optimized gradient times for 26–46% B gradients. Conditions as in Fig. 5 except where indicated otherwise.

resolution of group B (R_s = 1.2) obtained with this segment (in combination with the first segment) was close to that obtained in Fig. 7c (R_s = 1.5). Fine tuning of the gradient at this point did not result in any improvement of this two segment separation.

The optimal gradient slope for the final segment (to elute group C) is predicted from Fig. 7d to be about 0.076%. The addition of this segment to the first two again

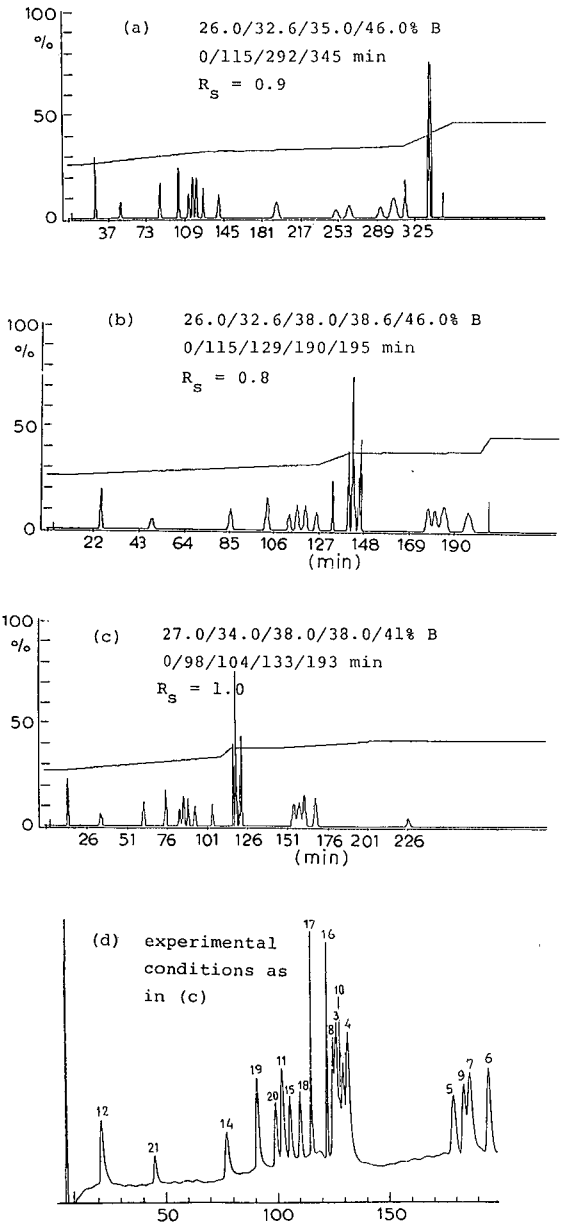

Fig. 8. Optimized separation of 30S ribosomal proteins using different gradients. See text for details.

gave a separation of group C that was inferior to that in Fig. 7d. However, fine tuning yielded an optimal gradient steepness of 0.21%/min, and this three segment gradient did provide a resolution of group C (R_s = 0.9) which is close to that predicted in Fig. 7d (R_s = 1.0).

The final three-segment gradient gave an overall minimum resolution of R_s = 0.9 (Fig. 8a) which is close to that inferred from Fig. 7 (R_s = 1.0). The separation in Fig. 8a is seen to be considerably better than is possible with any single-segment gradient (Fig. 6a, minimal resolution R_s = 0.7). The separation time (345 min total) is also less than that required for the best single-segment gradient (t_G = 500 min). The effort required to design this particular gradient (apart from the initial two experimental runs) amounted to a few hours of computer time. A similar procedure based on trial-and-error experimental runs would be impractical, probably requiring several weeks.

Elsewhere, we have reported the separation of all twenty components of this sample, using a complex four-segment gradient[4]. This gradient was developed by trial and error (computer simulations), before the recommendations arrived at in this study were implemented. It is interesting to see that this latter gradient (Fig. 8c) is actually superior (minimal R_s = 1.0) to that in Fig. 8a, and requires a much shorter time. This suggests that an experienced chromatographer can use (many) trial-and-error computer simulations to arrive at good final gradients. However, the systematic approach outlined above requires less effort (and experience) than the more empirical approach that resulted in the separation in Fig. 8c.

Comparison of the predicted separation in Fig. 8c with the actual chromatogram in Fig. 8d for these conditions shows only fair overall agreement. The observed minimal resolution was about R_s = 0.8 (*vs.* 1.0 predicted), and the retention times of earlier bands differ significantly, between experimental and predicted chromatograms. These errors in prediction are believed to be due to (a) rounding of the gradient by the equipment and (b) changes in column retention between the initial and final experimental runs. Attention to the recommendations in ref. 4 should result in better agreement in other instances.

Example of 32 50S ribosomal proteins

A similar approach to the above was next tried for the separation of the 32 50S ribosomal proteins, an even more complex sample. Details of this work will be described elsewhere, but Fig. 9 compares the predicted (optimal) separation using a four-segment gradient with the final experimental chromatogram*. As discussed in ref. 5, the agreement between these two chromatograms is good ($\pm$ 0.5% in t_g, $\pm$ 8% in R_s). The conditions for Fig. 9 allow the separation of 31 of the 32 proteins in this sample with a minimal resolution of about 0.8 (one band pair cannot be resolved with this column, regardless of the gradient conditions).

Other observations

Evaluating the chromatogram. The evaluation of a chromatogram during the design of a gradient by computer simulation is important to decisions made in the inevitable trial-and-error fine tuning of the gradient at each step. Some workers will

* Fig. 9b shows only the confirmed 50S ribosomal protein bands, which are numbered in Fig. 9c. Additional bands in Fig. 9c correspond to other compounds that were ignored in this study.

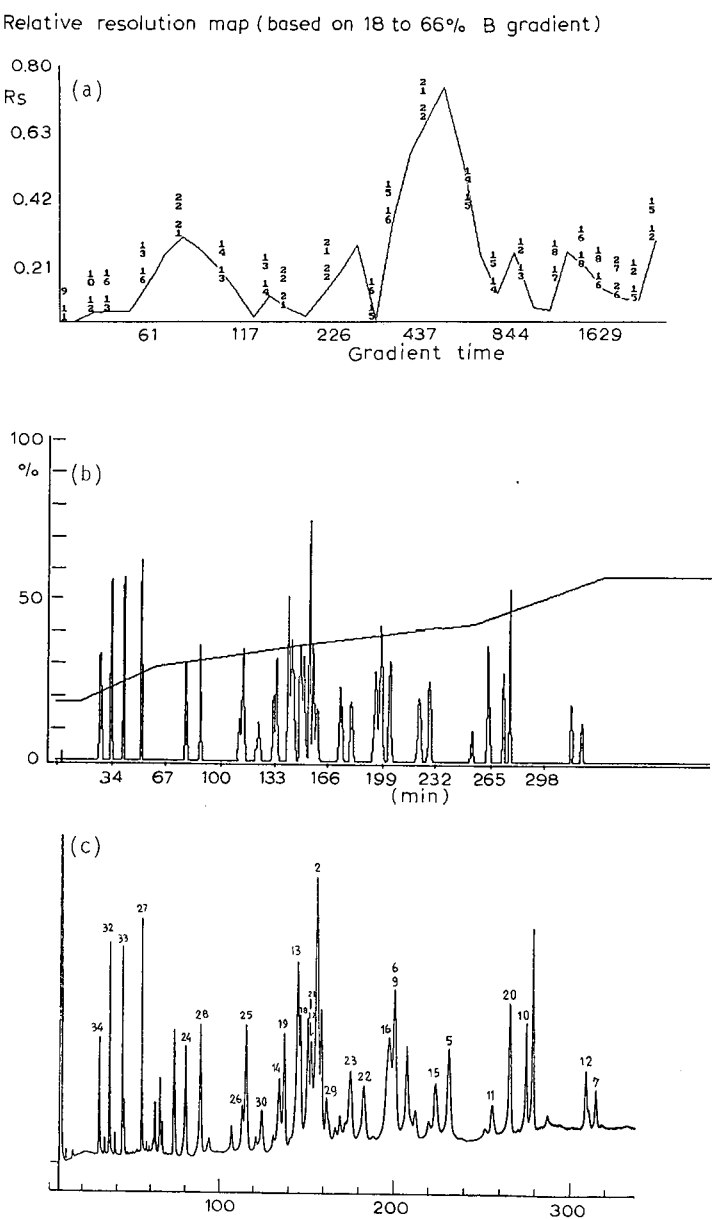

Fig. 9. Optimized separation of 50S ribosomal protein sample. (a) Resolution map; (b) simulated chromatography; (c) experimental chromatogram. Conditions: 18, 29, 37, 43, 58% B in 0, 46, 142, 241, 320 min; other conditions as in the Experimental section in ref. 4. $N = 900$.

prefer to use tables of R_s values for each band in the chromatogram (these are provided by DryLab G for each run, *e.g.*, as in Table I). Changes in the gradient usually lead to an increase in R_s for one or more critical bands and a decrease in resolution of other critical bands. Often the best choice of gradient will equalize the R_s values of two

critical band pairs, and tables of R_s values therefore inform us (a) in which direction a particular gradient should be changed for best results and (b) how close we are to an optimal result.

Other workers may prefer to examine the actual chromatograms that are predicted for each gradient to be evaluated. However, complex samples such as this often make visual interpretation of the chromatogram difficult. Overlapping bands combined with the low resolution of the computer screen can lead to generally confusing data. One means of improving this situation, which is not available experimentally, is to increase the predicted resolution of each separation by some large and arbitrary amount. This is illustrated in Fig. 10 for the group B bands (Fig. 11 of ref. 1) of the 30S ribosomal protein sample above. Here, the effect of gradient time (or steepness) on the separation (26–46% B gradients) is examined for a plate number of 160 000; these separations have a resolution that is eight times that observed experimentally. In the examples in Fig. 10 it is possible to see clearly changes in relative band position as the gradient steepness is changed; band 4 (marked with an asterisk) migrates from position 1 to position 4 as the gradient time is changed from 30 to 240 min. Bands 2 and 3 are initially well resolved (t_G = 30 min), but gradually approach each other and merge at a gradient time of 240 min.

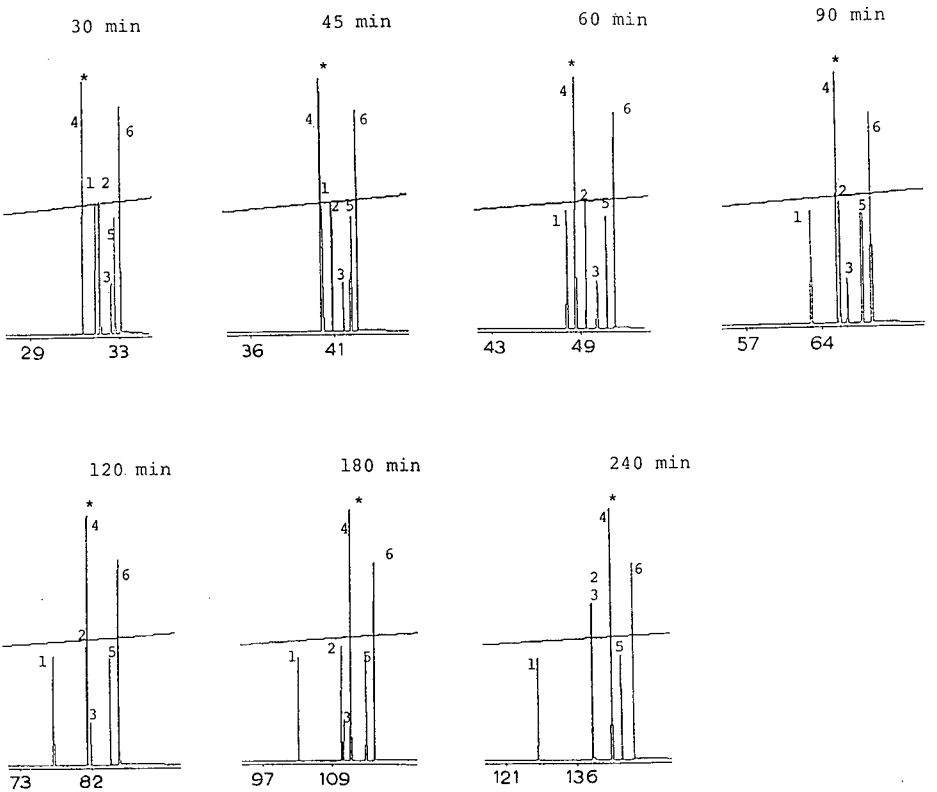

Fig. 10. Use of high-resolution computer simulations to track bands as the gradient time is varied. Ribosomal protein sample; conditions as in Fig. 5 except where indicated otherwise.

Alternative gradients. The examples in Fig. 8 suggest that more than one approach to gradient optimization may often be successful. In fact, the separation of a given sample such as this can usually be achieved (with similar resolution and in a similar time) by an almost endless number of gradients. For example, Fig. 6c suggests that group B can be separated with nearly adequate resolution (minimal $R_s = 0.8$) in a much shorter time ($t_G = 68$ min), as shown in Fig. 7b. This suggests adjusting the steepness of the second segment to a value of about 0.3% B/min, instead of the value of 0.017% B/min suggested by Fig. 7c. A similar approach to that for the development of the gradient in Fig. 8a yielded the predicted separation in Fig. 8b. An overall minimum resolution of $R_s = 0.8$ (*vs.* $R_s = 0.9$ in Fig. 8a) was obtained, in about half the total time (195 *vs.* 345 min). For some applications, this separation might prove preferable to that in Fig. 8a.

The considerable effort spent in designing the separation in Fig. 8a may not be necessary in all instances. The data in Fig. 6 lead immediately to the predicted separations of each group in Fig. 7. Depending on what compounds in the sample are of interest, any of these group separations might have been suitable for the desired application. However, with a little additional effort (*ca.* 1 h), a single separation (Fig. 8a) can provide equivalent results for the total sample.

Recommendations for designing an optimal gradient by computer simulation

Our experience in applying computer simulation to a number of different examples (described here and elsewhere) is summarized below. It is assumed that (a) the inital experimental data have been collected in such a way as to maximize the accuracy of computer predictions of separation, (b) the data have been entered into the computer correctly (bands matched between two initial runs) and (c) any discrepancies between the experimental and corresponding simulated chromatograms have been addressed (as in the example in Fig. 5). That is, we should first do everything possible to insure the success of computer simulation for the sample at hand. The individual computer simulation steps required to optimize the gradient conditions are as follows (assumes the use of DryLab G or equivalent software):

(1) First, examine a resolution map for the entire sample, *e.g.*, as in Fig. 4c for the PAH sample. Many samples (especially those with fewer than fifteen components) can be adequately resolved by using a linear (unsegmented) gradient with an optimal steepness or value of t_G. Other samples (case II) where the resolution decreases continuously from the beginning to the end of the chromatogram can be handled similarly, except that a two-segment gradient may provide marginally better resolution.

(2) Once an optimal gradient steepness has been chosen, trim the gradient range (reduce $\Delta\varphi$) to save time. This can be done by trial and error (as in Fig. 2 in ref. 1) or DryLab G will provide specific recommendations. Often it is necessary to re-optimize gradient time after the final gradient range is selected (repeat step 1).

(3) For more demanding samples, such as the case III examples described here, a segmented gradient will often be preferred. There are two possible approaches, illustrated by the PAH and ribosomal protein samples. Which approach should be followed depends on an initial examination of the experimental chromatograms. One approach (as in the 30S ribosomal protein example) is to divide the sample into distinct groups, *e.g.*, A–C in Fig. 11d in ref. 1, if this is possible. Alternatively (as with the PAH

sample), one can see whether there are a small number of critical band pairs in the sample. These can be identified initially on the basis of the RRM (Fig. 4c) and by looking for other marginally resolved band pairs (when t_G is varied). In the PAH example, band pairs 3–4, 9–10 and 14–15 were selected in this way.

(4) For samples such as the PAHs, it is recommended to first carry out computer simulations for those bands (only) prior to and including the first critical band pair. The gradient range and steepness for these compounds can then be optimized. In this connection, the use of an RRM (for the bands in question) can save time. This step is similar to step 1.

(5) A second segment can be added next, just following elution of the first critical band pair. The steepness of this segment can be varied in trial-and-error fashion to optimize the resolution of the second critical band pair. This procedure can be repeated as necessary for a third, fourth, etc., critical band pairs and associated gradient segments. During this process, one should be aware that an optimized preceding segment can compromise the resolution in the following segment. This will be less of a problem with protein samples, because of small values of $\varphi_e - \varphi^*$, and more of a problem with small molecules in the 200–500 Da molecular weight range. In these instances, it may be advantageous to de-optimize a preceding segment (*i.e.*, reduce the value of φ^* so as to allow a maximum value of minimum resolution for the two segments together).

(6) For samples that can be broken into distinct groups (especially samples of higher molecular weight), each group can be examined separately to determine an approximately optimal gradient steepness (%B/min). The use of RRMs is useful for this purpose, as illustrated in Fig. 6 for the ribosomal proteins. Now proceed in similar fashion as for steps 4 and 5 so as to build up a suitable multi-segmented gradient. Again it will sometimes be profitable to de-optimize a preceding segment in order to improve the resolution of a subsequent segment, so as to achieve a maximal value of minimal resolution (for both segments). Similarly, it is sometimes best to end a preceding segment prior to elution of the last band in that group, especially when the last band is well resolved from the critical band pair in this segment. That is, the value of φ^* should sometimes be smaller than the value required to elute the last band of a group.

These recommendations plus the discussion of the preceding two examples should facilitate the computer-assisted design of optimized gradients. Ideally, these rules could form the basis of a computer-assisted gradient-optimization scheme. However, it is not yet possible to reduce this procedure to sufficiently simple steps that can be programmed into a computer, as the overall process is still too complex and not yet well enough understood.

Procedures to avoid. In our experience, there are also some approaches or strategies which seem less useful. Attempting to understood the details surrounding the separation of critical band pairs in the chromatogram generally leads to "paralysis by analysis". Fig. 10 for one part of an actual chromatogram illustrates this point; one can easily imagine the incredible complexity of separation for this group of compounds as a function of (a) preceding gradient segments, (b) the starting point (φ^*) of the present segment and (c) the duration (t_G) of this segment (in which the sample group is eluted).

Another problem to avoid is attempting an overly precise adjustment of gradient conditions so as to maximize the minimal resolution. Improvements of less than 0.1

unit in R_s are generally not worthwhile, except as they accumulate to give greater improvements in separation. The actual experimental run will often deviate from the predicted separation by ± 0.1 R_s units. Also, a major advantage of computer simulation is its ability to suggest that further improvements in gradient conditions will not be useful, when several successive attempts at improving sample resolution prove unsuccessful.

CONCLUSIONS

Recommendations for the best approach to designing an optimal gradient for a given sample are provided, based on the use of computer simulation and DryLab software. Computer simulation greatly simplifies the task of obtaining an adequate separation of complex samples containing a large number of components (*e.g.*, fifteen or more compounds). The application of computer simulation appears especially worthwhile for biological samples containing peptides or proteins.

The design of acceptable gradients for some samples (case I) is straightforward; only the gradient steepness and range need to be optimized, and there are no changes in band spacing to confuse the chromatographer. Samples composed of homologous or oligomeric series (case II) are slightly more challenging, but again the proper choice of gradient steepness and range is usually adequate. In some instances a two-segment gradient will provide better overall resolution and/or a shorter run time; curved gradients are seldom required or worthwhile.

Samples that exhibit changes in band spacing when gradient conditions are varied (case III) offer the greatest opportunity for maximizing resolution by selecting the best gradient. Often such samples benefit from multi-segmented gradients, so that the gradient steepness (and band spacing) can be optimized at different parts of the chromatogram. Because separation within a given gradient segment is affected by previous segments in the gradient, the design of the overall gradient can be challenging. Various techniques for simplifying this procedure are described.

REFERENCES

1 B. F. D. Ghrist and L. R. Snyder, *J. Chromatogr.*, 459 (1988) 25.
2 J. W. Dolan, L. R. Snyder and M. A. Quarry, *Chromatographia*, 24 (1987) 261.
3 B. F. D. Ghrist, B. S. Cooperman and L. R. Snyder, in F. E. Regnier and K. M. Gooding (Editors), *HPLC of Biological Macromolecules: Methods and Applications*, Marcel Dekker, New York, 1989.
4 B. F. D. Ghrist, B. S. Cooperman and L. R. Snyder, *J. Chromatogr.*, 459 (1988) 1.
5 B. F. D. Ghrist, *Ph.D. Thesis*, University of Pennsylvania, Department of Biochemistry, 1988.

Journal of Chromatography, 459 (1988) 65–77
Elsevier Science Publishers B.V., Amsterdam — Printed in The Netherlands

CHROMSYMP. 1502

EFFECTS OF PEAK TAILING ON COMPUTER OPTIMISATION PROCEDURES FOR HIGH-PERFORMANCE LIQUID CHROMATOGRAPHY

I. CHARACTERISTICS OF TAILED PEAKS UNDER OPTIMISATION CONDITIONS

S. SEKULIC and P. R. HADDAD*
Department of Analytical Chemistry, University of New South Wales, P.O. Box 1, Kensington, N.S.W. 2033 (Australia)

SUMMARY

The effects of peak tailing were studied by sequential generation of exponentially modified Gaussian peaks and observation of the trends between percentage area overlap, resolution, and the τ to σ ratio (where τ is the time constant and σ the standard deviation of the peak). It was found that only tailing of the first peak in a peak pair increased the percentage area overlap, whereas in other cases the area overlap was slightly decreased. When the heights of the component peaks in a peak pair were unequal, a swamping zone of total area overlap was introduced and the resolution (R_s) was required to attain a threshold value before separation in terms of area overlap was observed.

The dependence of peak tailing on the nature of solvent modifiers was determined experimentally, using five sympathomimetic amines as solutes and mixtures of methanol, acetonitrile, and tetrahydrofuran with water as solvents. When binary mobile phases of water with one modifier were considered, the amount of tailing exhibited by a peak was independent of the concentration of the modifier in the eluent, but was dependent on the nature of the modifier. For ternary mobile phases, formed from linear combinations of the above binary mixtures, the degree of tailing followed an approximately linear relationship with mobile phase composition.

INTRODUCTION

It is generally agreed that the occurrence of purely Gaussian peaks in high-performance liquid chromatography (HPLC) is rare[1–3], due to intra-column and extra-column factors which contribute to peak asymmetry. Intra-column factors include overload, system mismatch, and poorly packed columns, whereas extra-column asymmetry generally results from sample dispersion created by movement through the sample injector, detector cell, or the tubing between the column and these units. More detail on these factors can be found elsewhere[3–5]. The peak shapes occurring in HPLC may be accurately modelled by using the exponentially modified Gaussian (EMG) function. The EMG function consists of a Gaussian peak profile,

0021-9673/88/$03.50

convoluted with an exponential decay function. The development, characterisation, and experimental justification of this model has been thoroughly reviewed[2,3].

Computer optimisation procedures for HPLC can be defined as computer-based methods for selection of the optimal chromatographic conditions pertinent to a desired separation. Such procedures are currently undergoing intensive development and hold enormous potential for simplifying the process of chromatographic methods development. In most cases, computer optimisation is directed towards selection of the optimal mobile phase composition, and a crucial step in this process is the evaluation of the quality of chromatograms arising from all mobile phases to be considered in the optimisation. This evaluation is accomplished with the aid of a mathematical criterion which assigns a numerical value to a chromatogram as an indicator of its quality.

Many criteria are based on an initial calculation of the resolution between all the peak pairs in a chromatogram, which is then followed by appropriate mathematical manipulations in order to calculate the desired criterion. If this calculation of resolution is inaccurate, the error will be propagated to the calculation of the criterion and may result in the final selection of a mobile phase composition which is not optimal. Our experience suggests that optimisation procedures are prone to failure when one or more solutes in the mixture to be separated exhibit peak tailing. This failure arises from the fact that peaks are assumed to be Gaussian, and the area overlap of adjacent peaks is consequently assumed to be less than that existing in practice.

In this paper, we report a study of the effects that tailed peaks have on optimisation procedures in which criteria calculations are based predominantly on resolution values. Detailed calculations are made for the degree of area overlap between peak pairs which show tailing, and the manner in which peak tailing varies with changing mobile phase composition is also examined. These results form the foundation for a modified optimisation procedure which accommodates peak tailing, and this procedure is described in a subsequent paper[6].

THEORY

Computer generation of peak profiles

In order to study the area overlap characteristics of tailed peaks, it was necessary to computer-generate both Gaussian and tailed peaks. Gaussian peaks[7] were generated from eqn. 1

$$h(t) = h_{max} \exp\left[\frac{-1}{2}\left(\frac{t - t_G}{\sigma}\right)^2\right] \tag{1}$$

where $h(t)$ is the peak height at time t, t_G is the time of the peak maximum, h_{max} is the maximum peak height, and σ is the standard deviation of the peak. Peak profiles were generated by plotting points at constant time intervals of 0.01 min, with $\sigma = 1$ min and a maximum peak height of 1 unit.

Tailed peaks were generated from the EMG function[2], according to the equation

$$h(t) = \frac{A}{\tau} \exp\left[\frac{1}{2}\left(\frac{\tau}{\sigma}\right)^2 - \frac{(t - t_G)}{\tau}\right] \int_{-\infty}^{z} \exp\left[\frac{(-x^2/2)dx}{\sqrt{2\pi}}\right] \tag{2}$$

where A is the peak area, and Z is given by the expression

$$Z = \left[\frac{(t - t_G)}{\sigma} - \frac{\sigma}{\tau}\right]$$

The EMG function produces a Gaussian profile which has been distorted by an exponential function of time constant τ. The distorted (tailed) peak has the same peak area as its parent Gaussian curve, but it is characterised by a shift in area toward the trailing edge of the peak. Other characteristics include a decrease in peak height and a shift of the peak maximum toward the trailing edge of the peak, relative to that observed for the parent Gaussian peak. The extent of tailing is determined by the ratio between the time constant, τ, and the standard deviation, σ, of the respective peak. The greater the τ to σ ratio, the greater the degree of tailing of the peak.

In order to generate EMG peaks with a large negative Z value ($Z < -4$) or small τ values, it was necessary (because of computer memory limitations) to use an approximate asymptotic relationship[8] for the error function integral. Thus, for the leading edge of the peak, eqn. 2 reduces to

$$h(t) = \frac{h_{max}\sigma}{\tau} \exp\left[\frac{1}{2}\left(\frac{t - t_G}{\sigma}\right)^2\right] \Big/ \left[\frac{\sigma}{\tau} - \frac{(t - t_G)}{\sigma}\right] \tag{3}$$

Also, for large positive values of $Z (Z > 10)$, the following approximation[8] was used

$$h(t) = 2h_{max}\frac{\sigma}{\tau}\sqrt{\frac{\pi}{2}} \exp\left[\frac{1}{2}\left(\frac{\sigma}{\tau}\right)^2 - \frac{(t - t_G)}{\tau}\right] \tag{4}$$

The τ to σ range covered in this study was 0 to 10.0.

Calculation of R_s and percentage area overlap

In this work, resolution (R_s) was calculated from

$$R_s = 2(t_{R_{i+1}} - t_{R_i})/(4\sigma_i + 4\sigma_{i+1}) \tag{5}$$

where t_R is the time of the peak maximum (*i.e.* t_G in the case of a Gaussian peak). For calculation of R_s when either peak was tailed, the time of the peak maximum, calculated from the EMG function, was used rather than t_G for the parent Gaussian function.

The percentage area overlap (%AO) between adjacent peaks was determined by first locating the point of intersection of the peaks, and then calculating the area fraction of each peak involved in the overlap, expressed as a percentage of total area

$$\%AO = 100\left(\frac{O_i}{A_i} + \frac{O_j}{A_j}\right) \tag{6}$$

where O_i is the area of peak i which is overlapped, and A_i is the total area of peak i. Symbols with the subscript j have similar meanings. The value of %AO was calculated by integration over discrete intervals of 0.01 min.

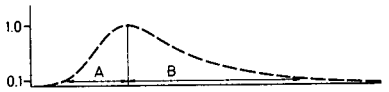

Fig. 1. Measurement of B/A at a peak height fraction of 0.1. A is the width of the leading half, and B is the width of the trailing half of the peak.

Experimental determination of τ to σ ratios

The simplest way to determine the degree of tailing exhibited by a peak is to measure the width of the leading half (A) and the trailing half (B) of the peak, and to calculate the ratio B/A. This ratio may be measured at any peak height level, but previous authors[2,9] have concentrated on 0.1, 0.3, and 0.5 of the maximum peak height, with the majority of their calculations centering on 0.1 of the peak height. The ratio calculated in this way is denoted $B/A_{0.1}$, and Fig. 1 shows the manner in which measurements are taken. Throughout this work, only $B/A_{0.1}$ ratios were used.

$B/A_{0.1}$ ratios can be converted to τ/σ values by using eqns. 7–10[9]. These equations can be used to construct a calibration curve for simple, graphic conversion of $B/A_{0.1}$ ratios to τ to σ values.

$$W = A + B \tag{7}$$

$$M = \frac{W^2}{\left[7.35 + 22.6 \exp\left(-0.708\frac{B}{A}\right)\right]} \tag{8}$$

$$\sigma = \frac{W}{\left(3.38\frac{B}{A} + 0.969\right)} \tag{9}$$

$$\tau = \sqrt{M - \sigma^2} \tag{10}$$

EXPERIMENTAL

Instrumentation

The peak generation work was performed on an Apple II+ microcomputer (Apple, Cupertino, CA, U.S.A.), containing a Digicard 80-column expansion card (Maclagan Wright Assoc., Eltham, Australia), fitted with twin floppy-disk drives, and interfaced to a BMC Model BX80 dot matrix printer (BMC International, Japan).

The liquid chromatograph consisted of a Waters Millipore (Milford, MA, U.S.A.) Model M590 pump, Model U6K injector, Model M441 UV detector (operated at 254 nm), and a Model M730 data module. The column was a Waters reversed-phase C_{18} Nova-Pak column (150 × 3.9 mm I.D.).

Reagents

Chromatography-grade solvents were used for the preparation of all mobile phases. The required amounts of organic solvents and water were measured by burette,

and the resulting solution was mixed thoroughly, filtered through a 0.45-μm membrane filter, and degassed in an ultrasonic bath before use. All mobile phases contained 5 m*M* sodium heptanesulphonate (Ajax Chemicals, Sydney, Australia) and 1% acetic acid, and were prepared freshly as required.

Amphetamine sulphate (AMPH) was obtained from U.S.V. Pharmaceuticals (Sydney, Australia), and 2-phenethylamine hydrochloride (PEA) and phenylpropanolamine hydrochloride (PPA) were obtained from Sigma (St. Louis, MO, U.S.A.). N-Methyl-2-phenethylamine hydrochloride (N-MePEA) and N,N-dimethyl-2-phenethylamine hydrochloride (N,N-diMePEA) were synthesised and checked for purity as previously reported[10].

RESULTS AND DISCUSSION

Area overlap characteristics for peaks of equal height

R_s values should indicate the extent of separation between two adjacent peaks, as determined by the degree of area overlap present. When R_s is calculated by using eqn. 5, it is assumed that the peaks are Gaussian in shape. However, if peak tailing is present the R_s value calculated in the above manner may not be indicative of the actual degree of area overlap existing between the two peaks concerned. This area overlap, and not the calculated R_s value, is the decisive factor which ultimately determines the quality of separation.

The effects of peak tailing on area overlap were determined by generating peak pairs at different R_s values and with differing degrees of peak tailing. For a particular pair of peaks, the possible combinations of peak shapes are: (i) both peaks Gaussian (G–G); (ii) a Gaussian peak followed by a tailed peak (G–T); (iii) a tailed peak followed by a Gaussian peak (T–G); (iv) both peaks tailed (T–T). The area overlap for each of these possibilities is discussed below, using the particular case where the heights of both peaks under consideration are the same.

(i) Both peaks Gaussian (G–G). This case is used as a reference for the determination of changes in the amount of area overlap resulting from the tailing of one or both peaks. The results of the G–G peak combination are represented by solid lines in Figs. 2 and 3, and a zero value for the τ to σ ratio indicates a Gaussian peak. The solid line in Fig. 2 shows the relationship between R_s (calculated according to eqn. 5) and the percentage area overlap of the two Gaussian peaks in a peak pair. The area overlap is reduced to zero for $R_s > 1.5$.

(ii) Gaussian peak with a tailed trailing peak (G–T). Fig. 2 also shows the relationship between R_s and area overlap as the τ to σ ratio for the second eluted peak is increased. Comparison of these results for the G–G peak combination illustrates that tailing of the second peak results in a decrease in the amount of overlap of the peak pair. The extent of this reduction in area overlap increases with increased tailing of the second peak. This effect is more pronounced in the low resolution region (R_s = 0–0.6), where a larger fraction of the area of each peak is involved in overlap. At higher values of R_s (0.6–1.5), the effects of tailing of the second peak are much less evident.

(iii) Tailed peak with a trailing Gaussian peak (T–G). With this peak combination, the expected trend is an increase in area overlap, resulting from the area shift of the leading tailed peak toward the overlap region. This behaviour is illustrated in Fig. 3. The increase in area overlap is governed by the degree of tailing imposed on

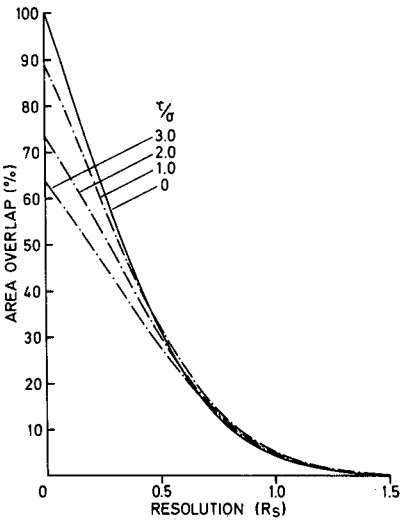

Fig. 2. Observed trends in percentage area overlap and resolution (R_s) for varying degrees of tailing imposed on the trailing peak in a peak pair (G–T case). First peak: Gaussian. Second peak: varying distortions. The solid line represents the case where both peaks are Gaussian (G–G).

the leading peak. At any given value of R_s, the area overlap of the peak pair increases with increased tailing of the leading peak. Thus, to obtain the same degree of area overlap for a T–G peak pair and a G–G peak pair, the distance between the peak maxima of the T–G pair must be increased. As the amount of tailing in the first peak is increased, greater R_s values are required to obtain zero area overlap. This can be

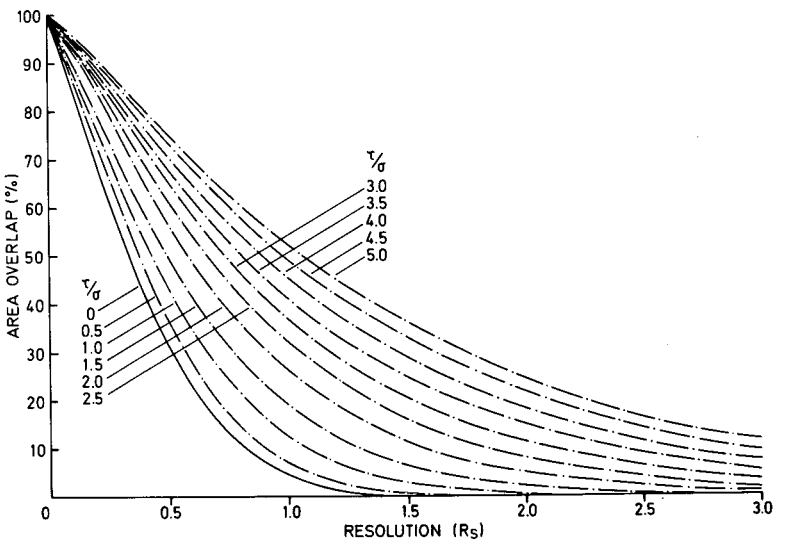

Fig. 3. Observed trends in percentage area overlap and resolution (R_s) for varying degrees of tailing imposed on the leading peak in a peak pair (T–G case). First peak: varying distortions. Second peak: Gaussian. The solid line represents the case where both peaks are Gaussian (G–G).

illustrated with an example from Fig. 3: the G–G pair of peaks are fully resolved at $R_s = 1.5$, but when the first peak is tailed by $\tau/\sigma = 1.0$, the R_s value needs to reach 2.15 before the T–G pair of peaks is fully resolved.

(iv) Both peaks tailed (T–T). In this instance, the trends in area overlap *versus* R_s (Figs. 4 and 5) were a mixture of those observed for the G–T and T–G cases above. At lower values of R_s (0–0.6), Fig. 4 shows that the amount of overlap was determined by the degree of tailing of the second peak. When the distortion of this second peak exceeded that of the first peak, there was a decrease in area overlap, resulting from simultaneous area shifts of the two peaks into and out of the overlap region. In the case shown in Fig. 4, the shift of the second peak out of the overlap region was greater than the shift of the first peak into the overlap region. At $R_s > 0.6$, the opposite trend occurred, and area overlap was slightly increased. Note that the solid line in Fig. 4 represents a peak combination where the leading peak has $\tau/\sigma = 0.5$ and the trailing peak is Gaussian.

Fig. 5 shows the case where the first peak has $\tau/\sigma = 3.0$. The solid line shows the area overlap characteristics when the trailing peak is Gaussian, and the broken line is the T–T case where $\tau/\sigma = 3.0$ for both peaks. Only very slight differences are observed between these two and this further illustrates that the τ to σ ratio for the first peak must exceed that of the second peak for increased area overlap to be observed.

From the above results it was concluded that peak tailing resulted in significantly increased area overlap of adjacent peak pairs only when the first peak was tailed. Tailing of the second peak often decreased the area overlap, and in instances where it

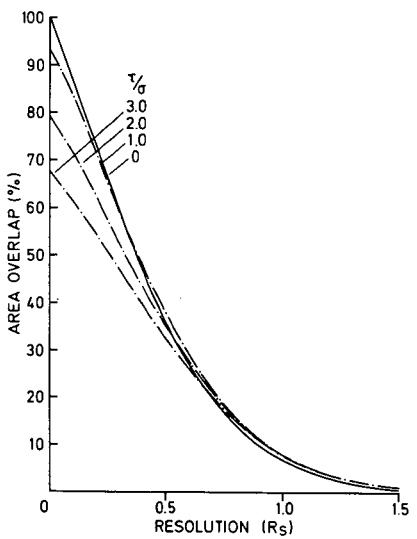

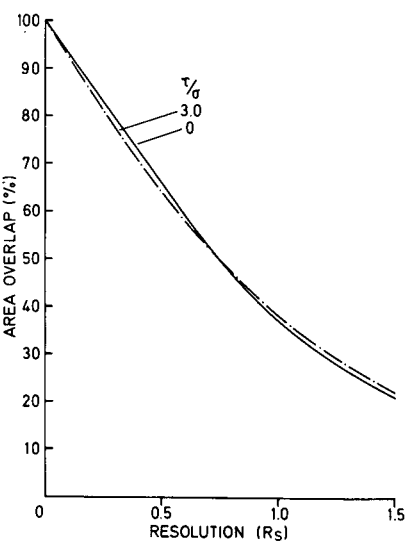

Fig. 4. Example of the observed trends in percentage area overlap and resolution (R_s) when both peaks in a peak pair are tailed (T–T case). In this instance, the tailing of the leading peak was maintained at $\tau/\sigma = 0.5$, while the degree of tailing of the trailing peak was varied as shown. The solid line represents the case where the trailing peak was Gaussian.

Fig. 5. Further example of the T–T case, where the first peak has $\tau/\sigma = 3.0$. The indicated values of τ/σ are for the second peak.

did not, the area overlap was similar to that observed when the second peak was Gaussian. These findings suggest that, when peak tailing is to be considered for optimisation purposes, increases in area overlap due to peak tailing can be assumed to arise from tailing of the first peak only.

Area overlap characteristics for peaks with varying height ratios

The above conclusions indicated that this section could be confined to consideration of the T–G case, the G–G combination again being used as a reference for comparison of results. Fig. 6 shows the relationship between R_s and area overlap for the G–G case, when the first peak is largest (Fig. 6A) and when the second peak is largest (Fig. 6B). Both figures show a noticeable swamping effect, in which R_s must be increased to a certain critical value (determined by the peak height ratio) before any separation occurs.

Similar results for the T–G case at several peak height ratios are given in Fig. 7. Fig. 7A shows that the swamping region extends to larger values of R_s when the height of the first peak is increased with respect to that of the second peak. On the other hand, when the second peak is larger, the area overlap increases with increasing τ to σ ratio of the first peak (Fig. 7B), in a similar manner to that observed for the T–G case for peaks of equal height (see Fig. 3).

The chief outcome of varying the relative peak heights is the introduction of the swamping zone at low values of R_s. However, in the region of most concern for optimisation purposes, *i.e.* R_s values of 1–1.5, the observations are very similar to those for the 1:1 peak height ratio.

Effects of solvent modifiers on peak shape

The foregoing results have highlighted the effects of peak tailing on the

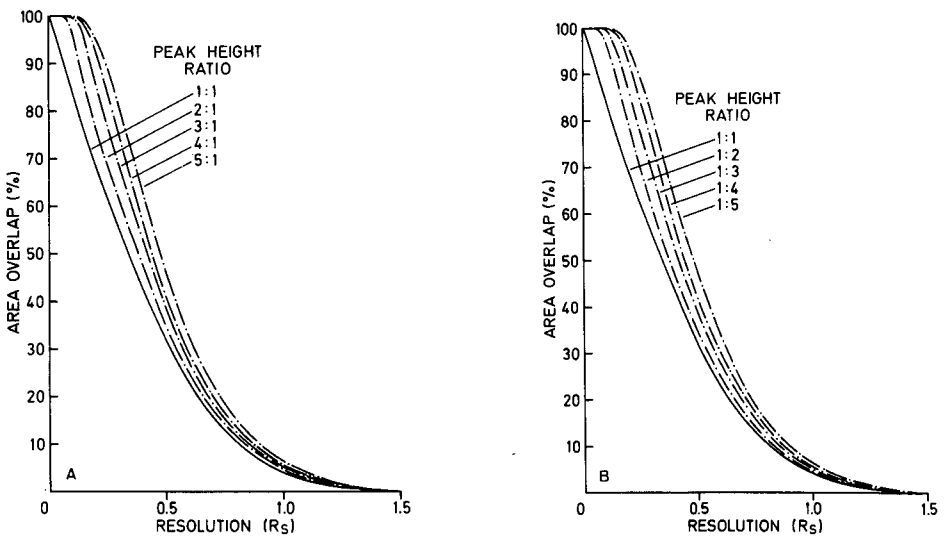

Fig. 6. Observed trends in percentage area overlap and resolution (R_s) for Gaussian peaks of varying peak height ratios, where (A) the leading peak height is largest, and (B) the trailing peak height is largest.

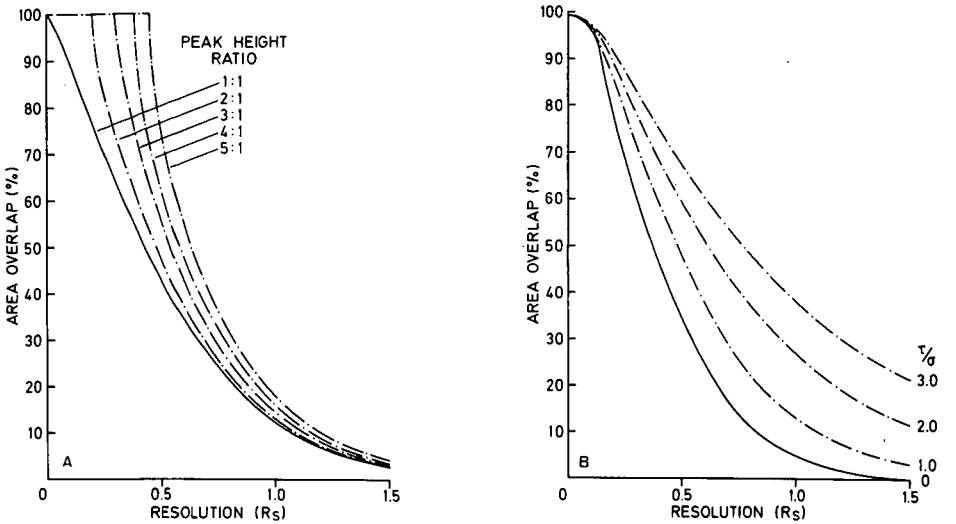

Fig. 7. Observed trends in percentage area overlap and resolution (R_s) for the T–G case with peaks of unequal height. (A) The τ to σ ratio for the first peak is constant (1.0) and peak height ratio is varied. (B) The peak height ratio is constant (1:2) and the τ to σ ratio for the first peak is varied. Both (A) and (B): second peak is Gaussian.

resolution between peak pairs. The extent of this effect is dependent on the tailing and on whether it is the leading or trailing peak that shows tailing. These findings have obvious ramifications for optimisation procedures in which Gaussian peak shapes are assumed. It is possible to devise a new optimisation criterion which gives due consideration to peak tailing effects, but the manner in which peak tailing varies under changing mobile phase conditions must first be established. Peak tailing can be ascribed to various extra-column and intra-column factors. Those factors which arise from purely physical effects can be expected to remain constant in the course of an optimisation procedure, but this may not be true of chemical factors, such as interaction of the solutes with silanol sites on the stationary phase.

Optimisation procedures for reversed-phase liquid chromatography (RPLC) generally involve the exploitation of selectivity effects occurring when mobile phases are prepared from combinations of water with methanol, acetonitrile, and tetrahydrofuran (THF). Binary (water plus one modifier), ternary (water plus two modifiers), or quaternary (water plus all three modifiers) mobile phases may be used, although ternary mobile phases usually provide sufficient selectivity to separate most sample mixtures. In order to correct successfully for peak tailing effects in optimisation processes, it is therefore necessary to examine the variation of peak tailing with changing mobile phase composition, at least for binary and ternary mobile phases.

To study these effects, careful peak shape measurements were made on five sympathomimetic amines known to exhibit tailing. The peak profile of each solute was recorded in a variety of binary mixtures of water with methanol, acetonitrile or THF. The concentration of organic solvents was varied in order to obtain peak profiles of each solute covering the approximate capacity factor range $1 \leqslant k' \leqslant 10$, which is the retention range usually applicable to optimisation procedures. Peak asymmetry was

measured, and τ/σ values were calculated for each peak from eqns. 7–10. The τ to σ ratios obtained for all five solutes are listed in Table I and a graphic representation of the results for one of the solutes (N,N-diMePEA) is presented in Fig. 8. This figure shows that τ to σ ratios for a particular binary mobile phase were essentially constant as the eluotropic strength of the mobile phase (and hence the capacity factor of the solute) was varied. However, striking differences in τ to σ ratios existed between the different modifiers. They can be attributed to differences in the interaction of these modifiers with the solutes and the stationary phase. For the series of solutes studied, tailing was least in the THF–water binary and greatest in the acetonitrile–water binary mobile phases. It is expected that this trend would vary with the nature of the solutes involved. The slight scatter of points in Table I is due to the error inherent in the B/A measurements. It should be pointed out that the accuracy of these measurements decreases with decreasing capacity factor.

The variation of peak tailing was also investigated, using ternary mobile phase

TABLE I

VARIATION OF τ TO σ RATIOS IN BINARY MOBILE PHASES OF WATER WITH METHANOL, ACETONITRILE OR THF

Solute identities are given in the Experimental section.

Solute	*Methanol*		*Acetonitrile*		*THF*	
	k'	τ/σ	k'	τ/σ	k'	τ/σ
PPA	0.6	2.6	0.9	3.1	1.1	2.3
	1.0	2.8	1.4	3.1	2.7	2.3
	1.3	2.6	3.5	2.9	3.9	2.3
	7.1	2.5	4.6	2.9	4.4	2.1
	11.7	2.8	11.9	3.1	9.5	2.1
PEA	0.6	3.4	1.1	5.1	1.2	2.6
	1.0	3.4	1.9	5.0	2.7	2.8
	1.4	3.5	4.6	4.8	4.4	2.8
	7.5	3.7	6.1	5.1	9.9	2.5
	12.8	3.7	15.5	4.8	14.0	2.9
N-MePEA	0.6	2.9	1.4	8.4	1.1	3.2
	1.1	3.2	2.4	8.8	2.4	3.2
	1.4	3.1	5.7	8.8	4.0	2.9
	7.3	3.1	7.5	8.7	8.8	2.9
	13.1	3.2	9.6	8.8	12.6	3.2
N,N-diMePEA	0.6	4.8	1.7	9.6	1.0	3.2
	1.2	4.7	2.8	9.5	2.2	3.4
	1.3	4.8	3.0	9.3	3.6	3.2
	6.8	4.7	7.4	9.5	7.9	3.1
	12.3	5.0	9.7	9.5	11.6	3.5
AMPH	0.6	3.7	1.4	6.5	1.4	2.1
	1.5	3.4	2.3	6.4	3.5	2.2
	1.7	3.4	2.5	6.4	6.1	1.8
	7.8	3.5	6.8	6.4	9.8	2.0
	11.4	3.5	9.1	6.4	14.7	2.1

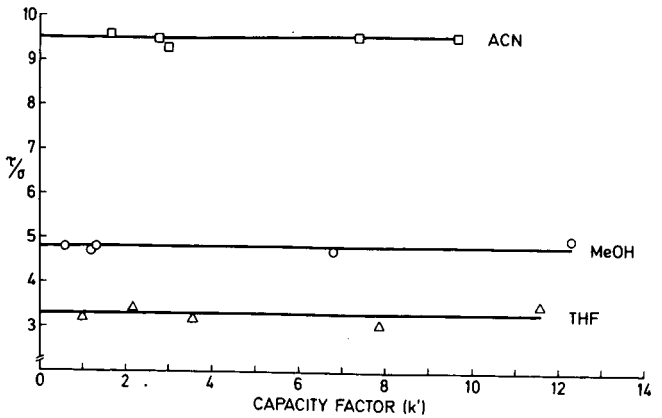

Fig. 8. Variation of τ to σ ratios for N,N-diMePEA in binary mobile phases. See Table I for information on other solutes studied. ACN = Acetonitrile; MeOH = methanol.

compositions. A hypothetical optimisation search area was defined by the three binary mobile phase compositions: methanol–water (60:40), acetonitrile–water (30:70) and THF–water (30:70). τ/σ values for the five sympathomimetic amines were determined at these three binary compositions and at ternary compositions produced from linear combinations of the binary mobile phases. Our aim was to ascertain the manner in which peak tailing varied over a typical optimisation search area.

Table II lists the mobile-phase compositions examined, together with the resultant τ/σ values for the five solutes, whilst Fig. 9 provides a graphic depiction of the results for PEA and N,N-diMePEA, which are representative of the group of solutes used. Fig. 9 shows that for ternary mobile phases τ/σ varied in an approximately linear manner with mobile phase composition. In some circumstances a slight curvature in

TABLE II

VARIATION OF τ TO σ RATIOS IN TERNARY MOBILE PHASES

Solute identities are given in the Experimental section.

Mobile phase composition				*τ to σ ratio*				
Methanol	*Acetonitrile*	*THF*	*Water*	*PPA*	*PEA*	*N-MePEA*	*N,N-diMePEA*	*AMPH*
60	0	0	40	2.7	3.5	3.1	4.8	3.5
45	7.5	0	47.5	2.9	3.5	4.1	5.8	3.5
30	15	0	55	3.2	4.4	4.8	7.1	3.8
15	22.5	0	62.5	3.2	4.4	6.4	8.1	5.0
0	30	0	70	3.0	5.0	8.7	9.5	6.4
0	22.5	7.5	70	3.1	4.8	7.3	7.1	5.3
0	15	15	70	2.8	3.7	5.4	5.3	3.9
0	7.5	22.5	70	2.5	3.4	4.4	4.4	2.8
0	0	30	70	2.2	2.7	3.1	3.3	2.0
15	0	22.5	62.5	2.5	2.5	2.8	3.8	2.3
30	0	15	55	2.9	2.9	3.2	4.4	2.5
45	0	7.5	47.5	2.9	3.2	3.2	4.5	2.8
60	0	0	40	2.7	3.5	3.1	4.8	3.5

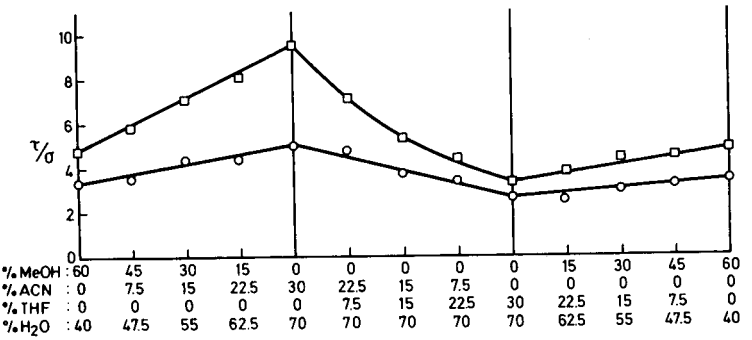

Fig. 9. Variation of τ/σ for PEA (○) and N,N-diMePEA (□) in ternary mobile phases. Data for further solutes can be found in Table II. MeOH = Methanol; ACN = acetonitrile.

the plots was observed, *e.g.*, N,N-diMePEA in acetonitrile–THF–water ternary mobile phases, but it is difficult to conclude whether this is a true trend or a propagation of the B/A measurement error mentioned earlier. In either case, the curvature is not extensive, and the relationship between τ/σ and mobile phase composition can be approximated by a straight line.

Suitability of the EMG model

The large number of chromatographic peaks generated in the above studies of the effect of solvent modifier on peak shapes provided ample data for assessment of the suitability of the EMG model for the simulation of tailed peaks. For a number of the experimental peaks, the width of the leading half (A) and the trailing half (B) were measured and used to calculate τ/σ using eqns. 7–10. The values so determined were then used to generate EMG peaks of the same height as the experimental peaks. When the experimental and computer-generated peaks were overlaid, it was found that they were virtually superimposable in every case examined. The closeness of fit obtained with the EMG model was considered to be strong evidence of the suitability of this model for simulating experimentally obtained tailed peaks.

CONCLUSIONS

This study has provided quantitative information on the degree of area overlap existing between peak pairs in which tailing is evident. From a comparison of tailed peak pairs with Gaussian peaks having the same retention times, it has been shown that area overlap in the tailed case is increased significantly, relative to the Gaussian peaks, only when the first peak in a pair is tailed. For the solutes tested, the degree of tailing exhibited was constant in binary mobile phases of water and one of the solvent modifiers methanol, acetonitrile or THF, regardless of the eluotropic strength of the mobile phase used. Differences were noted in the degree of tailing observed for the same solute when the nature of the modifier in the binary mobile phase was varied. The τ to σ ratios were found to follow an approximately linear relationship with the mobile phase composition for ternary mobile phases formed from linear combinations of the binary compositions referred to above.

These results have direct application to computer optimisation procedures for

HPLC in that they provide a basis for predicting the manner in which peak tailing can be expected to vary over the range of mobile phases to be considered in the optimisation process. In turn, this knowledge permits accurate calculation of the degree of area overlap of each sample peak with its neighbouring later-eluted peak, and therefore provides a realistic assessment of the separation achieved. A new optimisation procedure which incorporates these features is discussed elsewhere[6].

REFERENCES

1 W. E. Barber and P. W. Carr, *Anal. Chem.*, 53 (1981) 1939.
2 J. P. Foley and J. G. Dorsey, *Anal. Chem.*, 55 (1983) 730.
3 R. E. Pauls and L. B. Rogers, *Anal. Chem.*, 49 (1977) 625.
4 V. Maynard and E. Grushka, *Anal. Chem.*, 44 (1972) 1427.
5 E. Grushka, *Anal. Chem.*, 44 (1972) 1733.
6 P. R. Haddad and S. Sekulic, *J. Chromatogr.*, 459 (1988) 79.
7 A. S. Said, *Theory and Mathematics of Chromatography*, Hüthig, Heidelberg, 1981, p. 75.
8 I. G. McWilliam and H. C. Bolton, *Anal. Chem.*, 41 (1969) 1755.
9 D. J. Anderson and R. R. Walters, *J. Chromatogr. Sci.*, 22 (1984) 353.
10 S. Sekulic , P. R. Haddad and C. J. Lamberton, *J. Chromatogr.*, 363 (1986) 125.

Journal of Chromatography, 459 (1988) 79–90
Elsevier Science Publishers B.V., Amsterdam — Printed in The Netherlands

CHROMSYMP. 1503

EFFECTS OF PEAK TAILING ON COMPUTER OPTIMISATION PROCEDURES FOR HIGH-PERFORMANCE LIQUID CHROMATOGRAPHY

II. AN OPTIMISATION ROUTINE FOR TAILED PEAKS

P. R. HADDAD* and S. SEKULIC
Department of Analytical Chemistry, University of New South Wales, P.O. Box 1, Kensington, N.S.W. 2033 (Australia)

SUMMARY

An optimisation program is proposed as a means of compensating for the loss of resolution resulting from peak tailing. A mobile phase search area of ternary compositions of water with two of the three solvents, methanol, acetonitrile, and tetrahydrofuran, is defined by isoeluotropic binary mobile phases of water with each of the above three modifiers. Retention and peak shape (τ/σ) data are obtained for each solute in the mixture to be separated, using the three isoeluotropic binary mobile phases. These data are used to interpolate retention and peak shape data for intermediate ternary mobile phases. The area overlap for each peak pair is calculated, and the resolution of a pair of Gaussian peaks with the same degree of area overlap is determined. This value is then used for calculation of an optimisation criterion and the ultimate selection of the optimal mobile phase. The program was computer-validated by using a hypothetical case. It was then experimentally tested by using a mixture of six compounds, giving both symmetrical and tailed peaks. In both cases, the use of the proposed program resulted in the selection of a mobile phase that gave a chromatogram superior to that obtained without considering peak tailing effects.

INTRODUCTION

Computer optimisation of mobile phase composition in high-performance liquid chromatography (HPLC) involves selection of an optimal mobile phase on the basis of the quality of the chromatogram produced by that mobile phase. Quality is assessed using a of mathematical criterion which assigns a numerical value to the chromatogram, dependent on the degree of separation achieved. The optimisation criterion is therefore a crucial parameter in determining the ultimate success of the optimisation process.

Schoenmakers[1] has recently reviewed optimisation criteria, and has defined "elemental criteria" as those which may be used to quantify the separation between a pair of adjacent peaks in a chromatogram. Elemental criteria include peak-valley ratio (P)[2,3], valley-to-top ratio (P_v)[4], fractional peak overlap (FO), resolution (R_s),

0021-9673/88/$03.50

and the separation factor (S)[5,6]. Some elemental criteria have been compared[7,8] and it is apparent that their characteristics differ markedly. R_s and S do not reflect changes in the peak shape or the ratio of peak areas, but their values are relatively easily calculated and are transferable to other columns. On the other hand, P, P_v, and FO are often more difficult to measure, but they accurately reflect the actual separation and vary with changes in peak shape and area ratio. Ease of calculation is of paramount importance in the practical implementation of optimisation procedures, and therefore R_s is by far the most commonly employed elemental criterion.

Since a chromatogram generally consists of more than two peaks, the quality of the entire chromatogram must be assessed by some combination of elemental criteria for adjacent peak pairs. A simple example is use of the R_s value for the peak pair in the chromatogram with the poorest resolution (*i.e.* $R_{s_{min}}$) as an indicator of the quality of the entire chromatogram. Summation of elemental criteria, such as R_s and S, has been suggested[9,10], but this sum is strongly influenced by the largest value of the elemental criterion in a chromatogram, and therefore it may not accurately indicate the degree of separation of less-resolved peak pairs. Product criteria, in which the values of the elemental criteria for each peak pair are multiplied, have also been proposed[5,11]. These have proven to be particularly useful, especially when the product is normalised to account for the length of the chromatogram. Composite criteria which consider factors other than separation, such as analysis time, have also been suggested[12].

The chief drawback of R_s as an elemental criterion, and hence of the composite criteria that use R_s for their calculation, is that peaks are considered to be Gaussian in shape. The utility of R_s in optimisation procedures would therefore be enhanced considerably if a new criterion could be devised based on R_s values (and thus taking advantage of the simplicity of calculation for this parameter), which can also make allowances for non-Gaussian peaks. In this paper, we propose such a criterion which expresses the resolution of tailed peaks in terms of the equivalent area overlap of Gaussian peaks. The new procedure is first computer-validated and then applied to the separation of a mixture of six aromatic compounds.

EXPERIMENTAL

Instrumentation

The optimisation programs used in this work were operated on a Macintosh Plus microcomputer (Apple, Cupertino, CA, U.S.A.) with 1 Mb RAM, fitted with an external disk drive and an Apple Imagewriter II printer. The liquid chromatograph consisted of a Waters Millipore (Milford, MA, U.S.A.) Model M590 pump, Model U6K injector, Model M441 UV detector (operated at 254 nm), and a Model M730 data module. The column was a Waters reversed-phase C_{18} Nova-Pak column (150 × 3.9 mm I.D.).

Reagents

Binary and ternary mobile phases used for the optimisation procedure were prepared by measuring the required volumes of chromatography-grade solvents and water with a burette into a suitable container, mixing the resultant solution thoroughly, filtering through a 0.45-μm membrane filter, and degassing in an ultrasonic bath before use. The mobile phases also contained 5 mM sodium heptanesulphonate

(Ajax Chemicals, Sydney, Australia) and 1% acetic acid. Analytical-grade solutes were obtained from the following sources: toluene from May & Baker (Dagenham, U.K.), *p*-iodophenol from Fluka (Buchs, Switzerland), and doxepin and propranolol from Sigma (St. Louis, MO, U.S.A.). N-*n*-Butyl-2-phenethylamine hydrochloride and 2,2'-diphenethylamine hydrochloride were synthesised and checked for purity as previously reported[13].

Optimisation software (prior to any changes)

The optimisation method was based on the iterative procedure reported by Schoenmakers *et al.*[5] and Drouen *et al.*[6]. In this procedure, retention data obtained for three isoeluotropic binary mobile phases are used to predict retention times for the ternary solvent mixtures formed from linear combinations of the binary mobile phases. All possible chromatograms within a mobile phase search area bound by the three isoeluotropic binary mobile phases are then assessed on the basis of a mathematical criterion[14] and the optimal mobile phase is selected. Retention data for this mobile phase are then measured and added to the data file in the computer. The calculation of the criterion is repeated, and a new optimal mobile phase selected. This process continues until the same optimum is selected in successive calculations or a previously measured mobile phase composition is assigned to be the optimum. Full details of the operational procedure and theoretical basis of this method are given elsewhere[5,6,15].

RESULTS AND DISCUSSION

Effects of peak tailing on calculations of criteria

As outlined in the Introduction, the ability of an optimisation procedure to locate the optimal mobile phase is dependent on an accurate assessment of the quality of a chromatogram through the use of a mathematical criterion. The criteria used in this work were the resolution product, ΠR_s, or the relative resolution product, r, which can be defined as[1]

$$\prod R_s = \prod_{i=1}^{n-1} R_{s_{i,i+1}} \tag{1}$$

$$r = \prod_{i=1}^{n-1} \left[\frac{R_{s_{i,i+1}}}{\frac{1}{n-1} \sum_{i=1}^{n-1} R_{s_{i,i+1}}} \right] \tag{2}$$

R_s for adjacent peaks (denoted by i and $i+1$) is calculated from the equation

$$R_s = \frac{\sqrt{N}}{2} \frac{(t_{R_{i+1}} - t_{R_i})}{(t_{R_i} + t_{R_{i+1}})} \tag{3}$$

where t_R represents the retention time of a peak, and N is the efficiency of the chromatographic column used. Whilst eqn. 3 assumes that the peaks involved are Gaussian in shape, it is nevertheless very useful for optimisation procedures, since it

permits R_s to be calculated on the basis of column efficiency and retention times for solutes in the mixture to be optimised. If a relationship between retention time and mobile phase composition is known or assumed, it becomes possible to predict retention times for any desired mobile phase composition and, hence, to calculate a criterion value for the chromatogram that would be produced with that particular mobile phase. In this way, the optimal mobile phase can be selected.

This approach operates well when the component solutes of the mixture to be separated give symmetrical peaks for which the R_s values calculated from eqn. 3 accurately reflect the actual degree of separation of the two peaks concerned. When peak tailing is evident, the value of R_s calculated for each peak pair from eqn. 3, and hence the value of the optimisation criterion, will be unchanged, despite the fact that the area overlap of the peaks may have increased. This is illustrated in Fig. 1, which shows a chromatogram of five fully resolved Gaussian peaks (Fig. 1A), whilst Fig. 1B shows five tailed peaks ($\tau/\sigma = 3.0$ for each peak) eluted at the same retention times. Despite the fact that the separation is clearly poorer in Fig. 1B, both chromatograms have identical values for the ΠR_s and r criteria.

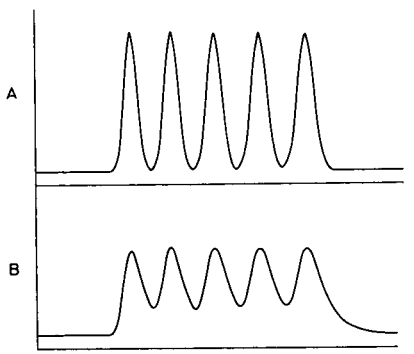

Fig. 1. Effect of peak tailing on area overlap. Retention times are the same for both chromatograms, but peaks are Gaussian in A and have $\tau/\sigma = 3.0$ in B.

Characteristics of tailed peaks in optimisation procedures

The aim of our work was to devise an optimisation program which would be capable of reliable prediction of optimal mobile phases for mixtures of solutes giving tailed peaks. The characteristics of tailed peaks that are of importance to optimisation procedures have been evaluated[16], and the results obtained can be summarised as:

(i) When a peak pair is considered, tailing of the leading peak causes a significant increase in the area overlap between the peaks, whereas tailing of the trailing peak generally results in a decrease in area overlap. When evaluating the separation of such a peak pair for an optimisation procedure, it is therefore necessary to consider the tailing exhibited by the leading peak only, and the trailing peak can be assumed to be Gaussian.

(ii) If the components of a peak pair are of different heights, the trends in area overlap are similar to those observed for peaks of equal height, except that a swamping region is introduced within which total area overlap is maintained until R_s reaches

a threshold value, dependent on the height ratio of the two peaks concerned. In the R_s region that is of most concern to optimisation procedures (*i.e.* 1–1.5), disparate height ratios do not exert a significant effect on area overlap. This factor, and the limitation on computer memory available for the optimisation program, lead to the necessity to assume that all peaks in a chromatogram are of equal height. Some loss of accuracy can be expected as a result of this assumption.

(iii) Peak asymmetry values, as given by τ/σ ratios, differ in binary mobile phases [water with methanol, acetonitrile or tetrahydrofuran (THF)]. A linear relationship between τ/σ and the mobile phase composition exists for ternary mobile phases, formed from linear combination of the above binary mobile phases. Thus, if the τ to σ ratio is known for each solute in the binary mobile phase compositions used to define the mobile phase search area in the optimisation, it becomes possible to calculate τ to σ ratios for ternary mobile phases within that search area.

(iv) The exponentially modified Gaussian function, which was used to generate tailed peaks in this study, is a good approximation for the actual peak shapes obtained experimentally.

Optimisation software for tailed peaks

Based on the above results, a new procedure was developed for the calculation of peak separation values, based on area overlap, which could be used for the determination of realistic criteria in cases of solutes giving tailed peaks. To achieve this goal, the optimisation program currently in use in our laboratory was modified in two ways.

In the first modification, the operator is asked to provide geometric information for each peak in the mixture, measured for each of the isoeluotropic binary mobile phases. The widths of the leading half (A) and the trailing half (B) of the peak, measured at 10% of peak height, are used to calculate the peak asymmetry ($B/A_{0.1}$) and, thence, the τ to σ ratio, from previously reported equations[16] or from a calibration curve, such as that shown in Fig. 2. The slope of an assumed linear relationship between τ/σ and Φ, the mobile phase composition, is then calculated for ternary mobile phases, comprising the search area defined by linear combinations of the isoeluotropic binary mobile phases. This permits calculation of τ to σ ratios for each solute in any mobile phase composition within the search area.

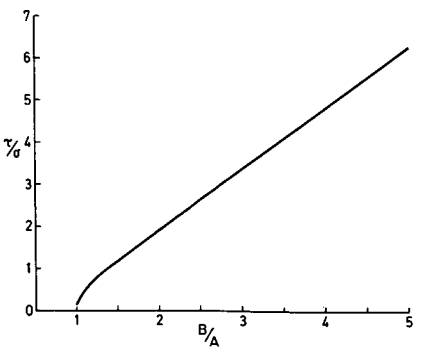

Fig. 2. Calibration plot for graphic conversion of asymmetry factors (B/A) into τ/σ values.

TABLE I

FOURTH-ORDER POLYNOMIAL COEFFICIENTS FOR EQUATIONS DESCRIBING THE RELATIONSHIP BETWEEN R_s AND PERCENTAGE AREA OVERLAP FOR PEAK PAIRS IN WHICH THE FIRST PEAK HAS THE INDICATED VALUE OF τ/σ

The coefficients are for the equaton $Ax^4 + Bx^3 + Cx^2 + Dx + E = 0$.

τ/σ	A	B	C	D	E	*Correlation coefficient*
0.0	−24.42	52.10	44.37	−168.48	100.38	0.9999
0.1	−42.56	91.03	22.09	−166.39	100.15	0.9999
0.2	−44.70	94.65	21.06	−167.36	100.20	0.9999
0.3	−21.90	40.15	58.45	−172.29	99.76	0.9999
0.4	−23.44	48.54	44.64	−164.31	99.90	0.9999
0.5	−28.40	71.64	10.41	−148.30	101.16	0.9999
0.6	−21.04	52.74	23.01	−148.13	100.58	0.9999
0.7	−10.36	18.54	57.23	−157.84	100.38	0.9999
0.8	−12.75	32.73	30.16	−141.33	100.65	0.9999
0.9	− 9.90	22.02	41.68	−143.50	100.16	0.9999
1.0	− 6.84	15.30	41.07	−138.88	101.58	0.9997
1.1	−10.03	31.30	13.91	−122.49	101.24	0.9997
1.2	− 3.71	5.00	47.66	−134.39	100.46	0.9999
1.3	− 4.01	8.65	36.74	−125.34	100.96	0.9998
1.4	− 6.43	20.17	18.71	−114.98	100.86	0.9999
1.5	− 1.67	−0.27	44.54	−123.61	100.74	0.9997
1.6	− 4.78	15.34	19.44	−109.25	100.30	0.9999
1.7	− 2.37	7.06	23.49	−105.20	100.79	0.9995
1.8	− 0.93	−1.35	38.78	−113.64	100.82	0.9997
1.9	− 1.28	1.79	30.39	−106.18	100.82	0.9996
2.0	− 0.73	−1.08	33.99	−106.29	101.25	0.9995
2.1	− 1.93	6.67	17.86	− 94.85	100.90	0.9995
2.2	− 0.19	−3.72	36.96	−105.30	100.99	0.9997
2.3	− 0.38	−2.21	32.77	−101.29	101.16	0.9996
2.4	0.12	−4.59	35.13	−100.21	101.35	0.9995
2.5	− 0.08	−2.90	30.21	− 95.13	101.10	0.9995
2.6	− 0.04	−2.97	29.43	− 93.36	101.51	0.9995
2.7	0.02	−3.47	30.49	− 93.54	101.21	0.9997
2.8	0.16	−4.11	30.89	− 92.98	101.85	0.9997
2.9	0.16	−3.97	29.55	− 90.10	101.53	0.9996
3.0	0.13	−3.52	27.56	− 86.83	100.74	0.9997
3.1	− 0.02	−2.20	23.72	− 83.43	101.52	0.9995
3.2	− 0.08	−1.61	21.60	− 80.75	101.56	0.9995
3.3	0.20	−3.89	27.49	− 85.23	101.51	0.9997
3.4	0.19	−3.72	26.32	− 82.91	101.28	0.9998
3.5	0.20	−3.74	26.02	− 82.12	101.79	0.9997
3.6	0.18	−3.40	24.38	− 79.47	101.46	0.9997
3.7	0.16	−3.12	23.14	− 77.58	101.52	0.9997
3.8	0.14	−2.85	22.09	− 76.24	101.95	0.9996
3.9	0.12	−2.61	20.81	− 73.93	101.59	0.9997
4.0	0.13	−2.67	20.90	− 73.49	100.95	0.9997
4.1	0.12	−2.57	20.28	− 72.34	101.23	0.9998
4.2	0.11	−2.36	19.28	− 70.73	101.27	0.9998
4.3	0.11	−2.32	18.96	− 70.15	101.79	0.9997
4.4	0.10	−2.21	18.18	− 68.35	101.40	0.9998
4.5	0.08	−1.91	16.85	− 66.34	101.22	0.9997
4.6	0.08	−1.94	16.77	− 65.77	101.48	0.9998
4.7	0.08	−1.81	16.08	− 64.50	101.51	0.9998

TABLE I *(continued)*

τ/σ	A	B	C	D	E	*Correlation coefficient*
4.8	0.06	−1.63	15.32	− 63.57	101.99	0.9996
4.9	0.08	−1.80	15.72	− 63.18	101.11	0.9999
5.0	0.07	−1.73	15.36	− 62.63	101.60	0.9998
5.1	− 0.21	0.74	8.29	− 55.49	100.79	0.9998
5.2	− 0.22	0.91	7.52	− 54.22	100.81	0.9999
5.3	− 0.24	1.09	6.78	− 52.98	100.83	0.9999
5.4	− 0.25	1.25	6.07	− 51.78	100.84	0.9999
5.5	− 0.24	1.16	6.38	− 51.95	100.96	0.9999
5.6	− 0.28	1.56	4.69	− 49.43	100.81	0.9999
5.7	− 0.28	1.68	4.12	− 48.38	100.82	0.9999
5.8	− 0.29	1.81	3.52	− 47.31	100.83	0.9999
5.9	− 0.31	1.95	2.90	− 46.26	100.83	0.9999
6.0	− 0.21	1.08	5.52	− 48.47	100.41	0.9999
6.1	− 0.09	0.14	7.52	− 49.40	100.53	0.9999
6.2	− 0.13	0.51	6.34	− 47.97	100.52	0.9999
6.3	− 0.14	0.61	5.87	− 47.07	100.53	0.9999
6.4	− 0.14	0.70	5.41	− 46.20	100.55	0.9999
6.5	− 0.15	0.79	4.94	− 45.28	100.51	0.9999
6.6	− 0.16	0.87	4.54	− 44.47	100.53	0.9999
6.7	− 0.16	0.96	4.10	− 43.64	100.54	0.9999
6.8	− 0.17	1.03	3.73	− 42.87	100.55	0.9999
6.9	− 0.17	1.11	3.34	− 42.10	100.56	0.9999
7.0	− 0.17	1.13	3.14	− 41.48	100.57	0.9999
7.1	− 0.18	1.19	2.80	− 40.77	100.59	0.9999
7.2	− 0.18	1.27	2.43	− 40.03	100.59	0.9999
7.3	− 0.19	1.33	2.10	− 39.35	100.60	0.9999
7.4	− 0.15	0.97	3.19	− 40.18	100.29	0.9999
7.5	− 0.16	1.04	2.89	− 39.49	100.29	0.9999
8.0	− 0.17	1.19	1.83	− 36.83	100.35	0.9999
8.5	− 0.18	1.39	0.67	− 34.11	100.38	0.9999
9.0	− 0.16	1.31	0.32	− 32.16	100.41	0.9999
9.5	− 0.16	1.27	0.33	− 31.22	100.03	0.9999
10.0	− 0.09	0.77	1.15	− 30.40	100.12	0.9999

Secondly, use is made of the relationships observed between % area overlap and R_s for a peak pair in which the leading peak exhibits tailing. These relationships have been reported previously[16] for τ/σ values in the range 0 to 10.0, and can be fitted[17] to fourth-order polynomial curves. The data for these polynomial functions are given in Table I, and are stored as part of the optimisation program. Thus, if the retention times of the components of a peak pair and τ/σ for the first-eluted peak are known, then R_s can be calculated from eqn. 3, and the percentage area overlap of the two peaks can be calculated by solving the equation in Table I for the appropriate τ/σ value.

This calculated area overlap can then be substituted into the polynomial expression for two Gaussian peaks (*i.e.* $\tau/\sigma = 0$ in Table I) to determine the R_s value which would be exhibited by two Gaussian peaks with the same degree of area overlap. The value calculated in this manner is described as the "Gaussian equivalent resolution", R_s'. Fig. 3 gives a graphic representation of the process involved for a peak

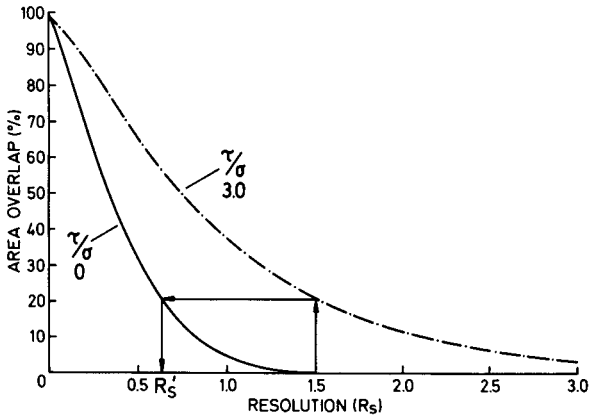

Fig. 3. Calculation of R_s', the Gaussian equivalent resolution, for a pair of peaks where $R_s = 1.5$ and the leading peak is tailed by $\tau/\sigma = 3.0$.

pair in which the first peak has $\tau/\sigma = 3.0$, the R_s calculated from eqn. 3 is 1.5 and the value of R_s' for the same peak pair is 0.63. Criteria values may then be calculated from R_s' values rather than R_s values, and criteria calculated in this way are identified in this paper as $\Pi R_s'$ and r'. The predicted optimal mobile phase composition is then determined and reported, together with a listing of the calculated R_s' values for each peak pair. A flow diagram of the entire process is presented in Fig. 4.

This modified optimisation program provides the operator with the option of including or excluding the consideration of peak tailing, so that when all solutes in a mixture give symmetrical peaks, it is not necessary to enforce the additional calculation time required in case of peak tailing.

Computer validation of the proposed procedure

It can be envisaged that peak tailing effects would exert the greatest influence in the situations described below, and it is in these cases that the modified optimisation procedure could be expected to show the most benefit:

(i) When the degree of tailing of solutes in the mixture varies widely; *e.g.*, one or two tailing solutes in a mixture, where solutes give symmetrical peaks.

(ii) When the order of elution of a tailed solute alters over the search area. Here, mobile phases in which a tailed peak is eluted last in a critical peak pair may be preferred to those in which the tailed peak is eluted first.

(iii) When solutes under consideration exhibit a significantly smaller degree of tailing with two of the modifiers, then ternary combination of those modifiers with water may be favoured.

In each of these situations, the use of R_s' values for criteria calculations would provide a more accurate appraisal of peak separation than that gained from the use of R_s values. A hypothetical retention file for three solutes in methanol–acetonitrile–water ternary mobile phases was used to validate the modified optimisation program. Table II lists the retention and peak shape data, and shows that only one solute (solute 1) exhibits peak tailing. The optimum was selected by using the relative resolution product criterion which gives preference to chromatograms in which peaks are evenly

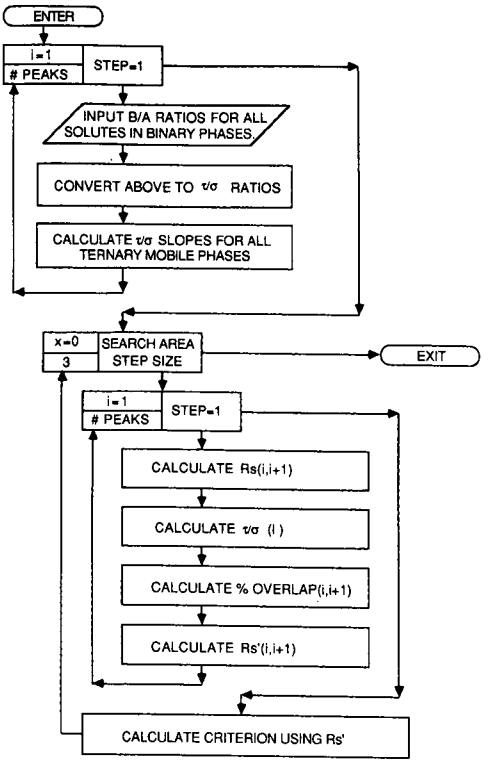

Fig. 4. Flow diagram of the steps incorporated into the optimisation program to compensate for peak tailing.

spaced. Using Eqn. 3 to calculate R_s values, the predicted optimal mobile-phase composition is calculated to be methanol–acetonitrile–water (17.5:22.5:60), with a criterion value of $r = 1$. Assuming Gaussian peak shapes, the optimal chromatogram is shown in Fig. 5a, whilst the actual chromatogram for this mobile phase composition is given in Fig. 5b. In its unmodified form, the optimisation software cannot

TABLE II

RETENTION AND PEAK SHAPE DATA FOR A HYPOTHETICAL TEST MIXTURE USED TO VALIDATE THE MODIFIED OPTIMISATION PROCEDURE

Solute	*Mobile phase: methanol–acetonitrile–water*			
	50:0:50		*0:35:65*	
	Retention time (min)	*Peak shape data (τ/σ)*	*Retention time (min)*	*Peak shape data (τ/σ)*
1	6.5	3.3	6.7	3.3
2	7.1	0	8.2	0
3	9.8	0	8.9	0

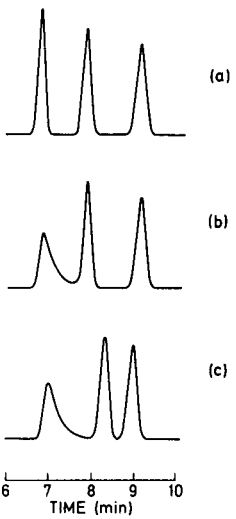

Fig. 5. Hypothetical test case for evaluation of the modified optimisation program. The data file in Table II was used. (a) Optimal chromatogram selected when peak tailing is not considered. (b) Actual chromatogram for this mobile phase. (c) Actual chromatogram selected by the modified program. Solute 1 has $\tau/\sigma = 3.3$.

distinguish between these two chromatograms, and does not recognise the area overlap existing between peaks 1 and 2 in Fig. 5b. When the same optimisation is repeated with the modified program, the predicted optimum mobile phase is acetonitrile–water (35:65), with a criterion value of $r' = 0.95$. The optimal chromatogram is shown in Fig. 5c, in which there is no area overlap between adjacent peaks. The chromatogram selected by the modified program shows superior resolution, despite the fact that the criterion values given above suggest that the reverse should be true.

Experimental validation of the proposed procedure

The performance of the modified software was evaluated by using a real sample mixture, comprising N-butylphenethylamine (N-BuPEA), 2,2′-diphenethylamine (di-PEA), propranolol, *p*-iodophenol (p-I-phenol), doxepin, and toluene. The optimisation search area of isoeluotropic mobile phases in which these solutes are eluted in the approximate capacity factor range $1 \leqslant k' \leqslant 10$ was found to be bounded by the binary mobile phases methanol–water (60:40), acetonitrile–water (44:56) and THF–water (42:58). Retention and peak shape data for each solute in these binary mobile phases were determined and are shown in Table III.

Optimisation without consideration of peak tailing yielded an optimal mobile phase composition of methanol–THF–water (36:17:47). The chromatogram obtained with this mobile phase is shown in Fig. 6. This separation attained a criterion value of $r = 0.84$, but it is clearly deficient in resolution between the two tailed peaks of propranolol and doxepin. The modified optimisation program was applied to the same search area and predicted the methanol–water (60:40) binary mobile phase to be optimal, giving a criterion value of $r' = 0.63$. The chromatogram obtained with this optimal mobile phase is shown in Fig. 7. It is clearly superior to the chromatogram shown in Fig. 6. This improvement is attributable partly to the exploitation of changes

TABLE III

RETENTION AND PEAK SHAPE DATA FOR TEST SOLUTES USED FOR EXPERIMENTAL VALIDATION OF THE MODIFIED OPTIMISATION PROCEDURE

Solute identities are given in the text.

Solute	*Mobile phase: methanol–acetonitrile–THF–water*					
	60:0:0:40		*0:0:42:58*		*0:44:0:56*	
	Retention time (min)	*Peak shape data (τ/σ)*	*Retention time (min)*	*Peak shape data (τ/σ)*	*Retention time (min)*	*Peak shape data (τ/σ)*
N-BuPEA	2.75	5.2	1.66	5.0	2.01	5.3
di-PEA	3.86	5.5	1.66	5.3	2.01	5.3
Propranolol	5.1	6.8	2.1	6.3	3.06	5.5
p-I-phenol	3.45	0	3.36	0	3.43	0
Doxepin	7.38	7.5	2.1	7.2	7.0	6.3
Toluene	6.46	0	5.13	0	8.15	0

in the order of elution of the solutes, particularly the tailed peak of doxepin, and is typical of case (ii) described in the previous section. Not only is the resultant chromatogram improved in terms of area overlap, but the optimal mobile phase was selected in one iteration of the optimisation procedure less than that required when peak tailing effects were not considered. It is clear that the modified program can be used successfully when tailed peaks are encountered, at the cost of some increase in computation time.

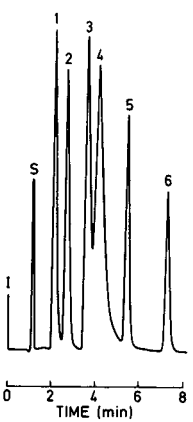

Fig. 6. Chromatogram obtained for the test mixture with the mobile phase selected by the unmodified optimisation program [*i.e.*, methanol–THF–water (36:17:47)]. The data file in Table III was used. Solute identities: 1 = N-BuPEA; 2 = diPEA; 3 = propranolol; 4 = doxepin; 5 = p-I-phenol; 6 = toluene; S = solvent peak.

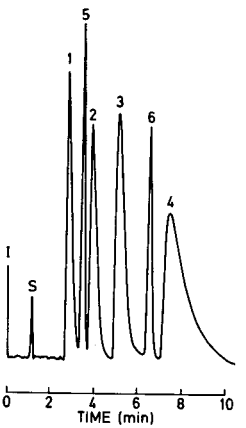

Fig. 7. Chromatogram obtained for the test mixture with the mobile phase selected by the modified optimisation program [*i.e.* methanol–water (60:40)]. The data file in Table III was used. Solute identities as for Fig. 6.

CONCLUSIONS

It has been demonstrated that when peak tailing effects are taken into consideration, better predictions of optimal mobile phase composition can be achieved. The proposed modifications are not extensive and with the aid of the coefficients listed in Table I, any existing optimisation program in which R_s values are used for the calculation of criterion values can be modified. Manual application of the techniques outlined in this paper is also possible when the calibration graph shown in Fig. 2 for conversion of $B/A_{0.1}$ values to τ to σ ratios is used, together with manual solution of the equations presented in Table I or use of the graphic relationships between R_s and percentage area overlap which we have reported previously[16].

REFERENCES

1 P. J. Schoenmakers, *Optimization of Chromatographic Selectivity (Journal of Chromatography Library*, Vol. 35), Elsevier, Amsterdam, 1986, Ch. 4.
2 R. Kaiser, *Gas-chromatographie*, Geest und Portig, Leibzig, 1960, p. 33.
3 O. E. Schupp, III, *Gas Chromatography*, Wiley, New York, 1968, p. 22.
4 A. B. Christophe, *Chromatographia*, 4 (1971) 455.
5 P. J. Schoenmakers, A. C. J. H. Drouen, H. A. H. Billiet and L. de Galan, *Chromatographia*, 15 (1982) 688.
6 A. C. J. H. Drouen, P. J. Schoenmakers, H. A. H. Billiet and L. de Galan, *Chromatographia*, 16 (1982) 48.
7 J. E. Knoll and M. R. Midgett, *J. Chromatogr. Sci.*, 20 (1982) 221.
8 H. J. G. Debets, B. L. Bajema and D. A. Doornbos, *Anal. Chim. Acta*, 151 (1983) 131.
9 J. Berridge, *J. Chromatogr.*, 244 (1982) 1.
10 P. Jones and C. A. Wellington, *J. Chromatogr.*, 213 (1981) 357.
11 J. L. Glajch, J. J. Kirkland, K. M. Squire and J. M. Minor, *J. Chromatogr.*, 199 (1980) 57.
12 P. R. Haddad, A. C. J. H. Drouen, H. A. H. Billiet and L. de Galan, *J. Chromatogr.*, 282 (1983) 71.
13 S. Sekulic, P. R. Haddad and C. J. Lamberton, *J. Chromatogr.*, 363 (1986) 125.
14 R. F. Nystron, *J. Am. Chem. Soc.*, 77 (1955) 2544.
15 A. C. J. H. Drouen, *Ph. D. Dissertation*, Technical University Delft, Delft, 1985.
16 S. Sekulic and P. R. Haddad, *J. Chromatogr.*, 459 (1988) 65.
17 *Manual for Scientific Plotter II*, Interactive Microware, Inc., Nalco Industries, Dundas, 1983.

Journal of Chromatography, 459 (1988) 91–107
Elsevier Science Publishers B.V., Amsterdam — Printed in The Netherlands

CHROMSYMP. 1487

UNIVERSAL DETECTION AND QUANTITATION OF SURFACTANTS BY HIGH-PERFORMANCE LIQUID CHROMATOGRAPHY BY MEANS OF THE EVAPORATIVE LIGHT-SCATTERING DETECTOR

G. R. BEAR*
Texaco Inc., Exploration and Production Technology Division, P.O. Box 425, Bellaire, TX 77401 (U.S.A.)

SUMMARY

The evaporative light-scattering (ELS) detector was evaluated for the quantitation of various types of surfactant. High-performance liquid chromatography techniques coupled with the ELS detector were developed for the quantitative analyses of commercially prepared ethoxylated alcohols, alkyl ether sulfates, and alkyl sulfonates, alkylbenzene sulfonates, and petroleum sulfonates. These analyses demonstrate the first direct techniques for separation and universal detection of a wide range of surfactants with a common detector. The ELS detector was ideal for the detection and quantitation of all species including those which do not contain chromophores. The detector provides an equal and linear response factor for each class of surfactant that is independent of molecular weight. The detection limits are in the low nmole range. The standard deviation of all the analyses was less than 1%.

INTRODUCTION

Surfactants are widely used for a variety of purposes including surface wetting agents, detergents, emulsifiers, lubricants, gasoline additives and enhanced oil recovery agents. The type of surfactant selected for a particular application often depends on the chemical and physical properties required and on economics or other considerations such as environmental concerns. To meet these requirements a typical surfactant formulation may contain blends of a variety of commercial products, which could include ionic and non-ionic ethoxylated surfactants, alkyl- and alkylarylsulfonates (synthetic sulfonates) and petroleum sulfonates.

Commercial surfactants contain mixtures of isomers and homologues, and may also contain variable amounts of unreacted starting material or extraneous oil that is added as a diluent or thinning agent. Variable amounts of water and inorganic salts are commonly present in these products. In order to maintain quality assurance, considerable effort must be devoted to developing reliable quantitative techniques for characterizing components present in these surfactants. Several publications and lit-

* Current address: Shell Development Co., Westhollow Research Center, P.O. Box 1380, Houston, TX 77251, U.S.A.

0021-9673/88/$03.50

erature reviews are available that describe techniques developed for surfactant analysis[1–6].

Difficulties are often encountered in many analytical methods due to the complex nature of the mixture and the lack of adequate detection capabilities, thus leading to poor quantitation techniques. For routine separation of a broad range of surfactants, high-performance liquid chromatography (HPLC) appears to be most promising[7–18]. UV and fluorescence detectors are commonly used in HPLC analysis of surfactants because of their compatibility with separation schemes requiring gradient elution. However, these detectors have two inherent limitations: (1) the detector response is dependent on molecular structure, *i.e.* the degree of aromaticity and type of substitution, and (2) only species with a chromophore can be detected. To overcome these limitations, post-column reaction detectors, based on extraction of fluorescent ion-pairs, were introduced for on-line detection of alkylsulfonates in HPLC[19–22]. However, the ion-pair formation and extraction efficiency were still dependent on the molecular structure and could not easily be used for quantitation.

Recently, the evaporative light-scattering (ELS) detector, also known as the mass detector, was introduced as a universal detector for non-volatile compounds in liquid streams[23–25]. The detector measures light refracted by the non-volatile particles after the effluent from the HPLC column is nebulized and the carrier solvent is evaporated. The amount of refracted light is proportional to the concentration of the analyte species. The ELS detector has been used to detect proteins[26], polymers[27], coal derivatives[28] and petroleum fractions[29] in HPLC separations. This paper reports the first direct techniques for separation and quantitation of surfactants by HPLC by means of the ELS detector for universal detection. The following surfactants were examined in this study: (a) non-ionic ethoxylated alcohols; (b) alkyl ether sulfates; and (c) synthetic and petroleum sulfonates.

EXPERIMENTAL

Apparatus

HPLC was performed with a Hewlett-Packard 1090 chromatograph (Hewlett-Packard, Atlanta, GA, U.S.A.) equipped with a ternary solvent delivery system, an auto-injector with a 0–25-μl injection loop, an oven compartment, and a diode-array UV detector. An ELS detector (Applied Chromatography Systems, Luton, U.K.) was connected in series to the UV detector. Signals from both detectors were processed with a VG 11-250 Multichrom chromatography data system (VG Instruments, Manchester, U.K.).

Reagents

All solvents were of HPLC-reagent grade (Burdick & Jackson Labs., Muskegon, MI, U.S.A.) and were filtered through a 0.45-μm glass fiber filter (Gelman Sciences, Ann Arbor, MI, U.S.A.). Hexane, 2-propanol and water were used for the analysis of non ionic ethoxylated surfactants. Water and tetrahydrofuran (THF) were used for the analysis of anionic surfactants.

Samples

All commercial surfactants used in this study are listed in Table I. No prelimi-

TABLE I

MODEL SURFACTANTS

Surfactant	*Abbreviation*
Nonylphenolethoxyalcohol	
$C_9H_{19}PhO(CH_2\ CH_2O)_{11}H$	NP11
Alkylethoxyalcohols	
$C_{12}H_{25}$–$C_{14}\ H_{29}O(CH_2CH_2O)_5H$	AE5
$C_{12}H_{25}$–$C_{14}\ H_{29}O(CH_2CH_2O)_7H$	AE7
$C_{12}H_{25}$–$C_{14}\ H_{29}O(CH_2CH_2O)_{11}H$	AE11
$C_{12}H_{25}O(CH_2\ CH_2O)_{12}H$	AE12
$C_{13}H_{27}O(CH_2\ CH_2O)_7H$	b-AE7
$C_{13}H_{27}O(CH_2\ CH_2O)_{11}H$	b-AE11
Alkyl ether sulfates	
$C_{12}H_{25}(CH_2\ CH_2O)_6OSO_3Na$	LN-60COS
$C_{12}H_{25}(CH_2\ CH_2O)_8OSO_3Na$	LN-80COS
$C_{12}H_{25}(CH_2\ CH_2O)_{12}OSO_3Na$	LN-120COS
$C_4H_9(C_4H_8O)\ _6(C_2H_4O)_2OSO\ _3Na$	BU-6B2ECOS
$C_4H_9(C_4H_8O)\ _6(C_2H_4O)_7OSO\ _3Na$	BU-6B7ECOS
Alkylsulfonate	
$C_{12}H_{25}SO_3Na$	1-C12
Alkylbenzenesulfonates	
$C_{12}H_{25}PhSO_3Na$	b-PhC12
$C_{16}H_{33}PhSO_3Na$	b-PhC16
Alkylarylsulfonates	
Sodium petroleum sulfonate 1	NaPS-1
Sodium petroleum sulfonate 2	NaPS-2
Calcium petroleum sulfonate 1	CaPS-1
Calcium petroleum sulfonate 2	CaPS-2
Calcium petroleum sulfonate 3	CaPS-3
Calcium petroleum sulfonate 4	CaPS-4

nary sample preparation was needed other than dilution. The non-ionic ethoxylated surfactants were diluted 1:40 (v/v) with hexane. The anionic surfactants (alkyl ether sulfates and synthetic and petroleum sulfonates) were diluted 1:20 (v/v) with water–THF (50:50). The calcium sulfonate surfactants were diluted 1:20 (v/v) with a THF–38% hydrochloric acid solution of pH *ca.* 1. Hydrochloric acid (reagent grade) was required to prevent salt precipitation by converting any excess water-insoluble calcium carbonate into water-soluble calcium chloride. All diluted samples were filtered through a 0.2-μm filter (Gelman Acrodisc CR) directly into the injector vials.

Chromatographic procedures

The non-ionic ethoxylates were separated according to the number of ethylene oxide (EO) groups (n) using normal-phase chromatography. The separation was achieved on an amino column (DuPont Zorbax NH_2, 25 cm × 4.6 cm I.D., 5 μm particle size). A precolumn (Zorbax BP NH_2, 2.5 cm × 0.2 cm I.D.) was connected to

TABLE II

GRADIENT ELUTION PROGRAM FOR NORMAL-PHASE HPLC OF NON-IONIC ETHOXYLATED SURFACTANTS

Time (min)	*Hexane (%)*	*2-Propanol (%)*	*Water (%)*
0	100	0	0
55	37	60	3

the amino column. The solvent system was a gradient of hexane, 2-propanol and water. The 55-min gradient program is summarized in Table II.

Components of the alkyl ether sulfate surfactants were separated into inorganic salt, sulfates and unreacted alchohol using a rapid reversed-phase chromatography. The column used for this separation was a 2.5 cm × 0.2 cm I.D. column packed with 10-μm C_{18}. The solvent system was a 4-min gradient program of water and THF, which is summarized in Table III. The synthetic and petroleum sulfonate components were separated into inorganic salt, sulfonates and unreacted oil by the same reversed-phase chromatographic method.

In all analyses the flow-rate was 1 ml/min and the column compartment was kept at 40°C.

Detection

The diode-array UV and ELS detectors were connected in series. The UV signals were monitored at 230 and 254 nm. The operating conditions of the ELS detector were optimized for maximum detector response and stable baseline. Surfactants with UV absorbance were detected by both detectors, while the UV-transparent surfactants could only be detected by the ELS detector.

The two basic parameters available for optimization of the ELS detector output are the nebulizer gas nitrogen flow-rate and the evaporator tube temperature. During normal-phase chromatography of non-ionic ethoxylates, the nitrogen pressure was 45 p.s.i. and the evaporator tube temperature was *ca.* 35°C. For the reversed-phase chromatography of alkyl ether sulfates and sulfonate surfactants, the nitrogen pressure was 20 p.s.i. and the evaporator tube temperature was *ca.* 50°C.

TABLE III

GRADIENT ELUTION PROGRAM FOR REVERSED-PHASE HPLC OF ALKYL ETHER SULFATE AND SYNTHETIC AND PETROLEUM SULFONATE SURFACTANTS

Time (min)	*Water (%)*	*THF (%)*	*Mode of operation*
0.0	90	10	Normal flow
0.5	90	10	Normal flow
1.0	40	60	Normal flow
2.5	40	60	Normal flow
2.6	0	100	Backflush
4.0	90	10	Backflush

RESULTS AND DISCUSSION

The ELS detector

In the ELS detector operation, the eluent from HPLC column is introduced into the top of a heated evaporator tube where it is nebulized by a stream of nitrogen. Droplets formed at the nebulizer pass through the heated tube. The solvent is vaporized and an aerosol is formed from the non-volatile solute particles contained in the eluent. The particles pass through a light path and the light scattered is detected at a fixed angle. The amount of scattered light is proportional to concentration.

The detector has many desirable features. It is inexpensive, stable and easy to operate. Most important, the detector is not subject to solvent interference and is insensitive to the chemical composition of detected species. The characteristics of the ELS detector in terms of nebulization and light-scattering theories have been studied in detail[25]. It has been shown that detector linearity and detection limits are directly related to the size, shape and number of particles formed in the evaporator tube. Under fixed nebulization and evaporation conditions, the detector response is dependent on the density and refractive index of the aerosol particles. For samples with similar densities and refractive indexes, the response is proportional to the mass of material present in each sample and independent of molecular weight. These characteristics allowed the ELS detector to be used as a universal detector for surfactants.

Analysis of non-ionic ethoxylates

Aliphatic and aromatic non-ionic ethoxylated surfactants, $RO(CH_2CH_2O)_nH$, were analyzed to determine the distribution of the ethoxylate oligomers. Oligomers with different numbers of EO groups were separated by normal-phase HPLC method as summarized in Table II. The separated components were monitored by both the ELS and UV detectors. Signals obtained by both detectors were compared, and normalized peak areas were used to calculate the percent composition of each oligomer.

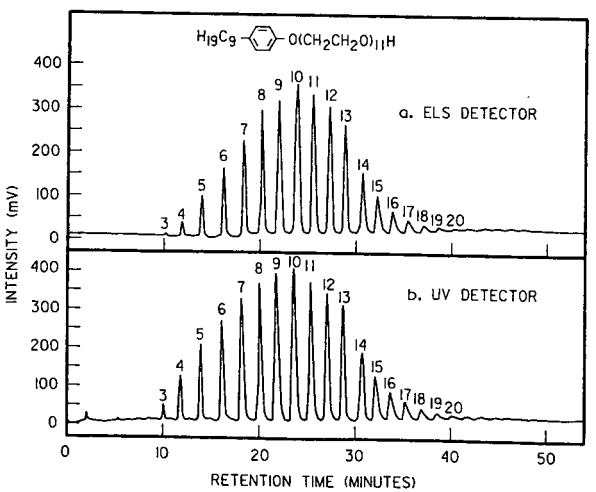

Fig. 1. HPLC analysis of nonylphenolethoxyalcohol oligomers: (a) ELS detector; (b) UV detector.

TABLE IV

QUANTITATIVE ANALYSIS OF NP11 OLIGOMERS WITH THE UV AND ELS DETECTORS

Number of EO groups, n	*Composition (%)*	
	UV	*ELS*
3	0.83	0.01
4	2.30	0.71
5	4.16	2.16
6	6.24	4.25
7	8.54	7.27
8	10.51	10.65
9	11.76	12.78
10	11.91	13.72
11	11.05	13.07
12	9.46	11.30
13	7.66	8.95
14	5.84	6.19
15	4.02	3.92
16	2.60	2.39
17	1.60	1.38
18	0.95	0.80
19	0.56	0.40

An example is shown in Fig. 1. The figure shows the high resolution of components in a nonylphenolethoxyalcohol, NP11, revealing a range of oligomers from n = 3 to 20. Quantitation of NP11 oligomers from these data is shown in Table IV. Comparison of signals obtained by both detectors (Fig. 1a and b) shows that the sensitivity of the ELS detector is comparable to that of a UV detector. Although the distribution profiles obtained by both detectors appeared similar, careful examination of the figures shows that the UV detector gives a higher response for lower-molecular-weight components, *i.e.* for components with $n \leqslant 7$. As shown in Table IV, the difference between the UV and the ELS response is large for $n = 3$, but decreases as n increases. This is due to the change in UV absorbance as a function of molecular structure. At the monitored wavelength (230 nm), the shorter the EO chain, the higher the absorbance[13]. As shown below, the ELS detector was found to provide a uniform linear response for ethoxylates, independent of n.

An especially important feature of the ELS detector was that it could be used for the detection and quantitation of ethoxylates not amenable to UV detection. Fig. 2 shows the distribution profiles of linear alkylethoxyalcohols AE5, AE7, and AE11. The general formula for these alcohol surfactants is $RO(CH_2CH_2O)_nH$, where R is $C_{12}H_{25}$ or $C_{14}H_{29}$ and the average value for n (mean, or $\bar{n}$) is 5 for AE5, 7 for AE7 and 11 for AE11. Using this technique it was possible to separate components of each product according to n. For example, in Fig. 2a, the AE5 components are separated into groups according to n, 1–10. Within each group, components are further separated according to the length of the alkyl chain, *i.e.* C_{12} and C_{14}. A similar separation is shown in Fig. 2b for AE7 and in Fig. 2c for AE11, where the n distribution ranged from 3–11 and 6–16, respectively.

Fig. 3 shows the distribution profiles obtained for the branched alkylethoxyal-

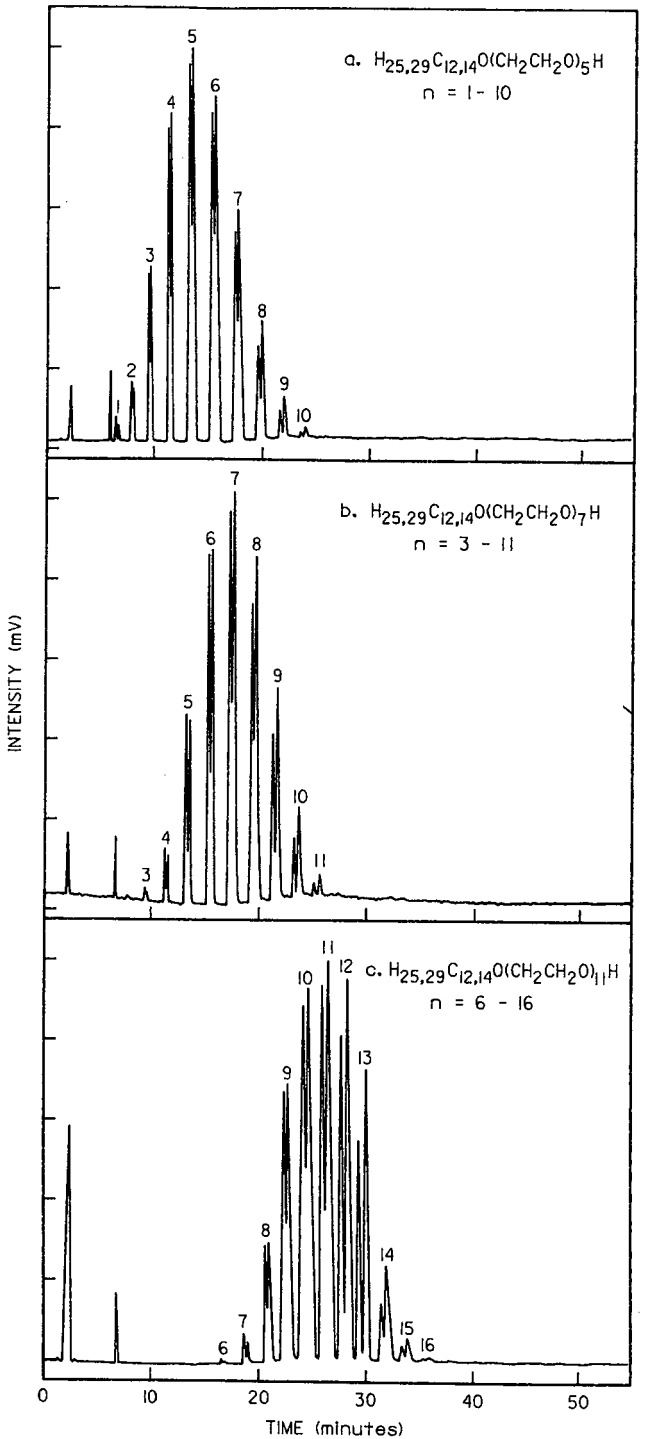

Fig. 2. HPLC analysis of linear alkylethoxyalcohol oligomers: (a) AE5; (b) AE7; (c) AE11.

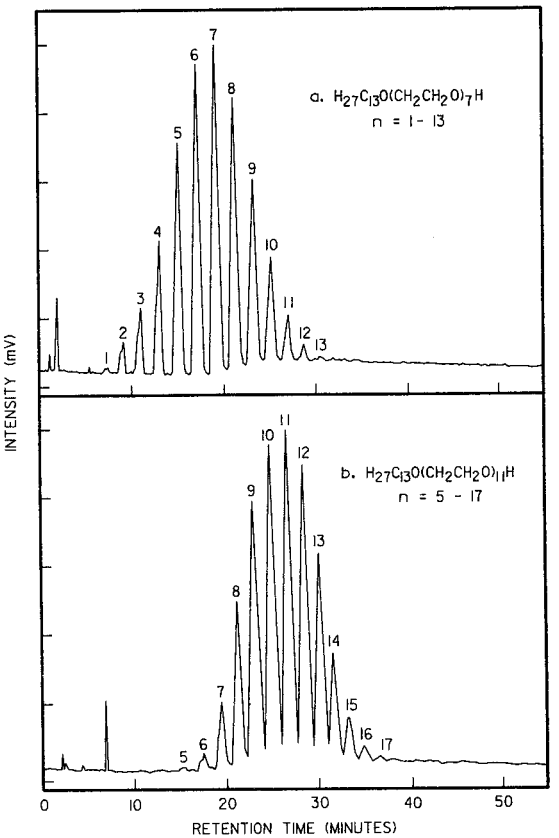

Fig. 3. HPLC analysis of branched alkylethoxyalcohol oligomers: (a) b-AE7; (b) b-AE11.

TABLE V

COMPARISON OF RESULTS OBTAINED BY THE HPLC–ELS METHOD WITH THE MANUFACTURER'S SPECIFICATIONS FOR THE QUANTITATIVE ANALYSIS OF AE11 OLIGOMERS

Number of EO groups, n	*Composition (%)*	
	Manufact. spec.	*ELS detector*
7	1.8	0.8
8	5.0	5.1
9	11.5	12.9
10	19.1	20.0
11	22.4	22.5
12	19.3	19.2
13	12.5	12.5
14	6.2	5.7
15	2.1	1.3

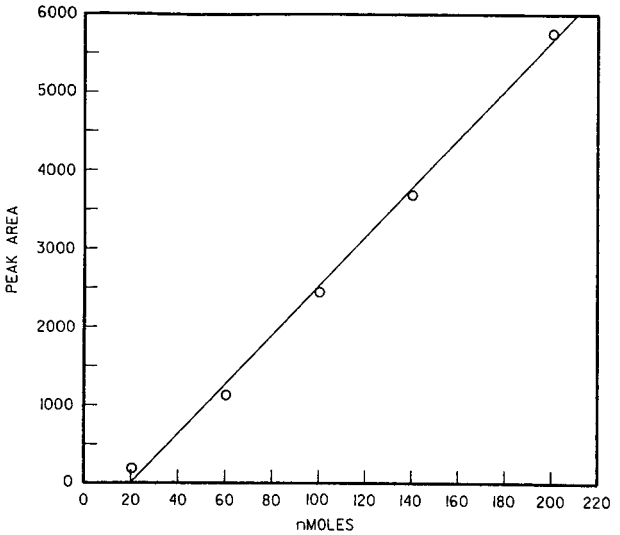

Fig. 4. Calibration curve of alkylethoxyalcohol surfactant, $C_{12}H_{25}O(CH_2CH_2O)_8H$.

cohols $C_{13}H_{27}O(CH_2CH_2O)_nH$, b-AE7 and b-AE11. The EO distribution is shown to be between 1 and 13 with $n = 7$ for b-AE7, and between 5 and 17 with $n = 11$ for b-AE11. In comparison with the linear ethoxylated alcohols shown in Fig. 2, the retention times were longer and peaks were broader due to the alkyl chain branching.

The percent composition of ethoxylate oligomers obtained with the ELS detector was verified by comparison with product specifications derived from flame ionization detection (FID). An example is shown in Table V for AE11. A similar comparison was obtained for other ethoxylated surfactants indicating close agreement between data obtained with the two detectors. The data illustrate that the ELS detector responds uniformly to these surfactants and is independent of the EO chain length. It also demonstrates the high accuracy of the HPLC–ELS method for quantitating ethoxylated oligomers. In these examples the standard deviation of the HPLC–ELS method was less than 1%.

The linearity and limit of detection of the ELS detector were determined with the ethoxyalcohol $C_{12}H_{25}O(CH_2CH_2O)_8H$. The calibration curve was linear over the concentration range shown in Fig. 4. The detection limit was found to be 20 nmol.

Analysis of alkyl ether sulfates

Anionic alkyl ether sulfate surfactants are produced by sulfating non-ionic alcohol polyalkyloxylates such as the ethoxylated surfactants discussed above. The sulfated products generally contain variable amounts of unconverted alcohols and even inorganic salts as reaction byproducts. Determination of the ratio of anionic to non-ionic components in surfactant mixtures is frequently desired for quality control and performance evaluation.

An HPLC–ELS method was developed to quantitate the ionic alkyl ether sulfates and unconverted non-ionic alcohol components present in the product mixtures. Separation of the ionic sulfate and non-ionic alcohol components was achieved by the reversed-phase chromatographic method summarized in Table III. This method com-

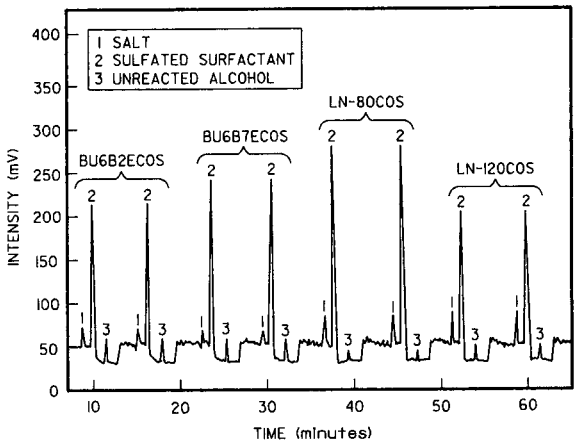

Fig. 5. HPLC analysis of (1) inorganic salt, (2) sulfated surfactant, and (3) unreacted alcohol in alkyl ether sulfate surfactants.

bined with ELS detection provided a fast and accurate technique for on-line separation and quantitation of the ionic and non-ionic alkyloxylate surfactant species.

Analysis of four alkyl ether sulfate surfactants is shown in Fig. 5. This figure shows the separation of each sample into three components, using two injections per sample. The first component is inorganic salt eluted with 90% water and 10% THF (Peak 1). As the THF concentration increases to 60%, the ionic sulfate surfactant components are eluted (Peak 2). After elution of these ionics, the non-ionic components are backflushed with 100% THF (Peak 3). All peaks are sharp and well resolved. The analysis time is 4 min per sample.

The ELS detector response was slightly higher for the non-ionic than for the ionic components. Fig. 6 shows the calibration curves obtained for the linear alkylethoxysulfate standard LN-80COS and the corresponding alkylethoxyalcohol LN-80. Both curves are linear with detection limits of *ca.* 20 nmol for the ionics and

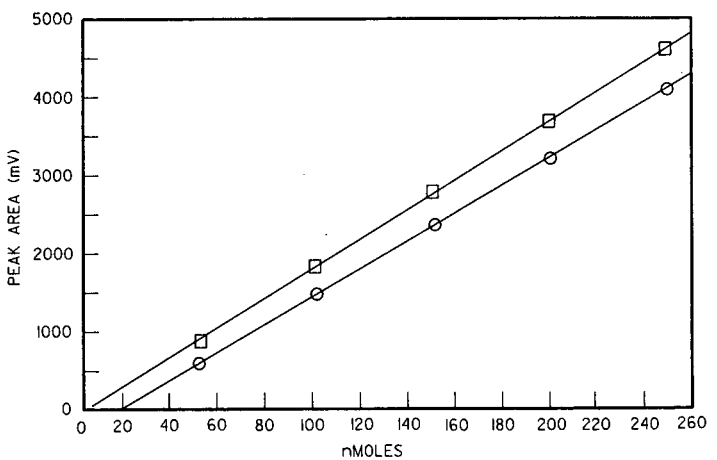

Fig. 6. Calibration curves of alkylethoxysulfate, LN-80COS (○) and alkylethoxyalcohol, LN-80 (□).

ca. 5 nmol for the non-ionics. Similar to the non-ionic ethoxylated surfactants discussed above, the detector response for the ionics was independent of the alkyl and ethoxy or butoxy chain lengths. The concentrations of ionic sulfates and non-ionic alcohols in the mixtures can be calculated directly from peak areas and the calibration curves.

Table VI lists the concentrations of alkyl ether sulfate samples obtained by HPLC–ELS and the standard mixed-indicator two-phase titration methods[30]. A comparison of the results shows good agreement between the two methods except for the highly water-soluble surfactants, BU-6B7ECOS and LN-120COS. The lower concentrations reported by the two-phase titration can be attributed to incomplete titration of these highly water soluble surfactants[30], a limitation of the titration method. Therefore, concentrations calculated from the ELS detector response for BU-6B7ECOS and LN-120COS are believed to be more accurate.

TABLE VI

QUANTITATION OF IONIC ALKYL ETHER SULFATE SURFACTANTS BY THE HPLC–ELS AND TWO-PHASE TITRATION METHODS

Surfactant	*Two-phase titration (mmol)*	*ELS detector (mmol)*
LN-60COS	9.9	10.0
LN-80COS	9.6	9.1
LN-120COS	7.1	8.6
BU-6B2ECOS	7.3	7.5
BU-6B7ECOS	6.6	8.0

Analysis of synthetic and petroleum sulfonates

Synthetic and petroleum sulfonates were analysed by the reversed-phase chromatographic procedure established for the analysis of alkyl ether sulfate surfactants (Table III). Similar to alkyl ether sulfates, the sulfonate mixtures were separated into three fractions: (1) inorganic salt; (2) sulfonates; and (3) unreacted oil. The ELS detector was used for the detection of the separated fractions and for the quantitation of sulfonates. The results were compared with those obtained by the standard titration methods[30,31].

Results from the HPLC–ELS analysis of a linear sodium alkylsulfonate standard, $C_{12}H_{25}SO_3Na$, are shown in Fig. 7. The response shown in Fig. 7 resulted from various injection volumes of 0.017 *M* C_{12} alkylsulfonate solution, *i.e.* 25 to 2 μl. The analyses of two branched sodium alkylbenzenesulfonate standards, $C_{12}H_{25}PhSO_3Na$ and $C_{16}H_{33}PhSO_3Na$, are shown in Fig. 8. The alkylbenzenesulfonate standards were at concentrations of 0.01 *M*, and the injection volumes ranged from 25 to 4μl. As shown in the chromatograms, all standard solutions contained only sulfonate; no salt or oil was present.

Fig. 9 shows the linear calibration curve obtained for alkylsulfonate and alkylbenzenesulfonate standards. As shown, the sulfonate detection limit is *ca.* 25 nmol and the ELS detector response factor is essentially the same for all the three sulfonate

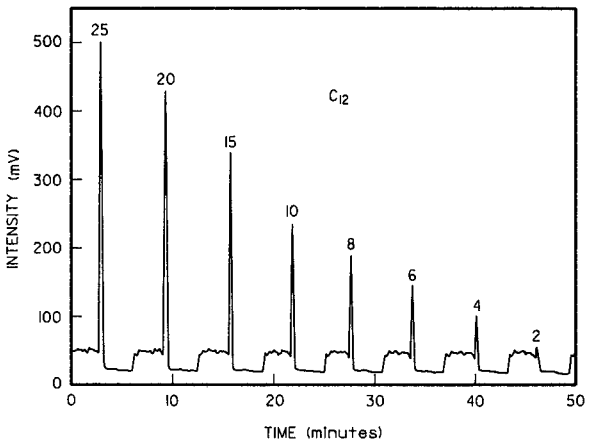

Fig. 7. ELS detector response to injections of 25–2 μl of 0.017 *M* linear sodium alkylsulfonate $C_{12}H_{25}SO_3Na$.

standards. Thus, the response is the same for both aliphatic and aromatic sulfonates and independent of the alkyl chain length.

The analyses of two petroleum sulfonates, NaPS-1 and NaPS-2, are shown in Fig. 10. The response to five injection volumes ranging from 25 to 5 μl for each surfactant is shown. Good separation was achieved between the inorganic salt and the sulfonated components. The oil present in NaPS-1 and NaPS-2 surfactants consisted of low-molecular-weight components, which were totally volatile under the detector operating conditions and, therefore, could not be detected. These two sulfonates are considerably different in molecular structure distribution. Nevertheless, their elution characteristics were the same as those observed for the synthetic single

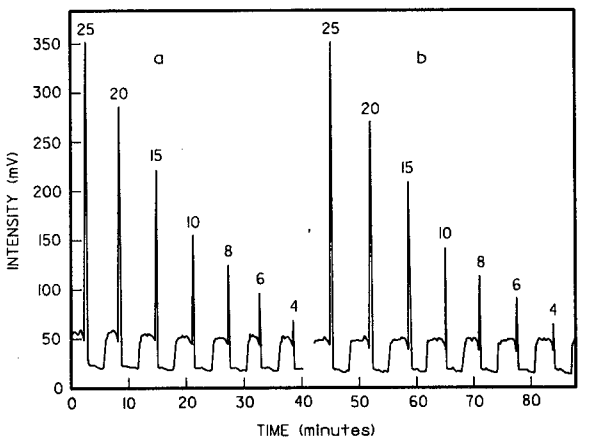

Fig. 8. ELS detector response to injections of 25–4 μl 0.01 *M* branched sodium alkylbenzenesulfonates: (a) $C_{12}H_{25}PhSO_3Na$; (b) $C_{16}H_{33}PhSO_3Na$; (Ph = C_6H_4).

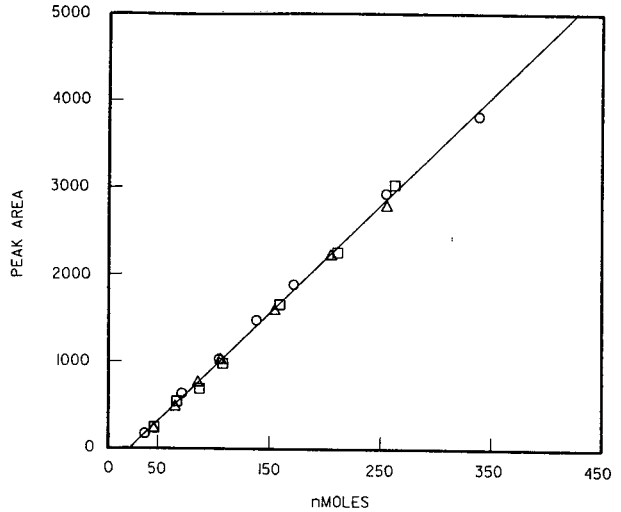

Fig. 9. Calibration curve of synthetic sulfonates, $C_{12}H_{25}SO_3Na$ (○); $C_{12}H_{25}PhSO_3Na$ (△); and $C_{16}H_{33}PhSO_3Na$ (□); (Ph = C_6H_4).

component sulfonates, *i.e.* a single, narrow, well defined peak for the sulfonate constituents. Fig. 11 shows the calibration curve obtained for both NaPS-1 and NaPS-2. This curve is the same as that obtained for C_{12} alkyl sulfonates. Therefore, the ELS detector response was the same for both synthetic and petroleum sulfonates and independent of molecular weight.

The concentrations of synthetic and petroleum sulfonates were calculated directly from peak areas using the sulfonate calibration curve shown in Fig. 9. Table VII summarizes the quantitative results calculated from the ELS detector response

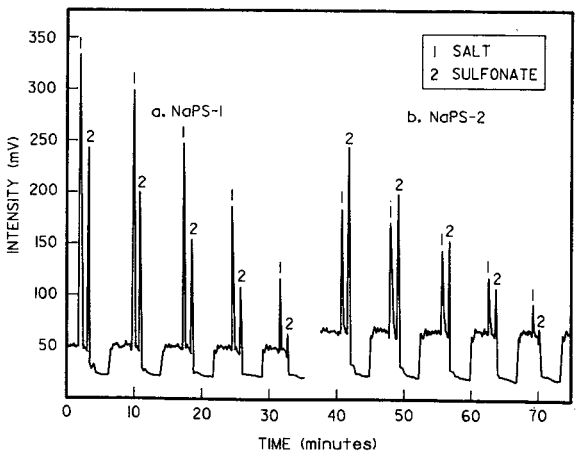

Fig. 10. HPLC analysis of (1) inorganic salt and (2) sulfonates present in sodium petroleum sulfonates: (a) NaPS-1; (b) NaPS-2. Injection volumes: 25, 20, 15, 10 and 5 μl of each.

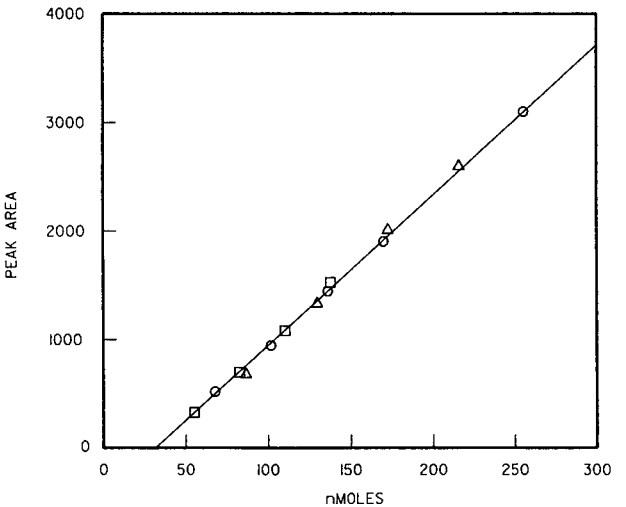

Fig. 11. Calibration curve of synthetic sulfonate $C_{12}H_{25}SO_3Na$ (○) and petroleum sulfonates NaPS-1 (△) and NaPS-2 (□).

TABLE VII

QUANTITATION OF SYNTHETIC AND PETROLEUM SULFONATES BY THE HPLC–ELS AND TWO-PHASE TITRATION METHODS

Surfactant	*Two-phase titration (mmol)*	*ELS detector (mmol)*
1-C_{12}	16.9	17.0
b-PhC_{12}	10.2	10.0
b-PhC_{16}	10.5	10.7
NaPS-1	8.5	8.6
NaPS-2	5.8	5.5

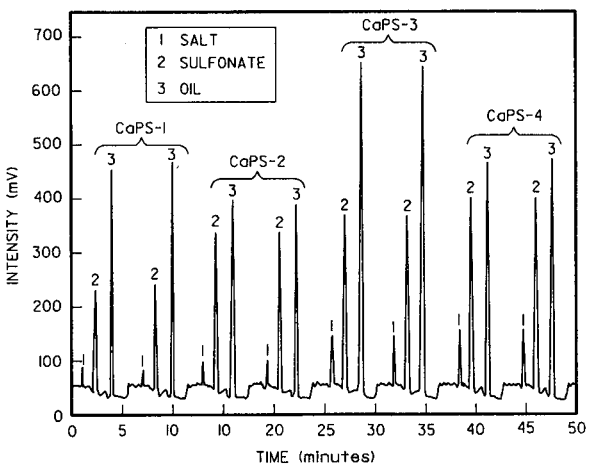

Fig. 12. HPLC analysis of (1) inorganic salt, (2) sulfonates, and (3) oil present in calcium petroleum sulfonates CaPS-1, CaPS-2, CaPS-3 and CaPS-4.

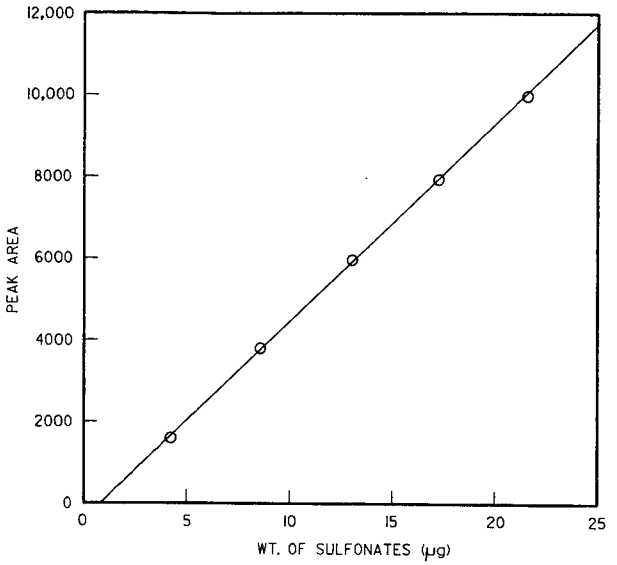

Fig. 13. Calibration curve of calcium petroleum sulfonate CaPS-1.

and those obtained by the two-phase titration method. Excellent agreement was found between results from the two methods (correlation coefficient = 0.9999). This agreement demonstrates the high accuracy of the HPLC–ELS method.

The analyses of four calcium petroleum sulfonate surfactants, CaPS-1, CaPS-2, CaPS-3, and CaPS-4, which are used as lubricating oil additives, are presented in Fig. 12. As shown, the surfactant components are separated into inorganic salt, sulfonated species, and unreacted oil. A baseline separation was obtained for all components and the repeatability was excellent.

The ELS detector response factor was found to be higher for these calcium-based surfactants than for the sodium sulfonates. This is not surprising in view of the structural differences between these two types of surfactant. Calcium-based sulfonates contain two sulfonate moieties per molecule in contrast to only one as in the sodium based compounds. Clearly, this difference in structure affects the properties of

TABLE VIII

QUANTITATION OF CALCIUM PETROLEUM SULFONATE SURFACTANTS BY THE HPLC–ELS AND METHYLENE BLUE TITRATION METHODS

Surfactant	*Activity (%)*	
	MB titration	*ELS detector*
CaPS-1	45.3	45.3
CaPS-2	44.9	45.6
CaPS-3	19.3	18.5
CaPS-4	30.9	30.6

the aerosol particles, *i.e.* size, shape, and number of particles formed in the evaporator tube, resulting in a higher response factor for the calcium-based class of surfactants. Fig. 13 shows the relationship between the injected quantity of CaPS-1 sulfonate and peak area. The response is linear with a detection limit of *ca.* 1 μg and a standard deviation of less than 1%.

The sulfonate peak areas and the calibration curve shown in Fig. 13 were used to calculate the percent activity (sulfonate weight percent) of each surfactant mixture. The calcium petroleum sulfonate activities obtained in this manner are listed in Table VIII, along with the activities obtained by the standard methylene blue titration[31]. Again, the comparison of the two techniques demonstrated a uniform response for the ELS detector and the high accuracy of the HPLC–ELS method.

For all analyses of the sodium and calcium synthetic and for the petroleum sulfonates presented here the standard deviation of the HPLC–ELS method was less than 1%. A correlation coefficient greater than 0.999 was found in comparison with the standard titration methods.

CONCLUSIONS

Examination of a wide range of non-ionic and anionic ethoxylated surfactants, $RO(CH_2CH_2O)_nH$ and $R(CH_2CH_2O)_nOSO_3Na$, where R ranged from C_6 to C_{14} alkyl or alkylbenzene and n varied from 1 to 20, showed no measurable change in detector response with the change in molecular weight. The ELS detector also exhibited an equal response factor for both synthetic and petroleum sulfonates, *i.e.* alkyl-, alkylbenzene- and alkylarylpetroleum sulfonates, that was independent of the alkyl chain length and the degree of aromaticity. The detector provided a uniform linear response for each class of surfactant, with detection limits in the low nmole range.

The HPLC procedures presented here provide effective separation and quantitation of components in commercial surfactant products. In comparison with conventional assays of surfactant activity, HPLC–ELS methods are simple, rapid, accurate, reproducible, and free from interferences.

ACKNOWLEDGEMENTS

The author thanks Texaco Inc. for permission to publish this paper. Also special acknowledgement goes to Drs. J. B. Allison and S. R. Missler for reviewing the manuscript.

REFERENCES

1 D. Hummel, *Identification and Analysis of Surface-Active Agents*, Interscience, New York, 1962.
2 M. J. Rosen and H. A. Goldsmith, *Systematic Analysis of Surface Active Agents*, Wiley-Interscience, New York, 1972.
3 G. F. Longman, *The Analysis of Detergents and Detergent Products*, Wiley, New York, 1976.
4 M. Kuo and H.A. Mottola, *CRC Crit. Rev. Anal. Chem.*, 9 (1980) 297.
5 R. A. Llenado and R. A. Jamieson, *Anal. Chem.*, 53 (1981) 174R.
6 R. A. Llenado and T. A. Neubecker, *Anal. Chem.*, 55 (1983) 93R.
7 P. Jandera and J. Churáček, *J. Chromatogr.*, 197 (1980) 181.
8 A. Nakae, K. Tsuji and M. Yamanaka, *Anal. Chem.*, 53 (1981) 1818.
9 G. R. Bear, C. W. Lawley and R. M. Riddle, *J. Chromatogr.*, 302 (1984) 65.

10 M. Ahel and W. Giger, *Anal. Chem.*, 57 (1985) 2584.
11 K. Levsen, W. Wagner-Redeker, K. H. Schäfer and P. Dobberstein, *J. Chromatogr.*, 323 (1985) 135.
12 I. Zeman, *J. Chromatogr.*, 363 (1986) 223.
13 M. S. Holt, E.H. McKerrell, J. Perry, and R. J. Watkinson, *J. Chromatogr.*, 362 (1986) 419.
14 G. R. Bear, *J. Chromatogr.*, 371 (1986) 387.
15 A. Marcomini, S. Capri and W. Giger, *J. Chromatogr.*, 403 (1987) 243.
16 A. Marcomini and W. Giger, *Anal. Chem.*, 59 (1987) 1709.
17 J. A. Pilc and P. A. Sermon, *J. Chromatogr.*, 398 (1987) 375.
18 R. H. Schreuder and A. Martijn, *J. Chromatogr.*, 435 (1988) 73.
19 J. F. Lawrence, U. A. Th. Brinkman and R. W. Frei, *J. Chromatogr.*, 185 (1979) 473.
20 W. M. A. Niessen, J. F. Lawrence, C. E. Werkhoven-Goewie, U. A. Th. Brinkman and R. W. Frei, *Int. J. Environ. Anal. Chem.*, 9 (1981) 45.
21 F. Smedes, J. C. Kraak, C. F. Werkhoven-Goewie, U. A. Th. Brinkman and R. W. Frei, *J. Chromatogr.*, 247 (1982) 123.
22 Y. Hirai and K. Tomokumi, *Anal. Chim. Acta*, 167 (1985) 409.
23 D. L. Ford, W. Kennard, *J. Oil Colour Chem. Assoc.*, 49 (1966) 299.
24 J. M. Charlesworth, *Anal. Chem.*, 50 (1978) 1414.
25 T. H. Morey and L. E. Oppenheimer, *Anal. Chem.*, 56 (1984) 2427.
26 W. W. Christie, *J. Chromatogr.*, 361 (1986) 396.
27 T. H. Mourey, *J. Chromatogr.*, 357 (1986) 101.
28 K. D. Bartle, M. J. Mulligan, N. Taylor, T. G. Martin and C. E. Snape, *Fuel*, 63 (1984) 1556.
29 S. Coulombe, *J. Chromatogr. Sci.*, 26 (1988) 1.
30 V. W. Reid, G. F. Longman and E. Heinerth, *Tenside*, 4 (1967) 292.
31 *1987 Annual Book of ASTM Standards*, Vol. 15.04, American Society for Testing and Materials, Philadelphia, PA, 1987, method ASTM D 1681-83.

Journal of Chromatography, 459 (1988) 109–118
Elsevier Science Publishers B.V., Amsterdam — Printed in The Netherlands

CHROMSYMP. 1469

ENHANCED PERFORMANCE OF A LASER-INDUCED FLUORESCENCE LIQUID CHROMATOGRAPHIC APPARATUS: A SYSTEMS APPROACH

THOMAS J. EDKINS and DENNIS C. SHELLY*
Department of Chemistry and Chemical Engineering, Stevens Institute of Technology, Hoboken, NJ 07030 (U.S.A.)

SUMMARY

A laser-induced fluorescence liquid chromatographic apparatus has been developed, using a systems approach, resulting in enhanced overall performance. Supporting evidence will be shown concerning four factors that impact most on these types of systems: (1) increasing sample introduction efficiency; (2) achieving high chromatographic efficiency; (3) maintaining maximum illumination efficiency; and (4) obtaining the greatest possible detectivity. Specific examples include a continuously purged injection valve, columns packed with constant-packing-rate conditions, efficient optical imaging using lightguide technology and photon counting detection electronics.

INTRODUCTION

The use of laser-induced fluorescence as a detection scheme for liquid chromatography (LC) is well documented[1]. Lasers are ideal for fluorescence detection because of the well known direct proportionality between the intensities of the source and resulting fluorescent signal[2]. Other advantages of lasers include high photon flux, beam collimation and monochromaticity; the last two combine to permit the beam to be focused to a very small spot[3]. This last point is very important when considering microcolumn LC, which requires a very small flow-cell volume for optimum analytical utility.

Microcolumn LC has been developed into a highly efficient analytical technique for many separations, as illustrated in a recent review[4]. Several papers [5–7] describe the combination of microcolumns, which provide significant solute concentration enhancement, with laser-induced fluorescence, which is a highly selective and sensitive detection technique. Most of these applications are characterized by the use of expensive, high power lasers, sophisticated optics, and complicated detection/signal processing electronics. Nonetheless, minimum detectable amounts in the 10^{-18}–10^{-15} g range have been reported.

Optical interferences may be regarded as fundamental barriers to improved sensitivity in these systems. Generally, two types of interferences are seen, scattered or reflected laser light (Rayleigh scattering) and background luminescence (Raman scat-

tering and ubiquitous molecular fluorescence). Rayleigh scattering can often be rejected through the use of optical filters; but Raman bands from the solvent (or the optics) are more difficult to reduce, particularly when the scattering overlaps the emission band of the analyte[2]. After achieving the required wavelength selectivity in the emission signal (often resulting in diminished signal strength), one approach to improving detectivity is the use of a signal-to-noise (S/N) enhancement technique, such as lock-in amplification[6] or photon counting[8].

Our work will focus on improving detectability while still maintaining a very modest cost (under $10 000) for the laser, optics and all electronics (*i.e.* the detection system). We will meet this goal through improvements in injection efficiency, an improved column packing technique, employment of lightguide technologies and effective use of a novel photon counting circuit. These efforts have resulted in a very efficient LC measurement system.

EXPERIMENTAL

Sampling/injection system

The injection system consisted of an electronically actuated Valco CI4W valve, with a 60-nl internal loop (Houston, TX, U.S.A.). A constant purge device was developed, in-house, to reduce chemical contamination of the sample loop. This unit,

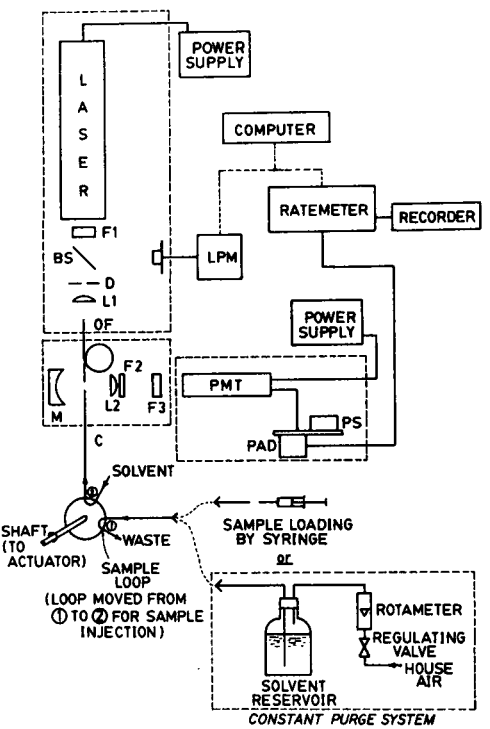

Fig. 1. Schematic diagram of the injection, separation and detection systems: F1 = liquid filter; BS = beamsplitter; D = diaphragm; L1 = planoconvex lens; OF = optical fiber; M = mirror; C = column; L2 = planoconvex lens; F2 = blocking (cut-in) filter; F3 = liquid filter; PMT = phtomultiplier tube; PAD = preamplifier/discriminator; PS = power supply; LPM = laser power meter.

displayed at the bottom of Fig. 1, was based on a compressed-air-driven gas displacement pump design. A bottle of solvent [tetrahydrofuran (THF)] was connected to the injection valve with a length of 250 μm I.D. fused-silica tubing (Polymicro Technologies, Phoenix, AZ, U.S.A.), with a small gauge (22S) needle cemented at the valve end. This needle was only removed from the valve when making an injection, hence continuous washing of the loop was provided.

Chromatographic system

The construction of the microcolumns, as well as the details of the packing study, have been described in a previous study[9]. All columns were packed and evaluated on an ISCO μLC-500 pump (Lincoln, NE, U.S.A.) using either 3-μm ODS Shandon Hypersil (Keystone Scientific, State College, PA, U.S.A.) or 5-μm Spherisorb S50DS2 (Alltech Assoc., Waukegan, IL, U.S.A.). For the test mixture and for the polynuclear aromatic hydrocarbon (PAH) mixture, we used a 750-mm fused-silica column (0.25 mm I.D.) packed with 5-μm Spherisorb.

Perylene was chosen as the standard for experiments at 442 nm, while pyrene was used at 325 nm. These standards, as well as a sixteen-component PAH mixture, were analytical grade and were purchased from Chem Service (West Chester, PA, U.S.A.). All solvents for the mobile phase were HPLC-grade and were obtained from Burdick & Jackson (Muskegon, MI, U.S.A.).

The flow-cell was a *ca.* 1-mm section of the column end connection, and was formed by acid etching of the polyimide coating with hot, concentrated sulphuric acid. This length restricts the flow-cell volume to only 75 nl, minimizing extra-column effects. The end connection was positioned inside a 0.0625-in. O.D aperture tube and was fastened inside a brass flow-cell body. The entire assembly was mounted in a Physitec (Norfolk, MA, U.S.A.) adapter plate/microbench.

Excitation and detection system

The excitation and detection system, as seen in Fig. 1, consists of six major components: (1) excitation source; (2) excitation optics; (3) emission optics; (4) detector and photon counting electronics; (5) ratemeter; and (6) recorder or computer.

A Liconix (Sunnyvale, CA, U.S.A.) 4210 NB helium–cadmium laser provided the incident radiation, and generated output powers of *ca.* 2.5 mW at 325 nm (beam diameter 1.1 mm, TEM_{01}) and *ca.* 15 mW at 442 nm (beam diameter 1.1 mm, TEM_{00}). The laser light was then transmitted through four optical components: a 10-mm pathlength liquid filter (cobalt sulfate for 325 nm, copper nitrate for 442 nm) a 0.25-mm thick quartz beamsplitter (Wilmad Glass, Buena Vista, NJ, U.S.A.), a 2-mm I.D. iris diaphragm (Physitec) and a 10-mm diameter, 19-mm focal length quartz planoconvex lens (Oriel, Stratford, CT, U.S.A.). For efficient transfer of either excitation or emission light, we chose a UV-grade optical fiber (Polymicro Technologies). This material had a core diameter of 120 μm, an O.D. of 200 μm, and provided 45–50% transmission efficiency for both 325 and 442 nm. A Model 45-PM laser power meter (Liconix) was used to make all laser power measurements as well as to provide continuous monitoring of laser output.

The fluorescence signal was then passed through the emission optical components. A quartz planoconvex lens, 10 mm diameter and 15 mm focal length (Physitec) was placed adjacent to the flow-cell. Next, a glass, cut-in filter (Oriel) was used to

isolate the emission signal from the laser radiation. A liquid filter (copper nitrate for 325 nm, copper chloride–calcium chloride for 442 nm) was placed between the glass filter and the transducer for additional isolation of the two signals.

The resulting collimated fluorescence beam was directly imaged onto a miniature photomultiplier tube (PMT) (Hamamatsu, Middlesex, NJ, U.S.A.), Model R-1635-02. This transducer, operating at a bias of −1250 V, provides a quantum efficiency of 14.2% at 420 nm (pyrene emission) and 7.45% at 500 nm (perylene emission)[10]. Virtually all of the 8-mm diameter photocathode was illuminated. The output of the PMT was connected to an Amptek (Bedford, MA, U.S.A.) Model A-101 preamplifier/discriminator assembly, which we used as our photon counting circuit. This device is a unique, hybrid microelectronic charge-sensitive preamplifier/discriminator, all incorporated into a single transistor package. The adjustment of discriminator level in this circuit has been described[8]. The pulse output of this circuit was directed to the TTL input of a Model PRM-100S ratemeter (Modern Instrumentation Technology, Port Matilda, PA, U.S.A.), which had both analog and digital (8-bit parallel) outputs. The analog output signal was connected to a Type LS recorder (Linseis, Princeton-Jct, NJ, U.S.A.), and the digital signal was sent to a Leading Edge Model D computer (Canton, MA, U.S.A.). We chose the recorder for all our detector Figure-Of-Merit determinations, and we used a 10-s analog output filter time constant on the ratemeter. More importantly, the ratemeter gate-time was fixed at 100 ms.

We evaluated two different optical configurations to achieve optimum detection system performance. Configuration 1, where the optical fiber carries the laser light to the flow-cell, is shown in Fig. 1. This alignment includes a 22-mm diameter, 8-mm focal length mirror to retro-reflect any fluorescence from the flow-cell. Configuration 2, where the fiber carries the fluorescent signal to the PMT, is shown in Fig. 2 and is similar to a design used by Sepaniak and Yeung[11]. The excitation optics are similar to those in configuration 1, but the placement of the flow-cell is different. Here, the laser is directly imaged into the flow-cell, and the subsequent emission is transmitted through the fiber to the planoconvex lens, cut-in (blocking) filter and solution filter of the emission optics. Therefore, the role of the fiber is reversed in configuration 2 from that of configuration 1. The laser power meter was used to make the power distribution measurements.

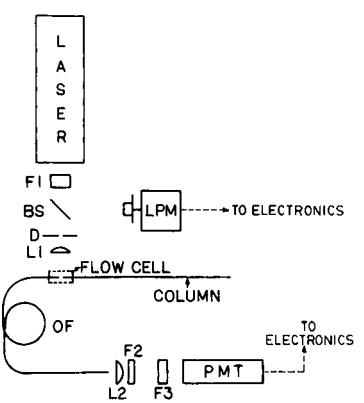

Fig. 2. Optical configuration 2: abbreviations as in Fig. 1.

RESULTS AND DISCUSSION

Evaluation of the sampling/injection system

We have recently utilized several procedures to enhance the ease of injection, as well as improve injection efficiency. Referring again to the constant purge device in Fig. 1, we have observed dramatic reductions in the washout problem associated with these valves when injecting non-aqueous solutes. For example, we found only negligible carryover with a blank injection that was preceded by an injection of 10^{-4} *M* perylene. Prior to using this device, we experienced washout problems that persisted for as long as 24 h for both pyrene and perylene[12].

Two other procedures have resulted in reductions of extra-column effects at the injection valve: (1) inserting the column into the pump channel of the valve (instead of the column channel); and (2) using a moving injection technique. Fig. 3 is a cutaway drawing of the Valco CI4W valve. Noting that the pump channel is 0.006 in. wider than the column channel, the column may be inserted through the wider channel (Fig. 3B). A Teflon sleeve is used to position the column in this channel, as shown. The column inlet is extended to within *ca.* 0.003 in. of the loop. The result of the new connection is that the particles at the column head are much closer to the loop than the previous arrangement (Fig. 3A), producing minimal unswept volume and more efficient solute transfer. This column connection (Fig. 3B) was developed with the aid of several consultations with scientists at Valco[13] and Brigham Young University[14].

Presently, an electronic actuator is being used to facilitate injection, in a "moving loop' technique. Timing of the injection cycle, combined with a 2-s injection period, has nearly eliminated exponential washout, a common feature of these valves. Based on a paper by Harvey and Stearns[15], we estimate a 30% injection of the total loop volume (18 nl for a 60-nl loop).

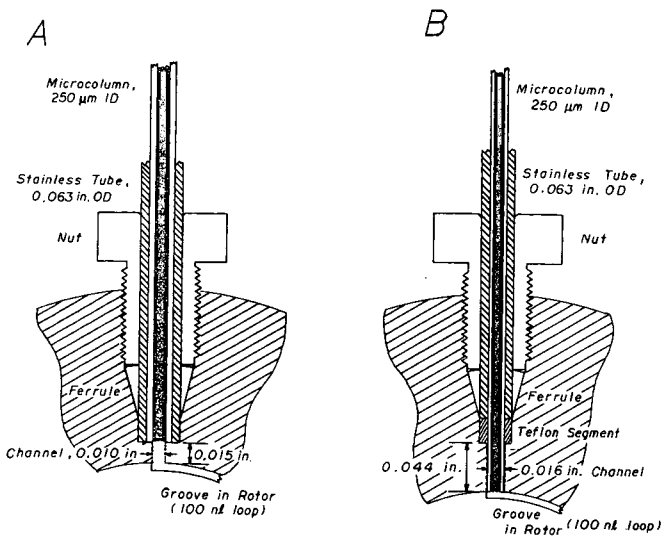

Fig. 3. Detail of column–valve connections: (A) column port attachment, end of column extends to port opening; (B) pump port attachment, end of column extends through port opening to rotor.

Optimization of the chromatographic system

Most recent efforts have focused on optimizing the pump pressure *vs.* packing (filtration) rate programs. These programs were employed by manually increasing the pump pressure control by a fixed amount every 30 s, simultaneously measuring bed height with a meter stick. This constant time interval enabled the packing rate to be determined, in a straightforward manner. A linear pressurization regime will likely result in a more uniform, more efficient bed. Following the technique proposed by Andreolini *et al.*[16], we obtained a constant packing rate (using 5-μm Spherisorb) after the first minute, but showed non-linearity prior to the first minute. However, we achieved minimum reduced plate heights (h_{min}) of 2.63–2.67. Although most of these packing studies were completed some time ago[9], the constant filtration rate work is still in its early stages and is a topic for a separate paper[17]. We hope to achieve more complete control of the pressure-time profile by computer interfacing the pump, thus enabling us to determine relationships between filtration rate, longitudinal bed uniformity and chromatographic efficiency.

Detector performance

Table I displays a comparison between detector performance at 325 and 442 nm for the two different optical configurations. The power distrubution data show that the two configurations were similar in their ability to deliver a respectable power level to the flow-cell. These measurements do not reflect the actual spot diameters, however. Therefore, it is reasonable to expect that the flow-cell power level for configuration 2 was actually *ca.* ten times that for configuration 1, since the lens (configuration 2) provided a much smaller spot diameter than the optical fiber (configuration 1). We used an equation, given by Scott[18], to determine detector minimum detectable quantities (MDQs). Use of this equation assumes a Gaussian profile, with the solute concentration at the peak maximum taken to be twice the average concentration. Lower detection limits were seen for 442 nm, which can be partially attributed to the higher power density at this wavelength. The fact that perylene has a higher quantum efficiency than pyrene (Φ_F for perylene = 0.94 and Φ_F for pyrene = 0.32[19]) certainly contributed to the results. The improvement in MDQ at 442-2 (442 nm excitation line, configuration 2) compared to 442-1 (442 nm excitation line, configuration 1) is partially due to the fact that a more efficient column was used for the configuration 2 measurements. However, it is interesting that the background count

TABLE I

DETECTION SYSTEM PERFORMANCE DATA

	Perylene		*Pyrene*	
	442-1	*442-2*	*325-1*	*325-2*
Power at laser (mW)	14.0	15.5	3.10	2.05
Power through filter (mW)	10.0	11.3	2.08	1.65
Power at flow-cell (mW)	6.20	6.65	1.55	1.10
R_b (kHz)	500–600	0.1–0.2	1000–1100	0.1–0.3
MDQ detector (fg)	10	1.7	540	180

rate (R_b) in the second configuration was nearly 10^4 *lower*. Experiments using the 325-nm excitation line yielded similar results: 325-2 gave almost a 10^4 decrease in R_b compared to 325-1, and 325-2 gave somewhat better detector performance as well. The high background count rate for configuration 1 can not be attributed to varying chromatographic conditions, because open tube measurements were performed for both configurations (at 442 nm), yielding the same background rates as for the packed column experiment. It has been thought that for best performance, photon counting needed to be accomplished at low count rates, yet our data show that we achieved somewhat lower MDQs with the high background configuration. This can be attributed to the large bandwidths of both the preamplifier/discriminator (4 MHz) and the ratemeter (100 MHz) as well as the fast rise-time of the PMT (0.8 ns, which corresponds to a bandwidth of *ca.* 4 GHz). More work must be done to completely characterize the kinetic performance of the photon counting electronics.

These data in Table I prompted us to investigate the source of the high background count rate for configuration 1. A test mixture containing acetone, sodium chloride and pyrene was formulated in order to study the optical response characteristics of the flow-cell. This mixture was chosen because acetone absorbs strongly at 325 nm, sodium chloride can function as a refractive index (RI) probe, and pyrene was previously used as a fluorescent analyte for excitation at 325 nm. As shown in Fig. 4, peak 1, occurring at *ca.* 3 min, was mainly due to the RI change of the sample solvent and sodium chloride. Peak 2, the acetone peak, eluted just after 3 min and generated only a refractive index change. Upon elution into an emission detector, a UV-absorbing solute should generate an inverted peak, provided that the excitation and background wavelengths are the same. Since acetone displayed only an RI

Fig. 4. Chromatogram of flow-cell performance test mixture. Components: acetone, 1%; sodium chloride, 250 ng/ml; pyrene, 1000 ng/ml in acetonitrile–water (65:35). Mobile phase, 100% acetonitrile.

change, reflected laser light, occurring outside the flow-cell in the emission optics, may be reaching the PMT. We can not conclude that the flow-cell is relatively immune to RI effects because sodium chloride has a similar RI to acetonitrile. It is interesting that only positive-going peaks were seen for sodium chloride and acetone. This may be due to the unique optical arrangement of configuration 1 compared to absorption-type detectors, which generate characteristic positive/negative RI peaks. Peak 3 was the usual pyrene peak, eluting at *ca.* 7 min.

We investigated the possibility that reflected/scattered light, arising from the optical fiber, was contributing to the high background of configuration 1. Reflected laser light, that exits from the optical fiber without passing through the flow-cell, may be collected by the emission optics. This light could originate in cladding or buffer modes or in a poorly-cleaved fiber end-face. We coiled the fiber in a small-diameter loop and meticulously cleaved and cleaned the fiber end-face, producing both improved transmission efficiency and a slight reduction in background count rate. The mirror-lens combination in configuration 1 produces nearly a 1.5 stearadian collection angle compared to the small 25.4 degree acceptance cone of the optical fiber in configuration 2. Therefore, the emission optics of configuration 2 are much more selective than those of configuration 1. However, it is unlikely that collection efficiency alone would account for the large background count rate. Additionally, Raman scattering that originates within the fiber may be reaching the PMT. Though we have made preliminary measurements of the background emission spectra for configuration 1, the results are inconclusive. Raman scattering from solvent within the flow-cell has been a complicating factor, as well as the difficult optical alignment necessary to carry out these measurements. We are exploring these aspects in more detail.

In spite of the slight performance advantage of configuration 2, as evidenced in Table I, it is unclear which configuration is preferred when considering linear dynamic range performance. We have observed a linear dynamic range of two orders of magnitude for configuration 1, whereas for configuration 2 linearity was observed for one decade of concentration, at best. Some of these features may be attributed to photophysical phenomena, such as excimer emission, delayed fluorescence or E-type (eosin) fluorescence, as described by Parker[20], that contribute to different extents in the two configurations. Probably these small linear calibrations are limited at high concentration by primary absorption, as defined by Christman *et al.*[21]. Wider linear dynamic ranges will result from a combination of several factors: (1) reduction in R_b; (2) identification of the source of detrimental photophysical effects; and (3) improved detectability through optical/electronic improvements.

Evidence of an overall highly efficient LC apparatus is presented in Fig. 5, which shows a PAH separation in which thirteen of the sixteen components were detected in 15 min (30 pg injected). A subsequent injection of only 3 pg of the same mixture resulted in detection of several peaks. For the pyrene peak, this would represent an MDQ below 200 fg, a very good result considering the low excitation power level and modest total cost of *ca.* $10 000 for the detection system. Another noteworthy aspect of Fig. 5 is the efficiency of the peaks, reflected in their widths. High efficiency chromatography demands fast, accurate detection electronics; and it is apparent that the photon counting system was adequately following the solute elution profile, characteristic of an efficient separation. We have not explicitly evaluated the

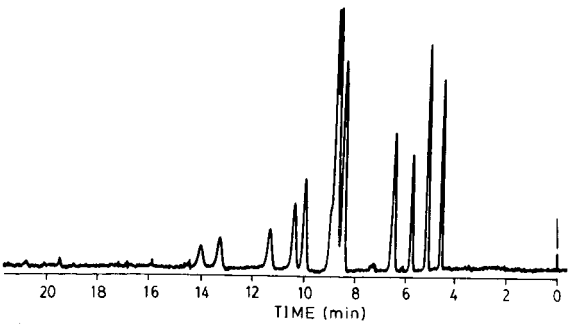

Fig. 5. Chromatogram of polynuclear aromatic hydrocarbon mixture: 30 pg injected amount for each of sixteen components. Mobile phase, acetonitrile–water (92:8).

temporal response characteristics of the detector. However, it must be remembered that the detection technique is digital and therefore not subject to the same distortion that RC-analog systems impart to fast signals. Thus, our photon counting system is quite appropriate for signals on the chromatographic time-scale. This aspect of detector operation will be included in a future paper.

CONCLUSIONS

We have demonstrated good overall system performance of our laser-induced fluorescence LC apparatus by critically evaluating the sampling/injection, chromatographic and detector systems. Modifications in our injection valve have resulted in two improvements: (1) almost no carryover from previous injections (no memory effects); and (2) more efficient solute transfer due to a near-zero dead volume column connection. Improvements in the chromatographic system, through a constant packing rate, have resulted in more uniformly packed columns and better efficiencies. In addition, we have obtained very good detector MDQs for both optical configurations, while operating under the constraints of low cost and low laser power. Most importantly, we have shown that a systems approach to instrument optimization, where improving each subsystem in the apparatus with constant consideration of the interrelationships between them, will enhance overall performance.

Some of our future work will include spectrometer measurements that identify the source of the high background count rate for configuration 1, and a critical evaluation of the small linearity in configuration 2. Because photon counting is most advantageous at low light levels, the configuration which will perform best is the one that exhibits both a low background count rate and wide linearity. We will also improve detector performance through greater utility of photon counting. One of our goals is to make this unique detection technique more useful for analytical separations.

ACKNOWLEDGEMENTS

We are indebted to M. Harvey of Valco Instruments for lending us the electronic valve actuator, R. Henry of Keystone Scientific for donating much of the packing

material and T.J. Dalton of Stevens for writing the software programs. This work was partially supported by the Governor's Commission on Science and Technology of New Jersey Innovative Partnership Program.

REFERENCES

1 E. S. Yeung, in E. H. Piepmeier (Editor), *Analytical Applications of Lasers*, Wiley, New York, 1986, Ch. 17.
2 R. B. Green, *Anal. Chem.*, 55 (1983) 20–32 A.
3 V. L. McGuffin, in P. Sandra (Editor), *Proc. Sixth Int. Symp. Capillary Chromatogr.*, Huetig, Heidelberg, 1985, pp. 800–808.
4 M. Novotny, *Anal. Chem.*, 60 (1988) 500–510 A.
5 S. F. Folestad, L. Johnson and B. Josefsson, *Anal. Chem.*, 54 (1982) 925–929.
6 J. Gluckman, D. Shelly and M. Novotný, *J. Chromatogr.*, 317 (1984) 443–453.
7 E. J. Guthrie, J. W. Jorgenson and P. R. Dluzneski, *J. Chromatogr. Sci.*, 22 (1984) 171–176.
8 D. C. Shelly and T. J. Edkins, *Proc. SPIE*, 910 (1988) 116–122.
9 D. C. Shelly and T. J. Edkins, *J. Chromatogr.*, 411 (1987) 185–199.
10 Hamamatsu Technical Data Sheet, *3/8 Diameter Series Photomultiplier Tubes*, Hamamatsu Corp., Middlesex, NJ.
11 M. J. Sepaniak and E. S. Yeung, *J. Chromatogr.*, 190 (1980) 377–383.
12 T. J. Edkins and D. C. Shelly, unpublished results, 1987.
13 M. Harvey, personal communication, 1987.
14 K. Markides, personal communication, 1987.
15 M. C. Harvey and S. D. Stearns, *J. Chromatogr. Sci.*, 21 (1983) 473–477.
16 F. Andreolini, C. Borra and M. Novotny, *Anal. Chem.*, 59 (1987) 2428–2432.
17 D. C. Shelly, V. L. Antonucci, T. J. Edkins and T. J. Dalton, *J. Chromatogr.*, 458 (1988) 267–279.
18 R. P. W. Scott, *Liquid Chromatography Detectors* (*Journal of Chromatography Library*, Vol. 33), Elsevier, Amsterdam, 2nd ed., 1986.
19 I. B. Berlman, *Handbook of Fluorescence Spectra of Aromatic Molecules*, Academic Press, New York, 2nd ed., 1971.
20 C. A. Parker, *Photoluminescence of Solutions*, Elsevier, Amsterdam, 1968.
21 D. R. Christman, S. R. Crouch, J. F. Holland and A. Timnick, *Anal. Chem.*, 52 (1980) 291–295.

Journal of Chromatography, 459 (1988) 119–138
Elsevier Science Publishers B.V., Amsterdam — Printed in The Netherlands

CHROMSYMP. 1467

EXPERIMENTAL AND THEORETICAL MODEL OF REFRACTIVE INDEX ARTIFACTS IN ABSORBANCE DETECTION

CHRISTINE E. EVANS, JOHN G. SHABUSHNIG* and VICTORIA L. McGUFFIN*
Department of Chemistry, Michigan State University, East Lansing, MI 48824 (U.S.A.)

SUMMARY

An anomalous signal is often observed upon sample injection in both liquid chromatography and flow-injection analysis using high-sensitivity absorbance detectors. This characteristic detector response, unrelated to sample absorbance, appears to arise from the change in refractive index within the flowcell. The factors affecting the refractive index gradient have been incorporated in a ray-tracing model, where the flowcell is regarded as a dynamic lens. The response predicted by this model correlates well with experimental measurement of the general shape, magnitude, and direction of the refractive index artifact. The proposed model should have wide ranging implications for both flowcell design and chromatographic interpretation of these anomalous signals.

INTRODUCTION

Detection systems based on absorption of electromagnetic radiation in the ultraviolet or visible region are among the most widely used in liquid chromatography (LC). Ideally, absorbance detectors respond only to substances which absorb the source radiation at a specific wavelength. However, an anomalous and non-specific response is commonly observed in high-sensitivity applications due to refractive index effects. A change in refractive index within the flowcell causes reflection and refraction of source radiation, resulting in a change in light intensity at the photodiode detector. This anomalous response is observed under a variety of experimental conditions, including sample injection (Fig. 1), stepwise or linear gradient elution, and other rapid changes in solvent composition. These refractive index artifacts can interfere with solute detection, leading to confusion or misinterpretation of chromatographic data.

Although commonly observed in LC[1] as well as flow-injection applications[2], the exact nature of the refractive index artifact is not clearly understood. Many factors are thought to affect the shape, magnitude, and direction of this response. The influence of flowcell geometry has been examined for cylindrical and square capillaries[3–7], sheath flowcells[6,8], and U- or Z-pattern flowcells[2,9–11]. Design of the external optical system also influences the response, since source radiation may be convergent, divergent, or

* Present address: The Upjohn Company, Kalamazoo, MI 49001, U.S.A.

0021-9673/88/$03.50

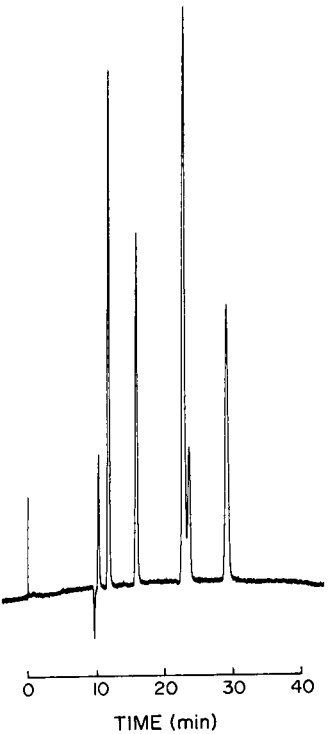

Fig. 1. Chromatogram illustrating refractive index artifact occurring in absorbance detection upon injection of standard test mixture dissolved in methanol into a methanol–water (75:25, v/v) mobile phase. Characteristic derivative-shaped response from absorbance anomaly is seen at a retention time of 10 min.

collimated as it enters the flowcell[10]. Finally, the absolute refractive index and refractive index gradient within the flowcell appear to have a substantial effect[10,11].

Although theoretical evaluations of the refractive index dependence of flowcells have been presented[2–11], attempts to correlate theoretical predictions and experimental results have been notably scarce in the literature. In this work, a three-fold approach is used to elucidate this detection anomaly. First, an absorbance detector with Z-pattern flowcell is utilized to measure the experimental shape, magnitude, and direction of the refractive index response occurring upon injection. Second, the change in light throughput in the flowcell is monitored by direct visual and photographic inspection to determine the origin of the detector response. Finally, optical ray-tracing techniques are employed to simulate the image diameter and intensity resulting from the refractive index gradient in the flowcell. Although the development presented here is limited to injection profiles in the Z-pattern flowcell, this approach should be applicable to any gradient or flowcell of interest.

THEORY

At the interface between two homogeneous media of differing refractive index (n), an incident light ray is deflected at an angle (θ) according to Snell's law:

$$n_1 \sin\theta_1 = n_2 \sin\theta_2 \quad (1)$$

When a flowcell is an integral part of an optical system, the refractive index properties within the cell determine the angular deflection of incident light. This deflection determines the size of the detected image and, if the flowcell is the limiting aperture in the system, the overall intensity of that image. Accordingly, in a flowcell containing a static or flowing solution of constant composition, the resulting transmittance depends on the absolute refractive index of the medium. However, when a zone of different composition is injected into the flowing stream, concentration gradients are formed by laminar flow, diffusion, and mixing phenomena. Because refractive index is a function of concentration, a corresponding refractive index profile is generated with components both radial and axial to the direction of flow. As the zone traverses the flowcell, the angular deflection of the incident light rays varies continuously in time and space, causing the flowcell to act as a dynamic gradient-index lens. The resultant response in such a dynamic system depends on the gradient of refractive index present in the flowcell, not on the absolute refractive index. Thus, determination of the final image size and intensity requires knowledge of both radial and axial contributions to the refractive index gradient.

The mathematical form of the radial gradient (dn/dr), which is perpendicular to the axis of flow, can be expressed as the product:

$$\frac{dn}{dr} = \frac{dn}{dC} \cdot \frac{dC}{dr} \tag{2}$$

where dn/dC represents the change in refractive index with concentration, and dC/dr is the change in concentration across the flowcell radius. Similarly, the axial gradient (dn/dz) can be determined from the change in concentration parallel to the axis of flow (dC/dz):

$$\frac{dn}{dz} = \frac{dn}{dC} \cdot \frac{dC}{dz} \tag{3}$$

Detailed knowledge of the form of the individual differential equations, as described below, is necessary to determine the radial and axial refractive index gradients.

Evaluation of dn/dC

According to simple solution theory, the refractive index of binary mixtures is a linear function of concentration[12], so that dn/dC is a constant. However, such ideal behavior is rarely observed for the polar, highly interacting solvents of interest in liquid chromatography (Fig. 2). For non-ideal solvent mixtures, dn/dC must be calculated from the tangential slope of the graph of refractive index *versus* concentration. This is achieved by reducing the experimental data to a polynomial equation and, subsequently, calculating the derivative (dn/dC) as a function of concentration.

Evaluation of dC/dr

For a flowcell of cylindrical geometry, the radial concentration gradient (dC/dr) can be determined from the equation derived by Taylor[13]:

$$C = C_0 + \frac{R^2 u}{4D_m}\left(\frac{r^2}{R^2} - \frac{r^4}{2R^4}\right)\frac{dC_0}{dz} \tag{4}$$

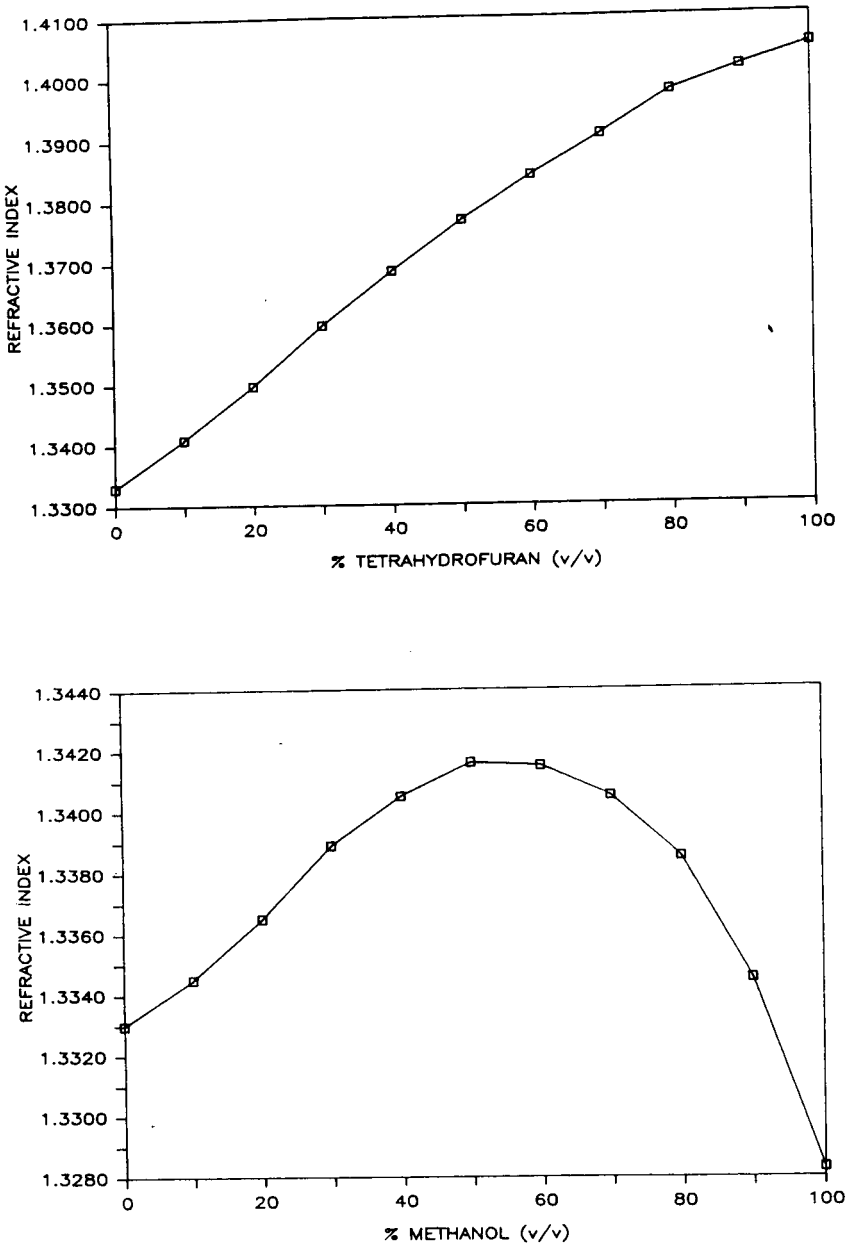

Fig. 2. Refractive index measurements for aqueous binary mixtures of tetrahydrofuran and methanol.

where the concentration (C) at a given radial distance (r) is evaluated as a function of the concentration (C_0) and axial concentration gradient (dC_0/dz) at the tube center, the tube radius (R), linear velocity (u), and diffusion coefficient (D_m). If the residence time in the flowcell is short, the concentration profile may be modelled as a parabola by

neglecting the second term of the parenthetical expression in eqn. 4. The derivative (dC/dr) is then evaluated as a function of the radial position.

Evaluation of dC/dz

The axial concentration function can take various forms for the injection and gradient elution profiles encountered in liquid chromatography. For an ideal injection, the concentration profile upon leaving the chromatographic column can be modelled as a Gaussian function:

$$C = \frac{M}{(2\pi\sigma_L^2)^{1/2}(\pi R^2)} \exp\left(\frac{-z^2}{2\sigma_L^2}\right) \quad (5)$$

where M is the injected sample mass, and z is the axial distance from the center of a zone with length variance σ_L^2. The length variance of the zone can be estimated from the Golay equation[14] for an open-tubular column, or from the Van Deemter[15] or Knox[16] equations for a packed column. The concentration gradient (dC/dz) is then calculated as a function of the axial position.

For the ideal conditions described herein, the radial refractive index gradient (dn/dr) can be determined by eqn. 2 from the derivative of the radial concentration profile (dC/dr) given in eqn. 4 and the dependence of refractive index on concentration (dn/dC). Similarly, the axial refractive index gradient (dn/dz) can be calculated by eqn. 3 from the axial concentration gradient (dC/dz) for injection given by eqn. 5 and the (dn/dC) relationship. Consequently, the absolute refractive index at specific coordinates (r,z) in the flowcell can be determined by integration, and the angular deflection subsequently calculated by using Snell's law (eqn. 1). Unfortunately, these differential equations are not readily amenable to analytical solution. In this paper, we have approached this problem by incorporating the calculated gradients into a simulation model based on optical ray tracing, where the flowcell is regarded as a dynamic lens. Although the assumed form of these gradients is greatly simplified, this model allows the direct comparison of theoretical predictions with experimental measurements of refractive index artifacts present in absorbance detection.

EXPERIMENTAL

Reagents

All organic solvents were high-purity, distilled-in-glass grade (Burdick and Jackson, Muskegon, MI, U.S.A.). Water was deionized and doubly distilled in glass (Model MP-3A, Corning Glass Works, Corning, NY, U.S.A.). Binary aqueous solutions of the organic solvents, ranging from 0 to 100% (v/v) were prepared by thoroughly mixing known volumes of each component.

Refractive index measurements

Measurements of refractive index were performed in triplicate utilizing an Abbe refractometer (Model Abbe-3L, Bausch and Lomb, Rochester, NY, U.S.A.), maintained at 25.0°C. Reproducibility was better than ± 0.0001 relative standard deviation (R.S.D.) for replicate measurements of a single sample as well as for replicate samples. Results of the refractive index measurements for binary mixtures of tetrahydrofuran–water and methanol–water are summarized in Fig. 2.

Chromatographic detection

A schematic diagram of the experimental system is shown in Fig. 3. A syringe pump (Model μLC-500, Isco, Lincoln, NE, U.S.A.) was utilized for solvent delivery at a constant flow-rate of 50 μl/min. Samples were introduced with a 1-μl injection valve (Model C14W1, Valco Instruments, Houston, TX, U.S.A.), which was connected directly to the detector by using an open tube of 46 cm × 0.025 cm I.D. A commercially available absorbance detector (Model Uvidec 100-V, Jasco, Tokyo, Japan), with a 1-μl Z-pattern flowcell, was employed at a monochromator wavelength of 589 nm with a 500-nm high-pass cutoff filter. This wavelength was chosen to allow the anomalous response due to refractive index to be distinguished from true sample absorbance. The apparent absorbance signal, resulting only from refractive index artifacts, was displayed on a chart recorder (Model 585, Linear Instruments, Reno, NV, U.S.A.) and was converted to transmittance by manual calculation.

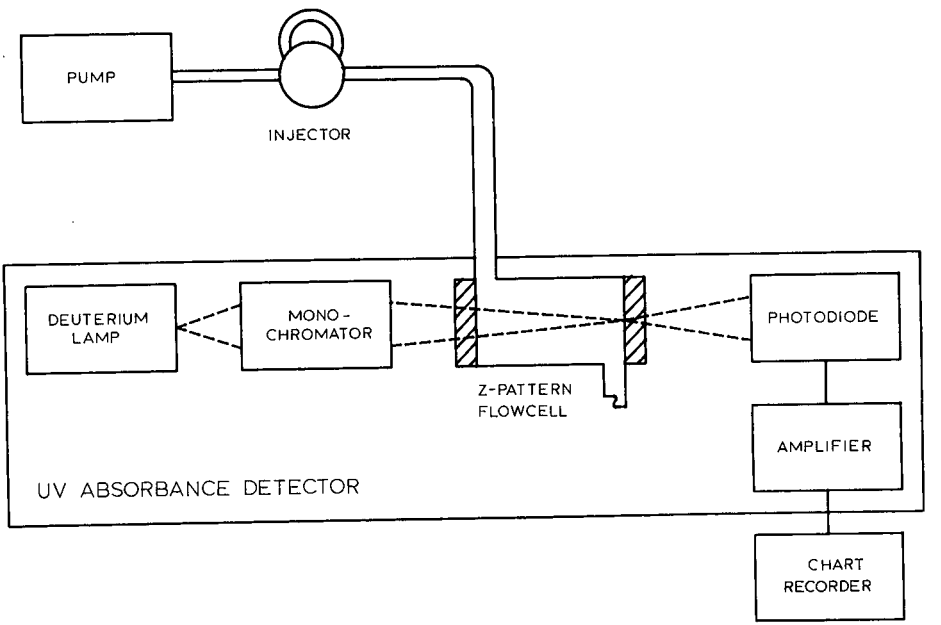

Fig. 3. Schematic diagram of liquid chromatographic absorbance detector. A 500-nm high-pass cutoff filter was placed between the source and monochromator, and measurements performed at 589 nm to isolate the refractive index artifact from response due to absorption of source radiation.

Visual detection

The Z-pattern flowcell was removed from the commercial detector, allowing direct probing of the cell with a helium–neon laser (Model 155, Spectra-Physics, Mountain View, CA, U.S.A.). The laser radiation was focussed on the cell utilizing a quartz lens (1.0 in. focal length, 1.0 in. diameter). The transmitted light was displayed on a viewing screen, placed 85 cm from the flowcell, for direct visual and photographic inspection.

Simulation

The simulation of refractive index artifacts was performed on an IBM-XT microcomputer (International Business Machines, Boca Raton, FL, U.S.A.) with a commercially available software package (Beam3, Stellar Software, Berkeley, CA, U.S.A.). This software allows the placement of optical sources, refracting and reflecting optical elements, apertures, and viewing screens at arbitrary positions. The resultant optical system is then analyzed using a three-dimensional ray-tracing algorithm.

In this simulation, a point source at 589 nm wavelength was located 0.5 mm from the front surface of a Z-pattern flowcell. The flowcell, shown in Fig. 4, was modelled as a pair of quartz windows ($n_D = 1.4570$) of 1.0 mm thickness and 0.5 mm aperture diameter. These parallel windows were separated by a distance of 5.0 mm, within which a flowing solution was contained. Finally, a screen was positioned 25 mm from the rear window of the flowcell to simulate the photodiode.

The flowing solution was modelled as a dynamic lens with continuously varying refractive index in both radial and axial directions. The radial contribution to the

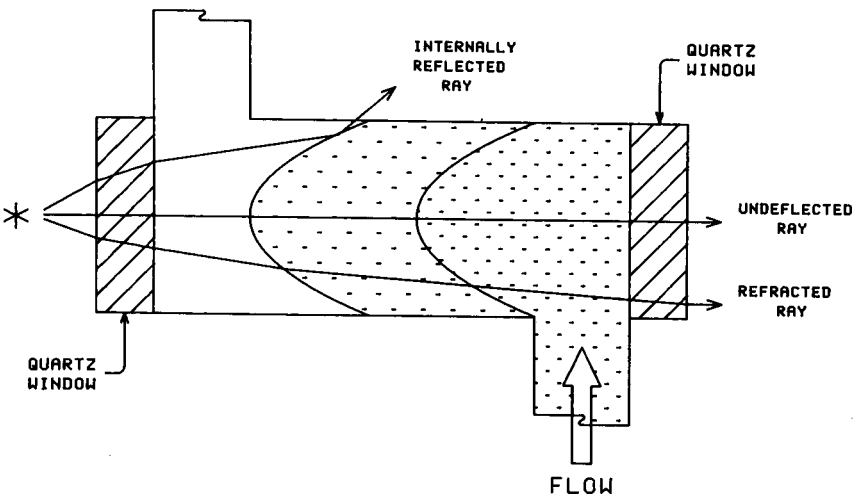

Fig. 4. Illustration of a Z-pattern flowcell with both radial and axial refractive index gradients.

refractive index gradient, which is parabolic in form, was calculated using eqn. 4 neglecting the $r^4/2R^4$ term. This expression defines the shape and curvature of the surfaces of constant concentration $[(C-C_0)/(dC_0/dz)]$, and hence, of constant refractive index, if dC_0/dz is considered constant in the flowcell at any point in time. The curvature of the parabolic profile, which characterizes the radial refractive index gradient, is given in eqn. 4 by the constant $(R^2u/4D_m)$. In this simulation, the flowcell radius ($R = 0.025$ cm) as well as mobile-phase velocity in the flowcell ($u = 0.4$ cm/s) were taken from experimentally measured values. Diffusion coefficients (D_m) were estimated utilizing the Wilke–Chang equation[17] to be $1.08 \cdot 10^{-5}$ cm^2/s for tetrahydrofuran in water and $1.64 \cdot 10^{-5}$ cm^2/s for methanol in water at 25°C.

The axial refractive index gradient was determined from the corresponding axial concentration gradient in eqn. 5, which is Gaussian in form. In order to accomplish this determination, the zone variance (σ_L^2) was first estimated for the open tube connecting the injector and detector using the familiar Taylor–Aris equation[13,18]:

$$\sigma_L^2 = \frac{R_t^2 \; u \; L_t}{24 \; D_m} \tag{6}$$

In this calculation, the tube radius ($R_t = 0.0125$ cm), length ($L_t = 46$ cm), and mobile phase velocity ($u = 1.7$ cm/s) were taken from experimental measurements. The length variance determined for the tetrahydrofuran–water solvent system was 50.8 cm^2 in the connecting tube, which corresponds to 3.17 cm^2 in the cell, while that for the methanol–water system was 31.0 cm^2 in the tube and 1.93 cm^2 in the cell. Subsequently, concentration values were calculated across the Gaussian profile using eqn. 5, in which the sample mass (M) was determined for a 1-μl injection volume, and all other experimental parameters were as previously defined. The limits of the Gaussian profile were assumed to be $6\sigma_L$, where the concentration is 1% of the maximum value at the zone center. Finally, the corresponding refractive indices were determined by interpolation from the concentration values (Fig. 2) as a function of the axial distance along the Gaussian profile.

After calculation of the radial and axial refractive index gradients was completed, the simulation was performed by sequentially incrementing the calculated axial refractive index profile through the flowcell in a stepwise manner. A minimum of 40 points was evenly distributed across the Gaussian profile at a constant axial interval of 2 mm, which corresponds to approximately 0.15 σ_L. At each point, both the final image size and intensity were assessed with the Beam3 ray-tracing software. The diameter of the image was determined by evaluating the position of a single peripheral ray on the detection screen. Image intensity values were calculated by allowing 1000 rays (I_0) of randomly distributed angles to be incident on the entrance of the flowcell. The number of rays transmitted through the cell (I) was subsequently determined and

TABLE I
COMPARISON OF NORMALIZED EXPERIMENTAL AND SIMULATED IMAGE INTENSITY AND SIZE FOR INJECTION RESPONSE OF TETRAHYDROFURAN–WATER SYSTEM

		Tetrahydrofuran injected into water		*Water injected into tetrahydrofuran*	
		First deflection	*Second deflection*	*First deflection*	*Second deflection*
Image intensity	Experimental	1.14	0.85	0.91	1.04
	Simulated	1.36	0.76	0.83	1.12
Image size	Experimental	0.56	1.53	1.10	0.91
	Simulated	0.81	1.20	1.09	0.91

TABLE II

COMPARISON OF NORMALIZED EXPERIMENTAL AND SIMULATED IMAGE INTENSITY AND SIZE FOR INJECTION RESPONSE OF METHANOL–WATER SYSTEM

		Methanol injected into water		*Water injected into methanol*	
		First deflection	*Second deflection*	*First deflection*	*Second deflection*
Image intensity	Experimental	1.05	0.97	1.10	0.89
	Simulated	1.06	0.96	1.24	0.82
Image size	Experimental	0.82	1.14	0.90	1.30
	Simulated	0.96	1.04	0.84	1.16

the image intensity ratio (I/I_0) calculated. This simulated intensity ratio was then normalized to that for the mobile-phase solvent. Because transmittance (T) is defined as the ratio of the transmitted power (P) to the incident power (P_0), intensity ratios predicted from the simulation (I/I_0) can be directly compared with experimental measurements of transmittance (P/P_0), which have been likewise normalized (Table I and II).

RESULTS AND DISCUSSION

In order to examine refractive index artifacts in absorbance detection, systematic experimental and theoretical studies of the response occurring upon injection were undertaken. The two solvent systems chosen for these studies, tetrahydrofuran–water and methanol–water, are representative of the wide variety of refractive index conditions encountered in reversed-phase LC. Not only is the range of absolute refractive indices among these solvents substantial (1.3328 for methanol, 1.3330 for water, and 1.4051 for tetrahydrofuran at 25°C), but the dependence of refractive index on concentration is notably different for the two solvent systems (Fig. 2). Aqueous mixtures of tetrahydrofuran show nearly ideal, linear refractive index response as a function of concentration, while aqueous methanol mixtures exhibit distinctly non-ideal behavior. Thus, these two solvent systems allow the characterization of this anomaly under the variety of refractive index conditions encountered in reversed-phase separations.

Experimental results

A commercially available absorbance detector equipped with a Z-pattern flowcell was utilized to evaluate the anomalous refractive index signal occurring upon injection of pure solvents. The detector response, displayed as the transmittance relative to that of the mobile phase, is shown in Fig. 5 for the tetrahydrofuran–water system. Upon injection of tetrahydrofuran into water (Fig. 5A), a derivative-shaped signal was observed with an absolute magnitude of approximately 0.08 absorbance units peak to peak. The direction of this signal shows first an increase (+) then

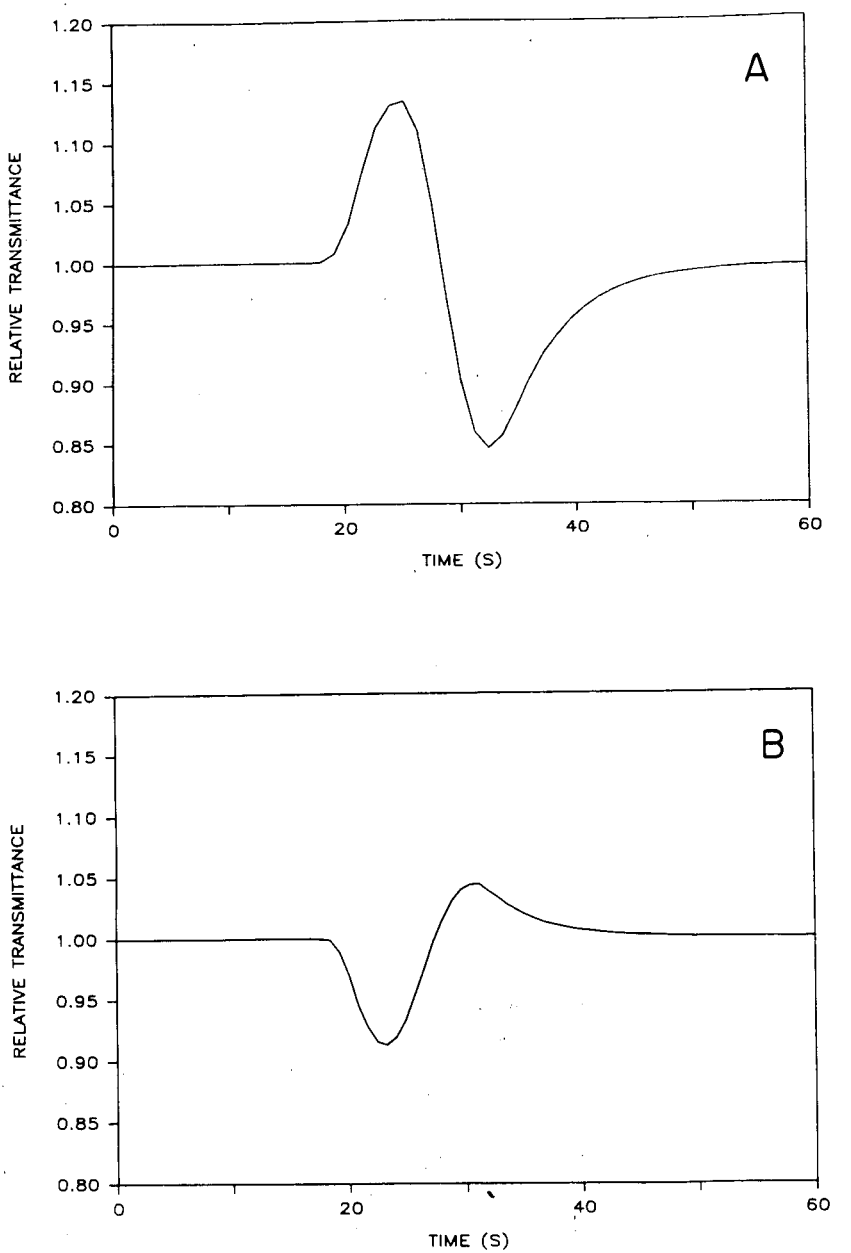

Fig. 5. Experimentally measured relative transmittance response occurring upon injection of (A) tetrahydrofuran into water and (B) water into tetrahydrofuran. Injection volume, 1 μl; flow-rate, 50 μl/min; detector volume, 1 μl; monochromator wavelength, 589 nm.

a decrease (−) in the relative transmittance. In contrast, when water was injected into tetrahydrofuran (Fig. 5B), the magnitude of the signal was reduced and the direction of signal deflection was reversed (−/+). The first and second deflection, measured at the

extremes of these derivative-shaped signals, are summarized as the normalized intensity in Table I.

Further investigations of this phenomenon were accomplished for the methanol–water system and are summarized in Fig. 6 and Table II. The refractive index

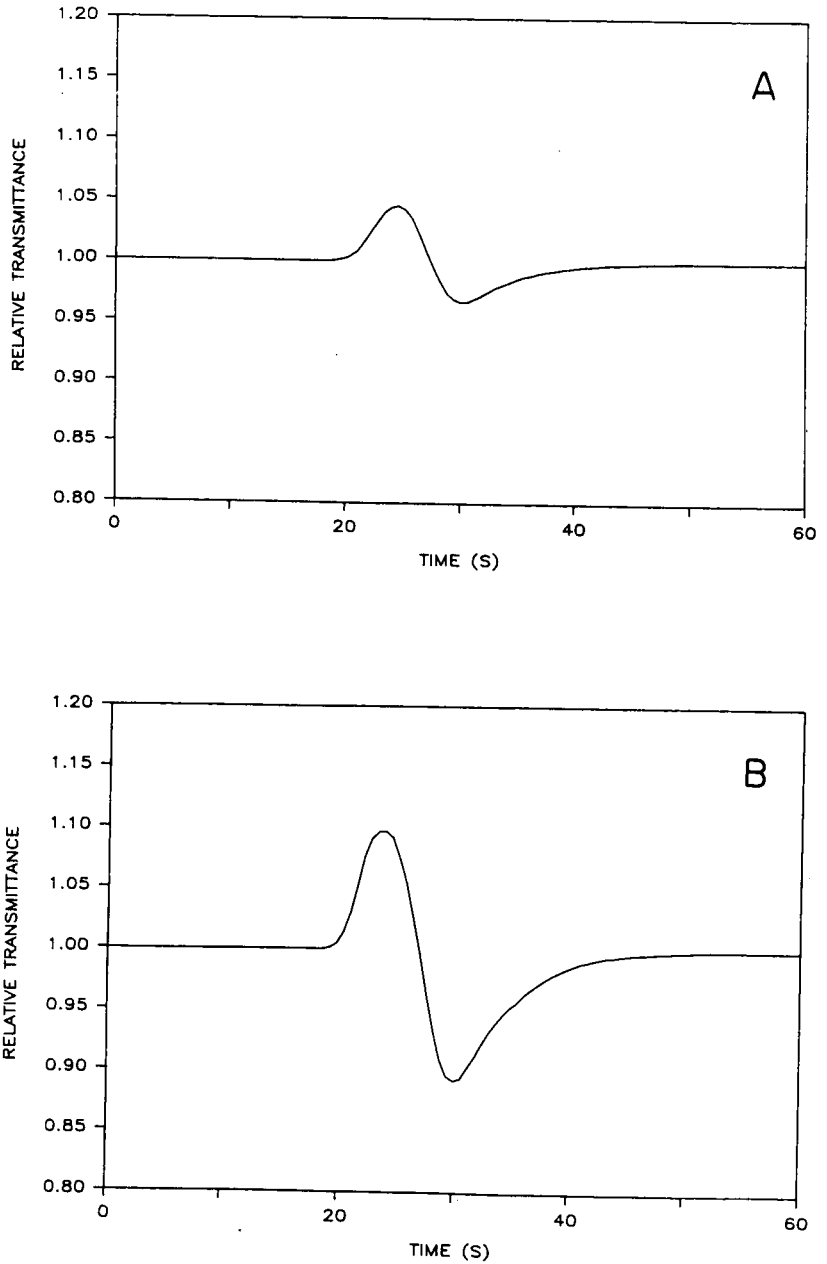

Fig. 6. Experimentally measured relative transmittance response occurring upon injection of (A) methanol into water and (B) water into methanol. Conditions same as for Fig. 5.

artifact observed experimentally was comparable to that of the tetrahydrofuran–water system in both shape and magnitude. In contrast to the tetrahydrofuran–water system, the signals observed for methanol injected into water (Fig. 6A) and water injected into methanol (Fig. 6B) were identical in direction (+/−). This result would not be expected if the response were determined solely by the absolute refractive index of the individual components. Moreover, the characteristic, derivative-shape response is not predictable for either system based on considerations of absolute refractive index alone.

To characterize the source of this derivative-shaped response in greater detail, the Z-pattern flowcell was removed from the absorbance detector and used for direct observation of this phenomenon. Visual detection was accomplished by focussing a helium–neon laser onto the Z-pattern flowcell and viewing the transmitted image on a screen as the zone eluted. Direct photographic monitoring of the injection of tetrahydrofuran into water is shown in a discontinuous time sequence in Fig. 7. The image of the transmitted radiation showed a substantial change in both size and intensity as the tetrahydrofuran zone passed through the flowcell. An initial decrease followed by an increase in image diameter was apparent during elution of the zone. Concurrently, the local light intensity was observed to increase then decrease, consistent with the detector response shown in Fig. 5A. Thus, the anomalous response may result from a change in intensity due to variations in image size or in overall throughput. Since no movement in the position of the resultant spot was visible, these two factors appear to be the primary contributions to detector response.

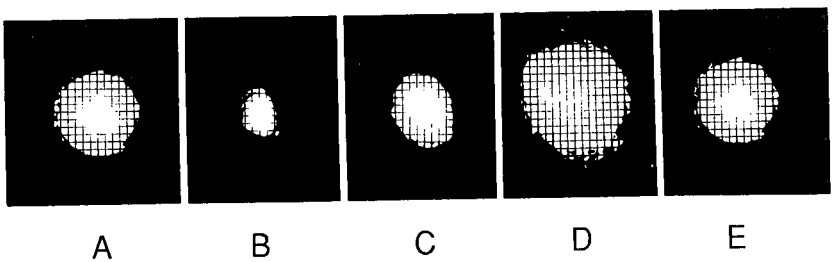

Fig. 7. Time sequence of photographs showing the change in light transmitted through the Z-pattern flowcell upon injection of tetrahydrofuran into a water mobile phase (Fig. 5A), (A) water mobile phase, 17 s; (B) first deflection, 25 s; (C) transition, 29 s; (D) second deflection, 33 s; (E) water mobile phase, 50 s.

Simulation results

Further elucidation of this anomaly was accomplished by computer simulation of the injection process in the Z-pattern flowcell. Dynamic refractive index gradients induced by the concentration profile formed upon injection were simulated with an optical ray-tracing model. This model incorporated refractive index gradients within the cell in both radial and axial directions relative to the axis of flow. In all simulations, the radial refractive index gradient was assumed to be of the parabolic form described by eqn. 4, neglecting the $r^4/2R^4$ term. The axial component of the gradient was determined based on the ideal Gaussian profile given in eqn. 5.

Simulation results are shown for the injection of tetrahydrofuran into water (Fig. 8) and water into tetrahydrofuran (Fig. 9) *versus* normalized axial position (z/σ_L).

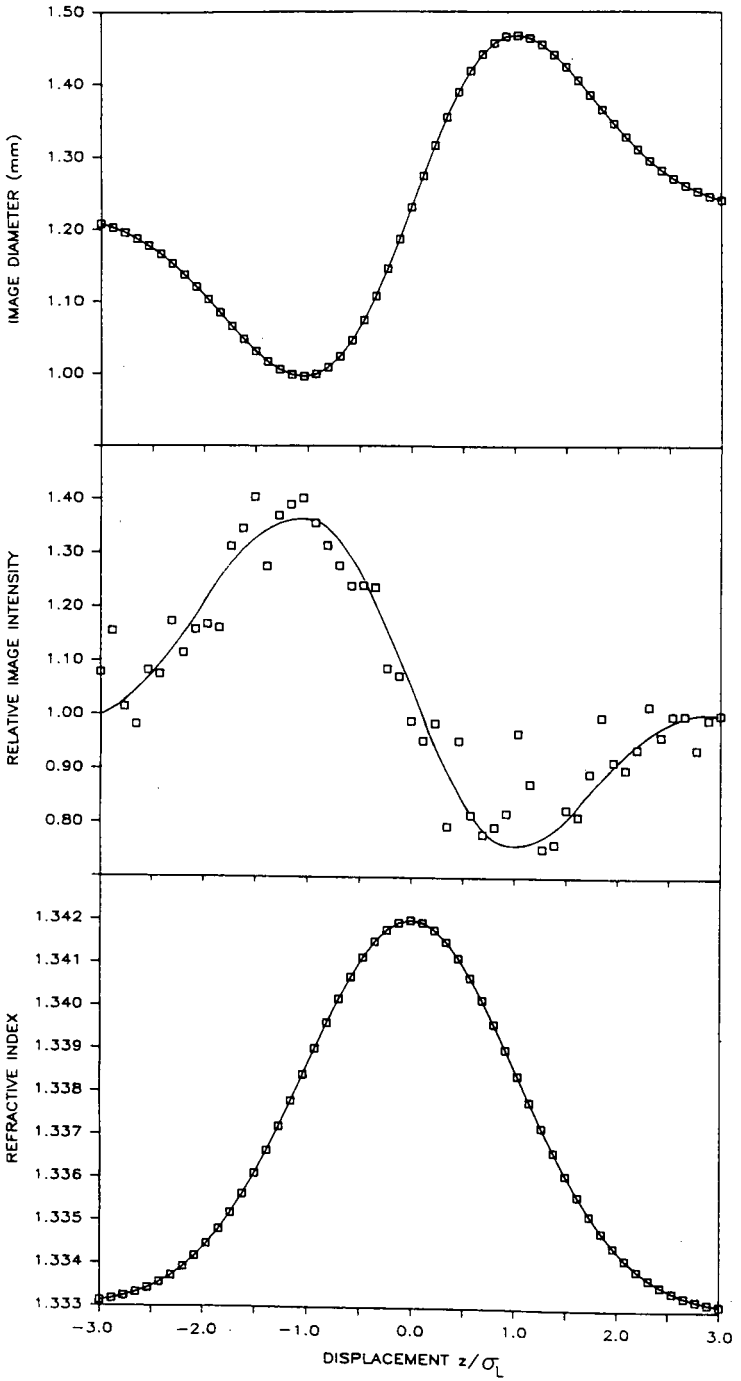

Fig. 8. Simulation results for tetrahydrofuran injected into water. Image diameter and overall relative intensity predicted for axial gradient shown at bottom of figure. Input parameters same as for Fig. 5.

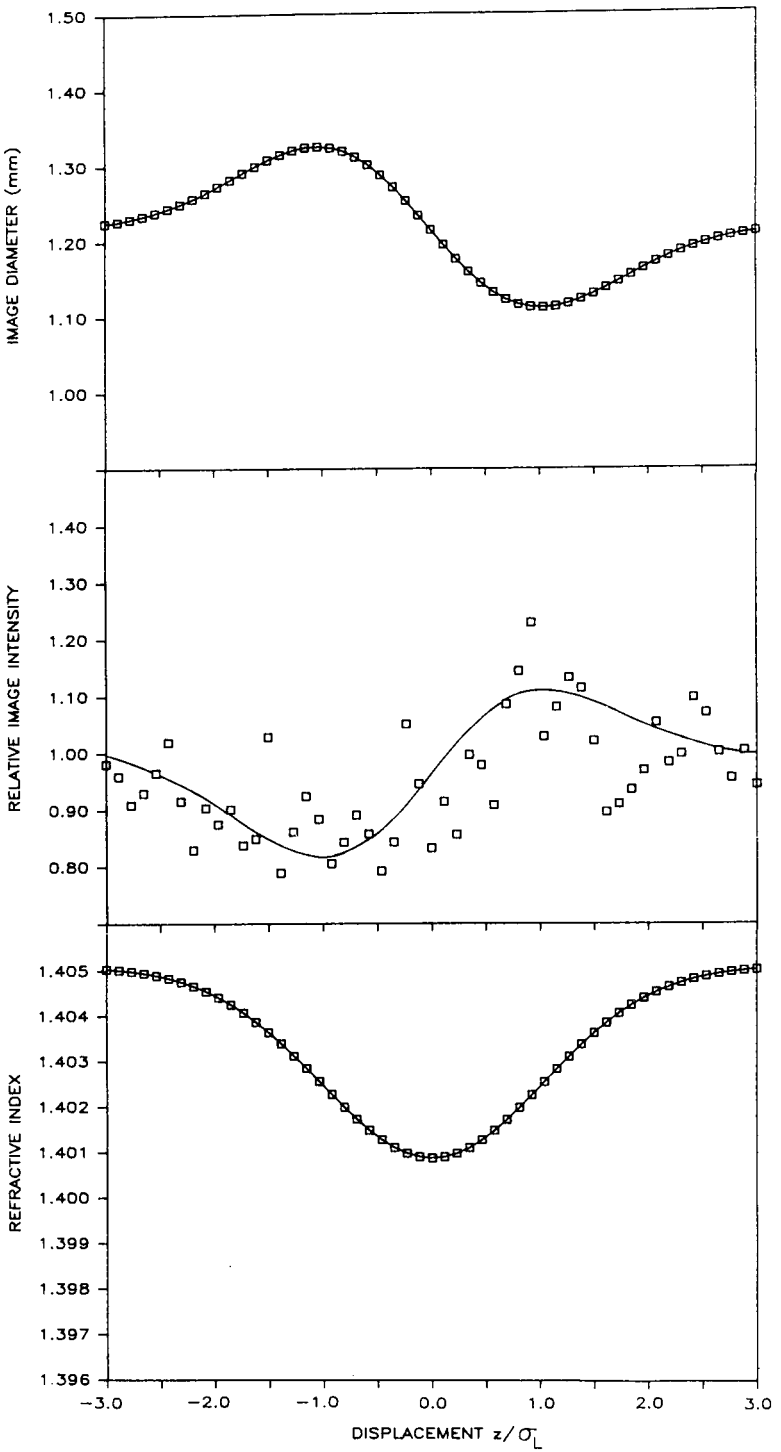

Fig. 9. Simulation results for water injected into tetrahydrofuran. Image diameter and overall relative intensity predicted for axial gradient shown at bottom of figure. Input parameters same as for Fig. 5.

The calculated axial function of refractive index, utilized as input to the simulation, is included along the bottom of each figure for clarity. Predictions of image size (figure top) and overall intensity (figure center) based on this simulation model show the characteristic derivative shape of the refractive index artifact. Relative image size predicted by the model shows good correlation with that determined by visual inspection. These results are summarized in Table I, where the experimental and theoretical relative image sizes are compared at the first and second deflection of the derivative-shaped response. In addition, excellent agreement of predicted and experimental image intensity is apparent by qualitative comparison of Figs. 8 and 9 with Fig. 5, and by quantitative comparison in Table I. Fluctuation in the predicted intensity values (R.S.D. = 6%) is due to variability in the random-number generator utilized for the simulation. Despite this imprecision, these results clearly indicate that changes in both image size and intensity are responsible for the observed refractive index artifacts. The comparison of image size and intensity in Table I provides quantitative confirmation of the accuracy of the simulation model.

As the simulation results for the tetrahydrofuran–water system indicate, the predicted detector response is a direct outcome of the changing focal properties of the "solvent lens" within the cell. At any time during the simulation, only a fraction (7%) of the total axial gradient is contained within the flowcell. Therefore, the steepness of the axial gradient within the flowcell is continuously changing as different portions of the zone traverse the cell. This varying axial gradient, together with a constant radial gradient, continuously alters the angle of light rays traversing the cell. If both components of the gradient are positive, the result based on Snell's law (eqn. 1) is a decrease in image size. When the axial gradient is reversed, as occurs after the midpoint of the Gaussian function, the size of the resultant image becomes larger. This process defines the derivative-shaped response, showing first a decrease followed by an increase in size when the injection profile shows a maximum in refractive index. Under conditions of constant radial gradient (constant flow-rate), the magnitude of this change in size is directly dependent on the magnitude of the axial gradient (dn/dz). This supposition, based on optical considerations, is confirmed in both the simulation and experimental results for the tetrahydrofuran–water system. Although this system has a nearly linear dependence of refractive index on concentration, the magnitude of dn/dC and, hence, dn/dz is greater for injections of tetrahydrofuran into water than for water into tetrahydrofuran (Fig. 2), and the resulting change in image size is proportionally larger. Intensity changes are also directly related to the variations in the angle of the light rays during elution. For the light conditions simulated here, two factors contribute to the change in throughput of the cell. First, the acceptance angle of the cell is directly proportional to the axial refractive index gradient. Because this model utilizes a point source of radiation, as the gradient increases, the amount of light allowed into the cell also increases. Second, the exit of the flowcell can act as the aperture stop, limiting the angle of light rays leaving the flowcell. For an increase in the axial gradient, both these factors lead to an increased light throughput. Thus, the changes in the axial refractive index gradient within the cell alter the angle of light rays, resulting in variations in both the size and intensity of the detected image. Although the dynamic nature of the axial gradient causes these changes in the resultant image, both axial and radial gradients are necessary for this "solvent lens" effect.

To test the versatility of this model, further simulations employed the non-ideal

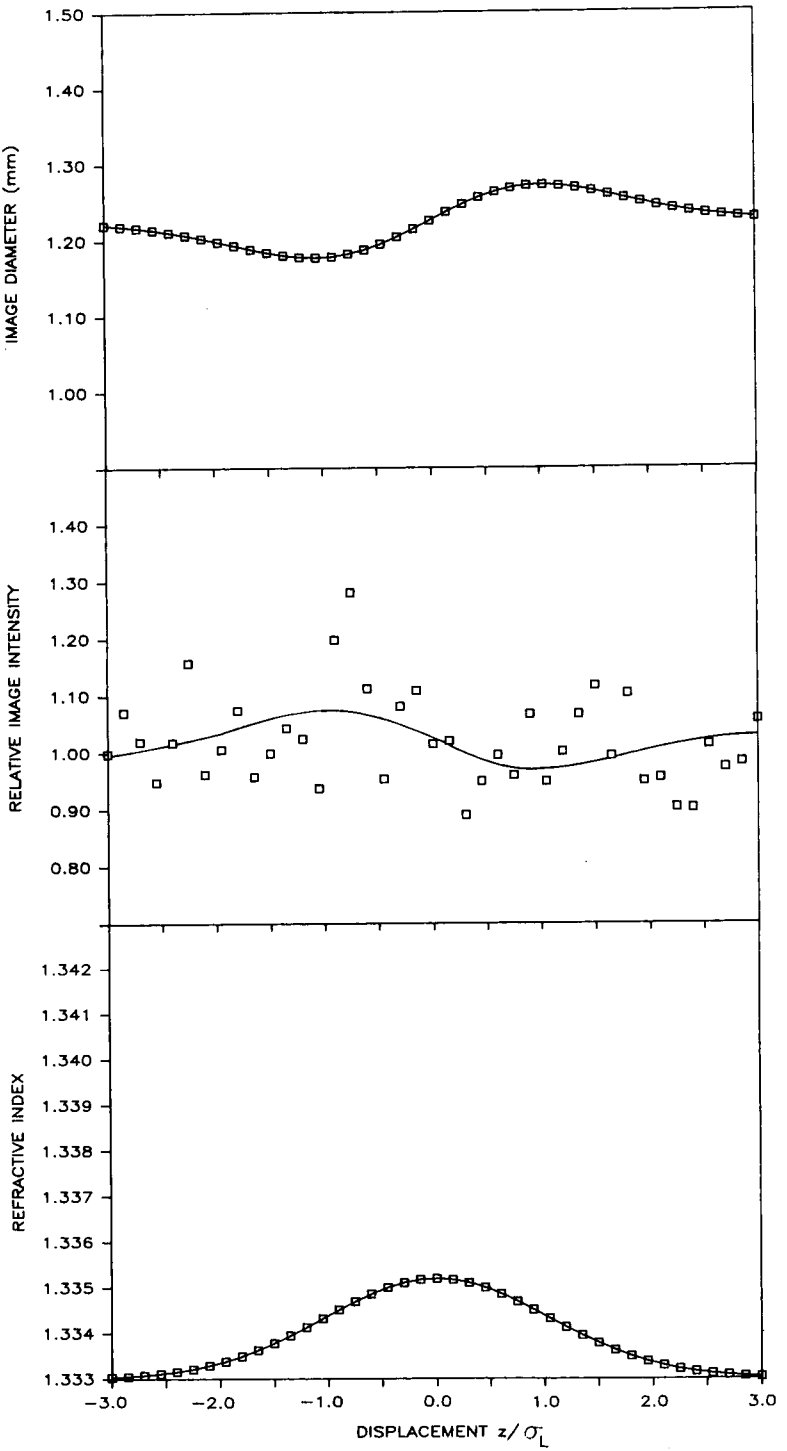

Fig. 10. Simulation results for methanol injected into water. Image diameter and overall relative intensity predicted for axial gradient shown at bottom of figure. Input parameters same as for Fig. 6.

methanol–water solvent system. In contrast to tetrahydrofuran–water, methanol–water exhibits a maximum in refractive index with concentration which is substantially greater than that of either pure solvent (Fig. 2). Yet, the predicted response illustrated in Figs. 10 and 11 shows excellent agreement in general shape and magnitude with the experimental response in Fig. 6. The quantitative comparison of image size and intensity for experimental measurement and theoretical prediction is given in Table II. The most interesting feature of the methanol–water system is that the direction of response (+/−), whether predicted (Figs. 10 and 11) or experimentally observed (Fig. 6), is identical for injection of methanol into water and *vice versa*. This similarity of response direction is a result of the maximum in refractive index *versus* concentration for the methanol–water solvent system. For this system, dn/dC is always positive when the zone profile at the detector has a concentration maximum less than 50% (v/v), even though methanol has a lower absolute refractive index than water. Dispersion of the plug injection for the methanol–water system results in a calculated concentration maximum of 14.6%. Because dC/dz is identical regardless of injection order (methanol–water or water–methanol), dn/dC determines both the sign and magnitude of the axial refractive index gradient (dn/dz). Consequently, dn/dz will always be of the same sign and the refractive index artifact will always be in the same direction. Thus, accurate prediction of even non-ideal solvent systems is possible with this gradient index model.

Limitations of the simulation model

As with any model, some simplifying assumptions are necessary to simulate experimental conditions. In this particular model, most assumptions arise from the flow conditions needed to describe the refractive index gradients induced upon injection of a pure solvent into a flowing stream. Whenever possible, all flow parameters have been chosen to be consistent with those experimentally examined. Concentration gradients are assumed to form from axial dispersion of an instantaneous injection described by the Taylor expression (eqns. 5 and 6). In practice, however, no injection is an ideal delta function and the resultant concentration profile may deviate from the predicted Gaussian shape. Moreover, any exponential mixing occurring in the region between the connecting tube and the flowcell will result in a modified Gaussian profile. A modified profile may indeed be expected due to the change in diameter between the tubing and the flowcell, as well as the right-angle entrance and exit of the Z-pattern flowcell. This abrupt change in flow path may influence not only the axial gradient, but the radial component as well. The Z-pattern design can give rise to an apparent bimodal flow path through the cell which results in complex radial gradients within the detector volume[19]. These gradients are not well understood or well characterized, therefore simulation of flow within the cell is limited at the present time to the parabolic profile described for a straight, round-bore tube.

External optical conditions also play a role in determining the intensity and size of the resultant image. For the simulation presented here, light incident on the flowcell was assumed to be divergent, effectively overfilling the entrance aperture. This is similar to many absorbance detector designs, where the exit of the monochromator acts as a point source of radiation for the flowcell. These light conditions, while true of the present detection system, are not representative of all systems. The model, however, can be adapted to the external optical configuration of any detector design.

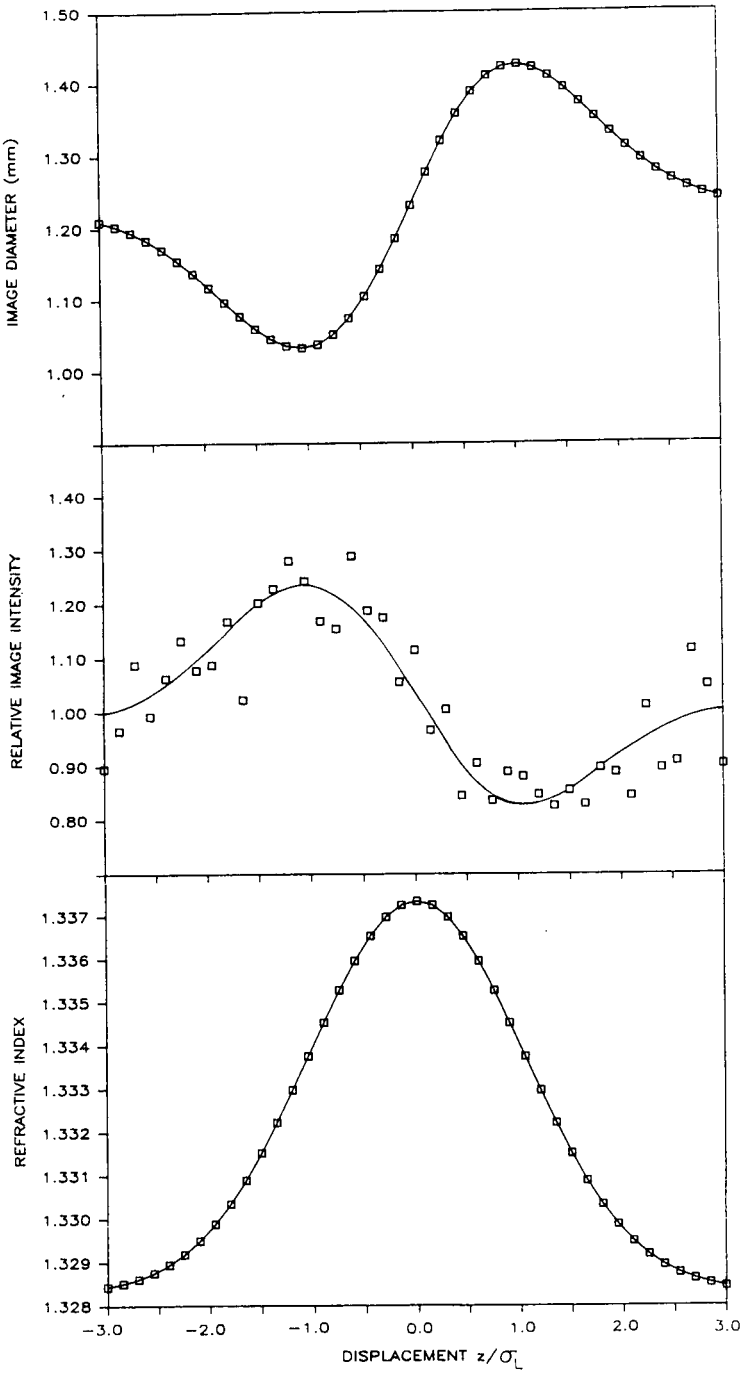

Fig. 11. Simulation results for water injected into methanol. Image diameter and overall relative intensity predicted for axial gradient shown at bottom of figure. Input parameters same as for Fig. 6.

Although the above assumptions have been necessary to describe flow and optical conditions in the detection system, a few additional assumptions have been necessitated by the software package utilized in the simulation. The Beam3 software requires that light rays strike all optical elements in the system in order to be detected. This restriction limits the simulation by not allowing light incident on the flowcell walls to continue through the simulated optical system. This is not true in many real flowcell designs, which contain polished interior walls allowing reflection of light. This assumption should result in attenuation of the simulated response, but the shape and direction of the signal would remain unchanged. In addition, the Beam3 software requires that the axial gradient be sequentially incremented, rather than continuously varied, through the flowcell. It is assumed that the minimum of 40 points across a profile accurately represents the continuous changes present under experimental conditions.

Finally, the basis of this model is that concentration gradients formed upon injection are the sole source of refractive index gradients within the flowcell. This cannot be entirely true due to the change in heat upon mixing of these polar solvents coupled with the temperature dependence of refractive index. The possible influence of temperature was investigated by injection of solvents at different temperatures. No visible change in the image size or intensity was observed with temperature fluctuation, and thus the predominant factor influencing the refractive index gradient in these studies was assumed to be the concentration gradient. However, with the knowledge of the refractive index dependence on temperature[20], this model could be modified to investigate this source of detector variability.

CONCLUSIONS

The refractive index response predicted by the dynamic-lens model shows excellent agreement in shape, magnitude, and direction with experimental measurement. This model provides a clearer understanding of the origins of this artifact, which will enable the development of improved flowcell designs for LC. For example, predicted changes in the image size emphasize the practical importance of photodetector size and alignment. In addition, the uniformity of response across the photodiode surface becomes essential when the detected image size and intensity are changing. This model makes possible the evaluation of such practical considerations as source alignment, illumination and collection optics, non-parallel windows and alternate flowcell designs. Equally important is the detailed understanding provided by this model of the factors influencing the refractive index signal. When these artifacts are used for chromatographic measurements, careful interpretation of the signal profile is required. If the peak maximum is used as a measure of retention time, for example, the characterization of column void volume or chromatographic system peaks will be substantially in error. This model is not limited to the simple injection profiles described herein, but is also applicable to more complex profiles arising from stepwise or linear gradient elution[21].

ACKNOWLEDGEMENTS

The authors are grateful to Julie Johnson (Michigan State University) for

technical assistance in implementation of the simulation model, to Jon Wahl (MSU) for the use of the chromatogram in Fig. 1, and to Hugh Montgomery (The Anspec Co.) for the kind loan of the solvent delivery system.

REFERENCES

1 L. R. Snyder and J. J. Kirkland, *Introduction to Modern Liquid Chromatography*, Wiley, New York, NY, 1979, p. 133.
2 D. Betteridge, E. L. Dagless, B. Fields and N. F. Graves, *Analyst (London)*, 103 (1978) 897.
3 D. J. Bornhop and N. J. Dovichi, *Anal. Chem.*, 58 (1986) 504.
4 J. Pawliszyn, *Anal. Chem.*, 58 (1986) 243.
5 J. W. Lyons and L. R. Faulkner, *Anal. Chem.*, 54 (1982) 1960.
6 J. Pawliszyn, *Anal. Chem.*, 58 (1986) 3207.
7 R. Synovec, *Anal. Chem.*, 59 (1987) 2877.
8 Y. F. Cheng and N. J. Dovichi, *Mikrochim. Acta*, 1986III (1986) 351.
9 J. N. Little and G. J. Fallick, *J. Chromatogr.*, 112 (1975) 389.
10 J. E. Stewart, *Appl. Opt.*, 20 (1981) 654.
11 J. E. Stewart, *Anal. Chem.*, 53 (1981) 1125.
12 W. Heller, *J. Phys. Chem.*, 69 (1965) 1123.
13 G. Taylor, *Proc. Roy. Soc. (London)*, A219 (1953) 186.
14 M. J. E. Golay, in D. H. Desty (Editor), *Gas Chromatography 1958*, Academic Press, New York, NY, 1958, p. 36.
15 J. J. VanDeemter, F. J. Zuiderweg and A. Klinkenberg, *Chem. Eng. Sci.*, 5 (1956) 271.
16 J. H. Knox, *J. Chromatogr. Sci.*, 15 (1977) 352.
17 C. R. Wilke and P. Chang, *AIChE J.*, 1 (1955) 264.
18 R. Aris, *Proc. Roy. Soc. (London)*, A235 (1956) 67.
19 K. Peck and M. D. Morris, *J. Chromatogr.*, 448 (1988) 193.
20 N. J. Dovichi, T. G. Nolan and W. A. Weimer, *Anal. Chem.*, 56 (1984) 1700.
21 C. E. Evans and V. L. McGuffin, in preparation.

Journal of Chromatography, 459 (1988) 139–149
Elsevier Science Publishers B.V., Amsterdam — Printed in The Netherlands

CHROMSYMP. 1477

RHODAMINE LABELLING REAGENT FOR THE DETERMINATION OF CHLOROPHENOLS BY LIQUID CHROMATOGRAPHY WITH PEROXY-OXALATE CHEMILUMINESCENCE DETECTION

P. J. M. KWAKMAN, J. G. J. MOL, D. A. KAMMINGA, R. W. FREI, U. A. Th. BRINKMAN and G. J. DE JONG*

Department of Analytical Chemistry, Free University, De Boelelaan 1083, 1081 HV Amsterdam (The Netherlands)

SUMMARY

Lissamine Rhodamine B sulphonyl chloride was applied as a pre-column labelling reagent for the peroxyoxalate chemiluminescence detection of phenolic compounds. The advantages of rhodamine labels are the high quantum yield, the long wavelength emission (>550 nm), which permits a considerable reduction of the chemiluminescence background, and the fact that electronegative heavy atom substituents do not quench the chemiluminescence.

By using a two-phase derivatization, the labelling procedure for chlorophenols can be made quantitative in 1 min at room temperature. The sensitivity of the method is limited by contaminants present even in the purified reagent and the formation of by-products during derivatization. For reversed-phase liquid chromatography, the oxalate and hydrogen peroxide were premixed in acetonitrile and added to the column effluent. For normal-phase liquid chromatography studies, the oxalate was dissolved in toluene–acetonitrile and pumped through a perhydrit reactor before its addition to the column effluent. The detection limits for several chlorophenols in both the reversed- and normal-phase systems are in the low picogram range.

INTRODUCTION

Peroxyoxalate chemiluminescence (CL) detection has been shown to be a highly sensitive detection principle for column liquid chromatography (LC)[1–7]. However, most analytes do not possess good chemiluminescence properties and derivatization is therefore necessary. Polycyclic aromatic compounds which exhibit good fluorescence properties, such as perylene derivatives[4,8], or small aromatic ring systems with electron-donating substituents, such as dimethylaminonaphthalene derivatives[1–3,6,7,9], are suitable labels for CL detection. Generally, the CL labels should have a low oxidation potential and a singlet excitation energy lower than about 105 kcal/mol, *i.e.*, an excitation wavelength higher than about 272 nm[10].

Sigvardson and Birks[5] investigated the inherent CL background emission and concluded that a weak emission occurs with a maximum at 440 nm. This background

0021-9673/88/$03.50

emission appears to be the main factor which limits the sensitivity of the method. Unfortunately, the major part of the background emission occurs in the wavelength region where most CL labels emit themselves. Therefore, it would be advantageous to apply labels with emission maxima at wavelengths of 550 nm or longer. In this case the CL background can be efficiently reduced by using a suitable filter. Recently, Metrione[11] described the application of Lissamine Rhodamine B sulphonyl chloride (laryl chloride) as a fluorescent label for the LC and thin-layer chromatographic (TLC) detection of amino acids. These rhodamine-type derivatives have an emission maximum at 595 nm and are well known for their excellent CL properties[4].

In this paper the application of laryl chloride as a pre-column labelling reagent for phenolic compounds in LC with peroxyoxalate CL detection is described. The labelling procedure involves ion-pair extraction of the deprotonated phenol with a tetrabutylammonium counter ion to an organic phase in which the non-polar derivatization reagent is dissolved[12]. CL detection was not only coupled with reversed-phase LC, but also a CL detection system for normal-phase LC was developed. The latter system seemed promising because, in general, luminescence detection is favoured by the use of relatively non-polar media[13].

EXPERIMENTAL

Chemicals

HPLC-grade solvents were purchased from Baker (Deventer, The Netherlands). Bis (2,4,6-trichlorophenyl) oxalate (TCPO), bis(2-nitrophenyl) oxalate (2-NPO) and bis(2,4-dinitrophenyl)oxalate (DNPO) were synthesized as described in the literature[14]. Lissamine Rhodamine B sulphonyl chloride (laryl chloride, see Fig. 1) was purchased from Kodak (Weesp, The Netherlands). Tetrabutylammonium iodide and perhydrit tablets (hydrogen peroxide held on a urea support) were bought from Merck (Darmstadt, F.R.G.), 3,5-dichlorophenol, 2,4,6-trichlorophenol and 2,3,4,5-tetrachlorophenol from Aldrich (Beerse, Belgium) and pentachlorophenol from Merck. All other chemicals were of analytical-reagent grade.

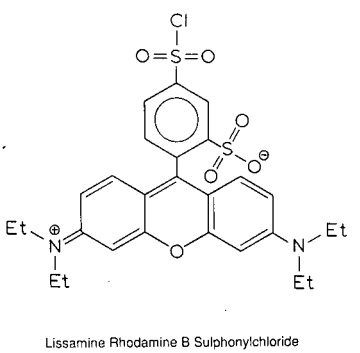

Fig. 1. Structure of Lissamine Rhodamine B sulphonyl chloride. Et = C_2H_5.

Column liquid chromatography

In the reversed-phase system the mobile phase was delivered by a Gilson Model 302 pump equipped with a Gilson Model 308 manometric module (Gilson, Villiers-le Bel, France). A Valco injection valve with a 25-μl loop was used for the introduction of samples on to a 150 × 3.1 mm I.D. analytical column packed by a slurry technique with 5-μm LiChrosorb RP-18 (Merck). Reversed-phase LC was carried out with acetonitrile–imidazole nitrate buffer (10 m*M* pH 7.0) (75:25, v/v) at a flow-rate of 0.5 ml/min as the eluent. In the normal-phase system, a Gilson Model 302 pump was used to deliver the LC mobile phase. A Valco injection valve with a 14-μl loop was used for injection on to a 250 × 3.1 mm I.D. 5-μm LiChrosorb Si 60 (Merck) silica column. Chromatography was carried out using a mobile phase of toluene–acetonitrile–methanol (60:40:5, v/v/v) containing 5 m*M* imidazole.

Detection systems

The reversed-phase system is shown schematically in Fig. 2a. Hydrogen peroxide and 2-NPO dissolved in acetonitrile at final concentrations of 50 and 10 m*M*, respectively, were mixed just before use and added to the column effluent with a

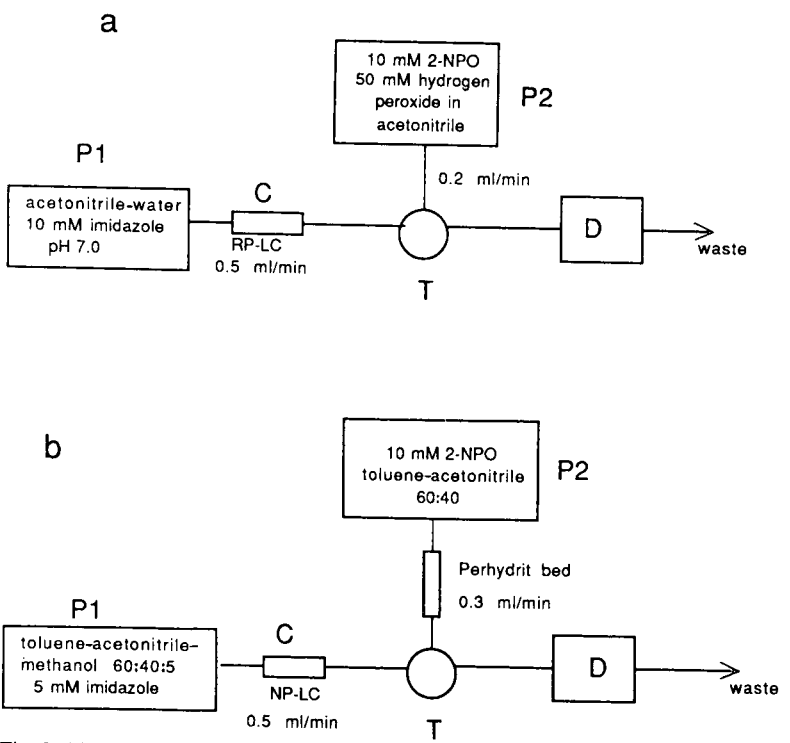

Fig. 2. (a) Schematic diagram of reversed-phase (RP) system: P1 = LC pump; C = LC column; P2 = pulseless syringe pump; T = tee-piece; D = Kratos detector. (b) Schematic diagram of normal-phase (NP) system: P1 = LC pump; C = LC column; P2 = pulseless syringe pump with perhydrit bed in-line; T = tee-piece; D = photomultiplier housing with 80-μl flow cell. For chromatographic details, see Experimental.

pulseless Isco (Lincoln, NE, U.S.A.) μLC-500 syringe pump. The mobile phase (0.5 ml/min) and the reagent (0.2–0.4 ml/min) were mixed using a standard Valco T-piece immediately in front of the detector. A Kratos (Ramsey, NJ, U.S.A.) FS 970 fluorescence detector equipped with a 2π steradian mirror, with the lamp turned off, a laboratory-made 50-μl flow cell[15] and a 580-nm emission cut-off filter were used for detection.

The set-up for the normal-phase system is shown schematically in Fig. 2b. A laboratory-made pulseless syringe pump delivered a 10 m*M* solution of oxalate (TCPO or 2-NPO) in toluene–acetonitrile (60:40, v/v). This solution was pumped through a 100 × 4.6 mm I.D. perhydrit column (containing *ca.* 1.7 g of perhydrit) and added to the LC column effluent. The flow-rates of the mobile phase and the reagent stream were 0.5 and 0.3 ml/min, respectively. A laboratory-made photomultiplier housing with an Oriel 7070 power supply[16] and a laboratory-made 80-μl quartz flow cell with a 570-nm cut-off filter were used. The Model RCA 1P-28 photomultiplier tube was typically operated at 750 V.

Labelling of chlorophenols with laryl chloride

To 500 μl of a solution of chlorophenols in a 0.02 *M* carbonate buffer (pH 9.0), 100 μl of 0.2 *M* tetrabutylammonium iodide in acetone–water (1:1, v/v) were added, then 500 μl of a 0.5 mg/ml solution laryl chloride in hexane–toluene–acetonitrile (4:3:1, v/v/v) were added and the two-phase mixture was whirl-mixed for 60 s. For trace-level analysis the 0.5 mg/ml laryl chloride solution was diluted 10-fold. Next, 50 μl of a concentrated (*ca.* 2 *M*) propylamine solution in water were added to remove the unreacted laryl chloride and the solution was mixed for a further 60 s, then 400 μl of the organic layer were evaporated to dryness and the residue was dissolved in 500 μl of mobile phase.

RESULTS AND DISCUSSION

Derivatization conditions

In the literature[17], the derivatization of phenolic compounds with dansyl chloride is usually carried out in acetone for about 30 min at elevated temperatures with, *e.g.*, solid potassium carbonate as a base. Recently, De Ruiter *et al.*[12] have developed a fast two-phase derivatization for the selective dansylation of chlorophenols. The chlorophenols, in their nucleophilic anionic form, are extracted as a tetrabutylammonium ion-pair from an aqueous solution into an organic phase containing the fluorescent label. This procedure allows a rapid derivatization and an easy separation of the analyte of interest from the intensely fluorescent hydrolysis product, which remains in the aqueous phase. In principle this system works for every apolar label able to react with extracted nucleophiles.

By making minor adjustments to the procedure in ref. 12, it was possible to apply laryl chloride as a highly chemiluminescent label for chlorophenols. Dissolving laryl chloride in dichloromethane or chloroform gave rise to very large interfering peaks; therefore, toluene–hexane mixtures were used instead. In addition, a small percentage of acetonitrile had to be added to improve the solubility of laryl chloride; an organic phase of hexane–toluene–acetonitrile (4:3:1) appeared to be the best choice. The derivatization time was optimized by varying the mixing time prior to the

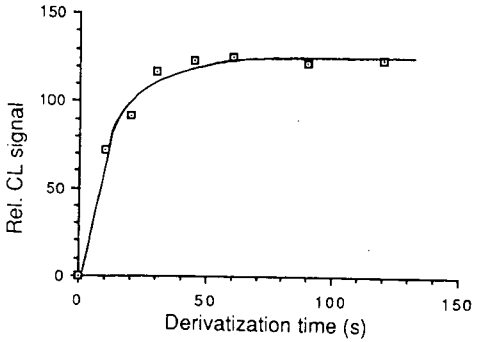

Fig. 3. Dependence of laryl derivative formation on reaction time. The derivatization time was varied by changing the addition time of the concentrated aqueous propylamine solution for removal of the excess of laryl chloride.

addition of the propylamine solution. After about 60 s of whirl-mixing at room temperature no further gain in signal was obtained (see Fig. 3).

Characteristics of laryl chloride as a CL label

The main advantage of rhodamine-type compounds is the high CL quantum yield[4] combined with its red emission wavelength (λ_{em} = 595 nm), which allows the use of an emission filter with a cut-off above 550 nm and, hence, a reduction of the CL background. When using the filter, a signal-to-noise (S/N) gain by a factor of 10 was obtained in the reversed-phase system and by a factor of 5 in the normal-phase system. Also, ultrapure and expensive solvents are no longer required, because the presence of impurities emitting above 550 nm is unlikely. In the reversed-phase system, which uses acetonitrile and water as solvents, it was sufficient to distil the LC column effluent only once (as its acetonitrile–water azeotrope) to be able to re-use it as the LC mobile phase with the same noise level as before.

A further advantage of the laryl chloride label is that, in principle, the CL (and the fluorescence) quantum yield will be the same for every chlorophenol derivative. With dansylated chlorophenols the number and position of the chlorine atoms strongly influence the fluorescence quantum yield; for example, chlorine atoms in the positions *ortho* to the hydroxyl group act as strong quenchers, and derivatives with four or five chlorine atoms hardly fluoresce at all[18]. With laryl chloride, the luminescence characteristics will be mainly determined by the heterocyclic ring system and not by the side ringe which is used for derivatization. Therefore, the CL quantum yield of a pentachlorophenol derivative will be equal to that of, *e.g.*, a disubstituted phenol derivative. In other words, a single calibration graph for each LC system (in peak area units) should, in principle, be sufficient for all chlorophenols. This was confirmed experimentally in both reversed-phase and normal-phase LC by measuring the peak areas for the laryl derivatives of 3,5-dichloro-, 2,4,6-trichloro-, 2,3,4,5-tetrachloro- and pentachlorophenol. For all laryl derivatives the ratio of peak area to moles of chlorophenol was the same, within experimental error.

A serious disadvantage of the present label is its impurity and the formation of by-products during derivatization. For purification of the reagent simple approaches

such as recrystallization and filtration were applied without any real success. Preparative LC on a 200 × 3.1 mm I.D. cyano-bonded column with acetonitrile as the mobile phase led to only a minor improvement in the reagent purity. Finally, it was found that 10-fold dilution of the laryl chloride solution dramatically reduced the interfering peaks. This was partly caused by the simple fact of diluting the impurities present in the reagent and partly by slower by-product formation. The amount of the (unknown) by-products formed not only increases with increasing time of derivatization, but obviously also with increasing laryl chloride concentration. As a result, for trace levels (1–400 ppb*) of chlorophenols, the use of a diluted laryl chloride solution is recommended; for concentrations of over 400 ppb the undiluted laryl chloride solution (see Experimental) should be used.

Chemiluminescence detection

Reversed-phase LC. In order to elute the apolar laryl derivatives of the chlorophenols with acceptable peak shape and retention, the mobile phase acetonitrile–water (75:25, v/v) was used. Usually the addition of a solution of TCPO in ethyl acetate to an aqueous mobile phase causes mixing and precipitation problems. These problems were avoided by dissolving 2-NPO (10 m*M*) and hydrogen peroxide (50 m*M*) in acetonitrile. 2-NPO was chosen because of its high CL intensity, slow decay of signal intensity, good solubility in acetonitrile and high stability[4].

The rate of the CL reaction mainly depends on the concentration of imidazole in the mobile phase[7]. This concentration was varied from 25 to 2.5 m*M* at a pH of 7.0 (see Fig. 4). The best S/N ratio was obtained with 10 m*M* imidazole and this concentration was maintained throughout all reversed-phase LC experiments. The 2-NPO concentration in the reagent stream was varied between 1 and 20 m*M* (see Fig. 5). The CL signal first increases rapidly with increasing 2-NPO concentration, but between 10 and 20 m*M* the increase is nearly negligible. In order to prevent possible precipitation of 20 m*M* 2-NPO its addition to the aqueous mobile phase, 10 m*M* was chosen for all further work. The hydrogen peroxide concentration was varied between 500 and 25

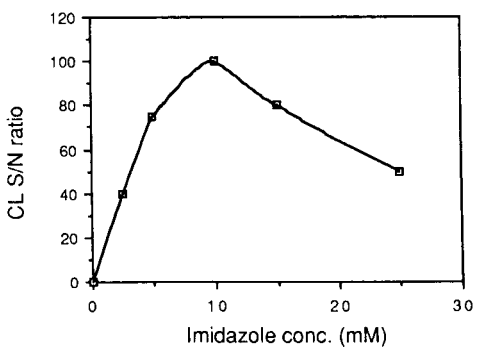

Fig. 4. Effect of imidazole concentration in the mobile phase on CL S/N ratio (10 m*M* 2-NPO; 50 m*M* hydrogen peroxide; 1.7 ng of laryl-2,4,6-trichlorophenol). For other conditions, see Experimental.

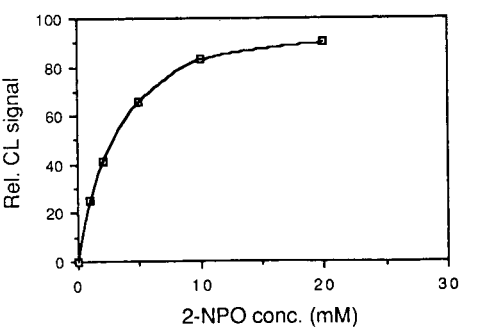

Fig. 5. Influence of oxalate concentration in the reagent stream on CL intensity (50 m*M* hydrogen peroxide; 10 m*M* imidazole; 1.7 ng of laryl-2,4,6-trichlorophenol). For other conditions, see Experimental.

* Throughout the article the American billion (10^9) is meant.

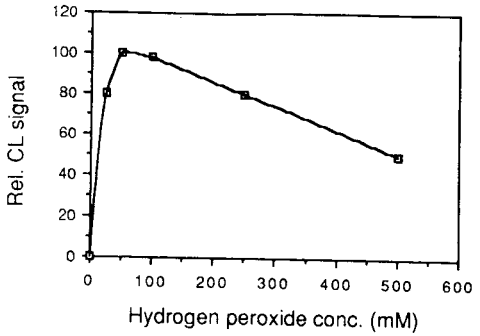

Fig. 6. Effect of hydrogen peroxide concentration in the reagent stream on CL intensity (10 m*M* 2-NPO; 10 m*M* imidazole; 1.7 ng of laryl-2,4,6-trichlorophenol). For other conditions, see Experimental.

m*M*, and an optimum was found at 50 m*M* (see Fig. 6). The rate of the CL reaction at high hydrogen peroxide concentrations seemed to be too fast, which resulted in the loss of a major part of the CL signal prior to the flow cell[15]. In addition, the mixture of 2-NPO and hydrogen peroxide turned out to be less stable at higher hydrogen peroxide (and hence water) concentrations. The solution of 10 m*M* 2-NPO and 50 m*M* hydrogen peroxide in acetonitrile was stable for at least 4 h at room temperature. It could even be stored overnight at −20°C with less than 1% loss in CL intensity, as measured by the injection of a standard rhodamine solution. Varying the flow-rate of the reagent mixture from 0.5 to 0.2 ml/min did not reduce the S/N ratio; 0.2 ml/min was preferred, because the 50-ml syringe pump volume then needed refilling only once every 4 h.

Normal-phase LC. In normal-phase solvents such as hexane and chloroform the fluorescence quantum yield is often higher than under reversed-phase conditions. In the present system, with a fairly high percentage of acetonitrile a small percentage of methanol was also necessary in order to elute the laryl derivatives with acceptable capacity factors and peak shape. Consequently, the polarity of the mobile phase was not as low as required for a real gain in CL quantum yield and, as is reported below, the limits of detection turned out to be essentially the same in both the reversed- and normal-phase systems.

Recently, Nozaki *et al.*[19] described a normal-phase LC system with peroxyoxalate CL detection, using separate pumps for the addition of the hydrogen peroxide and oxalate solutions. An aqueous hydrogen peroxide solution was added to methanol containing an acetate buffer; that is, the CL detection was still carried out under semi-aqueous conditions. In the non-aqueous system described in this paper, it sufficed to use only one reagent pump, *viz.*, by inserting the perhydrit column already described in an earlier paper[9]. A hydrogen peroxide concentration of about 13 m*M* was obtained by pumping a solution of 2-NPO or TCPO [10 m*M* in toluene–acetonitrile (60:40, v/v)] through a 100 × 4.6 mm I.D. perhydrit column; the oxalate concentration had been optimized by varying it between 2.5 and 20 m*M*. DNPO could not be used because of the rapid hydrolysis of this ester in the perhydrit column, as shown by the appearance of an intense yellow colour. Changing the toluene–acetonitrile ratio from 60:40 to 40:60 was expected to increase the hydrogen peroxide

concentration in the reagent stream. However, no increase in signal was found; therefore, it can be concluded that the concentration of hydrogen peroxide was already optimal at 40% acetonitrile.

The hydrogen peroxide concentration of 13 m*M* was calculated by running parallel experiments with a known amount of aqueous hydrogen peroxide in the reagent solution. This method of adding hydrogen peroxide could not be used routinely, because of the frequent formation of precipitates in the capillary inserted after the T-piece. The concentration of 13 m*M* hydrogen peroxide is in sharp contrast with the 600 m*M* concentration utilized in the normal-phase system described by Nozaki *et al.*[19] A direct comparison between both normal-phase systems cannot be made, because the systems are essentially different regarding, *e.g.*, the mobile phase modifiers, the amount of water in the solvent stream passing the flow-cell and the type of catalyst.

As with the reversed-phase system, the rate of the CL reaction is influenced most by the imidazole concentration in the mobile phase. Varying this concentration between 20 and 2.5 m*M* showed 5 m*M* imidazole to be the optimal concentration. Under these conditions the rate of the CL reaction is in the same range (less than about 30 s) as in the reversed-phase system.

Analytical data

In both the reversed- and normal-phase systems the linearity was measured by diluting a solution of derivatized 2,4,6-trichlorophenol in the range 5–500 ppb of trichlorophenol. The systems showed excellent linearity over more than two orders of magnitude (normal-phase system, $n = 9$, $r = 0.9998$; reversed-phase system, $n = 9$, $r = 0.9995$). The limits of detection (S/N = 3) were 3–4 pg (15–20 fmol) in both LC systems.

The performance of the laboratory-made photomultiplier housing was checked by comparing this detection system with the Kratos FS 970 detector with a 2π steradian mirror. Surprisingly, the S/N ratio was the same for both detection systems. This indicates that expensive fluorimeters are not really required for CL measurements.

The linearity of the derivatization reaction was tested by varying the chlorophenol concentration from 500 to 5 ppb. Initially, detection in the low-ppb range was limited by the appearance of large interfering peaks in the chromatogram. Use of the 0.05 mg/ml laryl chloride solution (see above) considerably reduced these interferences without influencing the linearity (normal-phase system, $N = 7$, $r = 0.9993$; reversed-phase system, $n = 7$, $r = 0.9991$).

A normal-phase chromatogram of 40 pg of the derivatized 2,4,6-trichlorophenol (obtained by 100-fold dilution of the derivative) is shown in Fig. 7a and the result of a direct derivatization of a 5-ppb trichlorophenol solution (66-pg loop injection) in Fig. 7b. A reversed-phase chromatogram of 44 pg of the derivatized 2,4,6-trichlorophenol (obtained by 50-fold dilution of the derivative) is shown in Fig. 8a and a direct derivatization of a 9-ppb solution (225-pg loop injection) in Fig. 8b. It is obvious that the chromatograms in Figs. 7b and 8b contain more interfering peaks than those in Figs. 7a and 8a. In practice, the detection limits of the various chlorophenols are about three times higher than those obtained when diluting a relatively concentrated stock solution, *i.e.*, they are about 10 pg (50 fmol).

As an application, Fig. 9 shows the reversed-phase LC analysis of Amstel river

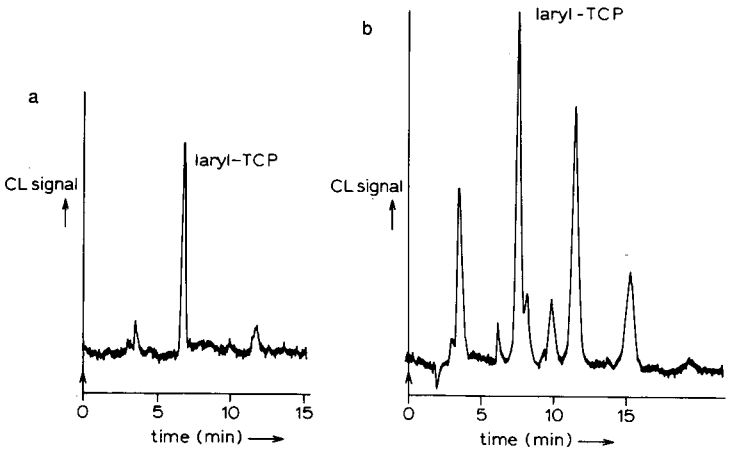

Fig. 7. (a) Normal-phase chromatogram of 40 pg of the laryl derivative of 2,4,6-trichlorophenol (laryl-TCP), obtained by 100-fold dilution of a relatively concentrated stock solution. (b) Normal-phase chromatogram of 66 pg of laryl-TCP, obtained by direct derivatization of a 5-ppb chlorophenol solution. For derivatization and LC conditions, see Experimental.

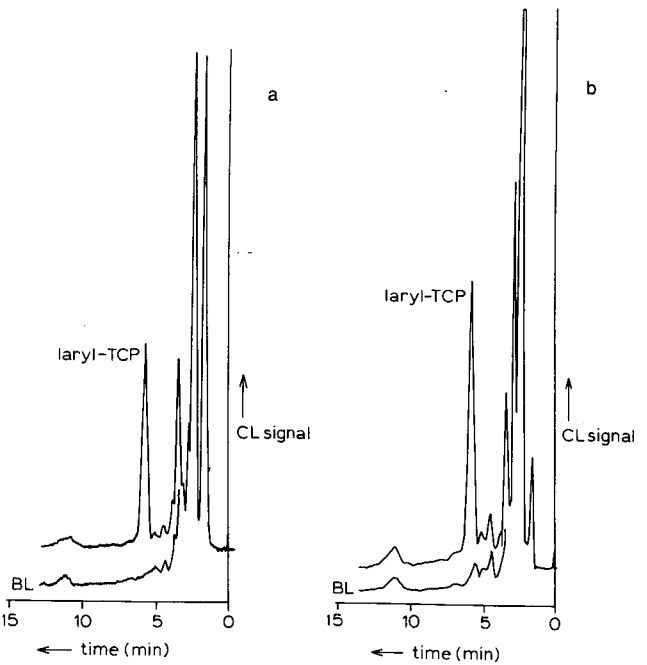

Fig. 8. (a) Reversed-phase chromatogram of 44 pg of laryl-TCP, obtained by 50-fold dilution of a relatively concentrated stock solution. The sensitivity of the detector is about three times higher than that in Fig. 8b. (b) Reversed-phase chromatogram of 225 pg of laryl-TCP, obtained by direct derivatization of a 9-ppb chlorophenol solution. Blanks (BL) are shown as reference. For derivatization and LC conditions, see Experimental.

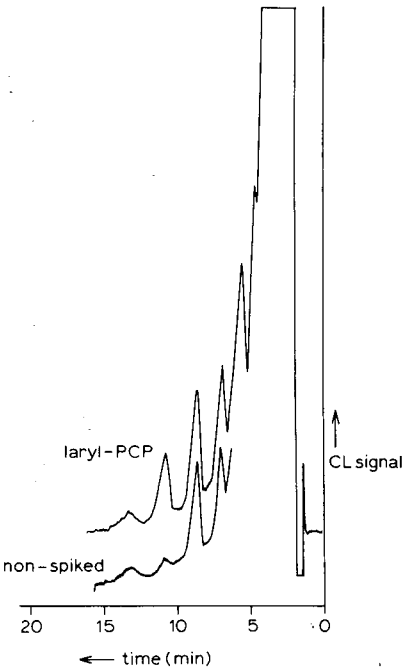

Fig. 9. Reversed-phase chromatogram of Amstel river water without and with 0.8 ppb pentachlorophenol spike; 200-μl loop injection (derivative indicated as laryl-PCP). For derivatization and LC conditions, see Experimental.

water spiked with 0.8 ppb of pentachlorophenol. The derivatization was carried out directly on the sample without any preconcentration or clean-up step(s). Peak compression occurring on the top of the analytical column allowed the use of a 200-μl injection volume (10% acetonitrile in water), which yielded an 8-fold higher sensitivity than with our conventional 25-μl loop injections. Under these conditions, the detection limit of pentachlorophenol in Amstel water is about 0.2 ppb when using only a 0.5-ml sample. If necessary, the result can be further improved by combining preconcentration with clean-up, *e.g.*, on a C_{18} precolumn.

CONCLUSIONS

Laryl chloride can be utilized as a sensitive labelling reagent for the selective two-phase derivatization of chlorophenols with subsequent CL detection. Detection limits in both the reversed- and normal-phase modes are in the low picogram range.

The main advantages of the rhodamine-type labels are the possibility of filtering out part of the CL background and the fact that electronegative heavy-atom substituents do not quench the CL signal. With laryl chloride, the presence of impurities and the formation of by-products still limit its applicability and other types of rhodamines are therefore currently being studied.

Although peroxyoxalate CL detection in normal-phase LC systems is, in principle, a promising approach, the results of this work do not show any gain in sensitivity

compared with reversed-phase systems. This is probably due to the high polarity of the label, which is caused by the presence of the second sulphonate group, which necessitates the addition of relatively large amounts of polar modifiers to the mobile phase. In other words, the gain in CL quantum yield should be more pronounced when working with less polar labels, which will allow LC elution with, *e.g.*, hexane–chloroform mixtures (provided that optimal hydrogen peroxide concentrations can be reached). Future research will deal with this aspect.

ACKNOWLEDGEMENTS

The authors are grateful to J. H. M. van den Berg and N. G. F. M. Lammers of Duphar B.V. and C. de Ruiter for stimulating discussions. This work was supported by Duphar B.V. and the Dutch Foundation of Technical Sciences (S.T.W.) under grant No. 700-349-1301.

REFERENCES

1 K. Kobayashi and K. Imai, *Anal. Chem.*, 52 (1980) 424.
2 K. Miyaguchi, K. Honda and K. Imai, *J. Chromatogr.*, 303 (1984) 173.
3 K. Imai, Y. Matsunaga, Y. Tsukamoto and A. Nishitani, *J. Chromatogr.*, 400 (1987) 169.
4 K. Honda, K. Miyaguchi and K. Imai, *Anal. Chim. Acta*, 177 (1985) 104 and 111.
5 K. W. Sigvardson and J. W. Birks, *Anal. Chem.*, 55 (1983) 432.
6 T. Koziol, M. L. Grayeski and R. Weinberger, *J. Chromatogr.*, 317 (1984) 355.
7 G. J. de Jong, N. Lammers, F. J. Spruit, C. Dewaele and M. Verzele, *Anal. Chem.*, 59 (1987) 1458.
8 B. Mann and M. L. Grayeski, *J. Chromatogr.*, 386 (1987) 149.
9 P. J. M. Kwakman, U. A. Th. Brinkman, R. W. Frei, G. J. de Jong, F. J. Spruit, N. G. F. M. Lammers and J. H. M. van den Berg, *Chromatographia*, 24 (1987) 395.
10 C. L. R. Catherall, T. F. Palmer and R. B. Cundall, *J. Chem. Soc., Faraday Trans. 2*, 80 (1984) 823.
11 R. M. Metrione, *J. Chromatogr.*, 363 (1986) 337.
12 C. de Ruiter, R. R. Otten, U. A. Th. Brinkman and R. W. Frei, *J. Chromatogr.*, 436 (1988) 429.
13 M. Zander, *Fluorimetrie*, Springer, Berlin, 1981, Ch. 3.
14 A. G. Mohan and N. J. Turro, *J. Chem. Educ.*, 51 (1974) 528.
15 G. J. de Jong, N. Lammers, F. J. Spruit, R. W. Frei and U. A. Th. Brinkman, *J. Chromatogr.*, 353 (1986) 249.
16 G. Gübitz, P. van Zoonen, C. Gooijer, N. H. Velthorst and R. W. Frei, *Anal. Chem.*, 57 (1985) 2071.
17 L. A. Sternson, in R. W. Frei and J. F. Lawrence (Editors), *Chemical Derivatization in Analytical Chemistry*, Plenum Press, New York 1981.
18 C. de Ruiter, J. F. Bohle, G. J. de Jong, U. A. Th. Brinkman and R. W. Frei, *Anal. Chem.*, 60 (1988) 666.
19 O. Nozaki, Y. Ohba and K. Imai, *Anal. Chim. Acta*, 205 (1988) 255.

Journal of Chromatography, 459 (1988) 151–162
Elsevier Science Publishers B.V., Amsterdam — Printed in The Netherlands

CHROMSYMP. 1463

OXIDATIVE DETECTION OF COULOMETRICALLY REDUCED ORGANONITRO PESTICIDES IN REVERSED-PHASE HIGH-PERFORMANCE LIQUID CHROMATOGRAPHY

RICHARD T. KRAUSE* and YI WANG*
Division of Contaminants Chemistry, Food and Drug Administration, Washington, DC 20204 (U.S.A.)

SUMMARY

A high-performance liquid chromatographic system is presented for determination of organonitro pesticides, metabolites and industrial chemicals having a variety of chemical structures. The compounds are chromatographed on a C_8 column with an acetonitrile–aqueous ammonium monochloroacetate gradient. The chromatographic responses of the compounds are monitored indirectly by oxidative detection of the coulometrically reduced organonitro functionality by means of a porous-graphite detector. Three nitrophenols (2,4-dinitrophenol, 4,6-dinitro-*o*-cresol and dinoseb), a dinitrophenyl aliphatic ester (binapacryl) and a nitroaniline (dicloran) were detected at low nanogram levels (3–10 ng for 50% recorder full-scale deflection). This technique overcomes the problems of high background currents and oxygen interference, observed in the direct reductive detection of organonitro compounds.

INTRODUCTION

The determination of analytes at residue levels in complex matrices requires a technique which separates the individual analytes and selectively detects the compounds of interest. Such multiresidue analytical approaches have been applied to the gas–liquid chromatographic (GLC) separation and selective detection of volatile organohalogen, organophosphorus and organonitrogen pesticides in food[1]. The electroconductivity detector in the halogen mode and the flame photometric detector in the phosphorus mode are highly selective for detection of organohalogen and organophosphorus pesticides, respectively. Volatile organonitrogen pesticides can be detected with the electroconductivity detector in the nitrogen mode. However, because of the large number of natural and man-made organonitrogen compounds, the practical selectivity is less than that desired. In addition, many toxic organonitrogen contaminants are not amenable to GLC since they are non-volatile and/or heat labile. This problem was solved for the N-methylcarbamate insecticides by using high-performance liquid chromatography (HPLC) to separate the heat-labile compounds; the N-

* Guest Scientist, The Institute of Plant Protection, Beijing, China.

0021-9673/88/$03.50

methylcarbamate moiety was selectively detected by a post-column fluorometric labeling technique[2–4].

The nitro functionality is contained in numerous pesticides, toxic metabolites, and industrial pollutants. A determinative technique was desired which could separate these organonitro compounds (nitrophenols, nitroanilines, nitrophorothioates, nitrodiphenyl ethers and nitrophenyl aliphatic esters) and selectively detect the nitro functionality at residue levels. A few organonitro pesticides and industrial chemicals can be determined by multiresidue methods (*e.g.* binapacryl[5,6], dicloran[1,5], parathion[5–7], dinoseb[6] and 4-nitrocresol[8]). However, the detection techniques (electron-capture, flame-photometric and thermionic detectors) do not selectively detect the nitro functionality, or the detector responds to another functionality in the compound. In addition, nitrophenols require derivatization[6,8] before determination by GLC. The nitrophenols have been chromatographed directly by HPLC, and the eluted compounds were monitored with a UV detector[9,10]. However, because of the multitude of UV-absorbing compounds, the UV detector does not have the selectivity needed for a residue determinative technique.

Organonitro compounds are electrochemically reducible and can therefore be detected by electrochemical detection (ED). Only a few other functionalities (azo, imine, N-oxide, quinone and nitrosamine) undergo electrochemical reduction[11]. Thus ED can provide a fair degree of selectivity for the nitro functionality. The purpose of the work reported here was to determine the feasibility of using HPLC to separate a variety of organonitro pesticides, toxic metabolites, and industrial chemicals, and of detecting the eluted analytes by ED.

EXPERIMENTAL

Chemicals

The organonitro compounds were obtained from the Environmental Protection Agency, Pesticide and Industrial Chemicals Repository (Research Triangle Park, NC, U.S.A.). All organonitro compounds were dissolved and dilutions were made in distilled-in-glass-grade methanol (Burdick & Jackson Labs., Muskegon, MI, U.S.A.). The acetonitrile was Burdick & Jackson distilled-in-glass UV grade. HPLC water was produced by a Milli-Q water system (Millipore, Bedford, MA, U.S.A.), consisting of prefilter, charcoal, ion-exchange and Organex cartridges. Monochloroacetic acid (MCA), Fisher Certified grade (Fisher Scientific, Fairlawn, NJ, U.S.A.), ammonium hydroxide (30%), Baker Analyzed Reagent grade (J.T. Baker, Phillipsburg, NJ, U.S.A.) and Milli-Q-purified water were used to prepare the aqueous 0.5 *M* MCA solution, adjusted to pH 2.70 with ammonium hydroxide.

Apparatus

Initial electrochemical data for the organonitro compounds were obtained with a Model CV-27 cyclic voltammograph (Bioanalytical Systems, West Lafayette, IN, U.S.A.). A glassy-carbon working electrode, palladium reference electrode, and platinum auxiliary electrode were used.

The mobile phase solutions of the HPLC systems were contained in Ultraware HPLC solvent reservoirs (Kontes, Vineland, NJ, U.S.A.) and degassed with helium (99.9955%), purified with in-line Hydro-Purge II and Oxy-Purge traps (Alltech As-

soc./Applied Science Labs., Deerfield, IL, U.S.A.). These solutions were delivered with a Model SP 8700XR pump (Spectra-Physics, San Jose, CA, U.S.A.). Injections were made into the column with a Spectra-Physics Model SP 8780XR autosampler, fitted with a 20-μl loop. The stainless-steel guard column (2 cm × 2 mm I.D.) was packed with 30- to 40-μm Perisorb RP pellicular packing material (Upchurch Scientific, Oak Harbor, WA, U.S.A.). The stainless-steel analytical column (25 cm × 4.6 mm I.D.) was packed with 6-μm spherical Zorbax C_8 packing material (DuPont, Wilmington, DE, U.S.A.). The guard and analytical columns were contained in a Model 2080 HPLC column oven (Varian, Palo Alto, CA, U.S.A.). The effluent from the column was passed through a Model 5020 guard ED cell (ESA, Bedford, MA, U.S.A.) with potential applied by an ESA Model 5100A Coulochem electrochemical controller. All chromatograms were recorded on a Spectra-Physics Model 4200 computing integrator. ESA filters containing 0.2-μm porous-graphite filter elements were placed in-line after the pump and immediately ahead of the guard cell.

HPLC operating parameters

The column oven was operated at 35°C. The mobile phase flow-rate was adjusted to 1.50 ± 0.02 ml/min with water–acetonitrile–aq. 0.5 *M* MCA (4:5:1) (aq. 0.5 *M* MCA, adjusted to pH 2.70 with ammonium hydroxide). The system was equilibrated at 20% acetonitrile (mobile phase components, 7:2:1) for 10 min before injection of the analyte solution. Immediately after injection, a 30-min linear gradient to 90% acetonitrile (mobile phase components, 0:9:1) was begun. The concentration of the aq. 0.5 *M* MCA solution in the mobile phase was kept constant at 10%.

The ED guard cell was set at −1.4 V to reduce the organonitro compounds. Detectors 1 and 2 of the analytical cell were set at −0.20 and +0.70 V, respectively. The multiplier gain switch was set to × 10, and the gain thumbpot switch was set to 10. The computing integrator was set at an attenuation of 8. The time constant was set at 0.4 s.

RESULTS AND DISCUSSION

A variety of organonitro pesticides, metabolites and industrial chemicals are listed in Table I. The electrochemical and liquid chromatographic characteristics of a number of these compounds were examined. The HPLC–ED investigations were conducted with nine organonitro compounds: binapacryl, bifenox, dicloran, dinoseb, 2,4-dinitrophenol, 4,6-dinitro-*o*-cresol (DNOC), 2-nitrophenol, oryzalin and parathion.

Electrochemical characteristics

Cyclic voltammetric data were collected to determine the effect of solution pH, electrolyte, organic solvent concentration and organonitro compound structure on the reduction and oxidation peak potentials. An acetonitrile–aq. 0.2 *M* electrolyte (1:1) solution was used, unless otherwise indicated, to simulate a mobile phase.

The pH of the electrolyte solution (measured before addition of organic solvent) greatly affects the reduction peak potentials of the organonitro compounds. As the pH was decreased from 12 (sodium hydroxide solution) to 2 (phosphoric acid solution), the reduction peak potentials became less negative by 150–400 mV and the

TABLE I

ORGANONITRO COMPOUNDS GROUPED BY STRUCTURE

Dinitroanilines
- Benefin
- Butralin
- Dinitramine
- Fluchloralin
- Isopropalin
- Nitralin
- Oryzalin*
- Pendimethalin
- Penoxalin
- Profluralin
- Trifluralin

Dinitroaromatics
- 2,4-Dinitrotoluene
- 2,6-Dinitrotoluene

Dinitrodiphenyl ethers
- Fluorodifen

Dinitrophenols
- 2,4-Dinitrophenol*
- Dinoseb*
- DNOC*

Dinitrophenylaliphatic esters
- Binapacryl*

Dinitro compounds, miscellaneous
- Dinocap
- Korax

Mononitroanilines
- Dicloran*

Mononitroaromatics
- Nitrobenzene
- Nitrotoluene
- Quintozene (PCNB)

Mononitrodiphenyl ethers
- Acifluorfen
- Bifenox*
- Nitrofen
- Oxyfluorfen

Mononitrophenols
- 2-Nitrophenol*
- 4-Nitrophenol

Mononitroorganophosphates
- O-Ethyl O-*p*-nitrophenyl benzenethiophosphonate (EPN)
- Fenitrothion
- Methyl parathion
- Paraoxon
- Parathion*

* Organonitro compounds used in HPLC–ED studies.

reduction peaks were better defined and showed greater detector response (peak height). Generally, a pH of less than 4 was required to obtain well-defined reduction peaks. Oxidation peak potentials of the reduction products of nitrophenols increased by 50–150 mV as the pH was decreased from 3.5 to 2.

Phosphoric acid and MCA were considered as potential acidic electrolytes because of their buffering capacity around pH 2–3.5. Both acids are good electrolytes; however, MCA is of advantage because its salts (formed on addition of base to adjust the pH) are more readily soluble in acetonitrile. To reduce problems with particulates and to minimize metal impurities, ammonium hydroxide was used to adjust the pH of the aqueous acidic solution before addition of the organic solvent. Cyclic voltammetric data showed that addition of sodium perchlorate to the MCA solution decreased the reduction peak potentials of the nitrophenols by 100–150 mV and increased the detector response by 10–20%.

The organic solvent concentration was found to affect the reduction peak potentials of the organonitro compounds. As the organic solvent concentration was

increased from 20 to 90%, the reduction peak potentials of the organonitro compounds became more negative by 100–300 mV. In the absence of a salt in the 90% acetonitrile–aq. acidic solution, the electrochemical reduction reaction was greatly reduced for bifenox, binapacryl and dicloran.

The location and number of nitro groups and other substituents on the phenyl ring affect reduction peak potentials, as shown by the cyclic voltammograms in Fig. 1. The 2,4- and 4,6-dinitro-substituted compounds (binapacryl, dinocap, dinoseb and 2,4-dinitrophenol) produced two well-defined reduction peaks. The first reduction peak occurs at *ca.* −0.9 V. The second reduction peak is at *ca.* −1.3 V for the dinitrophenols, and at −1.1 V for the two dinitrophenyl aliphatic esters, binapacryl and dinocap. The 2,6-dinitroaniline, oryzalin, did not produce two well-defined reduction peaks, but rather a reduction peak with a slight shoulder at a potential of −1.1 V. The mononitro-substituted compounds had reduction potentials ranging from −1.0 V for bifenox and parathion to −1.2 V for 4-nitrophenol. This range of reduction potentials could be used to advantage in providing added detection selectivity. Also, the data show that a large negative potential is required to monitor all organonitro compounds eluted from a chromatographic column.

Chromatographic characteristics

The organonitro compounds were initially chromatographed on a C_8 column by using an acetonitrile–water gradient. Table II shows the retention times of the

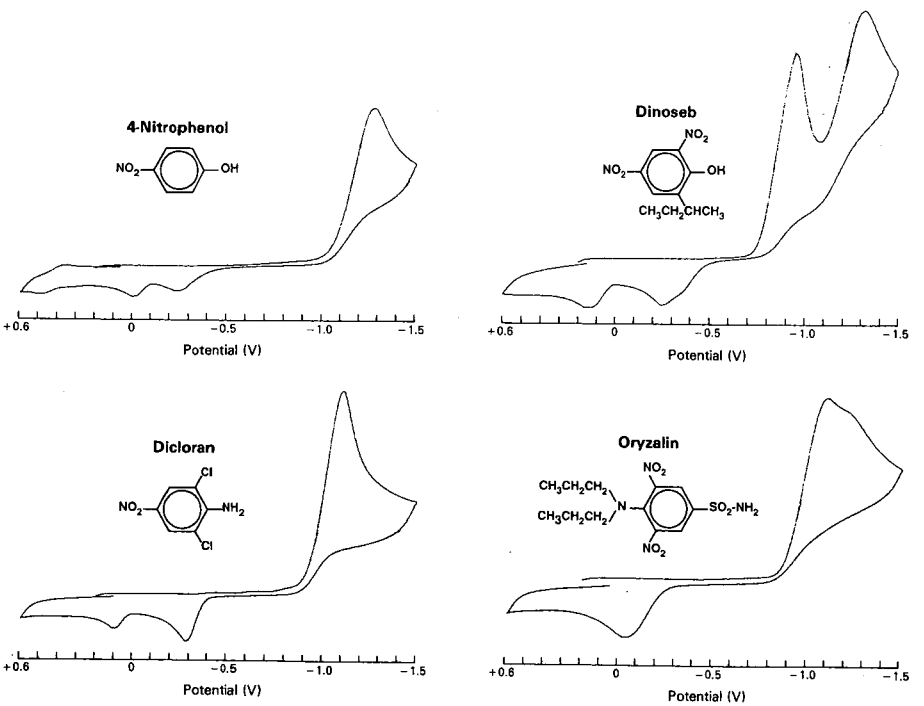

Fig. 1. Cyclic voltammograms of four organonitro compounds. Analyte concentration, 1 m*M*; scan range, +0.6 to −1.5 V; scan rate, 250 mV/s; working electrode, porous graphite; reference electrode, palladium; auxiliary electrode, platinum; electrolyte solution, acetonitrile–aq. 0.2 *M* MCA (pH 2.7, 1:1).

TABLE II

CHROMATOGRAPHIC CHARACTERISTICS OF ORGANONITRO COMPOUNDS ON A C_8 COLUMN WITH NEUTRAL AND ACIDIC MOBILE PHASES

Compound	*Mobile phases*			
	Acetonitrile–water		*Acetonitrile–aq. MCA*	
	Retention time (s)	*RRT**	*Retention time (s)*	*RRT**
2,4-Dinitrophenol	350	0.24	715	0.47
DNOC	598	0.41	971	0.64
4-Nitrophenol	678	0.46	615	0.41
2-Nitrophenol	814	0.56	782	0.52
Paraoxon	982	0.67		
Dicloran	1043	0.71	1039	0.68
Dinoseb	1043	0.72	1384	0.91
Methyl parathion	1214	0.83		
Oryzalin	1270	0.87	1289	0.85
Fenitrothion	1282	0.88		
Parathion	1383	0.95	1434	0.95
Bifenox	1462	1.00	1517	1.00
Nitrofen	1488	1.02		
EPN	1494	1.02		
Fluchloralin	1545	1.06		
Binapacryl	1549	1.06	1634	1.08
PCNB	1550	1.06		
Oxyfluorfen	1578	1.08	1657	1.09
Pendimethalin	1598	1.09		
Trifluralin	1636	1.12		
Benefin	1638	1.12		
Butralin	1646	1.13		
Isopropalin	1741	1.19		
Dinocap**	1746	1.19	1855	1.22
	1764	1.21	1876	1.24

* Retention time relative to bifenox.
** Dinocap contains two major isomers.

compounds (relative to bifenox). Sharp symmetrical peaks were obtained for all compounds except the nitrophenols, which produced broad peaks. Hsu *et al.*[12] and other authors have reported that an organic acid is necessary to diminish any interactions between phenols and residual silanol groups of silica-based reversed-phase packings, as well as to suppress dissociation of the phenols and thereby to improve chromatographic peak shape. In these studies, MCA was used as the organic acid. Its effect on the retention time of the nitrophenols and other organonitro compounds is shown in Table II. The use of MCA at pH 2.7 produced sharp symmetrical peaks for all organonitro compounds, including the nitrophenols. MCA appeared to have little, if any, effect on the relative retention times of the non-phenolic compounds. The relative retention times of 2-nitrophenol and 4-nitrophenol were slightly less with MCA in the mobile phase. However, for 2,4-dinitrophenol, dinoseb and DNOC the relative retention times were considerably longer with MCA in the mobile phase. The reten-

tion times of the phenols in the two mobile phases were found to be related to the pK_a values of the phenols. 2-Nitrophenol and 4-nitrophenol have pK_a values of *ca.* 7.2, whereas 2,4-dinitrophenol, dinoseb and DNOC have pK_a values of 4–4.5. In the acidic mobile phase (pH 2.7) ionization of all the phenols is suppressed, whereas in the acetonitrile–water (pH 6) mobile phase, ionization of the dinitro compounds is increased, resulting in shorter retention times.

HPLC–ED direct detection of nitro functionality

The determination of organonitro compounds by HPLC with direct reductive ED of the nitro functionality was determined to be infeasible. Extremely high background currents were produced at a potential of -1.0 V, which resulted in excessive baseline noise and a large change in the baseline during gradient elution. Also, oxygen in the non-degassed sample produced a large, off-scale, tailing peak, which obscured the responses of numerous organonitro compounds. Attempts to reduce the background current and eliminate oxygen from the sample during injection were unsuccessful.

HPLC–ED indirect detection of nitro functionality

Reduction of organonitro compounds results in formation of such products as anilines and hydroxyanilines. These products are electrochemically active and can be oxidized, as shown in Fig. 1 by the oxidation peaks in the cyclic voltammograms. Thus, it is possible to detect the nitro functionality indirectly.

Nitro polynuclear aromatic hydrocarbons (PAHs) have been reduced in post-column zinc[13] and platinum–rhodium[14] catalyst columns. The reduced nitro-PAHs were reported to be detected fluorometrically. The catalytic reduction of the various organonitro compounds reported here was investigated, using the platinum–rhodium catalyst reported by Tejada *et al.*[14]. Because the reduction takes place in the presence of methanol and not acetonitrile, a methanol–aq. MCA (pH 2.7) mobile phase was used. The ESA coulometric detector was used after the catalytic column to detect the reduction products in the oxidative mode. Although the organonitro compounds were indirectly detected in this manner, after a few hours of use, the electrochemical detector would become "poisoned" and would no longer respond to the reduction products. Although the detector could be reactivated by passing 6 *M* nitric acid through the porous-graphite electrodes, it would soon become "poisoned" when used again.

The design of the ESA coulometric detection cells and electronic controller prompted an investigation of the Model 5020 coulometric guard cell for reduction of the organonitro compounds (post-column) and the Model 5010 analytical cell for detection of the reduction products through electrochemical oxidation. The guard cell has its own potentiostat, which allows a current of 1000 μA to be applied before it becomes overloaded, and this enables operation at high potentials and background currents. Also, because analytes in the total flowing stream are reduced in the porous-graphite cell, no sensitivity is lost at the oxidation electrode. This solves the problem posed by amperometric thin-layer cells of reduced sensitivity at the second electrode due to diffusion of the 2–5% of analyte that has reacted at the surface of the first electrode.

Hydrodynamic voltammetric data were obtained with the HPLC–ED system

for selecting the detector-operating reduction and oxidation potentials. Hydrodynamic voltammograms (HDVs) were first obtained by changing the applied reduction potential on the guard cell while monitoring the response of detector 2 of the analytical cell, maintained at a constant oxidation potential. HDVs were obtained for nine organonitro compounds. Fig. 2 shows the HDVs obtained for five of the compounds. The dinitrophenols (2,4-dinitrophenol, dinoseb and DNOC) were most easily reduced, reaching a maximum detector response between -0.9 and -1.2 V. Binapacryl, bifenox and dicloran approached the maximum response near -1.7 V. 2-Nitrophenol, oryzalin, and parathion appeared to be incompletely reduced, even at a reduction potential of -1.7 V. Sodium perchlorate was added to the mobile phase in an attempt to lessen the reduction potentials of the organonitro compounds, as was observed in cyclic voltammetric studies. However, the reagent-grade sodium perchlorate produced extremely high background currents (possibly due to metal impurities), which negated its use for reducing reduction peak potentials of the organonitro compounds. Because of rapidly increasing background currents above -1.5 V, -1.4 V was selected as the reduction potential for the guard cell.

HDVs were also obtained by changing the oxidation potential of detector 2 and maintaining the guard cell reduction potential at -1.4 V. HDVs for five of the nine compounds are shown in Fig. 3. Near maximum response was obtained at $+0.50$ V for six compounds (bifenox, dicloran, 2,4-dinitrophenol, dinoseb, DNOC and parathion). The detector response for 2-nitrophenol reached a plateau near $+0.6$ V and

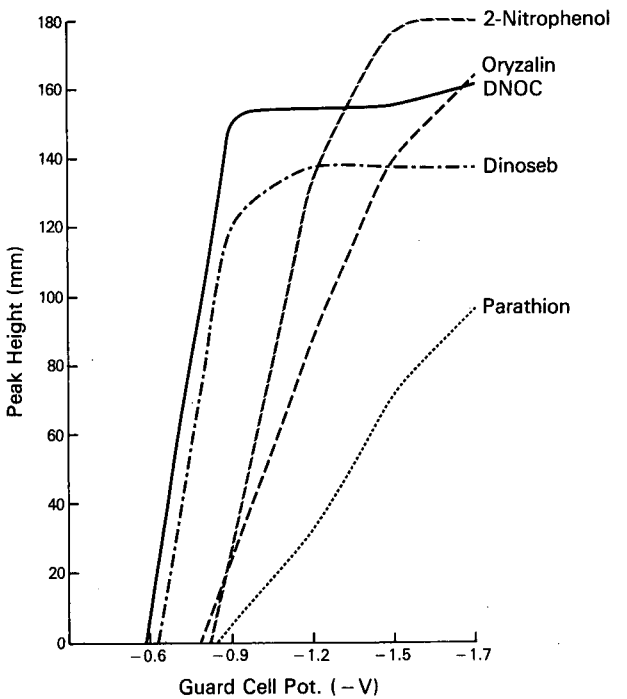

Fig. 2. Hydrodynamic voltammograms with the reductive potential (Pot.) on the guard cell changed. See text for instrument parameters.

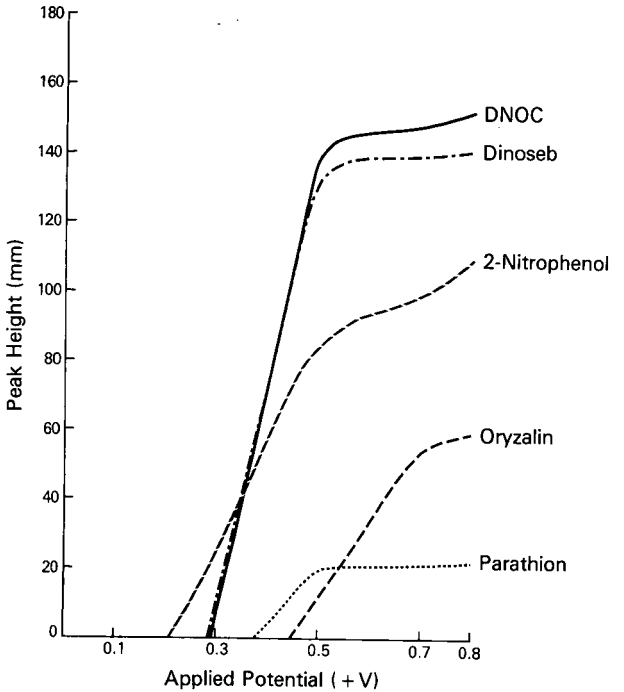

Fig. 3. Hydrodynamic voltammograms with the oxidative potential on the analytical cell changed. See text for instrument parameters.

then increased again, possibly because of the oxidation of the phenol. The maximum detector response for binapacryl and oryzalin was obtained near +0.7 V. An oxidation potential of +0.7 V was selected.

In the HDV oxidation studies, an interesting phenomenon was observed for binapacryl. At potentials of less than +0.3 V, a negative peak was observed; however, binapacryl is not reduced until a potential of *ca.* −0.8 V is applied. Negative peaks were also observed for binapacryl, DNOC and oryzalin at −0.2 V. Baizer[15] has reported that if an amino or hydroxyl group is situated *ortho* or *para* to the nitro group, the intermediate phenylhydroxylamine very rapidly loses water to form the easily reducible quinone, or the mono- or diimine. The loss of water is reported to take place most quickly in acid or alkaline solution. The hydroxyl group in DNOC and the ether group in binapacryl are *ortho* and *para* to the two nitro groups of each compound. Oryzalin contains two nitro groups, which are both *ortho* to the amine functional group. However, it should be noted that the nitro group(s) for the other six compounds are also in the *ortho* and/or *para* position, and for these compounds no change in response was noted when detector 1 was turned off or a potential of −0.20 V was applied. The electrochemical reduction products formed and/or the presence or absence of other functional groups on the phenyl ring may influence the effect on the reduction products of setting detector 1 at −0.2 V. It was observed that by operating detector 1 at −0.2 V, the oxidation response at detector 2 for DNOC, binapacryl and

oryzalin increased by 30, 20 and 10%, respectively, without any change in response for the other six compounds. Therefore, detector 1 was operated at −0.2 V.

A chromatogram obtained at the selected reduction and oxidation potentials is shown in Fig. 4. The sharp chromatographic peaks indicate good flow-through design of the guard and analytical cells. The organonitro peaks in the chromatogram represent 5–20 ng of a specific compound, indicating good detector response. The solvent peak and apparent "oxygen" peak are adequately separated from the peaks of the organonitro compounds. Although the magnitude of the gradient is large (20–90% acetonitrile in water), the change in the baseline has been minimized by maintaining a constant concentration of the electrolyte in the mobile phase. It should also be emphasized that periodic cleaning of the cell required that the cell first be cleaned with dilute nitric acid solution and then dilute sodium hydroxide solution. When the cell was washed with only nitric acid, severe negative peaks were observed immediately after the positive analyte peak. The reason for this phenomenon is unknown.

During our investigations it was necessary to make several injections of the organonitro compounds to obtain stable responses by the detection system. Table III shows the short-term response stability obtained for the nine compounds after the detection system has been "equilibrated". The average coefficient of variation (C.V.)

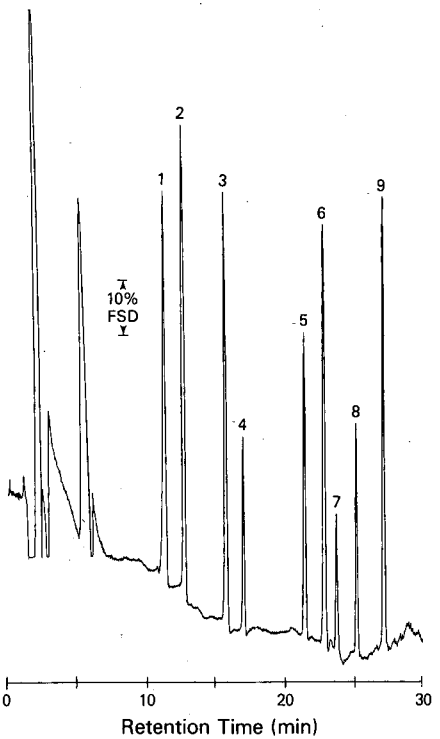

Fig. 4. HPLC–ED chromatogram of nine organonitro compounds. Peaks: 1 = 2,4-dinitrophenol, 5 ng; 2 = 2-nitrophenol, 10 ng; 3 = DNOC, 5 ng; 4 = dicloran, 10 ng; 5 = oryzalin, 20 ng; 6 = dinoseb, 5 ng; 7 = parathion, 20 ng; 8 = bifenox, 20 ng; 9 = binapacryl, 10 ng. See text for instrument parameters.

TABLE III

SHORT-TERM STABILITY OF DETECTOR RESPONSE FOR NINE ORGANONITRO COMPOUNDS

Compound	*Peak height**	*Av. peak height*	*C.V. (%)*
Binapacryl	6885 6789 6904	6859	0.9
Bifenox	3547 3341 3352	3413	3.4
Dicloran	6515 6605 6521	6547	0.8
Dinoseb	6317 6365 6371	6351	0.5
2,4-Dinitrophenol	5895 5870 6002	5922	1.2
DNOC	3004 2959 2967	2977	0.8
2-Nitrophenol	7345 7355 7443	7381	0.7
Oryzalin	4528 4520 4640	4563	1.5
Parathion	2036 2053 1979	2023	1.9

* Peak height units for the Spectra-Physics computing integrator.

in response is 1.3% for the triplicate injections of the nine compounds shown in Table III. Bergens[16] recently reported a similar indirect HPLC–ED system with dual amperometric electrodes for the indirect detection of nitrodiphenylamines.

ACKNOWLEDGEMENT

The authors thank Dr. Tejada, Environmental Protection Agency, Research Triangle Park, NC, U.S.A., for supplying the platinum–rhodium catalyst.

REFERENCES

1 M. A. Luke, J. E. Froberg, G. M. Doose and H. T. Masumoto, *J. Assoc. Off. Anal. Chem.*, 64 (1981) 1187.

2 R. T. Krause, *J. Assoc. Off. Anal. Chem.*, 68 (1985) 726.
3 H. A. Moye, S. J. Scherer and P. A. St. John, *Anal. Lett.*, 10 (1977) 1049.
4 R. T. Krause, *J. Chromatogr.*, 185 (1979) 615.
5 A. Andersson and B. Ohlin, *Var Foeda*, 38 (1986) 79.
6 C. E. Johansson, *Pestic. Sci.*, 9 (1978) 313.
7 P. T. Holland and T. K. McBhie, *J. Assoc. Off. Anal. Chem.*, 66 (1983) 1003.
8 T. M. Shafik, H. C. Sullivan and H. R. Enos, *J. Agric. Food Chem.*, 21 (1973) 295.
9 H. Roseboom, C. J. Berkhoff, J. I. Wammes and R. C. C. Wegman, *J. Chromatogr.*, 208 (1981) 331.
10 N. G. Buckman, J.O. Hill, R. J. Magee and M. J. McCormick, *J. Chromatogr.*, 284 (1984) 441.
11 K. Bratin and P. T. Kissinger, *J. Liq. Chromatogr.*, 4 (1981) 321.
12 A. J. Hsu, R. J. Laub and S. J. Madden, *J. Liq. Chromatogr.*, 7 (1984) 615.
13 W. A. MacCrehan and W. E. May, *Anal. Chem.*, 56 (1984) 625.
14 S. B. Tejada, R. B. Zweidinger and J. E. Siesby, Jr., *Anal. Chem.*, 58 (1986) 1827.
15 M. M. Baizer (Editor), *Organic Electrochemistry*, Marcel Dekker, New York, 1973, p. 331.
16 A. Bergens, *J. Chromatogr.*, 410 (1987) 437.

Journal of Chromatography, 459 (1988) 163–172
Elsevier Science Publishers B.V., Amsterdam — Printed in The Netherlands

CHROMSYMP. 1488

CARBON–POLYMER CHIPS AS SENSITIVE ELECTROCHEMICAL DETECTORS FOR MICRO-LIQUID CHROMATOGRAPHY

L. J. NAGELS*
Laboratory of Organic Chemistry, Rijksuniversitair Centrum Antwerpen, Groenenborgerlaan 171, B-2020 Antwerp (Belgium)
J. M. KAUFFMANN
Institut de Pharmacie, Université Libre de Bruxelles, Campus Plaine, 1050 Brussels (Belgium)
G. SCHUDDINCK and C. DEWAELE
Laboratory of Organic Chemistry, Rijksuniversiteit Ghent, Krijgslaan 281 (S4), B-9000 Ghent (Belgium)
G. J. PATRIARCHE
Institut de Pharmacie, Université Libre de Bruxelles, Campus Plaine, 1050 Brussels (Belgium)
and
M. VERZELE
Laboratory of Organic Chemistry, Rijksuniversiteit Gent, Krijgslaan 281 (S4), B-9000 Ghent (Belgium)

SUMMARY

The construction and characterization of an on-line electrochemical detector especially suited for flow-rates in the order of a few microlitres per minute is described. The working electrode is tubular, of length 15 mm and I.D. 90 μm (effective volume 100 nl). It is made of a small carbon–polymer chip, giving an inexpensive, practical and disposable construction. When used with packed fused-silica liquid chromatographic columns of 0.3 mm I.D., sub-picogram detection limits are obtained. The detector is linear for amounts up to 1 ng. An exceptional feature of this detector is that it stabilizes in a few seconds after potential onset (no baseline drift). The noise level is very constant and predictable. Some examples are given of the oxidative determination of phenolic compounds and catecholamines. Coulometric efficiencies, response *versus* flow-rate behaviour and peak dispersion characteristics are given.

INTRODUCTION

Chromatographic methods are rapidly expanding towards the use of small-diameter columns (less than 1 mm I.D.). The benefits are a lower cost of stationary-phase material and eluents and applicability to very small sample volumes. In our work, a method was needed for the determination of catecholamines in small biological samples. The use of sub-1-mm I.D. packed capillary liquid chromatographic (micro-LC) columns with electrochemical detection (ED) was appropriate for the problem, but a detector that fits these requirements could not be found.

0021-9673/88/$03.50

Flow-through electrochemical detectors have been the subject of intensive research, especially for the determination of organic molecules in the oxidative mode[1]. Their use and characteristics are very well documented for conventional high-performance liquid chromatographic (HPLC) methods (column diameter larger than 1 mm)[2,3].

Small column diameters and low flow-rates pose new problems in the construction of detectors. A few electrochemical detectors have been described for microbore LC systems[4–6], for open-tubular capillary LC[7] and for micro-LC columns[8–13]. In the last instance, detection limits of 10 pg[10] were mentioned for detectors based on planar electrode systems. Therefore, our first experiments were directed towards laboratory-made wall-jet detectors, which have been used succesfully in our laboratories for conventional HPLC systems (detection limits in the low-picogram range for 4.6 mm I.D. columns). With such detectors, good results were obtained for micro-LC also, but the baseline noise and drift were not reproducible. This phenomenon was ascribed to hydrodynamic conditions that are difficult to control at low flow-rates when planar glassy carbon electrodes are used. Miniaturization of the working electrode diameter from 3 mm to 1.5 and 0.8 mm and reduction of the working electrode–counter electrode distance from 50 μm to a few micrometres dit not improve this situation. For these reasons, a tubular electrode was designed in which carbon composite materials were used.

Such materials have already been used in planar[14] and in tubular[15–17] flow-through detectors for use with conventional HPLC columns (large internal volumes). For the latter type of detectors, a hole must be drilled into the material, which restricts the diameter and results in rough internal surfaces. For these reasons, and because reliable and sensitive planar electrode constructions are available for conventional HPLC systems (column I.D. larger than 1 mm), tubular detectors have never been competitive in this area. For the drastically reduced flow-rates used in micro-LC systems, planar working electrodes may well prove unsatisfactory. It was felt that narrow-bore tubular electrodes could provide good flow characteristics even at low flow-rates. Very narrow channels can be more easily produced in this material than in hard materials, such as glassy carbon. Further, carbon–polymer electrodes exhibit large accessible potential ranges, small and constant residual currents and reproducible surface activities[18–20]. On the other hand, their kinetic parameters are less favourable than those of freshly polished glassy carbon. We selected an ethylene–vinyl acetate copolymer containing 9% of vinyl acetate because of its high chemical inertness and its good electrochemical behaviour[14,21]. This paper describes the use of such a copolymer in a disposable tubular electrochemical sensor for application at low flow-rates.

EXPERIMENTAL

Chromatographic equipment

The chromatographic setup consisted of a high-pressure pump (Model M6000A; Waters Assoc., Milford, MA, U.S.A.), a 60-nl internal volume injector (Valco CV6U; VICI, Houston, TX, U.S.A.) and a 25 cm × 0.32 mm I.D. micro-LC column of the fused-silica type, filled with 5-μm C_{18} (RSL-Alltech, Eke, Belgium). All eluents were continuously degassed with helium. A conventional HPLC column (25

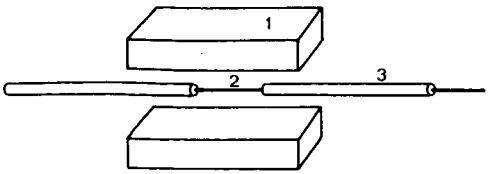

Fig. 1. Construction of a carbon–polymer tubular electrode. 1 = Piece of copolymer; 2 = stainless-steel wire of 90 μm diameter; 3 = polymide-coated fused-silica quartz capillary of 100 μm I.D.

cm × 4.6 mm I.D.) served as a solvent by-pass. A splitter was placed between the pump and the conventional + micro-LC systems. Using this system, a flow-rate of 1–2 ml min^{-1} could be maintained with the HPLC pump.

Electrochemical detector

The working electrode was made of an ethylene–vinyl acetate copolymer containing 9% of vinyl acetate, mixed with 20% (w/w) of carbon. This material is obtained as sheets of thickness 1.3 mm, as described in refs. 20 and 21. For the fabrication of a working electrode chip, two rectangular pieces (5 × 25 mm) were cut out of these sheets (see Fig. 1). A metal wire of 90 μm thickness (stainless-steel syringe-cleaning wires from Hamilton, Reno, NV, U.S.A.) was inserted into two fused-silica capillaries of 100 μm I.D., which coated with a polyimide layer, are readily available (RSL-Alltech). The inlet and outlet capillaries were 80 and 35 mm long, respectively, and the distance between them was 15 mm. The two capillaries must be inspected under a light microscope; they should not contain dust particles in the interior and the capillary ends contacting the plastic must be squarely cut. After cutting the capillaries with a glass cutter, the ends were polished with silicon carbide grinding paper (grit 600, Carbimet; Buehler, Lake Bluff, U.S.A.). Residual silicon carbide particles were removed from the capillaries by flushing with water. The capillaries and steel wire were placed between the two copolymer pieces and this construction was placed on an aluminium foil, and then on a hot-plate (200°C). A second hot-plate (200°C) was pressed manually against the upper piece of copolymer (also covered with aluminium foil to avoid contact of the plastic with the hot-plate). Application of pressure for a few seconds was sufficient to compress a chip to 1 mm thick.

The moulded assembly was removed from the hot-plates and allowed to cool in air for *ca.* 30 s. The steel wire was then pulled out and the tubular working electrode could be used as shown in Fig. 2. The short capillary dipped into a conducting solution (3.5 *M* potassium chloride was found to be appropriate for our experiments). A combined calomel reference electrode and platinum counter electrode was used to complete the detector (PT62 type; Schott Geräte, Hofheim a.Ts., F.R.G.). The contact points between the fused-silica capillaries and the copolymer were shock-protected by a drop of silicone rubber.

RESULTS AND DISCUSSION

Potential response behaviour: hydrodynamic voltammograms

Electrochemical detectors are highly selective when compared with, *e.g.*, UV detectors[22]. Especially steep, well resolved voltammograms give added possibilities

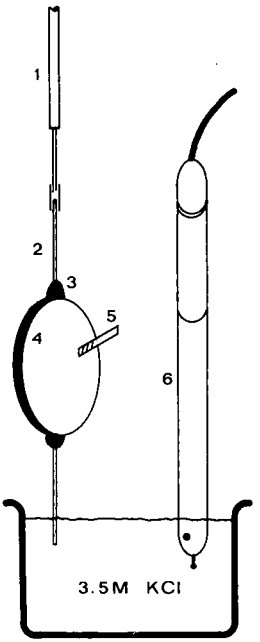

Fig. 2. Construction of electrochemical detector. 1 = Micro-LC column; 2 = quartz capillary; 3 = silicone rubber; 4 = carbon-composite working electrode; 5 = electrical contact; 6 = combined calomel–platinum counter electrode.

for differentiating between electroactive species. The shape of the voltammograms depends on the reaction kinetics, the iR drop (i = current; R = resistance) and the homogeneity of the electric field between the working and counter electrodes. Whereas the reaction kinetics depend on the electrode material used, the last two phenomena are strongly influenced by cell geometry.

In Fig. 3, hydrodynamic voltammograms (HDVs) obtained on a chip-type electrode are compared with those measured with a classical wall-jet type of detector. Curves a and b are the HDVs of caffeic acid (a reversibly and rapidly oxidized *o*-

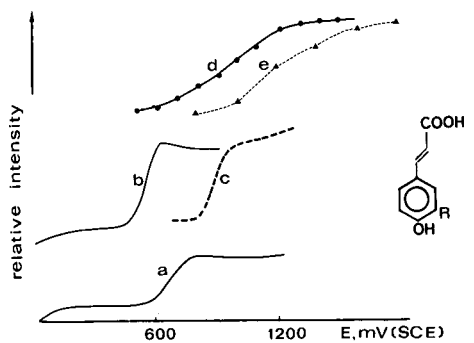

Fig. 3. Hydrodynamic voltammograms of caffeic acid (R = OH) and *p*-coumaric acid (R = H) in micro-LC systems.

dihydroxyphenolic acid) on a planar copolymer electrode (3 mm I.D., 20% carbon) and on a planar glassy carbon electrode (3 mm I.D.), respectively. Both electrodes were mounted in the same wall-jet cell so that the observed differences are due only to the electrode material, and not to the cell geometry. This detector had the working and counter electrodes in a parallel opposed configuration; the stainless-steel inlet line was used as the counter electrode. The reaction kinetics are faster on the planar glassy carbon (curve b) than on the planar copolymer electrode (curve a). Curves a and b were recorded by on-line rapid-scanning (1 V s^{-1}) staircase voltammetry. This technique (see also ref. 23), which is expected to become increasingly used in routine HPLC detection, is very sensitive to the *iR* drop and cell geometry. The same HDVs were obtained with a more cumbersome method in which repetitive injections and manual changes of electrode potential were used. The latter method was used to record the voltammograms in Fig. 3d and e for caffeic acid and *p*-coumaric acid respectively, with the tubular copolymer detector shown in Fig. 2. When this cell geometry is used, the HDVs are considerably shifted towards apparently higher applied potentials. However, these "overpotentials" can only partly be ascribed to sluggish electrode kinetics, as the copolymer electrode showed good kinetic behaviour when used in a planar form (curve a). They are ascribed to the special geometric configuration of the working and counter electrodes. This results in a reduced resolving power; the caffeic acid–*p*-coumaric acid pair is better resolved with the glassy carbon wall-jet detector (curves b and c, respectively) than with the plastic chip detector (curves d and e).

Linearity

When used with micro-LC columns, the detector shows a linear response behaviour for injected amounts from 5 to 1000 pg (Fig. 4a). Above 1 ng, deviations from linearity begin to occur. The above concentration range (three decades) can be considered as the working range for organic trace analysis with micro-LC methods. For use with conventional HPLC methods (4.6 mm I.D. columns, 1 ml min^{-1} flow-rate), a

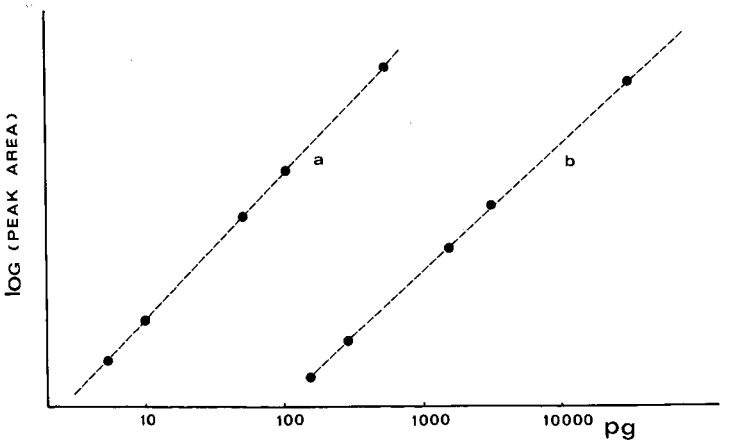

Fig. 4. Calibration graphs for the tubular electrode in (a) micro-LC and (b) conventional HPLC (C_{18} column, 25 cm × 4.6 mm I.D.). 3,4-Dihydroxybenzoic acid was used as a test substance. The eluent composition was methanol–0.01 *M* orthophosphoric acid (30:70). Flow-rate: (a) 0.005 and (b) 1 ml min^{-1}.

linear response behaviour was obtained from 0.1 to 50 ng (Fig. 4b, and other measurements). On a non-logarithmic (linear) scale, the calibration graphs show a zero intercept.

Detection limits and baseline stability

Chromatographic detection is easily and reproducibly obtained in the picogram range, as shown in Fig. 5 for phenolic compounds (A) and catecholamines (B). On the basis of the gallic acid peak in Fig. 5A (peak a), the detection limit was calculated to be 500 fg. This is far below the detection limits reported by Goto *et al.*[10] (10 pg) for planar glassy carbon electrodes used in micro-LC systems. The response of the catecholamines as a function of the applied working electrode potential declines for potentials above 1200 mV. This behaviour was also observed by Yoshiura *et al.* with glassy carbon electrodes (ref. 24, Fig. 3).

Fig. 5C shows that the tubular copolymer detectors can also be used succesfully with conventional HPLC systems. The three phenolic compounds were injected in the 100–200-pg range. However, at these flow-rates, the glassy carbon-based wall-jet detector had even better signal-to-noise characteristics (results not shown). Unfortunately, a great disadvantage of the latter detectors is the long stabilization time required to measure these low amounts (baseline dift).

For the small currents measured in Fig. 5A and B, the noise level was unaffected by external events, such as touching the glass beaker (Fig. 2) or the reference electrode. Such effects, which are due to high cell impedances, are frequently observed for many classical cell designs. The "chip" electrode described here allows the use of a reference electrode with a platinum fibre junction. This has distinct advantages over ceramic membrane types, as the latter occasionally tend to give high impedances because of deposition of solid potassium chloride.

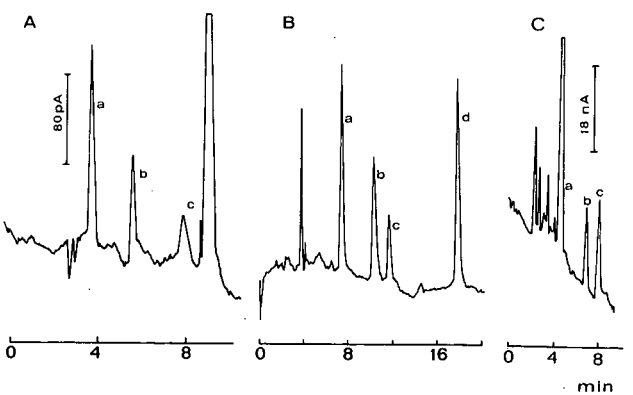

Fig. 5. Application of carbon–copolymer tubular electrodes in (A and B) micro-LC and (C) conventional HPLC. (A) Separation of (a) 8.2 pg of gallic acid, (b) 6.6 pg of 3,4-dihydroxybenzoic acid and (c) 6 pg of 3,4-dihydroxybenzaldehyde in the micro-LC system. Eluent, methanol–0.01 *M* phosphoric acid (30:70). Detector potential, +1600 mV [*vs.* a saturated calomel electrode (SCE)]. (B) Separation of 10–20-pg amounts of (a) noradrenalin, (b) adrenalin, (c) 3,4-dihydroxybenzylamine and (d) dopamine. Eluent, 3 m*M* heptanesulphonate + 100 mg/l EDTA + disodium hydrogenphosphate–citric acid buffer pH 3.5, 10^{-2} *M* + 5% acetonitrile. Column, see text; detector potential, +900 mV (*vs.* SCE). (C) Separation of (a) 240 pg of gallic acid, (b) 190 pg of 3,4-dihydroxybenzoic acid and (c) 210 pg of 3,4-dihydroxybenzaldehyde on a conventional C_{18} column (25 cm × 4.6 mm I.D.). Eluent, methanol–0.01 *M* orthophoshoric acid (30:70); detector potential, +1600 mV (*vs.* SCE).

Faraday-cage shielding of the detector components was not required. The measured currents are still considerably higher than those which are measured with ED in open-tubular capillary systems, where shielding is necessary[7]. In our study of the tubular "chip" electrode, external noise pick-up did occur occassionally when the working electrode was fouled or clogged, or when the calomel electrode junction was disrupted. Noise was also due to a non-grounded pneumatic pump; grounding immediately eliminated the noise. Adhesion of gases to the electrode surface occasionally reduced the coulometric efficiency. This was quickly remedied by placing the chip plus inlet and outlet capillaries in a test-tube filled with methanol and applying a vacuum for a few minutes.

An interesting advantage of the tubular micro-LC detector is the almost total lack of baseline drift (such drifts are a common phenomenon with glassy carbon working electrodes). The detector can be used a few seconds after application of the electrode potential. This potential can even be changed during analysis without excessively disturbing the chromatogram. The latter behaviour is very exceptional for an electrochemical detector. With the tubular "chip" electrodes, automatic disruption of the applied potential at very high current densities becomes very feasible. This would protect the electrode from accidental fouling by abnormally high concentrations of substances.

After a 14-day period of uninterrupted analysis (3,4-dihydroxybenzoic acid was injected 5–10 times daily in 600-pg amounts under the conditions stated for Fig. 5A), no significant change in the detector response could be observed. During this work, fifteen "chip"-type electrodes were assembled and tested, and all yielded results comparable to those shown in Fig. 5.

Coulometric efficiency

Coulometric efficiencies decrease when increasing concentrations of organic solvents are used in the mobile phase (Fig. 6A), and this also occurs with the glassy

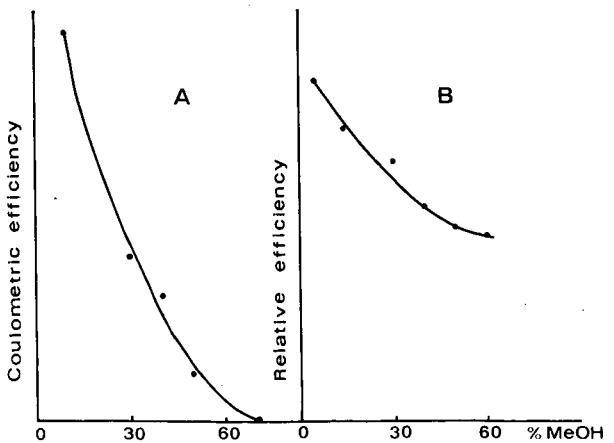

Fig. 6. Decrease of the response of (A) a tubular carbon–copolymer detector and (B) a wall-jet glassy carbon detector with increasing methanol concentrations in the eluent (methanol–0.01 *M* orthophosphoric acid). (A) Recorded under micro-LC conditions; (B) recorded under conventional HPLC conditions. Gallic acid was used in both systems. MeOH = Methanol.

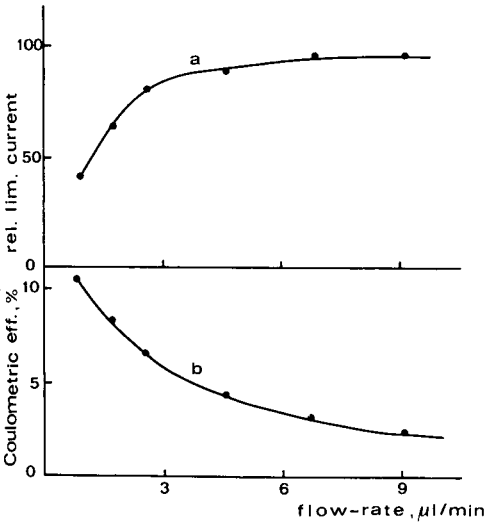

Fig. 7. Variation of (a) the limiting (lim.) current and (b) the coulometric efficiency (eff.) with flow-rate under micro-LC conditions. The curves were recorded with 3,4-dihydroxybenzoic acid as the test substance. Eluent, methanol–0.01 *M* orthophosphoric acid (30:70).

carbon-based wall-jet detector (Fig. 6B). In Fig. 6A, the real coulometric efficiency of the "chip"-type detector is shown. It is as high as 30% for organic solvents in 10% (v/v) concentration. For the measurements shown in Fig. 6A, the conductivities of all chromatographic eluents were adjusted to 2 mmho with potassium chloride to minimize differences in the *iR* drop). Such high efficiencies at low flow-rates were also noted by Goto *et al.*[10]. The coulometric efficiency of the detector also decreases with increasing flow-rate (see Fig. 7b); a decrease from 10% to 2% occurs when the flow-rate is increased from 1 to 12 µl/min for an eluent containing 30% of organic solvent. Electrochemical detectors with high or low coulometric efficiencies are usually classified as coulometric or amperometric devices, respectively. The first are mass-sensitive, whereas the second are concentration-sensitive. With the micro-tubular detectors that were used in this study at low-flow rates, some intermediate behaviour is to be expected.

Another important feature of electrochemical detectors is the dependence of limiting currents on flow-rates. For the tubular detector described here, this dependence is given in Fig. 7a. Limiting currents were obtained by measuring peak heights. As the chromatographic column was part of the system, a normalization was applied to this peak height to account for the variation in peak broadening (normalization to the same peak volume). After an initial increase in the limiting current with increasing flow-rate, this current becomes almost flow-insensitive. A 50% decrease in limiting current occurred when the flow-rate was decreased from 5 to 1 µl/min. Such dependences have been the subject of several studies, and mathematical expressions have been formulated for hypothetical systems[25]. As was stated by Roosendaal and Poppe[26], much remains to be done to cope with realistic situations, such as electrodes in flow-through detectors. The experimental conditions used in this study (small diameters, low flow-rates and high coulometric efficiencies) provide new material for such

TABLE I

PEAK VARIANCE (nl) AFTER INJECTING NORADRENALIN IN DIFFERENT VOLUMES IN A FLOW-INJECTION SETUP, CONSISTING OF A WALL-JET DETECTOR (EQUIPPED WITH 1.5 AND 3 mm DIAMETER GLASSY CARBON ELECTRODES) AND A CHIP-TYPE CARBON–POLYMER DETECTOR

Detector type	*Injection volume (nl)*		
	60	*20*	*500*
Wall-jet (1.5 mm)	285	372	593
Wall-jet (3 mm)	306	427	467
Chip	244	337	354

studies. A curve such as Fig. 7a also yields practical information on the flow-rates that are still useful with 90 μm I.D. tubular electrodes from the point of view of detector sensitivity. The curves compare well with those obtained in a slightly different way by Goto *et al.* on planar glassy carbon working electrodes used under micro-LC conditions (ref. 10, Fig. 7).

Other working electrode dimensions and materials

Tubular working electrodes of I.D. 40 and 200 μm and with lengths varying from 2 to 20 mm were also tested. The smaller inner diameter gave a considerably higher baseline noise but had little effect on peak height. The 200-μm I.D. electrodes showed substantially the same behaviour as the 90-μm I.D. electrodes (signal-to-noise ratio, linearity, voltammogram shape, baseline stability and response *versus* flow characteristics). The 90-μm I.D. electrodes gave less peak broadening and were therefore found to be the most satisfactory. The use of copolymer material with higher carbon contents (30%) was not found to be satisfactory, as cracking of the electrode material and subsequent leaking of the cell occurred.

Peak broadening

Extra peak dispersion was determined by measuring the total variance (in nanolitres) after the injection of different volumes of catecholamine solutions in a flow-injection setup (injector + detector only). This variance was calculated by using moment analysis to account for peak shapes deviating from Gaussian forms. Table I compares the results obtained with a wall-jet detector (3 and 1.5 mm diameter working electrodes), and the results obtained with a tubular "chip" detector. In this respect also the tubular detector had better characteristics than the wall-jet detector. This is not surprising, as the working electrode has a smaller inner diameter than the quartz connector tubing.

CONCLUSIONS

Tubular detectors made of carbon–polymer material are very useful for micro-LC. Sub-picogram detection limits are obtained and the response is linear up to 1 ng. The discriminating power for different electroactive compounds is lower than with

planar glassy carbon-type detectors. Because they are easy to use and have reliable performance characteristics, these tubular detectors are very convenient for application at low flow-rates. They can also be used at higher flow-rates (up to 2 ml min^{-1}), but in this instance the demands are not as great because classical glassy carbon detectors perform very well in this range. It is to be expected that the new detectors will be useful in applications other than HPLC. Biosensors seem likely candidates, especially when electrode-coupled enzymes are envisaged, because low flow-rates may well prove to be compatible with efficient enzymatic product conversion. Another area of application could be the analysis of small sample volumes in flow-injection methods at microlitres per minute flow-rates (possibly with micro-pump systems[27]).

ACKNOWLEDGEMENTS

The authors thank Mr. J. Everaert and Mrs. L. Van Roy for valuable help. C.D. thanks the I.W.O.N.L. for a grant.

REFERENCES

1 C. M. Selavka and I. S. Krull, *J. Liq. Chromatogr.*, 10 (1987) 345.
2 D. C. Johnson, S. G. Weber, A. M. Bond, R. M. Wightman, R. E. Shoup and I. S. Krull, *Anal. Chim. Acta*, 180 (1986) 187.
3 K. Stulik and V. Pacakova, *Crit. Rev. Anal. Chem.*, 14 (1984) 297.
4 A. Carlsson and K. Lundström, *J. Chromatogr.*, 350 (1985) 169.
5 J. Caliguri, P. Capella, L. Bottari and I. N. Mefford, *Anal. Chem.*, 57 (1985) 2423.
6 K. Slais, *J. Chromatogr. Sci.*, 24 (1986) 321.
7 R. L. St. Claire, III, and J. W. Jorgenson, *J. Chromatogr. Sci.*, 23 (1985) 186.
8 N. Sagliano, Jr., and R. A. Hartwick, *J. Chromatogr. Sci.*, 24 (1986) 506.
9 M. Goto, T. Nakamura and D. Ishii, *J. Chromatogr.*, 226 (1981) 33.
10 M. Goto, Y. Koyanagi and D. Ishii, *J. Chromatogr.*, 208 (1981) 261.
11 M. Goto, E. Sakurai and D. Ishii, *J. Chromatogr.*, 238 (1982) 357.
12 M. Goto, in M. V. Novotny and D. Ishii (Editors), *Microcolumn Separations —Columns, Instrumentation and Ancillany Techniques (Journal of Chromatography Library*, Vol. 30), Elsevier, Amsterdam, Oxford, New York, Tokyo, 1985, p. 309.
13 M. Goto and K. Shimada, *Chromatographia*, 21 (1986) 6631.
14 J. M. Kauffmann, C. R. Linders, G. J. Patriarche and M. R. Smyth, *Talanta*, 35 (1988) 179.
15 A. Liberti, C. Morgia and M. Mascini, *Anal. Chim. Acta*, 173 (1985) 157.
16 J. D. McLean, *Anal. Chem.*, 54 (1982) 1169.
17 D. N. Armentrout, J. D. McLean and M. W. Long, *Anal. Chem.*, 51 (1979) 1039.
18 G. J. Patriarche, J. M. Kauffmann and J. C. Vire, *J. Pharm. Biomed. Anal.*, 1 (1983) 469.
19 J. M. Kauffmann, M. P. Prete, J. C. Vire and G. J. Patriarche, *Fresenius Z. Anal. Chem.*, 321 (1985) 172.
20 G. J. Patriarche, *J. Pharm. Biomed. Anal.*, 4 (1986) 789.
21 M. P. Prete, J. M. Kauffmann, J. C. Vire, G. J. Patriarche, B. Debye and G. Geuskens, *Anal. Lett.*, 17(B12) (1984) 1391.
22 L. J. Nagels and W. L. Creten, *Anal. Chem.*, 57 (1985) 2706.
23 J. G. White, R. L. St. Claire, III, and J. W. Jorgenson, *Anal. Chem.*, 58 (1986) 293.
24 M. Yoshiura, T. Iwamoto, K. Iriyama and T. Kuwana, *J. Liq. Chromatogr.*, 10 (1987) 3141.
25 S. Prabhu and J. L. Anderson, *Anal. Chem.*, 59 (1987) 157.
26 E. M. M. Roosendaal and H. Poppe, *Anal. Chim. Acta*, 158 (1984) 323.
27 R. E. Dessy, *Anal. Chem.*, 57 (1985) 1188A.

Journal of Chromatography, 459 (1988) 173–181
Elsevier Science Publishers B.V., Amsterdam — Printed in The Netherlands

CHROMSYMP. 1430

WATER AS A STATIONARY PHASE MODIFIER IN PACKED-COLUMN SUPERCRITICAL FLUID CHROMATOGRAPHY

I. SEPARATION OF FREE FATTY ACIDS

F. O. GEISER
Geiser Scientific, Glen Mills, PA 19342 (U.S.A.)
and
S. G. YOCKLOVICH*, S.M. LURCOTT, J. W. GUTHRIE and E.J. LEVY
Computer Chemical Systems, Inc., Rt. 41 & Newark Road, P.O. Box 683, Avondale, PA 19311 (U.S.A.)

SUMMARY

A procedure is described for supercritical fluid chromatography (SFC) of free fatty acids (lauric, myristic, palmitic, stearic and arachidic acid) with either dry carbon dioxide or water-saturated carbon dioxide as the mobile phase and with flame-ionization detection. Seven stationary phases were evaluated with water-saturated and dry carbon dioxide under otherwise identical conditions. The retention time for lauric acid with water-saturated carbon dioxide varied from 5.6 min ($k' = 8.7$) for Deltabond™ Octyl to 23.6 min ($k' = 39.7$) for YMC-Gel PVA-Sil™. The range of stationary phase polarity reported in this study should enable an investigator to adjust SFC conditions to resolution requirements for various solute mixtures. Water-saturated carbon dioxide improved the chromatographic resolution and sensitivity of all seven stationary phases, particularly of covalently bonded phases.

INTRODUCTION

Saturation of supercritical carbon dioxide with water or with water–formic acid has been reported to improve significantly the resolution of polar solutes such as long-chain free fatty acids in packed-column supercritical fluid chromatography (SFC)[1]. This technique has been shown to be compatible with universal detection methods such as flame ionization detection (FID), thereby enabling the separation of free fatty acids and related natural products which are not easily separated by conventional liquid or gas chromatographic methods, especially at the low concentrations typically found in pharmaceutical formulations or in biological samples.

Earlier reports of equipment for saturating carbon dioxide have described the use of a precolumn (150 × 4.6 mm I.D.) packed with silica gel (100–200 mesh) and inserted between the pump and the sample injection port. The silica gel precolumn was saturated with about 40% (w/w) water. As carbon dioxide passed through the precolumn at 25°C, water was desorbed from silica gel, thereby saturating the carbon

0021-9673/88/$03.50

dioxide with an estimated 0.15–0.18% (w/w) water at 25°C at 1800–5500 p.s.i. carbon dioxide[1,2].

Although prior investigators have proposed a mechanism by which polar organic modifiers (*e.g.* methanol) in low concentration deactivates packed-column stationary phases[3–5], we are not aware of studies in which commercially available packed-column stationary phases were tested in separations with "dry" and water-saturated supercritical carbon dioxide in combination with FID. Such a technique should prove useful for the rapid screening and quality control of suitable packed column SFC and high-performance liquid chromatographic (HPLC) stationary phases.

The objectives of our investigation were: (1) to automate the water saturation of supercritical carbon dioxide so that SFC could be conducted easily with and without water, (2) to screen a variety of silica-based stationary phases using free fatty acids as model polar solutes, (3) to propose a mechanism for the observed chromatographic improvement with water-saturated carbon dioxide, and (4) to use this mechanistic model to propose "ideal" packed-column SFC stationary phases, and to examine qualitatively the relative polarity of a variety of commercially available packed-column stationary phases so that investigators could adjust SFC conditions to the resolution requirements of various sample mixtures.

In this study, saturated free fatty acids (lauric, myristic, palmitic, stearic, arachidic acid) were separated sequentially on seven silica-based stationary phases, using "dry" and water-saturated supercritical carbon dioxide as the mobile phase. The stationary phases selected for the study included: four stationary phases previously identified[6] as suitable for SFC (Deltabond Methyl, Deltabond Octyl, Deltabond Cyano, and Nucleosil Cyano), and three stationary phases for which SFC separations have not been reported in the literature (YMC-Gel phenyl, YMC-Gel silica, and YMC-Gel PVA-Sil). YMC-Gel PVA-Sil was of particular interest to us since it is reported to exhibit long term stability at pH values as high as 13.5 even though it consists of a silica gel support, coated with polymerized polyvinyl alcohol[7]. We are not aware of published reports in which this unique stationary phase has been used in a non-aqueous chromatographic system, such as in SFC with carbon dioxide.

EXPERIMENTAL

SFC system

The SFC system consisted of a CCS 5000 SFC and CCS 727 data system (Computer Chemical Systems, Avondale, PA, U.S.A.). The CCS 5000 SFC system was equipped with a 0.1-μl injection loop, a post-column restrictor, calibrated to give an expanded gas flow-rate of 22 ml/min at 1800 p.s.i. to 90 ml/min at 6000 p.s.i. (column oven temperature, 70°C), a remotely actuated 8-port valve, which could be switched conveniently back and forth to the water-saturated precolumn, and a flame ionization detector set at 350°C.

Reagents

The following free fatty acids were purchased from Chem Services (West Chester, PA, U.S.A.): lauric acid ($C_{12}H_{24}O_2$), myristic acid ($C_{14}H_{28}O_2$), palmitic acid ($C_{16}H_{32}O_2$), stearic acid ($C_{18}H_{36}O_2$), arachidic acid ($C_{20}H_{40}O_2$), oleic acid

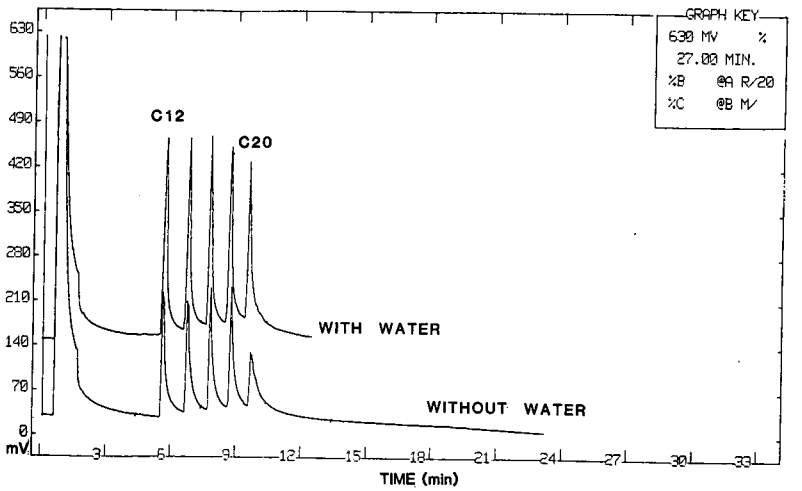

Fig. 1. SFC of C_{12}, C_{14}, C_{16}, C_{18}, C_{20} saturated free fatty acids. Carbon dioxide mobile phase at 70°C with and without water modifier. Column: 100 × 1 mm I.D. 5 μm Deltabond Octyl (300 Å) (C8). Conditions: 1800 p.s.i. for 2 min after injection; 1800 to 6000 p.s.i. at 100 p.s.i./min.

($C_{18}H_{34}O_2$), linoleic acid ($C_{18}H_{32}O_2$), and linolenic acid ($C_{18}H_{30}O_2$). Baker-analyzed HPLC-grade water was purchased form VWR Scientific (Philadelphia, PA, U.S.A.). SFC-grade liquid carbon dioxide was purchased from Scott Specialty Gases (Plumsteadville, PA, U.S.A.).

SFC columns

The water-saturation precolumn (100 × 6 mm I.D., nominal 5 μm, 100 Å) appropriately conditioned for SFC was supplied by Computer Chemical Systems. Three 100 × 1 mm I.D. columns packed with YMC-Gel PVA-Sil (silica gel encapsulated with polymeric polyvinyl alchohol), YMC-Gel phenyl (covalently-bonded diphenylmethyl-silyl), and YMC-Gel silica (non-bonded) stationary phases (all nominally 5 μm, 120 Å spherical) were supplied by YMC, Inc. (Morris Plains, NJ, U.S.A.). One 100 × 1 mm I.D. column packed with Nucleosil Cyano stationary phase (covalently-bonded cyanopropylsilyl, nominal 5 μm, 100 Å spherical), and three 100 × 1 mm I.D. columns packed with Deltabond Methyl (covalently bonded polymerically cross-linked methylsilyl), Deltabond Octyl (covalently bonded polymerically cross-linked octylsilyl), and Deltabond Cyano (covalently bonded polymerically cross-linked cyanopropylsilyl), stationary phases (all nominal 5 μm, 300 Å spherical) were purchased from Keystone Scientific (State College, PA, U.S.A.).

SFC column conditioning

All microbore columns (100 × 1 mm I.D.) were prepared for SFC by elution with 20 ml of methanol at a rate of 0.5 ml/min, followed by drying for at least 2 h at 150°C in the SFC oven with varying pressure increases from 1500 to 6000 p.s.i. carbon dioxide. YMC-Gel PVA-Sil was found not to tolerate exposure to 150°C and was therefore conditioned at 125°C for 12–16 h (overnight). When columns were

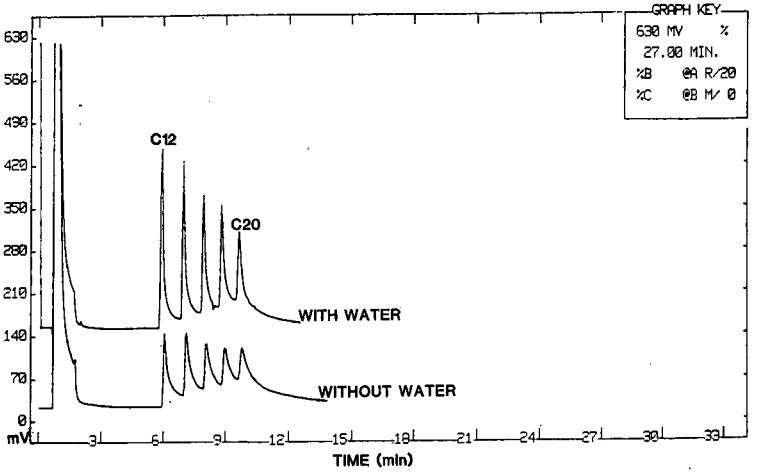

Fig. 2. SFC of C_{12}, C_{14}, C_{16}, C_{18}, C_{20} saturated free fatty acids. Conditions: as per Fig. 1. Carbon dioxide mobile phase at 70°C, with and without water modifier. Column: 100 × 1 mm I.D., 5 μm Deltabond Methyl (300 Å) (C1).

installed in the SFC system, the baseline FID response when pressurized to 6000 p.s.i. (at 90°C) did not exceed 100 mV.

Preparation of water saturation columns

The preconditioned water-saturation SFC column (100 × 6 mm I.D.) was connected to an 8-port valve, and 20 ml of HPLC-grade water was pumped into the column at a rate of 0.5 ml/min. The column was subsequently dried partially with gaseous carbon dioxide at 150 p.s.i. for 30 min. The valve was actuated in order to

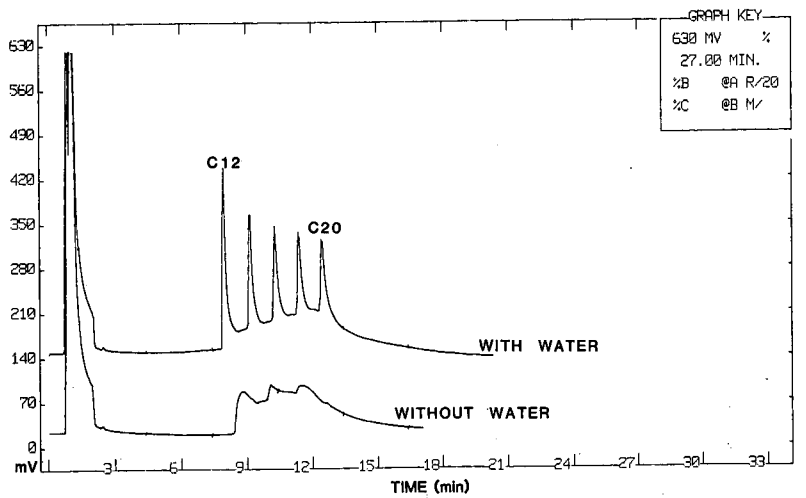

Fig. 3. SFC of C_{12}, C_{14}, C_{16}, C_{18}, C_{20} saturated free fatty acids. Conditions: as per Fig. 1. Carbon dioxide mobile phase at 70°C, with and without water modifier. Column: 100 × 1 mm I.D., 5 μm YMC Gel phenyl (120 Å) (PH).

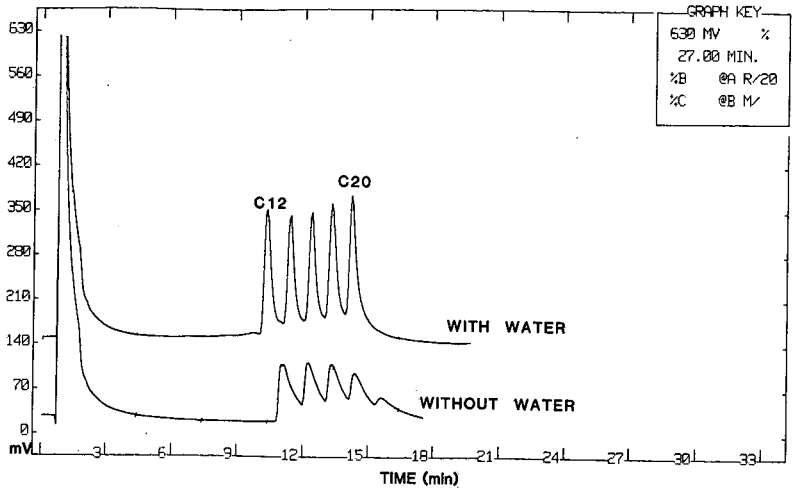

Fig. 4. SFC of C_{12}, C_{14}, C_{16}, C_{18}, C_{20} saturated free fatty acids. Conditions: as per Fig. 1. Carbon dioxide mobile phase at 70°C, with and without water modifier. Column: 100 × 1 mm I.D., 5 μm Deltabond Cyano (300 Å) (CN1).

allow carbon dioxide to flow through the water-saturated precolumn, and the pressure was raised from 1500 to 6000 p.s.i. at the rate 500 p.s.i./min and held at 6000 p.s.i. (at 90°C) until the FID baseline response did not exceed 100 mV.

RESULTS AND DISCUSSION

Screening of stationary phases: separation of saturated free fatty acids

The following chromatographic conditions were used for each stationary phase

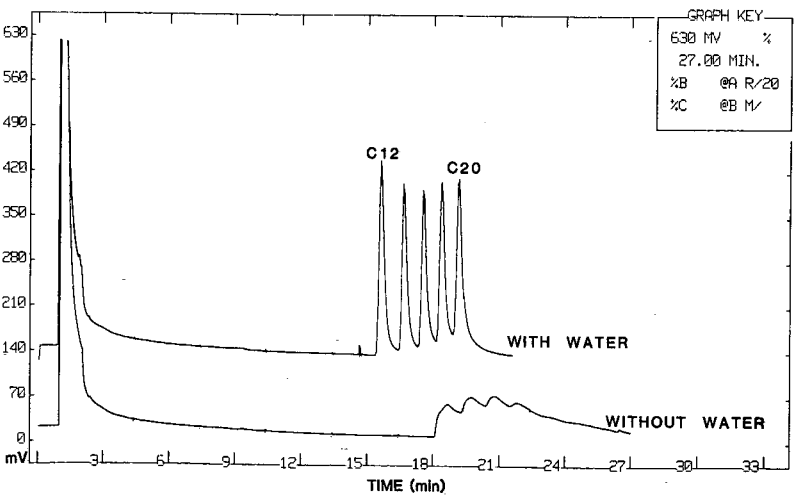

Fig. 5. SFC of C_{12}, C_{14}, C_{16}, C_{18}, C_{20} saturated free fatty acids. Conditions: as per Fig. 1. Carbon dioxide mobile phase at 70°C, with and without water modifier. Column: 100 × 1 mm I.D., 5 μm Nucleosil Cyano (100 Å) (CN2).

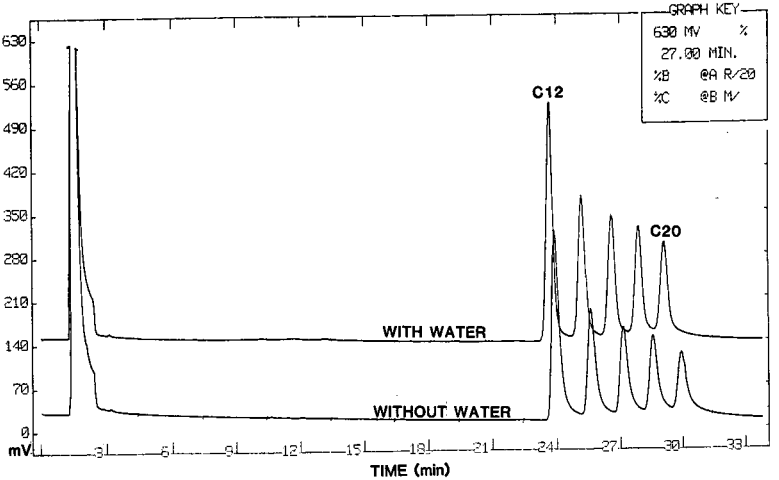

Fig. 6. SFC of C_{12}, C_{14}, C_{16}, C_{18}, C_{20} saturated free fatty acids. Conditions: as per Fig. 1. Carbon dioxide mobile phase at 70°C, with and without water modifier. Column: 100 × 1 mm I.D., YMC Gel PVA-Sil (120 Å) (PVA).

column: a solution of lauric, myristic, palmitic, stearic, and arachidic acids (*ca.* 5 mg/ml each in dichloromethane) was injected via the 0.1-μl injection loop. The column oven temperature was held at 70°C. After a 2-min hold at 1800 p.s.i., the carbon dioxide pressure was increased to 6000 p.s.i. at a rate of 100 p.s.i./min. Each column was tested in duplicate with dry carbon dioxide, and in duplicate with water-saturated carbon dioxide. Water was removed from the SFC columns by heating the column oven to 150°C for 15 min at 6000 p.s.i., then keeping them at 70°C for 10 min. Due to

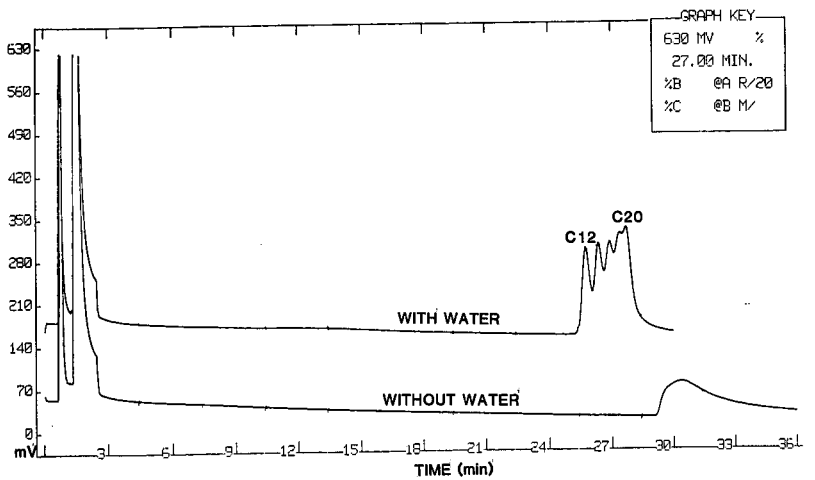

Fig. 7. SFC of C_{12}, C_{14}, C_{16}, C_{18}, C_{20} saturated free fatty acids. Conditions: as per Fig. 1. Carbon dioxide mobile phase at 70°C, with and without water modifier. Column: 100 × 1 mm I.D., YMC Gel Silica (120 Å) (SIL).

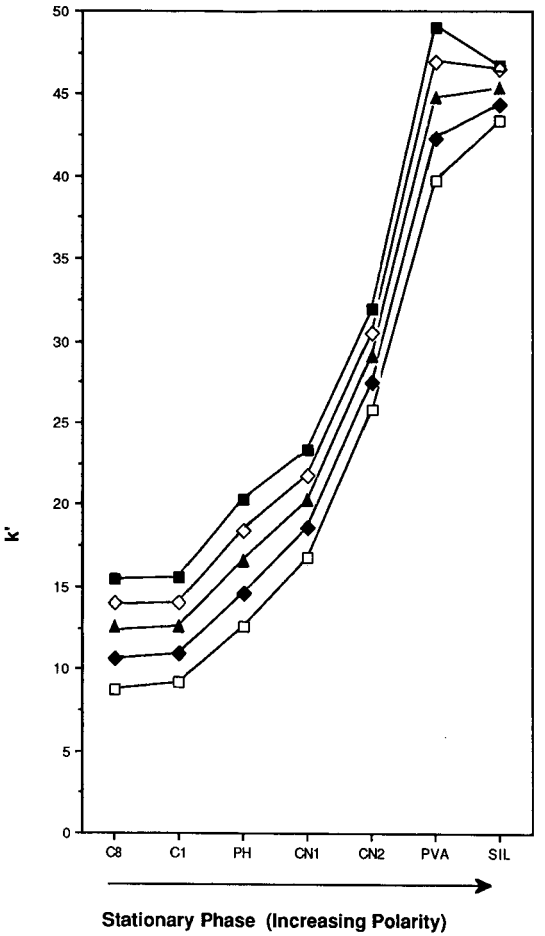

Fig. 8. Free fatty acid k' data *vs.* increasing stationary phase polarity for seven stationary phases. SFC conditions are the same as per Fig. 1, water-saturated carbon dioxide mobile phase, column oven 70°C. Stationary phase abbreviations are given in Figs. 1–7. Free fatty acid solutes were: (⊡) lauric (C_{12}), (◆) myristic (C_{14}), (▲) palmitic (C_{16}), (◇) stearic (C_{18}), (■) arachidic (C_{20}) acid.

the temperature limitations of YMC-Gel PVA-Sil, the drying conditions were modified to 125°C for 12–16 h (overnight).

Column performances with dry and with water-satuarted carbon dioxide are presented in Figs. 1–7 in the order of increasing retention time and stationary-phase polarity. To illustrate the polarity variations of the seven stationary phases futher, k' data for the five free fatty acids were plotted in Fig. 8. These results illustrate that an investigator could vary the retention of lauric acid from $k' = 8.7$ (5.6 min) for Deltabond Octyl to $k' = 39.7$ (23.6 min) for YMC-Gel PVA-Sil. The range of exhibited stationary phase polarities should enable an investigator to select a column based on the resolution requirements for a particular analysis.

Using the protocol presented, this technique should prove useful for rapid

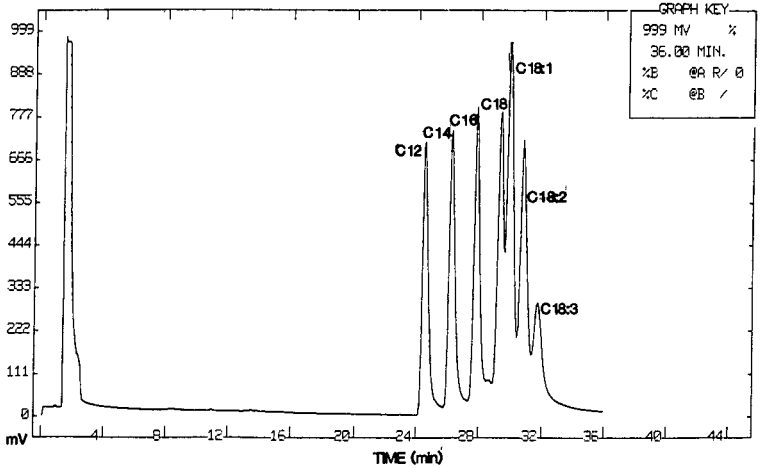

Fig. 9. SFC of saturated and unsaturated free fatty acids. Conditions: same as Figure 1. Water-saturated carbon dioxide mobile phase, column oven 70°C. Column: 100 × 1 mm I.D., 5 μm YMC Gel PVA-Sil. Unsaturated free fatty acids are oleic (C_{18}:1), linoleic (C_{18}:2) and linolenic (C_{18}:3) acid.

screening and selection of suitable packed column SFC stationary phases, and allow these phases to be compared with the performance of existing phases.

In a preliminary study on mixtures of saturated and unsaturated fatty acids, YMC-Gel PVA-Sil was selected for evaluation because of its superior resolving power. The results of the separation are given in Fig. 9 in which oleic, linoleic, and linolenic free fatty acids were separated from a mixture of lauric, myristic, palmitic, and stearic acids under the chromatographic conditions used in Figs. 1–7. Since the unsaturated free fatty acids are model compounds for potent natural products, such as prostanoids, leukotrienes, and thromboxanes, additional research will be directed to evaluating packed-column SFC stationary phases which would enable the FID detection of these important classes of compounds.

CONCLUSIONS

Water-saturated carbon dioxide improved the chromatographic performance of all seven packed-column stationary phases evaluated in the study: (A) peak shape and resolution were improved for covalently-bonded stationary phases (YMC-Gel Phenyl and Nucleosil Cyano) and for non-bonded silica gel (YMC-Gel Silica); (B) peak height and sensitivity were increased for polymer-coated stationary phases (Deltabond Methyl, Octyl, and Cyano, and YMC-Gel PVA-Sil).

A mechanism is proposed which attributes the primary benefit of water-saturated carbon dioxide to masking of undesirable sites (probably unreacted silanol) on the stationary phase. From these results we conclude that packed column SFC stationary phase research should be directed to the manufacture of stationary phases that minimize the requirement for masking of unwanted sites by modifiers. These stationary phases would be expected to exhibit the highest reproducibility and utility, especially in the separation of non-chromophoric solutes requiring the use of FID.

From the qualitative data presented in this study, we conclude that YMC-Gel PVA-Sil (Fig. 6) and Deltabond C8 (Fig. 1) are suitable models for packed-column SFC stationary phases. We recommend that conditions for packed-column SFC separation conditions should routinely include the use of water-saturated carbon dioxide, because of its clear enhancement of chromatographic resolution and sensitivity, especially with polar solutes.

ACKNOWLEDGEMENTS

The authors wish to acknowledge R. Hartwick and R. Blaine for packing of microbore columns, M. Simms and M. Klee for helpful technical discussions, and J. Watkins for invaluable assistance in conditioning the columns and in reviewing experimental data.

REFERENCES

1 H. E. Schwartz, *Fresenius Z. Anal. Chem.*, 330 (1988) 204.
2 B.W. Wright and R. D. Smith, *J. Chromatogr.*, 355 (1986) 367.
3 R. Board, D. McManigill, H. Weaver and D. Gere, *J. Chem. Soc. South Africa*, June (1983) 17.
4 A. L. Blilie and T. Greibrokk, *Anal. Chem.*, 57 (1985) 2239.
5 J. M. Levy and W. M. Richey, *J. High Resolut. Chromatogr. Chromatogr. Commun.*, 8 (1984) 503.
6 R. E. Majors, *LC · GC, Mag. Liq. Gas Chromatogr.*, 6 (1988) 462.
7 M. Tsuboi, R. Yammamura, K. Kitagawa, R. S. Cooley, *Abstracts of the Pittsburgh Conference on Analytical Chemistry and Applied Spectroscopy, Atlantic City, NJ, March 9–13, 1987*, Abstract No. 721.

Journal of Chromatography, 459 (1988) 183–191
Elsevier Science Publishers B.V., Amsterdam — Printed in The Netherlands

CHROMSYMP. 1462

EFFECT OF THE PARTIAL MOLAR VOLUME OF THE SOLUTE IN THE STATIONARY PHASE ON RETENTION IN SUPERCRITICAL FLUID CHROMATOGRAPHY

CLEMENT R. YONKER* and RICHARD D. SMITH
Chemical Methods and Separations Group, Chemical Sciences Department, Pacific Northwest Laboratory (Operated by Battelle Memorial Institute), Richland, WA 99352 (U.S.A.)

SUMMARY

Retention in supercritical fluid chromatography is a dynamic mechanism, involving intermolecular interactions in the mobile and stationary phases. A simple thermodynamic model, describing solute retention, has been investigated on the basis of macroscopic thermodynamic variables of the solute partial molar volume in the stationary and mobile phases. Solute–solvent interactions in the mobile phase are dominant at lower pressures. Solute–stationary phase interactions have an important role in solute retention in capillary supercritical fluid chromatography. The interaction of the solute with the five different stationary phases reflects the polarizability differences between these phases, as shown by the partial molar volume of the solute in the stationary phase.

INTRODUCTION

Retention in supercritical fluid chromatography (SFC) is a complex function of temperature, density, eluent composition and the intermolecular interactions between the solute and the mobile and stationary phases. Solute–solvent interactions in the fluid mobile phase can be expressed on the basis of the macroscopic thermodynamic quantity of the partial molar volume of the solute in the mobile phase at infinite dilution, $\bar{v}_i^{mp,\infty}$. Pressure effects on solute retention in SFC are well established. This parameter incorporates changes in chemical potential of the solute with pressure $(\partial\mu_i/\partial P)_{T,n}$. In supercritical fluid solutions the chemical potential of the solute can be changed dramatically by small variations of pressure[1,2]. Interaction of the solute with the stationary phase can be described by the fundamental solution property of the partial molar volume of the solute in the stationary phase at infinite dilution, $\bar{v}_i^{sp,\infty}$.

A simple thermodynamic model for solute retention in SFC has been proposed by Van Wasen and co-workers[3,4] and Yonker and co-workers[5,6], based on the macroscopic thermodynamic parameters of $\bar{v}_i^{mp,\infty}$ and $\bar{v}_i^{sp,\infty}$. Martire and Boehm[7,8] have outlined a unified theory of adsorption chromatography, applied to gas, liquid and supercritical mobile phases, based on a more complex statistical thermodynamic model describing solute retention. The thermodynamic model of Yonker and

0021-9673/88/$03.50

co-workers[5,6] has been used to correlate solute retention as a function of pressure, based on the solution thermodynamic parameters of the partial molar volume ($\bar{v}_i^{mp,\infty}$, $\bar{v}_i^{sp,\infty}$). Both approaches provide similar insights into the SFC retention process.

In this paper, development of the retention model is extended by studies of various bonded stationary phases in capillary SFC over a wide range of pressures. The roles of both the mobile and stationary phases on retention were studied experimentally. The partial molar volume of the solute in the stationary phase has been used to determine whether the retention process is based on adsorption or partitioning into the bonded phase. Both fundamental solution parameters, $\bar{v}_i^{mp,\infty}$ and $\bar{v}_i^{sp,\infty}$, have been studied to gain a greater insight into the retention mechanism in SFC.

THEORY

Solute retention in SFC as a function of pressure at constant temperature for a pure fluid mobile phase is expressed by[3,5]

$$(\partial \ln k'/\partial P)_T = \frac{1}{RT}(\bar{v}_i^{mp,\infty} - \bar{v}_i^{sp,\infty}) - K \tag{1}$$

where k' is the solute capacity factor, P is the mobile-phase pressure, R is the gas constant, T is the absolute temperature and K is the isothermal compressibility of the fluid solution. The solute concentration is considered to be at infinite dilution and solute retention will therefore be independent of concentration. Thus, the partial molar volumes are determined at infinite dilution of the solute in the fluid mobile phase ($\bar{v}_i^{mp,\infty}$) and stationary phase ($\bar{v}_i^{sp,\infty}$). The assumptions made in eqn. 1 are that the molar volume of the stationary phase and the volumes of the stationary phase and mobile phase are independent of pressure. Under infinite dilution conditions, generally relevant to SFC, the isothermal compressibility of the fluid solution is equal to the isothermal compressibility of the pure mobile phase.

The partial molar volume of the solute in the mobile phase at infinite dilution can be evaluated by

$$\bar{v}_i^{mp,\infty} = (\partial V/\partial n_1)_{T,P,n_2} = K_2 V_2 (\partial P/\partial n_1)_{T,P,n_2} \tag{2}$$

where V is the volume of the binary solution, n_1 and n_2 are the number of moles of solute and solvent, respectively, K_2 is the isothermal compressibility of the pure fluid and V_2 is the molar volume of the pure fluid[6]. The partial molar volume of the solute in the mobile phase can be divided into two parts: K_2V_2, which is dependent on the pure fluid, and $(\partial P/\partial n_1)_{T,P,n_2}$, which is dependent on the attractive or repulsive intermolecular interactions in the binary solution.

There are three pressure regimes of interest to retention in eqn. 1. The first regime exists at low pressures, where $|\bar{v}_i^{mp,\infty}| \gg |\bar{v}_i^{sp,\infty}|$. As the isothermal compressibility of the fluid is greatest in the low-pressure region near the critical point of the fluid, a minimum in $\bar{v}_i^{mp,\infty}$ is observed where K_2 is a maximum[4,9–11]. Eqn. 1 for this pressure region is reduced to

$$(\partial \ln k'/\partial P)_T \approx \bar{v}_i^{mp,\infty}/RT - K \tag{3}$$

The derivative $(\partial P/\partial n_1)_{T,P,n_2}$ in eqn. 2 will be negative at low pressure because as a solute is added to the fluid at constant volume and temperature, the overall pressure of the system decreases with attractive solute–fluid intermolecular interactions. Negative partial molar volumes have been observed for supercritical fluids[1,2,4,11]. Therefore the slope of retention calculated from eqn. 3 would be negative.

The second pressure region of importance occurs when $\bar{v}_i^{mp,\infty} = \bar{v}_i^{sp,\infty}$; then eqn. 1 is reduced to

$$(\partial \ln k'/\partial P) \approx -K \tag{4}$$

In this case, the slope of solute retention is similar to the isothermal compressibility of the fluid. At these pressures the compressibility of the fluid is small; therefore the slope in eqn. 4 will be approximately zero.

The final pressure region of interest is at higher pressures, where $\bar{v}_i^{mp,\infty}$ is positive and greater than $\bar{v}_i^{sp,\infty}$. This pressure region is defined when the reduced density for the fluid is greater than 1.6. In this region, K_2 and K are very small, and $\bar{v}_i^{mp,\infty}$ has a small positive value[1]. Eqn. 1 cannot be simplified, as both $\bar{v}_i^{mp,\infty}$ and $\bar{v}_i^{sp,\infty}$ play a role in solute retention. With $\bar{v}_i^{mp,\infty}$ being positive at higher pressures, the derivative $(\partial P/\partial n_1)_{T,P,n_2}$ is positive. Under these conditions, $(\partial P/\partial n_1)_{T,P,n_2}$ represents possible repulsive interactions occurring in the fluid mobile phase at higher densities. If the value of $\bar{v}_i^{sp,\infty}$ reflects attractive interactions between the solute and the bonded stationary phase, then $\bar{v}_i^{sp,\infty} < V_i$ (where V_i is the molar volume of the solute). When repulsive interactions between the solute and stationary phase occur, it is possible for $\bar{v}_i^{sp,\infty} > V_i$. Finally, if the solute is adsorbed on the surface of the bonded stationary phase, then $\bar{v}_i^{sp,\infty} \approx V_i$, because the solute mainly interacts with itself.

Solute retention for naphthalene as a function of pressure with carbon dioxide as the mobile phase was studied with various column types at 35 and 45°C. The $\bar{v}_i^{sp,\infty}$ values are regressed from the least-squares fit of the experimental data to the calculated theoretical data to determine the apparent retention mechanism and the role of the stationary phase in solute retention in SFC.

EXPERIMENTAL

The experimental system and approach has been described in detail elsewhere[12]. The capacity factors for naphthalene at 35 and 45°C in carbon dioxide from 80 to 350 atm with SE-33, OV-17, DB-5, OV-1 and SE-54 were measured. The chemical composition of the stationary phases in the capillaries is given in Table I. The dimensions of the capillary columns were 10 m × 100 μm I.D. A Varian (Walnut Creek, CA, U.S.A.) 8500 microprocessor-controlled high-pressure syringe pump provided a pulse-free mobile-phase flow and accurate fluid pressure. The column temperature was controlled with a constant-temperature air-bath to an accuracy of ±0.1°C. The system pressure was measured with a Bourdon tube-type pressure gauge in line between the pump and the capillary column in the oven. The retention time of naphthalene as a function of pressure was measured with a reporting integrator, having an accuracy of 0.1 s. The elution time of dichloromethane, which was the solvent used for naphthalene, was used for the t_0 measurement in the determination of k' for naphthalene at all pressures studied. The solute sample was injected with a Valco

TABLE I

PARTIAL MOLAR VOLUME OF NAPHTHALENE IN DIFFERENT STATIONARY PHASES ($\bar{v}_i^{sp,\infty}$ ± PROBABLE ERROR) FROM THE LEAST-SQUARES FIT OF EXPERIMENTAL RETENTION DATA

Column type	*Phenyl-to-methyl ratio of the polysiloxane stationary phase*	*Partial molar volume (cm^3/mole)*		*Film thickness (μm)*
		35°C	*45°C*	
OV-1	0:100	197 ± 22	377 ± 3	0.20
DB-5	5:95	124 ± 9	284 ± 32	0.20
SE-54	5:95	84 ± 16	149 ± 11	0.20
OV-17	50:50	22 ± 20	244 ± 20	0.10
SE-33	0:100	347 ± 26	300 ± 23	0.20
		149 ± 30	299 ± 16	0.30
		68 ± 16	144 ± 10	0.40
V_i (naphthalene)		126.4	127.4	

(Houston, TX, U.S.A.) C14W HPLC injection value (0.2 μl rotor volume), which was mounted outside the oven. A flow restrictor was connected to the end of the capillary and controlled the flow of the mobile phase through the column. After expansion through the restrictor, the solute was detected with a flame ionization detector.

RESULTS AND DISCUSSION

Experimental partial molar volume data for naphthalene in carbon dioxide are available[2]. They permit the calculation of $\bar{v}_i^{mp,\infty}$ by means of a two-parameter cubic equation of state (EOS), such as the Peng–Robinson EOS[1,2,6]. The accuracy of the fit of the experimental data as one nears the critical point of the fluid becomes suspect, but further from the critical point the fit is improved. The binary interaction parameters for the calculation of $\bar{v}_i^{mp,\infty}$ of naphthalene calculated with the Peng–Robinson EOS were regressed from solubility data of naphthalene in carbon dioxide at 35 and 45°C[2]. The experimental data[1] and $\bar{v}_i^{mp,\infty}$ calculated from the Peng–Robinson EOS for naphthalene at 35 and 45°C are shown in Fig. 1. The trends in $\bar{v}_i^{mp,\infty}$ are similar to that reported by Van Wasen and Schneider[11] as a function of pressure and temperature determined from experimental retention studies in packed-column SFC. The calculation of solute retention in SFC is similar to that described by the authors previously[6]. In this work the partial molar volume of the solute in the stationary phase was obtained by a least-squares fit of the experimental data to eqn. 1. The data in Fig. 1 show a large negative $\bar{v}_i^{mp,\infty}$ value at 35°C for naphthalene. This is because the derivative $(\partial P/\partial n_1)_{T,P,n_2}$ in eqn. 2 is negative. As discussed in the Theory section, attractive intermolecular interactions between the solute and the solvent would cause $(\partial P/\partial n_1)_{T,P,n_2}$ to be negative. Therefore, carbon dioxide can be considered to cluster about naphthalene at these low pressures near the critical point. This affects the solubility of naphthalene in carbon dioxide[1,10]. At 45°C, $\bar{v}_i^{mp,\infty}$ is not as negative as at 35°C; therefore one might expect the slope of solute retention to be not as steep at 45°C as for naphthalene at 35°C. This is indeed seen for the cases studied in this work and was also reported by Van Wasen and Schneider[11] for packed-column SFC. The

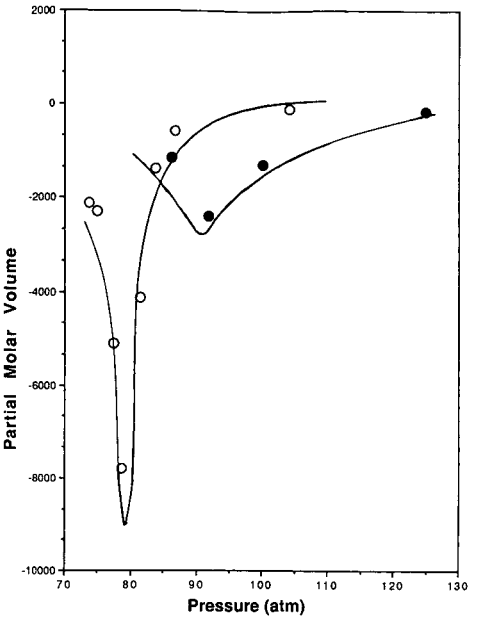

Fig. 1. Plot of the partial molar volume (in cm^3/mole) of naphthalene in carbon dioxide as a function of pressure at (○) 35 and (●) 45°C. Symbols, experimental data; lines, calculated data.

$\bar{v}_i^{mp,\infty}$ values in Fig. 1 become less negative and finally positive as pressure increases, thus reflecting the onset of possible repulsive interactions between the solute and solvent as pressure increases $[(\partial P/\partial n_1)_{T,P,n_2} > 0]$.

In Fig 2, with DB-5 (phenylmethylpolysiloxane with a phenyl/methyl ratio of 95:5) at 35°C, naphthalene retention is plotted as a function of pressure. The solid line is calculated from eqn. 3, assuming $\bar{v}_i^{mp,\infty}$ is dominant, and is fixed to the first experimental data point. The Peng–Robinson EOS was used to calculate $\bar{v}_i^{mp,\infty}$ at 35°C. The experimental data and the solid line correlate fairly well at low pressures, but as the pressure increases the predicted slope becomes zero, and with still further increases in pressure the theoretical slope becomes positive. A positive slope indicates a net increase in solute retention (increased k') with pressure.

The experimental results do not bear out this postulated retention mechanism at higher pressures. As pressure increased, the naphthalene retention asymptotically decreased, approaching a k' value of zero in all cases studied. Further increases in pressure up to 350 atm did not show the retention reversal theoretically calculated for Fig. 2. The theoretical retention reversal is caused by the overemphasis of the repulsive interactions between the solute and the fluid mobile phase in $\bar{v}_i^{mp,\infty}$ $[(\partial P/\partial n_1)_{T,P,n_2} > 0]$ as pressure increases.

The experimental results for the DB-5 capillary column were used again with the theoretical retention slope calculated from eqn. 1, allowing $\bar{v}_i^{sp,\infty}$ to assume a value giving the best least-squares fit to the experimental data. These results are shown in Fig. 3. The least-squares value for $\bar{v}_i^{sp,\infty}$ was 124 cm^3/mole for naphthalene in this polyphenylmethylsiloxane stationary phase. The theoretical slope of retention fits the

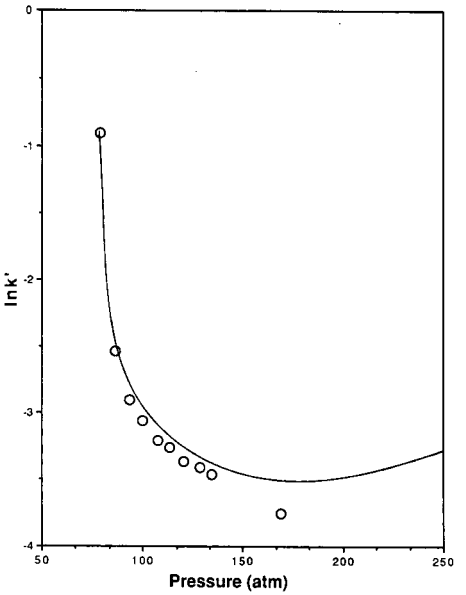

Fig. 2. Plot of experimental ln k' *versus* pressure for DB-5 at 35°C. The solid line was calculated from eqn. 3.

experimental data fairly accurately over the entire pressure range studied. In this instance at 35°C, no retention minimum is predicted for the retention of naphthalene with carbon dioxide. Therefore, the mobile phase alone does not control solute retention. The stationary phase has a role in the retention mechanism in SFC but the

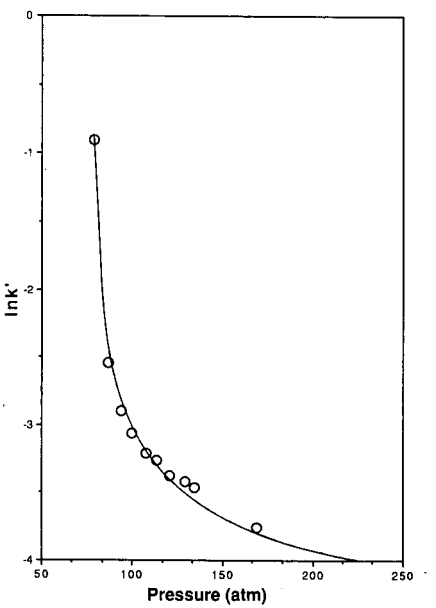

Fig. 3. Plot of experimental ln k' *versus* pressure for DB-5 at 35°C. The solid line was calculated from eqn. 1 with the least-squares value for $\bar{v}_i^{sp,\infty} = 124$ cm^3/mole.

exact role, be it an adsorption or partitioning process, remains to be defined.

Similar results at 45°C for naphthalene eluted from a capillary bonded with OV-17 by carbon dioxide are shown in Fig. 4. The calculated slope is based on a $\bar{v}_i^{sp,\infty}$ of 244 cm^3/mole, which was obtained from the least-squares fit to the experimental data. Once again, the data are fitted fairly accurately by the calculated slope over the entire pressure range studied. Similar results were obtained with all columns studied at both 35 and 45°C, as shown in Figs. 3 and 4 for naphthalene and carbon dioxide. No retention minimum was seen in the experimental solute retention values with increasing pressure up to and including 350 atm.

The partial molar volume of the solute in the stationary phase is an important thermodynamic parameter, related to the solute environment in the bonded polymeric phase. If there are no intermolecular interactions between the bonded polymeric stationary phase and the solute, then the solute is adsorbed on the interface region between the stationary phase and the fluid mobile phase. Solute adsorption on the surface of the polymer should give a $\bar{v}_i^{sp,\infty}$ value equal to the molar volume of the pure solute (V_i). This is because the solute is only capable of interacting with itself when it is adsorbed on the stationary phase. If the solute can partition into the bonded polymeric phase, then the possibility exists for attractive or repulsive intermolecular interactions between the solute and the stationary phase. If the intermolecular interactions are more attractive than in the pure solute, then $\bar{v}_i^{sp,\infty} < V_i$ would be expected to occur. On the other hand, if the intermolecular interactions are slightly repulsive (less attractive) between the solute and the stationary phase, then the total volume for the stationary phase–solute solution will increase with $\bar{v}_i^{sp,\infty} > V_i$. Through the study of $\bar{v}_i^{sp,\infty}$ under

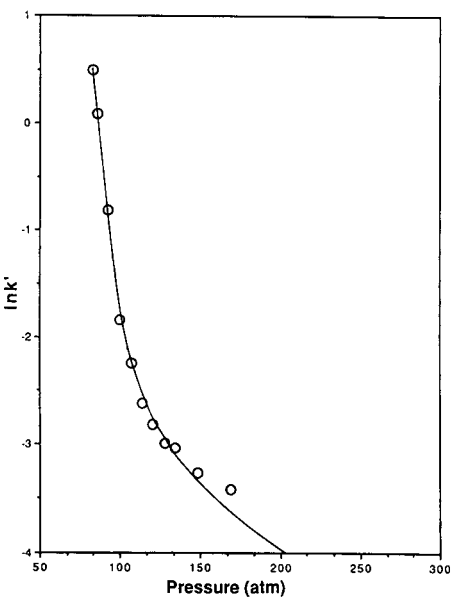

Fig. 4. Plot of experimental ln k' *versus* pressure for OV-17 at 45°C. The solid line was calculated from eqn. 1 with the least-squares value for $\bar{v}_i^{sp,\infty}$ = 244 cm^3/mole.

SFC conditions, a greater in-depth understanding of the intermolecular interactions between the solute and stationary phase can be obtained.

Table I contains the least-squares regressed $\bar{v}_i^{sp,\infty}$ values, obtained from fitting eqn. 1 to the experimental data for the five stationary phases studied by capillary SFC. Naphthalene should be able to interact more effectively with a polarizable stationary phase, such as OV-17, owing to the larger phenyl content of the bonded polymer. The ranking of naphthalene interactions with these five stationary phases is qualitatively OV-17 > SE-54 ≈ DB-5 > OV-1 ≈ SE-33. This is based on the decreasing percentage of phenyl groups in the bonded polymer (*cf.*, Table I). Intermolecular interactions between the solute and stationary phase are reflected in the $\bar{v}_i^{sp,\infty}$, regressed from the experimental data by means of eqn. 1. Naphthalene can interact very effectively with OV-17, and one obtains $\bar{v}_i^{mp,\infty} < V_i$. The least effective interaction should be with OV-1 and SE-33, as evidenced by $\bar{v}_i^{sp,\infty} > V_i$. A similar trend in $\bar{v}_i^{sp,\infty}$ is seen at 45°C, where $\bar{v}_i^{sp,\infty}$ decreases as the solute–stationary phase interaction increases. The qualitative agreement between $\bar{v}_i^{sp,\infty}$ from the proposed thermodynamic retention model and the postulated extent of intermolecular interaction between the solute and stationary phase is remarkable. The difference in $\bar{v}_i^{sp,\infty}$ as a function of temperature is probably due to the increased thermal energy in the system which contributes to higher thermal random motion in the polymer phase. This thermal motion precludes as effective of an intermolecular interaction between the solute and stationary phase at the higher temperature. This is reflected in the larger $\bar{v}_i^{sp,\infty}$ values at 45°C compared with 35°C. These results seem to establish the partitioning of the naphthalene solute into the bonded polymeric phase. This fact is also borne out when comparing the $\bar{v}_i^{sp,\infty}$ results for SE-33 as a function of stationary-phase film thickness. As the film thickness increases the bonded polymer would be a better solvent for the solute. This is reflected in the decrease in $\bar{v}_i^{sp,\infty}$ and an increase in solute retention with increasing film thickness for the SE-33 stationary phase.

Experimental data and $\bar{v}_i^{sp,\infty}$ values have been reported with a packed column (10-μm Whatman Partisil ODS-2) and carbon dioxide at 40°C by Brown *et al.*[13]. They reported an adsorption retention mechanism for naphthalene on the octadecyl-bonded stationary phase because they found that $\bar{v}_i^{sp,\infty} \approx V_i$ in this system. Studies performed by these workers on other solutes proved in conclusive owing to relatively large experimental uncertainties. The lack of accurate experimental $\bar{v}_i^{mp,\infty}$ values for different solutes as a function of pressure precludes the accurate extension of this technique to different solute–solvent–stationary phase systems[13]. The experimental methodology and theoretical retention calculation based on eqn. 1 do suggest the important potential for studying the intermolecular interactions of dilute solute-bonded polymeric phases.

CONCLUSIONS

Determination of $\bar{v}_i^{sp,\infty}$ on the basis of theory and the methodology discussed in this paper provides insights concerning the role of adsorption or partitioning processes in retention during SFC. If $\bar{v}_i^{sp,\infty} = V_i$, then solute adsorption at the stationary phase interface probably occurs. If $\bar{v}_i^{sp,\infty} > V_i$ or $\bar{v}_i^{sp,\infty} < V_i$ then a partition-like retention process must occur with slightly repulsive or attractive intermolecular interactions between the solute and stationary phase. The results presented in this paper are

consistent with the extent of intermolecular interaction between naphthalene and the polarizable stationary phases studied. The extension of this work to different solutes awaits more accurate $\bar{v}_i^{mp,\infty}$ determinations.

ACKNOWLEDGEMENT

The authors acknowledge the support of the U.S. Department of Energy, Division of Chemical Science Office of Basic Energy Sciences, under Contract DE-AC06-76RLO 1830.

REFERENCES

1 C. A. Eckert, D. H. Ziger, K. P. Johnston and S. Kim, *J. Phys. Chem.*, 90 (1986) 2738.
2 D. H. Ziger, *Ph. D. Dissertation*, University of Illinois, Urbana, IL, 1983.
3 U. van Wasen and G. M. Schneider, *Chromatographia.*, 8 (1975) 274.
4 U. van Wasen, I. Swaid and G. M. Schneider, *Angew. Chem., Int. Ed. Engl.*, 19 (1980) 575.
5 C. R. Yonker, R. W. Gale and R. D. Smith, *J. Phys. Chem.*, 91 (1987) 3333.
6 C. R. Yonker and R. D. Smith, *J. Phys. Chem.*, 92 (1988) 1664.
7 D. E. Martire, *J. Liq. Chromatogr.*, 10 (1987) 1569.
8 D. E. Martire and R. D. Boehm, *J. Phys. Chem.*, 91 (1987) 2433.
9 R. B. Gitterman and I. Procaccia, *J. Chem. Phys.*, 78 (1983) 2648.
10 P. G. Debenedetti and S. K. Kumar, *AIChE J.*, 34 (1988) 645.
11 U. van Wasen and G. M. Schneider, *J. Phys. Chem.*, 84 (1980) 229.
12 R. D. Smith, H. T. Kalinoski, H. R. Udseth and B. W. Wright, *Anal. Chem.*, 56 (1984) 2476.
13 B. O. Brown, A. J. Keshbaugh and M. E. Paulaitis, *Fluid Phase Equilib.*, 36 (1987) 247.

Journal of Chromatography, 459 (1988) 193–200
Elsevier Science Publishers B.V., Amsterdam — Printed in The Netherlands

CHROMSYMP. 1414

USE OF TWO SIMULTANEOUS DETECTORS IN CAPILLARY SUPERCRITICAL FLUID CHROMATOGRAPHY

DARRYL J. BORNHOP*, STAFFAN SCHMIDT* and NATHAN L. PORTER
Lee Scientific Inc., 4426 S. Century Drive, Salt Lake City, UT 84123 (U.S.A.)

SUMMARY

A simple splitter device was incorporated into a capillary supercritical fluid chromatographic system to allow simultaneous detection with both a universal detector (flame ionization detector) and a selective detector (ultraviolet–visible absorbance detector). The technique is quantitative and reproducible while maintaining the high resolution normally obtainable with a capillary column. The advantage of using two detectors simultaneously is demonstrated. The technique enables the analyst to obtain additional information in the analysis of complex matrices.

INTRODUCTION

Supercritical fluid chromatography (SFC) is a separation technique that is gaining wide acceptance for many applications. Among the attributes of SFC, especially capillary column SFC, are a high separation efficiency[1–3], applicability to thermally labile molecules[4,5] and multi-detector compatibility[6–12]. The high separation efficiency is attributed to the properties of the supercritical fluid employed, which has gas-like diffusivity and liquid-like solvating characteristics. These mobile phase properties, combined with advantages realized by utilizing open-tubular wall-coated capillaries as columns, produce a separation technique with a high resolution similar to that of capillary gas chromatography (GC) and an applicability potentially comparable to that of high-performance liquid chromatography (HPLC). The disadvantage of using small-volume fused-silica capillary columns is that the post- and pre-column dead volume constraints are severe. Detector dead volume constraints are particularly serious when conventional optical detection methods are employed with capillary SFC[13,14].

Carbon dioxide is the most commonly used fluid in SFC because it is supercritical at moderate temperature (*ca.* 35°C) and pressure (*ca.* 75 atm), is non-toxic and is inexpensive to obtain in high purity. These moderate supercritical conditions allow the chromatographer to analyze thermally labile species, such as carbamate

* Present address: Department of Analytical Chemistry, Arrhenius Laboratory, University of Stockholm, S-10691 Stockholm, Sweden.

0021-9673/88/$03.50

pesticides[15], without the decomposition that accompanies GC. In addition, many non-volatile species that are not amenable to GC or do not not have UV-absorbing chromophores, and are thus poor candidates for LC, can be chromatographed and detected using capillary SFC systems with a flame ionization detector[16,17]. As decompression can be performed either before or after UV detection, various fluid phase detectors are also applicable in SFC[12–14,18].

Multi-detector compatibility is certainly one of the key attributes of SFC, especially capillary SFC. As illustated by Later *et al.*[12], UV–VIS, flame ionization (FID), Fourier transform infrared (FT-IR) and mass spectrometry (MS) are among the detection techniques that have been applied to SFC analysis. Other commonly used GC and LC detection methods used in SFC include nitrogen–phosphorus detection (NPD)[19], scanning fluorescence detection[18], photodiode array-based scanning UV–VIS detection[20] and dual flame photometric detection (FPD)[21].

There are several advantages in using two or more detectors simultaneously, including (1) a reduced analysis time as a result of obtaining two chromatograms of the same component in a single run and (2) detection yielding two forms of information[22] (universal, *e.g.*, in FID, and specific, *e.g.*, in UV detection) for elucidating the identity of solutes found in complex matrices. So far, no report has appeared that describes the use of FID and UV detection simultaneously. Raynor *et al.*[23] employed a splitter to monitor FID while diverting a portion of the sample to a potassium bromides window for subsequent scanning and spectral analysis with an IR microscope. Levy *et al.*[24] attached a flame ionization and a UV detector in series for the detection of the effluent from a 4.6-mm I.D. packed column in SFC. Finally, a low-dead-volume T-piece has been used in capillary SFC for simultaneous detection by FID and MS[25].

We describe here a splitting device that is very simple and allows simultaneous detection with two detectors in capillary SFC. Detection limits, chromatographic performance and analytical applications are discussed.

EXPERIMENTAL

Apparatus

The experiments were performed on a Model 501 supercritical fluid chromatographic system (Lee Scientific, Salt Lake City, UT, U.S.A.). This system was equipped with a Model 501 UV detector especially designed for capillary SFC[14]. The flame ionization detector was not modified and was operated as prescribed by the instrument manufacturer. In all instances, SFC-gade carbon dioxide (Scott Speciality Gases, Plumsteadville, PA, U.S.A.) was used as the mobile phase. The columns employed were 3 m × 50 μm I.D., SB-Methyl-50 and 10 m × 100 μm I.D. SB-Methyl-100 (Lee Scientific), each with a 0.25-μm film. Split injections were made with a 200-nl internal loop air-actuated Valco (Houston, TX, U.S.A.) injection valve. The injection time was 2 s.

Our splitter is a modification of the SGE (Austin, TX, U.S.A.) Model VSOS-1:1, made especially for the high pressures and low dead volumes utilized in capillary SFC. The transfer lines were varied as described under Results and Discussion, but in most instances the FID transfer line consisted of an 18 cm × 50 μm I.D. frit restrictor (Lee Scientific) and the UV transfer line was a portion of deactivated fused-silica capillary tubing. These transfer lines were connected with a two hole graphite–Vespel ferrule. In all experiments the UV restrictor was mounted after the UV detector flow-cell cuvette.

Chemicals

All chemicals were of analytical-reagent grade or better. Test and calibration solutions were prepared in dichloromethane. Calibration and height equivalent to a theoretical plate (HETP) test solutions consisted of *n*-hexadecane (C_{16}) and *n*-tetracosane (C_{24}) and the polycyclic aromatic hydrocarbon (PAH) species anthracene and pyrene. A number of dilutions of the stock solution were prepared in order to construct calibration graphs.

RESULTS AND DISCUSSION

A calibration graph was constructed for the four test solutes, anthacene, pyrene, C_{16} and C_{24}, with FID and for anthracene and pyrene with UV–VIS detection. The results are summarized in Table I. Both calibration graphs were linear ($r > 0.99$) over at least three orders of magnitude with detection limits of *ca.* 5 ppm for UV–VIS detection and *ca.* 1000 ppm for FID. No decrease in linearity was observed with the highest concentration solution investigated, but it is expected that chromatographic overloading will limit the upper end of the concentration range suitable for this system. As indicated in Table I, the detection limits are only modest, but the concentration (mass) detection limits are fairly good. The mass sensitivity enhancement is expected as predicted by theory for micro-separation schemes and observed experimentally[26–28]. It was found that the splitting ratio is primarily dependent on the amount of restriction used at each detector. By controlling this flow parameter it is possible to vary the relative amount of analyte sent to each of the two detectors.

The detection limits obtained in the simultaneous mode are comparable to, but slightly higher than, those found in the operation of each detector individually. A direct comparison is difficult for the UV detector as different columns of different diameters were used in this study, which was aimed at developing a capillary UV–SFC interface. As peak height was used as an indicator of response in both stand-alone UV experiments[14] and the present experiments, changes in the chromatographic conditions could contribute significantly to differences in the observed detection limits. Ideally, an integrator should be employed so that chromatographic band-broadening

TABLE I

LIMITS OF DETECTION FOR UV–VIS DETECTION AND FID

Conditions: injection, 200 nl before split; injection splitting ratio, 7:1; UV–VIS flow-rate, 3.3 × FID flow-rate; FID at 350°C, UV–VIS detection at 254 nm.

Solute	*Detection limit**	
	UV–VIS	*FID*
Anthracene	4 ppm, 90 pg**	15 ppm, 90 pg**
Pyrene	10 ppm, 200 pg**	10 ppm, 60 pg**
C_{16}	–	10 ppm, 60 pg**
C_{24}	–	8 ppm, 50 pg**

* Detection limits are two standard deviations larger than the noise in the background signal.

** On-column mass detection limits compensated for injection split and split flows.

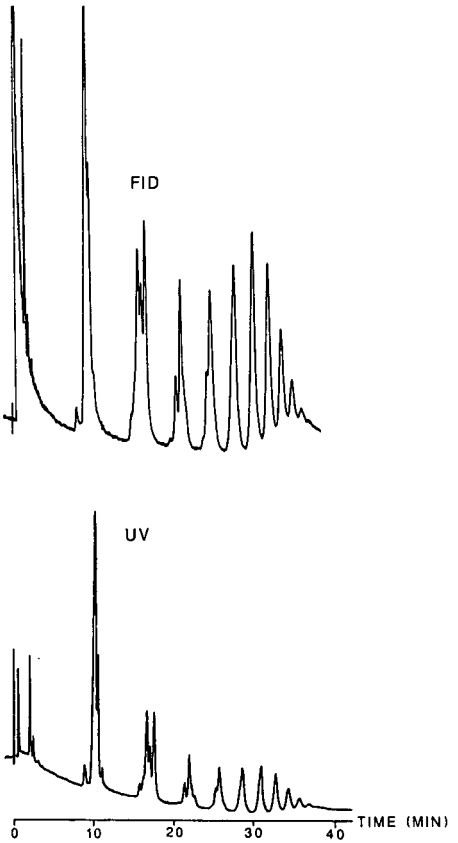

Fig. 1. Chromatograms of phenylhydropolysiloxane. Column temperature, 120°C. The UV trace was obtained at 210 nm. The FID trace was obtained at an attenuation of 2^6 and a detector temperature of 400°C.

contributions to a decrease in detection limits are minimized. The FID mass detection limits compare well with those suggested by the instrument manufacturers, who report an on-column detection limit for *n*-alkanes in the range 50–100 pg. In general, the concentration and mass detection limits are good and the simultaneous detection interface is suitable for most normal capillary SFC applications. Concentration detection limits could possibly be improved upon by careful control of the split flow and by an increase in the column loadability.

When such a device is incorporated into a capillary-based SFC system it is important to know whether the introduction of a post-column detector volume will contribute significantly to chromatographic band broadening. To answer this question we determined HETP values for the *n*-alkane and PAH test mixture used for calibration. This test solution contained solutes that gave k' values from 0.46 for C_{16} to 3.2 for C_{24} under the chromatographic conditions used. The reduced plate height (H) values for the system varied from 0.52 to 1.35 μm. Although the H values for UV detection are slightly lower than those for FID (the volume of the UV detector is less

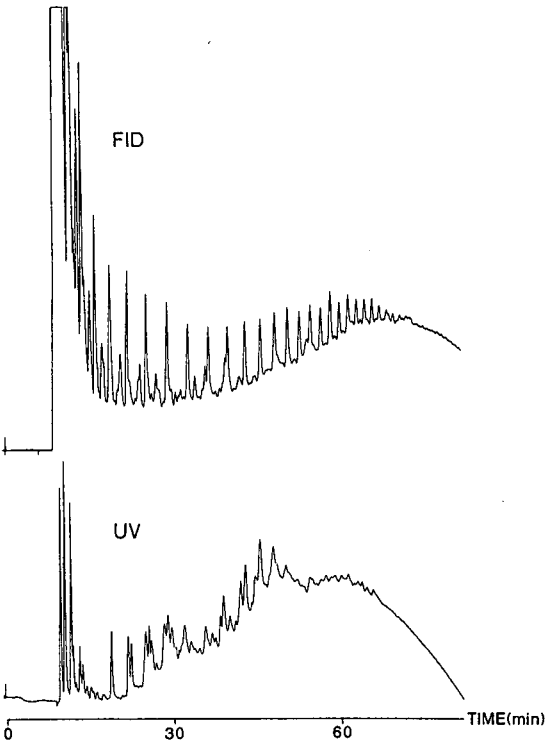

Fig. 2. Chromatogams of a Levelland oil/separation oil. Column temperature, 100°C. UV detection at 254 nm and employing baseline compensation. The FID trace was obtained at an attenuation of 2^6 and a detector temperature of 415°C.

than 60 nl), the H values for the two detectors compare well. Values obtained with the 100-μm I.D. column in the manufacturing test (*ca.* 3000 plates/m) and those obtained with the simultaneous detection method (*ca.* 2900 plates/m) show that the interface device contributes little to post-column dispersion. That high chromatographic efficiency is retained is further illustated by the chromatograms presented in this paper.

A few comments should be made concerning the practical aspects of this experiment. First, because the SFC system operates at high pressure, it is important to ensure that no leaks exist in the system. Any such leaks could result in a loss of pressure before the detectors and a subsequent decrease in the density of the mobile phase. Such a decrease would result in a solubility change, causing a possible loss of chromatographic resolution. Second, because the system is based on a capillary column, pre- and post-column dead-volume constraints are severe, and dead volumes must be kept to the minimum. Finally, a comment should be made about the use of 50-μm I.D. columns. These are the narrowest commercially available separation columns and have very small volumes even when very long. We were unsuccessful with a short piece (3 m) of 50-μm I.D. column, but we believe that the simultaneous detection interface could be used with 10- or 20-m columns, as their larger volumes impose less severe dead-volume constraints. The best results are expected with 100-μm I.D. capillary columns.

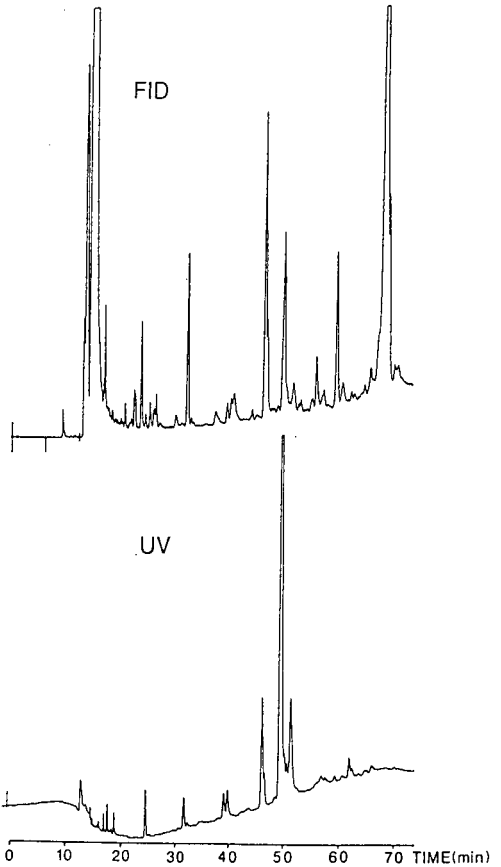

Fig. 3. Chromatogram of a neat sample of a cold-pressed grapefruit oil. Column temperature, 100°C. UV trace at 254 nm. The FID trace was obtained at an attenuation of 2^6 and a detector temperature of 415°C.

Fig. 1 shows the FID and UV capillary chromatograms of a polyphenylhydrosiloxane with the dual-detector split interface. The chromatogram illustrates the effectiveness of transfer of the higher molecular weight oligomers. If the concentration of the sample or the splitting ratio were modified so that the UV detector received more of the sample, the UV trace would be almost identical with that obtained using FID.

Figs. 2 and 3 further illustate the advantages gained by employing two detection methods simultaneously for the analysis of a complex mixture. The oil sample shown in Fig. 2 is a complex mixture of aliphatic and aromatic hydrocarbons. The FID trace alone shows the *n*-alkane distribution, as expected, but gives no selective information about the UV-absorbing species in the sample. Close comparison of the retention times obtained with UV detection and FID shows that there are unresolved peaks, or closely eluted peaks, that are detected by both the flame ionization detector (universal) and the UV detector (selective at 254 nm). These compounds probably correspond to species other than *n*-alkanes and are most likely the aromatic or polycyclic species expected in this type of oil. In addition, the simplified UV trace gives information that is

unattainable with FID alone, and the FID trace represents virtually all organic compounds present. Of particular interest is the formation gained with respect to the early eluting species. As illustrated in Fig. 2, there are at least three major compounds that absorb strongly at 254 nm. They would not be detected if only FID were employed. These components are significant in concentration and certainly contribute substantially to the chemical nature of the sample.

A third example of the utility of the simultaneous detection method is shown in the analysis of a grapefruit oil. Note the excellent chromatographic performance illustrated in Fig. 3. In this sample, the advantage of the two-detector approach is shown by the absence of the major component seen in the UV trace which is eluted late in the FID trace. The presence and concentration of the component eluted mid-way in the UV trace suggests that this species is an aromatic component characteristic of the sample.

In this paper we have illustrated that an interface device, based on a splitter, can be employed in capillary SFC with simultaneous FID and UV–VIS detection. Chromatographic performance is maintained, and the relative amount sent to each detector can be quantified. Calibration for each of the detectors remains linear, while the splitting ratio is controlled by setting the relative restriction used at each flow channel. This simultaneous measurement allows the analyst to obtain additional information, which facilitates the elucidation of complex matrices. We are currently investigating other detector combinations for selective and universal detection.

ACKNOWLEDGEMENTS

The authors thank all members of the research group at Lee Scientific for their helpful discussions, in particular Dr. Brian Jones, Dr. Frank Yang, Dr. Bruce Richter and Dr. Douglas Later. Special thanks are due to Tony Weaver of SGE for help with the modification of the transfer device. This work was funded in part by an SBIR Grant from the USDA (86-SBIR-0-0130).

REFERENCES

1 J. C. Fjeldsted and M. L. Lee, *Anal. Chem.*, 56 (1984) 619A.
2 P. A. Peaden and M. L. Lee, *J. Chromatogr.*, 259 (1983) 1–6.
3 M. Novotny, S. R. Springston, P. A. Peaden, J. C. Fjeldsted and M. L. Lee, *Anal. Chem.*, 53 (1981) 407A–414A.
4 B. E. Richter, *J. High Resolut. Chromatogr. Chromatogr. Commun.*, (1985) 8.
5 C. M. White and R. K. Houck, *J. High Resolut. Chromatogr. Chromatogr. Commun.*, 8 (1985) 293.
6 K. E. Markides, S. M. Fields and M. L. Lee, *J. Chromatogr. Sci.*, 24 (1986) 254–257.
7 D. R. Gere, *Science (Washington, D.C.)*, 222 (1983) 253–259.
8 S. Rokushika, H. Hatano and H. H. Hill, *Anal. Chem.*, 59 (1987) 8–12.
9 J. C. Fjeldsted, B. E. Richter, W. P. Jackson and M. L. Lee, *J. Chromatogr.*, 279 (1983) 423–430.
10 W. R. West and M. L. Lee, *J. High Resolut. Chromatogr. Chromatogr. Commun.*, 9 (1988) 161–166.
11 S. L. Pentoney, K. H. Schafer and P. R. Griffiths, *J. High Resolut. Chromatogr. Chromatogr. Commun.*, 9 (1986) 168–171.
12 D. W. Later, D. J. Bornhop, E. D. Lee, J. D. Henion and R. C. Weibolt, *LC · GC Mag. Liq. Gas Chromatogr.*, 5 (1987) 804–810.
13 S. M. Fields, K. E. Markides and M. L. Lee, *Anal. Chem.*, 60 (1988) 802–806.
14 D. J. Bornhop, B. E. Richter and D. W. Later, *J. Chromatogr. Sci.*, submitted for publication.
15 B. W. Wright and R. D. Smith, *J. High Resolut. Chromatogr. Chromatogr. Commun.*, 8 (1985) 8–11.
16 B. E. Richter, *Chromatogr. Forum*, 1 (1986) 52–54.

17 D. W. Later, B. E. Richter and M. R. Anderson, *LC · GC Mag. Liq. Gas Chomatogr.*, 4 (1986) 992–1003.
18 J. C. Fjeldsted, B. E. Richter, W. P. Jackson and M. L. Lee, *J. Chromatogr.*, 279 (1983) 423–430.
19 W. R. West and M. L. Lee, *J. High Resolut. Chromatogr. Chromatogr. Commun.*, 9 (1986) 161–167.
20 K. Jinno, T. Hoshino, T. Hondon, M. Saito and M. Senda, *Anal. Chem.*, 58 (1986) 2696–2699.
21 K. E. Markides, E. D. Lee, R. Bolick and M. L. Lee, *Anal. Chem.*, 54 (1986) 740–743.
22 T. Hershfeild, *Anal. Chem.*, 48 (1976) 16A–24A.
23 M. W. Raynor, I. L. Davies, K. D. Bartel, A. Williams, J. M. Chalmers and B. W. Cook, *Eur. Chromatogr. News*, 1 (1987) 18–22.
24 J. M. Levy, J. P. Guzowski and W. E. Huhak, *J. High Resolut. Chromatogr. Chromatogr. Commun.*, 10 (1987) 337–341.
25 G. Holzer, S. Deluca and K. J. Voorhees, *J. High Resolut. Chromatogr. Chromatogr. Commun.*, 8 (1985) 528–531.
26 M. Novotny, *Anal. Chem.*, 53 (1981) 1294A–1308A.
27 R. P. W. Scott, *J. Chromatogr. Sci.*, 18 (1980) 49–54.
28 J. W. Jorgenson and E. J. Guthrie, *J. Chromatogr.*, 255 (1983) 335–348.

Journal of Chromatography, 459 (1988) 201–213
Elsevier Science Publishers B.V., Amsterdam — Printed in The Netherlands

CHROMSYMP. 1441

EFFECT OF SAMPLE SIZE ON RETENTION IN PACKED COLUMN SUPERCRITICAL FLUID CHROMATOGRAPHY

A METHOD FOR CHARACTERIZING STATIONARY PHASE HOMOGENEITY

PETER J. SCHOENMAKERS*, LOUIS G. M. UUNK and PIETER K. DE BOKX
Philips Research Laboratories, P.O. Box 80000, 5600 JA Eindhoven (The Netherlands)

SUMMARY

Retention was measured as a function of the amount of solute injected in packed column supercritical fluid chromatography with three different chemically bonded stationary phases and with carbon dioxide as the mobile phase. The retention was found to decrease with increasing sample size. The effect was more pronounced for polar solutes.

A mixed retention mechanism is postulated to explain the results. Both the chemically bonded groups on the surface and the residual silanol groups are assumed to contribute to the retention. The former type of interaction is assumed to be independent of the solute concentration (*i.e.*, a constant distribution coefficient). The adsorption on silanol groups is described by a Langmuir isotherm. By assuming that the observed capacity factor is proportional to the distribution coefficient, an equation can be fitted to the experimental data. The resulting coefficients can be used to characterize the extent to which residual silanols contribute to the retention process. When methanol is added as a modifier to the mobile phase, the effect of sample size on retention disappears, suggesting that preferential adsorption of modifier deactivates the silanol groups on the surface.

INTRODUCTION

There are many good reasons for preferring carbon dioxide as the mobile phase for supercritical fluid chromatography (SFC)[1], including its favourable critical properties ($T_c \approx 31°C$ and $p_c \approx 73$ atm) and its excellent compatibility with detection devices, such as flame ionization and UV detectors. The fact that carbon dioxide is non-toxic and non-flammable also needs to be stressed. The use of carbon dioxide as a cheap, clean and safe solvent is one of the potential advantages of SFC over contemporary liquid chromatography.

However, if carbon dioxide is used as the mobile phase in combination with chemically bonded stationary phases (*e.g.*, octadecyl-modified silica) in packed column SFC, poorly shaped peaks are often observed for hydrogen-bonding solutes.

0021-9673/88/$03.50

For example, in a study concerning the applicability of SFC for the analysis of liquid crystal mixtures[2] we found sharp, symmetrical peaks for solutes containing hydrocarbon (alkyl, cyclohexyl, phenyl) and cyano groups, but strongly asymmetric peaks for solutes containing ether or ester groups in the molecular structure. The tentative explanation for these observations is a heterogeneous surface, on which the solute molecules interact with active sites. Chemically bonded stationary phases (CBPs) are prepared by a reaction of the surface of silica particles with a bonding agent. In this reaction silanol (SiOH) groups on the surface are replaced by other functional groups (polar or non-polar). If only because of the size of the bonding agent, not more than about half of the silanol groups can react, so that residual silanols will always be present on the surface. The presence of these silanol groups, the extent to which they are accessible to solute molecules and their actual state at the surface determine the nature and magnitude of their effect on retention and selectivity in chromatography.

If the number of silanol groups at the surface is reduced as much as possible by a prolonged reaction with small silylating agents (so-called "end-capping"), better peak shapes and shorter retention times can be observed for solutes of intermediate polarity[3]. However, in our opinion, chemically bonded stationary phases formed by the reaction of small molecules with the silica surface may differ in degree rather than in kind. In other words, the effect of residual silanol groups may be reduced, but not eliminated, by better bonding procedures.

The actual state of the silanol groups at the surface is determined by their location and by their environment. The environment of the silanol groups may be changed by the presence of adsorbed molecules, such as water or other polar molecules. This latter effect is frequently employed in packed column SFC when polar modifiers are added to the mobile phase (*e.g.*, ref. 3). If silanol groups and bonded groups contribute independently to retention in packed column SFC, a mixed retention mechanism will prevail. This will not by definition result in poor peak shapes, but it will (i) if the two mechanisms have very different kinetics, for example if one of them is a slow exchange between adsorbed molecules on the surface, or (ii) if the two mechanisms result in different types of adsorption isotherms. Because packed column SFC with carbon dioxide as the mobile phase can be performed on chemically bonded stationary phases as well as on bare silica[4], we consider the first possibility to be unlikely. We have assumed the second possibility to be valid. This hypothesis is supported by our experimental results (see below).

The surface heterogeneity can be studied from the shapes of the experimentally obtained peaks. This is difficult in SFC, because of (i) the lack of rigorous theories for the dispersion in ideal situations (on homogeneous surfaces) and (ii) the exceptionally bad peak shapes that may be observed under some conditions in non-ideal situations. The purpose of this work was to establish a much simpler pragmatic method for characterizing the homogeneity of stationary phases, based on the observed variation of retention with sample size. Developing homogeneous stationary phases may be a general goal for packed column SFC, but it was not one of the aims of this work.

Adsorption isotherms

In this paper we present a model for the adsorption isotherm in SFC based on a mixed retention mechanism, to which the bonded groups and the silanol groups contribute independently. The adsorption isotherm is assumed to be linear for the first

interaction, because of the relatively large sample capacity of chemically bonded phases[5]. Because of the number of accessible silanol groups on the surface is limited, we assume a Langmuir-type isotherm for the contribution of silanol groups to solute retention. This model is then assumed to apply to observed capacity factors in addition to distribution coefficients.

The distribution coefficient in terms of concentrations (K_c) is defined by

$$K_c = c_s/c_m \tag{1}$$

where c_s and c_m are the concentrations of the solute in the stationary and the mobile phase, respectively. If K_c is independent of c_m, we speak of a linear distribution isotherm. In this case, the capacity factor (k) of the solute in a chromatographic experiment is related to the distribution coefficient by

$$k = Q_s/Q_m = (c_s V_s)/(c_m V_m) = K_c(V_s/V_m) \tag{2}$$

where Q is the total mass of solute in either phase and V is the total volume of the indicated phase in the column. In chromatography the distribution isotherm is ideally linear. For very small sample sizes this is usually a reasonable approximation. A non-linear adsorption isotherm causes the distribution coefficient to vary with the concentration. This will affect the shape of chromatographic peaks. If the distribution coefficient is lower at higher solute concentrations (concave isotherm), the top of the peak will move more quickly than the edges, so that the top will tend to catch up with the front and tailing results. Such concave isotherms can be interpreted as an overloading of the stationary phase. The reverse effect, convex isotherms, caused (for example) by mobile-phase overloading, leads to fronting.

Yonker *et al.*[6] studied the effect of solute concentration on retention in capillary SFC. The results obtained with large amounts of sample (up to 8 μg) may be interpreted as mobile phase overloading. In packed column SFC the solubility of the solute in the mobile phase is unlikely to cause problems, because of the much higher volumetric flow-rates. We can estimate the concentration at the top of the column by assuming that the solute is introduced on the first theoretical plate. For a plate height of 0.5 mm in a 50-μm I.D. capillary column (a reduced plate height of 10), the plate volume is about 1 nl. For a packed column of 4.6 mm I.D. and a plate height of 15 μm (reduced plate height of 3 with 5-μm particles) the mobile phase volume per plate is about 150 nl. We consider amounts of solute exceeding 1 μg to be large, even for packed column SFC on 4.6 mm I.D. columns. The study of Yonker *et al.* was conducted at a much higher range of C_m values than in this work.

THEORY

If we consider the adsorption of solute molecules at active sites (silanol groups) on the surface and if we assume that only one solute molecule can be adsorbed on a given site, and that the adsorbed molecules do not affect each other (constant adsorption energy), then a Langmuir-type equation can be used to describe the distribution isotherm, *i.e.*,

$$c_{s,SiOH} = ac_m/(bc_m + 1) \tag{3}$$

where $c_{s,SiOH}$ is the concentration of the solute on the silanols (mol/m^2) and a and b are coefficients that depend on the solute and the stationary phase. Also, different values for a and b may be found with different mobile phases or at different pressures and temperatures. The distribution coefficient, in terms of concentrations, for the distribution of the solute between the silanol groups and the mobile phase ($K_{c,SiOH}$) follows from

$$K_{c,SiOH} = c_{s,SiOH}/c_m = a/(bc_m + 1) \tag{4}$$

For the distribution of the solute between the chemically bonded groups and the mobile phase we assume a linear distribution isotherm, *i.e.*, $K_{c,CBP}$ is independent of the concentration. The effective distribution coefficient, $K_{c,Tot}$, is the sum of the two individual contributions:

$$K_{c,Tot} = (c_{s,SiOH} + c_{s,CBP})/c_m = K_{c,SiOH} + K_{c,CBP} \tag{5}$$

or, in terms of the (dimensionless) chromatographic capacity factor (k)[7,8],

$$k = \varphi_{SiOH}K_{c,SiOH} + \varphi_{CBP}K_{c,CBP} \tag{6}$$

where φ_{SiOH} and φ_{CBP} are phase ratios for the two distribution processes. The dimension and, therefore, the value of φ depends on the definition of c_s. In the present situation we shall define c_s as the adsorbed amount per unit area of stationary phase (mol/m^2), in which case

$$\varphi_{SiOH} = \varphi_{CBP} = A_s/V_m \tag{7}$$

where A_s is the total surface area of stationary phase in the column (specific surface area × weight of stationary phase in the column) and V_m the total volume of mobile phase in the column.

Eqn. 5 describes the distribution coefficient for the adsorption of the solute on two different sites. If the assumed model is correct, the capacity factor at any time and place in the column will follow eqn. 6. However, in chromatography we do not measure a single ("static") value of the distribution coefficient, but rather a capacity factor, which corresponds to an integrated ("dynamic") value of the distribution coefficient. The capacity factor is determined by the entire process in the column. If the distribution coefficient is independent of time and place in the column, the static and dynamic values are identical. In the present situation (p = 255 bar and T = 35°C), the density does not decrease significantly along the column[9]. However, the capacity factor does vary with the concentration of the solute. We shall therefore write the observed capacity factor k_{obs} as

$$k_{obs} = \varphi_{SiOH}\bar{K}_{c,SiOH} + \varphi_{CBP}\bar{K}_{c,CBP} = \frac{aA_s}{V_m(b\bar{c}_m + 1)} + \frac{\bar{K}_{c,CBP}A_s}{V_m} \tag{8}$$

In eqn. 8 $\bar{c}_m$ is an effective average value of the concentration of the solute in the mobile phase and $\bar{K}$ denotes a corresponding average distribution coefficient. The actual

concentration will vary both along the column (due to dilution of the chromatographic peak) and along the profile of the peak. $\bar{c}_m$ will be related to the injected amount of solute (Q_i, mol) by

$$\bar{c}_m = \beta(Q_i)Q_i \tag{9}$$

where the proportionality factor, β, is a function of Q_i and has a dimension of l^{-1}. Combining eqns. 8 and 9 yields

$$k_{obs} = \frac{aA_s}{V_m(b\beta(Q_i)Q_i + 1)} + \frac{\bar{K}_{c,CBP}A_s}{V_m} \tag{10}$$

We shall now make the most rigorous approximation in the present model by assuming "quasi-static" behaviour, *i.e.*, β does not vary with Q_i. If k values and peak shapes vary with Q_i, an effect of Q_i on the dilution of the peak during its migration through the column may also be anticipated. According to eqn. 10, increasing amounts of solute may lead to reduced capacity factors and, hence, to less dilution. Limiting ourselves to first-order effects, eqn. 10 assumes the form

$$k_{obs} = a'/(b'Q_i + 1) + d' \tag{11}$$

with

$$a' = aA_s/V_m \tag{12}$$

$$b' = \beta b \tag{13}$$

and

$$d' = K_{c,CBP}A_s/V_m = k_{CBP} \tag{14}$$

where k_{CBP} is the capacity factor that would be observed if the contribution of the silanol groups to the retenton were negligible.

In eqn. 3 the ratio a/b is the number of silanol groups available for interaction. From eqns. 12 and 13 we find

$$a/b = (a'/b')(V_m\beta/A_s) \tag{15}$$

Also, b in eqn. 3 and therefore b' in eqn. 11 are a measure of the strength of the interaction. Because the parameter β is not known, we cannot obtain estimates for a/b and b, but we may use the values of a/b' and b' as indications for the *relative* numbers of accessible silanol groups on different stationary phases and for the *relative* strength of the interactions, respectively.

EXPERIMENTAL

The SFC instrument used in this study has been described previously[10–12]. Carbon dioxide (99.8%) (Philips Gasfabriek, Eindhoven, The Netherlands) was used as the mobile phase. The purity was judged to be sufficient in combination with UV detection. When methanol (analytical-reagent grade; Merck, Darmstadt, F.R.G.) was added as a modifier to the mobile phase, this was done by means of a second pump (PU 4015; Philips Scientific, Cambridge, U.K.). The proportional flow-rates of the two pumps were kept constant, while the total flow-rate was controlled by a constant-pressure feedback circuit. The effluent streams of the two pumps were combined in a standard T-piece and fed into a 4100-type cyclonic mixing chamber (Philips Scientific) at low temperatures (liquid state) and the combined stream was led into a temperature equilibration coil in the oven prior to injection.

Retention times were measured from the tops of the peaks. Chromatograms were recorded at constant inlet and outlet pressures of 255 and 240 bar, respectively, in order to avoid a bias due to pressure-drop effects[11]. The retention time of dichloromethane was used as t_0.

Four different liquid-crystal components were used as the test solutes. Their structures are shown in Fig. 1. These solutes were selected on the basis of our own practical experience with packed column SFC. It was not our intention to develop a coherent set of test solutes. Solutes were injected as individual standard solutions of varying concentrations. By simultaneously varying the injection volume and the dilution factor, it was verified that identical results were obtained for identical amounts (mass units) of solute injected. Injection of a mixture of solutes led to different results. This, we believe, is due to competition for the active sites between the different solutes.

Stationary phases

A commercial octadecylsilyl column (Chromspher C_{18}, 5-μm particles) (Chrompack, Middelburg, The Netherlands) of 150 mm × 4.6 mm I.D. was used.

Two additional stationary phases were synthesized in our laboratory. A perfluorooctyl phase ("Fluoro column") was prepared by "chemically drying" the surface of Chromspher silica (Chrompack, particle size 5 μm) with thionyl chloride[13], followed by a reaction with (heptadecafluoro-1,1,2,2-tetrahydrodecyl)-1-trichlorosilane, refluxing in dry toluene under an argon atmosphere for about 15 h with pyridine as a scavenger (for HCl). A trimethylsilyl phase ("TMS column") was prepared by the reaction of a sample of the same silica with diethyl-1,1,1-trimethylsilylamine for 2 h in dry toluene. The structures of the bonded groups are listed in Table I. Columns (100 mm × 4.6 mm I.D.) were packed with the two synthesized phases using slurries in 2-propanol.

For each of the three phases the carbon percentage was determined by elemental

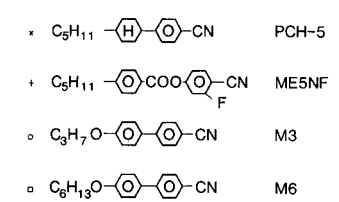

Fig. 1. Molecular structure and identification codes of solutes used in this study.

TABLE I
STRUCTURES AND COVERAGES OF THE STATIONARY PHASES USED
Specific surface area of the silica, 176 m^2/g.

Column	*Bonded group*	*Coverage*		
		C (%)	*Å²/group*	*μmol/m²*
C_{18}	$-Si(CH_3)_2C_{18}H_{37}$	13.3	43	3.86
Fluoro	$\equiv Si(CH_2)_2C_8F_{17}$	3.6	82	2.02
TMS	$-Si(CH_3)_3$	1.9	53	3.10

analysis.Together with the specific surface area obtained from nitrogen-adsorption measurements, these figures were used to calculate the coverage according to ref. 14 (Table I). The coverage of the C_{18} column of 3.86 $\mu mol/m^2$ implies that about half of the silanol groups present on the surface (*ca.* 8 $\mu mol/m^2$)[14] had reacted. A secondary ("end-capping") reaction carried out by the manufacturer may cause the actual number of reacted silanol groups to be slightly higher than the calculated coverage.

The Fluoro column was included in the study as an example of a stationary phase with a low surface coverage. Therefore, a much larger number of silanol groups remains present on the surface. The TMS column has a fairly high surface coverage, but the small size of the bonded group (methyl rather than octadecyl groups) may imply that the remaining silanols can be more easily accessible to solute molecules.

The three stationary phases used in this study were selected to demonstrate the variation of retention with sample size as a means of characterizing surface homogeneity. Batch-to-batch variability was not tested, as it was beyond the scope of this study.

RESULTS

Fig. 2 shows the variation of the observed capacity factor with the amount of solute injected for the four solutes shown in Fig. 1 on the C_{18} column. Here and in subsequent figures, the drawn lines represent the best fit according to eqn. 11. A significant variation in k_{obs} with varying Q_i was found for all solutes, but the effect was largest for the two ethers M3 and M6 (see Fig. 1). This is not simply because of the higher capacity factors of these two solutes, because at high concentrations the capacity factors of M3 and PCH-5 are about equal. The estimates of the limiting capacity factors at very high concentrations (d' in eqn. 11) for M3 and M6 are indicated in Fig. 2. For the two other solutes d' is virtually reached within the experimental range.

Fig. 3 shows the effect of sample size on the observed capacity factor for two solutes on the Fluoro column and Fig. 4 that for the same two solutes on the TMS columns. A very substantial variation of k with Q_i is observed in all four instances. Especially for PCH-5, the magnitudes of the observed differences in k are greater on the Fluoro and TMS columns than on the C_{18} column.

The magnitude of the effect of the sample size on the capacity factor can be quantified by use of the data in Table II, which gives the coefficients obtained by fitting

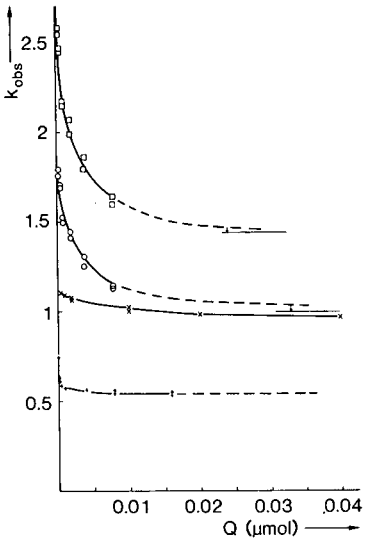

Fig. 2. Variation of the observed capacity factor with the amount of solute injected for the four solutes shown in Fig. 1 on the C_{18} column. The drawn lines represent the best fit according to eqn. 11. Solutes: (□) M6; (○) M3; (×) PCH-5; (+) ME5NF. Mobile phase, CO_2; column inlet pressure, 255 bar; outlet pressure, 240 bar: temperature, 35°C.

eqn. 11 to the data shown in Figs. 2–5. The highest capacity factor for ($Q \downarrow 0$) corresponds to $a' + d'$, whereas d' is the lowest possible value (for $Q_i \rightarrow \infty$). According to the present model, the ratio a'/d' is representative of the possible variation in k due to the silanol-group effect relative to the retention caused by the chemically bonded groups. The coefficient b' is an indication of the interaction of the solute molecules with the active sites on the surface (silanol groups). In addition to a', b' and d', Table II also lists a calculated value of a/b', which may serve as an indication of the number of silanol groups accessible to the solute molecules.

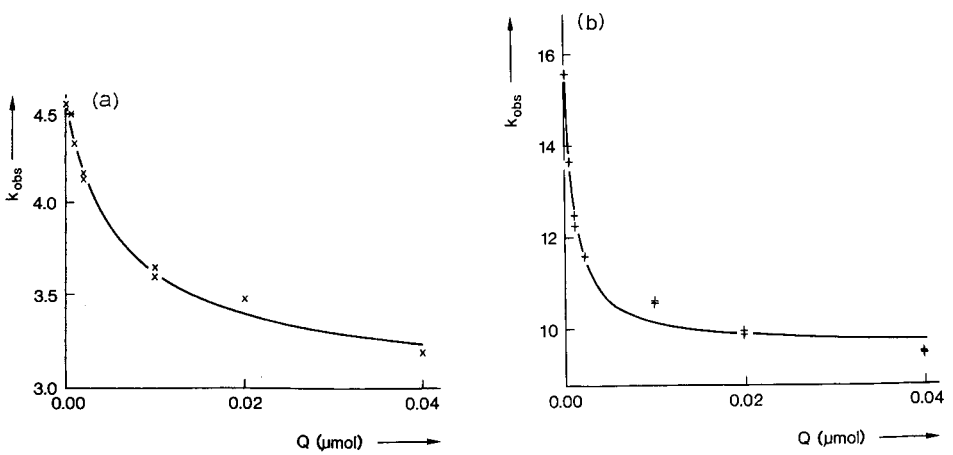

Fig. 3. As Fig. 2 for (a) PCH-5 and (b) ME5NF on the Fluoro column.

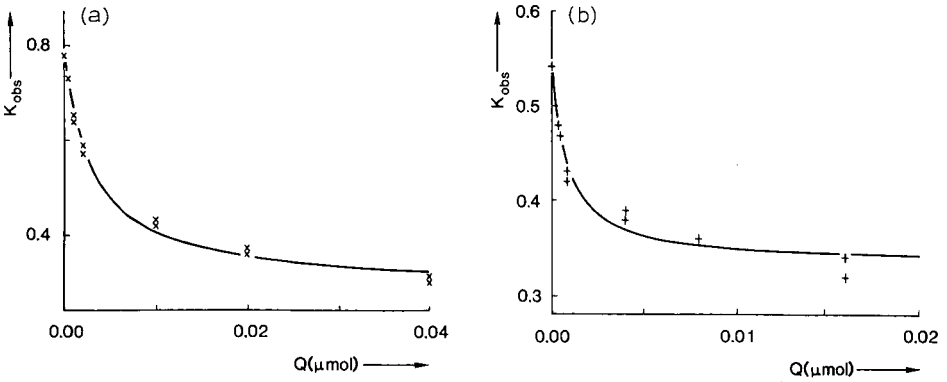

Fig. 4. As Fig. 2 for (a) PCH-5 and (b) ME5NF on the TMS column.

Fig. 5 illustrates the effect of the addition of about 5% (v/v) of methanol to the mobile phase. With the polar modifier present in the mobile phase, no effect of sample size on capacity factors can be measured. Also, a considerable reduction in the observed capacity factors (see d' values in Table II) and an improved peak shape and

TABLE II

COEFFICIENTS FOUND BY FITTING EQN. 11 TO THE DATA SHOWN IN FIGS. 2–5

Column inlet pressure, 255 bar; outlet pressure, 240 bar; temperature, 35°C, except for mobile phases containing methanol (50°C). Figures in parentheses indicate the precision of the parameter estimates [relative standard deviation (R.S.D.), %].

Stationary phase	*Mobile phase*	*Solute*	a'	b' (mol^{-1})	d'	a/b'* ($lmol/m^2$)
C_{18}	CO_2	PCH-5	0.17	2.0×10^8	0.95	7.3×10^{-15}
			(4)	(21)	(0.7)	(23)**
C_{18}	CO_2	ME5NF	0.16	6.0×10^9	0.54	2.3×10^{-16}
			(46)	(80)	(0.8)	(36)
C_{18}	CO_2	M3	0.89	6.0×10^8	1.00	1.3×10^{-14}
			(4)	(22)	(5)	(23)
C_{18}	CO_2	M6	1.31	6.6×10^8	1.44	1.7×10^{-14}
			(4)	(23)	(5)	(24)
C_{18}	CO_2–methanol	PCH-5	0	–	0.40	–
C_{18}	CO_2–methanol	ME5NF	0	–	0.21	–
Fluoro	CO_2	PCH-5	1.51	1.6×10^8	3.04	8.4×10^{-14}
			(4)	(21)	(2)	(23)
Fluoro	CO_2	ME5NF	5.84	1.0×10^9	9.65	5.0×10^{-14}
			(13)	(34)	(2)	(23)
TMS	CO_2	PCH-5	0.49	3.2×10^8	0.29	1.3×10^{-14}
			(4)	(23)	(6)	(21)
TMS	CO_2	ME5NF	0.20	1.2×10^9	0.34	1.4×10^{-14}
			(10)	(40)	(3)	(34)

* Calulated by using eqn. 12. $A_s = 146\ m^2$ was calculated from a specific surface area of 176 m^2/g, a packing density of 0.5 g/ml and a column volume of 1.66 ml. $V_m = 1.3$ ml.

** Calculated from the equation

$$\text{R.S.D.}_{a/b} = (b/a)\sqrt{(1/b^2)\text{var}_a + (a^2/b^4)\text{var}_b - (2a/b^3)\text{cov}_{ab}}$$

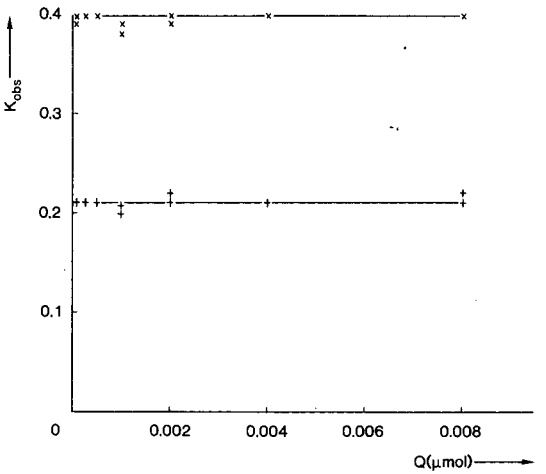

Fig. 5. As Fig. 2 for (×) PCH-5 and (+) ME5NF. Mobile phase, CO_2, with *ca.* 5% (v/v) of methanol; temperature, 50°C.

efficiency were obtained. Both of these effects are well documented (*e.g.*, ref. 3) and will not be discussed further in this paper.

DISCUSSION

Eqn. 11 can be seen to provide a good representation of the experimental data on the variaton of retention with sample size. This suggests that the shape of the distribution term may be described by eqn. 8, and that our hypothesis of a mixed retention mechanism is not unreasonable. On the C_{18} column the differences between the model equation and the experimental data are smaller than on the Fluoro and TMS columns. In the range of large amounts of sample on the latter two columns the capacity factor varies more strongly with Q_i than suggested by the model. A possible explanation is that a constant distribution coefficient (linear isotherm) is a valid assumption for the retention on the C_{18} phase (featuring a relatively large number of long chains on the surface), but is not rigorously correct for either the Fluoro column (small number of chains) or for the TMS column (short chains). Nevertheless, eqn. 11 does provide a reasonable description of the experimental data.

An indication of the precision of the coefficients in Table II is provided by the relative standard deviations (shown in parentheses). These figures show that when b' is large both a' and b' cannot be determined with a high precision. However, the observed variations in b' are definitely significant within the constraints of the model. Because inprecise values for a' and b' tend to coincide with large values for the covariance, the precision of the ratio a/b' is always between 20 and 40%. Therefore, differences between a/b' values larger than about a factor of two are significant.

The coefficients in Table II can be used to characterize the suitability of stationary phases for packed column SFC. The parameters a' and b' represent the extent to which k_{obs} varies with Q_i. By differentiating eqn. 11 we find that at small sample amounts (for $Q_i \downarrow 0$) the variation of k with Q_i (dk/dQ_i) equals $-a'b'$, whereas

at high concentrations (for $Q_i \rightarrow \infty$) dk/dQ_i approaches $-a'/b'$. The extent to which k varies with Q_i will determine the shape of the chromatographic peaks. For example, on the C_{18} column ME5NF yielded sharp peaks (calculated plate counts between 6000 and 9000), despite a large value for b' (see Table II), owing to the low value for a'. The ethers M3 and M6 show lower values for b', but much higher values for a', leading to poor peak shapes, especially at higher concentrations.

The relatively strong interaction of the ME5NF ester with the silanol groups on the surface (high b' value) is coupled to a (relatively) low number of accessible silanol groups (low value for a/b'). This may be due to the molecular structure (Fig. 1), which shows the ester group to be "hidden" between two phenyl rings. In contrast, the two ethers (M3 and M6), in which the ether group may be more easily accessible, appear to interact with a much larger number of silanols on the surface. The magnitude of the interaction (b') and the number of accessible silanol groups are approximately the same for the two ethers. The cyano compound (PCH-5) showed the weakest interaction with the silanol groups. This is in agreement with our previous observations of good peak shapes for these compounds in packed column SFC with carbon dioxide as the mobile phase[1].

The Fluoro column, which has the lowest surface coverage in terms of $\mu mol/m^2$, yields much higher values for the accessible number of silanol groups (a/b' in Table II). The magnitude of the interaction is similar to that on the C_{18} column for PCH-5, but is a factor of six lower for ME5NF. This suggests that the interaction is different (and weaker) with the more readily accessible silanol groups in between the relatively scarce perfluorooctyl chains than with the isolated silanol groups surrounded by long octadecyl chains.

The values for the accessible number of silanol groups on the TMS column are between those for the other two columns. This is a reasonable result, considering that the surface coverage is higher than on the Fluoro column, but that the chain length and, hence, the extent of shielding per bonded group is less than on the C_{18} column. The magnitude of the interaction with the silanol groups is similar to that on the Fluoro column for ME5NF, but larger by a factor of two for PCH-5.

The values of a' and d' in Table II give an indication of the extent to which k varies with sample size. For the first two solutes on the C_{18} column k may increase by 20% (for PCH-5) to 30% (for ME5NF) over the value obtained with very large samples (d'). For the same two solutes on the Fluoro column the increase is about 50%, whereas on the TMS column the respective values are about 170 and 60%. This also suggests that of the three columns considered, the C_{18} column is the most suitable for these solutes. However, even on this column, the two ethers (M3 and M6) show increases in k of almost 100% on going from very large amounts of sample ($k = d'$) to very small amounts ($k = a' + d'$). The capacity factors at high concentrations (d') are much higher on the Fluoro column than on the C_{18} column, wich in turn shows more retention than the TMS column. The difference in selectivity ($\alpha_\infty = d'_{\text{PCH-5}}/d'_{\text{ME5NF}}$) between the three different phases is remarkable, with values of 1.76, 0.32, and 0.85 for the C_{18}, Fluoro and TMS columns, respectively. However, stationary phase selectivity is not the subject of this paper and we plan to discuss it in a future publication.

The addition of about 5% (v/v) of methanol to the mobile phase caused the effect of the sample size on the observed capacity factor to disappear completely. Apparently, the stationary phase behaves as a homogeneous surface (*i.e.*, $a' = 0$). This

supports the assumption that polar modifiers, such as methanol, provide a dynamic coating of surface silanol groups. The retention is much lower than with pure carbon dioxide as the mobile phase, even when compared with the (extrapolated) capacity factors for very large sample sizes (d'). The experiments with methanol in the mobile phase were performed at a higher temperature (50 rather than 35°C) in order to stay above the critical temperature of the mixture. At a temperature of 35°C the capacity factors would have been even lower with the methanol–carbon dioxide mixture. This illustrates that the effect of the addition of methanol on retention is not due exclusively to a dynamic coverage of the silanol groups, because in that event we would expect a capacity factor close to the d' value observed with pure carbon dioxide. A change in the nature of the mobile phase also appears to contribute to a reduction of the observed capacity factors. This conclusion can be supported by spectroscopic data[15,16].

CONCLUSIONS

(1) Retention in packed column SFC with carbon dioxide as the mobile phase and silica-based chemically bonded stationary phases may be strongly dependent on the amount of sample injected.

(2) The variation of the observed capacity factor with the sample size can be described by a model assuming a mixed retention mechanism. In this model, silanol groups are assumed to contribute to retention according to a Langmuir isotherm, whereas the chemically bonded groups on the surface are assumed to give rise to a linear isotherm.

(3) The coefficients found from the above model give an indication of the relative number of accessible silanol groups on the surface of different stationary phases and of the relative strength of the interaction between these groups and the solute molecules. Therefore, the variation of the observed capacity factor with the amount of sample injected can be used to characterize the homogeneity of stationary phases.

(4) The hydrogen-bonding properties of the solute, the surface coverage and the accessibility of active sites are all reflected in the coefficients of the above model.

(5) On the basis of conclusions 3 and 4, the variation of the observed capacity factor with the amount of sample injected can be used to characterize the homogeneity of stationary phases.

(6) The addition of *ca.* 5% (v/v) of methanol to the mobile phase caused the effect of sample size on retention to vanish completely.

ACKNOWLEDGEMENTS

The fluoroalkyl and trimethylsilyl phases were synthesized by Jan Ponjeé and Fred Touwslager of our laboratory. Columns were packed at the laboratory for Instrumental Analysis of the Technical University of Delft (Hugo Billiet).

REFERENCES

1 P. J. Schoenmakers and L. G. M. Uunk, *Adv. Chromatogr.*, 30 (1989) in press.
2 P. J. Schoenmakers, F. C. C. J. G. Verhoeven and H. M. van den Bogaert, *J. Chromatogr.*, 371 (1986) 121.
3 A. L. Blilie and T. Grybrokk, *Anal. Chem.*, 57 (1985) 2239.

4 P. Mourier, P. Sassiat, M. Caude and R. Rosset, *J. Chromatogr.*, 353 (1986) 61.
5 C. E. Goewie, *Thesis*, Free University, Amsterdam, 1983.
6 C. R. Yonker, R. W. Gale and R. D. Smith, *J. Chromatogr.*, 389 (1987) 433.
7 A. Nahum and Cs. Horváth, *J. Chromatogr.*, 201 (1981) 53.
8 K. E. Bij, Cs. Horváth, W. R. Melander and A. Nahum, *J. Chromatogr.*, 203 (1981) 65.
9 P. J. Schoenmakers, P. E. Rothfusz and F. C. C. J. G. Verhoeven, *J. Chromatogr.*, 395 (1987) 91.
10 P. J. Schoenmakers and F. C. C. J. G. Verhoeven, *Trends Anal. Chem.*, 6 (1987) 10.
11 P. J. Schoenmakers and F. C. C. J. G. Verhoeven, *J. Chromatogr.*, 352 (1986) 315.
12 P. J. Schoenmakers and L. G. M. Uunk, *Chromatographia*, 24 (1987) 51.
13 J. M. J. Vankan, J. J. Ponjeé, J. W. de Haan and L. J. M. van de Ven, *J. Colloid Interface Sci.*, in press.
14 G. E. Berendsen and L. de Galan, *J. Liq. Chromatogr.*, 1 (1978) 561.
15 S. Kim and K. P. Johnston, *AIChE J.*, 33 (1987) 1603.
16 C. R. Yonker and R. D. Smith, *J. Phys. Chem.*, 92 (1988) 2374.

Journal of Chromatography, 459 (1988) 215–220
Elsevier Science Publishers B.V., Amsterdam — Printed in The Netherlands

CHROMSYMP. 1490

DETERMINATION OF A NEW INOTROPIC AGENT IN HUMAN PLASMA BY HIGH-PERFORMANCE LIQUID CHROMATOGRAPHY

SHIH-HSIEN HSU*, TERRI L. KOERPER, BARBARA J. TOMLINSON, JOY R. MIKSIC and PETER E. GREBOW

Rorer Central Research, 800 Business Center Drive Building 2, Horsham, PA 19044 (U.S.A.)

SUMMARY

A new orally active inotropic agent, 6-[3,4-dihydro-3-methyl-(2H)-2-oxo-quinozolinyl)]-4,5-dihydro-3-(2H)-pyridazinone (I), is currently under investigation[1,2]. In support of clinical studies, a HPLC assay for the analysis of compound I in human plasma has been developed. The method involved a solid-phase extraction using C_{18} cartridge columns washed with methanol–water (20:80) and eluted with acetonitrile–water (70:30). The eluate was then extracted with dichloromethane. A reversed-phase alkylphenyl-bonded column was used as the analytical column. The mobile phase was a mixture of methanol, acetonitrile, 2-propanol and phosphate buffer (pH 4.6). A wavelength of 311 nm was used for detection. The limit of detection of the assay was 2 ng/ml, and the limit of quantitation was 5 ng/ml. A linear calibration range of 5 ng/ml to 1200 ng/ml was obtained with a correlation coefficient > 0.99. The precision and accuracy were evaluated by analyzing samples of three different concentrations ($n = 5$), 40, 200 and 800 ng/ml in plasma. The coefficients of variation and the differences from nominal values were less than 10%. The average recovery for 5, 50 and 100 ng/ml of analyte in plasma was about 90%. This assay has been applied to clinical studies with satisfactory performance and to plasma of different species in preclinical studies.

INTRODUCTION

A new, potent, orally active inotropic agent, 6-[3,4-dihydro-3-methyl-(2H)-2-oxoquinozolinyl)]-4,5-dihydro-3-(2H)-pyridazinone (I), is currently under preclinical and clinical investigation[1,2]. In support of these studies, a highly specific and sensitive method for the determination of the drug in biological matrices was required. This report describes a high-performance liquid chromatographic (HPLC) assay for analysis of compound I in human plasma. The assay involved both solid-phase and liquid–liquid extractions for sample purification prior to HPLC analysis. The method has been successfully applied to plasma from non-human species as well as in human pharmacokinetic studies.

0021-9673/88/$03.50

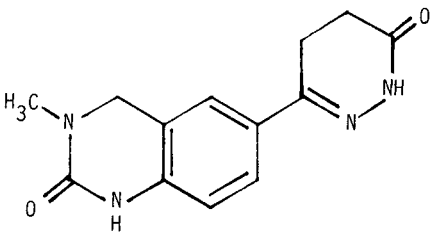

I

EXPERIMENTAL

Materials

HPLC-grade methanol, acetonitrile, 2-propanol and dichloromethane, and analytical-grade sodium phosphate (monobasic, ACS certified) were obtained from Fisher Scientific (Pittsburgh, PA, U.S.A.). The 3-ml (500 mg) C_{18} Bond Elut cartridge columns were obtained from Analytichem (Harbor City, CA, U.S.A.). Pooled blank human plasma with sodium heparin as an anticoagulant was obtained from Biological Specialty Corp. (Lansdale, PA, U.S.A.). The analyte (I), and the internal standard [1,3-dihydro-3,3-dimethyl-5-(1,4,5,6-tetrahydro-6-oxo-3-pyridazinyl)-2H-indol-2-one], were synthesized at Rorer Central Research.

Preparation of the standard solutions

All stock solutions [10 μg/ml of compound I and 0.2 mg/ml of internal standard (IS)] were prepared with methanol–water (50:50). The working IS solution (1 μg/ml) was prepared by diluting the stock solution (0.2 mg/ml) with methanol–water (50:50). All other human plasma standards (0, 5, 10, 50, 100, 300, 600 and 1200 ng/ml of compound I) for standard curves were prepared by diluting the stock solutions with plasma.

Instrumentation

The HPLC system used consisted of a Waters (Milford, MA, U.S.A.) Model 510 dual-piston pump, a Waters intelligent sample processor (WISP), Model 710B and a Kratos (Ramsey, NJ, U.S.A.) Model 773 spectroflow UV detector. A Waters recording integrator, Model 730 data module, and a Nelson Analytical (Cupertino, CA, U.S.A.) Model 2600 data acquisition system, on a Compaq DeskPro 386 were also used in this study.

Extraction procedure

Frozen plasma samples, standards, or controls were placed in a warm water bath (40–45°C) for 10 min. To 1.00 ml of sample, standard or control in a 10 × 130 mm polypropylene tube, 100 μl of an internal standard solution (1 μg/ml) were added. After mixing, the samples were passed through a 3-ml (500-mg) C_{18} solid-phase extraction column with the aid of a vacuum. The extraction column was activated with one column volume of methanol and then water prior to performing the extraction. After the samples passed through the extraction column, the column was washed with

500 μl of methanol–water (20:80), and then eluted with two 500-μl volumes of acetonitrile–water (70:30).

To the 1 ml of eluate, 5 ml of dichloromethane was added. The solution was well mixed in a vortex mixer (approximately 0.5 min) and centrifuged at 1300 *g* (3000 rpm) for 5 min. The aqueous layer was aspirated and the organic layer was evaporated to dryness at 35°C under a gentle stream of nitrogen. The residue was dissolved in 100 μl of mobile phase, and a 40-μl aliquot was injected into the HPLC system.

Chromatography

An ES Industries (Marlton, NJ, U.S.A.) 150 × 4.6 mm I.D. column, packed with 5-μm particle size, 60-Å pore size, alkylphenyl reversed-phase material was used as the analytical column. An Upchurch Scientific (Oak Harbor, WA, U.S.A.) guard column, packed with Alltech–Applied Science (Deerfield, IL, U.S.A.) pellicular phenyl was used to protect the analytical column. The mobile phase consisted of methanol–2-propanol–acetonitrile–0.02 *M* sodium phosphate (monobasic) (15:6:7:72, v/v). A flow-rate of 1 ml/min and ambient temperature were used for the separation. The detection wavelength was 311 nm.

Quantitation and calibration

The standard curves were constructed by the peak-height ratios (I to IS) *vs.* concentration of the standards. Concentration values of samples were calculated by using non-weighted linear regression parameters from the standard curve. The calibration standards contained 0, 5, 10, 50, 100, 300, 600 and 1200 ng/ml of compound I in plasma. Due to the large concentration range, the calibration was divided into two curves; low range (0–100 ng/ml) and high range (0–1200 ng/ml). Concentrations of 100 ng/ml or below were interpolated from the low-range curve and any concentration value exceeding this was interpolated from the high-range curve.

Validation procedures

The method was validated to assess linearity, precision, sensitivity, accuracy, specificity, and viability of extracted samples on storage overnight. Three different concentrations (40, 200 and 800 ng/ml) of compound I-spiked human plasma samples (spiked control samples) were prepared in addition to the human plasma standards. On the first day of validation, human plasma standards were analyzed in triplicate along with the three concentrations of spiked controls samples ($n = 5$ for each concentration). Analyses of the standard and spiked control samples on subsequent days were used to assess within-day variability in the standard curve and the day-to-day precision and accuracy. Specificity of the analyses was demonstrated by comparing blank samples ($n = 3$) with I-spiked samples for each day of validation. Extraction recoveries for I and IS were determined by a peak-height comparison of extracted human plasma standards at 5, 50 and 100 ng/ml ($n = 3$ for each concentration) with the peak heights of comparable non-extracted aqueous standard (prepared with mobile phase).

Clinical samples

A single rising-dose safety study was performed in normal volunteers ($n = 16$, all male). For the determination of drug plasma levels, blood was drawn, following

a 10-mg and 15-mg oral dose (capsule). Subjects received active I at 4- to 5-day intervals to allow adequate washout of the previous dose. The plasma samples (heparinized) were collected at 0, 0.5, 1.5, 3.0, 6.0, 10 and 24 h after dosing, and were assayed, as described.

RESULTS AND DISCUSSION

A 2 ng/ml of analyte in plasma was found to be the detection limit which was determined by the signal-to-noise (S/N) ratio larger than five (Fig. 1). The standard curve was found to be linear between 5 and 1200 ng/ml, with correlation coefficients greater than 0.9957 for within-day analysis. A mean correlation coefficient $\pm$ S.D. of 0.9985 $\pm$ 0.0025 was obtained for the analyses ($n = 3$) of three days. The coefficient of variation (C.V.) of the slope (over three analysis days) was less than 3.3% (Table I).

Sample chromatograms (Fig. 1) of a human plasma blank and sample show the separation of the analyte and the internal standard. Although there is an unidentified peak at 6 min, the chromatogram showed no significant interferences, either with the analyte or with the internal standard. The retention times of compound I and IS are approximately 7.5 and 9.5 min, respectively.

The within-day precision of the plasma assay was assessed from five replicate extractions of control plasma standards at the three levels (Table II). The within-day C.V. ranged from 5.14 to 5.49% at concentrations of 40, 200 and 800 ng/ml in the plasma.

The day-to-day precision was determined over three consecutive days using the I-spiked plasma samples ($n = 5$ for each analysis day) of each concentration level (Table II). The C.V. of the interpolated I concentration were 1.56% for the low level (40 ng/ml), 2.97% for the mid level (200 ng/ml), and 2.35% for the high level (800 ng/ml).

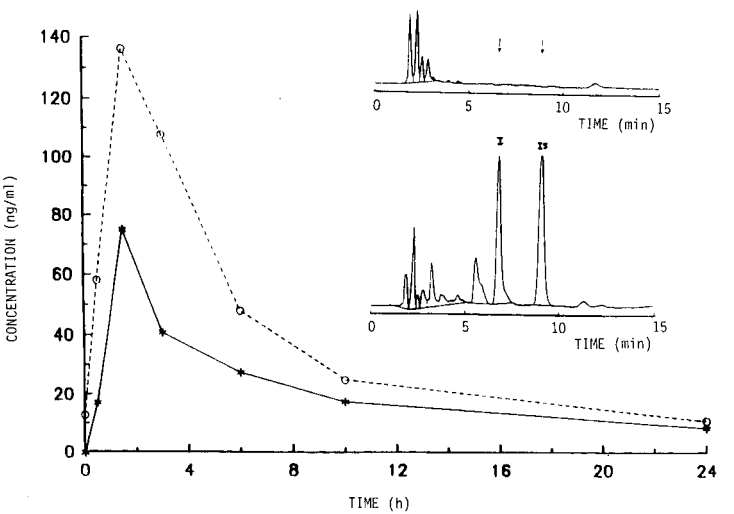

Fig. 1. Plasma concentrations of compound I as a function of time up to 24 h in a volunteer after a single oral dose (capsule) of 10 mg (lower curve) and 15 mg (upper curve). Chromatograms show the blank human plasma samples (upper chromatogram) and plasma samples drawn at 1.5 h after 10-mg capsule oral dose, plasma level is approximately 40 ng/ml. See text for the chromatographic conditions.

TABLE I

REGRESSION PARAMETERS FOR THREE DAYS ANALYSIS

Date	*Low-range curve (0–100 ng/ml)*			*High-range curve (100–1200 ng/ml)*		
	Slope	*Intercept*	*Correlation coefficient*	*Slope*	*Intercept*	*Correlation coefficient*
Day 1*	0.011453	0.011682	0.9993	0.011394	0.011987	1.0000
Day 2*	0.011682	0.0043388	0.9995	0.011278	−0.139970	0.9957
Day 3*	0.012209	−0.0046443	0.9996	0.011562	0.024990	0.9999
$\bar{x}$	0.011781	0.003792	0.9995	0.011411	−0.034331	0.9985
S.D.	0.000388	0.008177	0.0002	0.000143	0.091717	0.0025
C.V. (%)	3.29		0.02	1.25		0.25

* Single standard curve for each day.

Accuracy of the within-day analyses was determined by interpolation of the I-spiked plasma concentrations from the standard curve (Table II). The within-day difference between the mean and nominal values ranged between −2.75% and 2.00% for the control samples.

TABLE II

WITHIN-DAY PRECISION AND ACCURACY FOR CONTROLS INTERPOLATED FROM A STANDARD CURVE (A) AND DAY-TO-DAY PRECISION FROM THREE ANALYSIS DAYS (B)

MQL = Minimum quantitation level (n = 3).

	MQL, 5 ng/ml	*Low level, 40 ng/ml*	*Mid level, 200 ng/ml*	*High level, 800 ng/ml*
(A) Within-day				
1	4.85	37.7	198	795
2	4.70	36.0	190	738
3	4.36	40.8	206	850
4	–	39.8	206	834
5	–	40.2	219	791
$\bar{x}$	4.64	38.9	204	802
S.D.	0.25	2.0	11	44
C.V. (%)	5.39	5.14	5.39	5.49
Difference (%)	−7.20	−2.75	2.00	0.25
(B) Day-to-day				
Day 1		37.7	198	795
Day 2		38.9	209	832
Day 3		38.6	200	803
$\bar{x}$		38.4	202	810
S.D.		0.6	6	19
C.V. (%)		1.56	2.97	2.35
Difference (%)		−4.00	1.00	1.25

The recovery studies for compound I were performed in triplicate at three different concentrations (5, 50 and 100 ng/ml). The average recovery was approximately 92% (n = 9, S.D. = 13.6%, C.V. = 14.8%). The recovery for the IS at 1.0 μg/ml was 96.7% (n = 9, S.D. = 6.11%, C.V. = 6.32%).

This assay has been used for human plasma samples and different animal (rat, dog, and monkey) plasma samples with satisfactory performance. Fig. 1 presents the plasma profile of compound I in one patient who orally received active I (capsule) 10 mg or 15 mg once-a-day. Although, there is an unexplainable level of I at 0 h of 15-mg dose on this subject, it was not shown on most of the subjects. The incident is currently under investigation. Mean plasma concentrations of compound I in human subjects receiving a single 10-mg dose were between 5.74 and 48.0 ng/ml for the first 24 h after drug administration, suggesting that the sensitivity of the method is sufficient for monitoring the pharmacokinetic profiles after these doses.

ACKNOWLEDGEMENT

The authors gratefully acknowledge Dr. R. Riley of the Clinical Department of Rorer Central Research for his assistance in obtaining the human plasma samples for this work.

REFERENCES

1 R. G. Pendleton, J. A. Barrett, K. Bauer and M. H. Perrone, *Pharmacologist*, 29 (1987) 136.
2 J. A. Barrett, C. Kaisewokie, R. Swillo, R. Waltmann, W. C. Faith, R. G. Pendleton and M. H. Perrone, *Pharmacologist*, 29 (1987) 135.

Journal of Chromatography, 459 (1988) 221–227
Elsevier Science Publishers B.V., Amsterdam — Printed in The Netherlands

CHROMSYMP. 1485

SEPARATION OF FATTY ACID BINDING PROTEIN BY HIGH-PERFORMANCE MIXED-MODE CHROMATOGRAPHY

ARABINDA SAMANTA, GERALD A. CORDIS, M. RENUKA PRASAD and DIPAK K. DAS*
Cardiovascular Division, Department of Surgery, University of Connecticut School of Medicine, Farmington, CT 06032 (U.S.A.)

SUMMARY

Fatty acid binding protein (FABP) (14 kDa), can regulate the levels of tissue free fatty acids by binding them with high affinity. Since free fatty acids are known to accumulate in the ischemic myocardium, it is likely that FABP has a significant role in regulating their concentration in ischemic heart. FABP has recently been purified from other proteins, but the method requires several hours and special techniques. In this report, we describe a rapid high-performance liquid chromatographic method for separating and isolating the FABP from myocardial tissue biopsies.

About 25–50 μg of rat heart cytosol was incubated with 2 nmol of the potassium salt of [9,10-^{3}H]oleate (25 000 cpm) for 10 min at 37°C. This was then injected onto a Bio-Rad (Richmond, CA, U.S.A.) TSK-125 column. The sample was run using a low-salt isocratic mobile phase containing 10 m*M* potassium phosphate buffer (pH 7) and 1 m*M* dithiothreitol, and at a flow-rate of 0.8 ml/min. The heart cytosol, when incubated with isotopic oleate, was resolved into two radioactive peaks, one eluting in the area of serum albumin (retention time 9.6 min) and the other corresponding to a retention time of 12.9 min. The sodium dodecyl sulfate polyacrylamide gel electrophoretic profile of the later peak revealed a major protein band of *ca.* 14 kDa. Rat heart FABP purified by gel filtration and ion-exchange chromatography coeluted with the second radioactive peak. When increasing concentrations of cytosol were incubated with radioactive oleate and analyzed by high-performance liquid chromatography, a linear increase in the radioactive oleate-bound FABP peak (retention time 12.9 min) was obtained. These results suggest that FABP was separated from other proteins using the TSK-125 column, and hence this method can be used for a rapid recovery of FABP from biological tissues.

INTRODUCTION

Fatty acid binding protein (FABP), an intracellular non-enzymatic protein, has recently been found to possess several unique properties in controlling the levels of tissue free fatty acids (FFAs) and their thioesters by binding them with high affinity[1,2]. FABP has recently been isolated and characterized from several tissues, including heart, liver, kidney, adipose tissue, and intestinal mucosa, and found to possess a molecular weight of *ca.* 14 kDa[1,2].

0021-9673/88/$03.50

The purification of FABP requires skill and is time-consuming. The most common method of its purification includes G-75 gel-filtration followed by DEAE anion-exchange chromatography[3–5]. When eluted by potassium chloride gradient on DEAE chromatography, the FABP occasionally needs another gel-filtration step. The final purity is judged by sodium dodecyl sulfate polyacrylamide gel electrophoresis (SDS-PAGE).

In this report, we describe a rapid method for separating the FABP from myocardial tissue using high-performance liquid chromatography (HPLC). The Bio-Rad TSK-125 column used in this study behaved as both gel filtration column and ion exchanger under our experimental conditions. This method can thus be used as a rapid single-step recovery of FABP from biological tissues such as heart.

EXPERIMENTAL

Materials

Fatty acid-free bovine serum albumin (BSA) and Sephadex G-75 were purchased from Pharmacia (Piscataway, NJ, U.S.A.). DE-52 was purchased from Whatman (Clifton, NJ, U.S.A.). Myoglobin standard was obtained from Bio-Rad (Richmond, CA, U.S.A.), and [9,10-^{3}H]oleate and Aquasol were from New England Nuclear (Boston, MA, U.S.A.). Dithiothreitol was obtained from Sigma (St. Louis, MO, U.S.A.), and Lipidex-1000 from Packard Instrument (Downers Grove, IL, U.S.A.). HPLC-grade water was obtained from a Millipore water system (Millipore, Bedford, MA, U.S.A.). Nylon-66 (0.45 μm) filters were purchased from Rainin Instrument (Woburn, MA, U.S.A.).

Equipment

A Waters Assoc. (Milford, MA, U.S.A.) HPLC system was used in this study. The system consisted of a WISP Model 710B injector, Model 720 system Controller, Model 730 data module, Model 490 programmable multi-wavelength UV detector, and Model 6000A pump. A Bio-Rad (Richmond, CA, U.S.A.) Bio-Sil TSK-125 HPLC column (30 cm × 7.5 mm I.D.) equipped with a Bio-Sil TSK guard column (7.5 cm × 7.5 mm I.D.) was used for the FABP separations.

Methods

Purification of rat heart cytosolic FABP. Isolation and purification of FABP from rat heart cytosol was performed according to the methods described by Fournier *et al.*[3] and Glatz *et al.*[6]. In short, hearts were obtained from pentobarbital (10 mg per rat intraperitoneal) anaesthetized male Sprague-Dawley rats weighing 300–325 g. Hearts were perfused with a buffer mixture containing 0.25 *M* sucrose, 10 m*M* potassium phosphate (pH 7.0), and 1 m*M* dithiothreitol (DTT). Hearts were then excised, blotted, minced, and homogenized in 3 ml of 10 m*M* potassium phosphate buffer containing 1 m*M* DTT, using a PTFE-glass Potter-Elvehjem tissue homogenizer (Kontes, Vineland, NJ, U.S.A.). The homogenates were centrifuged at 800 *g* for 15 min to remove nuclear fractions and cell debris, followed by centrifugation at 12 500 *g* for 20 min to remove mitochondria and 105 000 *g* for 60 min to settle the microsomes. The 105 000 *g* supernatant served as the source of FABP.

The FABP was then purified to homogeneity according to Ockner *et al.*[5] by

employing G-75 gel-filtration and DEAE anion-exchange chromatography. The FABP eluted with a potassium chloride gradient from the DEAE column was further purified by a second G-75 gel-filtration. The FABP fractions were collected, and SDS-PAGE was carried out under reduced and denaturing conditions using 4.0% stacking gel (pH 6.8) and 15% separating gel in SDS. The electrophoretic buffer contained 0.025 *M* Tris (pH 8.8), 0.192 *M* glycine, and 0.1% SDS. Gels of 15% were run at 10 mA/gel for 4–5 h, after which they were fixed and stained in a solution of 0.2% Coomassie brilliant blue in methanol–water–acetic acid (5:5:1). The relative mobility of purified FABP was compared with that of protein standards to determine molecular weight.

Preparation of heart cytosol for HPLC. The 105 000 *g* supernatant was used for HPLC. Cytosol (6–60 μg) was incubated with 2 nmol of the potassium salt of [9,10-^{3}H]oleate (*ca.* 25 000 cpm) for 10 min at 37°C, and a 25-μl volume was injected onto a TSK-125 column. A low-salt isocratic mobile phase was used, which contained 10 m*M* potassium phosphate buffer (pH 7) and 1 m*M* DTT. Using a flow-rate of 0.8 ml/min, the effluent was monitored at 280 nm, and 0.4-ml fractions were collected for scintillation counting.

Highly purified FABP standard, obtained as described above, as well as BSA and myoglobin (horse) standards, were also injected on the TSK-125 column and chromatographed separately under identical conditions. These peaks were compared with those obtained from chromatography of cytosol FABP.

Delipidation of purified FABP and assay of fatty acid binding. The purified FABP was subjected to delipidation using Lipidex 1000 as described by Glatz *et al.*[6]. In brief, 2 mg of FABP were loaded on a column of Lipidex (5 cm × 0.5 cm I.D.) and equilibrated with 100 m*M* Tris–HCl buffer (pH 7.4) at 37°C. The delipidated FABP emerged in the void volume. The oleate binding was determined essentially according to the procedure described by Offner *et al.*[7]. The reaction mixture contained increasing amounts of oleic acid (sodium salt), 24 μg of FABP, 1.5 m*M* DTT, and 100 m*M* Tris–HCl (pH 7.4) in a total volume of 0.35 ml. The binding was allowed to continue for 5 min at 37°C, after which the test-tubes were cooled in ice. The unbound fatty acid was removed by mixing with 200 μl of ice-cold Lipidex-1000 and buffer suspension (1:1, v/v) for 10 min at 0°C. The radioactivity remaining in the supernatant was determined to calculate the nmoles of oleate bound per nmole of FABP[7].

RESULTS

Separation and identification of FABP from other proteins

About 37.5 μg of rat heart cytosol was incubated with 3 nmol of [9,10-^{3}H]oleate and injected onto a TSK-125 column as described in *Methods*. The effluent, monitored at 280 nm, revealed three major peaks, as shown in Fig. 1. Purified FABP, BSA, and myoglobin standards were injected separately on the same column and run under identical conditions. The tracings of these peaks were overlaid on the rat heart cytosol chromatogram shown in Fig. 1. As observed in the figure, the ^{3}H-labeled heart cytosols are resolved into two radioactive peaks, one eluting in the area of the BSA standard (t_R = 9.6 min) and the other corresponding to the area of the purified FABP peak (t_R = 12.9 min).

The later effluents corresponding to FABP peak were collected and SDS-PAGE

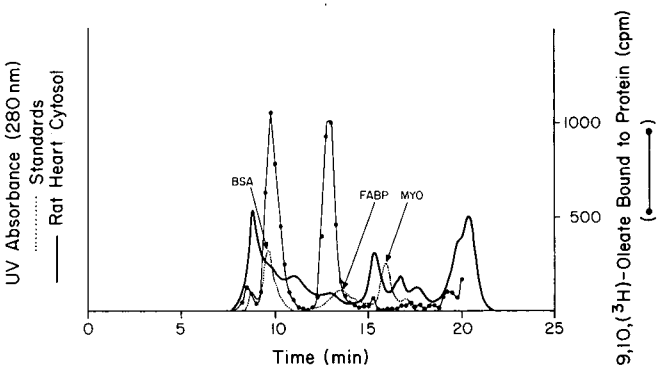

Fig. 1. HPLC chromatogram of rat heart cytosol and protein standards. Rat heart cytosol (37.5 μg) was prepared, incubated with 3 nmol of [9,10-^{3}H]oleate, and chromatographed as described in Experimental. A 25-μl volume of protein standards (BSA = bovine serum albumin, 10 μg; FABP = fatty acid binding protein, 5 μg; MYO = horse myoglobin, 6 μg) was run separately and the tracing overlaid on the rat heart cytosol chromatogram. Fractions were collected and counted for [9,10-^{3}H]oleate bound to rat heart cytosol as described in Experimental. UV absorbance of cytosol at 280 nm (———), UV absorbance of protein standards at 280 nm (– – –), and radioactivity bound to cytosol (●—●) were plotted against time (min).

was run on this sample. The SDS-PAGE profile revealed a major band of *ca.* 14 kDa molecular weight (Fig. 2), which corresponds to the molecular weight of rat heart FABP reported in the literature[1–7].

Binding of purified FABP with fatty acid

In order to confirm whether the peak identified as FABP in Fig. 1 is indeed FABP capable of binding FFAs, we assayed for oleate binding on the delipidated sample, as described in *Methods*. As shown in Fig. 3, when the sodium oleate concentration was increased, increasing amounts of oleate were bound to FABP and the saturation was reached at a value of 2 nmol of oleate bound per nmol of FABP. This binding is similar to the value recently reported in the literature[4,7]. The affinity of binding for [^{14}C]oleic acid with FABP was analyzed from a Scatchard plot. From the Scatchard analysis (Fig. 4), the maximum binding capacity for oleic acid was determined as 2.0 nmol/n mol FABP. The apparent dissociation constant (K_d) value was 0.48 μM for oleic acid. This K_d value compares favorably with those reported in the literature[6].

We also challenged the cytosol with radioactive oleate by incubating various concentrations of the cytosol (6 μg, 12.5 μg, 25 μg, 37.5 μg, 50 μg, and 60 μg) with a constant amount (2 nmol) of [^{3}H]oleate, followed by HPLC. The radioactivity found in the FABP peak was plotted against the concentration of cytosol. As shown in Fig. 5, we found a linear response in the radioactive oleate-bound FABP peak (t_R = 12.9 min) when increasing amounts of cytosolic protein (6–60 μg) were used.

DISCUSSION

The abundant presence of FABP in the cytosolic compartments of many biological tissues, including heart, kidney, liver, lung, brain, intestine, skeletal muscle,

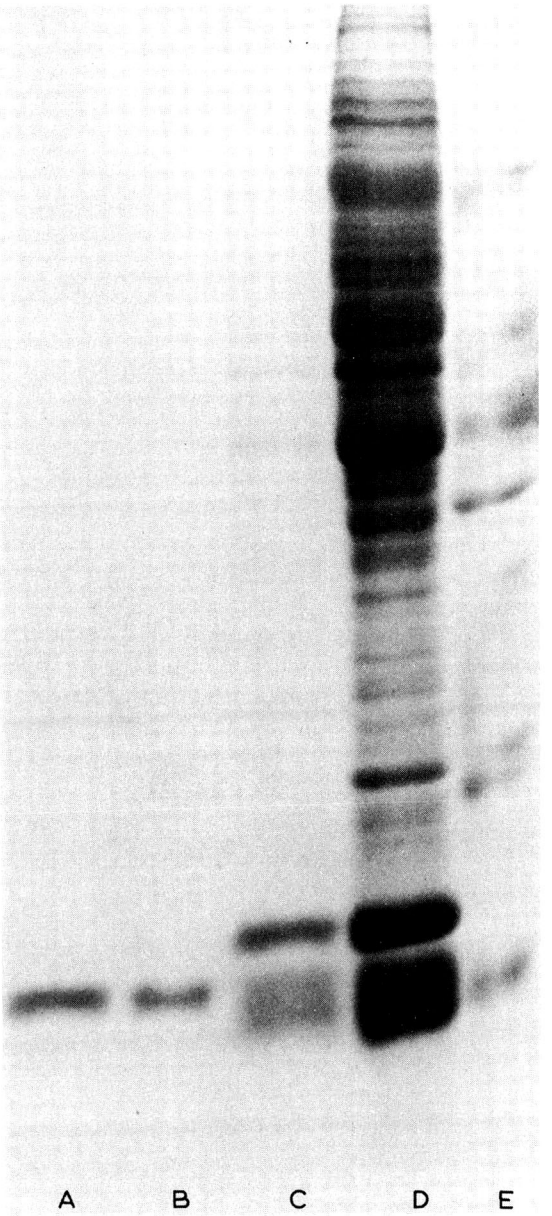

Fig. 2. SDS-PAGE profiles. (A) Effluent from TSK-125 column corresponding to FABP peak; (B) FABP standard purified by gel-filtration and anion-exchange chromatography; (C) G-75 pooled during purification of FABP (purified protein is given in B); (D) rat cytosolic proteins (this protein was then subjected to G-75 gel-filtration as shown in B, and subsequently purified to homogeneity as in (A); (E) marker proteins (67 kDa, 45 kDa, 36 kDa, 29 kDa, 24 kDa, 20 kDa, 14 kDa).

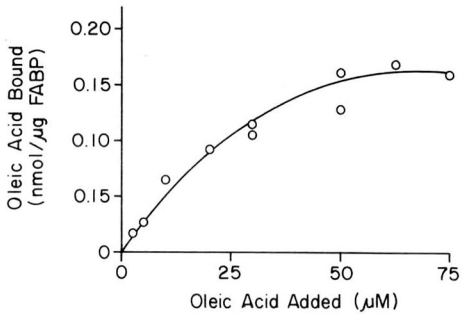

Fig. 3. Binding of radiolabeled oleic acid to rat heart FABP. Varying amounts of oleic acid were incubated with 24 μg of FABP for 5 min at 37°C. After equilibration, protein-bound and unbound oleic acids were separated by the use of Lipidex at 0°C as described in Experimental. Values have been corrected for non-specific binding at each point and represent an average of four experiments.

and adipose tissue, suggest some physiological significance of this protein in tissue[1]. However, most of the significance still remains under speculation, except that FABP has been found to bind with high affinity with FFAs and their esters and to shuttle them through the cytosolic compartment[7].

FFAs and their esters are known to accumulate in the biological tissue in a variety of disease processes. For example, prolonged ischemic insult results in the accumulation of FFAs[8]. Accumulation of FFAs is a common occurrence in myocardial infarction or during open-heart surgery[9]. Accumulation of FFAs and their es-

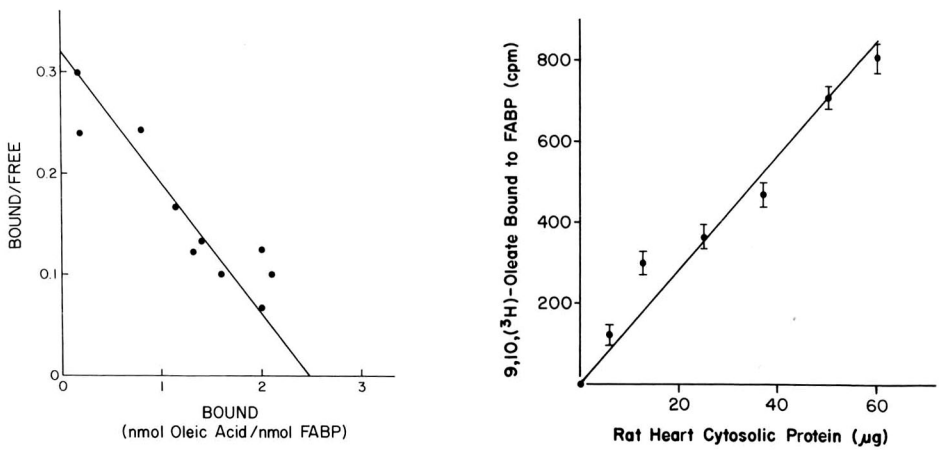

Fig. 4. Scatchard analysis of the saturation curve shown in Fig. 3. Values have been corrected for non-specific binding determined at each point and represent an average of four experiments.

Fig. 5. Incorporation of [9,10-^{3}H]oleate into FABP of rat heart cytosol. Increasing amounts of rat heart cytosol was incubated with [^{3}H]oleate and chromatographed as described in Experimental. Values have been corrected for non-specific binding determined at each point and represent an average of three experiments. The radioactivity found in the FABP peak was plotted against the concentration of cytosol used in the assay.

ters, particularly the long-chain thioesters, tends to cause myocardial dysfunction by their detergent-like action and enzyme-inhibitory properties[10]. Although serum albumin also binds to fatty acids, this protein, being of extracellular origin, is incapable of binding with the intracellularly accumulated FFAs and their esters. FABP, on the other hand, can not only bind them, presumably protecting the tissue from the detrimental effects of FFAs, but also shuttle them through the cytosolic compartment[5].

The separation and detection of FABP is a necessary step for performing any experiment concerning the physiological or biochemical roles of FABP. As mentioned earlier, the only method available for the separation of FABP involves several sophisticated chromatographic steps, including gel filtrations and anion-exchange chromatography. In addition, these techniques take over 24 h to separate FABP from the cytosol. The method described in this report is an extremely simple HPLC technique. The sample is run with an isocratic mobile phase by a single-step elution. The total separation time is 22 min.

In addition, the results of our study also suggest that Bio-Rad TSK-125, a gel filtration column, also behaves as an ion exchanger under our experimental conditions supporting the results from a previous study[11]. In the present study, at low ionic strength, myoglobin with a higher molecular weight than FABP eluted later from the column. This method can thus be used for a rapid single-step quantitation of FABP from biological tissues such as heart.

ACKNOWLEDGEMENTS

This study was supported by USPHS NIH HL 22559, HL 33889, and HL 34360. We thank Randall Jones and Howard Young for obtaining the necessary rat heart biopsies, and Joanne D'Aprile for her skillful secretarial assistance.

REFERENCES

1 J. F. C. Glatz, G. J. Vander Vusse and J. H. Veerkamp, *News Physiol. Sci.*, 30 (2985) 41.
2 R. J. A. Paulussen, G. P. M. Jansen and J. H. Veerkamp, *Biochim. Biophys. Acta*, 877 (1985) 342.
3 N. C. Fournier, M. Zucker, R. E. Williams and I. C. P. Smith, *Biochemistry*, 22 (1983) 1863.
4 A. Samanta, M. R. Prasad, R. M. Engelman and D. K. Das, *J. Mol. Cell. Cardiol.*, 19 (1987) 219.
5 R. K. Ockner, J. A. Manning and J. P. Kane, *J. Biol. Chem.*, 257 (1982) 7872.
6 J. F. C. Glatz, C. C. F. Baerwaldt, J. H. Veerkamp and H. J. M. Kempen, *J. Biol. Chem.*, 259 (1984) 4295.
7 G. D. Offner, R. F. Troxler and P. Brecher, *J. Biol. Chem.*, 261 (1986) 5584.
8 K. R. Chien, A. Han, A. Sen, L. M. Buja and J. T. Willerson, *Circ. Res.*, 54 (1984) 313.
9 G. A. Cordis, M. R. Prasad, H. Otani, R. M. Engelman and D. K. Das, *Chromatographia*, 24 (1987) 687.
10 A. M. Katz and F. C. Messineo, *Circ. Res.*, 48 (1981) 1.
11 E. Pfannkoch, K. C. Lu, F. E. Regnier and H. G. Barth, *J. Chromatogr. Sci.*, 18 (1980) 430.

Journal of Chromatography, 459 (1988) 229–236
Elsevier Science Publishers B.V., Amsterdam — Printed in The Netherlands

CHROMSYMP. 1486

NOVEL DUAL-WAVELENGTH MONITORING APPROACH FOR THE IMPROVED RAPID SEPARATION AND ESTIMATION OF ADENINE NUCLEOTIDES AND CREATINE PHOSPHATE BY HIGH-PERFORMANCE LIQUID CHROMATOGRAPHY

GERALD A. CORDIS
Cardiovascular Division, Department of Surgery, University of Connecticut School of Medicine, Farmington, CT 06032 (U.S.A.)
RICHARD M. ENGELMAN
Department of Surgery, Baystate Medical Center, Springfield, MA 01107 (U.S.A.)
and
DIPAK K. DAS*
Cardiovascular Division, Department of Surgery, University of Connecticut School of Medicine, Farmington, CT 06032 (U.S.A)

SUMMARY

A rapid and improved method for the simultaneous quantification of adenine nucleotides, including adenosine triphosphate, adenosine diphosphate, adenosine monophosphate, as well as creatine phosphate by high-performance liquid chromatography is described. A programmable multi-wavelength UV detector was used to monitor the effluent initially at 210 nm for 4 min to measure creative phosphate, and then at 259 nm for 6 min to quantitate adenosine mono-, di- and triphosphate. The method is, thus, not only rapid, but also extremely sensitive because of the utilization of corresponding absorption maxima for creatine phosphate and adenine nucleotides, rather than measuring all of them at a single wavelength. In addition, computer-generated standard curves were used to estimate these compounds, thereby improving the accuracy of the measurements.

Since myocardial high-energy phosphate levels are widely measured because they are reliable parameters for myocardial preservation during ischemia, these compounds were assayed in pig heart prior to and following ischemia. The results were compared with those obtained by conventional high-performance liquid chromatographic assay methods in order to examine the validity of this method. Our results indicate that this is indeed a novel method, which is more rapid as well as sensitive and accurate compared with other methods.

INTRODUCTION

Despite a number of methods now available for the separation and quantitative estimation of high energy phosphate compounds in biological tissues [1–6], a rapid and accurate method for the measurement of extremely low levels of these compounds is

0021-9673/88/$03.50

still lacking. In most of these methods, adenine nucleotides are measured at 254 nm, whereas creatine phospate (CP) is measured at 210 nm, in which the respective absorption maxima are observed [1]. These methods, thus, require relatively more time because of the necessity of the separate injections of the samples onto the high-performance liquid chromatographic (HPLC) column, with a subsequent change in wavelength and mobile phase in order to measure CP and to achieve complete separation of adenosine triphosphate (ATP), adenosine diphosphate (ADP), and adenosine monophosphate (AMP). Ion-exchange HPLC methods[2] allow simultaneous determination, but all the compounds are measured at 210 nm. The method is lengthy, the baseline drifts due to the gradient, and baseline separation of AMP is not achieved. Reversed-phase methods[3] also allow simultaneous analysis; however, CP and the adenine nucleotides are measured at 214 nm, and baseline separation of ADP and ATP in myocardial extracts is not achieved. Recently we[4] and others[5,6] have developed methods which allow simultaneous measurement of ATP, ADP, AMP, and CP. However, these methods utilize a wavelength of 210 nm, where only CP shows absorption maxima; hence, extremely low levels of adenine nucleotides are not adequately resolved. The same investigators [5,6] used rapid isocratic methods for their simultaneous analysis of adenine nucleotide and CP. However, baseline separation of CP from various bases and nucleosides in a myocardial extract and subsequent accurate quantitation can only be achieved by the absence of an organic solvent in the initial mobile phase. We, therefore, used the gradient system in order to subsequently elute the adenine nucleotides in our separation.

Since the preservation of high-energy phosphate compounds, including ATP and CP, during ischemic insult such as myocardial infarction or open-heart surgery, is considered to be one of the most important determinants for the functional recovery of heart[7], rapid and accurate measurements of extremely low levels of these compounds are necessary to predict the appropriate therapeutic interventions[8,9]. In this report, we describe a rapid HPLC technique aided by computer to use 210 nm and 259 nm wavelengths for estimating pmole amounts of high-energy phosphate compounds in myocardial tissue with rapidity and high precision.

EXPERIMENTAL

Materials

Adenine nucleotides and creatine phosphate used as chromatographic standards were purchased from Sigma (St. Louis, MO, U.S.A.). Tetrabutylammonium phosphate was purchased as PIC Reagent Low UV A from Waters Assoc. (Milford, MA, U.S.A.). UV spectrograde acetonitrile was obtained from Burdick & Jackson Labs. (Muskegon, MI, U.S.A.) HPLC-grade water was obtained from a Millipore water system (Millipore, Bedford, MA, U.S.A.). Centrifugal 0.45-μm nylon microfilters were from Schleicher & Schuell (Keene, NH, U.S.A.). Solvent 0.45-μm Nylon-66 filters were purchased from Rainin Instrument (Woborn, MA, U.S.A.).

Equipment

Two Waters Assoc. HPLC systems were used. The first system consisted of a WISP Model 710B injector, Model 720 system controller, Model 730 data module, Model 490 programmable multi-wavelength UV detector, Model 6000A pump, Mod-

el 45 pump, μBondapak C_{18} Guard-Pak precolumn, Z-Module, and a Radial-Pak Nova-Pak C_{18} (10 cm × 5 mm I.D., 4 μm particle size) radial compression cartridge. The second HPLC system consisted of Model 820 full control MAXIMA computer system, Satellite WISP Model 700 injector, Model 490 programmable multi-wavelength UV Detector, two Model 510 pumps, μBondapak C_{18} Guard-Pak precolumn, Z-Module, and a Radial-Pak Nova-Pak C_{18} (10 cm × 5 mm I.D., 4 μm particle size) radial compression cartridge.

Methods

Myocardial left ventricular biopsies from anesthetized 20-kg pigs of either sex were obtained using a high-speed dental drill fitted with a vacuum line for rapid removal of tissue. The samples were immediately immersed in liquid nitrogen and stored at –73°C until extracted. The biopsy specimens were homogenized in 6% perchloric acid using a Polytron tissue homogenizer (Brinkman Instruments, Westbury, NY, U.S.A.), centrifuged, neutralized to pH 7.0 with 5 *M* potassium carbonate, and filtered for HPLC, as described previously[4].

A volume of 25 μl of a filtered, neutralized, perchloric acid extract was injected onto a Nova-Pak C_{18} column with a degassed initial mobile phase of 48 m*M* monobasic potassium phosphate, 1 m*M* tetrabutylammonium phosphate (pH 5.8, with potassium hydroxide) at a flow-rate of 2 ml/min. Using a Waters Assoc. Model 490 programmable multi-wavelength UV detector, the effluent was monitored at 210 nm for 4 min to measure CP, and then monitored at 259 nm for 6 min to measure the adenine nucleotides. The initial mobile phase was used for 4 min, followed by a step gradient to 20% acetonitrile in the degassed initial buffer. After the 10 min run, the column was equilibrated with the initial mobile phase for 25 min prior to the next injection. The UV detector was auto-zeroed upon injection and during the change in wavelength. A blank was initially run and used for baseline substraction.

A calibration curve was produced using MAXIMA 820 software (Waters) system for each of the high-energy phosphate compounds. Using external standards, six different concentrations ranging from 10 μ*M* to 1 m*M* were used. A response factor was then calculated from the slope of each curve.

The MAXIMA 820 software and the I-200 system interface module controlled the two HPLC pumps and the auto-injector. The computer system also acquired and stored data from the UV detector. Data processing allowed editing of the integration and production of calibration curves. The M-490 UV detector was used for changing the wavelength, auto-zeroing, and for baseline subtraction.

RESULTS

Separation of ATP, ADP, AMP, and CP using two different wavelengths

High-energy phosphate compounds were separated according to previously described methods[4]. These methods utilize a single wavelength of 210 nm to monitor compounds eluted. The retention times of CP, AMP, ADP, and ATP were 5.7 min, 18.5 min, 22.6 min, and 28.1 min, respectively, making a total run time of *ca.* 35 min (Fig. 1A).

CP and the adenine nucleotides were then separated utilizing the two-wavelength approach. As described in *Methods*, the effluent was initially monitored at 210

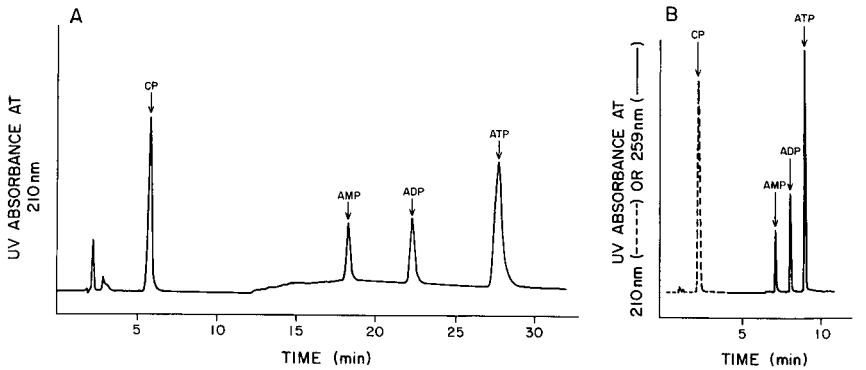

Fig. 1. Separation of CP, AMP, ADP, and ATP standards by ion-pair reversed-phase HPLC. A volume of 25 μl of standard solution of 1 m*M* CP, 0.1 m*M* AMP, 0.15 m*M* ADP, and 0.5 m*M* ATP was injected onto a C_{18} column equipped with a programmable multi-wavelength detector. (A) Conventional method using a 10-μm particle size C_{18} column and a linear gradient as described elsewhere[4]. (B) Modified method using a 4-μm particle size C_{18} column, step gradient, baseline subtraction, and wavelength shift as described in Experimental (- - - -) 210 nm; (——) 259 nm.

nm for 4 min when CP was detected with a retention time of 2.2 min (Fig. 1B). The UV detector was pre-programmed, such that after 4 min the wavelength was changed to 259 nm when AMP, ADP, and ATP showed up with retention times of 7.1 min, 8.1 min, and 9.0 min, respectively. The peaks were identified by comparison with the authentic standards.

Construction of calibration curve

Using the second HPLC system described in Experimental, and employing the MAXIMA 820 software, a calibration curve and response factor were produced for each of the CP and adenine nucleotide standards. Six different concentrations in a ten-fold range for each standard were injected and chromatographed as described in Experimental. In Fig. 2, the concentrations of each standard, (A) CP, (B) AMP, (C) ADP, and (D) ATP, were plotted against the peak area obtained. A response factor was obtained from the slope of each curve. The calculated response factors for CP, AMP, ADP, and ATP were $2.234\,481 \cdot 10^7$, $1.167\,666 \cdot 10^7$, $1.270\,137 \cdot 10^7$, and $1.392\,313 \cdot 10^7$, respectively. The differences between the respective response factors can be explained because of the changes in peak shape as the component is retained on the column. In each case, however, the calibration curve was linear, with all points having a small standard deviation and falling on the curve. The *r* value was very close to 1 in each case.

Quantitative estimation of high-energy phosphate compounds in pig heart

Since the high-energy phosphate compounds are extremely susceptible to ischemic insult, we assayed ATP, ADP, AMP, and CP from pig heart prior to and after 60 min of normothermic ischemia, as well as after 60 min of ischemia followed by 60 min of revascularization. The quick-frozen myocardial biopsies were processed as described in *Methods*, and loaded onto the HPLC column equipped with programmable multi-wavelength UV detector. The results from control pre-ischemic heart

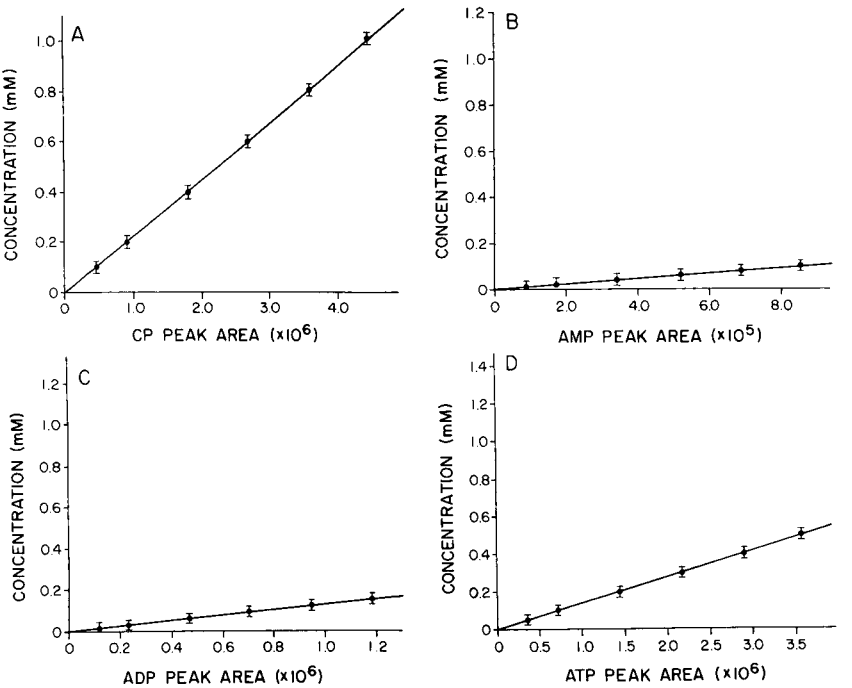

Fig. 2. Calibration curves for CP, AMP, ADP, and ATP standards. Six different concentrations of each standard, as indicated on the graph, were injected onto a C_{18} column as described in Experimental, and the different concentrations were plotted against the peak area. Each value represents mean ± S.E. of at least three different experimental results. The r values are: CP = 0.999 859 58; AMP = 0.999 860 05; ADP = 0.999 948 50; ATP = 0.999 768 51 . (A) CP; (B) AMP; (C) ADP; (D) ATP.

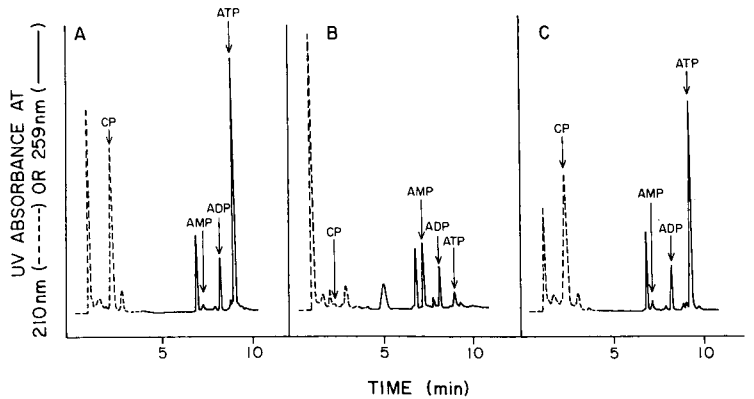

Fig. 3. Separation of CP, AMP, ADP, and ATP in porcine myocardial perchloric acid extracts, filtered and neutralized, as described in Experimental. Each injection consisted of 25 μl of neutralized perchloric acid extract containing 1 mg of tissue biopsy. The UV detector was set at 0.8 a.u.f.s. (A) Control heart; (B) ischemic heart; (C) reperfused heart.

TABLE I

LIMIT OF DETECTION FOR ATP, ADP, AMP AND CP BY HPLC

Standards of each component were injected onto a C_{18} column as described in Experimental using the UV detector set at 0.001 a.u.f.s.

	Lowest limit of detection (pmol)	*S/N ratio*
CP	10.0	4.0
AMP	1.5	4.0
ADP	2.0	4.0
ATP	1.0	4.0

biopsies are shown in Fig. 3A, whereas the results from ischemic heart biopsies are demonstrated in Fig. 3B. As shown in the figure, even though the amounts of CP and ATP were extremely low, they were still detected with reasonable peak heights, enough to obtain accurate estimates. Peak-shift studies were done as described previously[4]. A porcine myocardial extract was acidified with hydrochloric acid and then heated to 50°C. This resulted in complete decrease in the CP peak and subsequent increase in the creatine peak. Addition of 5′-adenylic deaminase to the extract caused a disappearance of the AMP peak, with an increase in the inosine monophosphate (IMP) peak. Myokinase converted ADP to AMP and ATP, and adenosine 5′-triphosphatase caused the decrease of ATP and an increase in ADP. Close examination of Fig. 3 indicates the presence of another peak in close proximity to AMP. This peak, with a retention time of 6.8 min, indicates the presence of NADH, which is known to decrease during ischemia and increase to the preischemic value after reperfusion. Fig. 3 also shows the appearance of a peak only in the ischemic heart, which disappears after reperfusion. This peak, with a retention time of 5.0 min, was identified as IMP. Reperfusion following ischemia is generally associated with the rebouncing of the values towards the pre-ischemic levels[7–9]. As expected, the values of these compounds were much higher in the reprefused hearts then ischemic hearts, as evidenced by the relatively higher peaks shown in Fig. 3C. Accuracy of the method was determined by standard addition technique. Additions of even 10 pmol of ATP, 20 pmol of ADP and AMP, and 50 pmol of CP were accurately reflected in the peak heights. The lowest limit of detection for the adenine nucleotides and CP and corresponding signal-to-noise (S/N) ratios are given in Table I. Within-run and inter-animal variations were 1% and 5%, respectively.

DISCUSSION

High-energy phosphate compounds, including ATP and CP, are considered as one of the most important biochemical gauges for proper functioning of mammalian heart. Myocardial infarction and open-heart surgery are usually associated with prolonged episodes of ischemic insult. During ischemia, depletion of the ATP level by adenylate kinase occurs, resulting in an extremely low level of ATP with a corresponding rise in tissue ADP and AMP[7]. CP also suffers appreciable loss, often becoming almost negligible after severe ischemic insult. Since CP serves as an "energy

buffer" and plays a significant role in the energy transport process between various cellular compartments, it is important to know the exact amounts of CP during the ischemic episode. At the onset of reperfusion, redistribution of adenine nucleotides usually takes place, which is reflected in the value of adenylate energy charge. Accordingly, ATP and CP, particularly the latter, often rise to the pre-ischemic levels[7].

It is, therefore, conceivable that extremely low levels, of ATP, ADP, AMP, and CP must be measured in the heart during ischemia with the utmost accuracy in order to be able to predict the functional recovery after the revascularization. In addition, issue size is also an important factor to be considered, because often only an extremely small amount of biopsy (less than 50 mg) may be obtained to measure the high-energy phosphate compounds.

In the present method, with less than a 50-mg biopsy we were able to accurately measure the levels of adenine nucleotides and CP during ischemia. We used standard addition technique to examine the accuracy of the method. The success of the method primarily depends on the fact that we measured CP and adenine nucleotides at two different wavelengths, corresponding to respective absorption maxima, instead of measuring at a single wavelength.

Another important feature of this method is the rapidity of the separation. The complete separation of CP, ATP, ADP, and AMP was achieved within 10 min, instead of *ca.* 35 min separation time for another previously described method[4]. The 25-min period of equilibration, however, remained unchanged. Such rapid determination is often very useful, because the results of the tissue levels of the high-energy phosphate compounds may be obtained prior to the initiation of reperfusion.

This computer-assisted method not only detected very low levels of high-energy phosphate compounds, but it also estimated them with a high degree of precision (within-run and inter-animal variations were 1% and 5%, respectively). Using a Waters Model 820 full-control MAXIMA computer, calibration curves were constructed for each compound. When various concentrations were plotted against the peak area, straight lines were obtained which, when extrapolated, passed through zero. Response factors for each compound were derived from these standard curves and used to calculate the unknown concentration of each compound in the pig heart extracts. This method thus increases the accuracy of the result significantly, as observed by the need for low amounts of standards in the standard addition technique (data not shown).

As mentioned earlier, the exact determination of high-energy phosphate compounds is of the utmost importance in evaluating proper myocardial performance during ischemia and reperfusion. Because of the great sensitivity, precision, and accuracy, as well as the rapidity, this computer-aided dual-wavelength method will be very useful in analyzing the tissue levels of ATP, ADP, AMP, and CP in ischemic and reperfused hearts. The method we report here should be easily adaptable for use with other tissues.

ACKNOWLEDGEMENTS

This study was supported by USPHS NIH HL 22559, HL 33889, and HL 34360. We thank Randall Jones and Howard Young for obtaining the necessary myocardial biopsies, and Joanne D'Aprile for her skillful secretarial assistance.

REFERENCES

1 E. Juengling and H. Kammermeier, *Anal. Biochem.*, 102 (1980) 358.
2 E. Harmsen, P. P. de Tombe and J. W. de Jong, *J. Chromatogr.*, 230 (1982) 131.
3 G. R. Dubyak and A. Scarpa, in H. A. Fozzard, E. Haber, R. B. Jennings, A. M. Katz and H. E. Morgan (Editors), *The Heart and Cardiovascular System, Vol. 1*, Raven Press, New York, 1986, Ch. 18, p. 303.
4 G. A. Cordis, R. M. Engelman and D. K. Das, *J. Chromatogr.*, 386 (1987) 283.
5 O. F. M. Sellevold, P. Jynge and K. Aarstad, *J. Mol. Cell. Cardiol.*, 18 (1986) 517.
6 T. Victor, A. M. Jordaan, A. J. Bester and A. Lochner, *J. Chromatogr.*, 389 (1987) 339.
7 D. K. Das, R. M. Engelman, H. Otani, J. A. Rousou, R. H. Breyer and S. Lemeshow, *Clin. Physiol. Biochem.*, 4 (1986) 187.
8 D. K. Das, R. M. Engelman, J. A. Rousou, R. H. Breyer, H. Otani and S. Lemeshow, *Am. J. Physiol.*, 251 (1986) H71.
9 D. K. Das, R. M. Engelman, J. A. Rousou, R. H. Breyer, H. Otani and S. Lemeshow, *Basic Res. Cardiol.*, 81 (1986) 155.

Journal of Chromatography, 459 (1988) 237–244
Elsevier Science Publishers B.V., Amsterdam — Printed in The Netherlands

CHROM. 1474

QUANTITATION OF FREE AMINO ACIDS IN BIOLOGICAL SAMPLES BY HIGH-PERFORMANCE LIQUID CHROMATOGRAPHY

APPLICATION OF THE METHOD IN EVALUATING AMINO ACID LEVELS IN CEREBROSPINAL FLUID AND PLASMA OF PATIENTS WITH MULTIPLE SCLEROSIS

G. ALI QURESHI* and M. SHAHID BAIG
Departments of Renal Medicine and Neurology, Karolinska Institute, Huddinge University Hospital, S-141 86 Huddinge (Sweden)

SUMMARY

An automatic on-line high-performance liquid chromatographic method based on a precolumn derivatization with *o*-phthalaldehyde has been developed to quantitate levels of free amino acids in cerebrospinal fluid (CSF) and plasma samples from 12 patients with multiple sclerosis (MS) and 12 controls. The analytical method gave reproducible results with relative standard deviations of 0.5–3% for all amino acids. The separation of 24 amino acids was performed on a reversed-phase C_{18} column, using two solvents and a multiple-step gradient. Each chromatographic experiment was completed within 40 min. The results showed higher levels of Glu, Gln, Gly and Ala and lower levels of Met, Val, Phe and Lys in plasma of MS patients. In CSF, increased levels of Gln, Arg, Ser and Tyr and decreased levels of Asp, Glu, Met, γ-aminobutyric acid and Phe were found in MS patients, whereas the levels of other amino acids remained more or the less same in both groups.

INTRODUCTION

It is well established that among the free amino acids, glutamic acid (Glu), aspartic acid (Asp), γ-aminobutyric acid (GABA), glycine (Gly), glutamine (Gln) and taurine (Tau) are prominent in mature brain and constitute 2/3 of the free α-amino nitrogen[1]. These amino acids possibly play an important rôle as neurotransmitters and/or neuromodulators[1–3].

It is known that the pattern of free amino acid concentrations in cerebrospinal fluid (CSF) reflects a complex equilibrium of amino acid transport at the various barriers between blood, CSF and brain, as well as metabolic processes in whole body and brain tissue[4,5]. Accordingly, abnormal concentrations of one or more free amino acids in CSF are found under various neurological conditions, such as central nervous system (CNS) infections, convulsions, extrapyramidal and in various neuropsychiatric disorders[4–12].

0021-9673/88/$03.50

Since the majority of identified neurotransmitters and putative neurotransmitters are either amino acids or their derivatives, the accurate and valid measurements of CSF amino acid levels would constitute a potentially useful method for investigating the CNS function. However, aside from GABA, systematic evaluation of basic parameters has not been adequately carried out, and this is reflected in the variability in CSF amino acid levels reported in the literature[10–16].

The quantitation of free amino acids and total amino acids in biological samples has traditionally been performed by classical ion-exchange chromatography followed by post-column derivatization with ninhydrin or a fluorescence reagent, such as *o*-phthalaldehyde (OPA)[17,18]. This technique is time consuming (2–3 h), requires relatively large sample volumes (100–300 μl) and yields unreliable results for labile amino acids such as Gln and Asn. Other problems encountered, including broadening of peaks, discrepancies in results in accurate quantitation of basic amino acid, buffer contamination, baseline shift and incorrect identification of amino acids in physiological samples, have recently been reviewed[19].

In recent years, the fluorogenic reaction between OPA, thiols and primary amines has been exploited in reversed-phase high-performance liquid chromatography (RP-HPLC). The reaction is highly specific and sensitive and is completed within a few minutes at ambient temperature. Various systems are utilized for HPLC analysis after OPA derivatization to quantitate amino acids in physiological fluids[20–24]. In this study, an automatic on-line HPLC system, based on precolumn derivatization with OPA, has been developed to quantitate free amino acids in CSF and plasma samples from twelve multiple sclerosis (MS) patients. This method gave highly reproducible results with standard deviations between 0.5 and 3% for all amino acids. The results obtained for MS patients were statistically compared with results for healthy controls.

EXPERIMENTAL

Materials

Individual crystalline samples of L-amino acids (standard kit No. 20065), 30% Brij and anhydrous OPA were obtained from Pierce Eurochemie, The Netherlands. Phosphoserine, 3-methylhistidine, citrulline, carnosine, α-, β- and γ-aminobutyric acid, taurine, asparagine, ornithine and 2-mercapthoethanol (2-ME) were obtained from Sigma (St. Louis, MO, U.S.A.). HPLC-grade methanol was obtained from Rathburn (Walkerburn, U.K.). Anhydrous sodium dihydrogenphosphate, disodium hydrogenphosphate, 5-sulphosalicylic acid, boric acid, sodium hydroxide and hydrochloric acid were all of analytical-reagent grade (Merck, Darmstadt, F.R.G.).

Individual standard stock solutions of amino acids in concentrations of 1 μmol/ml were prepared in doubly distilled water with the addition of a few drops of 0.1 *M* hydrochloric acid. A standard mixture containing 25 amino acids was prepared with similar concentrations of amino acids. This mixture was diluted to 0.1, 0.05, 0.03 and 0.02 μmol/ml to establish a relationship between the fluorescence intensity and the concentration of the individual amino acids. Water used for the preparation of buffers and standards was deionized and sterile (Milli-Q water purification system, Millipore).

The chromatographic system consisted of two solvent delivery pumps (6000A

and M45), a multiple sampler (WISP 710B), a data module, a system controller (730B) and a fluorescence detector (420-AC) with the monochromator set at 340 nm and a 450-nm cut-off filter, all supplied by Waters Assoc. (Milford, MA, U.S.A.).

Methods

The separation of the amino acids was performed on a 5-μm LiChrosorb C_{18} column (150 mm × 4 mm I.D.) obtained from Merck. A precolumn (4 mm × 4 mm I.D.), containing similar material, was inserted between the analytical column and the injector. The column was conditioned with 50% aq. methanol and then with solvent A for 1 h before use. For pump A, a mobile phase consisting of tetrahydrofuran–methanol – 0.02 *M* phosphate buffer (pH 6.8) (1:1:98) (eluent A), and for pump B, a mobile phase consisting of phosphate buffer–methanol (35:65) (eluent B) was used. Both these eluents were filtered through 0.45-μm filter-paper and sonicated for 10 min before use. Details of the OPA reagent and buffers were given in ref. 25. The gradient used is shown in Fig. 1.

Biological samples and their treatment

Lumbar CSF and venous blood samples were collected simultaneously between 9 and 11 a.m. from 12 control subjects (7 women and 5 men aged 36–67 years, mean 49.8 ± 8.8 years) and 12 patients with clinically defined MS (6 women and 6 men aged 25–65 years, mean 47 ± 11 years). None of the subjects was on any medication. The control subjects had complaints of headaches or dizziness, but no objective findings suggesting an involvement of the nervous system. All MS patients showed oligoclonal bands in their CSF and high intrathecal immunoglobulin (IgG) production (IgG index > 7). The blood samples were centrifuged at 1500 *g* for 15 min and the plasma was separated.

Prior to HPLC analysis, 100 μl of plasma or CSF samples were treated with an equal volume of cold 4% sulphosalicylic acid (SSA) and 50 μl of β-amonibutyric acid (50 nmol/ml) were added as an internal standard. The mixture was centrifuged at 1500 *g* for 15 min and the supernatant was collected and stored at −70°C if not analysed immediately. The derivatization of amino acids with OPA was carried out according to Qureshi *et al.*[21].

RESULTS AND DISCUSSION

Fig. 1 shows the chromatogram of the standard OPA-derivatized amino acids under our experimental conditions. Each peak represents 2.5 nmol of amino acid. The fluorescence intensity measured for all amino acids was linearly correlated with the amount injected over a range of 5–100 nmol giving $r^2 = 1$. By running five replicates of the standard (2.5 nmol/ml), each amino acid showed high reproducibility in terms of integrated areas and retention times, giving relative standard deviations (R.S.D.) between 0.5 and 3%. The detection limit for each amino acid was less than 1 pmol. The separation of the amino acids was completed within 40 min.

Figs. 2 and 3 show the chromatograms of plasma and CSF samples respectively from a MS patient.

Table I shows the mean plasma levels of free amino acids in controls and MS patients. Previous studies[26,27] on MS patients found increased plasma levels of Ala

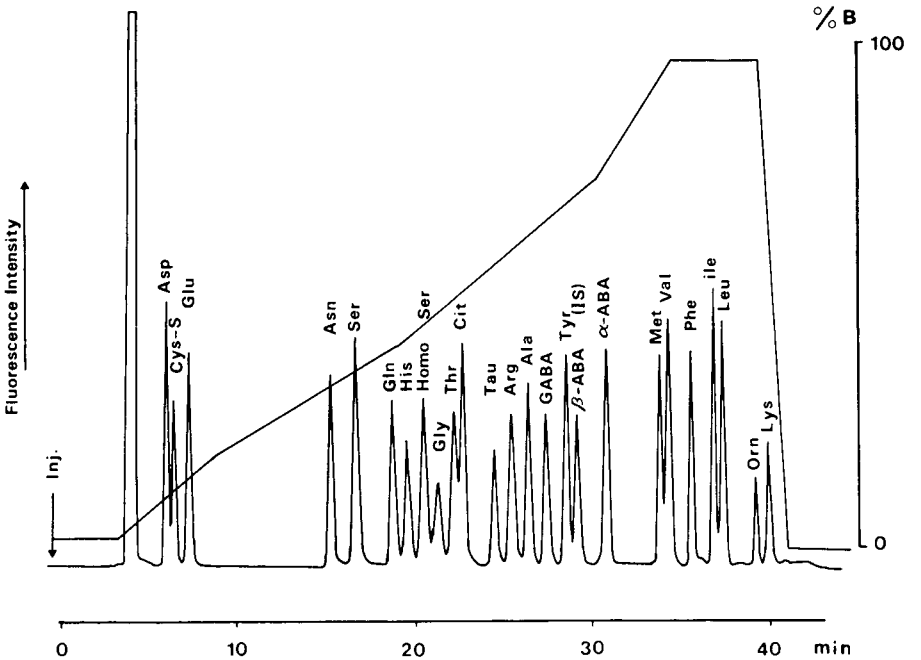

Fig. 1. Separation of standard (2.5 nmol/ml) OPA–2-ME-derivatized amino acids on 5-μm LiChrosorb C_{18} (150 mm × 4 mm I.D.) by the use of tetrahydrofuran–methanol–0.02 *M* phosphate buffer (pH 6.8) (1:1:98) (eluent A), and phosphate buffer–methanol (35:65) (eluent B). The gradient used is shown in %B. A flow-rate of 1 ml/min was maintained throughout except for the first 2 min when it was linearly increased from 0.2 to 1 ml/min. The detection was made at 340 excitation and 450 nm (emission).

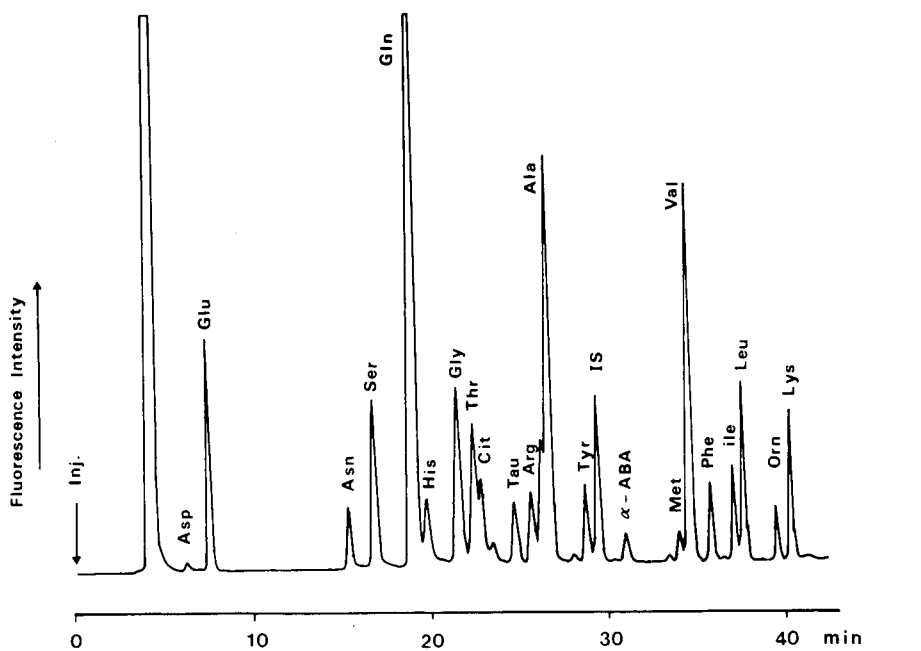

Fig. 2. Separation of OPA-amino acid derivatives in a plasma sample from an MS patient under experimental conditions identical to those in Fig. 1.

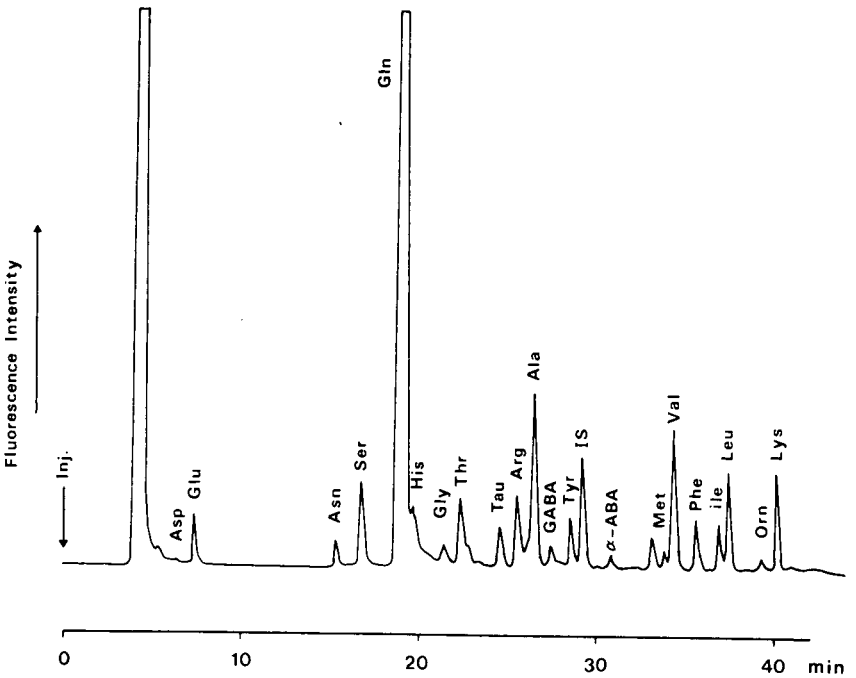

Fig. 3. Separation of OPA-amino acid derivatives in a CSF sample from an MS patient under experimental conditions identical to those in Fig. 1.

TABLE I

LEVELS OF FREE AMINO ACIDS IN PLASMA FROM 12 CONTROLS AND 12 PATIENTS WITH MULTIPLE SCLEROSIS

Amino acid	*Plasma levels, mean ± S.D. (n = 12) (μmol/l)*	
	Controls	*MS patients*
Asp	14.5 ± 4.3	11.9 ± 3.7*
Glu	29.2 ± 3.7	40.3 ± 4.3
Asn	53.3 ± 9.2	57.6 ± 12.7
Ser	102.3 ± 14.7	106.7 ± 16.7
Gln	490.2 ± 49.1	544.5 ± 48.0
His	81.3 ± 16.8	83.2 ± 13.7
Gly	210.2 ± 21.7	251.3 ± 32.1
Thr	112.3 ± 20.3	121.3 ± 23.7
Cit	32.9 ± 8.3	37.3 ± 6.8
Tau	66.1 ± 12.3	68.2 ± 10.2
Arg	110.4 ± 25.7	136.3 ± 32.1
Ala	230.7 ± 32.6	301.3 ± 47.2**
Tyr	55.3 ± 10.4	49.8 ± 4.6
Met	28.1 ± 5.8	23.3 ± 7.3*
Val	206.1 ± 27.6	179.8 ± 19.3*
Phe	67.6 ± 8.3	53.7 ± 11.8
Ile	69.1 ± 7.6	66.8 ± 10.7
Leu	137.2 ± 17.4	125.7 ± 25.2
Orn	63.1 ± 14.7	58.9 ± 5.6
Lys	196.3 ± 23.4	142.1 ± 17.6**

* $p < 0.05$.
** $p < 0.01$.

and Arg, and decreased levels of Leu, Ile, Val, Tyr and Phe, but these results were not confirmed by a third group[28]. However, elevated levels of Glu were shown in MS patients during relapses.

In our study, the levels of Glu, Asn, Gly, Arg and Ala were increased while the levels of Asp, Met, Val, Phe and Lys were decreased in MS patients. Among the amino acids Ala is known to function as a carrier for an amino base outside of brain tissue and this amino base may be overproduced in the course of an infection[29,30]. Under similar conditions, the increase as well as the decrease in certain amino acids may also be due to the selective disruption of the amino acid transport systems since the plasma or serum concentration of an amino acid is generally of the same order of magnitude as the binding constant for its transport into the brain.

Little information is available on CSF levels of amino acids in MS patients and few attempts[6,12,31,32] have been made to study the rôle of amino acids in this disorder. Table II shows the mean levels of amino acids for both groups. The levels of Ser, Gln, Tyr and Orn showed consistent increases, whereas Asp, Glu, GABA and Phe showed a tendency to decrease in MS patients. The levels of other amino acids remained more or less similar to those of the control group. Among the amino acids, the increase in Tyr in CSF in MS patients may be important as Tyr is involved in

TABLE II

LEVELS OF FREE AMINO ACIDS IN CSF FROM 12 CONTROLS AND 12 PATIENTS WITH MS

Amino acid	*CSF levels, mean ± S.D. (n = 12) (μmol/l)*	
	Controls	*MS Patients*
Asp	1.72 ± 0.24	1.11 ± 0.19*
Glu	26.13 ± 4.81	18.96 ± 3.85*
Asn	8.34 ± 1.76	10.14 ± 0.93
Ser	20.65 ± 3.37	23.84 ± 3.46
Gln	450.00 ± 38.18	561.17 ± 84.72**
His	19.31 ± 4.28	20.56 ± 6.34
Gly	11.76 ± 2.44	9.83 ± 1.78*
Thr	44.26 ± 11.63	48.80 ± 9.11
Cit	4.33 ± 1.63	4.18 ± 1.14
Tau	5.85 ± 1.91	4.52 ± 1.24
Arg	15.73 ± 5.21	20.78 ± 6.53*
Ala	26.26 ± 6.31	28.70 ± 4.71
GABA	0.12 ± 0.01	0.07 ± 0.01***
Tyr	14.17 ± 2.63	26.73 ± 4.76**
Met	6.08 ± 1.44	2.98 ± 0.54***
Val	23.63 ± 5.04	21.88 ± 4.45
Phe	15.86 ± 31.16	7.89 ± 2.94**
Ile	9.16 ± 2.34	8.04 ± 1.96
Leu	19.91 ± 3.46	20.94 ± 4.16
Orn	8.57 ± 1.99	9.63 ± 2.37
Lys	42.45 ± 4.30	42.81 ± 6.85

* $p < 0.05$.
** $p < 0.01$.
*** $p < 0.001$.

many metabolic pathways resulting in neurotransmitters such as catecholamines and their metabolites.

It is known that the amino acid concentrations of CSF are for the most part lower than in plasma or serum and moreover the ratio between CSF and plasma amino acids differs from one amino acid to another. Hence, it is postulated that either an active transport mechanism or a dynamic exchange exists within the blood–brain barrier[33]. Furthermore, it is also argued that various factors do participate in this transport and that the transport mechanisms differ according to various groups of amino acids. Hence, comparing the ratios of amino acids in CSF and plasma might provide a key to understanding either metabolic changes in blood and CNS or abnormalities in the transport mechanism to and from CSF.

Table III shows the ratios of amino acids in CSF and plasma in controls and MS patients. Apart from Val, Tyr, Orn and Lys, most of the ratios are lower or unchanged in MS patients. Comparing Tables I, II and III it is evident that it is not only the blood concentration of an amino acid which is of importance in influencing its concentration in CSF, but an additional local factor in the brain related to the MS condition may play a rôle. It may be the transport function of the blood–CSF barrier in MS patients which leads to the marked difference as compared to the control group.

TABLE III

RATIOS OF FREE AMINO ACIDS BETWEEN CSF AND PLASMA FROM 12 CONTROLS AND 12 PATIENTS WITH MS

Amino acid	*CSF/Plasma ratios, mean ± S.D. (n = 12)*	
	Controls	*MS Patients*
Asp	0.14 ± 0.02	0.10 ± 0.02*
Glu	0.89 ± 0.10	0.47 ± 0.05*
Asn	0.21 ± 0.02	0.18 ± 0.01
Ser	0.35 ± 0.02	0.31 ± 0.04
Gln	1.10 ± 0.11	1.00 ± 0.14
His	0.24 ± 0.04	0.26 ± 0.03
Gly	0.05 ± 0.01	0.04 ± 0.01
Thr	0.37 ± 0.09	0.36 ± 0.06
Cit	0.09 ± 0.01	0.09 ± 0.02
Tau	0.10 ± 0.01	0.07 ± 0.00*
Arg	0.18 ± 0.02	0.15 ± 0.01
Ala	0.12 ± 0.02	0.08 ± 0.01**
Tyr	0.23 ± 0.04	0.41 ± 0.08***
Met	0.17 ± 0.02	0.11 ± 0.01**
Val	0.10 ± 0.02	0.15 ± 0.01*
Phe	0.23 ± 0.04	0.16 ± 0.03
Ile	0.09 ± 0.01	0.10 ± 0.01
Leu	0.28 ± 0.04	0.21 ± 0.05
Orn	0.16 ± 0.03	0.18 ± 0.04
Lys	0.19 ± 0.03	0.24 ± 0.05*

* $p < 0.05$.
** $p < 0.01$.
*** $p < 0.001$.

The use of an automatic HPLC method giving rapid quantitation of amino acids has been effective in our study of the complex phenomena involved in the transport mechanisms of amino acids between blood and brain. In addition the method is programmed to make OPA react with amino acids automatically, thereby controlling the reaction kinetics and avoiding variations in results due to the instability encountered with the OPA derivatives. Special care was taken in the treatment of the biological samples including the use of milder conditions (4% SSA) resulting in complete deproteinization and giving highly reproducible results with R.S.D. $< 3\%$ for all amino acids.

REFERENCES

1 J. W. Wood, in A. Lajtha (Editor), *Handbook for Neurochemistry*, Vol. 3, Plenum, New York, 1982, pp. 415–487.
2 A. T. B. Moir, G. W. Asheroft and T. B. B. Crawford, *Brain*, 93 (1970) 357.
3 F. E. Bloom, *Neurosci. Res. Program Bull.*, 10 (1972) 127.
4 J. Piek, A. Boldt-Göth, D. Wieczorek and W. J. Bock, *Neurochirurgia*, 78 (1985) 33.
5 D. I. Heiblim, H. E. Evans, L. Glass and M. M. Agbayani, *Arch. Neurol.*, 35 (1978) 765.
6 K. Iijima, S. Takase, K. Tsumyraya, M. Enda and K. Itahara, *Tohoku J. Exp. Med.*, 126 (1978) 133.
7 A. W. Teelkenand and J. P. Lakye, in J. P. Lake (Editor), *Parkinson Disease*, Excerpta Medica, Amsterdam, 1977, pp. 85–112.
8 R. N. Corston, E. H. F. McGale, C. Stonier, E. C. Hutchinson and G. M. Aber, *J. Neurol., Neurosurg. Psychiatry*, 44 (1981) 86.
9 H. Briem, E. H. Hultman, M. E. Kalin and P. R. Lundberg, *J. Neurol., Neurosurg. Psychiatry*, 42 (1979) 881.
10 E. H. F. McGale, I. F. Pye, C. Stonier, E. Hutchinson and G. M. Aber, *J. Neurochem.*, 24 (1975) 587.
11 T. Kruse, H. Reiber and V. Neuhoff, *J. Neurol. Sci.*, 70 (1985) 129.
12 K. J. Scholt and D. Meier, *Acta Neurol. Scand.*, 75 (1978) 304.
13 T. N. Ferraro and T. A. Hare, *Brain Res.*, 338 (1985) 53.
14 P. J. Goodnick, H. E. Evans, D. L. Dunnar and R. R. Fiere, *Biol. Psychiat.*, 15 (1980) 557.
15 J. C. Dickinson and P. B. Hamilton, *J. Neurochem.*, 13 (1966) 1179.
16 T. L. Perry, S. Hansen and J. Kennedy, *J. Neurochem.*, 24 (1975) 587.
17 D. H. Spackman, W. H. Stein and S. Moore, *Anal. Chem.*, 30 (1958) 1190.
18 R. J. Benson and P. E. Hare, *Proc. Natl. Acad. Sci. U.S.A.*, 72 (1975) 619.
19 A. P. Williams, *J. Chromatogr.*, 373 (1986) 175.
20 J. D. Cooper and D. C. Turnell, *Clin. Chem.*, 28 (1982) 527.
21 G. A. Qureshi, L. Fohlin and J. Bergström, *J. Chromatogr.*, 297 (1984) 91.
22 H. Godel, T. Graser, P. Földi, P. Pfaender and P. Fürst, *J. Chromatogr.*, 297 (1984) 49.
23 R. J. Smith and K. A. Panico, *J. Liq. Chromatogr.*, 8 (1985) 1783.
24 H. R. Zielke, *J. Chromatogr.*, 347 (1985) 320.
25 G. A. Qureshi and P. Södersten, *J. Chromatogr.*, 400 (1987) 247.
26 F. Monaco, S. Fumero, A. Mondino and R. Mutani, *J. Neurol., Neurosurg. Psychiat.*, 42 (1979) 640.
27 F. C. Westall, A. Hawkin, G. M. Ellison and L. W. Myers, *J. Neurol. Sci.*, 47 (1980) 353.
28 A. Mori, *Amino Acids and Brain*, Chygai-Igakusha, Tokyo, 1976, p. 259.
29 W. H. Oldendorf and J. Szabo, *Am. J. Physiol.*, 230 (1976) 94.
30 W. M. Pardridge and W. H. Oldendorf, *Biochem. Biophys. Acta*, 401 (1975) 128.
31 J. J. Martin and W. Schole, *J. Neurol. Sci.*, 15 (1972) 49.
32 D. E. Lumsden and D. McAlpine, in D. E. Lumsden and E. D. Achesson (Editors), *Amino Acids in Multiple Sclerosis*, Livingstone, Edinburgh, 1972, pp. 433–441.
33 F. L. Hymoller, O.J. Mahler and M. M. Parker, *Int. J. Neuropsych.*, 2 (1966) 293.

Journal of Chromatography, 459 (1988) 245–249
Elsevier Science Publishers B.V., Amsterdam — Printed in The Netherlands

CHROMSYMP. 1456

DETERMINATION OF SALSOLINOL BY ION-EXCHANGE CHROMATOGRAPHY WITH GLYCYLGLYCINE AS THE POST-DERIVATIZING AGENT

TOKUICHIRO SEKI*
College of Bio-Medical Technology, Osaka University, 1-1, Machikaneyama-cho, Toyonaka-shi, Osaka 560 (Japan)
and
YUZO YANAGIHARA and KOHJI NOGUCHI
Asahi Chemical Ind. Co., Ltd., 1-3-2, Yakoo, Kawasaki-ku, Kawasaki-shi, Kanagawa 210 (Japan)

SUMMARY

The determination of salsolinol in human urine was carried out by ion-exchange chromatography on two coupled columns of a weakly acidic ion exchanger with a hydrophilic matrix (Asahipak ES-502C). Salsolinol was first isolated from urine by adsorption on Amberlite CG-50. It was eluted together with catecholamines by 2/3 *M* boric acid solution. The amines were then separated by isocratic elution from the first column of Asahipak with 0.05 *M* sodium succinate buffer (pH 5.5) containing 0.015 *M* borate and 0.5 m*M* ethylenediaminetetraacetate. Epinephrine, norepinephrine, dopamine and salsolinol were eluted in that order. The salsolinol-containing fraction was then transferred, by column switching, to a second Asahipak column and eluted with the same mobile phase. Salsolinol was determined fluorimetrically by reaction with glycylglycine in the presence of hexacyanoferrate(III) at pH 7.5–8 and 65°C. Samples could be analysed every 47 min. The detection limit for salsolinol was 2 pmol/ml.

INTRODUCTION

Salsolinol (1-methyl-6,7-dihydroxy-1,2,3,4-tetrahydroisoquinoline) has been found in urine[1], cerebrospinal fluid[2,3], rat and human brain tissue[4–6], and food and beverage samples[7]. The determination of salsolinol in these samples involved extraction by ion exchange[8] or alumina adsorption[1,7,9] and analysis by gas chromatography–mass spectrometry[7,9] or a radioenzymatic method[10]. Ion-pair reversed-phase liquid chromatography with electrochemical detection was also effective for the determination of salsolinol in human urine[8].

We have found that salsolinol reacts rapidly with glycylglycine at elevated temperatures and at pH 7.5–8 in the presence of potassium hexacyanoferrate(III) to give fluorescent compound(s), and that salsolinol could be separated from catecholamines on a column of hydrophilic cation-exchange resin (Asahipak ES-502C) by elution

0021-9673/88/$03.50

with a 0.05 *M* succinate buffer (pH 5.5) containing 0.015 *M* borate and 0.5 m*M* ethylenediaminetetraacetate.

These findings were applied to the determination of salsolinol in human urine by combining ion-exchange extraction, separation of the salsolinol fraction on two coupled columns of Asahipak ES-502C by column switching and fluorimetric determination of salsolinol in the eluate with glycylglycine as the post-derivatizing agent.

EXPERIMENTAL

Materials

Epinephrine bitartrate, norepinephrine bitartrate, dopamine hydrochloride and salsolinol were purchased from Sigma (St. Louis, MO, U.S.A.) and glycylglycine from Nakarai Chemicals (Kyoto, Japan). Other chemicals were of analytical-reagent grade from Yashima Pharmaceutical (Osaka, Japan). Stock solutions of amines (1 m*M*) were prepared in 0.01 *M* hydrochloric acid, and were diluted in 0.04 *M* succinate–0.4 *M* borate buffer (pH 5.3) containing 1 m*M* ethylenediaminetetraacetate to give standard solutions of various concentrations.

A constant-flow pump (Model Trirotar III and V; Jasco, Tokyo, Japan) was used to pump buffer through the chromatographic columns. A dual-head pump (Model SP-024-2; Jasco) was used to pump reagents and mix them with the elutate. A fluorimeter (Model FP-115; Jasco) equipped with a 30-μl flow cell was used to measure fluorescence. Samples were injected by an automatic injector (Model KSST-60J; Kyowa Seimitsu, Tokyo, Japan). A four-way automatic valve (Sanuki Kohgyoh, Tokyo, Japan) was used to connect two columns of Asahipak ES-502C in series.

Methods

Amberlite CG-50 was buffered and equilibrated with a 0.4 *M* phosphate buffer (pH 6.5) as described previously[11]. The buffered resin was poured into a tube (18 × 0.5 cm I.D. with a 20-ml reservoir) with 0.4 *M* phosphate buffer (pH 6.5) and allowed to settle under gravity to form a resin bed 12 cm high. The column was washed with 2 ml of water before use.

A 10.0-ml portion of filtered urine was mixed with 1.0 ml of a 2% solution of semicarbazide hydrochloride containing 0.5% each of sodium metabisulphite and disodium ethylenediaminetetraacetate dihydrate, and the mixture was adjusted to pH 6.3–6.4 with 0.5 *M* sodium hydrogencarbonate solution. The mixture was then applied to the Amberlite CG-50 column, which was first washed with 6 ml of deionized water and then with 2 ml of 2/3 *M* boric acid solution. A further 3 ml of boric acid solution were used to elute salsolinol from the column into a test-tube containing 1.95 ml of 0.1 *M* succinic acid solution and 0.05 ml of 0.1 *M* ethylenediaminetetraacetate solution containing 5% β-thiodiglycol. The salsolinol fraction was stored in a refrigerator.

A 0.3-ml of aliquot of this fraction was injected into the first column of Asahipak ES-502C (10 × 0.76 cm I.D.), kept at 35°C. The mobile phase (0.05 *M* succinate–0.015 *M* borate–0.5 m*M* ethylenediaminetetraacetate, pH 5.5) was pumped at a rate of 1.5 ml/min and the salsolinol fraction from the first column was switched to the second column of Asahipak ES-502C (10 × 0.76 cm I.D.), connected to the first column and kept at 60°C, and eluted with the same mobile phase at a flow-rate of 1.5

ml/min. The time to rotate the automatic valve in order to transfer the salsolinol fraction from the first to the second column was found by monitoring fluorimetrically the elution of salsolinol from the first column. When the timing of the rotation of the automatic valve is correct, the salsolinol peak in the elution pattern disappears.

The eluate from the second column was mixed with an equal mixture of reagents A and B; reagent A was a solution of 0.1 *M* glycylglycine (pH 6.5) containing 0.2 *M* boric acid and 0.05 *M* tartaric acid and reagent B was 0.25 *M* potassium borate buffer of pH 9.4 containing hexacyanoferrate(III) (0.01%, w/v). Each reagent was pumped at a flow-rate of 0.47 ml/min with a dual-head pump and mixed by using a T-shaped connector. The mixture of reagents was filtered through a guard column (15 × 0.6 cm I.D.) packed with 5-μm Shodex DS-613 polystyrene gel (Showa Denko, Tokyo, Japan) to remove fine particles that would cause background noise when passing through the flow cell. The filtered reagent mixture was mixed with the eluate, using a T-shaped connector and heated in a PTFE tube (50 m × 0.5 mm I.D.), immersed in a water-bath kept at 65°C. The fluorescence was measured with a fluorimeter using a UV-D36C as excitation light filter (transmittance maximum 365 nm) and a Y-44 as emission light filter (transparent to visible light of wavelength longer than 420 nm). Both filters were of coloured glass manufactured by Toshiba (Tokyo, Japan). A diagram of the equipment is shown in Fig. 1.

RESULTS AND DISCUSSION

Salsolinol was measured fluorimetrically by reaction with glycylglycine in the presence of hexacyanoferrate(III). This reaction is apparently analogous to that of glycylglycine with oxidized catecholamines. *e.g.*, adrenochrome[12]. The optimal pH for this reaction is 7.5–8 when performed at 65°C in a PTFE tube (50 m × 0.5 mm I.D.). The excitation and emission maxima were 360 and 490 nm, respectively.

The salsolinol fraction obtained by an ion-exchange method using Amberlite CG-50 (buffered at pH 6.5) as the adsorbent contains catecholamines. Therefore, a chromatographic system was developed which uses Asahipak ES-502C, a cross-linked vinyl–alcohol copolymer with carboxymethyl groups, as the stationary phase and

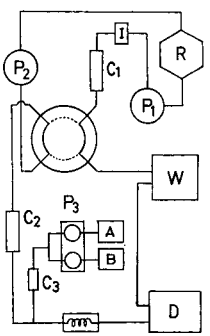

Fig. 1. Diagram of the column switching equipment. R, mobile phase reservoir; I, automatic injector; P_1, Trirotar III; P_2, Trirotar V; P_3, dual-head pump (Model SP-024-2, Jasco); C_1 and C_2, Asahipak ES-502C columns; C_3, guard column; D, fluorimeter (Model FP-115, Jasco); W, waste; A, reagent A reservoir; B, reagent B reservoir.

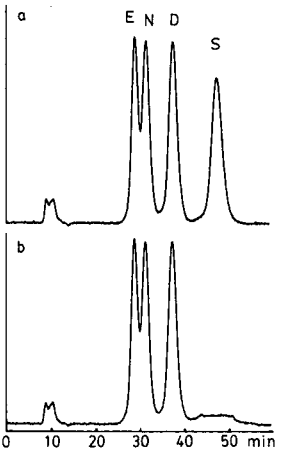

Fig. 2. Elution of standard samples from the first column. Amines in the elutate were monitored fluorimetrically. (a) Separation of epinephrine (E, 20 pmol/ml), norepinephrine (N, 20 pmol/ml), dopamine (D, 100 pmol/ml) and salsolinol (S, 50 pmol/ml); (b) after transfer of the salsolinol peak to the second column.

0.05 *M* succinate buffer (pH 5.5)–0.015 *M* borate–0.5 m*M* ethylenediaminetetraacetate as the mobile phase (Fig. 2a). Elution was performed at 35°C, and in order to separate impurities that would be eluted with salsolinol under these conditions the salsolinol peak from the first column was transferred to the second column of Asahipak ES-502C by using a four-way valve. The first column was connected to the second 36 min after sample injection, and 7.5 min later the columns were disconnected. The salsolinol peak disappeared from the elution pattern of the first column as shown in Fig. 2b. The salsolinol peak, transferred to the second column, was eluted with the same buffer as that used for the first column. The temperature of the second

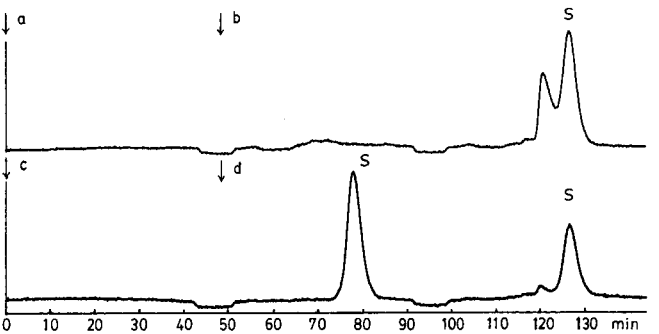

Fig. 3. Elution of a standard and urine samples transferred from the first to the second column. Arrows indicate the time of injection of a sample into the first column. The upper and lower curves represent different set of experiments. Standard salsolinol (50 pmol/ml, the first peak on the lower curve) was eluted from the second column 78 min after injection (at arrow c) into the first column. A urine sample was injected at d and 78 min after injection the salsolinol peak was eluted after a small impurity peak. A urine sample injected at a yielded no peak 78 min after injection, and the urine sample injected at b yielded a peak 78 min after injection (peak S on the upper curve).

column was 60°C, and the difference in temperature between the first and the second columns made it possible to separate salsolinol from impurities. The impurities were eluted faster than salsolinol, as shown in Fig. 3. Use of the same mobile phase for both stages of the HPLC separation (using two columns of Asahipak ES-502C) yielded a relatively stable baseline and a limit of detection of 2 pmol/ml for salsolinol.

A linear relationship between the peak height and the concentration of salsolinol added to the column was obtained between 5 and 200 pmol/ml. Samples could be analysed every 47 min. When salsolinol was added to a urine sample at a concentration of 10 pmol/ml, the mean recovery was 95 ± 3.2% (C.V., $n = 6$). When the concentration of free salsolinol was measured in normal human urine samples, the range of concentration was 0–30 pmol/ml. These values agree with the value of free salsolinol in the urine pool (11.2 ± 0.95 pmol/ml, $n = 10$) reported by Sjöquist and Ljungquist[9].

The results indicate that this method is suitable for the determination of salsolinol in human urine and other biological samples.

REFERENCES

1 M. A. Collins, W. P. Nijm, G. Teas, G. Borge and C. Goldfarb, *Science*, 206 (1979) 1184.
2 B. Sjöquist, S. Borg and H. Kvande, *Substance Alcohol Actions/Misuse*, 2 (1981) 63.
3 B. Sjöquist, S. Borg and H. Kvande, *Substance Alcohol Actions/Misuse*, 2 (1981) 73.
4 B. Sjöquist, S. Liljequist en J. Engel, *J. Neurochem.*, 39 (1982) 259.
5 W. D. Myers, L. Mackenzie, K. T. Ng, G. Singer, G. A. Smythe and M. W. Duncan, *Life Sci.*, 36 (1985) 309.
6 B. Sjöquist, E. Perdahl and B. Wimblad, *Drug Alcohol Depend.*, 12 (1983) 15.
7 M. W. Duncan, G. A. Smythe, M. V. Nicholson and P. S. Clezy, *J. Chromatogr.*, 336 (1984) 199.
8 J. Odink, H. Sandman and W. H. P. Schreurs, *J. Chromatogr.*, 377 (1986) 145.
9 B. Sjöquist and C. Ljungquist, *J. Chromatogr.*, 343 (1985) 1.
10 C. A. Nesterick and R. G. Rahwan, *J. Chromatogr.*, 164 (1979) 205.
11 T. Seki, Y. Yamaguchi, K. Noguchi and Y. Yanagihara, *J. Chromatogr.*, 332 (1985) 9.
12 T. Seki and Y. Yamaguchi, *J. Chromatogr.*, 287 (1984) 407.

Journal of Chromatography, 459 (1988) 251–260
Elsevier Science Publishers B.V., Amsterdam — Printed in The Netherlands

CHROMSYMP. 1422

SIMULTANEOUS QUANTITATION OF CATECHOLAMINES AND O-METHYLATED METABOLITES IN URINE BY ISOCRATIC ION-PAIRING HIGH-PERFORMANCE LIQUID CHROMATOGRAPHY WITH AMPEROMETRIC DETECTION

YING-PUI M. CHAN* and TAK-SING S. SIU

Clinical Biochemistry Unit, Queen Mary Hospital Compound, University of Hong Kong, Pokfulam (Hong Kong)

SUMMARY

A simple high-performance liquid chromatographic procedure was developed for the simultaneous determination of catecholamines and metanephrines in urine. One-step sample preparation was achieved with Bio-Rex 70 ion-exchange resin. The extract was assayed on a C_{18} reversed-phase column. Dihydroxybenzylamine was used as an internal standard. The eluent was monitored by an electrochemical detector with an oxidation potential of +0.85 V. The use of 1-heptanesulphonic acid in the mobile phase permitted the separation of norepinephrine, epinephrine, dopamine, normetanephrine and metanephrine in a single chromatogram. The corresponding detection limits were 5, 9, 14, 10 and 30 nmol/l, respectively. For the between-day precision, the coefficients of variation at physiological and pathological concentrations were less than 11%. Compounds with similar chemical structures and drugs commonly prescribed for the treatment of hypertension were assayed and found not to cause interferences in the chromatogram. The assay is reliable and is suitable for the analysis of clinical specimens. Reference values were established for normotensive Chinese patients with no neurological or endocrine disorders and also for patients suffering from essential hypertension.

INTRODUCTION

The measurement of the 24-h urinary excretion of cateholamines and their metabolites, metanephrines and vanillylmandelic acid (VMA) is recommended for the diagnosis of pheochromocytoma[1,2]. There is no general agreement as to which analyte is the most important for diagnosis. Several investigators favour VMA[3,4], while others recommend metanephrines[5,6] or norepinephrine[7,8]. A report in which the literature up to 1984 is reviewed indicated that no single urinary test is foolproof for the diagnosis of pheochromocytoma[9]. For every test, false positives have been reported for patients with essential hypertension, and false negatives have been reported for patients with confirmed pheochromocytoma. Some workers[10] recommend that all catecholamines and their metabolites be measured.

The quantitation of catecholamines and metanephrines by high-performance

0021-9673/88/$03.50

liquid chromatography (HPLC) coupled with electrochemical detection (ED) have largely replaced the older spectrophotometric, fluorimetric, radiometric and gas chromatographic procedures. However, most published methods permit the simultaneous measurement of only either norepinephrine (NE), epinephrine (EP) and dopamine (DA)[11,12]; normetanephrine (NM) and metanephrine (MN)[13,14]; or VMA and homovanillic acid (HVA)[15,16]. It would obviously be advantageous if several of these compounds could be assayed with a single sample preparation and chromatographic procedure. In this paper we describe a simple, reliable and rapid procedure for the simultaneous extraction and quantitation of urinary NE, EP, DA, NM and MN.

EXPERIMENTAL

Apparatus

The HPLC system consisted of an M6000A pump and data module (Waters Assoc., Milford, MA, U.S.A.), an LC-4B amperometric detector with a glassy carbon electrode and silver–silver chloride reference electrode (Bioanalytical Systems, West Lafayette, IN, U.S.A.) and an MS830 column heater and MS1660 autosampler (Kontron Instruments, Zurich, Switzerland). Separations were carried out on a 250 × 4 mm I.D. stainless-steel Hibar column, packed with 10-μm LiChrosorb C_{18} (Merck, Darmstadt, F.R.G.).

Chemicals

NE, EP, DA, NM, MN and 3,4-dihydroxybenzylamine hydrochloride (DHBA) were obtained from Sigma (St. Louis, MO, U.S.A.). 1-heptanesulphonic acid from Kodak (Rochester, NY, U.S.A.), acetonitrile from Fisher Scientific (Pittsburgh, PA, U.S.A.) and Bio-Rex 70 cation-exchange resin (100–200 mesh) from Bio-Rad Labs. (Richmond, CA, U.S.A.). Other chemicals were of analytical-reagent grade or better and were supplied by Merck.

Urine specimens

Twenty-four-hour urine specimens were collected from hospitalized Chinese patients. One group consisted of 40 patients who were normotensive and had no neurological or hormonal disorders. The other group consisted of 17 patients suffering from essential hypertension. Samples were collected in dark glass bottles containing 750 ml of 2 *M* sulphuric acid as a preservative. Sample were refrigerated during collection and thereafter at 4°C. Analysis was performed within 7 days after collection.

Sample preparation

Bio-Rex 70 cation-exchange resin was conditioned and converted to the NH_4^+ form by washing successively with 3 *M* hydrochloric acid, 3 *M* sodium hydroxide solution, 3 *M* acetic acid, 1 *M* ammonium acetate and 0.1 *M* ammonium acetate buffer (pH 6.5). It was buffered to pH 6.5 with 0.1 *M* ammonium acetate and stored at 4°C. The resin was then allowed to reach room temperature, and the slurry was packed into polystyrene tubes of 0.7 I.D. cm to form a resin bed 3 cm high. The columns were washed with 10 ml of deionized water and drained immediately prior to the application of urine.

A 5-ml aliquot of urine was transferred to a scintillation vial and mixed with 50 μl of internal standard (10 mg of DHBA in 10 ml of 0.1 *M* hydrochloric acid), 100 μl of Na_2EDTA solution (0.1 g/ml) and 100 μl of freshly prepared sodium metabisulphite solution (0.1 g/ml). The pH of the mixture was adjusted to 6.5 ± 0.1 by adding 5, 1 and 0.1 *M* sodium hydroxide solution successively. The mixture was transferred to a Bio-Rex 70 column and allowed to drain. The column was then washed with 10 ml of deionized water and eluted with 7 ml of 4 *M* formic acid. The eluate was collected and a 100-μl aliquot was injected directly into the column.

Chromatographic conditions

A buffer solution, composed of 300 m*M* sodium dihydrogenphosphate, 4 m*M* 1-heptanesulphonic acid and 0.2 g/l Na_2EDTA was titrated to pH 2.5 with orthophosphoric acid, then filtered throuh a 0.22-μm Type HA filter (Millipore, Bedford, MA, U.S.A.). The mobile phase was prepared by mixing 98 parts by volume of the above buffer with 2 parts of acetonitrile. The mobile phase was degassed by sparging with helium for *ca.* 1 min before use. A flow-rate of 2.2 ml/min was used. The column temperature was maintained at 40°C during the analysis. A potential of +0.85 V was applied across the electrode of the electrochemical detector.

Calculations

A set of calibration standard solutions, each containing 5, 20, 80, 200 or 400 μmol/l of NE, EP, DA, NM and MN, was prepared in 0.1 *M* hydrochloric acid and stored at −70°C. Working solutions were prepared by diluting 50 μl of each calibration standard solution with 50 μl of internal standard solution and 6.9 ml of 4 *M* formic acid. The working concentrations corresponded to those found in the eluate obtained from 5 ml of urine, with analyte concentrations in the range 50–4000 nmol/l. Calibration graphs and regression equations were constructed, based on peak-height ratios between catecholamines and the internal standard. The concentrations of catecholamines in urine specimens were calculated from the regression equation after adjusting for the relative recovery between each catecholamine and the internal standard.

Method validation

The absolute recovery was evaluated by adding known amounts of standards and DHBA to pooled urine at concentrations of 50, 200, 800 and 3200 nmol/l. Ten samples from each spiked preparation was extracted by the described procedure, except that the DHBA–4 *M* formic acid solution was replaced with 4 *M* formic acid. The peak heights were compared with those obtained by injecting standards of known concentrations.

The analytical recovery was assessed by adding known amounts of standards at four different concentrations to urine samples from twelve individuals. The results obtained were compared with those obtained with the original samples.

The within-run precision was determined by extracting and assaying replicate samples from three pools of urines with different concentrations of the compounds. The between-day precision was determined at three different concentrations by assaying aliquots of two pools of urine, which were stored at −70°C.

RESULTS AND DISCUSSION

Fig. 1 shows voltammograms obtained with the chromatographic parameters described. A potential of +0.85 V was chosen for maximum signal sensitivity and stability. Injections of standards, prepared in 4 *M* formic acid, indicated that the signals produced by the detector were linear at urine concentrations from 35 to 7000 nmol/l for each analyte (Fig. 2).

The one-step extraction procedure was reliable and reproducible. No significant difference in absolute recovery was observed at the different concentrations examined. The mean absolute recoveries ± the standard error of the mean for NE, EP, DA, NM, MN and DHBA were 79.7 ± 0.88%, 75.0 ± 1.26%, 89.7 ± 1.73%, 74.5 ± 1.42%, 62.1 ± 1.35% and 89.4 ± 0.77%, respectively. Analysis of duplicates urine samples with all five analytes at different concentrations demonstrated that the extraction procedure was linear for concentrations between 100 and 8000 nmol/l.

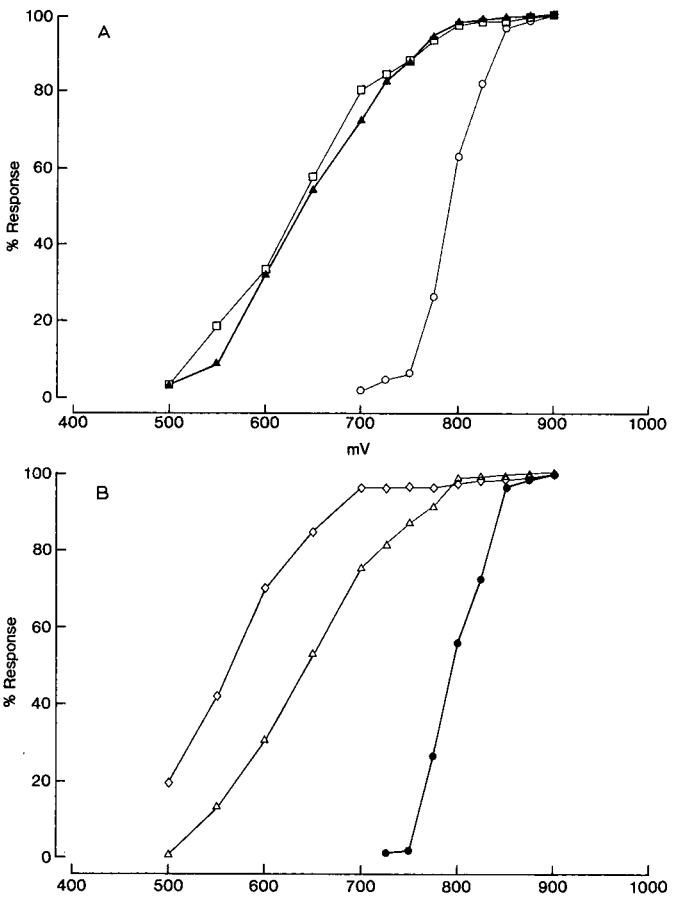

Fig. 1. Voltammograms of (A) NE (□), DHBA (▲) and NM (○); (B) DA (◇), EP (△) and MN (●). Units are expressed as a percentage of the maximum response, obtained at an applied potential of +0.9 V.

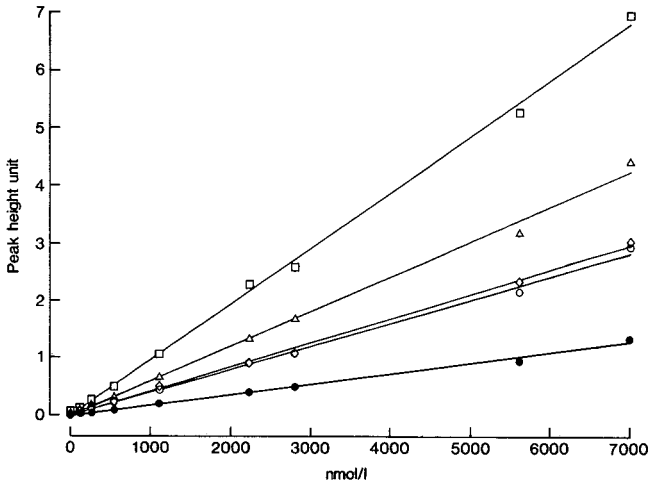

Fig. 2. Linearity of peak-height response relative to urinary concentrations from 35 to 7000 nmol/l. Chromatographic conditions as described in the text. (□) NE; (△) EP; (◇) DA; (○) NM; (●) MN.

The analytical recoveries of the compounds at different concentrations are presented in Table I. The mean analytical recoveries for NE, EP, DA, NM and MN were 99.7, 97.0, 89.5, 99.6 and 102.7%, respectively.

TABLE I

ANALYTICAL RECOVERY

Known amounts of standards were added at four different concentrations to twelve urine samples from different individuals. The results were compared with those obtained with the original specimens.

Compound	*Added concentration (nmol/l)*	*Recovery (%)*	*S.D. (%)*	*n*
NE	50	110.6	5.4	6
	200	96.3	6.4	12
	800	98.5	6.6	12
	2000	97.9	1.1	6
EP	50	90.8	8.9	6
	200	97.5	7.6	12
	800	98.8	3.3	12
	2000	98.7	1.8	6
DA	100	92.2	9.3	6
	400	92.3	9.9	12
	1600	88.5	6.8	12
	4000	86.0	2.4	6
NM	50	118.3	11.8	6
	200	95.2	9.5	12
	800	101.1	10.8	12
	2000	105.6	3.5	6
MN	100	110.5	6.9	6
	400	96.7	12.2	12
	1600	100.2	11.1	12
	4000	93.5	4.4	6

TABLE II

WITHIN-RUN PRECISION

Replicate samples from three pools of urine with different concentrations of compounds were assayed as a batch.

Compound	*n*	*Mean concentration (nmol/l)*	*Coefficient of variation (%)*
NE	10	120	6.6
	6	316	2.7
	6	932	3.7
EP	10	34.4	10.5
	6	224	3.9
	6	825	1.7
DA	10	755	3.9
	6	1121	3.7
	6	4193	2.3
NM	10	147	9.6
	6	329	5.3
	6	1011	3.6
MN	10	75.3	9.2
	6	447	6.6
	6	1665	3.7

Data on within-run and between-day precision are presented in Tables II and III, respectively. The coefficients of variation were all below 11%. A signal-to-noise ratio of 3 was adopted as the detection limit of the assay. The detection limits for NE, EP, DA, NM and MN in urine were 5, 9, 14, 10 and 30 nmol/l, respectively.

TABLE III

BETWEEN-DAY PRECISION

Aliquots of two pools of urine were stored at −70°C. Twenty-two sets were assayed over a period of 60 days.

Compound	*n*	*Mean concentration (nmol/l)*	*Coefficient of variation (%)*
NE	22	297	5.8
	22	799	6.3
EP	22	116	6.4
	22	423	5.4
DA	22	506	5.9
	22	2359	5.8
NM	22	268	10.1
	22	620	8.3
MN	22	151	8.9
	22	667	10.5

Twelve compounds with structures similar to those of catecholamines and drugs commonly prescribed for the treatment of hypertension were assayed by this procedure. Chlopromazine, L-DOPA, epinine, 5-hydroxytryptamine, labetalol, methyldopa, 3-metoxytyramine, 3-methoxytyrosine, metropolol, phenoxybenzamine, propanolol and tyramine were found to produce no interference with the specified method.

The method described is very robust. It has been employed in our laboratory for the routine analysis of patients urine for more than 8 months. Our workload consisted of 15–25 specimens per week. Urine samples for quality control were also assayed with each batch of analyses. During this period, no significant deterioration of the detector response was observed and repolishing or replacement of the glassy carbon electrode was not necessary. The C_{18} column continued to produce good separations after 8 months of service.

Reference values established with specimens obtained from 40 non-hypertensive Chinese adults having no neurological or hormonal disorders and from 17 patients with essential hypertension are presented in Table IV.

Fig. 3 shows typical chromatograms obtained with a 24-h urine sample from a healthy individual, extracted with and without added DHBA. No significant endogenous peak was found at the retention time of the internal standard (DHBA).

A chromatogram obtained from a patient with pheochromocytoma, confirmed by surgery, is presented in Fig. 4. The determination of NE, EP, DA, NM and MN was completed in 10 min. However, a total chromatography time of 25 min is recommended, because 5-hydroxytryptamine and 3-metoxytyramine were also extracted by this technique and appeared as late peaks with retention times of 20 and 23 min, respectively.

Pheochromocytoma is a rare neural-crest tumour, which in about 10% of cases is malignant. Early diagnosis and subsequent surgical removal usually lead to prompt recovery[2]. It is generally held that a predominant increase in EP indicates an adrenal tumour[17]. Although urinary-free dopamine mainly reflects renal conversion of plasma DOPA by renal tubular aromatic amino acid decarboxylase, an increase in urinary

TABLE IV

REFERENCE VALUES FOR URINARY CATECHOLAMINES AND METANEPHRINES

Analyses were performed on 24-h urine specimens collected from 40 Chinese patients who were normotensive and had no neurological or endocrine disorders and from 17 Chinese patients suffering from essential hypertension. The upper limits were calculated from the mean + 2 S.D.

Compound	*Normal (n=40)*		*Essential hypertension (n=17)*	
	Range (nmol per 24 h)	*Upper limit (nmol per 24 h)*	*Range (nmol per 24 h)*	*Upper limit (nmol per 24 h)*
NE	63–416	440	85–557	535
EP	19–113	110	13–137	145
NM	18–212	240	64–370	350
MN	38–315	275	38–420	370
DA	221–2410	2570	220–3603	3810

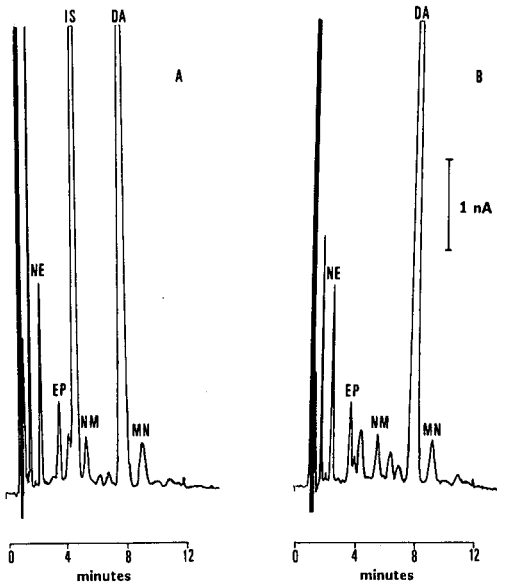

Fig. 3. (A) Representative chromatogram of a urine specimen obtained from a healthy individual, extracted after the addition of internal standard. (B) Chromatogram from the same specimen, extracted without added internal standard. Chromatographic conditions as described in the text.

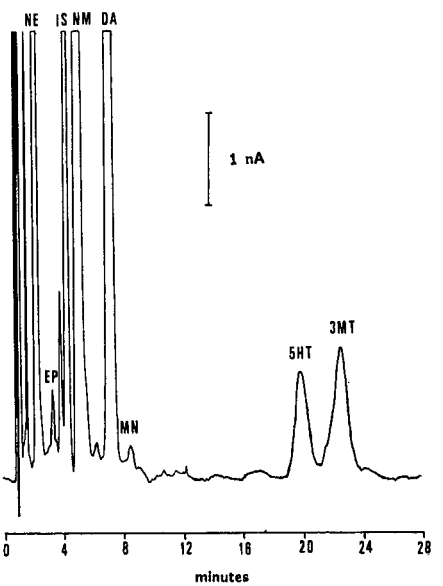

Fig. 4. Chromatogram of a urine specimen from a patient with surgically confirmed pheochromocytoma. The concentrations of NE, EP, DA, NM and MN were 7138, 87, 3713, 14245 and 59 nmol/l, respectively (urine volume, 1200 ml). 5HT = 5-hydroxytryptamine; 3MT = 3-metoxytyramine.

dopamine has been reported to be associated with malignancies[1,18]. As no single urine test has been proved to be completely reliable, screening for all urinary catecholamines and metabolites, namely EP, NE, DA, MN, NM, VMA and HVA, is recommended[10]. The development of a procedure that permits the simultaneous quantitation of most of these compounds is not simple. Differences in the chemical and partition characteristics of these compounds make it difficult to devise a single extraction and analytical procedure for their simultaneous quantitation. Different sorbents for the extraction of urinary catecholamines and metanephrines have been used, including alumina[19,20], cation-exchange resins[21,22] and boric acid gel[23,24], singly or in combination[22,25]. Other workers have used on-line sampling pre-treatment with adsorbents packed in small columns[26,27]. Odink *et al.*[28] used Bio-Rex 70 as adsorbent and boric acid as eluent, but failed to recover NM and MN. In our procedure, elution from Bio-Rex 70 with 4 *M* formic acid gave good recoveries of all of the catecholamines and metanephrines.

Parker *et al.*[29] developed an HPLC metod that is applicable to the analysis of NE, EP, MN, NM, VMA and 5-HIAA. However, three different methods of sample preparation were required, depending on the catecholamines or metabolites being quantitated. Joseph[30] employed butane boronic acid as a group-specific pairing agent by HPLC on a C_{18} column with ED and fluoresence detection and was able to quantitate eleven catecholamines, indoleamines and related precursors and metabolites in brain tissue, including NE, EP, VMA and HVA. Wester *et al.*[31] described the simultaneous determination of seventeen of the major monoamine neurotransmitters, precursors and metabolites, including NE, EP, DA, NM, MN, VMA and HVA. Their HPLC–ED procedure was applicable to extracts from brain tissue and cerebrospinal fluid[32]. However, the sample preparation procedure for urine was not described by either Joseph[30] or Wester *et al.*[31]. It is uncertain whether their procedures are applicable to urine which usually contains a large amount of endogenous metabolites and electroactive phenolic compounds. Only one method has been published on the simultaneous determination of urinary catecholamines and their O-methylated metabolites. Abeling *et al.*[33] employed Amberlite CG-50 and HPLC with fluoresence detection, which required a 10-fold concentration of the eluate by lyophilization prior to HPLC.

With the advantages of being simple, rapid, robust and capable of the simultaneous quantitation of NE, EP, DA, NM and MN, our method is ideal for application in clinical laboratories. The reference values in normotensive Chinese and hypertensive patients obtained in this study agree well with those reported previously[33].

ACKNOWLEDGEMENTS

This study was supported in part by grants from the University of Hong Kong (18-10005), the Wing Lung Bank Medical Research Fund (311-030-8009-69) and the World Health Organization (360-181-0604).

REFERENCES

1 D. F. Davidson, *Ann. Clin. Biochem.*, 24 (1987) 494.
2 N. A. Samaan and R. C. Hickey, *Semin. Oncol.*, 14 (1987) 297.
3 S. J. Soldin and J. G. Hill, *Clin. Chem.*, 26 (1980) 291.
4 D. Ratge, G. Baumgardt, E. Knoll and H. Wisser, *Clin. Chim. Acta*, 132 (1983) 229.
5 P. F. Plouin, J. M. Duclos, J. Menard, C. Bohuon and J. M. Alexandra, *Br. Med. J.*, 282 (1981) 853.
6 E. L. Bravo and R. W. Gifford, *N. Engl. J. Med.*, 311 (1984) 1298.
7 G. Stenstrom, B. Sjogren and J. Waldenstrom, *Acta Med. Scand.*, 214 (1983) 145.
8 M. J. Brown and D. J. Allison, *Br. J. Clin. Pharm.*, 12 (1981) 251.
9 P. Manu and L. A. Runge, *Am. J. Epidemiol.*, 120 (1984) 788.
10 B. Shapiro, J. C. Sisson, R. Lloyd, M. Nakajo, W. Satterlee and W. H. Beierwaltes, *Clin. Endocrinol.*, 20 (1984) 189.
11 K. Mori and K. Imai, *Anal. Biochem.*, 146 (1985) 283.
12 H. Tsuchiya, M. Tatsumi, N. Takagi, T. Koike, H. Yamaguchi and T. Hayashi, *Anal. Biochem.*, 155 (1986) 28.
13 L. M. Bertani-Dziedzic, A. M. Krstulovic, S. W. Dziedzic, S. E. Gitlow and S. Cerqueira, *Clin. Chim. Acta*, 110 (1981) 1.
14 J. G. Flood ad R. B. McComb, *Clin. Chem.*, 27 (1981) 1268.
15 Y. M. Chan and T. S. Siu, *Clin. Chem.*, 32 (1986) 1155.
16 A. Premel-Cabic, A. Turcant and P. Allain, *Clin. Chem.*, 32 (1986) 1585.
17 K. Engelman and W. G. Hammond, *Lancet*, i (1968) 609.
18 J. M. Polak and S. R. Bloom, *Endocrine Tumours*, Churchill Livingstone, New York, 1985, p. 271.
19 J. F. O'Hanlon, Jr., H. C. Campuzano and S. M. Horvath, *Anal. Biochem.*, 34 (1970) 560.
20 I. N. Mefford, M. Ota, M. Stipetic and W. Singleton, *J. Chromatogr.*, 420 (1987) 241.
21 R. E. Shoup and P. T. Kissinger, *Clin. Chem.*, 23 (1977) 1268.
22 G. M. Anderon, J. G. Young, P. I. Jatlow and D. J. Cohen, *Clin. Chem.*, 27 (1981) 2060.
23 T. P. Moyer, N. S. Jiang, G. M. Tyce and S. G. Sheps, *Clin. Chem.*, 25 (1979) 256.
24 K. Oka, M. Sekiya, H. Osada, K. Fujita, T. Kato and T. Nagatsu, *Clin. Chem.*, 28 (1982) 646.
25 A. H. B. Wu and T. G. Gornet, *Clin. Chem.*, 31 (1985) 298.
26 J. D. De Jong, A. J. F. Point and U. R. Tjaden, *J. Chromatogr.*, 414 (1987) 285.
27 M. Goto, G. Zou and D. Ishii, *J. Chromatogr.*, 275 (1983) 271.
28 J. Odink, H. Sandman and W. H. P. Schreurs, *J. Chromatogr.*, 377 (1986) 145.
29 N. C. Parker, C. B. Levtzow, P. W. Wright, L. L. Woodard and J. F. Chapman, *Clin. Chem.*, 32 (1986) 1473.
30 M. H. Joseph, *Curr. Sep.*, 7 (1985) 2.
31 P. Wester, J. Gottfries, K. Johansson, F. Klintebäck and B. Winblad, *J. Chromatogr.*, 415 (1987) 261.
32 P. Wester, J. Gottfries and B. Winblad, *J. Chromatogr.*, 415 (1987) 275.
33 N. G. Abelin, A. H. van Gennip, H. Overmars and P. A. Voute, *Clin. Chim. Acta*, 137 (1984) 211.

Journal of Chromatography, 459 (1988) 261–267
Elsevier Science Publishers B.V., Amsterdam — Printed in The Netherlands

CHROMSYMP. 1491

HIGH-PERFORMANCE LIQUID CHROMATOGRAPHIC ANALYSIS OF JOSAMYCIN IN SERUM AND URINE

M. SKINNER and I. KANFER*
School of Pharmaceutical Sciences, Rhodes University, Grahamstown 6140 (South Africa)

SUMMARY

A high-performance liquid chromatographic assay for the analysis of josamycin in human serum and urine is presented. The assay involves a simple solid-phase extraction procedure coupled with a phase separation step, separation on a reversed-phase C_{18} column with UV detection by a multi-wavelength programmable detector. The mobile phase was acetonitrile–0.015 *M* phosphate buffer, pH 6.0 (5:2) at a flow-rate of 1.2 ml/min. The column temperature was maintained at 35°C. Linear calibration curves over the concentration ranges 0.1–2.0 mg/l (serum) and 0.5–5 mg/l (urine) were obtained with correlation coefficients of 0.9983 and 1.0000, respectively. The relative standard deviations of five replicate samples at the upper and lower limits of each calibration curve were below 7%. The recoveries at the upper and lower ends of the calibration range for serum were 77% and 70%, respectively, and those for urine were 76% and 80%, respectively.

INTRODUCTION

Josamycin (Fig. 1), a relatively new macrolide antibiotic, is used mainly in the treatment of gram-positive infections[1–5]. Josamycin is reported to be more stable than erythromycin over the normal gastric pH range[6], and is well tolerated with a low incidence of side effects[7,8]. These properties, together with the decreased ability of certain bacteria to become resistant to josamycin compared with other macrolide antibiotics[9,10], confers certain advantages on this drug in the treatment of susceptible infections. Most of the pharmacokinetic data published to-date have been derived

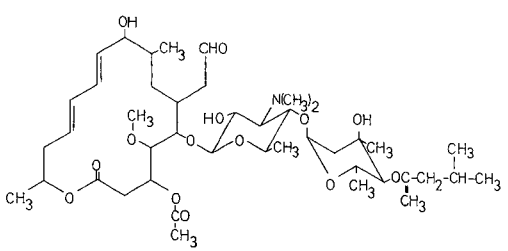

Fig. 1. Molecular structure of josamycin.

0021-9673/88/$03.50

from microbiological assay techniques[11–14], which are tedious to perform. Fourtillan *et al.*[15] adapted the high-performance liquid chromatographic (HPLC) assay of erythromycin developed by Tsuji[16] to assay josamycin in plasma. However, this method involves on-stream post-column derivatisation, extraction and fluorescence detection, requiring complex and expensive equipment. Ducci and Scalori[17] described an HPLC assay of josamycin with a detection limit of 0.3 mg/l, which is insufficiently sensitive for pharmacokinetic studies. Räder *et al.*[18] recently described a sensitive HPLC assay but a dual-pump system and expensive column-switching apparatus are required. The method described here is sufficiently sensitive for pharmacokinetic studies and requires only standard HPLC apparatus.

EXPERIMENTAL

Materials

The modular HPLC system consisted of a constant-flow pump (M45; Waters Assoc., Milford, MA, U.S.A.), an automated sample injector (Waters WISP 710B), a multi-wavelength programmable UV detector (Waters M490), and a dual-pen flatbed recorder (Model 561, Hitachi, Tokyo, Japan). The analysis was performed on a 25 cm × 3.9 mm I.D. stainless-steel column, packed in our laboratory with microparticulate bonded (10 μm) octadecylsilane (C_{18}) material (Techsil, HPLC Technology, Wilmslow, U.K.). The column temperature was maintained at 35°C by a Model LC-22 temperature controller (Bioanalytical Systems, W. Lafayette, IN, U.S.A.) to improve peak shape and resolution of josamycin from pre-eluting peaks observed in serum and urine samples. The solid-phase extractions were performed on 1-ml disposable C_{18} extraction columns (Bond-Elut; Analytichem, Harbour City, CA, U.S.A.).

All reagents were of at least analytical grade. The acetonitrile was of distilled-in-glass UV grade (Burdick & Jackson, Muskegon, MI, U.S.A.). Phosphoric acid and sodium hydroxide were both obtained from Merck (Johannesburg, South Africa). Josamycin was obtained from Yamanouchi (Tokyo, Japan) and oleandomycin phosphate from Pfizer (Pietermaritzburg, South Africa). Water used for extraction and chromatography was purified by filtration through a Milli-Q system (Millipore, Bedford, MA, U.S.A.).

The internal standard solution, containing 0.5 g/l oleandomycin phosphate (Fig. 2) was prepared by dissolving 10 mg oleandomycin phosphate in 2 ml of acetonitrile in a 20-ml volumetric flask and making up to volume with water.

An aqueous josamycin stock solution was prepared by dissolving 10 mg josamycin in 2 ml acetonitrile and making up to volume with water in a 10-ml volumetric flask (solution A). A 1-ml volume of solution A was then diluted to 10 ml with water

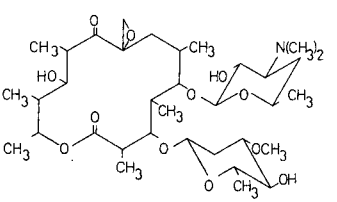

Fig. 2. Molecular structure of oleandomycin.

(solution B). Serum standards containing 0.1, 0.3, 0.6, 1.0, 1.5 and 2.0 mg/l josamycin were prepared by the serial dilution of a serum stock solution containing 1 ml solution B in 50 ml. Urine standards containing 0.25, 0.5, 1.0, 2.5 and 5.0 mg/l josamycin were prepared by the serial dilution of a urine stock solution containing 1 ml of solution B in 20 ml.

The mobile phase was acetonitrile–0.015 *M* phosphate buffer (5:2) degassed and filtered through a 0.4-μm HVLP Millipore filter prior to use. The buffer was prepared by making 0.96 ml phosphoric acid up to 1 l with water and adjusting the pH to 6.0 with sodium hydroxide pellets. The buffer used in the elution mixture (0.05 *M*) was prepared by making 3.2 ml phosphoric acid up to 1 l with water and adjusting the pH to 5.8 with sodium hydroxide pellets.

Methods

A 1-ml volume of sample (serum or urine) was mixed in a vortex mixer with 1 ml of acetonitrile for 5 s. Internal standard (200 μl) was added and mixed for an additional 5 s. Precipitated proteins were separated by centrifugation for 5 min at 1600 *g* and the supernatant was transferred to a 10-ml test-tube, containing 5 ml water. The diluted supernatant was then loaded onto a 1-ml disposable C_{18} extraction column which had been pretreated by wetting with 5 ml acetonitrile followed by 5 ml water, with the aid of a 20-ml custom-made glass reservoir. On completion of the loading process, the column was washed with 20 ml water followed by 4 ml acetonitrile–water (1:1). The column was then dried under vacuum (5–15 mmHg), using a Baker No. 10 extraction system (J. T. Baker, Phillipsburg, NJ, U.S.A.). Drug and internal standard were then eluted into a 2 ml tapered collection tube (Kimble, Owens-Illinois, IL, U.S.A.) with 3 × 0.5 ml aliquots of acetonitrile–0.05 *M* phosphate buffer, pH 5.8 (3:2), the column being dried under vacuum between each aliquot. The sample was evaporated to dryness under vacuum at 40°C in a rotary vacuum centrifuge (Savant, Hicksville, NY, U.S.A.). Reconstitution was effected by the addition of 20 μl of water, mixing for 1 min, addition of 50 μl of acetonitrile, mixing for an additional 1 min, and centrifugation for 30 s at 1600 *g*. An aliquot (30–40 μl) of the clean supernatant was transferred to a WISP limited-volume insert (Waters) with a microsyringe. Aliquots (2–10 μl) of this sample were injected into the chromatographic system. The flow-rate of the mobile phase was maintained at 1.2 ml/min for the analysis of both serum and urine samples, resulting in a pressure of 55 bar. Retention times for josamycin and internal standard (oleandomycin) were *ca.* 6.0 and 8.0 min, respectively. The eluate was monitored at 231 nm for the detection of josamycin (0.02 a.u.f.s. for serum and 0.06 a.u.f.s. for urine) and at 204 nm for the internal standard (0.06 a.u.f.s.). The time constants and threshold values for both wavelengths were 1.0 s and 0%, respectively. Chromatograms of extracts of serum and urine samples collected before and after the administration of 1 g josamycin to a human volunteer are shown in Figs. 3–6.

RESULTS

Calibration curves obtained by plotting the ratio of josamycin peak height to that of internal standard *vs.* josamycin concentration for serum and urine standards were found to be linear over the concentration ranges studied. The linear regression

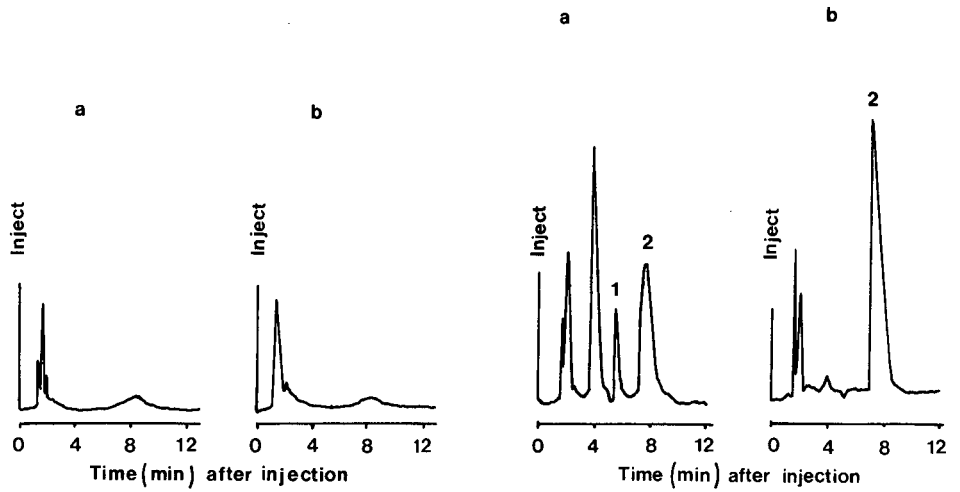

Fig. 3. Chromatograms of a blank serum extract, monitored at 231 nm (a) and 204 nm (b).

Fig. 4. Chromatograms of a serum extract, containing 0.29 mg/l josamycin (1) and internal standard (2), monitored at 231 nm (a) and 204 nm (b).

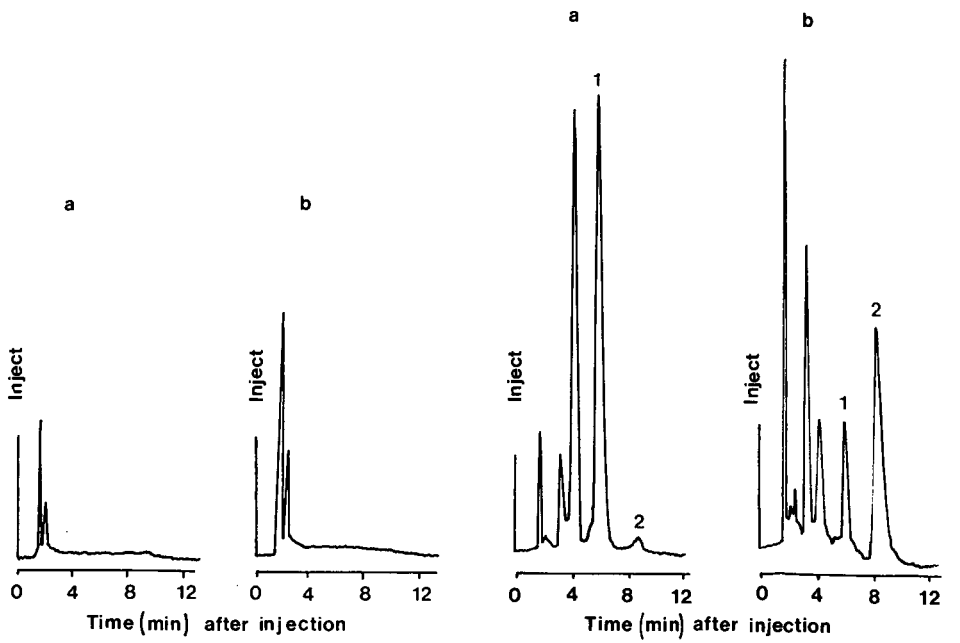

Fig. 5. Chromatograms of a blank urine extract, monitored at 231 nm (a) and 204 nm (b).

Fig. 6. Chromatograms of a urine extract, containing 5.28 mg/l josamycin (1) and internal standard (2), monitored at 231 nm (a) and 204 nm (b).

equations were $y = 1.0855x - 0.0237$ with a correlation coefficient of 0.9983 for serum and $y = 0.3142x - 0.0073$ with a correlation coefficient of 1.0000 for urine.

Accuracy and precision, determined at 0.30 and 1.82 mg/l in serum and 1.49 and 4.54 mg/l in urine, were found to be (mean ± S.D.; $n = 5$) 0.27 ± 0.01 and 1.78 ± 0.10 mg/l, and 1.43 ± 0.05 and 4.96 ± 0.17 mg/l, respectively. Although a slight baseline shift occurred in the area where the internal standard eluted (Fig. 3b), this relatively small aberation did not affect the analysis of serum samples.

The percentage recoveries from spiked serum and urine samples were assessed by extraction of five replicate samples at the upper and lower ends of the calibration ranges without the addition of internal standard. A phase separation was effected by the addition of 20 μl water and 50 μl acetonitrile followed by mixing for 1 min. Due to the partial miscibility of the two solvents after salting out, the volume of the supernatant is unknown. Therefore, as much of this layer as possible was transfered to a 2-ml collection tube, containing internal standard. Samples were then evaporated to dryness under vacuum at 40°C and reconstituted with 20 μl water and 50 μl acetonitrile. After mixing for 1 min, aliquots of this sample were injected into the chromatograph. Reference samples were prepared by the addition of that amount of josamycin equivalent to 100% recovery to collection tubes containing internal standard. Evaporation to dryness and reconstitution were effected as with test samples. The ratios of the peak height for josamycin to that of internal standard for the test samples were then compared with those of the reference samples. The percentage recoveries at the upper and lower ends of the calibration range for serum were 77% and 70%, respectively, and those for urine 76% and 80%, respectively.

The detection limit of josamycin in serum and urine was 0.025 mg/l, based on a signal-to-noise ratio of 3 and determined with a 10-μl injection volume and a channel 1 sensitivity setting of 0.01 a.u.f.s.

Analysis of serum samples stored at –15°C for 7, 14 and 28 days showed the samples to be stable and the method of analysis highly reproducible. Urine samples, on the other hand, showed evidence of degradation.

DISCUSSION

A rapid, sensitive assay with the accuracy and precision required for pharmacokinetic studies has been developed for the analysis of josamycin in human serum and urine. The major metabolite of josamycin is an hydroxylated compound which has been detected in serum and urine by the use of HPLC. Two other metabolites, a second hydroxylated compound and the deisovaleryl metabolite have only been detected in urine[15]. Chromatograms of serum samples collected after the administration of 1 g josamycin to healthy male volunteers show the appearance of an unknown peak at *ca.* 4 min (Fig. 4a). Chromatograms of urine samples collected from the same volunteers show the appearance of two extra peaks at *ca.* 3 min and 4 min (Fig. 6a). As pure samples of these metabolites were not available for chromatographic use, an HP 1040A diode array detector was utilised in an attempt to identify these unknown compounds. Data obtained show the eluting compounds to exhibit UV spectra almost superimposable on that of josamycin. These unknown peaks are therefore likely to be metabolites of josamycin indicating the separation of josamycin from its major and one minor metabolite.

With the aid of custom-built racks and reservoirs, and allowing the sample and washes to percolate through the extraction columns under gravity, over 80 samples can be extracted with ease during a normal working day and assayed overnight.

The utilisation of dual-wavelength monitoring enables the use of an internal standard which shows little or no UV absorbance at 231 nm, the wavelength of maximum absorption of the compound of interest. Chromatographically, oleandomycin is highly suitable as an internal standard in this assay and its use as such has been made possible by the application of dual-wavelength monitoring.

An important characteristic displayed by macrolides[19] when adsorbed on reversed-phase C_{18} material is they are easily eluted by an acetonitrile–buffer mixture but not by an acetonitrile–water mixture. A large water wash after loading is required for the removal of serum salts from the column and it is thus essential that this wash not become contaminated with ions from the diluted sample. Contamination can occur if pasteur pipettes used during loading to remove bubbles from the extraction column are also used during the 20-ml water-wash procedure, or from diluted sample remaining on the side of the reservoir after loading. It is therefore advisable to use clean pasteur pipettes and rinse the reservoirs with HPLC-grade water prior to the commencement of the 20-ml water wash. Contamination of this wash can lead to excessive loss of josamycin during the acetonitrile–water wash prior to elution and serious problems with accuracy and precision.

The composition of the mobile phase was critical for good separation of josamycin and internal standard. An increase in buffer concentration resulted in the more rapid elution of oleandomycin from C_{18} material, with little effect on the retention time of josamycin. Conversely, the retention of josamycin was more sensitive to the proportion of acetonitrile in the mobile phase. A high proportion of acetonitrile promoted rapid elution of josamycin. Good selectivity and resolution on a C_{18} column could easily be effected by manipulation of the molarity of the buffer used and the ratio of acetonitrile to buffer.

ACKNOWLEDGEMENTS

The authors would like to thank the Council for Scientific and Industrial Research for their financial support, Yamanouchi Pharmaceutical Co. for their generous donation of josamycin and Dr. C. Stubbs for his invaluable help.

REFERENCES

1 T. J. Cleary, S. Villa, L. Sands and T. Hoffman, *Curr. Ther. Res.*, 23 (1976) 351.
2 S. S. Long, S. Mueller and R. M. Swenson, *Antimicrob. Agents Chemother.*, 9 (1976) 859.
3 R. E. Reese, R. F. Betts, L. W. Goedde and R. G. Douglas, *Antimicrob. Agents Chemother.*, 10 (1976) 253.
4 L. J. Strausbaugh, J. A. Dilworth, J. M. Gwaltney and M. A. Sande, *Antimicrob. Agents Chemother.*, 9 (1976) 546.
5 E. L. Westerman, T. W. Williams and N. Moreland, *Antimicrob. Agents Chemother.*, 9 (1976) 988.
6 A. Horioka, Yamanouchi Pharmaceutical Co., Tokyo, Japan, personal communication.
7 G. Privitera, S. Bonino and S. Del Mastro, *Int. J. Clin. Pharm. Res.*, 4 (1984) 201.
8 L. J. Strausbaugh, W. K. Bolton, J. A. Dilworth, R. L. Guerrant and M. A. Sande, *Antimicrob. Agents Chemother.*, 10 (1976) 450.
9 C. Lam and E. Basalka, *Eur. J. Clin. Microbiol.*, 4 (1985) 279.

10 S. Mitsuahshi, *Drug Action and Drug Resistance in Bacteria,* University Park Press, Tokyo, 1971.
11 T. Bergan, P. Tolas and B. Oydvin, *Pharmacology,* 8 (1972) 336.
12 T. Bergan and B. Oydvin, *Pharmacology,* 7 (1972) 36.
13 F. Fraschini, P. C. Braga, V. Gagliardi, M. Falchi, F. Scaglione, G. Scarpazza, L. Tessari, G. Gattei and L. Pignanelli, *Drugs Exptl. Clin. Res.*, 9 (1983) 345.
14 F. Fraschini, P. C. Braga, G. Biella, F. Scaglione, C. Montoli and G. Scarpazza, *Int. J. Clin. Pharm. Res.*, 3 (1983) 203.
15 J. B. Fourtillan, M. A. Lefebvre and P. Gobin, *G. Ital. Chemioter.*, 29, Suppl. 1 (1982) 103.
16 K. Tsuji, *J. Chromatogr.*, 158 (1978) 337.
17 M. Ducci and V. Scalori, *Int. J. Clin. Pharm. Res.*, 4 (1984) 195.
18 K. Räder, A. Wildfeuer, A. Schwedass and H. Laufen, *J. Chromatogr.*, 344 (1985) 416.
19 C. Stubbs, J. M. Haigh and I. Kanfer, *J. Chromatogr.*, 353 (1986) 33.

Journal of Chromatography, 459 (1988) 269–273
Elsevier Science Publishers B.V., Amsterdam — Printed in The Netherlands

CHROMSYMP. 1457

HIGH-PERFORMANCE LIQUID CHROMATOGRAPHIC METHOD FOR THE DIRECT QUANTITATION OF OXY RADICALS IN MYOCARDIUM AND BLOOD BY MEANS OF 1,3-DIMETHYLTHIOUREA AND DIMETHYL SULFOXIDE

PARINAM S. RAO*, NISA RUJIKARN and JOHN M. LUBER, Jr.
Division of Cardiothoracic Surgery, Long Island Jewish Medical Center, New Hyde Park, NY 11042 (U.S.A.)

SUMMARY

A direct, sensitive (50–200 ng), simple and specific high-performance liquid chromatographic (HPLC) method is described for the quantitation of oxy radicals by means of the consumption of dimethyl sulfoxide (DMSO) by the hydroxy radical and dimethylthiourea (DMTU) by hydrogen peroxide. The specific scavengers catalase and L-methionine were used to quantitate hydrogen peroxide and OH, respectively. The DMSO and DMTU peaks were separated and identified by HPLC on a Waters C_{18} Resolve 10-μm Radial-Pak column with an isocratic mobile phase (5% aqueous methanol) at 2 ml/min with UV detection (DMSO, 214 nm; DMTU, 240 nm). The OH concentrations were extrapolated by a luminol chemiluminescence technique. A linear relationship was obtained for DMTU consumption by hydrogen peroxide in the range 0.25–0.40 mM with a coefficient of variation (C.V.) of 8.8 ± 2.1% and for DMSO consumption by hydroxy radicals in the range 0.1–3.2 μM OH, with a C.V. of 9.6 ± 3.6%. The limits of detection for this method were 50 ng of hydrogen peroxide for DMTU and 200 ng of OH for DMSO. Hydrogen peroxide averaged 10.5 ± 3.6 nmol/ml in blood and 56.4 ± 5.3 μmol/g wet weight in left ventricular (LV) tissue. The hydroxy radical concentration was 0.1 μM in blood and 0.3 μM in LV tissue.

INTRODUCTION

Based on indirect evidence from scavenging experiments, the oxygen metabolites superoxide (O_2^-), hydroxy (OH) and peroxy radicals (OOH) and hydrogen peroxide are present in variable concentrations in both normal and disease states[1–4]. Scavenging enzymes, such as superoxide dismutase (SOD) and catalase, are large, highly charged particles, which probably do not reach key intracellular locations when given exogenously. On the other hand, dimethylthiourea (DMTU) and dimethyl sulfoxide (DMSO), specific scavengers of hydrogen peroxide and OH, respectively, are small and highly mobile across cell membranes, affecting both intra- and extracellular compartments. As they are both relatively non-toxic, they may be suitable for use in biological systems as *in vivo* oxygen metabolite scavengers. DMTU at low concentra-

0021-9673/88/$03.50

tions (1 m*M*) consumes hydrogen peroxide without affecting OH. However, at 100 m*M* concentration it consumes approximately 23% of the OH available. DMSO, on the other hand, specifically scavenges OH but not hydrogen peroxide at 1 m*M*.

The use of DMTU and DMSO consumption as a marker for oxy radicals in biological systems was previously limited because the small amounts of hydrogen peroxide and OH that occur in these systems could not be measured[5,6]. We have developed a direct, simple and specific high-performance liquid chromatographic (HPLC) method with UV detection for the quantitation of the micromolar concentrations of OH and hydrogen peroxide produced in biological systems. This technique is based on their consumption by DMSO and DMTU. The concentrations of DMSO and DMTU selected (1 m*M*) produced no cross-scavenging of OH and hydrogen peroxide. Quantitative data were obtained by measuring the DMSO and DMTU consumption in the absence and presence of L-methionine and catalase, which are specific scavengers of OH and hydrogen peroxide, respectively.

EXPERIMENTAL

Materials

HPLC-grade methanol (Fisher, Springfield, NJ, U.S.A.) was used. Analytical-reagent grade chemicals were obtained from the following sources: DMTU (Lancaster Synthesis, Windham, NH, U.S.A.), DMSO (Aldrich, Milwaukee, WI, U.S.A.), hydrogen peroxide (Fisher), iron(II) sulfate, EDTA, catalase and L-methionine (Sigma, St. Louis, MO, U.S.A.). Water was purified with a Milli-Q filtration system (Millipore, Bedford, MA, U.S.A.).

The apparatus consisted of a Waters Model 510 liquid chromatograph, coupled to a Waters U6K injector and a 490 programmable multi-wavelength UV detector (Waters Assoc., Milford, MA, U.S.A.), A Digital 350 computer/controller and printer (LA 50) completed the system (Digital, Merrimack, NH, U.S.A.). The column used was a Waters Resolve C_{18} Radial-Pak 10-μm cartridge measuring 8 mm × 10 cm. Injections were made with a 25-μl Hamilton syringe (Waters Assoc.).

Methods

The mobile phase contained 5% methanol in Millipore water, routinely prepared, filtered through the Duropore filter (0.22 μm) (Waters Assoc.) and degassed the day of use. The flow-rate was 2 ml/min and the sample volume injected was 20 μl. Absorption spectra were recorded at 214 nm for DMSO and 240 nm for DMTU.

Standards of DMTU (0.25–4.0 m*M*), DMSO (0.5–3.5 m*M*), hydrogen peroxide (100–700 μM), catalase (200 μg/ml) and L-methionine (10 m*M*) were used on the day of preparation. Hydroxy radical (1.0 μM) was produced with Fenton's reagent[7] [1 m*M* iron(II) sulfate–0.4 m*M* hydrogen peroxide–1 m*M* EDTA] and quantitated by the luminal chemiluminescence technique[8].

Blood samples consisted of 100 μl of fresh heparinized blood, which was mixed with 50 μl of DMTU or DMSO (1 m*M*) and 50 μl of phosphate buffer (pH 7.4) within 1–2 s of collection. The samples were mixed in a Vortex mixer, centrifuged for 5 min (1100 *g*, 4°C) and a 20-μl sample was injected on to the column.

Left ventricular tissue (50 mg) was quickly frozen (1–2 s after harvest) in liquid nitrogen, powdered under dry nitrogen and mixed with 50 μl of DMTU or DMSO (1

m*M*) and 100 μl of phosphate buffer (pH 7.4). The mixture was again mixed for 3 min, centrifuged for 5 min (1100 *g*, 4°C) and a 20-μl sample was injected on to the column.

Scavenger data with L-methionine and catalase (50 μl of each) were obtained by incubation with the specimens for 1 min at room temperature. The scavenger solution volume replaced the phosphate buffer in these experiments.

RESULTS AN DISCUSSION

The calibration graphs for DMTU absorbance at 240 nm (0.25–4.0 m*M*) and for DMSO absorbance at 214 nm (0.5–3.5 m*M*) were linear. Linear regression analysis indicated the following characteristics for these curves: DMTU, slope = 192, r = 0.999, intercept = 1.6; DMSO, slope = 64, r = 1.000, intercept = 4. The actual chromatograms for 1 m*M* concentrations DMTU and DMSO are shown in Fig. 1.

The calibration graph for hydrogen peroxide concentration by means of DMTU (1 m*M*) consumption was also linear. Addition of catalase (200 μg/ml) completely inhibited DMTU consumption, confirming that hydrogen peroxide was responsible for the DMTU in both tissue and blood. As the DMTU consumption graph was linear, the peak-height difference represented the concentration of hydrogen peroxide in both standard and sample. Spiking the blood sample with 500 μM hydrogen peroxide yielded quantitative results with this method. The coefficient of variation for this technique was 8.8 ± 2.1% (n = 10) in the range 50–60 m*M* with recoveries of 99 ± 0.6% and a sensitivity of 50 ng.

In human blood, the hydrogen peroxide concentration was 10.5 ± 3.6 nmol/ml and in swine LV tissue 56.4 ± 5.3 μmol/g wet weight (Table I). The amount of hydrogen peroxide measured in human blood and tissue represents the concentration that exceeds the rate of turnover of native complex of the catalase.

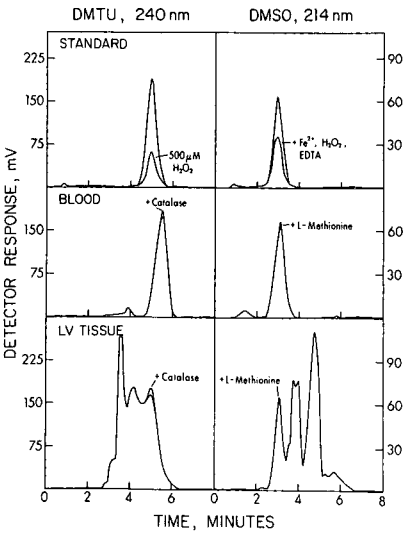

Fig. 1. Chromatogram of standards, human blood and swine LV tissue in the presence of DMTU (1 m*M*) and DMSO (1 m*M*).

TABLE I

HYDROGEN PEROXIDE CONCENTRATION IN STANDARDS, HUMAN BLOOD AND SWINE LV TISSUE DETERMINED BY HPLC FROM THE DMTU CONSUMPTION AND SCAVENGING BY CATALASE

Results are mean values (n = 10).

Sample	*Peak height (mV)*		*Hydrogen peroxide concentration (μM)*
	DMTU	*DMTU + catalase*	
DMTU (1m*M*)	185	185	0
Hydrogen peroxide (500 μ*M*)	182	60	496
Human blood + hydrogen peroxide (500 μ*M*)	181	55	512
Human blood	181	186	10.5
Swine LV tissue	173	185	56.4

TABLE II

PRECISION OF METHODOLOGY

Method	*Detects*	*Range (μM)*	*C.V. (%)*	*Sensitivity (ng)*
DMTU	H_2O_2 concentration	50–600	8.8 ± 2.1	50
DMSO	OH concentration	50–800	9.6 ± 3.6	200

TABLE III

HYDROXY RADICAL CONCENTRATION IN STANDARDS, HUMAN BLOOD AND SWINE LV TISSUE BY HPLC FROM THE DMSO CONSUMPTION AND SCAVENGING BY L-METHIONINE

Results are mean values (n = 10).

Sample	*Peak height (mV)*		*OH (hydrogen peroxide) concentration (μM)*
	DMSO	*DMSO + L-methionine*	
DMSO (1 m*M*)	62	62	0
OH (1 μ*M*)*	60	45	0.95
Human blood + OH (1 μ*M*)	60	44	1.07
Human blood	62	63	0.10
Swine LV tissue	60	63	0.30

* Fe^{2+} (1 m*M*)–hydrogen peroxide (0.4 m*M*)–EDTA (1 m*M*) with the luminal chemiluminescence technique yielded 1.0 μ*M* of OH radical equivalents.

DMSO (1 m*M*) consumption by OH radicals (produced with Fenton's reagent, and quantitated by luminol chemiluminescence) was directly proportional to the concentration of hydrogen peroxide in the reagent in the range 0.2–1.4 m*M*. L-Methionine (10 m*M*) quantitatively scavenged the OH radicals. The peak height difference in the chromatograms *vs.* OH concentration yielded a calibration graph for hydroxy radical concentration in a manner identical with the DMTU calibration. Spiking the blood sample with Fenton's reagent (1 μM OH) yielded quantitative data. The coefficient of variation (C.V.) for the OH determination was 9.6 ± 3.6% (n = 10) in the range 50–800 μM hydrogen peroxide (0.1–3.2 μM OH). The recovery was 95 ± 2.2% and the sensitivity was 20 ng (Table II). Neither blood nor LV tissue showed significant concentration of OH [0.011 ± 0.004 μM and 0.30 ± 0.08 μmol/g wet weight, respectively (Table III)]. The concentration of hydroxy radicals in blood (0.01 ± 0.004 μM) and in LV tissue (0.30 ± 0.08 μmol/g wet weight) were also negligible.

This HPLC method provides a direct, highly specific, sensitive and reproducible quantitation of hydroxy radicals and hydrogen peroxide in biological systems. The ability of the scavengers, DMSO and DMTU, to cross cell membranes and their relative non-toxicity indicates their value when used alone or in combination, at appropriate millimolar concentrations, to detect specific oxy-derived radicals and potentially protect a biological system *in vivo* from their damaging effects.

REFERENCES

1 J. M. McCord, *Ann. Intern. Med.*, 89 (1978) 122.
2 P. S. Rao and H. S. Mueller, in J. J. Spitzer (Editor), *Myocardial Injury*, Plenum Press, New York, 1983, p. 347.
3 J. F. Turrens, J. D. Crapo and B. A. Freeman, *J. Clin. Invest.*, 73 (1984) 879.
4 C. L. Myers, S. J. Weiss, M. M. Kirsch, B. M. Shepard and M. Schlafer, *J. Thorac. Cardiovasc. Surg.*, 91 (1986) 281.
5 J. H. Jackson, C. W. White, N. B. Parker, J. W. Ryan and J. E. Repine, *J. Appl. Physiol.*, 59 (1985) 1995.
6 N. B. Parker, E. M. Berger, W. E. Curtis, M. E. Muldrow, S. L. Linas and I. E. Repine, *J. Free Radicals Biol. Med.*, 1 (1985) 415.
7 H. J. H. Fenton, *J. Chem. Soc.*, 65 (1894) 899.
8 P. S. Rao, J. M. Luber, Jr., J. Milinowicz, P. Lalezari and H. S. Mueller, *Biochem. Biophys. Res. Commun.*, 150 (1988) 39.

Journal of Chromatography, 459 (1988) 275–279
Elsevier Science Publishers B.V., Amsterdam — Printed in The Netherlands

CHROMSYMP. 1500

Note

High-performance liquid chromatographic determination of indomethacin serum concentrations

YVONNE L. BROWN, ROBERT J. KANDROTAS, JEAN B. DOUGLAS and PETER GAL*,*
Clinical Pharmacology Research and Development Laboratory, The Moses H. Cone Memorial Hospital, 1200 North Elm Street, Greensboro, NC 27401 (U.S.A.)

Indomethacin has been used with varying success for closure of patent ductus arteriosis (PDA) in premature infants[1,2]. Successful PDA closure is particularly difficult in neonates below 1000 g, more than 14 days postnatal age, and with very large PDA[2]. Since the cause of the limited success may be due to inadequate indomethacin serum concentrations, the availability of a rapid, reliable indomethacin assay may be very helpful. We describe such an assay.

MATERIALS AND METHODS

Apparatus and chromatographic conditions

The high-performance liquid chromatography (HPLC) system (Waters Assoc., Milford, MA, U.S.A.) consisted of two Model 510 pumps controlled by an automated gradient controller (Model 680), a Model 441 fixed-wavelength ultraviolet detector (set at 254 nm and 0.01 a.u.f.s.), and a 710B WISP autosampler. The recorder used was a Model 740 data module and was set for a run time of 10 min. The analytical column used was a Nova Radial-Pak® C_{18} reversed-phase column (Waters) in a radial compression unit (Waters) with a C_{18} precolumn.

Chemicals

HPLC-grade acetonitrile was obtained from Burdick and Jackson (Muskegon, MI, U.S.A.) and indomethacin, flufenamic acid (the internal standard) and acetic acid were obtained from Sigma (St. Louis, MO, U.S.A.).

Standard solutions

Stock solutions of indomethacin (10 μg/ml) and the internal standard, flufenamic acid (40 μg/ml) were prepared in acetonitrile. Standards were prepared in drug-free serum using these solutions to formulate indomethacin concentrations of 0.25–5 μg/ml, each containing a final flufenamic concentration of 20 μg/ml. These

* Present address: Pharmacy Education and Research, Greensboro AHEC, 1200 North Elm Street, Greensboro, NC 27401, U.S.A.

0021-9673/88/$03.50

standards were found to be stable for 5 months if refrigerated at 4°C. Serum-based standards were compared to standards prepared in acetonitrile and shown to be identical, allowing the less expensive acetonitrile-based preparations to serve as standards for the assay.

The mobile phase was acetonitrile–water–acetic acid (54.2:45.2:0.6). This was achieved by combining solution A [water–acetonitrile–acetic acid (44:950:6)] and solution B [acetonitrile–water–acetic acid (950:44:6)] in a ratio of solution A–solution B = 55:45. The pH of the mobile phase is 3.6.

Sample preparation

The extraction method was tested at three different injection volumes: 25, 50 and 100 μl. To the appropriate amount of serum, an equivalent volume of internal standard solution (flufenamic acid, 40 μg/ml) was added in a conical centrifuge tube. Protein was then precipitated by adding 1 ml of acetonitrile to the mixture, then agitating it on a Vortex mixer for 1 min. The samples were then centrifuged at 9500 *g* for 2 min. The supernatant was separated into a glass test-tube and evaporated to dryness under a stream of nitrogen at 37°C. The residue from the supernatant was reconstituted with 100 μl of mobile phase, and 75 μl were injected.

Analytical recovery and extraction

The assay recovery was assessed for both indomethacin and flufenamic acid. Indomethacin was studied at 0.1, 0.4, 1.5 and 4 μg/ml. Flufenamic acid was studied at 1.5 and 4 μg/ml. Six serum samples containing indomethacin and flufenamic acid were extracted and injected. In addition, 6 samples of each drug at concentrations of 1.5 and 4 μg/ml were prepared in mobile phase and injected directly. Recovery was calculated based on the peak heights for drugs extracted from serum (Peak Extr) and the drugs dissolved in mobile phase and injected directly (Peak Dir), using the formula:

$$\% \text{ recovery} = \frac{\text{Peak Extr}}{\text{Peak Dir}} \times 100$$

RESULTS

Representative chromatograms of extractions of blank serum and a serum sample spiked to contain 2 μg/ml flufenamic acid are depicted in Fig. 1. The response of the detector was linear from 0.1 to 5.3 μg/ml with a sensitivity of 0.1 μg/ml. There was very little between-run or within-run variability for serum samples sizes ranging from 25 μl to 100 μl (Table I). Recovery ranged from 99 to 107% for concentrations ranging from 0.1 to 4 μg/ml. The percent error of the assay ranged from a low of 0.5% at 2 μg/ml to a high of 9% at 0.1 μg/ml (Table II).

Other drugs which are commonly used concurrently with indomethacin are listed in Table III, along with retention times and capacity factors. These drugs do not interfere with the indomethacin assay.

DISCUSSION

Indomethacin is the treatment of choice for PDA closures[1,2]. Efficacy is felt to be related to maintaining adequate indomethacin serum concentrations[2–5]. While an

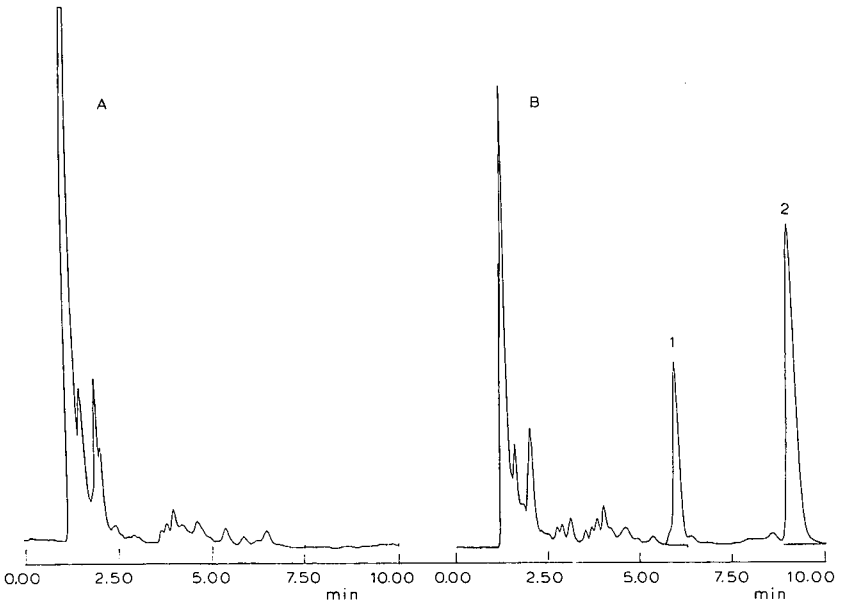

Fig. 1. Extracted blank serum (A) and serum spiked to contain 2.0 μg/ml indomethacin (1) and 20 μg/ml flufenamic acid (2) (B).

TABLE I

COMPARISON OF COEFFICIENTS OF VARIATION (C.V.) AND RECOVERIES USING DIFFERENT SERUM VOLUMES

	Volume (μl)		
	25	*50*	*100*
Within-day C.V. (%)	1.6	1.5	1.6
Between-day C.V. (%)	3.0	4.9	2.0
Recovery (%)	100	100	100

TABLE II

COMPARISON OF COEFFICIENTS OF VARIATION (C.V.) AND RECOVERIES USING 100 μl SERUM AT DIFFERENT INDOMETHACIN CONCENTRATIONS

Indomethacin concentration (μg/ml)	*C.V. (%)*	*Recovery (%)*
0.1	9.0	107
0.4	2.4	99
1.9	0.5	101
3.9	1.0	99

TABLE III

RETENTION TIMES AND CAPACITY FACTORS FOR OTHER DRUGS LIKELY TO BE PRESENT

Drug	*Retention time (min)*	*Capacity factor*
Indomethacin	6.07	3.82
Flufenamic acid	9.41	6.41
Ampicillin	Many peaks	<3.0
Dopamine HCl	3.15	1.47
Lorazepam	2.55	1.0
Gentamicin	3.15	1.47
Phenobarbital	2.78	1.18

optimal therapeutic range is unknown, several authors, using samples collected at times ranging from 2 to 24 h after a dose have cited[3–5] values from 0.25 to 3.5 μg/ml. Our approach has been to adjust each indomethacin dose based on available serum indomethacin concentrations and clinical response until PDA closure is achieved. Once PDA closure is achieved at a known indomethacin serum concentration, this "critical" concentration is maintained for 24 h. Using this approach, PDA closure was achieved in all 21 patients dosed to a critical concentration with one case of mild renal toxicity. This compared to only 64% PDA closure and up to 50% renal toxicity in two control groups[5].

The validity of this dosing approach depends on the rapid availability of the indomethacin concentration and limitation of the sample size required. This assay can be run on samples as small as 25 μl, although we have routinely used 100 μl. This compares to 200 μl or more for previously published assays[6–8]. The preparation and run time totals about 30 min, compared with 60 to 90 min for other methods we have utilized[6,7]. A final cost consideration is the reliability of standards prepared in acetonitrile rather than serum, and the stability of these standards for at least 5 months when refrigerated at 4°C.

CONCLUSION

The practicality of offering an indomethacin assay in the clinical laboratory depends on availability of an assay and relatively inexpensive assay which can be performed with speed and accuracy.

The assay we describe above meets these criteria. Most neonates require indomethacin serum concentrations of 0.5 to 2.5 μg/ml to close a PDA[9]. In this concentration range, the C.V. for our assay is below 2%. This new assay provides unique benefits making it particularly desirable for clinical laboratories wishing to provide this assay. Based on the increasing support for serum indomethacin concentration monitoring, we feel clinical laboratories will want to provide this assay.

REFERENCES

1 R. B. Cotton, *Clin. Perinatol.*, 14 (1987) 621.
2 S. M. Douidar, J. Richardson and W. R. Snodgrass, *Dev. Pharmacol. Ther.*, 11 (1988) 196.

3 A. R. Brash, D. E. Hickey, T. P. Graham, M. T. Stahlman, J. A. Oates and R. B. Cotton, *N. Engl. J. Med.*, 305 (1981) 67.
4 A. Leonhardt, V. Isken, P. G. Kuhl and H. W. Seyberth, *Eur. J. Pediatr.*, 146 (1987) 140.
5 M. M. Culhane, P. Gal, S. Schall, R. L. Weaver, J. L. Ransom, M. V. Miles, Y. L. Brown and A. A. Bird, *Drug Intell. Clin. Pharm.*, 21 (1987) 24A.
6 A. C. Mehta and R. T. Calvert, *Ther. Drug Monit.*, 5 (1983) 143.
7 C. N. Ou and V. L. Frawley, *Clin. Chem.*, 30 (1984) 898.
8 R. J. Stubbs, M. S. Schwartz, R. Chiou, L. A. Entwistle and W. F. Bayne, *J. Chromatogr.*, 383 (1986) 432.
9 P. Gal, J. L. Ransom, R. Weaver, S. A. Schall, Y. L. Bown and M. M. Culhane, *Pharmacotherapy*, 8 (1988) 74.

Journal of Chromatography, 459 (1988) 281–289
Elsevier Science Publishers B.V., Amsterdam — Printed in The Netherlands

CHROMSYMP. 1442

MEASUREMENT OF THE RELEASE OF ADENINE NUCLEOTIDES DURING PLATELET AGGREGATION BY SMALL-BORE-COLUMN ISOCRATIC HIGH-PERFORMANCE LIQUID CHROMATOGRAPHY

F. BODOLA and C. R. BENEDICT*
Division of Cardiology, E-53, Department of Internal Medicine, The University of Texas, Medical Branch, Galveston, TX 77550 (U.S.A.)

SUMMARY

This paper describes a simple and sensitive method for measuring adenosine, adenosine monophosphate, adenosine diphosphate, and adenosine triphosphate in plasma and tissues. This method involves sample preparation by perchloric acid extraction, followed by high-performance liquid chromatography on a small-bore column with UV detection at 254 nm. The minimum detectable amounts were adenosine, 0.60 pmol; adenosine monophosphate, 0.90 pmol; adenosine diphosphate, 1.5 pmol; and adenosine triphosphate, 2.5 pmol. The interassay coefficient of variation for the measurement of these compounds was less than 4%. The influence of varying the pH and the concentration of phosphate, acetonitrile, and ion-pairing reagent are described. This method can be used to measure adenine nucleotide release during platelet aggregation.

INTRODUCTION

Recent studies have brought to light the importance of thrombus formation in occlusive coronary artery disease. Qualitative angiography[1], postmortem coronary arterial studies[2–4], coronary angioscopy[5], and biochemical studies[6] indicate the importance of thrombosis, superimposed on ruptured atherosclerotic plaques in myocardial infarction. Platelet aggregation is intimately involved in the process of thrombus formation.

Studies intended to delineate the mechanisms of platelet aggregation during thrombus formation have been hampered by the lack of reliable methods to study *in vivo* platelet aggregation. Detection of circulating platelet aggregates was proposed as evidence of *in vivo* platelet aggregation, but this test is difficult to standardize and reproduce[7]. Other methods to detect platelet activation have focused on radioimmunoassays of platelet secretory products, such as Platelet Factor 4, β-thromboglobulin, and the arachidonic acid metabolite thromboxane B_2 (TxB_2). Studies in which Platelet Factor 4[8] or β-thromboglobulin[9,10] are used as markers for intravascular platelet activation have produced equivocal results. This is probably due to sampling problems, leading to release of these products from platelets. Similar artefactual changes due to sampling, combined with imprecise assay methods, have

0021-9673/88/$03.50

cast doubt on the validity of using TxB_2 as a marker for *in vivo* platelet aggregation[11,12]. To assess the involvement of platelets in thrombus formation, more sensitive and specific indices of platelet aggregation are necessary.

During platelet aggregation, adenosine diphosphate (ADP) and serotonin are released from dense granules. Unlike serotonin, ADP released from platelets into plasma is not taken up again by the intact non-aggregated platelets, and may serve as a useful index of platelet aggregation. Several methods have been published for the determination of adenine nucleotides in biological materials by high-performance liquid chromatography (HPLC) (see refs. 13–19 and references cited therein). However, because they lack sensitivity, none of these methods can be used reliably to measure the release of adenine nucleotides as an index of platelet aggregation. A sensitive isocratic method is described for the measurement of adenosine (ADE), adenosine monophosphate (AMP), ADP, and adenosine triphosphate (ATP) in plasma by the use of HPLC on a 2.1-mm I.D. reversed-phase C_{18} column with UV detection at 254 nm. This method is also applicable to studies of the metabolism of adenine nucleotides in tissues and cell cultures.

EXPERIMENTAL

HPLC

The system consisted of a Waters Assoc. 6000A (Milford, MA, U.S.A.) pump with microflow modifications, a Waters Assoc. U6K injector with a 20-μl injection loop, and a Kratos Spectroflow 783 UV detector (Kratos Analytical, Ramsey, NJ, U.S.A.), equipped with a 12-μl flow-cell, operated at 254 nm. A Brownlee (Santa Clara, CA, U.S.A.) RP-18 column (220 × 2.1 mm I.D.), attached to a Brownlee RP-18 (15 × 2.1 mm) guard precolumn was used for chromatographic separations. The connecting tubes between the injector, column, and detector were kept as short as possible. Data were collected and analyzed with IBM PC/XT and Nelson Analytical 2600 Series Chromatography software (Cupertino, CA, U.S.A.).

The chemicals used were of the highest grade available. Acetonitrile and perchloric acid were obtained from Aldrich (Milwaukee, WI, U.S.A.). Potassium dihydrogenphosphate, potassium hydroxide, tetrabutylammonium hydrogensulfate (TBAHS), and triethylamine (TEA) were obtained from Fluka (Ronkonkoma, NY, U.S.A.). Nucleotide standards and adenosine were obtained from Sigma (St. Louis, MO, U.S.A.). Milli-Q Water (Millipore, Bedford, MA, U.S.A.) was used for preparing the mobile phase. Standards were prepared by dissolving an accurately weighed amount of standard (10 mg) in 10 ml of 0.1 *M* phosphate buffer (pH 6.5), which was stored at −70°C.

Mobile phases were prepared fresh daily by adding 10 ml of acetonitrile to 450 ml of 0.125 *M* phosphate buffer (pH 6.5), containing 4 m*M* TBAHS, followed by 1 ml of TEA. The pH of the mobile phase was adjusted to 6.5 with 8 *M* potassium hydroxide, and finally the volume was made up to 500 ml with 0.125 *M* phosphate buffer (pH 6.5). The mobile phase was filtered through a 0.45-μm Nylon filter (Rainin Instruments, Woburn, MA, U.S.A.) and degassed for 5 min before use. This mobile phase contained 2% (v/v) acetonitrile 12.5 m*M* TEA, and 4 m*M* TBAHS, and produced excellent resoluion at pH 6.5. Chromatography was carried out at room temperature with a mobile phase flow-rate of 0.5 ml/min. Various flow-rates were tested. Slower

flow-rates led to a loss in resolution and higher flow-rates produced undesirable back pressure (> 3000 p.s.i.). Generally, equilibration of the column was assumed when a steady baseline was observed at a detector range of 0.002 a.u.f.s. with a 0.1-s rise time. When the column was not in use, the mobile phase was recycled through the column to keep the chromatographic conditions stable.

Platelet aggregation and sample preparation

For platelet aggregation studies, blood was collected in plastic tubes containing 3.8% sodium citrate (1 ml for 9 ml of blood), and platelet-rich plasma was separated immediately by centrifugation at 102 *g* for 15 min at room temperature. After removing the upper two-third of platelet-rich plasma, the remainder was again centrifuged at 4000 *g* for 10 min to yield platelet-poor plasma. Platelet-rich plasma samples were kept tightly capped at room temperature until analysed. For platelet aggregation, a platelet-rich plasma sample of 360 μl was prewarmed for 1 min by stirring in siliconized glass cuvettes placed in a Sienco dual-channel aggregometer (Morrison, CO, U.S.A.). Aggregation was induced by adding 10 μl of 120 m*M* solution of calcium chloride and 3 μg of collagen (Helena Labs., Beaumont, TX, U.S.A.) dissolved in 0.01 *M* Tris-buffered saline (pH 7.4). During aggregation, the percentage change in light transmission of platelet-rich plasma (set at 10%) relative to platelet-poor plasma (set at 90%) was monitored. When platelet aggregation was 60% completed (usually 2–3 min after adding collagen), the cuvette was plunged into ice–water and then centrifuged immediately at 4000 *g* for 10 min at 4°C to prepare platelet-poor plasma by removing the platelets. The nucleosides and nucleotides were extracted from platelet poor plasma by a modified perchloric acid method. To 500 μl of platelet-poor plasma, 500 μl of 10% (v/v) perchloric acid was added, followed by 50 μl of 1 *M* potassium dihydrogenphosphate, and mixed for 10 s on a vortex mixer. The sample was then centrifuged at 4000 *g* for 5 min at 4°C. A 500-μl aliquot of the clear supernatant was transferred to a 75 × 12 mm polypropylene tube, and 30 μl of 8 *M* potassium hydroxide was added. After mixing, the tube was placed in an ice-bath for 30 min. The precipitate formed was removed by centrifugation at 30 000 *g* for 10 min at 4°C. A 300-μl aliquot of the supernatant was transferred to another 75 × 12 mm polypropylene tube, and 30 μl of 1.5 *M* phosphate buffer (pH 6.5) was added to adjust the pH to 6–7.

A standard curve was constructed for each assay from four different amounts of adenosine, AMP, ADP, and ATP, added to 1 ml of platelet poor plasma (PPP) and carried through the entire procedure. The amount of standard added, covered the range from 1.25 ng to 10 ng.

RESULTS

When a mixture of standards, containing ADE, AMP, ADP, and ATP in 0.125 *M* phosphate buffer (pH 6.5) was injected, ADE was eluted at 5.90 min, AMP at 4.66 min, ADP at 8.97 min, and ATP at 17.53 min. The k' values were: ADE = 4.87, AMP = 3.63, ADP = 7.94, and ATP = 16.5, respectively (Fig. 1). When standards in phosphate buffer were extracted with perchloric acid and injected, identical results were obtained. The recovery was determined by injecting a known amount of the nucleotides in mobile phase and comparing the results with values obtained when the

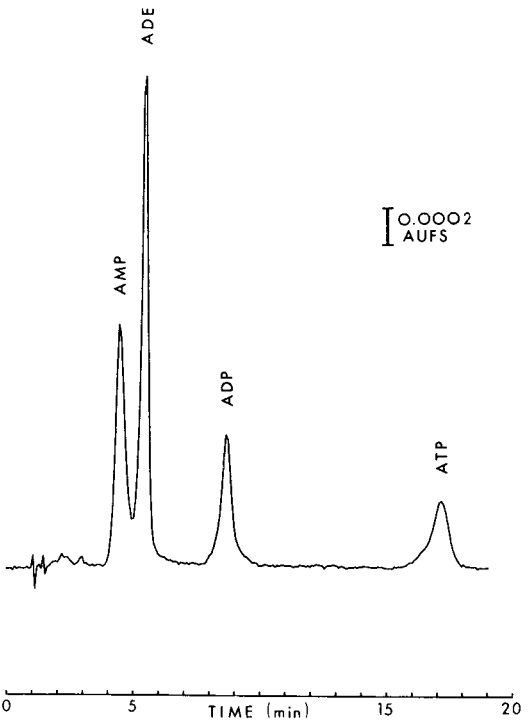

Fig. 1. Chromatogram showing the retention time for adenosine (ADE), adenosine monophosphate (AMP), adenosine diphosphate (ADP), and adenosine triphosphate (ATP). A 2-ng amount of each was dissolved in the mobile phase and injected. For conditions, see text.

same concentrations were added to platelet-poor plasma and carried through. The recovery for all four compounds was 92.6 ± 0.5% (mean ± S.D.) (n = 12). The standard curve was linear for all four compounds throughout the range tested (r = 0.99; $p < 0.001$). The sensitivity of the method (at a signal-to-noise ratio of 3) for ATP was 2.5 pmol, for ADP 1.5 pmol, for AMP 0.90 pmol, and for ADE 0.60 pmol (amount injected on the column). The inter-assay coefficient of variation was determined by adding 5 ng of ADE, AMP, ADP, and ATP to four different plasma samples and assaying on four different days. The value was less then 4% for all the compounds.

Platelet-poor plasma had no detectable levels of ADP or ATP, whereas low concentrations of AMP and ADE were detected (Fig. 2, Table I). With platelet aggregation, there was a significant increase in the concentation of AMP, ADP, and ATP in platelet poor-plasma (Fig. 3, Table I).

The purity of the detected ADE, AMP, ADP, and ATP peaks was determined by several methods: (1) the peak areas were increased in direct proportion to added ADE, AMP, ADP, and ATP; (2) no ADE, AMP, ADP, or ATP peaks were detected when samples were incubated with a mixture of hexokinase, myokinase, and adenylic acid deaminase, which metabolized the adenine nucleotides; (3) the absorption at 254 and 280 nm were compared for all four compounds. The mean $areas_{254}/areas_{280}$ ratio for all four compounds were similar for the sample peaks and the injected standards with a value of 3.42 for ADE, 3.49 for AMP, 3.83 for ADP, and 2.75 for ATP.

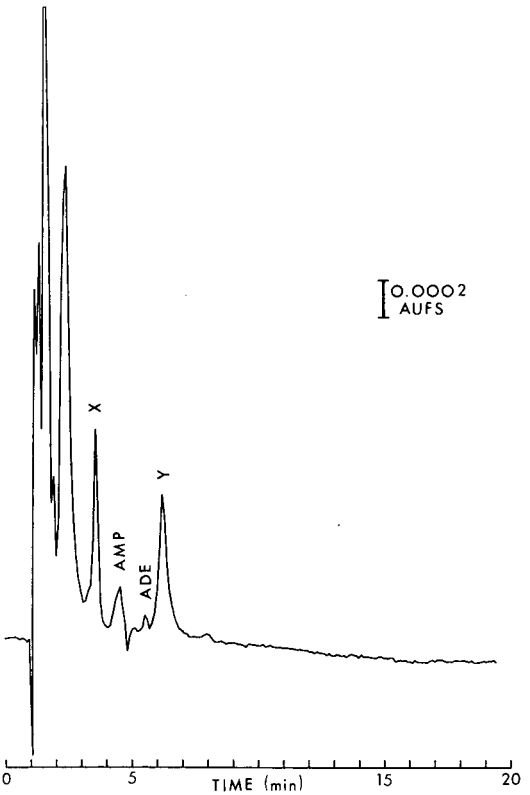

Fig. 2. Chromatogram of platelet-poor plasma. X and Y are unknown peaks.

Several chromatographic parameters were examined to determine their role in enhancing peak separation without significantly increasing the analysis time for each sample. The percentage of acetonitrile used (Fig. 4), the concentration of phosphate buffer used (Fig. 5), the concentration of TBAHS used (Fig. 6), and the pH (Fig. 7) had a major effect on retention characteristics of the adenine nucleotides. The pH selected for the mobile phase did not significantly alter the peak retention characteristics of the column, even after four months of continuous use ($>$ 1000 sample injections).

TABLE I

THE CHANGE IN PLASMA CONCENTRATION OF ADENOSINE (ADE), ADENOSINE MONOPHOSPHATE (AMP), ADENOSINE DIPHOSPHATE (ADP), AND ADENOSINE TRIPHOSPHATE (ATP) DURING PLATELET AGGREGATION

Concentrations are expressed as pmol/ml of plasma (n = 8) (mean ± S.D.).

	ADE	*AMP*	*ADP*	*ATP*
Pre-aggregation	2.4 ± 0.7	152 ± 21	<1.5	<2.5
Post-aggregation	3.1 ± 0.6	1396 ± 139*	2372 ± 212*	2601 ± 237*

* $p < 0.001$ (unpaired t test).

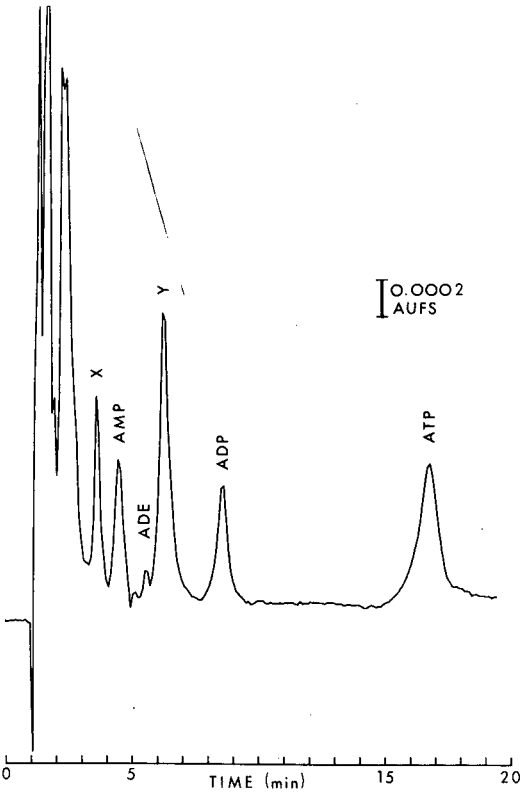

Fig. 3. Chromatogram of platelet-poor plasma, prepared from platelet-rich plasma following platelet aggregation. X and Y are unknown peaks.

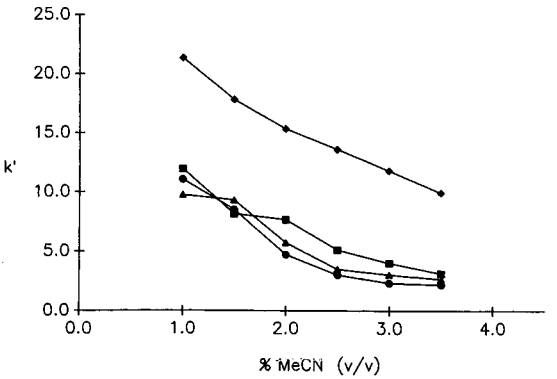

Fig. 4. Change in capacity factors (k') for ADE (▲), AMP (●), ADP (■), and ATP (◆) with variation in acetonitrile (MeCN) concentration. Other parameters were the same as in text.

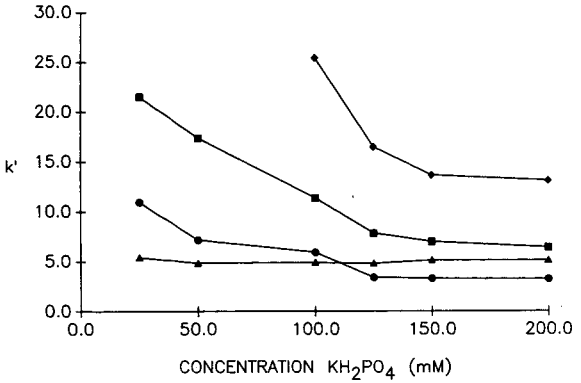

Fig. 5. Effect of potassium phosphate buffer concentration on capacity factors for ADE (▲), AMP (●), ADP (■), and ATP (◆). Other parameters were the same as in text.

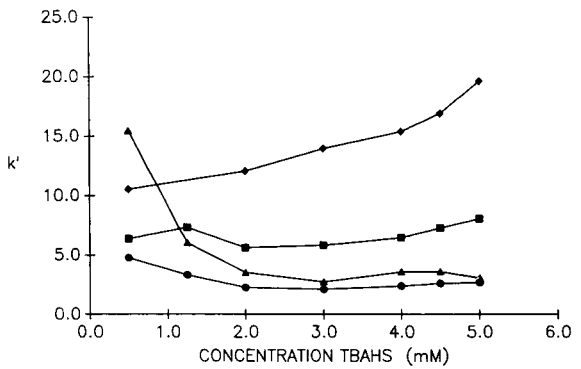

Fig. 6. Change in capacity factors for ADE (▲), AMP (●), ADP (■), and ATP (◆) with variation in TBAHS concentration. Other parameters were the same as in text.

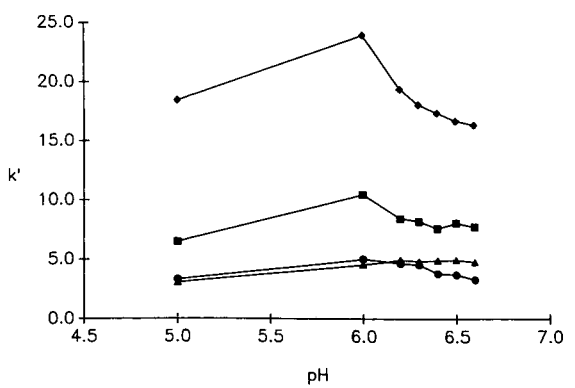

Fig. 7. Effect of pH changes on capacity factors for ADE (▲), AMP (●), ADP (■), and ATP (◆). Other parameters were the same as in text.

DISCUSSION

It is well known that application of gradient elution to routine quantitative analysis can impair reproducibility[20]. In fact, the column equilibrium between analyses easily results in peak shifting[21]. Further, these methods have limited sensitivity. Therefore, for the simultaneous measurement of ADE, AMP, ADP, and ATP, a highly sensitive isocratic reversed-phase method was developed by optimization of the condition of separation.

Tetrabutylammonium ions (TBA) bind to the stationary phase of the C_{18} column due to hydrophobic interactions of the aliphatic groups of the packing material with the butyl groups of TBA. Due to this interaction, positively charged groups arise on the stationary phase. This modulates the retention of nucleotides as a function of the number of negatively charged phosphate groups. Thus, k' tends to increase as the number of nucleotidyl phosphate groups increases (triphosphate > diphosphate > monophosphate) (Fig. 1).

An increase in TBA cation concentration increases the equilibrium concentration of TBA cations retained on the C_{18} column surface. Thus, as the concentration of TBAHS increases, the k' of ATP increases dramatically due to the association of the nucleotidyl phosphate groups with the increased number of TBA cations (Fig. 6). Below 2 m*M* TBAHS concentration, ADE showed large increases in k' due to greater hydrophobicity of the column as a result of the reduced equilibrium concentration of TBA cations retained. The k' values of AMP, ADP, and ATP do not increase substantially below 2 m*M* TBAHS, since the hydrophobic interactions with the column are reduced by the phosphate groups.

An increase in acetonitrile decreases the equilibrium concentration of TBA cations retained. This suggests a greater hydrophobic interaction of the butyl groups of the TBA cations with acetonitrile, thus decreasing the concentration of TBA on the stationary phase[22,23]. An increase in acetonitrile concentrations therefore leads to a reduction of the k' for all four compounds (Fig. 4).

Increasing the mobile-phase counter-anion concentration by addition of salt or buffer decreases the amount of nucleotide retained due to mass-action effects[22]. The degree of variation in retention is dependent on both the selectivity and concentration of the counter-anion. Therefore, increasing the concentration of potassium dihydrogenphosphate reduces the k' of all the nucleotides due to anion exchange of the dihydrogenphosphate anion with the TBA cations; effectively reducing the amount of TBA cations available for binding the nucleotidyl phosphate groups (Fig. 5).

In addition, lowering the pH reduces the k' of the nucleotides (Fig. 7). In this case, the nucleotidyl phosphate groups have a reduced interaction with the the TBA cations on the stationary phase because of partial protonation of the phosphate groups themselves.

When TEA was not added to the mobile phase, tailing of the peaks was observed, suggesting that the column was not fully endcapped. Use of 12.5 m*M* TEA decreased this effect. It is known that even after exhaustive endcapping, steric hindrance prevents derivatization of all the silanol groups. The effect of these functional groups was modified with TEA, which was routinely used in all experiments. To obtain high sensitivity, a 2.1 mm I.D. column was used. To minimize the peak broadening, the connecting tubes were kept as short as possible and the micro-bore manifold was

installed on the detector to connect the column directly to the detector cell.

The method is sensitive enough to measure nucleoside and nucleotide concentrations in 500 μl of plasma or less. Platelet-poor plasma showed non-detectable levels of ADP and ATP (Table I). With platelet aggregation, there was a marked increase in concentration of ATP, ADP, and AMP. This suggests that during platelet aggregation, all three nucleotides are released. This contrasts with previously published results[23]. However, the possibility cannot be excluded that the ADP and/or ATP released form platelets may be rapidly metabolized to produce AMP and may contribute to the observed results.

ACKNOWLEDGEMENTS

This work was supported by R01 HL 34837-03, R01 HL 39916-01 and R01 HL 39165-01. Claude R. Benedict is an Established Investigator of the American Heart Association. We wish to thank Richard Gayden for helpful comments.

REFERENCES

1 J. A. Ambrose, S. L. Winters, R. R. Arora, A. Eng, A. Riccio, R. Gorlin and V. Fuster, *J. Am. Coll. Cardiol.*, 7 (1986) 472.
2 D. C. Levin and J. T. Fallon, *Circulation*, 66 (1982) 316.
3 E. Falk, *Circulation*, 71 (1985) 699.
4 M. J. Davies and A. C. Thomas, *Br. Heart J.*, 53 (1985) 363.
5 C. T. Sherman, F. Litvack, W. Grundfest, M. Lee, A. Hickey, A. Chaux, R. Kass, C. Blanche, J. Mateloff, L. Morgenstern, W. Ganz, H. J. C. Swan and J. Forrester, *N. Engl. J. Med.*, 315 (1986) 913.
6 D. J. Fitzgerald, L. Roy, F. Catella and G. A. Fitzgerald, *N. Engl. J. Med.*, 315 (1986) 983.
7 M. A. Packham, *Thromb. Haemost.*, 40 (1978) 174.
8 G. C. White and A. A. Marouf, *J. Lab. Clin. Med.*, 97 (1981) 369.
9 M. D. Rubenstein, R. T. Wall, D. S. Bain and D. C. Harrison, *Am. Heart J.*, 102 (1981) 363.
10 C. W. Pumphrey and J. Dawes, *Am. J. Cardiol.*, 50 (1982) 1258.
11 G. A. Fitzgerald, A. K. Pedersen and C. Patrono, *Circulation*, 67 (1983) 1174.
12 A. K. Pedersen, M. L. Watson and G. A. Fitzgerald, *Thromb. Res.*, 33 (1983) 99.
13 E. Juengling and H. Kammermeier, *Anal. Biochem.*, 102 (1980) 358.
14 D. W. Nierenberg, A. L. Pogolotti, Jr. and D. V. Santi, *J. Chromatogr.*, 190 (1980) 212.
15 B. Levitt, R. J. Head and D. P. Westfall, *Anal. Biochem.*, 137 (1984) 93.
16 G. Crescentini and V. Stocchi, *J. Chromatogr.*, 290 (1984) 393.
17 G. K. Bedford and M. A. Chiong, *J. Chromatogr.*, 305 (1984) 183.
18 Z. Olempska-Beer and E. B. Freese, *Anal. Biochem.*, 140 (1984) 236.
19 J. L.-S. Au, M.-H. Su and M. G. Wientjes, *J. Chromatogr.*, 423 (1987) 308.
20 G. Lencini, E. Buzzi, M. Marcesca, M. Mazzei and A. Balbi, *Anal. Biochem.*, 165 (1987) 379.
21 N. A. Parris, *Instrumental Liquid Chromatography (Journal of Chromatography Library*, Vol. 27), Elsevier, Amsterdam, 2nd ed., 1984, p. 305.
22 P. G. Rigas and D. J. Pietrzyk, *Anal. Chem.*, 60 (1988)454.
23 A. M. Pimenov, Yu. V. Tikhonov and P. T. Toguzov, *J. Liq. Chromatogr.*, 9 (1986) 1003.
24 H. Holmsen, *Sem. Hematol.*, 22 (1985) 219.

Journal of Chromatography, 459 (1988) 291–300
Elsevier Science Publishers B.V., Amsterdam — Printed in The Netherlands

CHROMSYMP. 1421

RAPID ISOLATION OF THYMOSIN β_4 FROM THYMOSIN FRACTION 5 BY PREPARATIVE HIGH-PERFORMANCE LIQUID CHROMATOGRAPHY

MAHNAZ BADAMCHIAN*

Department of Biochemistry, The George Washington University, School of Medicine and Health Sciences, Washington, DC 20037 (U.S.A.)

M. PATRICIA STRICKLER and M. JUDE STONE

Waters Chromatography Division, Millipore Corporation, Life Science Application Laboratory, Fairfax, VA 22030 (U.S.A.)

and

ALLAN L. GOLDSTEIN

Department of Biochemistry, The George Washington University, School of Medicine and Health Sciences, Washington, DC 20037 (U.S.A.)

SUMMARY

We have developed a rapid, efficient, and reproducible two-step method for the purification of thymosin β_4 (Tβ_4) from thymosin fraction 5 (TF5). This purification is based on the use of high-performance preparative/semi-preparative and analytical reversed-phase (Delta-Pak C_{18}) chromatographic columns. Sodium dodecyl sulfate-polyacrylamide gel electrophoresis and amino acid compositional analysis have shown that natural, purified Tβ_4 is identical to synthetic Tβ_4. This procedure can be used to isolate other biologically active peptides from TF5 in sufficient quantity for characterization.

INTRODUCTION

A partially purified thymosin preparation from calf thymus termed "thymosin fraction 5" (TF5)[1] has been studied extensively for biological activity[2–8], and in clinical trials[9–13]. TF5 has been shown to modulate several *in vivo* and *in vitro* immune responses[13,14]. TF5 consists of a family of biologically active polypeptide components with hormone-like activities. Thymosin β_4 (Tβ_4) is one of several peptides that is present in TF5 and participates in the process of regulation, differentiation, and function of thymus-dependent thymocytes. Tβ_4 has been isolated from TF5 and completely characterized. Tβ_4 is composed of 43 amino acid residues and has a molecular weight of 4982 and p*I* of 5.1. The amino-terminus of the peptide is blocked by an acetyl group[14]. Tβ_4 has been purified from TF5 by conventional column techniques for large-scale purification using ion-exchange chromatography on a carboxymethyl-cellulose column, followed by gel chromatography on Sephadex G-50 in 6 *M* guanidinium chloride. The desalted Tβ_4 on Sephadex G-10 had a yield of 0.45%[15]. Tβ_4 has also been isolated by high-performance liquid chromatographic (HPLC)

0021-9673/88/$03.50

techniques for analytical purposes, using a μBondapak C_{18} column[16] with a recovery of 2–3%. Low recoveries have always been a problem in the isolation of TF5 peptides and have limited the amount of purified peptide available for further characterization and comparison of the different forms of the biologically active peptides. In the present study, we report a very fast, reproducible, and efficient large-scale isolation procedure as well as an analytical reversed-phase HPLC (RP-HPLC) procedure for the purification of $T\beta_4$ from TF5.

EXPERIMENTAL

Materials

Clinical-grade TF5 (Lot C114080-02) and synthetic $T\beta_4$ were provided as a gift from Alpha One Biomedicals (Washington, DC, U.S.A.). Delta-Pak C_{18} columns and chemicals for the Pico-Tag system were from Waters Chromatography Division of Millipore (Milford, MA, U.S.A.). Water for HPLC was purified with a Milli-Q water system (Millipore, Bedford, MA, U.S.A.) sodium dodecylsulfate-polyacrylamide gel electrophoresis (SDS-PAGE) chemicals were of molecular-biology grade and were purchased from Sigma (St. Louis, MO, U.S.A.). The SDS low-molecular-weight protein standards and silver-stain kit were purchased from Bio-Rad Lab. (Richmond, CA, U.S.A.). All buffers and solvents were of HPLC grade (Fisher Scientific, Pittsburgh, PA, U.S.A.). All HPLC solutions were filtered through a 0.45-μm membrane (Millipore) prior to use.

HPLC Methods

Optimization of reversed-phase chromatographic conditions for the fractionation of TF5 was carried out on a Model 600 HPLC system (Waters), equipped with a Model 490 multi-wavelength detector set at 280 nm and a 300 mm × 3.9 mm I.D. Delta-Pak, 300-Å, 15-μm, C_{18} column (Waters). Eluent A was 0.02 *M* ammonium acetate, (pH 6.8); eluent B was acetonitrile. A 60-min linear gradient from 0 to 80% B was run at a flow-rate of 0.5 ml/min. The sample was 900 μg of TF5, dissolved in the initial buffer.

Preparative-scale reversed-phase chromatography of TF5 (1.5 g) was performed on a Delta-Prep HPLC system (Waters), equipped with a Model 481 variable-wavelength detector with a semi-preparative flow-cell, set at 280 nm, and a 300 mm × 50 mm I.D. Delta-Pak, 300 Å, 15-μm C_{18} column (Waters). Eluent A was 0.02 *M* ammonium acetate (pH 6.8), and eluent B was acetonitrile. A 60-min linear gradient from 0 to 80% B was run at a flow-rate of 80 ml/min. TF5 was dissolved in eluent A and applied to the column through a port in the solvent delivery system. Fractions of 1 min were collected, and a 1-ml aliquot was used for radioimmunoassay (RIA).

Semi-preparative reversed-phase HPLC of an aliquot of a $T\beta_4$-active fraction No. 20 (5.6 mg) from the preparative separation, was carried out on a Model 600 HPLC system 1 equipped with a Model 490 multi-wavelength detector, set at 214 nm, and a 150 mm × 3.9 mm Delta-Pak, 300 Å, 5-μm C_{18} column (Waters). Eluent A was 0.1% phosphoric acid in water, and eluent B was acetonitrile containing 0.1% phosphoric acid. Separation of $T\beta_4$ was achieved with a 10-min linear gradient from 0 to 14% B, followed by a 10-min hold at 14% B and a 10-min linear gradient to 18% B at a flow-rate of 1 ml/min. Fractions of 1 min were collected and assayed by RIA for

Tβ_4. The peak of immunoreactive Tβ_4 (fraction 33, 100 μl) was diluted with 100 μl of water and rechromatographed under the same conditions. One half minute fractions were collected. Fractions 33 and 33.5, collected from this separation were pooled, reduced to a volume of 250 μl, diluted with 250 μl of water, and rechromatographed similarly. The peak was collected and subjected to amino acid analysis and SDS-PAGE.

A crude mixture, containing synthetic Tβ_4 (50 μg) was also chromatographed on the 5-μm Delta-Pak C_{18} column under the conditions described above. The major peak (33.5 min) was identified as Tβ_4 by RIA. Data from all the chromatographic procedures was collected with a Model 840 chromatography workstation (Waters).

Gel electrophoresis

SDS-PAGE was performed according to the method of Laemmli[17]. Tβ_4 samples were incubated at 90°C for 5 min before gel electrophoresis. Proteins were visualized by silver staining with the Bio-Rad silver-stain kit.

Amino acid analysis

This procedure was performed with the Pico-Tag amino acid analysis system of Waters-Millipore. The method is based on the formation of a phenylthiocarbamyl (PTC) derivative of the amino acids from acid-hydrolyzed proteins. The Tβ_4 samples (about 5–10 μg) were hydrolyzed in 200 μl of a constant-boiling hydrochloric acid atmosphere, containing 1% (v/v) phenol, at 110°C for 48 h in the Pico-Tag work station. The hydrolysates were dried and the amino acids were derivatized with phenylisothiocyanate (PITC) for 20 min at room temperature to yield the corresponding PTC derivatives[18]. These derivatives were analyzed with the Pico-Tag amino acid analysis system, which had been previously calibrated with a standard mixture of amino acids.

Protein determinations

Protein was estimated by the method of Lowry *et al.*[19] with bovine serum albumin (BSA) as standard in the case of crude preparations, and by amino acid analysis in the case of highly purified samples.

Radioimmunoassay

The RIA for Tβ_4 was performed according to the method of Naylor *et al.*[20]. Fractions collected from the HPLC separation were lyophilized and resuspended in 1 ml HPLC-grade water, and aliquots of these fractions were used for the RIA. RIA buffer (0.01 *M* sodium phosphate buffer (pH 7.4.), containing 0.165 *M* sodium chloride, 0.05% sodium azide, 0.01 m*M* EDTA, and 0.1% BSA was added to each tube to bring the volume to 400 μl. A 50-μl aliquot of stock antiserum and 50 μl of tracer-labeled tyrosine (Tyr^1–C13–Tβ_4) were added to each tube. The tubes were mixed in a vortex mixer and incubated for 24 h at 4°C. Separation of free from bound tracer was carried out by the addition of 50 μl of goat anti-rabbit IgG in 0.5 *M* phosphate buffer solution. After mixing, the tubes were incubated overnight at 4°C. The immunoprecipitates were pelleted by centrifugation at 1500 *g* for 25 min at 4°C. The supernatants were aspirated and discarded, and the radioactivity in the immunoprecipitates was measured in an automatic Beckman Gamma 4000 spectrometer (Columbia, MD, U.S.A.).

RESULTS AND DISCUSSION

The primary goal of our ongoing thymosin research program is to develop a rapid and efficient method for the isolation of the TF5 peptides. The isolated peptides will then be further characterized and their individual biological functions will be determined. In the present study, separation of thymic peptides in TF5 was carried out by RP-HPLC on the Delta-Pak columns.

Fig. 1 shows an analytical RP-HPLC separation of TF5. TF5 (900 μg) was fractionated on a 300 mm × 3.9 mm I.D. Delta-Pak, 300-Å, 15-μm C_{18} column under the conditions described in *HPLC methods*. Under these conditions many peptides were eluted as distinct peaks in the first half of the chromatogram, whereas a broad heteregeneous peak was eluted in the second half of the chromatogram. We were unable to improve the resolution of the 30–60 min region of TF5 by using different chromatographic conditions and HPLC columns, *e.g.*, ion-exchange, reversed-phase, size exclusion, chromatography, etc. (results are not shown). However, the fractionation of TF5 on the Delta-Pak, 300-Å, 15-μm C_{18} column generated the greatest number of peptide peaks compared to all other HPLC columns we have tried. Therefore, the Delta-Pak C_{18} column was selected as the initial step for the fractionation of TF5 peptides.

Preparative scale-up isolation of Tβ_4 from TF5 was achieved with a 300 mm × 50 mm I.D. preparative Delta-Pak 300-Å, 15-μm C_{18} column (Fig. 2). This was the initial step used for the fractionation of all the peptides in TF5. Isolation of Tβ_4 from this preparative chromatogram can be used as an example of the further isolation of new TF5 peptides. The RIA analysis of the fractionated TF5, as shown in Fig. 2,

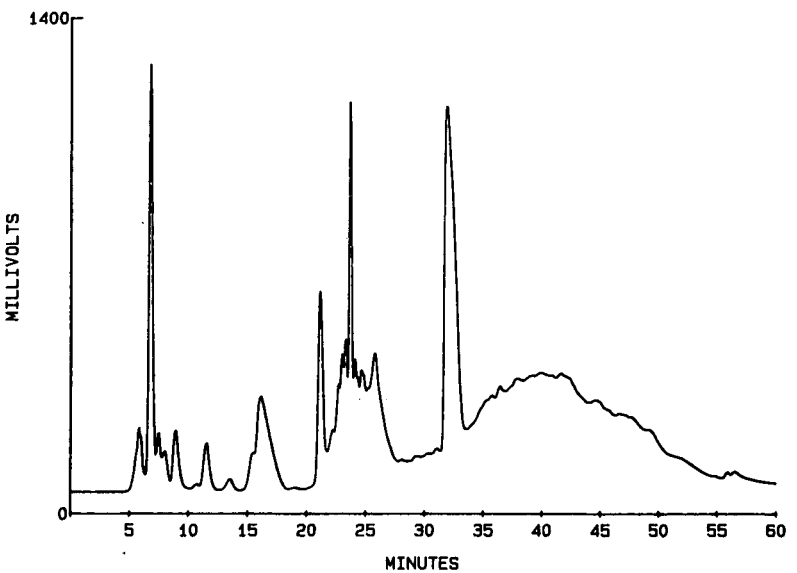

Fig. 1. RP-HPLC separation of 900 μg of TF5 on a 300 mm × 3.9 mm I.D. Delta-Pak, 300 Å. 15-μm, C_{18} column. Eluent A was 0.02 *M* ammonium acetate, (pH 6.8), and eluent B was acetonitrile. A 60-min linear gradient from 0 to 80% B was run at a flow-rate of 0.5 ml/min. Detection, 280 nm, 1.4 a.u.f.s.

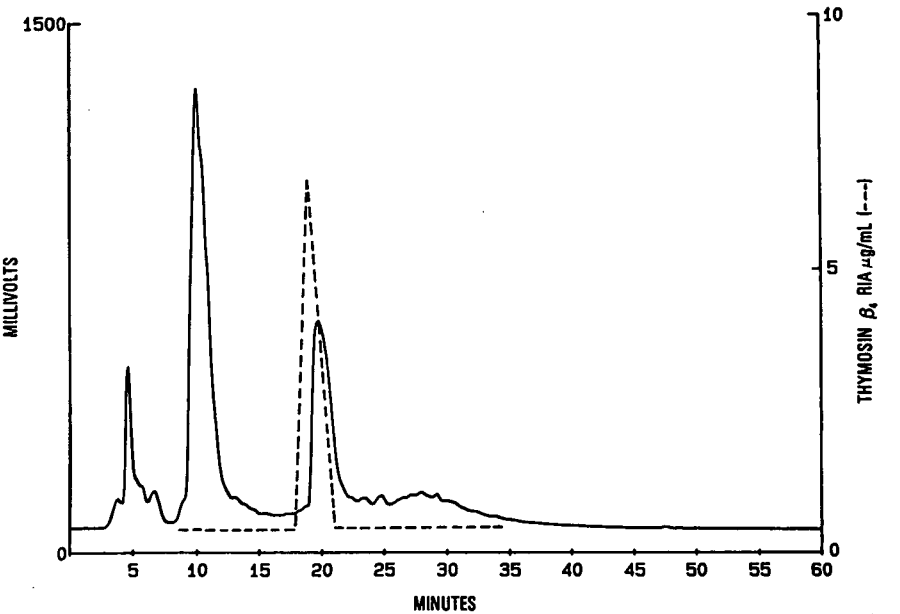

Fig. 2. RP-HPLC separation of 1.5 g of TF5 on a 300 mm × 50 mm I.D. Delta-Pak, 300-Å, 15-µm, C_{18} column. Eluent A was 0.02 *M* ammonium acetate, (pH 6.8) and eluent B was acetonitrile. A 60-min linear gradient from 0 to 80% B was run at a flow-rate of 80 ml/min. Detection, 280 nm at 1.5 a.u.f.s. Fractions were assayed for Tβ_4 by RIA. Results are superimposed on the chromatogram.

indicated that immunoreactive Tβ_4 was eluted between 18 and 21 min. Fraction 20 (F20) was used for further purification.

Optimal separation conditions for the F20 peptides were determined with a 150 mm × 3.9 mm I.D. analytical Delta-Pak, 300-Å, 5-µm, C_{18} column (Fig. 3). Our results indicated that the major peptide peak from the chromatographic separation of F20 was Tβ_4 (peak 1). When synthetic Tβ_4 was chromatographic under the same conditions, the major Tβ_4 peak had a retention time identical to that of peak 1 (results not shown). This chromatographic step can also be used for the identification and isolation of Tβ_4 for analytical purposes.

F20 (5.6 mg) from the preparative separation (Fig. 2) was further fractionated on a 150 mm × 3.9 mm I.D. Delta-Pak, 300 Å 5-µm, C_{18} column under the conditions described previously in *HPLC methods*. As shown in Fig. 4, the scale-up isolation of Tβ_4 from F20 did not lead to appreciable loss in resolution. The RIA analysis of the fractions indicated that the major peptide peak at a retention time of 33 min was Tβ_4. Rechromatography of immunoreactive fractions 32–34 under similar conditions revealed a single major peptide peak for fraction 33, (Fig. 5), and the presence of several minor contaminants. The other fractions (not shown) contained much less Tβ_4. Fraction 34 was contaminated by the shouldering peak shown on peak 1 in Figs. 3 and 4. Therefore, fractions 33 and 33.5 (from the rechromatography of fraction 33) were pooled, rechromatographed and used as the final Tβ_4 preparation for SDS-PAGE and amino acid composition analysis.

An estimate of the homogeneity of the isolated Tβ_4 was obtained by RP-HPLC. As shown in Fig. 6, the isolated Tβ_4 from TF5 (natural Tβ_4) gave a homogeneous

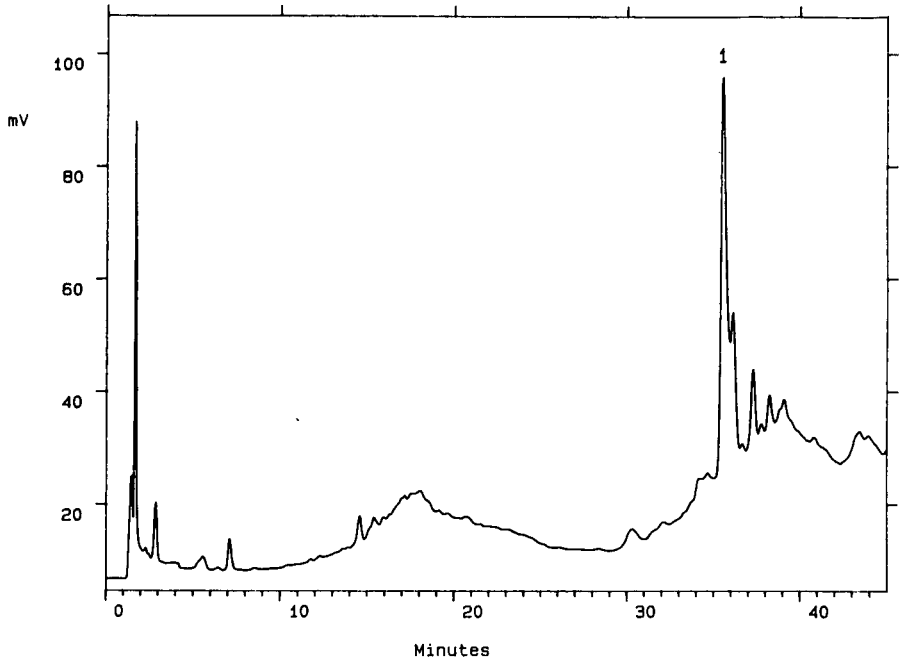

Fig. 3. RP-HPLC separation of 130 μg of fraction 20 from the 1.5 g separation of TF5 on a 150 mm × 3.9 mm I.D. Delta-Pak, 300-Å, 5-μm, C_{18} column. Eluent A was 0.1% phosphoric acid and eluent B was acetonitrile containing 0.1% phosphoric acid. Separation of Tβ_4 was achieved by a 10-min linear gradient to 14% B, followed by a 10-min hold at 14% B and a 10 min-gradient to 18% B. The flow-rate was 1 ml/min. Detection at 214 nm, 0.1 a.u.f.s.

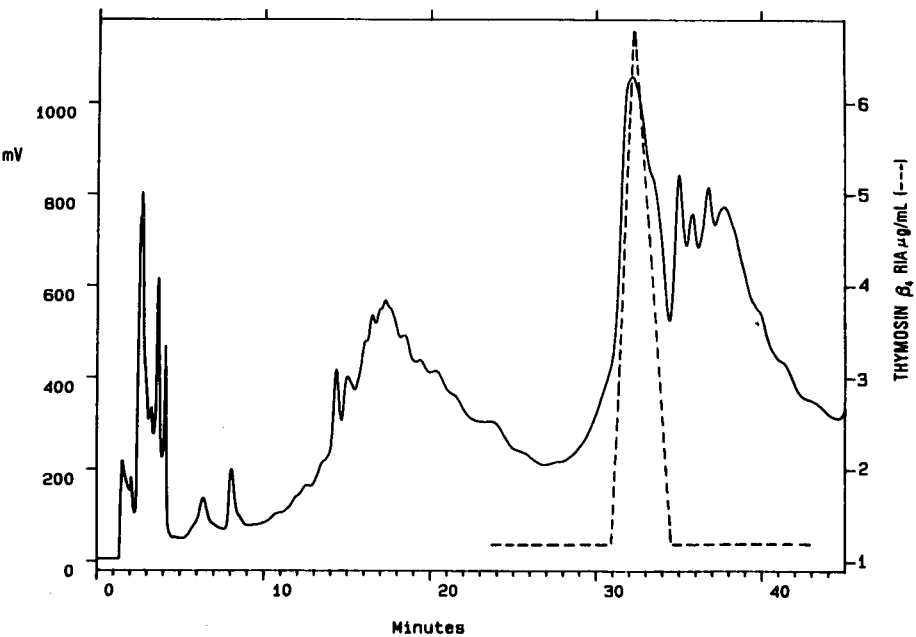

Fig. 4. RP-HPLC separation of 5.6 mg of fraction 20 from the 1.5 g separation of TF5 on a 150 mm × 3.9 mm I.D. Delta-Pak, 300-Å, 5-μm, C_{18} column, under the conditions described in Fig. 3. Detection, 214 nm, 1 a.u.f.s. Collected fractions were assayed for Tβ_4 by RIA. Results are superimposed on the chromatogram.

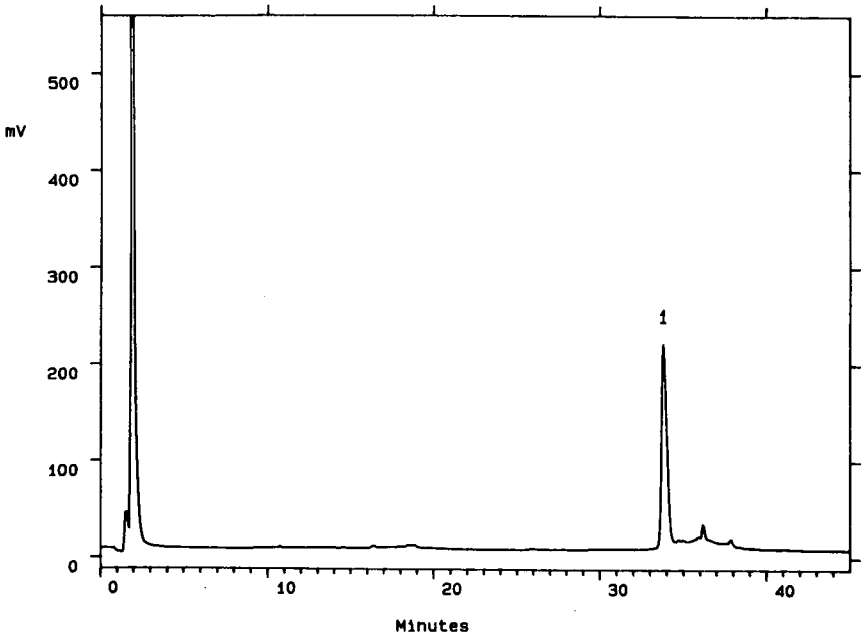

Fig. 5. Rechromatography of 100 μl of fraction 33 from the preparative separation of fraction 20. The sample was diluted with 100 μl of water and injected into the 150 mm × 3.9 mm I.D. Delta-Pak, 300-Å, 5-μm, C_{18} column, under the conditions described in Fig. 3. Detection, 214 nm, 0.5 a.u.f.s.

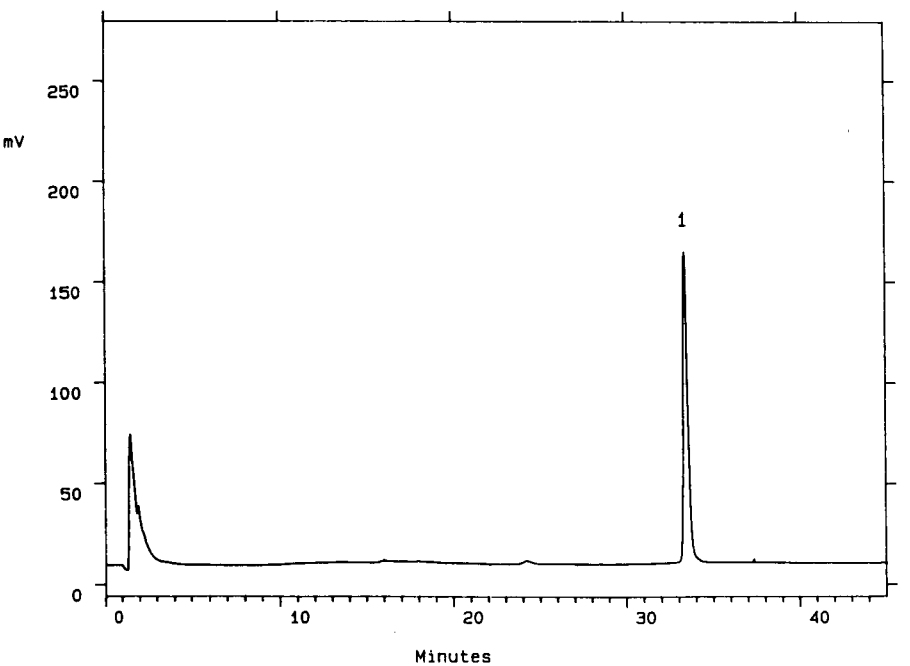

Fig. 6. Rechromatography of fractions 33 and 33.5 (from the purification of fraction 33). The sample was concentrated to 250 μl, diluted with water, and injected into the 150 mm × 3.9 mm I.D. Delta-Pak, 300-Å, 5-μm, C_{18} column, under the conditions described in Fig. 3. Detection, 214 nm, 0.5 a.u.f.s.

peak. Fig. 7 shows the comparison of the purified natural Tβ_4 by the two-step RP-HPLC procedure and the crude synthetic Tβ_4. Results indicate that natural and synthetic Tβ_4 have identical retention times.

SDS-PAGE analysis of the natural and HPLC purified synthetic Tβ_4, illustrated in Fig. 8, was carried out as described in *HPLC methods*. When the protein bands on SDS gels were initially stained with Coomassie Blue R-250, only a very faint band of Tβ_4 was evident. When the gel was then processed with the more sensitive silver stain, a single identical protein band with a low molecular weight was evident for both natural and synthetic Tβ_4 samples. Gel electrophoresis of Tβ_4 has in the past always been done by isoelectric focusing (IEF) using relatively huge amounts of Tβ_4 (200 μg). In addition, the Tβ_4 band on IEF gels was only visible during the fixing step of the gel by using 20% trichloroacetic acid, and it disappeared during subsequent staining and destaining procedures[10]. The SDS-PAGE and staining procedure used for the Tβ_4 peptide has two advantages over the previously reported IEF method: (1) it requires 10 times less protein and (2) the stained Tβ_4 band is intense and stable.

Amino acid analysis of the purified synthetic and natural Tβ_4 are shown in Tabel I. Our results indicate that the synthetic and purified natural Tβ_4 have the identical amino acid composition.

In summary, we were able to purify Tβ_4 from TF5 in a two-step RP-HPLC procedure. The presence of Tβ_4 was followed by RIA and HPLC retention time. In the first step of the purification the fractions containing Tβ_4 (18–21) were identified in the RIA. In the second step only F20 was selected for further purification. Fractions

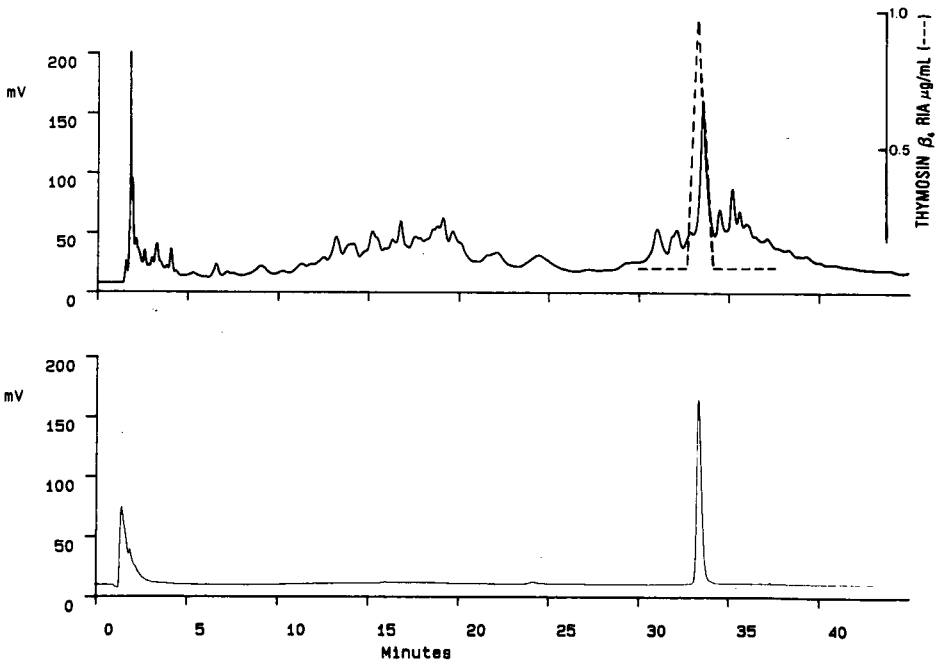

Fig. 7. Comparison of 50 μg of crude synthetic Tβ_4 and Tβ_4 isolated by the two-step RP-HPLC procedure on the 150 mm × 3.9 mm I.D. Delta-Pak, 300-Å, 5-μm column with the gradient described previously (Fig. 3). The synthetic Tβ_4 was identified by RIA, and the results are superimposed on the chromatogram.

TABLE I

AMINO ACID COMPOSITION OF NATURAL AND SYNTHETIC THYMOSIN β_4

Amino acid analysis was performed with a Pico-Tag amino acid analysis system. About 10-μg samples of synthetic and isolated Tβ_4 were hydrolyzed with 6 *M* hydrochloric acid, containing 1% (v/v) phenol at 110°C for 48 h. The hydrolysates were dried and used for amino acid analysis by the Pico-Tag standard procedure[18]. The data are presented as assumed numbers of residues per molecule.

Amino acid	*Synthetic Tβ_4*	*Natural Tβ_4*	*From reported sequence**
Asp	3.9	3.8	4
Glu	10.8	10.6	11
Ser	3.5	3.8	4
Gly	1.1	1.2	1
Thr	2.8	3.2	3
Ala	2.2	1.8	2
Pro	2.9	2.9	3
Met	0.8	0.7	1
Ile	1.6	1.9	2
Leu	1.6	2.2	2
Phe	0.9	0.8	1
Lys	8.5	8.6	9

* Number of residues obtained from the reported sequence result[14].

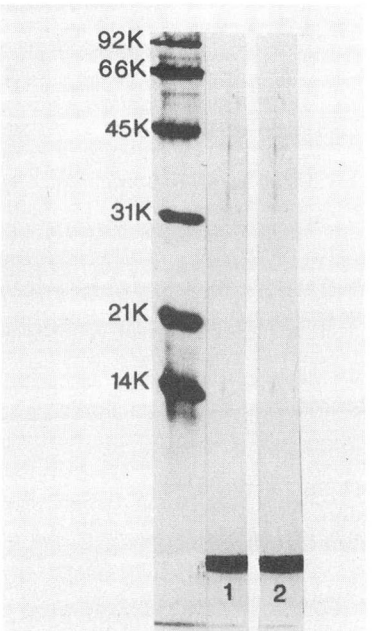

Fig. 8. SDS-PAGE of synthetic and isolated Tβ_4. About 10–20 μg of Tβ_4 samples were electrophoresed on a 1.5-mm 12% SDS-polyacrylamide gel according to the method of Laemmli[17] and stained with silver stain. Lanes 1 and 2, synthetic and natural Tβ_4, respectively. On the left are standard proteins. K = Kilodalton.

32–34 from F20 were immunoreactive. However, only the peak of immunoreactivity, (fraction 33), was used for further purification and analysis. From fraction 33 we obtained 5.1 mg of Tβ_4 which correlates well with 5.4 mg calculated by RIA. The mass recovery of Tβ_4 from F20 was greater than 80% as calculated by the peak area of Tβ_4 compared to the peak area of an HPLC purified synthetic β_4 standard. More Tβ_4 could be obtained from the other immunoreactive fractions (18, 19 and 21) from the preparative separation of TF5. Our goal, however, was to develop a simple procedure for the isolation of biologically active peptides from TF5 in sufficient quantity for characterization. The isolation of Tβ_4 is presented as an example.

ACKNOWLEDGEMENTS

This research was supported in part by a grant CA24974 from National Cancer Institute and by a gift from Alpha 1 Biomedicals.

REFERENCES

1 J. A. Hooper, M. C. McDaniel, G. B. Thurman, G. H. Cohen, R. S. Schulof and A. L. Goldstein, *Ann. N.Y. Acad. Sci.*, 249 (1975) 125.
2 G. B. Thurman, A. Ahmed, D. M. Strong, M. E. Gershuim, A. D. Steinberg and A. L. Goldstein, *Transplant. Proc.*, 7 (1975) 299.
3 J. F. Back, M. Dardenne, A. L. Goldstein, A. Guha and A. White, *Proc. Natl. Acad. Sci. U.S.A.*, 68 (1971) 2734.
4 M. J. Dauphinee, N. Talal, A. L. Goldstein and A. White, *Proc. Natl. Acad. Sci. U.S.A.*, 71 (1974) 2637.
5 M. Zisblatt, A. L. Goldstein, F. Lilly and A. White, *Proc. Natl. Acad. Sci. U.S.A.*, 66 (1970) 1170.
6 M. A. Hardy, M. Zisblatt, N. Levine, A. L. Goldstein, F. Lilly and A. White, *A. Transplant. Proc.*, 3 (1971) 926.
7 B. A. Khaw and A. H. Rule, *Br. J. Cancer*, 28 (1973) 288.
8 M. A. Scheinberg, A. L. Goldstein and E. S. Cathcart, *J. Immunol.*, 116 (1976) 156.
9 D. W. Ward, A. L. Goldstein, W. Doyle and A. Ammann, *N. Engl. J. Med.*, 292 (1955) 70.
10 A. L. Goldstein, G. H. Cohen, J. L. Rossio, G. B. Thurman, J. T. Ulrich and C. N. Brown, *Med. Clin. North Am.*, 60 (1976) 591.
11 L. A. Schafer, A. L. Goldstein, J. U. Gutterman and E. M. Hersh, *Ann. N.Y. Acad. Sci.*, 277 (1976) 607.
12 L. A. Schafer, J. U. Gutterman, E. M. Hersh, G. M. Mavligit and A. L. Goldstein, in S. O. Chirigos and A. Michael (Editors), *Progress in Cancer Research and Therapy*, Vol. 2, Raven Press, New York, 1977, p. 329.
13 A. L. Goldstein, T. L. K. Low, G. B. Thurman, M. M. Zatz, N. Hall, J. Chen, S. K. Hu, P. B. Naylor and J. E. McClure, *Recent Prog. Horm. Res.*, 37 (1981) 369.
14 T. L. K. Low, S. K. Hu and A. L. Goldstein, *Proc. Natl. Acad. Sci. U.S.A.*, 78 (1981) 1166.
15 T. L. K. Low and A. L. Goldstein, *J. Biol. Chem.*, 257 (1982) 1000.
16 T. L. K. Low and R. C. Mercer, *J. Chromatogr.*, 301 (1984) 221.
17 U. K. Laemmli, *Nature (London)*, 227 (1970) 680.
18 B. A. Bidlingmeyer, S. A. Cohen and S. L. Tarvin, *J. Chromatogr.*, 336 (1984) 93.
19 O. H. Lowry, N. J. Rosebrough, A. L. Farr and R. J. Randall, *J. Neurochem.*, 12 (1985) 253.
20 P. H. Naylor, J. E. McClure, B. L. Spangelo, T. L. K. Low and A. L. Goldstein, *Immunopharmacology*, 7 (1984) 9.

Journal of Chromatography, 459 (1988) 301–311
Elsevier Science Publishers B.V., Amsterdam — Printed in The Netherlands

CHROMSYMP. 1494

DETERMINATION OF NOSCAPINE AND ITS METABOLITES IN PLASMA BY COUPLED-COLUMN LIQUID CHROMATOGRAPHY

MARGARETA JOHANSSON, AGNETA TUFVESSON ALM, HEIDI FORSMO-BRUCE and SVEN JACOBSSON

ACO Läkemedel AB, Research and Development Dept., Box 3026, S-171 03 Solna (Sweden)

and

DOUGLAS WESTERLUND

Department of Analytical Pharmaceutical Chemistry, Uppsala University, Biomedical Center, P.O. Box 574, S-751 23 Uppsala (Sweden)

SUMMARY

Noscapine, narcotoline and cotarnine were quantified in deproteinized plasma samples by using a coupled-column liquid chromatographic system. The drug and the metabolites were first separated into two groups on a short polar precolumn (–CN) with an acidic mobile phase, containing a low content of acetonitrile. The metabolites were transferred to a hydrophobic analytical column (C_{18}) and separated with a mobile phase containing a counter ion and a co-ion in an acidic buffer with an high acetonitrile content. Noscapine was transferred to another hydrophobic analytical column (C_{18}) with a mobile phase containing a counter ion in an acidic buffer with an high acetonitrile content. Ultraviolet detection at 310 nm was used for all three compounds. The limits of quantitation were 9 ng/ml for noscapine, 13 ng/ml for cotarnine and 20 ng/ml for narcotoline. The within-day precisions were better than 6% (relative standard deviation), and the absolute recoveries were above 82%.

INTRODUCTION

Noscapine is a centrally active antitussive agent. The metabolism of the drug is not known in detail, but a few demethylated metabolites have been identified, *e.g.*, narcotoline[1], cotarnine, hydrocotarnine and meconine[2,3]. Plasma levels of noscapine have previously been determined using normal phase[4] or reversed-phase liquid chromatography[4–6]. The metabolites have been identified only in urine[2,3] and in rat liver microsomes[7].

In recent years the use of coupled columns for the analysis of drugs in biological material has increased rapidly[8,9]. The technique increases the sample throughput by minimizing the sample clean-up and by permitting automation[10]. Furthermore, it is an alternative to gradient elution for the determination of compounds with different polarities, *e.g.*, a drug and its metabolites[11,12].

Coupled-column systems, based on ion-pairing principles, have been evaluated

0021-9673/88/$03.50

for noscapine, narcotoline and cotarnine[13,14]. In this study the most suitable of the previous systems was applied to the quantitation of noscapine and its metabolites in plasma. The aims were to make the sample-work up as simple as possible, to develop a method with high reliability and to achieve the necessary selectivity and sensitivity.

EXPERIMENTAL

Chemicals

Noscapine base was obtained from Macfarlan Smith (Edinburgh, U.K.), cotarnine chloride dihydrate from EGA-Chemie (Albuch, F.R.G.) and narcotoline from Diosynth-Apeldorn (Oss, The Netherlands). The sodium salt of dodecyl sulphate (DDS) was obtained from Eastman Kodak (Rochester, NY, U.S.A.) and N,N-dimethyl-N-octylamine (DMOA) from ICN Pharmaceuticals (Plainview, NY, U.S.A.). The perchloric acid (suprapure quality) and the buffer substances (analytical quality) were obtained from Merck (Darmstadt, F.R.G.). The water in the precolumn mobile phase and the acetonitrile was of HPLC quality and obtained from Merck. The water used in the analytical column mobile phases was purified in a Milli-Q apparatus (Millipore, Bedford, MA, U.S.A.).

Apparatus

The liquid chromatographic system consisted of a Kontron Tracer MCS, 670 valve switching unit, with a Tracer timer 210 (Kontron, Zürich, Switzerland). The pumps were LKB 2150 (LKB, Bromma, Sweden) and Waters M-6000A (Waters Assoc., Milford, MA, U.S.A.). The samples were injected with a Waters WISP 710 B automatic injector. Noscapine was detected at 310 nm with a LDC/Milton Roy SM 4000 (Laboratory Data Control, Riviera Beach, FL, U.S.A.), narcotoline and cotarnine at 310 nm with a Spectroflow 783 (Kratos Analytical, Ramsey, NJ, U.S.A.). The output signal from the UV detectors was connected to two Shimadzu C-R3A-integrators (Shimadzu, Kyoto, Japan).

Liquid chromatographic system

The chromatographic system is shown in Fig. 1. The precolumn was a Brownlee Spheri-5 CN (30 mm × 4.6 mm, 5 μm; Brownlee Labs., Santa Clara, CA, U.S.A.) with a mobile phase containing 6–10% (v/v) of acetonitrile in a phosphate buffer (pH 2; ionic strength, $I = 0.05$). The analytical column for the metabolites was a laboratory-packed Nucleosil C_{18} (100 mm × 4.6 mm, 3 μm, Macherey-Nagel, Düren, F.R.G.) with a mobile phase containing 2 m*M* DDS–0.1 m*M* DMOA in a 35% (v/v) solution of acetonitrile in phosphate buffer (pH 2, $I = 0.05$). The analytical column for noscapine was a Spherisorb ODS-2 (100 mm × 4.6 mm, 3 μm; Phase Separations, Queensferry, U.K.) with a mobile phase containing 3 m*M* DDS in a 40% (v/v) solution of acetonitrile in phosphate buffer (pH 2, $I = 0.05$). An enrichment column for noscapine was inserted in the backflush mode in a switching valve between the precolumn and the analytical column. The enrichment column (20 mm × 3.8 mm) was laboratory-packed by the slurry technique with Spherisorb ODS-2, 3 μm. The flow-rate was always 1 ml/min. A single-column system was used for evaluation of the absolute recoveries of the protein precipitation. This column was a Spherisorb Ph (250 mm × 4.6 mm, 5 μm) with a mobile phase containing 32.5% (v/v) acetonitrile in phosphate buffer (pH 2, $I = 0.05$). The eluate was monitored at 310 nm.

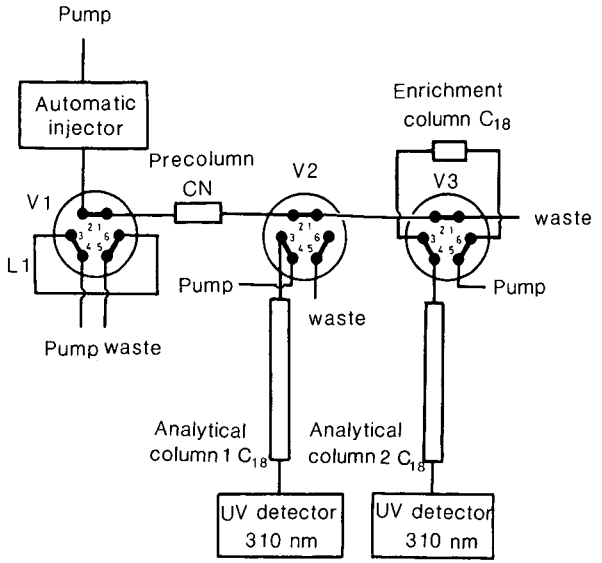

Fig. 1. Scheme of the chromatographic system. Chromatographic conditions: precolumn, Brownlee CN (5 μm, 30 mm × 4.6 mm); analytical column 1, Nucleosil C_{18} (3 μm, 100 mm × 4.6 mm); analytical column 2, Spherisorb ODS-2 (3 μm, 100 mm × 4.6 mm); enrichment column, Spherisorb ODS-2 (3 μm, 20 mm × 3.8 mm); precolumn eluent, 6–10% (v/v) acetonitrile in phosphate buffer (pH 2); analytical column 1 eluent, 2 m*M* DDS–0.1 m*M* DMOA in 35% (v/v) acetonitrile in phosphate buffer (pH 2); analytical column 2 eluent, 3 m*M* DDS in 40% (v/v) of acetonitrile in phosphate buffer (pH 2); detection wavelength, 310 nm; injection volume, 500 μl.

Column switching

Noscapine and the metabolites were first separated into two fractions on the precolumn. The metabolites were transferred to analytical column 1 for further separation. Noscapine was enriched on a short (C_{18}) column before being backflushed to analytical column 2. Between injections, the precolumn was cleaned by creating a step gradient of acetonitrile. A mixture of 50% (v/v) acetonitrile in phosphate buffer (pH 2, $I = 0.05$) was pumped into the loop (1.6 ml) through valve 1 with the pump in the Kontron unit. By switching the valve, the gradient was created. The timetable of the switching events is given as Table I.

Sample preparation

Plasma (1.000 ml) was mixed carefully with acetonitrile (0.125 ml) and perchloric acid (0.250 ml). The samples were centrifuged at 5000 rpm for 10 min. Then, the supernatant (0.800 ml) was adjusted to about pH 3, using 0.380 ml of a solution containing 1 *M* trisodium citrate and 5 *M* sodium hydroxide (1:4). A 500-μl sample was injected into the precolumn.

Mass spectrometry

Mass spectra were recorded in the electron impact (EI) (70 eV) or chemical ionization (CI) (ammonia) mode, using a Shimadzu QP 1000 mass spectrometer, equipped with a direct inlet probe. The probe temperature was programmed from

TABLE I

SWITCHING EVENTS

Time	*Valve*	*Event*
0		Plasma sample is injected
0.9 A*	V_2 on	Precolumn and analytical column 1 are connected in series and narcotoline and cotarnine are enriched on the top of analytical column 1
B**	V_2 off	Precolumn and analytical column 1 are disconnected. Elution of the metabolites starts
0.9 C***	V_3 on	Precolumn and enrichment column are connected in series and noscapine is enriched
D§	V_3 off	Enrichment column and analytical column are connected
D§ + 1.0	Kontron pump on	Loop is filled with 50% acetonitrile in acidic buffer
D§ + 1.6	Kontron pump off	
D§ + 2.1	V_1 on	Precolumn is purified with acetonitrile in acidic buffer
D§ + 3.6	V_1 off	Regeneration of the precolumn is completed

* A = Time for the start of the metabolite fraction, *e.g.*, 2.0 min.
** B = Time for the end of the metabolite fraction, *e.g.*, 3.5 min.
*** C = Time for the start of the noscapine fraction, *e.g.*, 6.0 min.
§ D = Time for the end of the noscapine fraction, *e.g.*, 8.5 min.

room temperature to 250°C at a rate of 40°C/min. The mass was scanned from *m/z* 40 to 450 (EI) and from *m/z* 100 to 450 (CI) with a cycle time of 4 s. Since the instrument has no direct facilities for reading the ion-source pressure, the conditions for chemical ionization were adjusted by setting the ratio of *m/z* 18:*m/z* 35 to approximatively 3:1. The presence of N-demethylated noscapine in the collected fraction was monitored by selected ion monitoring (SIM) of the ions *m/z* 191, 193 and 206 for the EI mode, and *m/z* 195, 204, 206 and 212 for CI mode. The time for collecting the N-demethylated fraction from the liquid chromatographic system was decided by UV monitoring at 310 nm. Four fractions, each containing about 180 ng, were collected and pooled. Then the pH was adjusted to about 8, using sodium hydroxide, and the pooled fraction was extracted for 15 min with 1.0 ml of 1% heptafluorobutanol in dichloromethane. After centrifugation, the organic phase was extracted with two portions of 2 ml 0.01 *M* sodium hydroxide. Finally, the organic phase was evaporated, and the residue was redissolved in 10 μl dichloromethane. A 3-μl sample was evaporated at the direct probe.

RESULTS AND DISCUSSION

Sample preparation

In aqueous solution, there is a pH-dependent equilibrium between noscapine lactone and noscapine acid[15]. At low pH, the lactone form prevails, and at an high pH the acid form. At pH 7.4, the two forms will exist in equal amounts. However, in blood and in 5% (w/v) albumin solution no measurable amount of noscapine was

TABLE II

ABSOLUTE RECOVERY OF NOSCAPINE, NARCOTOLINE AND COTARNINE AFTER ADDITION OF VARYING VOLUMES OF ACETONITRILE TO PLASMA BEFORE PROTEIN PRECIPITATION

Work-up procedure: 1.00 ml plasma was mixed with varying volumes of acetonitrile and 0.250 ml perchloric acid (11.4 *M*).

Added volume of acetonitrile (ml)	*Absolute recovery (%)*		
	Noscapine	*Narcotoline*	*Cotarnine*
0.050	81	63	79
0.075	80	74	85
0.100	81	76	84
0.125	90	91	92
0.150	89	88	91
0.200	76	83	72

converted into noscapine acid[4]. The reason for this is probably a strong protein binding of the lactone.

Isolation of noscapine from plasma has previously been performed by liquid–liquid extraction, both in tubes and on a solid phase[4]. By using a coupled-column system, a direct injection technique can be substituted for the manual isolation procedure. In order to minimize deterioration of the precolumn, the plasma proteins were precipitated before injection. Precipitation with 1 *M* perchloric acid (1.00 ml for 1.00 ml plasma) gave only *ca.* 50% recovery. Addition of acetonitrile to plasma before precipitation with perchloric acid increased the recoveries (Table II), until a maximum was reached at 0.125 ml. Dilution of perchloric acid before precipitation decreased the absolute recoveries (Table III). The use of 11.4 *M* perchloric acid for precipitation made pH adjustment of the supernatant necessary in order to avoid degradation of the analytes. At pH 3 the compounds were stable for at least 24 h. An increase to almost quantitative recoveries (> 95%) was obtained by diluting the plasma in phosphate buffer (pH 7.4) before precipitation (Table IV). However, with this high dilution a large injection volume was necessary in order to exceed the low

TABLE III

ABSOLUTE RECOVERY OF NOSCAPINE, NARCOTOLINE AND COTARNINE USING VARYING CONCENTRATIONS OF PERCHLORIC ACID

Work-up procedure: 1.00 ml plasma was mixed with 0.125 ml acetonitrile and 0.250 ml perchloric acid.

Concentration of perchloric acid (M)	*Absolute recovery (%)*		
	Noscapine	*Narcotoline*	*Cotarnine*
1.4	57	82	79
2.8	61	91	83
5.7	76	98	89
11.4	88	99	90

TABLE IV

ABSOLUTE RECOVERY OF NOSCAPINE, NARCOTOLINE AND COTARNINE AFTER DILUTION OF PLASMA BEFORE PRECIPITATION

Work-up procedure: plasma was diluted to 1.00 ml in phosphate buffer, pH 7.4 (I = 0.2) and mixed with 0.125 ml acetonitrile and 0.200 ml perchloric acid (11.4 M).

Volume plasma (ml)	*Absolute recovery (%)*		
	Noscapine	*Narcotoline*	*Cotarnine*
0.25	95	99	97
0.50	87	95	93
0.75	84	92	95
1.00	74	84	87

minimum determinable concentration. As a compromise, 0.125 ml acetonitrile and 0.250 ml 11.4 M perchloric acid were added to undiluted plasma and 500-μl sample was injected into the precolumn.

The reliability of the protein precipitation was checked by addition of albumin (3 mg/ml) and orosomucoid (2 mg/ml) to plasma. This did not affect the absolute recoveries of the analytes. Because lipophilic compounds, *e.g.*, 1 mg/ml cholesterol or 10 mg/ml oleic acid did not dissolve in plasma, the influence of plasma lipophilicity on absolute recoveries was checked by using plasma from fasted or fed persons. No differences in the absolute recoveries of the analytes were obtained.

Chromatography

The chromatography of noscapine and the metabolites has previously been studied in different coupled-column systems, based on the heart-cut technique[14]. Noscapine and the metabolites were separated into two fractions on a polar precolumn (–CN). Each fraction was then transferred to an analytical column for final separation. Transfer of the precolumn eluate produced system peaks in the analytical columns[14]. The system peaks are formed as a consequence of disturbed equilibria on the analytical column. Each deviating mobile phase component may give rise to a system peak, which contains the mobile phase component in deficiency or excess.

The system peaks were used to obtain high peak performance of the analytes on the analytical column, in order to improve the sensitivity. The precolumn eluent giving the best results with respect to separation, efficiency and production of system peaks had a low content of acetonitrile in an acidic buffer. By using an analytical column eluent containing an high content of acetonitrile and DDS (1 mM), a compressed noscapine peak was obtained when eluted together with an increasing gradient of the system peak[14]. However, when noscapine is co-eluted with the system peak, the selectivity for structurally related compounds, *e.g.*, metabolites is decreased[14]. By increasing the acetonitrile content to 40% (v/v) and the DDS concentration to 3 mM, the system peak and the noscapine peak were separated. This improved the separation of noscapine from the unidentified metabolite (Fig. 2). Furthermore, the peak performance of noscapine was unaffected, *i.e.*, neither band broadening nor peak compression was obtained.

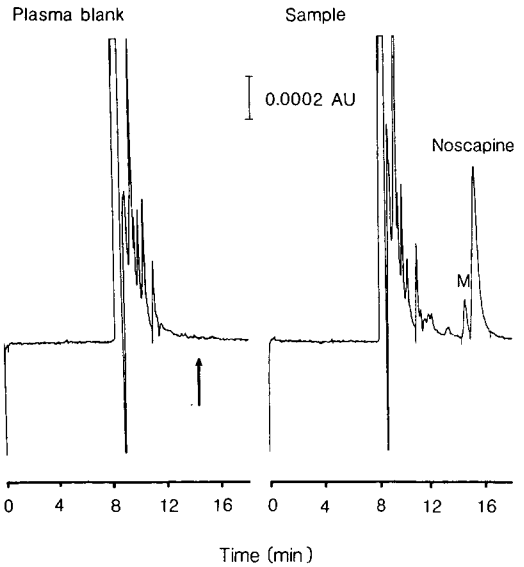

Fig. 2. Plasma blank and sample chromatogram. The plasma sample was taken after an oral dose of 200 mg noscapine. The noscapine concentration corresponds to 242 ng/ml plasma. Chromatographic conditions as in Fig. 1. The arrow indicates the retention time for noscapine. M = Unidentified metabolite.

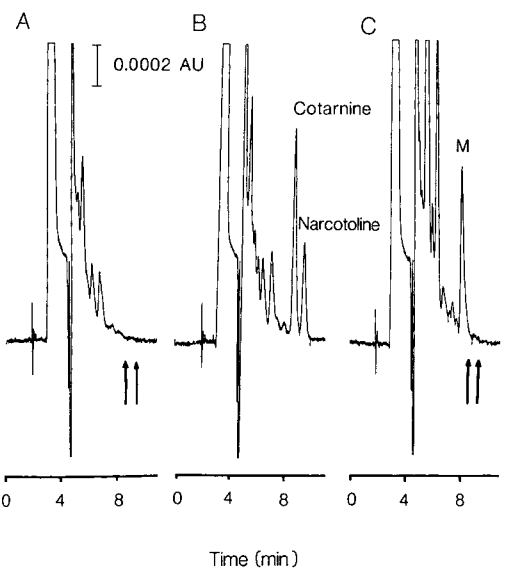

Fig. 3. Chromatogram of narcotoline and cotarnine. (A) Plasma blank; (B) plasma spiked with 99 ng/ml cotarnine and 102 ng/ml narcotoline; (C) plasma after an oral dose of 300 mg noscapine. Chromatographic conditions as in Fig. 1. The arrows indicate the retention times for cotarnine and narcotoline. M = Unidentified metabolite.

For the metabolites an eluent containing an high concentration of acetonitrile, DDS and DMOA was used. Even in this case, the system peak produced contained an excess of DDS[14]. The peak performance of the analytes was unaffected and no efforts were made to elute the metabolites together with the system peak for fear of lowering the selectivity. A good resolution of cotarnine, narcotoline and endogenous compounds in deproteinized plasma was obtained by using 2 m*M* DDS–0.1 m*M* DMOA in a solution of 35% (v/v) acetonitrile in an acidic buffer (Fig. 3). Another unidentified metabolite appeared (Fig. 3C) in plasma samples collected after an oral dose of the drug.

Tentative mass spectrometric identification of N-demethylated noscapine

The retention time of the unidentified metabolite on the noscapine column coincides with that of N-demethylated noscapine. The EI mass spectrum of N-demethylated noscapine produced an intense ion at *m/z* 206, orginating from the isoquinoline part. An ion at *m/z* 191 was probably produced by the loss of a methyl group from the ion at *m/z* 206. Furthermore, the ion at *m/z* 193 originated from the isobenzofuranone part. The LC eluate produced signals at *m/z* 191, 193 and 206 in the SIM analysis. The relationship of the relative intensities between the fragments in the eluate corresponded to the relative intensities of the reference compound. The abundance of the molecular ion at *m/z* 399 was very low and could not be registered, by EI or CI. CI with ammonia produced fragments at *m/z* 204 and 206 from the isoquinoline part and at *m/z* 195 and 212 (most likely from the isobenzofuranone part). The fragment at *m/z* 212 may be due to the addition of ammonia to the isobenzofuranone structure (*m/z* 196). The relative intensities of the fragments at *m/z* 195, 206, 212, but not *m/z* 204, in the eluate were in accordance with the intensities of the reference compound. A mass spectrum of the collected fraction could not be obtained by EI or CI, probably because the concentration of the metabolite was too low owing to losses during the work-up procedure. However, the data obtained indicate that the metabolite is N-demethylated noscapine. As pointed out earlier, the eluate from the column used for narcotoline and cotarnine also showed an unidentified metabolite (Fig. 3). In accordance with the above discussion, this peak may correspond to N-demethylated narcotoline or cotarnine. Further support for this is the retention behaviour of dextromethorphan and its N- and O-demethylated metabolites in a liquid chromatographic system[8] similar to the one used here for noscapine and its metabolites. Since no reference compounds for the O-demethylated metabolites are available, mass spectrometric identification is difficult. Furthermore, the main part of the O-demethylated metabolites probably exists in the form of conjugates.

Detection

An high detection selectivity and sensitivity is required when low levels of a drug must be determined in biological samples. Unfortunately, noscapine has no functional groups useful for derivatization. Oxidation of noscapine by bromine generated on-line has been tried, but the detection limit is too high (>20 ng)[16]. Oxidation with a coulometric detector (ESA, Coulochem Model 5100A) requires an high potential. The signal continuously increases up to the highest level tested, 1.2 V. At this high potential the background current is too high. The lowest detection limit of noscapine was obtained with UV detection at 211 nm, which was *ca.* 15 times better

TABLE V

DAY-TO-DAY VARIATION

R.S.D. = Relative standard deviation.

Compound	*Added (ng/ml)*	*R.S.D. (%)*	*Interval (days)*
Noscapine	15	9.5	9
	250	5.5	15
Narcotoline	26	15.6	10
	263	6.4	15
Cotarnine	14	17.6	12
	271	4.5	15

than that at 310 nm. The more selective fluorescence detection with a xenon lamp at 316/427 nm (Perkin-Elmer LS-4 fluorescence spectrometer) gave a four times lower signal-to-noise ratio than UV at 310 nm. Fluorescence detection with a deuterium lamp at 211/370 nm (Kratos 980 fluorescence detector) gave twice the signal-to-noise ratio of UV at 310 nm. However, when the main part of this study was performed only an UV detector was available. UV detection at 211 nm resulted in too much endogenous interference when 3 m*M* DDS was used. By increasing the DDS concentration, some interference disappeared, but another complication appeared —the resolution of noscapine and the unidentified metabolite was too low. Another way to decrease the endogenous interference was to increase the detection wavelength. Thus detection at 310 nm was used in the routine determinations. Injection of 2.00 ml of the supernatant instead of 0.5 ml gave only a small increase of the noscapine peak width from the precolumn. However, the amount of endogenous interference in the eluate from the analytical column increased considerably, limiting the injection volume to 0.5 ml of the supernatant.

Quantitation and stability of the system

The method has been used in an automated fashion for routine determinations. The samples were worked up manually (protein precipitation and buffering) and

TABLE VI

RELATIVE STANDARD DEVIATIONS AND ABSOLUTE RECOVERIES (%) OF NOSCAPINE, COTARNINE AND NARCOTOLINE

Compound	*Added (ng/ml)*	*R.S.D. (%)*	*Absolute recovery (%)*	*n*
Noscapine	9.3	5.9	84	7
	15	6.0	89	9
	250	1.2	86	7
Cotarnine	13	4.5	82	8
	241	1.5	88	9
Narcotoline	20	4.4	92	8
	263	2.5	95	9

injected automatically overnight. Before start-up, the retention times for the precolumn were checked daily, and the actual column-switching times were entered in the Tracer timer. The analyte peaks were integrated and evaluated by comparison with a standard curve, constructed from standards prepared like the samples. A calibration solution was injected as every tenth sample to ensure the stability of the system. The day-to-day variation is shown in Table V. The compounds were stable for more than 8 months at -20°C.

The absolute recoveries and the within-day precisions are shown in Table VI. The absolute recoveries were determined by comparison with direct injections into the precolumn of the compounds dissolved in a mixture containing phosphate buffer (pH 7.4), perchloric acid and acetonitrile (1.00 ml + 0.250 ml + 0.125 ml), adjusted to a pH of *ca.* 3. Plasma levels down to 9 ng/ml for noscapine, 13 ng/ml for cotarnine and 20 ng/ml for narcotoline were determined.

In general, 50–60 samples were analyzed overnight. The precolumn was used for about 3–4 days, corresponding to the injection of 45–60 ml of deproteinized plasma before the peaks became deformed and the resolution decreased. After change to a new precolumn, the retention time of the noscapine peak decreased by *ca.* 2–3 min after the first 5–7 plasma injections. Therefore, the time for the column switching event was determined after pretreatment of the column with 6–8 plasma injections. Between each day the retention time of noscapine on the precolumn decreased slightly. This was compensated by decreasing the acetonitrile content of the precolumn eluent by 1.0% for each day the precolumn was used.

CONCLUSION

Coupled-column liquid chromatography was used for quantitation of noscapine and its metabolites. Prior to injection on a short precolumn the plasma proteins were precipitated with acetonitrile and perchloric acid. Noscapine and the polar metabolites were separated into two groups on the precolumn and each group was transferred to an analytical column for further separation. The precolumn was used for about 45–60 ml of deproteinized plasma before the peaks deteriorated and the resolution decreased.

ACKNOWLEDGEMENT

We would like to thank Dr. Peter Lind for supplying the N-demethylated noscapine.

REFERENCES

1 N. Tsunoda, H. Yoshimura and H. Kozuka, *J. Hyg. Chem.*, 22 (1976) 280.
2 N. Tsunoda and H. Yoshimura, *Xenobiotica*, 9 (1979) 181.
3 N. Tsunoda and H. Yoshimura, *Xenobiotica*, 11 (1981) 23.
4 M. Johansson, S. Eksborg and A. Arbin, *J. Chromatogr.*, 275 (1983) 355.
5 K. Møller Jensen, *J. Chromatogr.*, 274 (1983) 381.
6 V. Haikala, *J. Chromatogr.*, 337 (1985) 429.
7 M. Karlsson, personal communication.
8 W. Roth, K. Beschke, R. Jauch, A. Zimmer and F. W. Koss, *J. Chromatogr.*, 222 (1981) 13.
9 A. Nazareth, L. Jaramillo, B. L. Karger, R. W. Giese and L. R. Snyder, *J. Chromatogr.*, 309 (1984) 357.

10 C. J. Little, D. J. Tomkins, O. Stahel, R. W. Frei and C. E. Werkhoven-Goewie, *J. Chromatogr.*, 264 (1983) 183.
11 M. Johansson and C. Svensson, *J. Pharm. Biomed. Anal.*, 6 (1988) 211.
12 J. W. Cox and R. H. Pullen, *J. Chromatogr.*, 307 (1984) 155.
13 M. Johansson and D. Westerlund, *J. Chromatogr.*, 452 (1988) 241.
14 M. Johansson, H. Forsmo-Bruce, A. Tufvesson Alm and D. Westerlund, *J. Pharm. Biomed. Anal.*, in press.
15 E. Pawelczyk and M. Zajac, *Pol. J. Pharmacol. Pharm.*, 27 (1975) 69.
16 W. Th. Kok, U. A. Th. Brinkman and R. W. Frei, *Anal. Chim. Acta*, 162 (1984) 19.

Journal of Chromatography, 459 (1988) 313–317
Elsevier Science Publishers B.V., Amsterdam — Printed in The Netherlands

CHROMSYMP. 1492

APPLICATION OF HIGH-PERFORMANCE LIQUID CHROMATOGRAPHY TO THE ANALYSIS OF PROPIONYL-L-CARNITINE BY A STEREOSPECIFIC ENZYME ASSAY

A. MARZO*, N. MONTI and M. RIPAMONTI
Real srl, Via Milano 7/9, 22079 Villaguardia, Como (Italy)
and
E. ARRIGONI MARTELLI
Sigma Tau SpA, Via Pontina Km. 30,400, 00040 Pomezia, Rome (Italy)

SUMMARY

Propionyl-L-carnitine was converted by chemical hydrolysis (0.3 *M* potassium hydroxide, pH 12.8, room temperature) into L-carnitine, which competes with crotonoylbetaine formation and can be quantitatively evaluated by an enzyme assay. Under the conditions selected, hydrolysis of propionyl-L-carnitine to L-carnitine was completed in a few minutes with less than 0.5% of crotonoylbetaine being formed. The method described is enantioselective and possesses the analytical requirements for assaying propionyl-L-carnitine during chemical synthesis procedures and in pharmaceutical formulations.

INTRODUCTION

Propionyl-L-carnitine (PLC) is an odd-carbon-number short-chain L-carnitine ester present in humans and animals as a minor component compared with L-carnitine and acetyl-L-carnitine (ALC)[1,2]. The interest in PLC results from the inotropic and fat-clearing activity that this substance has proved to possess in isolated perfused rat heart and in *in vivo* investigations of rats, dogs and humans. Hence a quantitative stereospecific assay is required in order to monitor the chemical synthesis of PLC and its presence in pharmaceutical formulations.

As the enzyme assay routinely used for L-carnitine and ALC[3–5] is not applicable to PLC, a method that involves alkaline hydrolysis of PLC to L-carnitine, with quantitative stereospecific determination of L-carnitine and high-performance liquid chromatographic (HPLC) monitoring to ascertain the complete hydrolysis of PLC and the net crotonoylbetaine (CB) formation, was developed and validated.

EXPERIMENTAL

Materials

Solvents and chemicals, all of analytical-reagent or HPLC grade, were supplied by Merck (Bracco, Milan, Italy), BDH (Milan, Italy) and Boehringer (Milan, Italy).

0021-9673/88/$03.50

L-Carnitine, PLC and CB were supplied by Sigma Tau (Rome, Italy).

A Varian Model DMS 70 spectrophotometer (Segrate, Milan, Italy) was used for the enzyme assay. A Hitachi Model 655A-11 liquid chromatograph, equipped with a Hitachi Model 655A variable-wavelength UV detector (Bracco, Milan, Italy), was used to monitor the hydrolysis. The statistical computations were performed on a Macintosh Plus personal computer (Apple, Reggio Emilia, Italy).

PLC hydrolysis

Hydrolysis, which allows the complete conversion of PLC into L-carnitine and the net formation of CB to be restricted to $\leq 0.5\%$, as monitored by HPLC, is achieved with 0.3 *M* potassium hydroxide solution (pH 12.8) at room temperature (20–25°C) in 15 min.

A number of hydrolysing agents at various concentrations and temperatures and with different times of assay were tested in order to obtain optimal conditions for PLC hydrolysis [0.5 *M* phosphate buffer at pH 8 and 10, room temperature, no hydrolysis; 0.2 *M* ammonia solution, pH 10 at 80°C, 55% hydrolysis after 2 h and 2% CB formation; 0.5 *M* ammonia solution, pH 11 at room temperature, 15% hydrolysis after 1 h and 1.5% CB formation; 0.1 *M* sodium hydrogencarbonate, pH 7.7 at 80°C, 15% hydrolysis after 2 h; 0.5 *M* potassium hydroxide solution, pH 13 at room temperature, 100% hydrolysis after 15 min but very large CB formation; 0.5 *M* 4-(2-hydroxyethyl)-1-piperazineethanesulphonic acid (HEPES) buffer, pH 10 at room temperature, no hydrolysis].

HPLC

A Supelcosil NH_2 (5 μm) column (250 × 4.6 mm I.D.) supplied by Supelco (Supelchem, Milan, Italy) was used. The mobile phase was acetonitrile–0.02 *M* phosphate buffer (pH 3) (75:25) at a flow-rate of 1 ml/min. Absorbance was monitored at 205 nm. The retention times were 2.15 min for PC, 4.80 min for PLC, 8.65 min for L-carnitine and 10.80 min for CB. Fig. 1 shows typical chromatograms of PLC before and after chemical hydrolysis.

Enzyme assay

L-Carnitine formed by alkaline hydrolysis of PLC was determined using an enzyme method based on a colorimetric reaction[6]. The addition of L-carnitine to a system containing carnitine acetyltransferase (CAT) and acetyl coenzyme A leads to the formation of CoASH and ALC. CoASH reduces dithionitrobenzoic acid, breaking the S–S bond and leading to 5-thio-2-nitrobenzoic acid with an absorption peak at 412 nm ($\varepsilon = 13\,600\ l\ mol^{-1}\ cm^{-1}$).

RESULTS

Linearity

The assay proved to be linear in the range 185–1110 nmoles/ml of L-carnitine, with a r^2 value of 0.9998 (Fig. 2). Linearity was also obtained for the overall procedure described, starting from PLC, over the range 250–1495 nmoles/ml.

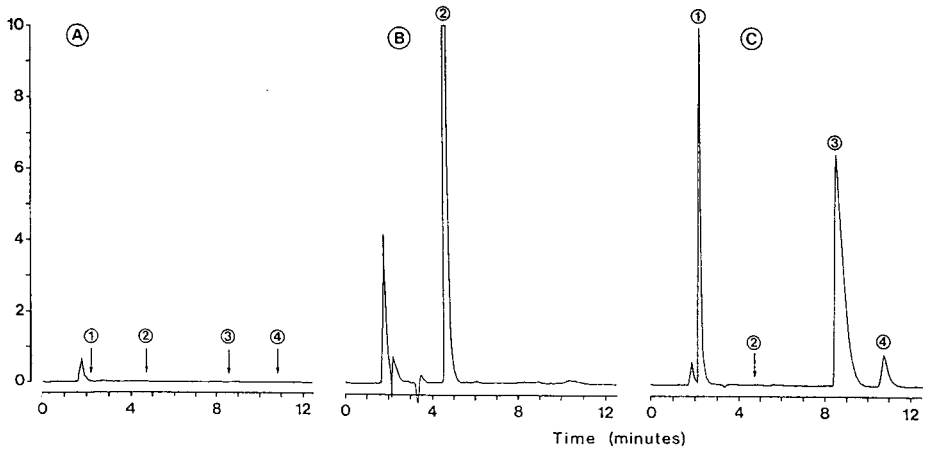

Fig. 1. Typical chromatograms obtained in monitoring PLC hydrolysis. (A) Solvent injection; (B) PLC before chemical hydrolysis; (C) PLC after chemical hydrolysis. Peaks: 1 = propionic acid; 2 = PLC; 3 = L-carnitine; 4 = CB.

Reproducibility

Reproducibility was investigated as the coefficient of variation (C.V.) over a series of 24 evaluations of PLC after hydrolysis to L-carnitine. The inter-assay C.V. was 1.04% (Table I).

Specificity

The method proved to be specific for the L-enantiomers of both carnitine and propionylcarnitine. When applied to L–D-enantiomer mixtures (1:0, 3:1, 1:1), the same results were obtained, indicating that the D-enantiomer does not interfere. Its specificity was tested by determining small amounts of L-carnitine in the presence of large amounts of PLC (Table II), in order to validate the method for the determination

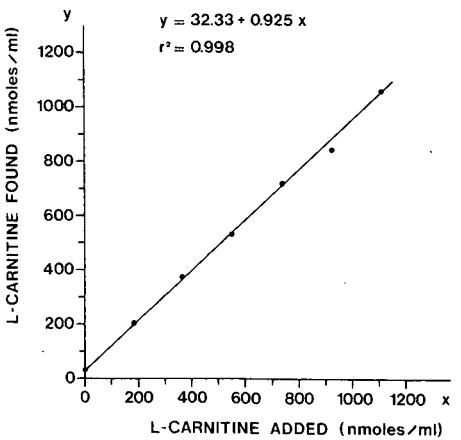

Fig. 2. Linearity of L-carnitine enzyme assay.

TABLE I

ANALYTICAL REPRODUCIBILITY OF LC ENZYME ASSAY

Six individual assays were carried out, each in quadruplicate.

Absorbance values	*Mean absorbance*	*S.D.*	*C.V. (%)*
0.512 0.507 0.505 0.513	0.509	0.0039	0.76
0.492 0.499 0.495 0.494	0.495	0.0029	0.59
0.502 0.495 0.505 0.494	0.499	0.0054	1.07
0.494 0.498 0.492 0.502	0.496	0.0044	0.89
0.499 0.496 0.491 0.500	0.496	0.0040	0.81
0.501 0.495 0.503 0.495	0.498	0.0041	0.83
Mean values	0.499	0.0052	1.04

TABLE II

SPECIFICITY OF THE ENZYME ASSAY FOR THE DETERMINATION OF SMALL AMOUNTS OF L-CARNITINE IN THE PRESENCE OF LARGE AMOUNTS OF PLC

Values in μmoles/ml.

L-Carnitine	*Propionyl-L-carnitine*	*Absorbance (mean of two determinations)*
0.19	3.0	0.134
0.19	5.9	0.135
0.19	11.8	0.132
0.19	23.7	0.131
		Mean: 0.133 S.D.: 0.0018 C.V. (%): 1.37

of L-carnitine when present as an impurity in PLC. In addition, the determination is not affected by the presence of propionic acid or potassium chloride in amounts equimolar to L-carnitine formed after PLC hydrolysis. In this respect, the method was validated for both PLC inner salt and hydrochloride.

DISCUSSION

We investigated the optimal hydrolysis conditions that convert PLC into L-carnitine by an enantiospecific enzyme assay. PLC hydrolysis proved to compete with CB formation, which in most instances was restricted to 0.2% and was never greater than 0.5%. The method also determines the L-carnitine before the hydrolysis as a likely impurity in PLC with high specificity. The percentage of PLC can be evaluated as follows:

$$[\text{PLC}] = A + B - \text{C}$$

where

$$A = \frac{A_c \cdot p_s \cdot 100 \cdot t}{A_s \cdot p_c};$$

A_c = absorbance of sample at 412 nm;
A_s = absorbance of standard at 412 nm;
p_c = weight of sample (mg);
p_s = weight of standard (mg);
t = fraction of reference standard title;
B = net percentage formation of CB;
C = percentage of L-carnitine in PLC raw material.

This method is therefore specific, selective, reproducible, sensitive and enantiospecific, allowing PLC to be determined in synthetic procedures and pharmaceutical formulations. It is also inexpensive, requiring only chemicals and enzymes that are readily available.

The method was not standardized for analyses of biological fluids, as the radioenzyme procedure proposed by Kerner and Bieber[7] seems to be more suitable for this purpose.

REFERENCES

1 J. Bremer, *Biochim. Biophys. Acta*, 48 (1961) 622.
2 N. Siliprandi, *Sci. Cult.*, 3 (1981) 3.
3 G. Cederblad and S. Lindsted, *Clin. Chim. Acta*, 37 (1972) 235.
4 J. D. McGarry and D. W. Foster, *J. Lipid Res.*, 17 (1976) 277.
5 S. V. Pande and M. N. Caramancion, *Anal. Biochem.*, 112 (1981) 30.
6 *Internal Report*, Sigma Tau, Rome, 1985.
7 J. Kerner and L. L. Bieber, *Anal. Biochem.*, 134 (1983) 459.

Journal of Chromatography, 459 (1988) 319–324
Elsevier Science Publishers B.V., Amsterdam — Printed in The Netherlands

CHROMSYMP. 1499

RAPID AND SENSITIVE METHOD FOR HIGH-PERFORMANCE LIQUID CHROMATOGRAPHIC ANALYSIS OF PTERINS IN BIOLOGICAL FLUIDS

I. ANTONOZZI*, C. CARDUCCI, L. VESTRI, A. PONTECORVI and F. MORETTI
Genetic-Metabolic Diseases Section, Department of Experimental Medicine, University "La Sapienza" of Rome, Rome (Italy)

SUMMARY

A rapid and sensitive high-performance liquid chromatographic (HPLC) method for the analysis of the most important urinary pterins is described. The method involves a preliminary sample oxidation to stabilize and convert pterins into their fluorescent forms and a purification by anion-exchange chromatography, followed by a short reversed-phase HPLC separation with fluorometric detection and quantitation of the different pterins. A complete HPLC analysis is accomplished in as little as 15 min. The sensitivity of the method allows the detection of as little as 20 pg of each pterin with a mean recovery greater than 99% for all pterins analysed. Reference values were obtained from 50 normal babies aged between 1 and 120 days. A significant correlation was found between urinary biopterin levels and the age of the babies ($r = 0.445$), while neopterin did not show any significant correlation with age. The "biopterin neopterin creatinine ratio" (BNCR index) was also significantly correlated with the age of the babies ($r = 0.428$). This rapid and sensitive method for pterin determination in biological fluids may be useful in the differential diagnosis of the various hyperphenylalaninemic conditions identified by neonatal mass screening programmes.

INTRODUCTION

Urinary pterin determination is receiving attention in several medical fields, including immunology, oncology, psychobiology and metabolic disorders[1–4].

One of the most important applications of this type of analysis is in the diagnosis of neonatal hyperphenylalaninemic conditions, caused by a metabolic block in the tetrahydrobiopterin biosynthetic or salvage pathway[5–7]. The diagnosis of these altered metabolic states which, if not recognized and treated early, may produce severe brain damage, requires a rapid and precise method for the determination of pterin levels in biological fluids. The establishment of an appropriate set of normal reference values is also important, since it has been demonstrated that pterin levels may vary with the age of the subject examined[6–8].

The aim of this work was: (1) to set up a rapid and sensitive method for high-performance liquid chromatographic (HPLC) analysis of urinary pterin levels

0021-9673/88/$03.50

and (2) to determine reference values for normal babies at the critical age interval between 1 and 120 days. The method may find application in the differential diagnosis of hyperphenylalaninemic conditions, detected by neonatal mass screening.

MATERIALS AND METHODS

All the reagents were of analytical grade and were used without further purification. Biopterin (B), neopterin (N), pterin (Pt) and 6-methylpterin (6-mPt) were obtained from Sigma (St. Louis, MO, U.S.A.), tetrahydrobiopterin (THB) and dihydrobiopterin (DHB) from Dr. B. Schirks (Wettsil a.A., Switzerland). To determine normal reference values, urines were collected from 50 normal babies (40 males and 10 females, age range 1–120 days), randomly selected from those attending a routine check-up visit.

Urines were collected in light-shielded containers, immediately acidified to pH 1 with 6 *M* hydrochloric acid and frozen in 1-ml aliquots at −70°C until analysed. A separate aliquot was used for a creatinine determination according to the method of Rossignol *et al.*[9].

Specimens were rapidly thawed at 40°C, and 100 μl of the internal standard (6-mPt, 28 μ*M*) were added to each aliquot. In order to measure the hydrogenated pterins THB and DHB, an oxidation to the more stable and fluorescent derivatives B and Pt was performed[11,12]. Two aliquots of the urine sample were subjected to differential oxidation in 0.1 ml of 0.5% iodine–1% potassium iodide either in alkaline solution, to convert DHB into B and THB in Pt (90 and 80% conversion, respectively), or in acidic solution, to convert both hydrogenated pterins into B (90% conversion). The difference between the amount of B derived from the two oxidative steps and the amount of B originally present in the urine sample before oxidation allows the determination of the hydrogenated pterins.

Samples were incubated in the dark at room temperature for 45 min and the reaction was stopped by the addition of 200 μl of 57 m*M* ascorbic acid. The oxidized samples were then purified by ion-exchange chromatography, using a solid-phase silica-bonded anion-exchange Bond-Elut column (Analytichem, Harbor City, CA, U.S.A.). After sample loading, the column was washed with 4 ml of water acidified to pH 4 with 1 *M* hydrochloric acid, and the analytes were eluted with 870 μl of 1 *M* potassium hydroxide–20% methanol. The analytes were then acidified by the addition of 130 μl of 6 *M* hydrochloric acid and then 20 μl were injected into a 25 cm × 0.46 cm I.D. RP-18 column (Macherey-Nagel, Duren, F.R.G.), in an 1084B liquid chromatograph (Hewlett-Packard, Avondale, PA, U.S.A.), equipped with a fluorometer FP-115 (Jasco, Hachioji, Tokio, Japan) or a SFM 25 spectrofluorometer (Kontron, Zurich, Switzerland) as detector. The wavelength settings were: excitation, 350 nm; emission, 410 nm.

The HPLC operating conditions were: eluent, water–methanol (97:3, v/v); oven temperature, 35°C; flow-rate, 0.7 ml/min. From 1.5 to 3 min after sample injection, a linear gradient was applied starting from 3 to 12% methanol. The quantitation of the analytes was performed according to the internal standard method.

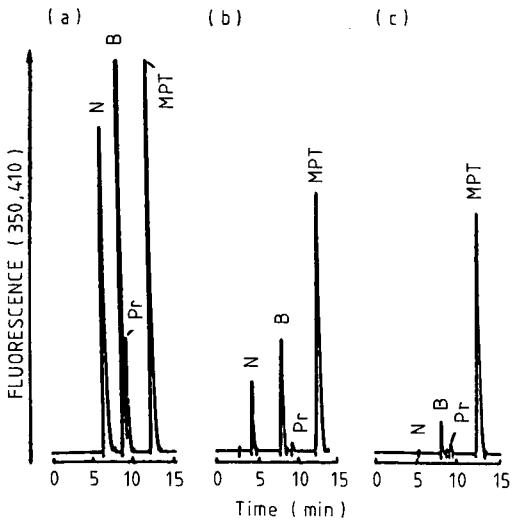

Fig. 1. Three typical chromatograms for (a) a standard mixture of B, N, Pt and 6-mPt, (b) a urine sample treated with acidic oxidation and (c) the same urine sample treated by alkaline oxidation.

RESULTS

Under our experimental conditions, a good separation between N, B, Pt and 6-mPt was achieved in 15 min (Fig. 1). The sensitivity of the method allowed the detection of as little as 20 pg of each pterin in an injection volume of 20 μl, with a linear dose–response curve over the range of 0.02–60 ng of pterins.

The recovery of the method was assessed by adding different quantities of each pterin to a known amount of urine. Fig. 2 shows the correlation between observed and expected values for the pterins indicated. The correlation cooefficient was highly significant ($r = 0.9994$) with a mean recovery of 101.4% for P, 99.6% for N and 99.5% for B.

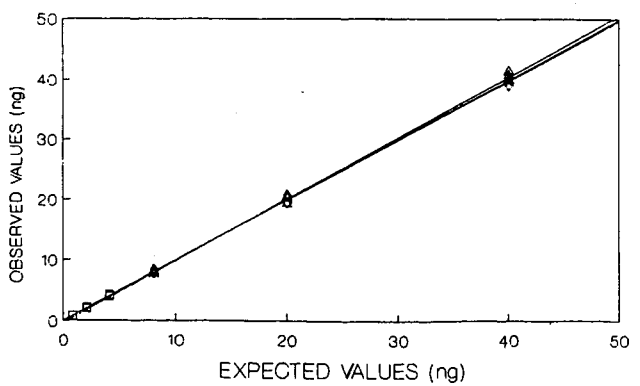

Fig. 2. Correlation between observed and expected values for the different pterins obtained in the analysis of an urine sample containing known amounts of each pterin. □, Pterin; △, neopterin; ◇, biopterin.

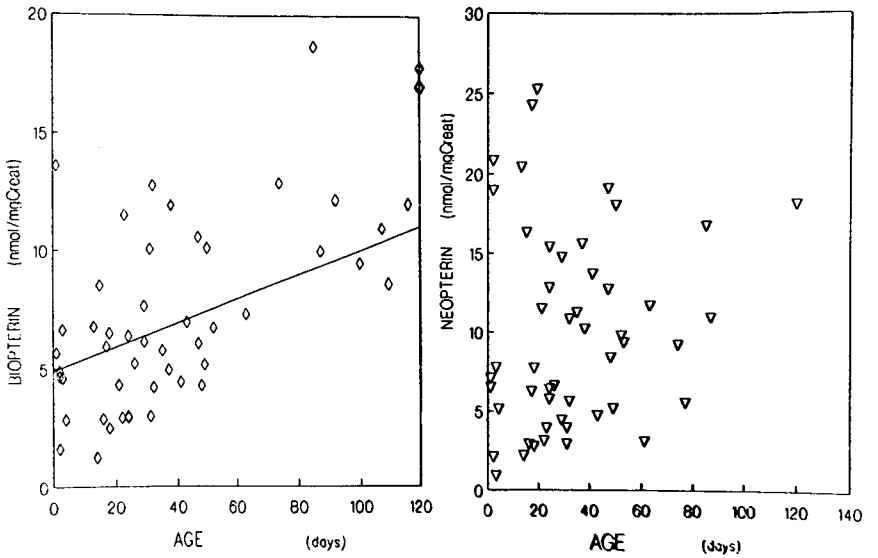

Fig. 3. Reference values for pterin urinary excretion: correlation between levels (nmol/mg creatinine) of N and B with the age of 50 normal babies. The urinary levels of B are significantly correlated with the age ($r = 0.445$ for $p < 0.0012$); the correlation between N and the age is not significant.

The precision of the method was assessed by processing 60 replicates of the same sample in three separate assays, resulting in a mean intra-assay coefficient of variation (C.V.) of 3.75% and a mean inter-assay C.V. of 4.3%.

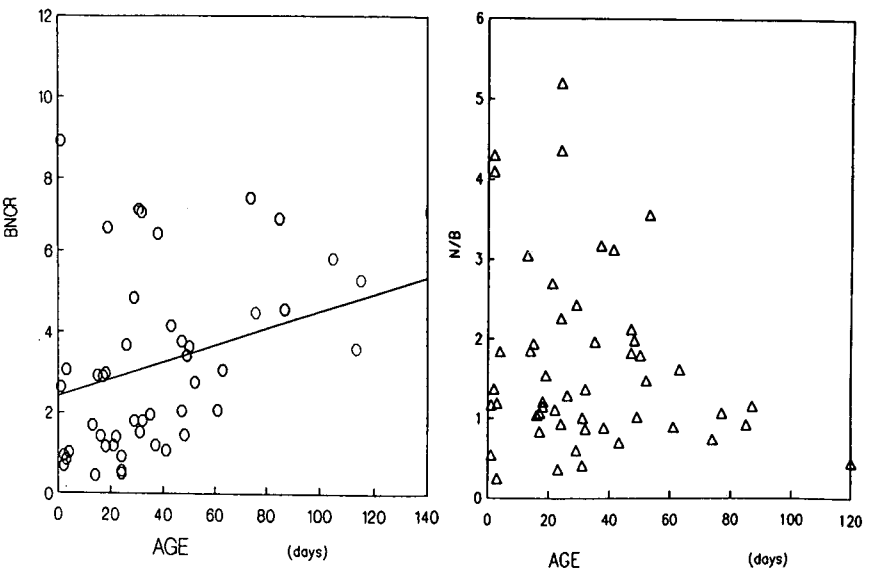

Fig. 4. Reference values for pterin urinary excretion: correlation between BNCR {[B/(N+B)] × (B/creatinine) · 10^5} and N/B with the age of 50 normal babies. BNCR is significantly correlated with age ($r = 0.428$ for $p < 0.002$); the correlation between N/B and age is not significant.

The method was also used in a preliminary field trial to establish urinary excretion levels of B and N in a group of 50 normal babies with ages ranging between 1 and 120 days. In Fig. 3 is shown the correlation between the age and urinary levels, expressed as nmol/mg creatinine. The levels of B were significantly correlated with the age of the babies ($r = 0.445$ for $p < 0.0012$) while the correlation between the levels of N and the age was not significant. The "biopterin neopterin creatinine ratio"[10] {BNCR index = $[B/(N + B)] \cdot (B/\text{creatinine}) \cdot 10^5$}, and the ratio between N and B (N/B), generally considered the best informative biochemical indices for the discrimination between phenylketonuria and the variant forms of hyperphenylalaninemia[10], were also determined for each sample on the basis of the excretion values of N and B. Fig. 4 shows the correlation between the BNCR index or the ratio N/B and the age of the babies: BNCR was significantly correlated with the age ($r = 0.427$ for $p < 0.002$), while N/B did not show any significant correlation.

DISCUSSION

In almost all the methods so far described the extraction of pterins from urine is accomplished by using ion-exchange chromatographic procedures[11–13]. On the contrary, the methods described for HPLC analysis of extracted samples are different, being based on either ion-exchange[14,15] or reversed-phase (RP) chromatography[13,16] with either fluorometric[13,14] or electrochemical detection[17]. Most of the methods so far described are also time consuming, requiring several purification steps, followed by an HPLC analysis that lasts *ca.* 20 min with RP columns[13] or even 30 min when ion-exchange columns are used[14].

The method described here allows HPLC analysis of the most important pterins (N and B) and of the hydrogenated forms THB and DHB in only 15 min, preceded by an extraction and purification step, taking *ca.* 10 min. The recovery, accuracy, precision and sensitivity of the method are in the range of other methods so far described[13–15].

The requirement of a proper set of reference values is important in the analysis of urinary pterins, since an age-dependent variation of urinary pterin excretion has been reported[18,19]. Since most blocks in pterin metabolism become evident during the first months of postnatal life, resulting in hyperphenylalaninemic conditions that are usually detected by means of neonatal screening programme, we applied this method to the determination of reference values in this critical age period. To our knowledge, reference values for this age interval have been extensively reported only by Dhondt *et al.*[18]. Our results are in good agreement with that report in terms of absolute values. The progressive increase with age of urinary B levels is in accordance with the results reported by Dhondt *et al.*[18] and by Niederwieser *et al.*[19]; moreover the lack of correlation between urinary N levels and age, in the first trimester of postnatal life, is not in contrast with the above mentioned reports that showed a decrease in urinary N levels starting only after the twelfth month of neonatal life. Our findings confirm the hypothesis that the age-dependent decline of N and the increase of B in children may be attributed to progressive maturation of the biopterin synthetic pathway, mainly of dihydrobiopterin synthetase (DHBS), in the first 3 months of life[10].

For these reasons, the variation in urinary pterin levels should be seriously considered when studying babies of this age.

In conclusion, we have described a rapid, sensitive and precise method for urinary pterin determination that can be applied to the differential diagnosis of the various hyperphenylalaninemic conditions together with mass neonatal screening for the metabolic disorder.

REFERENCES

1 A. M. G. Farci, F. Cabras, G. Cappai, L. Chessa, I. Pillosu, G. Tuveri, A. Lovisello, E. Atzeni, A. Mathieu, P. Usai, R. Laconi, A. Balestrieri, V. L. Garau, M. Tocco and D. Casula, in H. Wachter, H. Ch. Curtius and W. Pfeiderer (Editors), *Biochemical and Clinical Aspects of Pteridines*, Vol. 5, Walter de Gruyter, Berlin, New York, 1987, p. 193.
2 D. Schonitzer, M. Honlinger, D. Fuchs, A. Hausen, G. Reibnegger, E. R. Werner and H. Watcher, in H. Wachter, H. Ch. Curtius and W. Pfeiderer (Editors), *Biochemical and Clinical Aspects of Pteridines*, Vol. 5, Walter de Gruyter, Berlin, New York, 1987, p. 331.
3 S. A. Jones and J. A. Blair, in H. Wachter, H. Ch. Curtius and W. Pfeiderer (Editors), *Biochemical and Clinical Aspects of Pteridines*, Walter de Gruyter, Vol. 5, Berlin, New York, 1987, p. 365.
4 B. Stea, R. M. Halpern, B. C. Halpern and R. A. Smith, *Clin. Chim. Acta*, 113 (1981) 231.
5 S. Kaufman, *J. Pediatr.*, 109 (1986) 572.
6 R. Matalon, *J. Pediatr.*, 104 (1984) 579.
7 H. Ch. Curtius, M. Hausermann, A. Niederwieser and S. Ghisla, in H. Wachter, H. Ch. Curtius and W. Pfeiderer (Editors), *Biochemical and Clinical Aspects of Pteridines*, Vol. 1, Walter de Gruyter, Berlin, New York, 1982, p. 27.
8 J. L. Dhondt, *J. Pediatr.*, 104 (1984) 501.
9 B. Rossignol, D. Rossignol and C. Petitclerc, *Clin. Biochem.*, 17 (1987) 203.
10 A. Niederwieser, H. Ch. Curtius, R. Gitzelmann, A. Otten, K. Baerlocher, B. Blehova, S. Berlow, H. Grobe, F. Rey, J. Schaub, S. Scheibenreiter, H. Schmidt and M. Viscontini, *Helv. Paediatr. Acta*, 35 (1980) 335.
11 B. Stea, R. M. Halpern, B. C. Halpern and R. A. Smith, *J. Chromatogr.*, 188 (1980) 363.
12 T. Fukushima and J. C. Nixon, *Anal. Biochem.*, 102 (1980) 176.
13 A. Niederwieser, W. Staudenmann and E. Wetzel, *Biochemical and Clinical Aspects of Pteridines*, Vol. 1, Walter de Gruyter, Berlin, New York, 1982, p. 81.
14 B. Stea, R. M. Halpern and R. A. Smith, *J. Chromatogr.*, 168 (1979) 385.
15 J. L. Dhondt, C. Largilliere, P. Ardouin, J. P. Farriaux and M. Dautrevaux, *Clin. Chim. Acta*, 110 (1981) 58.
16 H. Rokos, K. Rokos, H. Frisius and H. J. Kirstaedter, *Clin. Chim. Acta*, 105 (1980) 275.
17 A. Niederwieser, W. Staudenmann and E. Wetzel, *J. Chromatogr.*, 290 (1984) 237.
18 J. L. Dhondt, P. Ardouin, J. M. Hayte and J. P. Farriaux, *Clin. Chim. Acta*, 116 (1981) 143.
19 A. Hausen, D. Fuchs, K. König and H. Wachter, *J. Chromatogr.*, 227 (1982) 61.

Journal of Chromatography, 459 (1988) 325–329
Elsevier Science Publishers B.V., Amsterdam — Printed in The Netherlands

CHROMSYMP. 1493

HIGH-PERFORMANCE LIQUID CHROMATOGRAPHIC EVALUATION OF SALICYLOYL PYRIDIXOL AND SYSTEMIC METABOLITES IN BIOLOGICAL SAMPLES

A. MARZO*, A. REINER, N. MONTI and M. RIPAMONTI
Real srl, Laboratory of Drug Metabolism and Pharmacokinetics, Via Milano 7/9, 22079 Villaguardia, Como (Italy)
and
C. LUCARELLI
Istituto Superiore di Sanità, Laboratory of Clinical Biochemistry, Viale Regina Elena 299, Rome (Italy)

SUMMARY

An high-performance liquid chromatographic analytical method, which allows quantitative evaluation of both salicyloyl pyridixol and its metabolite salicylic acid, is reported. This method has demonstrated to possess the required specifications in terms of linearity, sensitivity, extraction recovery, reproducibility and specificity for pharmacokinetic investigations in both human subjects and experimental animals. The results obtained from an investigation on the rat are briefly discussed.

INTRODUCTION

Salicyloyl pyridixol (SP) is a new non-steroid antiinflammatory agent which in previous pharmacotoxicological investigations has been shown to possess the activity of salicylates with very low gastrointestinal side-effects, in agreement with a series of previous investigations on drugs containing the carboxylate in esterified form[1–5].

SP is the product of esterification of salicylic acid (SA) and 3-pyridixol (or pyridoxine) (Fig. 1). Any pharmacokinetic investigation of an ester such as SP must be based on an analytical method capable of evaluating both the parent drug and its metabolite SA. This paper describes an analytical method which evaluates SP and SA in plasma, tissues and urine. Pharmacokinetic results in the rat are also discussed.

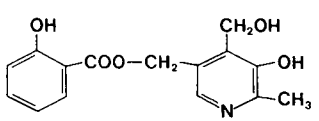

Fig. 1. Chemical structure of salicyloyl pyridixol (SP), $C_{15}H_{15}O_5N$. Molecular weight = 289.293.

0021-9673/88/$03.50

EXPERIMENTAL

Materials

The solvents and chemicals, all of analytical or HPLC grade, were supplied by Merck (Bracco, Milan, Italy), Fluka (Schrepfer, Milan, Italy) and Sigma (Prodotti Gianni, Milan, Italy).

SP was synthesized by Erregierre (S. Paolo D'Argon, Bergamo, Italy). SA was available in the Real laboratory and was shown to meet the USP XXI (1985) specifications. An Hitachi Model 655A-11 liquid chromatograph (Bracco) and an Hitachi Model 655A variable-wavelength UV detector were used for analysis. The column was a μBondapak C_{18}, 5 μm, 300 mm × 4.6 mm I.D., from Waters Assoc. (Millipore, Segrate, Milan, Italy). The statistical computations were performed on a Macintosh Plus personal computer (Apple, Reggio Emilia, Italy).

Methods

A 1-ml volume of plasma was diluted in 1 ml of phosphate–citrate buffer at pH 7.4. The tissues were homogenized with the same buffer at a tissue/buffer ratio of 1:4 (w/v), and 50 μl 30% perchloric acid and 0.5 ml methanol were then added to deproteinize the plasma or tissue sample. After stirring for 10 min and centrifuging at 2400 *g* for 5 min, an aliquot of the supernatant was separated. 3-Methylbenzoic acid was used as an internal standard (I.S.), added after extraction to monitor recovery and before extraction in the routine analysis. The mobile phase consisted of acetonitrile–1% phosphoric acid (17:83) at pH 3.25. The flow-rate was 2 ml/min. Absorbance was monitored at 238 nm. Retention times were 5.25 min for SA, 6.78 min for SP and 12.31 min for I.S. Fig. 2 shows typical chromatograms.

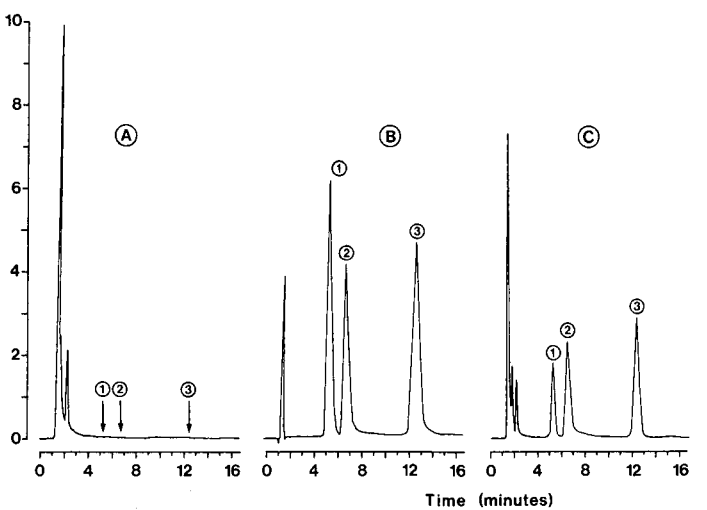

Fig. 2. HPLC of salicylic acid (1), salicyloyl pyridixol (2) and 3-methylbenzoic acid (I.S.) (3). (A) Blank plasma; (B) authentic standards; (C) plasma of a rat treated with the drug.

RESULTS AND DISCUSSION

Linearity was verified in terms of detector response factor for both the parent drug and SA in the 50–1000 ng range, five replications being performed. The intra-assay coefficient of variation was 1.12 for SP and 1.35 for SA.

The inter-assay coefficient of variation was 4.05 for SP and 4.37 for SA when a fixed analyte/I.S. ratio (1:1) was used. It was 4.78 for SP and 4.92 for SA when the method was validated at variable analyte/I.S. ratio ranging from 1:4 to 4:1 (Table I).

TABLE I

ANALYTICAL LINEARITY OF DETECTOR RESPONSE EVALUATED WITH BOTH A FIXED ANALYTE/I.S. RATIO OF 1:1 AND A VARIABLE RATIO RANGING FROM 1:4 TO 4:1

$$DRF = \frac{\text{analyte peak area}}{\text{I.S. peak area}} \cdot \frac{\text{I.S. concentration}}{\text{analyte concentration}}$$

Amount injected (ng)			*DRF*	
Analyte	*I.S.*		*SP*	*SA*
50	50		1.667	1.504
125	125		1.669	1.573
250	250		1.728 ± 0.0195 (S.D.)* (C.V. = 1.12%)	1.433 ± 0.0194 (S.D.)* (C.V. = 1.35%)
500	500		1.839	1.606
1000	1000		1.725	1.516
		Mean	1.726	1.526
		S.D.	0.0698	0.0668
		C.V. (%)	4.05	4.37
250	1000		1.850	1.443
500	1000		1.635	1.629
1000	1000		1.710	1.538
1000	500		1.682	1.580
1000	250		1.764	1.476
		Mean	1.728	1.533
		S.D.	0.0826	0.0755
		C.V. (%)	4.78	4.92

* Five replicates.

The recovery of SP and SA from rat plasma was investigated in the range from 10 to 100 μg/ml, the analysis being performed in quadruplicate at each concentration. The average recovery was 90.5% for SP and 91.5% for SA, with linear correlation coefficients, r^2, of 0.9928 and 0.9966 respectively (Table II). Extraction recovery in urine and tissues was very close to the values obtained in plasma.

This method has been used for a pharmacokinetic study of SP in the rat after oral administration of the drug at a dose of 100 mg/kg (48 mg/kg in terms of SA). Sprague-Dowley male rats, weighing 225–250 g, supplied by Charles River (Calco,

TABLE II

RECOVERY OF SP AND SA FROM RAT PLASMA IN QUADRUPLICATE ANALYSES

Internal standard was added in such a way as to have a drug/I.S. ratio of 1:1 both for SP and SA. During routine analysis, the internal standard used was such as to remain in a drug/I.S. ratio of 1:4–4:1.

	Amount added (= x) (μg/ml)	*Amount recovered (= y)*				*Recovery (%)*
		Mean (μg/ml)	*S.D.*	*C.V. (%)*		
SP	10	9.5	0.23	2.39		95.0
	20	18.6	0.63	3.40		93.0
	50	44.0	2.38	5.41		88.0
	100	86.0	5.26	6.11		86.0
					Mean	90.5
					S.D.	4.20
					C.V. (%)	4.64
SA	10	8.7	0.43	4.90		87.0
	20	18.0	0.51	2.83		90.0
	50	48.5	2.59	5.34		97.0
	100	92.0	2.07	2.25		92.0
					Mean	91.5
					S.D.	4.20
					C.V. (%)	4.59

Italy), were used. Fig. 3 shows the mean plasma SA concentration *vs.* time curve obtained according to the open one-compartment model for the oral route, using the non-linear fitting method. Table III shows the main pharmacokinetic parameters obtained from the mean plasma concentrations of SA in the rat.

The lowest detectable amount was 20 ng (1000 ng/ml in terms of plasma concentration) for SP and 10 ng (500 ng/ml) for SA.

Considerable care was given to specificity in terms of evaluating both the parent drug and SA, in that SP was hydrolysed at a very slow rate, giving a concentration of the drug as such in the gastric and intestine walls and of SA in the systemic circulation.

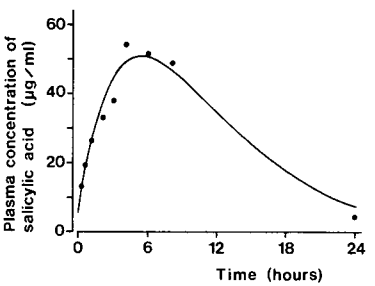

Fig. 3. Plasma concentration *vs.* time behaviour of salicylic acid after oral administration of salicyloyl pyridixol in the rat (100 mg/kg).

TABLE III

PHARMACOKINETIC PARAMETERS REFERRING TO THE PLASMA CONCENTRATION OF SA AFTER ORAL ADMINISTRATION OF SP (100 mg/kg, 48 mg/kg AS SA)

t_{max} = peak time; C_{max} = peak concentration; $t_{1/2}$ = half-life; K_a = absorption rate constant; K_{el} = elimination rate constant; AUC = area under the plasma concentration *vs.* time curve.

t_{max}	(h)	:	4
C_{max}	(μg/ml)	:	58.7
$t_{1/2}$	(h)	:	4.24
K_a	(h^{-1})	:	0.178
K_{el}	(h^{-1})	:	0.170
$AUC_{0-24\ h}$	(μg/ml · h)	:	770.78

In conclusion, the method described possesses the specifications required for pharmacokinetic and bioavailability investigations in human beings and in laboratory animals. It is rapid, requiring only one extraction for the parent drug and SA, and simple and inexpensive reagents. A skilful operator can process more than 25 analyses a day without an autosampling injector. The method is also proving to work very well in human pharmacokinetic studies, which are now in progress.

REFERENCES

1 T. Y. Shen, *J. Med. Chem.*, 24 (1981) 1.
2 M. W. Whitehouse and K. D. Rainsford, *J. Pharm. Pharmacol.*, 32 (1980) 795.
3 G. Y. Paris, D. L. Garmaise and D. G. Cimon, *J. Med. Chem.*, 22 (1979) 683.
4 G. W. Carter, P. R. Young, L. R. Swett and G. Y. Paris, *Agents Actions*, 10 (1980) 240.
5 K. Brune, *Am. J. Med.*, 14 (1983) 19.

Journal of Chromatography, 459 (1988) 331–335
Elsevier Science Publishers B.V., Amsterdam — Printed in The Netherlands

CHROMSYMP. 1465

RAPID IDENTIFICATION OF *BACTEROIDES* SPECIES BY HIGH-PERFORMANCE LIQUID CHROMATOGRAPHY

L. RADIN* and A. ARZESE
Istituto di Microbiologia, Università di Genova, Genoa (Italy)
C. LUCARELLI
Istituto Superiore di Sanità, Rome (Italy)
and
G. A. BOTTA
Istituto di Microbiologia, Università di Udine, Udine (Italy)

SUMMARY

High-performance liquid chromatography was evaluated for the rapid identification of *Bacteroides* species of clinical interest. Each isolate was inoculated into a defined chemical medium containing primarily carbohydrates and was incubated aerobically at 37°C for 1 h. After centrifugation, the supernatants were placed on ice to stop further enzymatic reactions. Specimens were injected into an Aminex HPX-87H column in order to determine carbohydrates and acid metabolic products. Peak areas of carbohydrates for each isolate were compared with those for uninoculated medium. As the utilization indexes of raffinose, lactose and arabinose were found to be particularly significant, the patterns of carbohydrate utilization could be used for the identification of *Bacteroides* species. This method can be adapted for diagnostic laboratory use and has good potential for automated microbial identification.

INTRODUCTION

Currently, there is considerable interest in the development of microtechniques and instrumental methods for the identification of anaerobic bacteria[1]. Many new microtest systems, such as the API 20 A (API System, Montalieu Vercieu, France) and the An-IDENT (API Analytab Products, Plainview, NY, U.S.A.), have been introduced to shorten the identification time. The use of instrumental methods for anaerobic bacteriology has involved mainly gas–liquid chromatography of volatile metabolic products and cellular fatty acids[2,3].

We have evaluated the applicability of high-performance liquid chromatography (HPLC) to the rapid identification of *Bacteroides* species by analysing changes in the composition of a defined chemical medium after aerobic incubation for 1 h.

0021-9673/88/$03.50

EXPERIMENTAL

Bacterial strains

Twelve *Bacteroides* isolates were obtained from the collection of the Institute of Microbiology, University of Genoa. The following species were tested: *B. fragilis* (three strains), *B. thetaiotaomicron* (three strains), *B. ovatus* (two strains), *B. vulgatus* (two strains) and *B. distasonis* (two strains). The *Bacteroides* were grown on blood agar plates in an anaerobic chamber for 24 h at 37°C.

Defined chemical medium

A defined chemical medium was formulated containing carbohydrates (raffinose, lactose, glucose, mannose, arabinose and salicin at final concentrations of 7.5, 7.5, 5.0, 2.5, 2.5 and 0.01 mg/ml, respectively) and the same trace factors as those reported by Harpold *et al.*[4]. All the components were dissolved in 20 m*M* potassium phosphate buffer (pH 7.0) and the medium was sterilized by passage through a filter of pore size 0.20 μm.

Aerobic incubation

Each *Bacteroides* isolate was inoculated into an aliquot (1 ml) of the filtered medium to approximately the turbidity of a No. 10 McFarland standard and incubated aerobically at 37°C for 1 h. Bacterial cells were removed by centrifugation, and the supernatants were placed on ice to stop further enzymatic reactions.

HPLC analysis

Samples (20 μl) were injected into the chromatograph for analysis. A modular system (Gynkotek, Munich, F.R.G.), equipped with an Aminex HPX-87H cation-exchange column (30 cm × 7.8 mm I.D.) for carbohydrate analysis (Bio-Rad Labs., Richmond, CA, U.S.A.) was used[5]. The column was kept at 20°C and 3.5 m*M* sulphuric acid was used as the mobile phase at a flow-rate of 0.4 ml/min. The spectrophotometer (SP-4; Gynkotek) was adjusted to 196 nm and 0.04 a.u.f.s. A Model 4290 integrator (Varian, Walnut Creek, CA, U.S.A.) was employed for peak-area quantitation.

Utilization index and production index

The carbohydrate utilization index was determined according to Harpold and Wasilauskas[6]. Lyxose was employed as an internal standard, as it was not metabolized by any of the *Bacteroides* species examined. Zero utilization of a carbohydrate would give an index value of 1 and complete utilization would give 0. A value of greater than 1 could occur if a metabolic product were eluted together with one of the carbohydrates. Indeed, some new compounds that were not present in the original medium were produced during incubation. Production indexes for these new peaks were determined by dividing their areas by that of the internal standard peak.

RESULTS

The HPLC profile of the individual carbohydrates for the uninoculated medium is shown in Fig. 1. Fig. 2 shows a chromatogram of the medium after inoculation

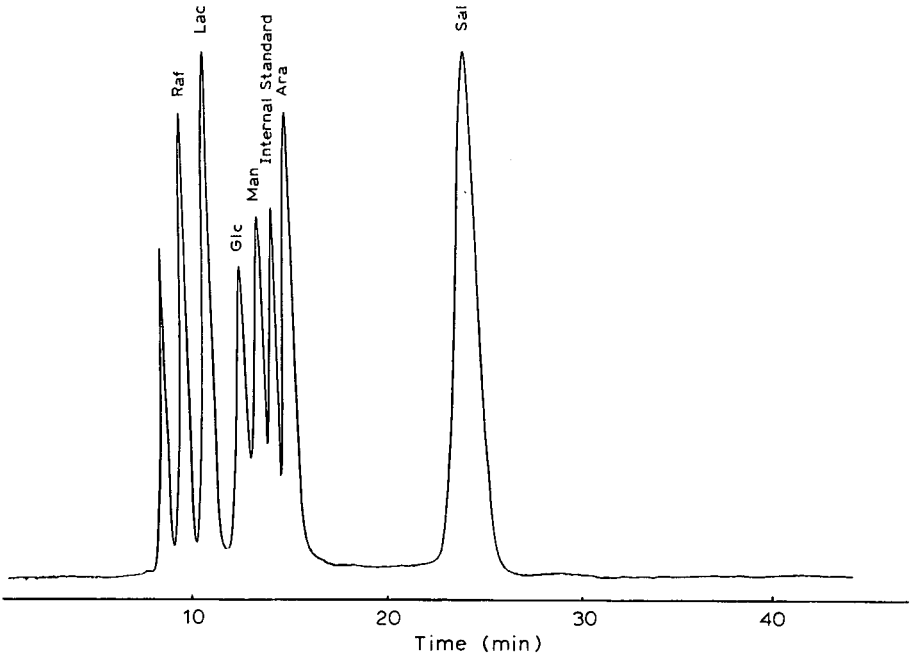

Fig. 1. HPLC profile of the defined chemical medium. Abbreviations as in Table I.

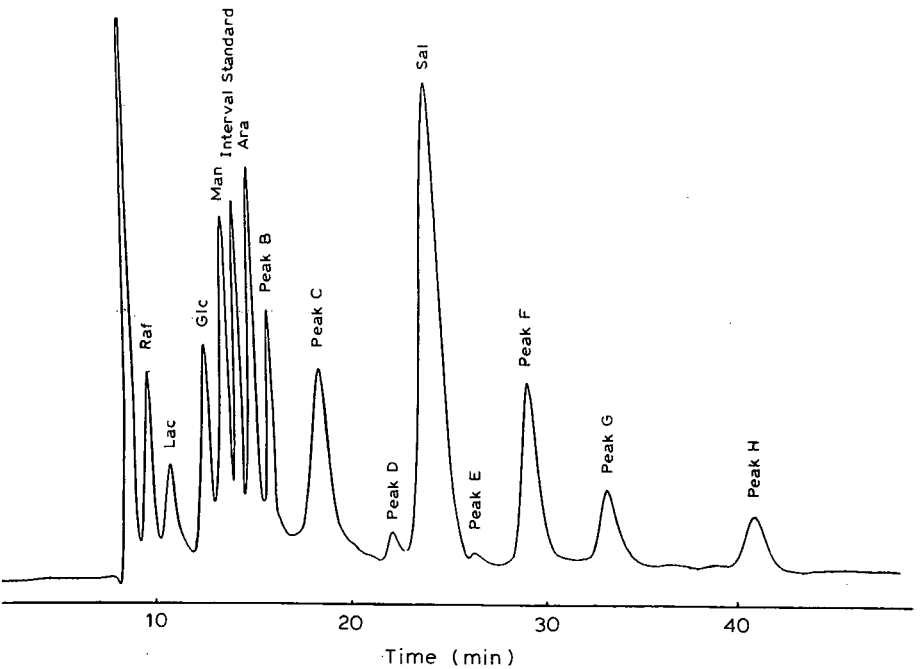

Fig. 2. HPLC profile of *B. fragilis* supernatant after aerobic incubation. Abbreviations as in Table I.

TABLE I

CARBOHYDRATE ULTILIZATION BY *BACTEROIDES*

Species	*Utilization index**					
	Raf	*Lac*	*Glc*	*Man*	*Ara*	*Sal*
B. fragilis	0.33	0.05	0.78	0.82	1.00	1.02
B. thetaiotaomicron	0.60	0.08	0.57	0.75	0.82	1.06
B. ovatus	0.85	0.75	0.65	0.85	0.58	0.78
B. vulgatus	0.12	0.52	0.82	N.D.	0.80	0.90
B. distasonis	0.90	0.84	0.74	0.78	1.02	0.82

* Data represent the mean values of the results obtained for the individual *Bacteroides* strains tested. Raf = raffinose; Lac = lactose; Glc = glucose; Man = mannose; Ara = arabinose; Sal = salicin.

with *B. fragilis,* which metabolized some carbohydrate and produced several new peaks. Each *Bacteroides* species produced typical HPLC patterns that could be used for taxonomic purposes. Table I shows utilization index data for the *Bacteroides* species examined. In addition to the carbohydrate peaks, eight significant new peaks (A–H) were produced. The production index data for these new peaks are shown in Table II. Peak A (retention time 14 min) was eluted between glucose and lyxose, peaks B, C and D (retention times 16, 19 and 23 min, respectively) were eluted between arabinose and salicin and peaks E, F, G and H (retention times 26, 30, 34 and 41 min, respectively) were eluted after salicin.

The *Bacteroides* species examined could be differentiated by their carbohydrate utilization patterns and the formation of new peaks. *B. vulgatus* was the only *Bacteroides* species that produced peak A whereas the production of peak H was a metabolic feature of *B. fragilis. B. ovatus* could be distinguished from the other species by the extent of its arabinose utilization. The remaining two species differed mainly with respect to lactose utilization, as the isolates of *B. thetaiotaomicron* strongly utilized lactose (utilization index 0.08) and those of *B. distasonis* only to a small extent.

TABLE II

NEW PEAKS PRODUCED BY *BACTEROIDES* SPECIES

Species	*Production index**							
	A	*B*	*C*	*D*	*E*	*F*	*G*	*H*
B. fragilis	0	1.07	2.83	0.77	0.55	2.55	1.33	1.99
B. thetaiotaomicron	0	0.69	2.25	0.73	2.08	2.77	0.67	0
B. ovatus	0	0.07	0.24	0.10	0.07	0.45	0.17	0
B. vulgatus	2.02	0.43	0.07	0.07	0.25	0.35	0.41	0
B. distasonis	0	0	0.03	0.01	0	0.07	0.01	0

* Data represent the mean values of the results obtained for the individual *Bacteroides* strains tested.

DISCUSSION

We have evaluated the HPLC monitoring of a chemically defined medium for the rapid identification of *Bacteroides* species. The medium was formulated on the basis of carbohydrate utilization results for *Bacteroides* species reported by other investigators[7]. Preformed enzymes appear to be responsible for carbohydrate utilization as all incubations were performed aerobically.

Utilization of the medium by *Bacteroides* resulted in the production of eight new peaks. Peak A, which was eluted with mannose, had the same retention time as pyruvic acid. Elimination of raffinose from the medium caused the size of peak A, produced by *B. vulgatus,* to decrease appreciably, suggesting that the formation of this peak could result from fermentation of raffinose. Peaks B, C and D have the same retention times as succinic, lactic and acetic acid, respectively. These acids are known to be metabolic products of *Bacteroides* species. Peaks F and G have retention times very close to those of isobutyric and butyric acid, respectively. However, peak F might correspond to a mixture of chemical entities, as the ultraviolet spectrum of the isolated component differed from that of a carboxylic acid.

This HPLC procedure offers the considerable advantage of yielding information about both the carbohydrate utilization and the metabolic end-products, simultaneously. To obtain similar information, it would be necessary to carry out both the biochemical tests of the API 20 A system and the gas chromatographic determination of fatty acids. Moreover, our procedure appears to be much more reliable than biochemical tests, mainly because the carbohydrate utilization by *Bacteroides* species can be determined quantitatively.

The possibility of increasing specificity and sensitivity by applying pre- or post-column derivatization reactions would enhance the utility of this method and provide a more precise identification of the metabolic products of a larger number of *Bacteroides* species[8,9].

REFERENCES

1 P. C. Appelbaum, C. S. Kaufmann, J. C. Keifer and H. J. Venbrux, *J. Clin. Microbiol.*, 18 (1983) 614.
2 T. Ezaki, N. Yamamoto, K. Ninomiya, S. Suzuki and E. Yabuuchi, *Int. J. Syst. Bacteriol.*, 33 (1983) 683.
3 M. A. S. Lambert and A. Y. Armfield, *J. Clin. Microbiol.*, 10 (1979) 464.
4 D. J. Harpold, B. L. Wasilauskas and M. L. O'Connor, *J. Clin. Microbiol.*, 22 (1985) 962.
5 G. Bonn, *J. Chromatogr.*, 322 (1985) 411.
6 D. J. Harpold and B. L. Wasilauskas, *J. Clin. Microbiol.*, 25 (1987) 996.
7 L. V. Holdeman, E. P. Cato and W. E. C. Moore (Editors), *Anaerobe Laboratory Manual,* Virginia Polytechnic Institute and State University, Blacksburg, VA, 4th ed., 1977.
8 N. Watanabe, *J. Chromatogr.*, 330 (1985) 333.
9 N. Takahashi, K. Abbe, S. Takahashi-Abbe and T. Yamada, *Infect. Immun.*, 55 (1987) 652.

Journal of Chromatography, 459 (1988) 337–340
Elsevier Science Publishers B.V., Amsterdam — Printed in The Netherlands

CHROMSYMP. 1497

Note

Improved high-performance liquid chromatographic determination of bacterial collagenase activity in ointments

PIER ANTONIO BIONDI*, FRANCESCA MANCA, ARMANDO NEGRI, CAMILLO SECCHI and GABRIELLA TEDESCHI

Istituto di Fisiologia Veterinaria e Biochimica, Via Celoria 10, 20133 Milan (Italy)

and

CLAUDIO LUCARELLI

Istituto Superiore di Sanità, V. le Regina Elena 299, 00161 Rome (Italy)

Bacterial collagenase (Clostridiopeptidase A, E.C. 3.4.24.3) has been shown to improve the antibiotic action when added to ointments used for topical treatment of ulcers. In order to quantify collagenase activity, labelled peptides have been introduced as substrates to bypass the time-consuming assays which use collagen as a substrate[1–3]. The rapid and simple spectrophotometric method of Wunsch and Heidrich[4] uses the N-protected pentapeptide 4-phenylazobenzyloxycarbonyl-L-Pro-L-Leu-Gly-L-Pro-D-Arg (PZ-peptide), which is hydrolysed by collagenase to PZ-Pro-Leu and then quantified at 320 nm. However, the presence in the tested ointments of compounds with chromophoric groups with a maximum absorption wavelength near 320 nm makes the spectrophotometric procedure unsuitable for collagenase assay. Recently, we devised a procedure to quantify accurately PZ-Pro-Leu, produced from PZ-peptide, by high-performance liquid chromatography (HPLC)[5]. In this study the method previously described was slightly changed and its suitability for collagenase analysis in ointments, where interfering substances are present, was tested.

EXPERIMENTAL

Materials

PZ-peptide, PZ-Pro-Leu and PZ-Pro-Phe were supplied by Serva (Heidelberg, F.R.G.). Ointments, containing collagenase and different antibiotics, were used as model formulations. Iruxol, containing collagenase and chloramphenicol, was supplied by Knoll (Liestal, Switzerland); ointments containing variable amounts of collagenase and rifamicin SV were a gift from Lepetit (Anagni, Italy).

A 2.5-m*M* solution of PZ-peptide was prepared by dissolving it in 2% final volume of methanol and diluting with 50 m*M* Tris–HCl (pH 7.5)–0.1 *M* sodium chloride–10 m*M* calcium acetate. This solution was prepared weekly and kept at −20°C when not used. The purity of PZ-peptide was checked every day by HPLC under the conditions described below. No PZ-Pro-Leu or any other spurious peak due to non-specific hydrolysis was detected even after repeated freezing and thawing cycles. A 0.1 m*M* solution of internal standard (PZ-Pro-Phe) was prepared in the HPLC eluent and maintained at 4°C.

0021-9673/88/$03.50

Chromatographic conditions

A Jasco (Tokyo, Japan) HPLC system, equipped with a Twincle pump and an Uvidec 100-III detector, set at 320 nm, was used. The a.u.f.s. setting of the detector varied between 0.01 and 0.04 depending on collagenase activity tested. Analyses were carried out on a cartridge (25 cm × 4 mm I.D.) packed with LiChrospher 100 RP-18 (5 μm) (Merck, Darmstadt, F.R.G.). A mixture of 0.1 *M* phosphoric acid (adjusted to pH 3 with triethylamine)–acetonitrile (40:60) was used as the eluent at a flow-rate of 0.8 ml/min.

Procedure

About 0.5 g of ointment in a screw-capped vial was extracted by end-over-end mixing for 30 min at 4°C with a mixture of 50 m*M* Tris–HCl (pH 7.5)–0.1 *M* sodium chloride–10 m*M* calcium acetate (2 ml) and light petroleum (b.p. 40–60°C) (3 ml). The aqueous phase was filtered using a Millipore HV 0.45-μm filter and 200 μl were kept at 25°C for 10 min. The enzymatic reaction was started with the addition of 2.5 m*M* PZ-peptide solution (50 μl). At timed intervals (5, 10 and 15 min), 50-μl aliquots were withdrawn and added to 100 μl of 0.1 m*M* PZ-Pro-Phe solution in the HPLC eluent mixture to stop the enzyme activity; 10 μl were finally analysed by HPLC.

PZ-Pro-Leu, produced by enzymatic hydrolysis, was quantitated from the peak height ratio PZ-Pro-Leu/PZ-Pro-Phe and the calibration graph obtained with the pure peptides, according to the procedure previously described[5].

RESULTS AND DISCUSSION

We introduced some slight modifications to the procedure recently described[5] in order to improve the sensitivity and the reproducibility of the method and to make it suitable for the analysis of ointments containing interfering compounds, like rifamycin SV. The HPLC eluent mixture was used to stop the enzyme reaction instead of aqueous citric acid. When the ointment containing rifamycin SV was analysed according to the method previously described, the final pH decrease brought about the precipitation of the antibiotic; consequently, the PZ-peptide peaks drastically decreased in the chromatographic profiles, due to their coprecipitation with rifamycin SV. In contrast, the presence of acetonitrile in the final mixture prevents any precipitation of PZ-peptide and assures total inactivation of the enzyme. The pH was increased from 7.0 to 7.5 following the study of the dependence of collagenase activity on pH, which showed that the maximum activity occurs at pH 7.5.

Another difference between the two procedures is the addition of the internal standard PZ-Pro-Phe at the end of enzyme incubation instead of at the beginning. The methanol used to make up standard stock solutions can cause a partial inactivation of the enzyme when added to the incubation mixture. Addition of the internal standard solution after the incubation allows the final methanol content in the assay mixture to be lowered to 0.4%, eliminating any possible interference with the enzyme action. The PZ-peptide content in the final reaction mixture was lowered from 1 to 0.5 m*M* to prevent partial precipitation when an extract of ointment containing rifamycin SV was analysed. It appears that PZ-peptide and rifamycin SV can interact also at neutral pH in highly concentrated aqueous solutions to give a precipitate which does not allow the enzyme incubation to be homogeneous. Fig. 1 shows two typical chro-

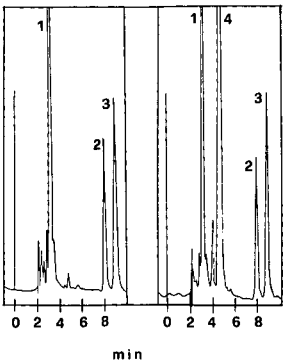

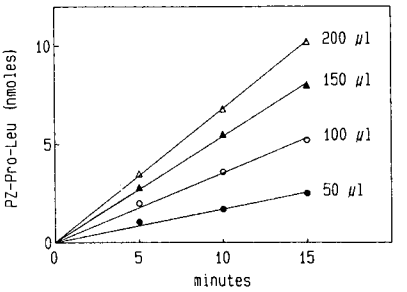

Fig. 1. Typical HPLC profiles, obtained from ointments containing chloramphenicol (left) or rifamycin SV (right), treated according the procedure described. Peaks: 1 = PZ-peptide; 2 = PZ-Pro-Leu; 3 = PZ-Pro-Phe; 4 = rifamycin SV.

Fig. 2. Time dependence of the production of PZ-Pro-Leu with different volumes of ointment extract.

matographic profiles obtained after collagenase extraction from ointments containing chloramphenicol or rifamycin SV. The latter antibiotic appears in the HPLC profile between PZ-peptide and PZ-Pro-Leu without interfering in the quantitative analysis of enzymatic activity.

It is noteworthy that PZ-Pro-Leu can be quantified by spectrophotometric analysis alone in the presence of chloramphenicol which does not significantly absorb at 320 nm but not in the presence of rifamycin SV, which has a maximum absorption wavelength at 314 nm.

In order to verify the possible interference of ointment extract with collagenase activity, the kinetics of the enzyme incubation was controlled. In Fig. 2 the time dependence of the appearance of PZ-Pro-Leu with different volumes of ointment extract is shown to be linear. No PZ-Pro-Leu peak was detected when eluent mixture and substrate solution were added simultaneously to ointment extracts, showing that no activity was detected at time zero. From these data, a linear relationship has been demonstrated between the measured activity and the extract volume for a four-fold range of extract volume (50–200 μl). The equation of the resulting regression line was $y = 0.0034 \cdot$ extract volume (μl) + 0.0075 ($r = 0.998$). The reproducibility of the method was studied by repeated analyses of samples of ointments containing chloramphenicol and rifamicyn SV. The collagenase activity contents were 8.1 ± 0.59 and 3.9 ± 0.26 mU/g (mean $\pm$ S.D., $n = 5$), respectively.

In conclusion, the superior selectivity and sensitivity of HPLC allows accurate measurements of collagenase activity even when interfering compounds are present and, therefore, other analytical procedures are inadequate. The method described appears suitable for routine determinations of the collagenase content in ointment and can be applied to stability studies and other pharmaceutical research problems.

ACKNOWLEDGEMENTS

This work was supported by grants from Ministero della Pubblica Istruzione (40 and 60% funds to P.A.B.).

REFERENCES

1 R. D. Gray, H. H. Saneii and A. F. Spatola, *Biochem. Biophys. Res. Commun.* , 101 (1981) 1251.
2 H. Weingarten and J. Feder, *Anal. Biochem.*, 147 (1985) 437.
3 M. D. Bond, D. S. Auld and R. R. Lobb, *Anal. Biochem.*, 155 (1986) 315.
4 E. Wunsch and H. G. Heidrich, *Hoppe-Seyler's Z. Physiol. Chem.*, 333 (1963) 149.
5 P.A. Biondi, F. Manca, A. Negri, A. Berrini, T. Simonic and C. Secchi, *Chromatographia*, 25 (1988) 659.

Journal of Chromatography, 459 (1988) 341–349
Elsevier Science Publishers B.V., Amsterdam — Printed in The Netherlands

CHROMSYMP. 1496

IMPROVED HIGH-PERFORMANCE LIQUID CHROMATOGRAPHIC ANALYSIS WITH DOUBLE DETECTION SYSTEM FOR L-DOPA, ITS METABOLITES AND CARBIDOPA IN PLASMA OF PARKINSONIAN PATIENTS UNDER L-DOPA THERAPY

P. BETTO, G. RICCIARELLO, M. GIAMBENEDETTI and C. LUCARELLI*
Istituto Superiore di Sanità, V. le Regina Elena 299, 00161 Rome (Italy)
and
S. RUGGERI and F. STOCCHI
I Clinica Neurologica, Università "La Sapienza", V. le dell'Università 30, 00161 Rome (Italy)

SUMMARY

An analytical method is described for measuring L-3,4-dihydroxyphenylalanine (L-DOPA), 3-O-methyl-DOPA, dihydroxyphenylacetic acid, free catecholamines and the peripheral DOPA decarboxylase inhibitor, carbidopa, in plasma samples of Parkinsonian patients by using high-performance liquid chromatography. A sample preparation method is presented for the isolation of the catecholamines and L-DOPA with its metabolites. Catecholamines are extracted by weak cation exchange on small columns and subsequent adsorption on alumina. L-DOPA, 3-O-methyl-DOPA, dihydroxyphenylacetic acid and carbidopa contained in the column effluents are directly injected in the chromatographic system. The eluates are separated on a reversed-phase column, monitored by both a coulometric electrochemical detector and a fluorescence detector, connected in series. Chromatographic peaks were identified on the basis of their retentions and response ratios of the two detectors. Two examples are presented of therapeutic drug monitoring in Parkinsonian patients treated with oral doses and continuous intravenous infusion of L-DOPA.

INTRODUCTION

After 5–7 years of L-3,4-dihydroxyphenylalanine (L-DOPA) therapy, 50–70% of Parkinsonian patients show signs and symptoms which have never been observed during the natural course of this disease. One of the earliest signs is a gradual decrease in efficacy of single-drug administration, clinically expressed by a shortening of the periods of good motor performance after which Parkinsonian symptoms re-emerge (wearing-off). These fluctuations frequently precede the onset of dyskynetic/dystonic involuntary movements, which appear at the beginning and at the end of the periods of efficacy of each single dose. Both the wearing-off and these dyphasic involuntary movements are strictly related to L-DOPA plasma levels. The pathogenesis of fluctuations in motor performance in Parkinson's disease is not fully understood[1,2]. Oscil-

lations in plasma L-DOPA levels and factors interfering with its transport into the brain have been pointed as major problems in the genesis of fluctuations. Maintenance of the L-DOPA plasma concentration is crucial. In fact, by maintaining the plasma level of the drug constant, it is possible to control most of the on/off phenomenon.[3,4].

The transport of L-DOPA through the blood–brain barrier is another important factor. Large neutral amino acids and some L-DOPA metabolites, such as 3-O-methyl-DOPA (OMD), can compete with L-DOPA for the utilization of the barrier carrier[5,6]. The detection of carbidopa (CD), a peripheral decarboxylase inhibitor, is also very important in ensuring that peripheral interferences remain minimal. Simultaneous monitoring of plasma levels of L-DOPA, its metabolites, catecholamines and CD is of great importance in the management of Parkinson's disease and thus there seem to be a definitive need for a simple method of quantitation of these compounds.

Investigation of the metabolism of L-DOPA has been facilitated by the introduction of high-performance liquid chromatography (HPLC), coupled with electrochemical detection (ED). The development of this analytical technique facilitated the establishment of highly sensitive and selective assay procedures for L-DOPA and its metabolites in plasma of Parkinsonian patients[7–21]. Under certain conditions, direct injection of deproteinized plasma into the HPLC system has been reported[11,13,14]. However, this is not applicable to the catecholamines, owing to their much lower levels. The use of C_{18} cartridges for plasma prepurification has also been described[15], but dopamine (DA) cannot be detected. Plasma extraction on alumina allows the determination of CD, L-DOPA, its metabolites and catecholamines, but the recovery is very low especially for dihydroxyphenylacetic acid (DOPAC) and CD[12,18], or OMD determination is not included[21].

Here, we report a purification procedure permitting a selective isolation of free L-DOPA, OMD, CD, DOPAC, norepinephrine (NE), epinephrine (E) and DA. The sample preparation involves extraction of catecholamines by ion exchange on small columns and subsequent adsorption on alumina. The ion-exchange column was washed with water to collect L-DOPA, OMD, DOPAC and CD. The eluate after deproteinization is directly injected in the chromatographic system. The use of the same mobile phase and column for the concurrent assays of catecholamines, L-DOPA and its metabolites increases the throughput of samples in the chromatographic system. Detection is achieved by a coulometric detector and a fluorescence detector, connected in series. Fluorimetric detection of catecholamines is a well known procedure that has been applied to HPLC assays[13,22,23]. The catecholamines, L-DOPA and its metabolites have been monitored by their natural fluorescence but at rather low sensitivity[13]. However during L-DOPA therapy, the levels of these compounds are high enough[19,20] so that detection by both detectors is possible. In regard to those compounds responding to both detectors, the specificity of our detection system, already rendered high thanks to the double potential barrier of the coulometric detector, is further enhanced by the presence of the second detector. The identity of L-DOPA, NE and DA was confirmed by the response ratios of the two detectors. The detection of the other compounds was performed only by ED (CD and DOPAC) or by fluorescence spectrometry (OMD).

EXPERIMENTAL

Materials

NE, E, DA, DOPAC and N-methyldopamine (NMDA, internal standard) were obtained from Sigma (St. Louis, MO, U.S.A.). L-DOPA and CD were gifts from Merck Sharp & Dohme (Darmstadt, F.R.G.). 1-Octanesulphonic acid sodium salt (OSA) and ethylene glycol-O,O′-bis(2-aminoethyl)-N,N,N′,N′-tetraacetic acid (EGTA) were obtained from Fluka (Buchs, Switzerland). Acetonitrile and methanol (HPLC grade) were obtained from Erba (Milan, Italy). Water was purified with the Milli-Q purification system (Millipore, Bedford, MA, U.S.A.). The column materials used for plasma purification were acid alumina AG-4, activated as described by Anton and Sayre[24], from Bio-Rad Labs. (Richmond, CA, U.S.A.) and CM-Sephadex from Pharmacia (Uppsala, Sweden). The anticoagulant/antioxidant solution used for sample treatment contained EGTA (60 mg/ml) and reduced glutathione (90 mg/ml), adjusted to pH 7 with 0.1 *M* sodium hydroxide.

The HPLC system consisted of a M-45 pump (Waters-Millipore, Bedford, MA, U.S.A.), an electrochemical detector (Coulochem 5100 A; ESA, Bedford, MA, U.S.A.) with a 5010 A analytical cell and a fluorescence spectrometer (LS-4; Perkin-Elmer, Norwalk, CT, U.S.A.). The two detectors were connected to a Chemresearch Chromatographic Data Management computer (ISCO, Lincoln, NE, U.S.A.). The samples were introduced with an injection valve (Rheodyne 7125, Berkely, CA, U.S.A.) having a 100-μl loop. The column was a 25 cm × 4.6 mm I.D. Nucleosil C_{18} (particle size 5 μm; Macherey-Nagel, Düren, F.R.G.).

Methods

The eluent was a mixture of 92% 0.025 *M* sodium acetate, 4% methanol and 4% acetonitrile, containing $2 \cdot 10^{-4}$ *M* OSA and $3 \cdot 10^{-4}$ *M* disodium EDTA. The eluent was adjusted to pH 3 with acetic acid. Isocratic elution was carried out at room temperature at a flow-rate of 0.9 ml/min. Potentials of +0.25 and –0.30 V were applied at the first and the second electrode of the analytical cell, respectively. The fluorescence was monitored using an excitation wavelength of 282 nm and an emission wavelength of 322 nm[13]. The two detectors were connected in series, with the fluorescence detector downstream, as its flow cell has a recommended maximum working pressure (450 p.s.i.)[25] lower than that of the ED flow cell (600 p.s.i.)[26].

Blood samples were drawn by venipuncture and transferred immediately to tubes containing 20 μl of EGTA–reduced glutathione solution per ml of blood. Samples were centrifuged at 4°C and the plasma was removed and stored at –80°C until analyzed. Plasma samples (1 ml) were spiked with 30 μl of internal standard solution (NMDA, 80 ng/ml) and applied to a small polypropylene column (2 cm × 0.5 cm) packed with CM-Sephadex pre-swollen in distilled water. Before use, the packed column was washed with 5 ml of 2 *M* hydrochloric acid and 10 ml of distilled water and buffered with 10 ml 0.1 *M* phosphate (pH 7). After sample application the column was rinsed with 5.5 ml of distilled water, discarding the first ml and collecting the next 4.5 ml of effluent in a conical tube, containing 0.5 ml of 0.5 *M* perchloric acid. After centrifugation of the deproteinized solution, the supernatant was removed and 10 μl of the solution were injected into the chromatograph for the determination of L-DOPA and its metabolites.

The catecholamines were eluted from the cation-exchange column with 3 ml of 0.5 *M* perchloric acid and the eluate was collected in 15-ml conical tubes. A 2-ml volume of Tris buffer (1.5 *M*, pH 9.3) containing 0.06 *M* EDTA and 20 mg of alumina were added. The tube was vortexed for 2 min, the supernatant was removed and the alumina was washed twice with 2 ml of water, centrifuging (3000 *g*) for 3 min between each washing. After the second washing, as much water as possible was removed. The catecholamines were eluted from the alumina with 100 µl of 0.1 *M* acetic acid after vortex mixing for 2 min. After centrifugation, the supernatant was removed and 25 µl were injected[27].

RESULTS AND DISCUSSION

The specific and sensitive method reported here for the determination of free L-DOPA, its metabolites and some catecholamines in human plasma employs HPLC with the use of two different detection systems (ED and fluorimetric detection) connected in series. The chromatographic conditions for all compounds of interest, expecially CD and OMD, were greatly improved compared with the case of only one detector. The retention times of these compounds, as described by other authors[20], were similar in a variety of previously used mobile phases, and their simultaneous determination was previously impossible in clinical samples without the use of the two detectors. This is evident from Fig. 1 A and B, where the separation of a standard

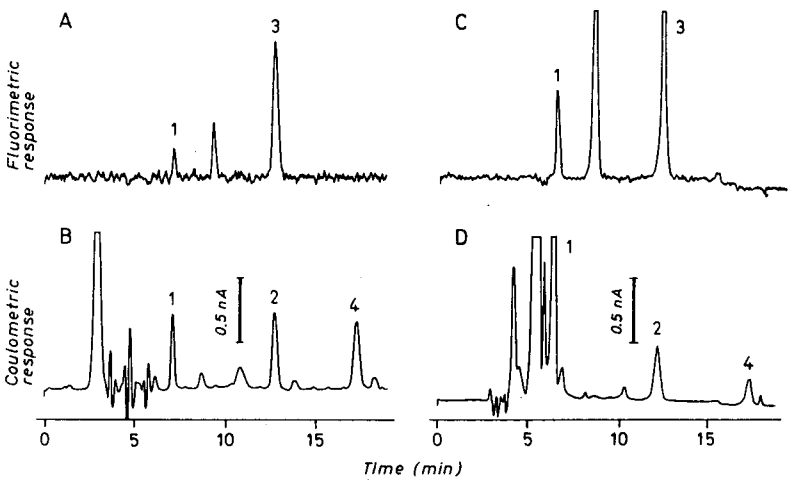

Fig. 1. Chromatograms of: (A),(B) 10 µl standard mixture of L-DOPA (20 ng/ml), CD (80 mg/ml), OMD (80 ng/ml) and DOPAC (20 ng/ml); (C),(D) 10 µl aqueous eluate obtained from the plasma of a patient undergoing L-DOPA therapy, according to the method described in the text. Peaks: 1 = L-DOPA; 2 = CD; 3 = OMD; 4 = DOPAC. The use of two detectors allowed the quantitative analysis of all compounds in the L-DOPA group. Since the retention times of OMD and CD were similar, we took advantage of their different detectabilities by the two detectors. Conditions: column, Nucleosil RP-C_{18}, 5 µm, 250 mm × 4.6 mm I.D.; room temperature; flow-rate, 0.9 ml/min; mobile phase, 0.0025 *M* sodium acetate–methanol–acetonitrile (92:4:4) (pH 3), detection, coulometric (E_1 +0.25 V, E_2 = −0.3 V), fluorimetric (excitation 282 nm, emission 322 nm). The signal-to-noise ratio of (C) seems to be different from that of (A) but really they are equal: it is simply the result of a stronger photoreduction of the original size, rendered necessary by the higher chart speed used in that experiment.

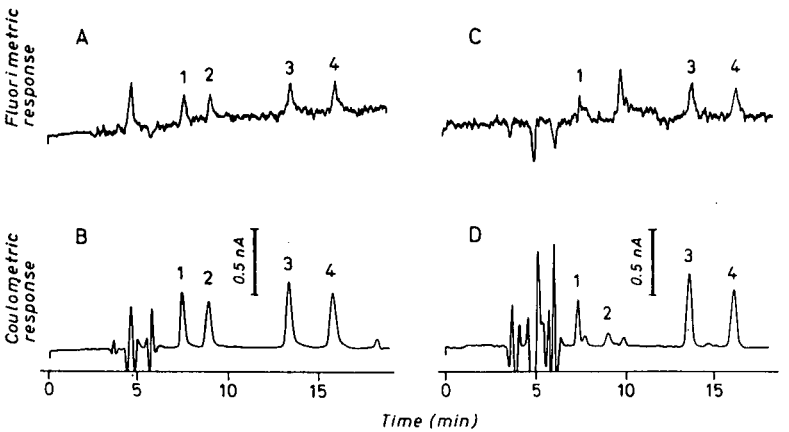

Fig. 2. Chromatograms of: (A),(B) 5 μl standard mixture of NE (34 ng/ml), E (13 ng/ml), DA (25 ng/ml) and NMDA (50 ng/ml, internal standard); (C),(D) 25 μl acetic eluate obtained from the plasma of a patient undergoing L-DOPA therapy according to the method described. For conditions see Fig. 1. Peaks: 1 = NE; 2 = E; 3 = DA; 4 = NMA.

mixture of L-DOPA, CD, OMD and DOPAC is shown. OMD and CD can be determined because the first is detected only by the fluorescence detector while the second is detected only by ED. The chromatograms were recorded at an expansion factor of 100 for the fluorescence detector and at a gain of × 5000 for the coulometric detector.

Fig. 2A and B show typical chromatograms of a standard solution of NE, E, DA and NMDA obtained with the two detectors. The chromatographic conditions were the same as in Fig. 1. Parts C and D of Figs. 1 and 2 show chromatograms of a plasma extract containing L-DOPA and its metabolites and the catecholamines, respectively.

The wide L-DOPA concentration range of the analyzed plasma samples (394–2351 ng/ml) forced us to utilize the coulometric detector with a gain not higher than × 5000. The low sensitivity allowed us to measure E, usually detectable in plasma by HPLC–ED[27], only in a few of the samples examined in this study. The case whose chromatogram is reported in Fig. 2C is one of them.

Recoveries of prepurification steps for L-DOPA, CD, DOPAC and NMDA were checked by analyzing plasma spiked with known amounts of substances ($n = 5$). As shown in Table I, the recoveries were nearly 100%. Consequently, the internal standard was not used routinely.

The reproducibility of the proposed method was established by the replicate analyses of a plasma pool, spiked with L-DOPA and its metabolites. Table II lists means, standard deviations and coefficients of variation ($n = 5$).

Linearity tests of L-DOPA, CD, OMD and DOPAC were performed by adding known amounts of the compounds to a pooled sample of plasma subjected to the complete preparation procedure. The detector response was linear for all compounds over the range 5–80 ng/ml for L-DOPA and DOPAC and 10–160 ng/ml for CD and OMD. Table III shows the regression lines for the four compounds. The values for catecholamines, absolute recovery, reproducibility and linearity, are in accord with data previously reported[27].

TABLE I

ABSOLUTE RECOVERY (%) AT DIFFERENT CONCENTRATIONS OF L-DOPA, OMD, DOPAC AND CD AFTER PURIFICATION BY USING A CATION-EXCHANGE COLUMN AND A DE-PROTEINIZATION PROCEDURE

Each value is the average of five analyses ± standard deviation.

Concentration (ng/ml)	*Recovery (%)*			
	L-DOPA	*DOPAC*	*CD*	*OMD*
5	99.1 ± 3.2	97.2 ± 4.0		
20	106.1 ± 2.7	93.2 ± 4.7	99.3 ± 4.7	97.6 ± 5.1
40	102.1 ± 4.5	99.8 ± 3.5		
80			108.0 ± 2.1	98.4 ± 5.4
160			102.2 ± 4.1	100.0 ± 5.1

The peaks of L-DOPA, its metabolites and catecholamines were identified by a combination of methods. The peak identification for all compounds was performed on the basis of the chromatographic retention time and by simultaneous injection of a standard. Secondly, for compounds detectable by both detectors (L-DOPA, NE, E, DA and NMDA), the ratios of ED/fluorimetric response were calculated and compared with those obtained with plasma samples. The peak-height ratios of reference compounds and those obtained with plasma samples are reported in Table IV. If a signal-to-noise ratio of 2 is assumed, the detection limits of L-DOPA, CD, OMD, DOPAC, NE, E, DA and NMDA were (expressed as pg) 20, 40, 40, 20, 10, 10, 10 and 10 respectively. As explained before (see Methods) we had to position the fluorescence detector downstream. We did not investigate whether peak components detected by fluorescence are electrolyzed products according to a coulometric detector or unelectrolyzed. Nevertheless, from the values of the potentials applied (+ 0.25 V, –0.30 V at the first and the second electrode, respectively), we considered an oxidation (first) counter balanced by a reduction (secondly) with a negligible final effect. Whatever the case, it is reasonable that if the influence of any reaction would not matter since the standards and plasma extracts are analyzed under perfectly identical conditions.

TABLE II

REPRODUCIBILITY OF THE METHOD

Mean values, standard deviations and coefficients of variation (C.V.) of plasma samples spiked with known quantities of L-DOPA, its metabolites and CD, $n = 5$.

	Fluorescence detector		*ED*	
	Plasma (ng/ml)	*C.V. (%)*	*Plasma (ng/ml)*	*C.V. (%)*
L-DOPA	19.2 ± 0.2	4.9	18.7 ± 0.7	3.5
CD	–	–	83.1 ± 3.1	3.6
OMD	78.4 ± 3.0	3.8	–	–
DOPAC	–	–	79.6 ± 3.8	5.6

TABLE III

LINEARITY OF RESPONSE AS A FUNCTION OF CONCENTRATION

y = peak heights of L-DOPA, CD, OMD and DOPAC; x = amount (ng/ml). Values for L-DOPA, CD and DOPAC obtained by ED, values for OMD obtained by fluorimetric detector.

	Range tested	*Regression equation*	*r*
L-DOPA	5–80	$y = 8.42x + 0.91$	0.9998
CD	10–160	$y = 1.85x + 1.75$	0.9992
OMD	10–160	$y = 3.89x + 0.99$	0.9983
DOPAC	5–80	$y = 7.43x + 0.25$	0.997

TABLE IV

PEAK-HEIGHT RATIOS

The values represent the ratio of peak height obtained with ED to that obtained with the fluorimetric detector for standard solutions and for plasma. The data are used to confirm peak identity. Results are the mean ± S.D. of ten experiments. The E level in the majority of plasma samples examined was too low to be measured under our operating conditions.

Compound	*Standards*	*Plasma*
L-DOPA	2.68 ± 0.21	2.62 ± 0.15
NE	1.95 ± 0.18	1.85 ± 0.27
E	2.05 ± 0.14	-
DA	2.58 ± 0.19	2.47 ± 0.15
NMDA	2.20 ± 0.18	2.31 ± 0.20

TABLE V

DETERMINATION OF L-DOPA METABOLITES AND CATECHOLAMINES IN PLASMA FROM PARKINSONIAN PATIENTS TREATED BY CONTINUOUS L-DOPA INFUSION

Each value represents the mean of three determinations. The values are expressed as ng/ml of plasma; n.d. = not detectable (< 0.5 ng/ml for the catecholamines and < 5 ng/ml for the other compounds). CD and DOPAC levels were not detectable (L-DOPA infusion rate = 80 mg/h).

Time (min)	*L-DOPA*	*OMD*	*NE*	*DA*
0	n.d.	2630 ± 210	n.d.	0.51 ± 0.03
30	394 ± 41	2036 ± 190	0.60 ± 0.05	0.74 ± 0.08
60	635 ± 38	2346 ± 244	0.51 ± 0.07	0.58 ± 0.04
90	563 ± 59	2012 ± 153	0.62 ± 0.04	0.92 ± 0.09
120	818 ± 57	2217 ± 124	0.52 ± 0.07	1.19 ± 0.07
180	979 ± 49	2700 ± 249	1.39 ± 0.06	2.94 ± 0.16
240	1114 ± 105	2752 ± 263	1.46 ± 0.0	2.97 ± 0.23

TABLE VI

DETERMINATION OF L-DOPA METABOLITES AND CATECHOLAMINES IN PLASMA FROM A PARKINSONIAN PATIENT FOLLOWING ORAL ADMINISTRATION (125 mg of L-DOPA + 12.5 mg of CD)

Each value represents the mean of three determinations. The values are expressed as ng/ml of plasma; n.d. = not detectable (< 0.5 ng/ml for catecholamines and 5 ng/ml for the other compounds).

Time	*L-DOPA*	*CD*	*OMD*	*DOPAC*	*NE*	*DA*
0	n.d.	n.d.	3000 ± 248	n.d.	0.97 ± 0.05	0.27 ± 0.02
30	500 ± 40	1212 ± 145	2453 ± 245	25 ± 1.5	0.82 ± 0.06	0.77 ± 0.06
60	2351 ± 180	295 ± 27	1325 ± 427	126 ± 11.1	1.21 ± 0.05	3.27 ± 0.26
90	2001 ± 160	n.d.	3388 ± 277	n.d.	0.71 ± 0.02	2.67 ± 0.16
120	1065 ± 115	800 ± 96	2548 ± 129	n.d.	0.71 ± 0.04	1.99 ± 0.18
180	866 ± 53	n.d.	3740 ± 411	75 ± 3.2	0.45 ± 0.04	0.88 ± 0.04
240	587 ± 37	n.d.	3969 ± 357	82 ± 6.6	n.d.	n.d.

Plasma samples from nine Parkinsonian patients, obtained during L-DOPA therapy, were analyzed. The results demonstrated large individual differences. Here, we report two cases as an example of the applicability of this method in the study of Parkinson patients. The case shown in Table V was treated by continuous L-DOPA infusion. From the L-DOPA plasma level it appears that this technique is able to maintain a constant level of the drug and thus control motor fluctuations. The level of OMD never reached the critical point (600 ng/ml), at which the action of L-DOPA is inhibited[28].

The second case (Table VI) shows the pharmacokinetics of oral L-DOPA, which produces a peak blood level after 60 min which then rapidly declines.

Our technique also allowed us to detected DA. The values obtained indicate that, despite the peripheral decarboxylase inhibitor, some DA is still present in the peripheral circulation.

REFERENCES

1 C. D. Marsden and J. D. Parkes, *Lancet*, i (1976) 292.
2 K. M. Shaw, A. J. Lees and G. M. Stern, *Q. J. Med.*, 49 (1980) 283.
3 J. G. Nutt, W. R. Woodward, J. P. Hammerstad, J. H. Carter and J. L. Anderson, *N. Engl. J. Med.*, 310 (1984) 483.
4 I. Shoulson, G. A. Glaubiger and T. N. Chase, *Neurology*, 25 (1975) 1144.
5 A. Reches and S. Fahn, *Ann. Neurol.*, 12 (1982) 267.
6 J. G. Nutt, W. R. Woodward and J. L. Anderson, *Ann. Neurol.*, 18 (1985) 537.
7 T. A. Hare, B. L. Beasley, R. A. Chambers, D. H. Boehme and W. H. Vogel, *Clin. Chim. Acta*, 45 (1973) 273.
8 R. M. Riggin, R. L. Alcorn and P. T. Kissinger, *Clin. Chem.*, 22 (1976) 782.
9 E. Nissinen and J. Taskinen, *J. Chromatogr.*, 231 (1982) 459.
10 R. C. Causon, M. J. Brown, K. L. Leenders and L. Wolfson, *J. Chromatogr.*, 277 (1983) 115.
11 M. F. Beers, M. Stern, H. Hurtig, G. Melvin and A. Scarpa, *J. Chromatogr.*, 336 (1984) 380.
12 D. S. Goldstein, R. Stull, R. Zimlichman, P. D. Levinson, H. Smith and H. R. Keiser, *Clin. Chem.*, 30 (1984) 815.
13 T. Ishimitsu and S. Hirose, *J. Chromatogr.*, 337 (1985) 239.
14 T. Ishimitsu and S. Hirose, *Anal. Biochem.*, 150 (1985) 300.
15 M. Gerlach, N. Klaunzer and H. Przuntek, *J. Chromatogr.*, 380 (1986) 379.

16 M. A. Mena, V. Muradas, E. Bazan, J. Reiriz and J. G. de Yebenes, *Adv. Neurol.*, 45 (1986) 481.
17 A. Baruzzi, M. Contin, F. Albani and R. Riva, *J. Chromatogr.*, 375 (1986) 165.
18 C. Lucarelli, P. Betto, M. Giambenedetti, G. Ricciarello, S. Ruggeri and F. Stocchi, *G. Ital. Chim. Clin.*, 12 (1987) 223.
19 Y. Michotte, M. Moors, D. Deleu, P. Herregodt and G. Ebinger, *J. Pharm. Biomed. Anal.*, 5 (1987) 659.
20 J. M. Cedarbaum, R. Williamsson and K. Hutt, *J. Chromatogr.*, 415 (1987) 393.
21 C. R. Freed and P. Asmus, *J. Neurochem.*, 32 (1979) 163.
22 A. M. Krstulovich, S. W. Dziedzic, L. Bertani-Dziedzic and D. E. Di Rico, *J. Chromatogr.*, 217 (1981) 523.
23 K. Mori, *J. Chromatogr.*, 218 (1981) 631.
24 A. H. Anton and D. F. Sayre, *J. Pharmacol. Exp. Ther.*, 138 (1962) 360.
25 *Model LS-4 Fluorescence spectrometer, Operator's manual,* Perkin-Elmer, Beaconsfield,
26 *The model 5100 A, Coulochem detector, Instruction manual,* ESA, Bedford, MA, 1986.
27 C. Lucarelli, P. Betto, G. Ricciarello, M. Giambenedetti, F. Sciarra, C. Tosti Croce and P. L. Mottironi, *Chromatographia,* 24 (1987) 423.
28 J. G. Nutt and Woodward, *Ann. Neurol.*, 21 (1987) 584.

Journal of Chromatography, 459 (1988) 351–360
Elsevier Science Publishers B.V., Amsterdam — Printed in The Netherlands

CHROMSYMP. 1473

DETERMINATION OF 5-HYDROXYTRYPTAMINE AND 5-HYDROXYINDOLEACETIC ACID IN PLASMA BY DIRECT INJECTION IN COUPLED-COLUMN LIQUID CHROMATOGRAPHY WITH ELECTROCHEMICAL DETECTION

BRITT-MARIE ERIKSSON* and BENGT-ARNE PERSSON
Bioanalytical Chemistry, AB Hässle, S-431 83 Mölndal (Sweden)

SUMMARY

A method is described that allows determination of 5-hydroxytryptamine (5-HT) and 5-hydroxyindoleacetic acid (5-HIAA) in platelet-poor human blood plasma after direct injection of 50–100 μl of plasma into a coupled-column liquid chromatographic system. The chromatographic system comprised an enrichment column and two separation columns with different selectivity properties. The samples were injected into the C_{18} enrichment column, which was eluted with a buffer solution as the mobile phase. 5-HT, 5-HIAA and the internal standard 5-hydroxy-N-methyltryptamine (5-HMT) were then desorbed by a stronger mobile phase and flushed into a cation exchanger, which separated 5-HT and 5-HMT. 5-HIAA passed straight through and was switched to a C_{18} column where it was retarded. After 5-HT and 5-HMT had been eluted from the cation exchanger and detected, the eluate from the C_{18} column was directed to the detector and 5-HIAA was determined. Basic plasma levels, about 4 n*M* for 5-HT and 30 n*M* for 5-HIAA, were measured with a relative standard deviation of about 5%.

INTRODUCTION

Blood platelets are a primary source of 5-hydroxytryptamine (5-HT), and measurements of intra- and extraplatelet concentrations of this biogenic amine are of interest in studies of haemostasis, thrombosis and different cardiovascular diseases[1,2].

A very sensitive method is needed for assaying platelet-poor plasma samples, where the concentration of 5-HT can be of the order of a few picomoles per ml. Various methods have been applied to the determination of 5-HT in biological fluids. Liquid chromatography with fluorometric[3,4] or electrochemical[5–8] detection provides high sensitivity. The assays often require precipitation of proteins[3,4] or sample purification and concentration steps, such as solvent extraction[6–8] or ion-exchange extraction[5]. Several authors have reported lowered recoveries after precipitation of proteins, probably due to co-precipitation of the compounds or decreased stability in the acidic environment[4,9–11].

We have developed a method for the concurrent measurement of 5-HT and its

0021-9673/88/$03.50

metabolite 5-hydroxyindoleacetic acid (5-HIAA) based on liquid chromatography with coupled column and electrochemical detection. The method is rapid and sensitive and does not require pre-purification of the plasma sample.

EXPERIMENTAL

Apparatus

The liquid chromatograph comprised three pumps, Model 2150 (LKB-Produkter, Bromma, Sweden), a pulse dampener (Touzart-Matignon, Vitry-sur-Seine, France), an automatic injector, ISS-100 (Perkin-Elmer, Überlingen, F.R.G.), with a refrigerated sample tray and injection vials (0.3 ml) of borosilicate glass (Chromacol, London, U.K), a Model 4270 integrator (Spectra-Physics, San Jose, CA, U.S.A.) and a M 460 electrochemical detector (Waters Assoc., Milford, MA, U.S.A.), in combination with a TL-5A thin-layer cell (Bioanalytical Systems, West Lafayette, IN, U.S.A.), comprising a glassy carbon working electrode, a stainless-steel auxiliary electrode and a silver–silver chloride reference electrode.

The switching events were controlled by the integrator and were performed by three pneumatically operated six-port valves, Model 7010 (Rheodyne, Berkeley, CA, U.S.A.) and an interface constructed by the Instrument Department, Hässle (Mölndal, Sweden). A refrigerated microcentrifuge, Model 154 RF (Ole Dich, Instrumentmakers, Hvidovre, Denmark), was used for centrifugation and a MSE (Crawley, U.K.) Soniprep 150 ultrasonic disintegrator for the disruption of platelets.

Chemicals

5-HT hydrochloride, 5-HIAA, 5-hydroxyindole-2-carboxylic acid (5-HICA), N-acetyl-5-hydroxytryptamine (Ac-5-HT), ethylene glycol bis (β-aminoethyl ether)-N′,N′-tetraacetic acid (EGTA) and reduced glutathione (GSH) were obtained from Sigma (St. Louis, MO, U.S.A.), 5-hydroxy-N-methyltryptamine (5-HMT) oxalate from EGA-Chemie (Steinheim, F.R.G.), 5-hydroxyindole-3-propionic acid (5-HIPA) and 5-hydroxytryptophol (5-HTOL) from Regis (Morton Grove, IL, U.S.A.) and hexanesulphonic acid sodium salt from Eastman Kodak (Rochester, NY, U.S.A.). Disodium ethylenediaminetetraacetate (EDTA), citric acid and all buffer substances and inorganic acids were of analytical reagent grade (E. Merck, Darmstadt, F.R.G.), and acetonitrile and methanol were of HPLC grade (Rathburn, Walkerburn, U.K.).

Chromatography

A schematic drawing of the chromatographic system is shown in Fig. 1, and a time schedule for the switching of the valves is presented in Table I. The enrichment column was a LiChroprep RP-18 column (50 mm × 4.6 mm I.D.) with 15–25 or 25–40 μm particles from E. Merck and 2-μm titanium frits from Upchurch (Oak Harbor, WA, U.S.A.). The separation columns were a Nucleosil 5 C_{18} column (150 mm × 4.6 mm I.D.) and a cation-exchange column, Nucleosil 5SA (50 mm × 3 mm I.D.), packed with particles from Macherey-Nagel (Düren, F.R.G.).

The enrichment and cation-exchange columns were packed with a viscosity slurry packing technique using methanol as the pressure liquid and a suspending liquid consisting of toluene–dioxane–cyclohexanol (1:1:4) and toluene–cyclohexanol (4:5), respectively[12]. The C_{18} column was obtained prepacked.

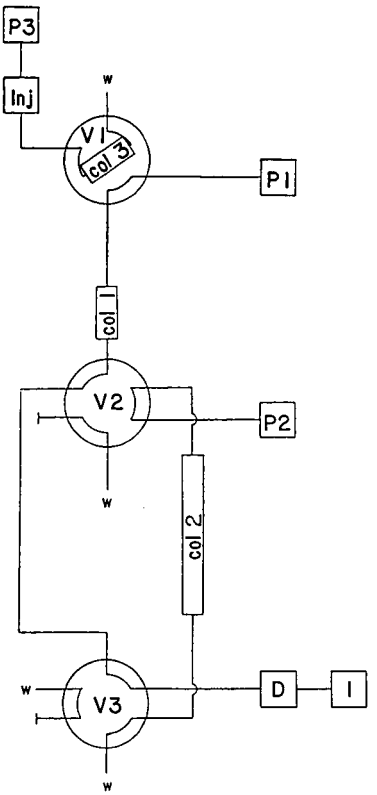

Fig. 1. Coupled-column liquid chromatographic system. P1, P2 and P3 = pumps with mobile phases 1 (citrate buffer, pH 5, $I=0.2$, containing 13% methanol), 2 (citrate buffer, pH 4.5, $I=0.2$, containing 10% methanol) and 3 (citrate buffer, pH 4, $I=0.1$); Inj = autoinjector; Col 1 = Nucleosil 5SA; Col 2 = Nucleosil $5C_{18}$; Col 3 = LiChroprep RP-18; V1, V2 and V3 = six-port valves; D = electrochemical detector; I = integrator; w = waste. For further details, see text.

TABLE I
TIME SCHEDULE FOR THE COLUMN SWITCHING

Time after injection (min)	*Switch valve No.*	*Comment*
0.0		The sample is injected into the enrichment column (3) with buffer for 3 min
3.0	1	The indoles are back-flushed from column to the cation-exchange column (1) with buffer containing methanol
3.6	2	5-HIAA is switched from column 1 to the C_{18} column (2) for 1.3 min
4.9	2 reset	The eluate from column 1 is recorded
14.0	3	The eluate from column 2 is recorded
14.1	1 reset	Column 3 is equilibrated with buffer
19.0	3 reset	The chromatogram is completed, and after recording the results, the next sample is injected

The mobile phases were citrate buffer (pH 4; ionic strength, $I=0.1$) for the enrichment column, citrate buffer (pH 5, $I=0.2$) containing 13% methanol for the separation on the cation exchanger and citrate buffer (pH 4.5, $I=0.2$) containing 10% methanol for the separation on the C_{18} column. The compositions of the buffers were 70 m*M* citric acid and 82 m*M* sodium hydroxide for pH 4, $I=0.1$, 70 m*M* citric acid and 131 m*M* sodium hydroxide for pH 5, $I=0.2$ and 95 m*M* citric acid and 145 m*M* sodium hydroxide for pH 4.5, $I=0.2$. Deionized and filtered water (Milli Q; Millipore, Bedford, MA, U.S.A.) was used for the mobile phases, which, prior to use, were degassed and filtered through a 0.45-μm MF Millipore filter. The flow-rate was 1 ml/min at ambient temperature and the eluent was monitored with an electrochemical detector, operated at +0.6 V. The detector cell was housed in a Faraday cage to avoid electrical disturbances.

Sample preparation

The blood samples were collected in chilled tubes of polypropylene, containing a small volume (20 μl/ml blood) of a solution (pH 5–7) of an anticoagulant, EGTA (0.2 *M*), and an antioxidant, GSH (0.2 *M*). These stabilizing agents are commonly used for catecholamines. After gentle mixing, the contents of the tubes were centrifuged at 10 000 *g* and 4°C for 10 min. The samples were stored at −70°C until analysed. After thawing and mixing of the sample, 100 μl of plasma and 20 μl of the internal standard, 5-HMT (2 μ*M*), were added to the injection vial which was capped and vortex-mixed before injection of 10–100 μl into the chromatographic system. Standard solutions of 5-HT, 5-HIAA and 5-HMT were prepared in phosphate buffer (pH 6), containing 5 m*M* EDTA, and when kept in portions at −70°C they were stable for 1 year. The buffer composition was 69 m*M* sodium dihydrogenphosphate and 10 m*M* disodium hydrogenphosphate.

Calibration was performed by injection of a mixture of 100 μl standard solution and 20 μl internal standard solution, and by measuring peak-height ratios. The median value of the calibration samples were used to calculate the concentrations of 5-HT and 5-HIAA in the unknown samples.

RESULTS AND DISCUSSION

Chromatography

Resolution of 5-HT, 5-HIAA and the internal standard, 5-HMT, was easily accomplished on a Nucleosil $5C_{18}$ column (150 mm × 4.6 mm I.D.) with a mobile phase of citrate buffer (pH 5, $I=0.1$) with 10% methanol as the organic modifier. Rabbit plasma samples containing *ca.* 100 n*M* of 5-HT and 5-HIAA were analyzed after direct injection of 10 μl of plasma. However, when an higher sensitivity was required, 5-HT was incompletely separated from interfering components originating from the plasma matrix. An increase in the retardation of 5-HT, by adding hexanesulphonate as counter ion to the mobile phase, did not adequately improve the selectivity.

Two-column system

By replacing the C_{18} column with a cation-exchange column, Nucleosil 5SA (50

mm × 3 mm I.D.), clean chromatograms of 5-HT were obtained while 5-HIAA was eluted too close to the front peak. This problem was solved by use of the cation-exchange column and the C_{18} column with a column-switching valve. After passage through the cation exchanger, 1.3 ml of the eluate, containing 5-HIAA, were switched to the C_{18} column, where 5-HIAA was retarded. The mobile phase for the cation exchanger was a citrate buffer (pH 5.0, $I=0.2$) containing 13% methanol.

After 5-HT and 5-HMT had been eluted from the cation exchanger and detected, the eluate from the C_{18} column was directed to the detector by a second valve and 5-HIAA was determined. To obtain a suitable retention time of 5-HIAA on the C_{18} column, a mobile phase, containing 10% methanol, an ionic strength of 0.2 and a pH of 4.5, was used.

This chromatographic system comprising two separation columns, a cation-exchange and a C_{18} column, was used for direct injection of rabbit plasma samples when 10 μl or less were sufficient to enable the measurement of 5-HT and 5-HIAA. A guard column (15 mm × 3 mm I.D.), containing 3-μm CN particles (Brownlee, Santa Clara, CA, U.S.A.), was inserted before the cation-exchange column and replaced when a total volume of about 400 μl of plasma had been injected into it. The cation exchanger was replaced when retention times became shorter, after assaying *ca.* 250 plasma samples. In Fig. 2 is shown a chromatogram obtained after injection of 10 μl of rabbit plasma into the two-column system.

We also performed experiments in which the cation exchanger was used in combinaton with an anion exchanger, Spherisorb SAX, 5-μm, 150 mm × 4.6 mm I.D. (PhaseSep, Norwalk, CT, U.S.A.). 5-HIAA was retarded on the anion exchanger, with

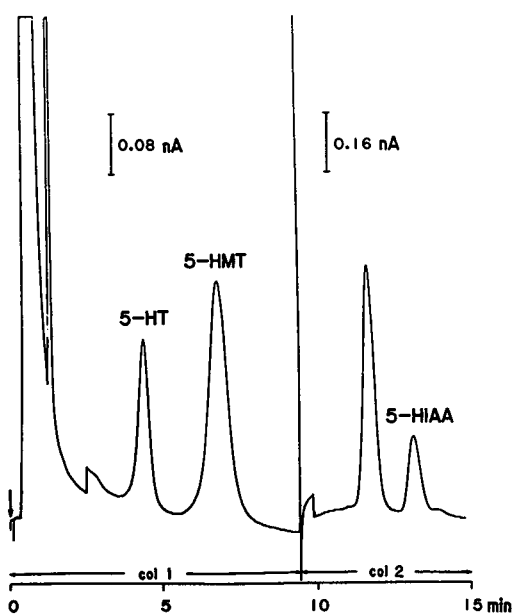

Fig. 2. Chromatogram of a rabbit plasma sample, containing 377 n*M* of 5-HT, 995 n*M* of 5-HMT and 354 n*M* of 5-HIAA, injected into the two-column liquid chromatographic system. Injection volume: 10 μl.

pure citrate buffer as the mobile phase, while 5-HT passed straight through and was switched to the cation exchanger. However, when plasma samples were injected directly into the anion-exchange column, we did not succeed in obtaining clean chromatograms of 5-HIAA.

Three-column system

For platelet-poor human plasma samples with very low concentration levels of 5-HT, injection volumes of 50–100 μl were required. To enable direct injection of these quantities of plasma, an enrichment column was placed in the loop position of a valve, and the plasma samples were applied to this column with a buffer solution as the mobile phase. After an appropriate time, 5-HT, 5-HIAA and 5-HMT were desorbed and backflushed with the stronger eluent into the cation exchanger, and the separations were performed as described above for the two-column system. While 5-HIAA was being measured, the buffer solution was switched back to the enrichment column to equilibrate it before the next injection. In Fig. 3 is shown a chromatogram obtained after injection of 100 μl of an human plasma sample into the three-column system.

Enrichment column

Precolumns with various packing materials were tested for their retardation ability and column efficiency. This was accomplished by connecting the detector directly to the effluent of the enrichment column. Columns containing packing materials with 5-μm particle diameters, *e.g.*, prepacked C_{18} columns (30 mm × 4.6 mm I.D.) from Brownlee gave too high a back pressure after injection of a total volume of a few hundred microlitres of plasma, and C_{18} columns (40 mm × 4.6 mm I.D.) containing particles of diameter 10 and 40 μm did not show any retardation of the

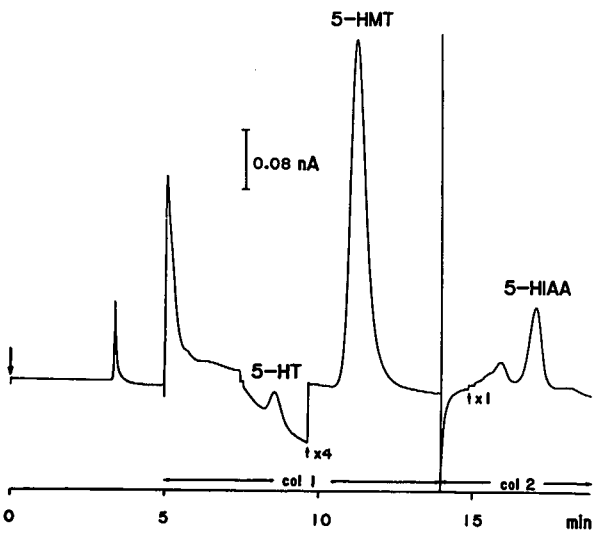

Fig. 3. Chromatogram of an human plasma sample, containing 3.8 n*M* of 5-HT, 238 n*M* of 5-HMT and 26.2 n*M* of 5-HIAA, injected into the three-column liquid chromatographic system. Injection volume: 100 μl.

solutes. We then packed columns (50 mm × 4.6 mm I.D.), equipped with titanium frits instead of steel frits, with various packing materials. According to reports in the literature, steel frits may interact with proteins, causing blockage and thus higher back pressure[13,14]. Another advantage of titanium frits, over steel frits, is that they gave a lower background current in electrochemical detection and can be used without any pretreatment. Steel frits had to be treated with a strong acid in an ultrasonic bath before use in order to lower the background current.

The packing materials LiChroprep RP-18, 15–25 and 25–40 μm, gave satisfactory results. A retention time of 9.5 min for 5-HT, the least retarded compound, was obtained with citrate buffer ($I=0.1$, pH 4) as the mobile phase. The buffer was passed through the column for 3 min, to wash out rapidly eluted compounds, before desorbing the solutes by backflushing with the stronger eluent. With citrate buffer as the mobile phase, the retardation of 5-HIAA reached a maximum at pH of *ca.* 4. At more acidic pH, less retardation was unexpectedly obtained. This might be due to displacement effects. A total plasma volume of about 5 ml was injected into the column before replacement.

Internal standard

An internal standard was added to compensate for variations in the injection volume and for minor fluctuations in the detector response during the analysis. Both acidic and basic substances were tested as internal standards. The degrees of protonation of the compounds and, hence, their retention times were altered by changing the pH of the mobile phase. The influence of pH on the capacity factors (k') is illustrated in Fig. 4. For the acidic substances, on the C_{18} column, the k' values decreased, not only when the pH of the mobile phase increased and the substances were

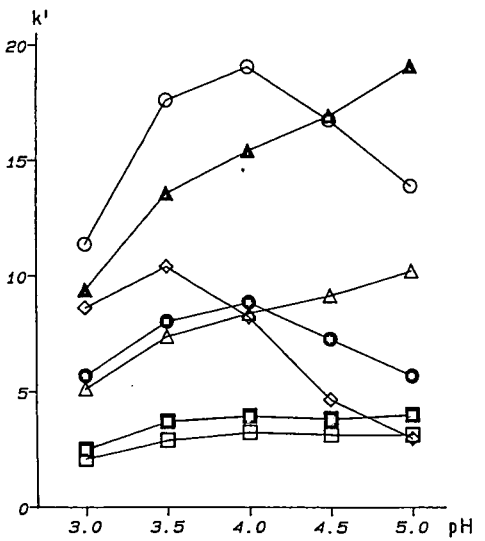

Fig. 4. Influence of the pH of the mobile phase on retention. Stationary phase: Nucleosil $5C_{18}$. Mobile phase: citrate buffer ($I=0.2$) containing 10% methanol. Key: □ = 5-HT; ■ = 5-HMT; △ = 5-HTOL; ● = 5-HIAA; ◇ = 5-HICA; ▲ = Ac-5-HT; ○ = 5-HIPA.

charged, but also, as mentioned above, at the lower pH of the citrate buffer. A maximum retardation was shown at a pH of about 3.5 for 5-HICA and at pH 4 for 5-HIAA and 5-HIPA. With 5-HICA as the internal standard, a pH of *ca.* 3 was suitable. However, at this pH the chromatogram of a plasma sample showed interferences with the 5-HIAA peak. Of the basic substances tested, 5-HMT was well separated from 5-HT on the cation exchanger and was therefore chosen as the internal standard.

Stability

5-HIAA was not stable in acidic solutions, *e.g.*, 0.01–0.1 *M* hydrochloric or perchloric acid, as also reported by others[15,16]; this is why we further examined the stability of 5-HT, 5-HMT and 5-HIAA in phosphate buffer at pH 6. Addition of EDTA (5 m*M*) improved the stability of the indole derivatives, their solutions being stable for at least 1 month when stored, in a dark place, at room temperature. At +4°C the solutions were stable, during this period, even in the absence of EDTA and at −70°C the solutions containing EDTA (5 m*M*) were stable for more than 1 year.

Accuracy

Precautions must be taken to prevent platelet breakdown during blood sampling, as 5-HT is mainly located within the platelets, and disrupted platelets will give rise to falsely increased plasma levels[4,17]. Fig. 5 shows that a centrifugation speed

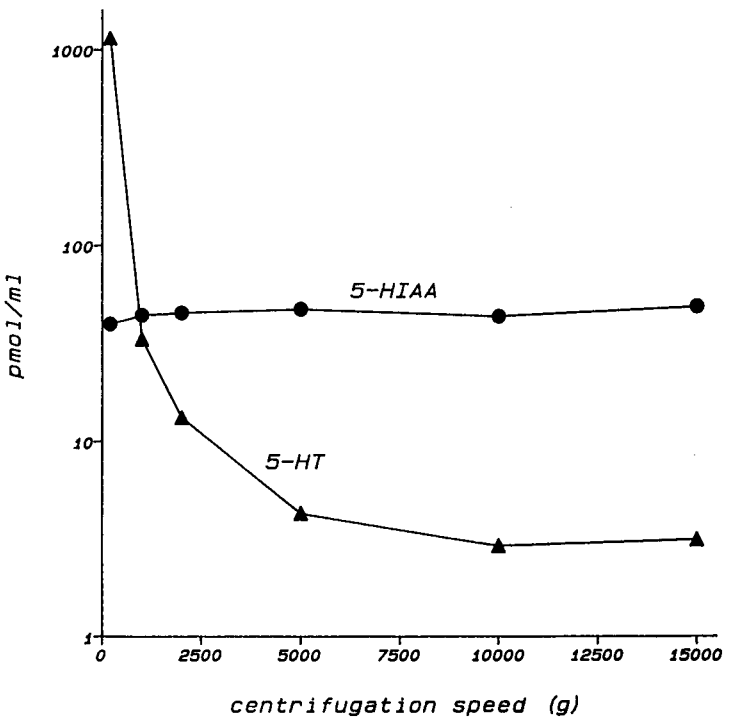

Fig. 5. Effect of centrifugation speed on the concentration of 5-HT in a plasma sample.

of 10 000 *g* was needed to obtain complete sedimentation of platelets. Centrifugation at 15 000 *g* gave the same result as centrifugation at 10 000 *g*, showing that no disruption of platelets occurred during centrifugation. This observation differs from that of Picard *et al.*[7], who found an higher concentration of 5-HT after centrifugation at 13 000 *g* than at 6000 *g*. 5-HIAA was not affected by the centrifugation speed, indicating that it is mainly located outside the platelets.

When plasma samples, containing intact platelets, were analyzed they were first treated with ultrasound or frozen at −70°C overnight to disrupt the platelets, otherwise most of the platelets adhered to the enrichment column, retaining their content of 5-HT. This gave falsely low values of the 5-HT concentration and caused contamination of subsequent chromatograms.

Many assays involve precipitation of proteins, but this leads to losses which must be compensated for in the calculation of the recovery[4,9–11]. After precipitation of proteins with perchloric acid, we observed losses of 5 to 10% for 5-HT and 5-HMT and *ca.* 30% for 5-HIAA.

Recovery and standard deviation

The recoveries of the indoles were determined by injecting standard solutions of the amines and the acid directly into the cation-exchange and reversed-phase column, respectively. The peak areas were compared with those obtained after injection into the coupled-column system. The recoveries were found to be 99.2 ± 1.2% for 5-HT, 97.3 ± 1.4% for 5-HMT and 101.6 ± 2.4% for 5-HIAA ($n=5$). Recoveries obtained when plasma samples were injected into the chromatographic system were 100.7 ± 2.6% and 98.2 ± 1.9% for 5-HT and 5-HIAA, respectively ($n=4$). For the concentration range tested (1–5000 n*M*) linearity was found for both 5-HT and 5-HIAA, in aqueous and plasma samples. The injection volume was 50 μl.

The relative standard deviations for injection of 10 μl of rabbit plasma into the two-column system were 2.4% for 5-HT and 3.9% for 5-HIAA ($n=10$) at a concentration of 380 n*M* of 5-HT and 270 n*M* of 5-HIAA. For a standard sample, the corresponding values were 1.1 and 1.6% at a concentration of 1.5 μ*M*. For a standard sample (100 μl), injected into the three-column system, the relative standard deviations were 3.4 and 3.0% for 5-HT and 5-HIAA, respectively ($n=5$), at a concentration of 26.1 n*M* for 5-HT and 36.3 n*M* for 5-HIAA. The corresponding values for an human plasma sample were 3.5% for 5-HT and 5.7% for 5-HIAA ($n=10$) at concentrations of 3.8 and 26.2 n*M*, respectively. The limit of detection was estimated as 1 n*M*.

The mean levels of 5-HT and 5-HIAA in platelet-poor plasma samples, obtained from normal controls ($n=5$), were 3.73 ± 0.65 and 30.5 ± 19.2 n*M*, respectively, in agreement with published results[4,11,18].

The concentrations of the plasma samples were calculated by comparing the peak-height ratios of 5-HT or 5-HIAA and the internal standard in the plasma samples with the ratios in the standard samples, which were prepared from aqueous standard solutions with known concentrations.

CONCLUSION

The chromatographic method described here permits quantification of 5-HT and 5-HIAA in less than 100 μl of a platelet-poor plasma sample. It is rapid and

relatively simple, requiring no pretreatment of the sample except for addition of the internal standard before injection. A recovery of about 100% was obtained, and the relative standard deviations were 3.5 and 5.7% for 5-HT and 5-HIAA, respectively, when an human plasma sample, containing 3.8 n*M* 5-HT and 26.2 n*M* 5-HIAA was analyzed.

REFERENCES

1 E. D. Frohlich, *J. Cardiovasc. Pharmacol.*, 10 (1987) 1.
2 P. M. Vanhoutte, *J. Cardiovasc. Pharmacol.*, 10 (1987) 8.
3 C. A. Palmerini, M. G. Cantelmi, A. Minelli, C. Fini, M. Zampino and A. Floridi, *J. Chromatogr.*, 417 (1987) 378.
4 G. M. Anderson, F. C. Feibel and D. J. Cohen, *Life Sci.*, 40 (1987) 1063.
5 D. D. Koch and P. T. Kissinger, in P. M. Kabra and L. J. Marton (Editors), *Clinical Liquid Chromatography*, Vol. 2, CRC Press, Boca Raton, FL, 1984, Ch. 31, p. 217.
6 B. Marasini, M. L. Biondi, P. Pietta and A. Agostoni, *Ric. Clin. Lab.*, 15 (1985) 63.
7 M. Picard, D. Olichon and J. Gombert, *J. Chromatogr.*, 341 (1985) 445.
8 M. Linnoila, K. A. Jacobson, T. H. Marshall, T. L. Miller and K. L. Kirk, *Life Sci.*, 38 (1986) 687.
9 O. C. Ingebretsen, A. M. Bakken and M. Farstad, *Clin. Chem.*, 31 (1985) 695.
10 E. R. Korpi, *Clin. Chem.*, 30 (1984) 487.
11 A. Minegishi and T. Ishizaki, *J. Chromatogr.*, 308 (1984) 55.
12 *High performance liquid chromatography*, Macherey-Nagel, Düren, 1987, p. 12.
13 C. T. Wehr, *J. Chromatogr.*, 418 (1987) 27.
14 N. Daoud, T. Arvidsson and K.-G. Wahlund, *J. Chromatogr.*, 385 (1987) 311.
15 N. Verbiese-Genard, M. Hanocq, C. Alvoet and L. Molle, *Anal Biochem.*, 134 (1983) 170.
16 B. Mohringe, O. Magnusson, G. Thorell and C. J. Fowler, *J. Chromatogr.*, 361 (1986) 291.
17 B. Petruccelli, G. Bakris, T. Miller, E. R. Korpi and M. Linnoila, *Acta Pharmacol. Toxicol.*, 51 (1982) 421.
18 F. Artigas, J. Ortiz, M. J. Sarrias, E. Martinez and E. Gelpi, *Clin. Chem.*, 32 (1986) 1985.

Journal of Chromatography, 459 (1988) 361–367
Elsevier Science Publishers B.V., Amsterdam — Printed in The Netherlands

CHROMSYMP. 1461

SCALE-UP METHODOLOGY FOR THE PREPARATIVE PURIFICATION OF PEPTIDE M

MARTHA KNIGHT*
Peptide Technologies Corporation, 125 Michigan Ave. N.E., Washington, DC 20017 (U.S.A.)
M. PATRICIA STRICKLER and M. JUDITH STONE
Waters Chromatography Division, Millipore, 3702 Pender Dr., Fairfax, VA 22030 (U.S.A.)
LINDA CHIODETTI and SARA GLUCH
Peptide Technologies Corporation, 125 Michigan Ave. N.E., Washington, DC 20017 (U.S.A.)
and
TOSHIMICHI SHINOHARA
National Eye Institute, National Institutes of Health, Bethesda, MD 20892 (U.S.A)

SUMMARY

An octadecapeptide, peptide M, the epitope of a retinal protein that induces experimental autoimmune uveitis, was synthesized and purified by preparative reversed-phase chromatography. The flow-rate and gradient conditions for maximum separation of impurities were determined on a 30 × 0.39 cm I.D. column of Delta Pak (15-μm spherical C_{18}-bonded silica with 300-Å pores). The maximum amount of peptide that was resolved under these conditions was then determined experimentally. Using a scale factor dependent on the square of the column diameters, the flow-rate and amount loaded were increased 164 times on a 30 × 5 cm I.D. column of the same packing. The same resolution was achieved. Batches of 200–342 mg were chromatographed with reproducible results, providing a total yield of 394 mg of pure peptide.

INTRODUCTION

S-antigen, a photoreceptor cell protein involved in the visual process, can produce autoimmune inflammatory disease[1]. An octadecapeptide sequence of the S-antigen is the pathogenic region of the protein which contains the epitope that induces experimental autoimmune uveitis, a T-cell mediated inflammation of the retinal cells and pineal gland. A synthetic peptide corresponding to this region of S-antigen has been confirmed to induce this disorder and is designated peptide M[2].

To make peptide M available for many studies, a large-scale synthesis was undertaken, and procedures for purifying relatively large amounts of the synthetic product had to be developed for one of the recently available preparative columns of 5 cm I.D. Applying proposed scale factors for sample load and flow-rate, the conditions determined on analytical columns of the same chromatographic material were systematically applied to a larger diameter column of the same length. Solid-phase

0021-9673/88/$03.50

synthesized peptides usually yield relatively heterogeneous products. Impurities can result from N to O acyl shifts, lack of removal of side-chain protecting groups or isomerization. The complexity of the task increases with increasing length of the synthesized peptide. Therefore, usually the major product of the synthesis needs to be isolated and characterized.

EXPERIMENTAL

Materials

Solvents and reagents used were of high-performance liquid chromatographic (HPLC) or analytical-reagent grade (Fisher Scientific, Pittsburgh, PA, U.S.A.). Dimethylformamide was obtained from Burdick & Jackson (Muskegon, MI, U.S.A.). Water was purified through the Millipore reverse-osmosis and cartridge filtration system (Millipore, Bedford, MA, U.S.A.). Peptide M (Asp–Thr–Asn–Leu–Ala–Ser–Ser–Thr–Ile–Ile–Lys–Glu–Gly–Ile–Asp–Arg–Thr–Val) was synthesized manually[3] starting with 7 g of Boc-Val phenylacetamidomethyl resin, 0.4 mequiv./g (Omni Biochem, National City, CA, U.S.A). The Boc-amino acid derivatives, including 2-Cl-carbobenzoxy (CBZ)-Lys, tosyl-Arg (Bachem, Torrance, CA, U.S.A.), benzyl ethers of Thr and Ser and the benzyl ester of Asp (U.S. Biochemical, Cleveland, OH, U.S.A.) were coupled as *in situ* generated active esters with equimolar amounts of dicyclohexylcarbodiimide and hydroxybenzotriazole. Deprotection was carried out by a 30-min reaction with 25% trifluoroacetic acid (TFA) in dichloromethane with 1 mg/ml indole and neutralization was effected with 10% triethylamine in dichloromethane. The peptide resin was washed between steps with 7 ml/g dichloromethane. After the assembly of the amino acids in the above sequence, the resulting peptide resin weighed 13.2 g. The peptide was liberated from the resin and side-groups were removed by treatment of the resin in two batches of 6.6 g, with 60 ml of hydrogen fluoride and 6 ml of anisole for 45 min at 0°C. After washing with ethyl acetate, extraction with water and lyophilization, 2.6 g of white powder resulted. Amino acid analysis using ion-exchange HPLC and *o*-phthalaldehyde post-column detection (St. John's Associates, Beltsville, MD, U.S.A.) of a 22-h hydrolysate gave the following molar ratios: Asp 2.95 : Thr 2.86 : Ser 1.99 : Glu 0.96 : Gly 0.89 : Ala 0.84 : Val 1.10 : Ile 2.56 : Leu 0.88 : Lys 1.05 : Arg 1.21.

Analytical chromatography

The peptide was chromatographed analytically to assess its purity and to develop the conditions for preparative chromatography. Solutions of 1 mg/ml of peptide in water were prepared and filtered, if necessary, through a 0.45-μm Durapore filter (Millipore). Crude peptide and the final purified peptide were chromatographed on μBondapak C_{18} (15 × 0.39 cm I.D. column) in 0.1% TFA or phosphoric acid in acetonitrile gradients at 1 ml/min for analytical characterization (not shown). The optimization of the separation of the crude peptide was carried out at a flow-rate of 0.5 ml/min on a 30 × 0.39 cm I.D. column of Delta Pak (C_{18}, 15 μm, 300 Å) (Waters, Milford, MA, U.S.A.) with two different volatile solvent systems: 0.02 *M* ammonium acetate (pH 6.8) and 0.1% acetic acid in acetonitrile or 0.1% aqueous TFA and 0.1% TFA in acetonitrile. The equipment used for analytical chromatography consisted of two Model 510 pumps, a WISP multiple-sample injector and a Model 481 variable-

wavelength detector, set at 214 nm, and data analysis was provided by a Model 840 Data Station. Methods development was performed on a Model 600 HPLC instrument, with a Model 490 multiwavelength detector, set at 214 nm, and the 840 data station (all from Waters). The solvents were sparged with helium.

Preparative chromatography

For preparative chromatography a 30 × 5 cm I.D. column of Delta Pak was used. The peptide was dissolved in water at a concentration of approximately 2 mg/ml and filtered through 0.45-μm Durapore filters. The solution of *ca.* 200–342 mg peptide was pumped into the column through a port on the solvent delivery system of a Delta-Prep instrument (Waters). The solvents were pumped at 80 ml/min with helium sparging. The effluent was passed through a preparative flow cell in a Model 481 detector, set at 214 nm, and connected to an 840 data station. Fractions were collected manually every 0.5 min. The fractions were analyzed by HPLC, and those containing pure peptide were lyophilized and combined. Some impure fractions were combined and rechromatographed to recover more pure peptide.

RESULTS AND DISCUSSION

The crude peptide was chromatographed on the 30 × 0.39 cm I.D. Delta-Pak column with two volatile solvent systems under various gradient conditions, as presented in Figs. 1 and 2. As all the components of the solvent systems are removable by lyophilization, no further steps in the purification were necessary. Maximum separation of impurities from the major peak was achieved with 0.1% TFA in water–acetonitrile eluents. In Fig. 1 are shown a series of linear gradients all starting at

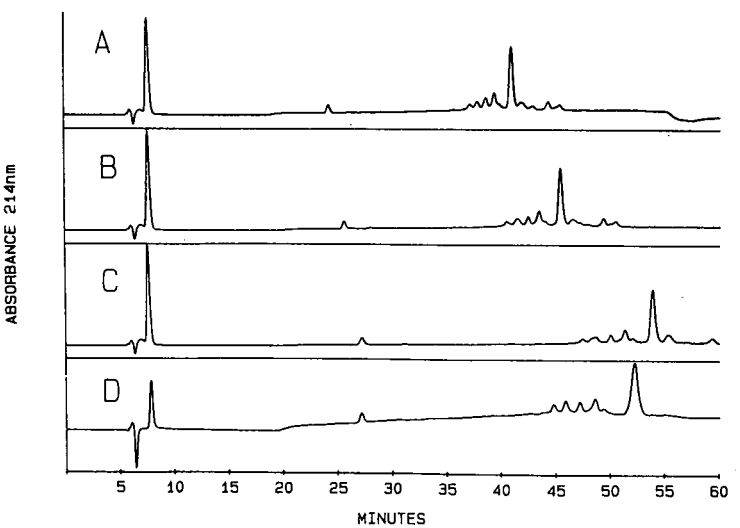

Fig. 1. Optimization of chromatographic conditions for the purification of synthetic peptide M on a 30 × 0.39 cm I.D. column of Delta Pak (C_{18}, 300 Å, 15 μm) with 0.1% TFA and acetonitrile gradients. Eluent A was 0.1% aqueous TFA and eluent B was 0.1% TFA in acetonitrile. The linear gradient for each chromatogram was as follows: A, 0–50% B in 40 min; B, 0–40% B in 40 min; C, 0–30% B in 40 min; D, 0–25% B in 30 min. Other conditions: flow-rate, 0.5 ml/min; detection, 214 nm. A.u.f.s.: A–C, 0.7; D, 0.6.

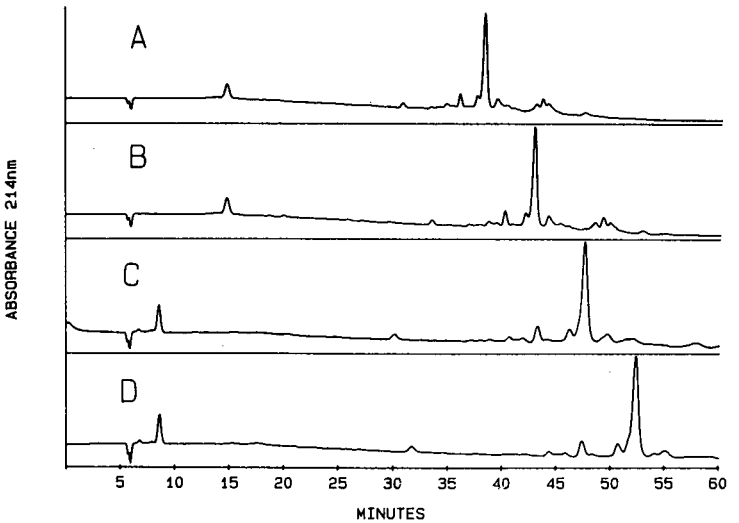

Fig. 2. Optimization of chromatographic conditions for the purification of synthetic peptide M on a 30 × 0.39 cm I.D. Delta Pak column. Eluent A was 0.02 *M* ammonium acetate (pH 6.8) and eluent B was 0.1% acetic acid in acetonitrile. The gradient conditions for each chromatogram were as follows: A, 0–30% B in 40 min; B, 0–25% B in 40 min; C, 0–20% B in 40 min; D, 5–18% B in 40 min. Flow-rate, 0.5 ml/min; detection, 214 nm. A.u.f.s.: A and B, 0.5; C and D, 0.3.

100% aqueous TFA and run with decreasing percentages of acetonitrile (50 to 25%). The 30-min gradient to 25% acetonitrile separates the hydrophilic impurities from the major peak while retaining the hydrophobic impurities on the column. Another volatile solvent system, 0.02 *M* ammonium acetate (pH 6.8), was tried to determine if a different selectivity would improve the resolution. As shown in Fig. 2, the impurities were not as well resolved from the major peak. At neutral pH the major peak is retained less than at acidic pH (compare Fig. 2A with Fig. 1C). The four acidic groups of the peptide are protonated at the low pH of TFA, making the peptide more hydrophobic, thus increasing the retention time. The increased retention time of the major peak more likely results from ion pairing of the TFA with the positive groups of the peptide[4,5].

The next step in methods development was to determine the capacity of the system without deterioration of resolution. Sample loads above 2.1 mg of crude peptide resulted in loss of resolution of the major peak from the hydrophilic impurities (Fig. 3). Also at loadings above 2.1 mg, the amount of peptide M recovered did not increase proportionately with the amount of crude material injected. Above a certain load the amount of soluble sample adsorbed on the bonded phase may be exceeded and the excess precipitates from the mobile phase. This precipitation of sample may or may not be irreversible. This is a possible explanation for the loss of material on reversed-phase columns and for the increase in column back-pressure that has been observed[6,7]. The flow-rate for a fixed linear velocity and mass for a fixed resolution applied to the preparative column are functions of cross-sectional area, and these can be increased as the squares of the diameters of the columns[8]. Using the

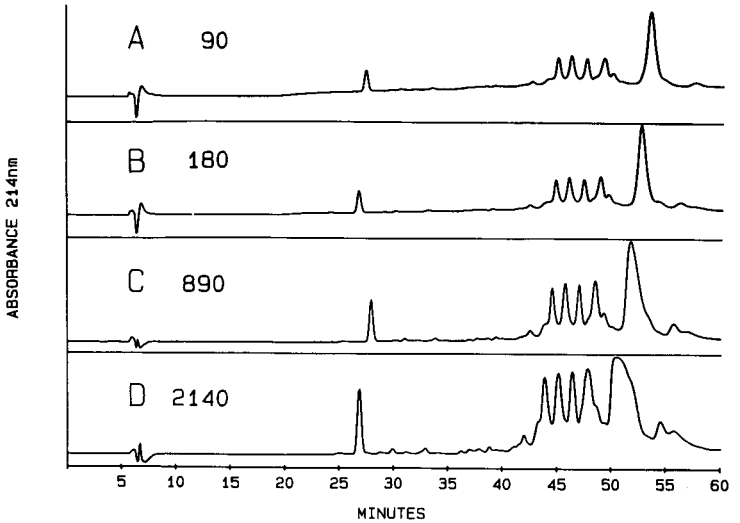

Fig. 3. Determination of load capacity. Chromatographic conditions: column, 30 × 0.39 cm I.D. Delta Pak; eluent A, 0.1% aqueous TFA; eluent B, 0.1% TFA in acetonitrile; linear gradient, 0–25% B in 30 min at a flow-rate of 0.5 ml/min. Amount (μg) of sample shown in each panel. Detection, 214 nm. A.u.f.s.: A, 0.25; B, 0.5; C, 1.5; D, 2.0.

scale factor of 164 increases the preparative flow-rate to 82 ml/min and the sample load to 345 mg.

The gradient duration was increased to compensate for the difference between the delay volumes of the analytical and preparative chromatographs. At analytical

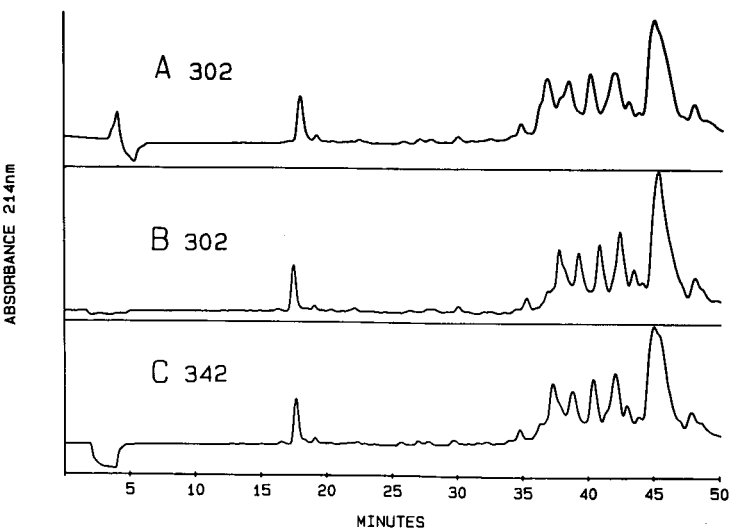

Fig. 4. Preparative chromatography of synthetic peptide M. Chromatographic conditions: column, 30 × 5 cm I.D. Delta Pak; eluent A, 0.1% aqueous TFA; eluent B, 0.1% TFA in acetonitrile. The sample was prepared and loaded as described under Experimental (sample load, mg, indicated in each panel). A 40-min linear gradient from 0 to 25% B was run at a flow-rate of 80 ml/min. Detection, 214 nm; sensitivity, 0.4 a.u.f.s.

flow-rates the time difference between the percentage of organic solvent delivered by the pumps and the percentage of organic solvent reaching the column is significant, whereas at preparative flow-rates it is almost negligible. In our experience using gradient elution, the retention time of a compound eluted from a preparative column has been observed to be less than its retention time from an analytical column even though the linear velocity was constant[9]. This and other factors, such as differences in the efficiency of the column packing, may be reponsible for the loss of resolution or decreased number of theoretical plates observed for wide-diameter columns of small particle (<20 μm) packing[10]. Therefore, to compensate for the gradient delay and to increase the resolution further, a gradient from 0 to 25% acetonitrile in 40 min was applied, 10 min longer than the analytical gradient duration. The results of three preparative separations of >300 mg each under these conditions are shown in Fig. 4. In these runs and others not shown, the major peak was eluted at 44 min. The mass of peptide recovered from 44 to 47 min averaged 24% of the mass of the crude sample loaded. The multiple preparative runs under these conditions were reproducible with respect to recovery and resolution, as shown in Fig. 4. At approximately 50 min, 50% acetonitrile was pumped to elute the hydrophobic impurities (not shown) followed by re-equilibration with 0.1% aqueous TFA for another injection. Each half-minute fraction during peak elution was analyzed by analytical HPLC, as shown in Fig. 5. The 45-min fraction was pure in this example (>99% relative peak area). The other fractions were combined with neighboring fractions of other runs and chromatographed to recover more of the pure peptide. By chromatography of most of the synthetic peptide, the final yield of biologically active peptide M was 394 mg or 24% (w/w) of crude peptide injected.

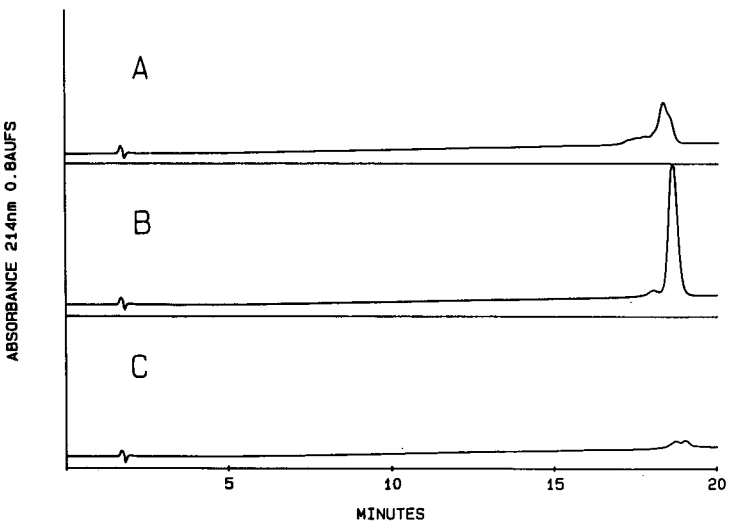

Fig. 5. Analytical rechromatography of fractions from the preparative separation (Fig. 4C) of 342 mg of synthetic peptide M on the 30 × 0.39 cm I.D. Delta Pak column. Eluent A, 0.1% aqueous TFA; eluent B, 0.1% TFA in acetonitrile. A 15-min linear gradient to 25% B was run at a flow-rate of 1 ml/min. Sample, 50-μl aliquots of the preparative fractions; detection, 214 nm; sensitivity, 0.8 a.u.f.s. A, Chromatogram of the fraction collected at 44.5 min; B, 45 min; C, 47 min. Peptide M was eluted in fractions 45–46.5.

REFERENCES

1 T. Shinohara, B. Dietzschold, C. M. Craft, G. Wistow, J. J. Early, L. A. Donoso, J. Horwitz and R. Tao, *Proc. Natl. Acad. Sci. U.S.A.*, 84 (1987) 6975.
2 L. A. Donoso, C. F. Merryman, T. W. Sery, T. Shinohara, B. Dietszschold, A. Smith and C. M. Kalsow, *Curr. Eye Res.*, 6 (1987) 1151.
3 J. M. Stewart and J. D. Young, *Solid Phase Peptide Synthesis*, Pierce, Rockford, IL, 2nd ed., 1984.
4 W. S. Hancock and D. R. K. Farthing, in W. S. Hancock (Editor), *Handbook of HPLC for the Separation of Amino Acids, Peptides and Proteins*, Vol. II, CRC Press, Boca Raton, FL, 1984, p. 3.
5 C. E. Dunlap, III, S. Gentleman and L. I. Lowney, *J. Chromatogr.*, 160 (1978) 191.
6 M. Knight, Y. Ito and T. N. Chase, *J. Chromatogr.*, 212 (1981) 356.
7 E. Henderson, R. Sowder and S. Oroszlan, in D. Liu, A. Schechter, R. L. Heinrikson and P. Condliffe (Editors), *Chemical Synthesis and Sequencing of Peptides and Proteins*, Elsevier/North-Holland, Amsterdam, 1981, p. 251.
8 C. Stacey, R. Brooks and M. Merion, *J. Anal. Purif.*, 2 (1987) 52.
9 M. P. Strickler, R. Neil, M. J. Stone, G. Tkalcevic, T. Grebas and P. Gemski, *7th International Symposium on HPLC of Peptides, Proteins and Polynucleotides, Washington, DC, 1987*, Abstract 829.
10 G. Espy, *Sep. Technol. Newsl.*, 1 (1988) 1.

Journal of Chromatography, 459 (1988) 369–378
Elsevier Science Publishers B.V., Amsterdam — Printed in The Netherlands

CHROMSYMP. 1479

PREPARATIVE-SCALE HIGH-PERFORMANCE LIQUID CHROMATOGRAPHY OF OMEGA-3 POLYUNSATURATED FATTY ACID ESTERS DERIVED FROM FISH OIL

JANET M. BEEBE and PHYLLIS R. BROWN*
Department of Chemistry, University of Rhode Island, Kingston, RI 02881 (U.S.A.)
and
JOSEPH G. TURCOTTE*
Department of Medicinal Chemistry, University of Rhode Island, Kingston, RI 02881 (U.S.A.)

SUMMARY

Marine triglyceride-derived omega-3 polyunsaturated fatty acid ethyl esters were separated by preparative high-performance liquid chromatography on a 25-μm octadecyl stationary phase using a ternary isocratic mobile phase of acetonitrile–tetrahydrofuran–water (466:233:300, v/v/v). The highest purity first-run fractions obtained were ethyl esters of the major marine polyunsaturates eicosapentaenoic acid (20:5ω3, 97.7%) and docosahexaenoic acid (22:6ω3, 93.7%), and the minor polyunsaturate octadecatetraenoic acid (18:4ω3, 98.1%).

INTRODUCTION

Interest in omega-3 polyunsaturated fatty acids initially was prompted by observations[1,2] that Greenland Eskimos experienced a significantly lower incidence of death from ischaemic heart disease than Western populations[2]. Results of subsequent studies indicated that this alleged or potential health benefit and other physiological effects[3–9] were due to a diet high in marine oils containing esterified omega-3 polyunsaturated fatty acids (PUFAs). The predominant marine triglyceride-derived omega-3 fatty acids are all-*cis*-5,8,11,14,17-eicosapentaenoic acid (20:5ω3, EPA) and all-*cis*-4,7,10,13-16,19-docosahexaenoic acid (22:6ω3, DHA).

Either native winterized or concentrated whole-body fish oils or fish liver oils have been utilized in most studies as dietary sources of EPA and DHA. Also, in many instances clinical subjects have been given relatively large doses of dietary fish oil supplements, for example, ranging from 18 to 50 g per day depending on the study[4–9]. Accordingly, the physiological effects and possible health benefits of administered fish oils generally have been attributed to either EPA or DHA alone, or to a synergistic effect between the two[10,11]. As a result, there has been controversy over the contribution of individual fish oil constituents to particular pharmacological actions and the optimal dosages required for achieving established and/or suspected beneficial effects.

0021-9673/88/$03.50

An obvious need exists, therefore, for amounts of pure EPA and DHA in usable form in order to study these polyunsaturates at all levels of investigation.

Over the past 15 years, long-chain fatty acids and their aromatic and aliphatic esters have been successfully separated by high-performance liquid chromatography (HPLC)[12–15]. Most of these analytical separations have been performed in the reversed-phase (RP) mode with an octadecyl stationary phase. A few reports[16–18] exist on the preparative-scale RP-HPLC of fish oil-derived methyl and ethyl esters of EPA and DHA, the major marine polyunsaturates. This paper describes the separation and purification of ethyl esters of EPA, DHA and the heretofore minor unreported polyunsaturate octadecatetraenoic acid (18:4ω3,OTA) on a preparative scale by modification of an analytical RP-HPLC procedure[19] which we used in preliminary work.

EXPERIMENTAL

Materials

Analytical-reagent grade anhydrous sodium sulfate, urea, potassium hydrogencarbonate, sodium metal and all solvents used for extraction and chromatography were obtained from Fisher Scientific (Springfield, NJ, U.S.A.); butylated hydroxytoluene (BHT) was obtained from Aldrich (Milwaukee, WI, U.S.A.). Promega™, which is commercially available in capsule form from the Parke-Davis Health Care Group (Morris Plains, NJ, U.S.A.), was utilized as a concentrated fish oil source. The concentrations of esterified EPA and DHA were 27.7% and 11.4%, respectively, as determined by gas chromatographic (GC) analysis of methyl esters derived from transesterification of the commercial oil (particular capsules); *ca.* 1% of minor polyunsaturates was also present.

Transesterification

Fish oil triglycerides were transesterified to ethyl esters by a modification of the previously described method of Christie[20]. The fish oil in six capsules (6 g) of Promega was removed with a syringe and immediately dissolved in 120 ml of peroxide-free tetrahydrofuran (THF); 240 ml of freshly prepared 0.5 *M* sodium ethoxide were added. After the reaction had proceeded at 50°C for 10 min, it was quenched by the addition of 12 ml of glacial acetic acid, followed immediately by 600 ml of distilled water. The aqueous phase was extracted twice with diethyl ether (300 ml) and the ether layer was dried over anhydrous sodium sulfate containing 10% solid potassium hydrogen bicarbonate. The resulting slurry was filtered and the solvent removed under reduced pressure to give a quantitative yield of ethyl esters.

Urea crystallization

Concentration of the polyunsatured fatty acid ethyl esters was accomplished using the procedure of Gunstone *et al.*[21] for methyl ester polyunsaturates. Following transesterification, the esters were dissolved in 24 ml of a 250 mg/ml solution of urea in ethanol. The urea crystallization was initiated at room temperature and then proceeded for 24 h at 4°C. On reaching ambient temperature, the resulting solid was washed with urea-saturated ethanol and filtered; the esters then were extracted twice from the filtrate with 50 ml of diethyl ether. The remaining solvent was removed

(rotary evaporator) under reduced pressure followed by addition of 6 ml of peroxide-free THF. Recovery experiments indicated that the yields after crystallization of 93% and 79% for EPA and DHA, respectively, were in agreement with literature values[21].

Optimization of high-performance liquid chromatography

The chromatographic system consisted of an M6000 pump, a U6K injector and an R401 differential refractometer operated at ambient temperature (Waters Division of Millipore, Milford, MA, U.S.A.) and an ST Macrobore® (Separations Technology, Wakefield, RI, U.S.A.) column (35.0 cm × 4.6 mm I.D.) of C_{18} reversed-phase material, 25-μm particle size. A guard column (30 mm × 4.6 mm I.D.) was dry-packed with Supelcosil LC-18 (40-μm) particles (Supelco, Bellefonte, PA, U.S.A.). Mobile phases were prepared by mixing appropriate volumes of acetonitrile, peroxide-free THF and water; all solvents were filtered through 0.45-μm nylon-66 filters (Rainin, Woburn, MA, U.S.A.) and degassed by saturation with helium. The esters were eluted with acetonitrile–THF–water (466:233:300, v/v/v) at a flow rate of 2.0 ml/min. Data were recorded on an Omniscribe strip-chart recorder (Houston Instruments, Austin, TX, U.S.A.). Peak areas were determined by triangulation. Following the transesterification and urea crystallization steps, the concentrated ethyl esters were dissolved in peroxide-free THF containing 0.005% (w/v) 8HT as an antioxidant. Solutions of esters were stored in Reactivials™ (Supelco) at 4°C blanketed with nitrogen. Samples of 10–50 μl containing 10–50 mg total fatty acid ethyl esters were injected with a 100-μl Hamilton (Reno, NV, U.S.A.) syringe.

Analytical high-performance liquid chromatography

Results of methods development experiments were monitored by analytical RP-HPLC of appropriate collected fractions. Prior to chromatography, the esters in each fraction were extracted from the eluent into hexane (2 ml) and the layers were separated. Next, the fractions were brought to dryness under a stream of nitrogen and reconstituted in 200 μl of peroxide-free THF containing 0.005% (w/v) BHT. Aliquots of 50 μl of these concentrates were then analyzed by RP-HPLC. The separations were performed on a Whatman ODS-3 RAC II column (100 mm × 4.6 mm I.D.) (Whatman, Clifton, NJ, U.S.A.); a guard column (30 mm × 4.6 mm I.D.) dry packed with Supelcosil LC-18 (40 μm) was also employed. The esters were eluted with acetonitrile–THF–water (360:200:440, v/v/v) at a flow-rate of 2.0 ml/min. Data were recorded on an Omniscribe strip-chart recorder. This procedure[19] was developed for the quantitative and qualitative analysis of PUFA methyl and ethyl esters derived from fish oil sources.

Preparative high-performance liquid chromatography

A Model ST/800A preparative chromatograph Separations Technology, (Wakefield, RI, U.S.A) fitted with an ST/2000-1 guard column (1 in. × 2 in. I.D.) and an ST/2000B preparative column (25 in. × 2 in. I.D.), each packed with ST Macrobore C_{18} (25 μm particle size), was employed for separation of esters. The system was equipped with a differential refractometer with a flowing reference (as opposed to an air-filled reference) in order to minimize baseline drift. The sensitivity was 8 × at 100 mV full-scale. Samples of 1 or 2 ml (equivalent to 0.8–1.6 g) of total esters were introduced into the system via a 10-ml syringe immediately followed by a 1-ml eluent

flush. The esters were eluted with acetonitrile–THF–water (466:233:300, v/v/v) at a flow-rate of 220 ml/min. Data were recorded with a strip-chart recorder at 12 cm/h. As the esters were eluted, typically 24 fractions of approximately 175 ml each were collected; the fractions were stored in tightly closed containers in a freezer at –60°C until analysed; an aliquot of each fraction was subsequently characterized by GC.

Capillary gas chromatography

Preparative HPLC fraction aliquots were analyzed by GC without further derivatization or purification. The gas chromatograph (Model 8500; Perkin-Elmer, Norwalk, CT, U.S.A.) was operated with an injection inlet temperature of 280°C, a flame ionization detector (splitting ratio 40:1) and a computer-interfaced integrator. The fused-silica capillary stationary phase was Perkin-Elmer BP-1 (12 m × 0.22 mm I.D.) with a 0.25-μm film thickness. The initial oven temperature of 100°C was held for 1 min, then the temperature was increased to 160°C at 32°C/min followed by a 2°C/min gradient to 210°C. The carrier gas linear velocity was 30 cm/s. The ethyl esters were identified by retention times compared with a Menhaden oil-derived ethyl ester standard mixture (Ocean Organics, Wakefield, RI, U.S.A.). Integrated peak areas were used to calculate the percentages of the various esters in each of the 24 fractions.

RESULTS AND DISCUSSION

The experimental conditions of the analytical RP-HPLC method[19] were found to be less than satisfactory for the optimization experiments. The peak shapes were too broad and not well defined; in addition, the analysis time was 2 h or longer. To compensate for the increased carbon load of the optimization packing (*ca.* 18%), as opposed to the carbon load of the analytical packing (*ca.* 10%), the amount of water in the mobile phase was reduced. The optimum mobile phase for use with the semi-preparative stationary phase was found to be acetonitrile–THF–water (466:233:300, v/v/v) at a flow-rate of 2.0 ml/min.

The effect of altering the flow-rate was also investigated in order to optimize the analysis time. Flow-rates of 1.0, 1.8, 2.0, 2.4 and 3.0 ml/min were evaluated. The optimum in terms of resolution and analysis time was found to be 2.0 ml/min. Although the analysis time could be considerably shortened (to 30 min at 3.0 ml/min), the resolution (R_s) of EPA and DHA was not acceptable (R_s = 0.6).

Fig. 1 shows a typical optimization chromatogram. The labeled fractions represent predominantly (A) ethyl octadecatetraenoate (OTA-Et), (B) ethyl eicosapentaenoate (EPA-Et) and (C) ethyl docosahexaenoate (DHA-Et). Fractions corresponding to the separated groups in the chromatogram were collected and subsequently characterized by analytical RP-HPLC[19]. The levels of EPA-Et and DHA-Et in the five fractions indicated in Fig. 1 are summarized in Table I; the fractions containing most EPA-Et and DHA-Et are fractions 3 and 4, respectively. A chromatogram of an analytical-scale separation of the components in fractions 3 and 4 is shown in Fig. 2. The chromatogram of fraction 3 shows that it consists mostly of EPA-Et and that of fraction 4 illustrates that it also contains EPA-Et; however, fraction 4 contains mainly DHA-Et. The relatively high content of DHA-Et in fraction 5 (Table I) is probably due to the tailing of peak C (Fig. 1).

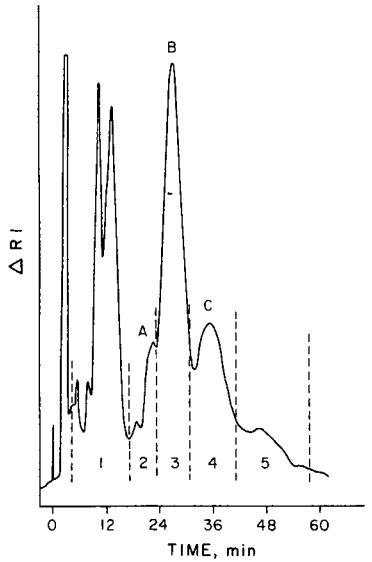

Fig. 1. Typical optimization chromatogram of fish oil-derived fatty acid ethyl esters. Conditions: mobile phase, acetonitrile–THF–water (466:233:300, v/v/v); stationary phase, ST Macrobore C_{18} (35 cm × 4.6 mm I.D., 25 μm); sample load, 35 mg total esters; detection, refractive index (RI) at 16×, ambient temperature with a trapped reference. Major peak components: (A) ethyl octatetraenoate; (B) ethyl eicosapentaenoate; (C) ethyl docosahexaenoate.

Overload experiments were carried out to determine the amount of sample that can be applied to the optimization column without exceeding the column linear capacity (mg of sample per gram of packing). When the column linear capacity is exceeded, overloading occurs[22]. The relationship between the sample load of EPA-Et and the capacity factor (k') is illustrated in Fig. 3. Column overloading occurs at approximately 4.0 mg sample per gram column packing, as is evidenced by the strong deviation in the linear decrease of k' which occurs when this sample load is reached. Hence approximately 36 mg of total fish oil esters may be applied to the optimization column per gram of packing without exceeding its linear capacity.

TABLE I

ANALYTICAL RP-HPLC ANALYSIS OF FRACTIONS FROM OPTIMIZATION EXPERIMENTS

See Fig. 1.

Fraction No.	*EPA-Et (area%)**	*DHA-Et (area%)*
1	0	0
2	1	0
3	93	0
4	2	82
5	0	50

* Values are expressed as area percentage of the sum of the areas of all of the peaks in the chromatogram (Fig. 2), except the solvent peak.

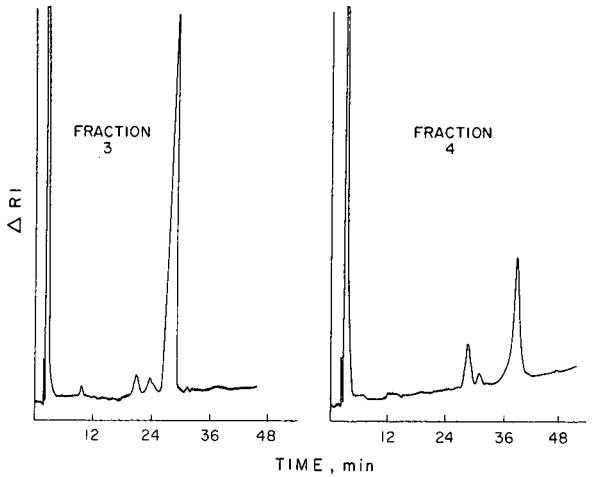

Fig. 2. Analytical RP-HPLC trace of collected fractions 3 and 4 from Fig. 1. Conditions: mobile phase, acetonitrile–THF–water (360:200:400, v/v/v); flow-rate; 2.0 ml/min; stationary phase, Whatman ODS-3 RAC II (100 mm × 4.6 mm I.D.); detection, refractive index at 8 ×, ambient temperature with a trapped reference; chart speed, 5 in./h.

The chromatographic effect of overloading is illustrated in Fig. 4. The chromatogram demonstrated by the broken line corresponds to a sample load of 25 mg of total fatty acid ethyl esters; thus it was obtained without exceeding the linear capacity of the column. On the other hand, the chromatogram (Fig. 4, solid line) obtained under conditions (sample load of a total of 50 mg of ethyl esters) that did exceed the linear capacity of the column showed that the peaks of EPA-Et and DHA-Et are not as well resolved.

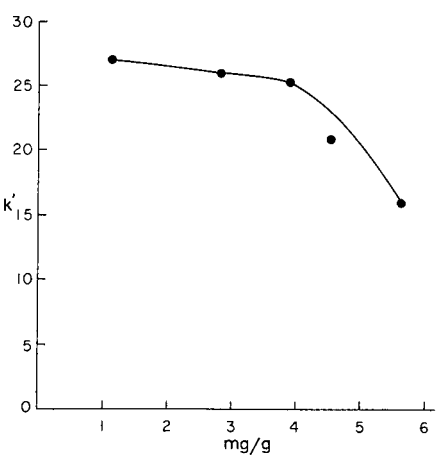

Fig. 3. Plot of *k' versus* sample load: mg/g = mg EPA-Et per gram of column packing. Overloading is defined[22] as the sample load where the solute capacity, *k'*, decreases by 10% from its constant value at smaller sample sizes.

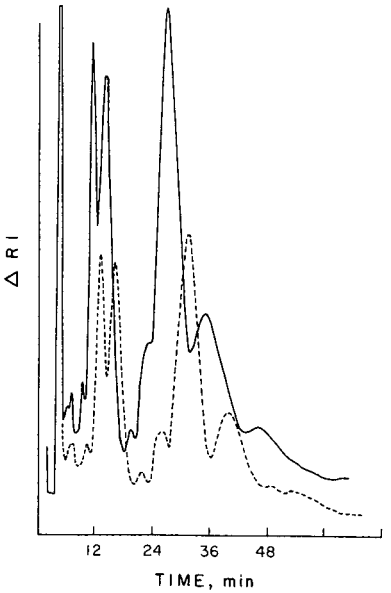

Fig. 4. Chromatographic effects of overloading: broken line, 25-mg fatty acid ethyl ester; solid line, 50-mg fatty acid ethyl ester. Mobile phase, acetonitrile–THF–water (466:233:300, v/v/v); flow-rate, 2.0 ml/min; stationary phase, ST Macrobore (350 mm × 4.6 mm I.D., 25 μm); detection, refractive index at 16×, ambient temperature with a trapped reference.

In the past, separating critical pairs (*i.e.*, fatty acids and esters with the same equivalent carbon length) by liquid chromatographic techniques with reversed-phase analytical, and especially semi-preparative or preparative stationary phases has been challenging. Most separations of fatty acids or their esters on the semi-preparative or preparative scale have required the implementation of argentation chromatography or recycling in order to obtain pure or enriched fractions of components. However, with the recent availability of more versatile semi-preparative and preparative packings of smaller particle sizes coupled with higher carbon loads, increased resolution of closely related compounds can be achieved. In this work, we successfully obtained enriched fractions of EPA-Et and DHA-Et of 93% and 82%, respectively, with a single pass through a Macrobore C_{18} column. Furthermore, results of our optimization studies were directly applicable to preparative-scale HPLC of the marine oil-derived omega-3 polyunsaturated ethyl esters.

Scale-up from the optimization studies gave baseline separation of three omega-3 fatty acid ethyl esters derived from the concentrated fish oil source in 40 min without recycling. A representative chromatogram of the esters with a 1.6-g sample is shown in Fig. 5. The three major peaks in order of elution correspond predominantly to (A) ethyl octadecatetraenoate (18:4ω3), (B) ethyl eicosapentaenoate (20:5ω3) and (C) ethyl docosahexaenoate (22:6ω3). The amounts of omega-3 PUFA ethyl esters in the highest purity (94%) fractions and the percentage composition of the respective esters (18:4ω3, 20:5ω3, 22:6ω3) in all fractions, as determined by capillary GC, are summarized in Table II. The minor omega-3 18:4ω3 ethyl ester eluted first and was found at high concentrations (94%) in fractions 1–4; fraction 3 was the most concen-

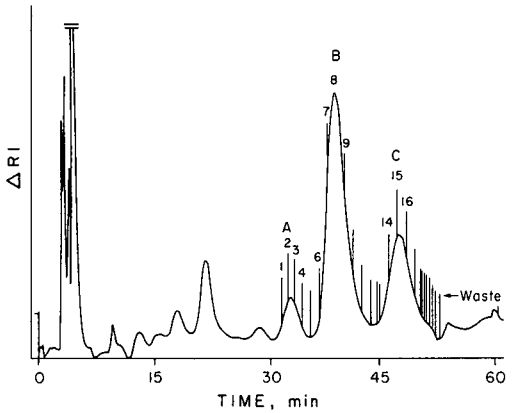

Fig. 5. Preparative HPLC trace of fatty acid ethyl esters derived from a fish oil concentrate. Conditions: sample, 1.6 g total ethyl esters; mobile phase, acetonitrile–THF–water (466:233:300, v/v/v); stationary phase, ST Macrobore C_{18} (25 in. × 2 in. I.D., 25 μm); detection, refractive index, 8 × at 100 mV full-scale, flowing reference at ambient temperature. Peak identification of predominant components: (A) ethyl octadecatetraenoate; (B) ethyl eicosapentaenoate; (C) ethyl docosahexaenoate. The vertical lines indicate fraction collection starting at fraction 1 continuing through fraction 24.

TABLE II

OMEGA-3 FATTY ACID ETHYL ESTER COMPOSITION OF MAJOR PREPARATIVE HPLC FRACTIONS DETERMINED BY GC

Fraction No.	*18:4ω3 (%)**	*20:5ω3 (%)**	*22:6ω3 (%)**	*22:5ω3 (%)**
1	(16)** 94.3			
2	(22) 94.8			
3	(12) 98.1			
4	(5) 95.3			
5	32.5	57.1		
6	1.8	(29)** 95.4		
7	0.2	(113) 97.7		
8		(87) 95.8		
9		(31) 95.9		
10		92.1		
11		86.1		
12		50.2		
13		13.4		
14		3.0		
15			12.5	
16			64.1	
17			86.4	1.5
18			91.1	13.9
19			93.7	1.5
20			84.8	0.5
21			60.7	1.5
22			72.2	3.2
23			70.9	3.8
24			63.6	1.3

* Data are expressed as a percentage of total GC analysis, *i.e.*, area%.
** Amount (mg) in parentheses.

trated at 98.1%. Most of the 20:5ω3 ethyl ester was found in five fractions (6–11), containing the ester at 86% concentration and greater. The highest concentration of 20:5ω3 ester was found in fraction 7 at 97.7%; lower concentrations of this ester occurred in fractions 5, 12, 13 and 14. The other major PUFA, 22:6ω3, ethyl ester was eluted immediately following the 20:5ω3 ethyl ester in fractions 15–24; the highest concentration was found in fraction 19 at 93.7%.

The results of these preliminary preparative HPLC studies, which are comparable[17,18] or superior[16] to previous reports, clearly demonstrate that very pure marine oil-derived polyunsaturates readily can be obtained in sufficient amounts for many laboratory-scale investigations. Optimization of sample load, coupled with repeated preparative runs, will allow the separation of multigram amounts of PUFAs. For example, 99+% pure ethyl eicosapentaenoate and ethyl octadecatetraenoate can be obtained on rechromatography of 94+% first-run eluate by using the present ternary mobile phase (acetonitrile–THF–water), or, preferably ethanol–water[17,18]. Although pure ethyl docosahexaenoate can also be obtained in the same manner, the corresponding free acid (DHA) may be generated in practical, large amounts via a chemical method (iodolactonization) developed by Wright *et al.*[23]. In our studies, the preparation, of ethyl octadecatetraenoate of purity up to 98% (first run), reported for the first time, is significant in view of the paucity of biological data on this minor marine oil-derived omega-3 PUFA.

ACKNOWLEDGEMENTS

This work was sponsored in part by NOAA Office of Sea Grant, U.S. Department of Commerce, under Grant No. NA85AA-D-56094. The authors thank Nicholas N. Sinchuk, Ocean Organics, Wakefield, RI, U.S.A. for the analysis (GC, fatty acid methyl ester) of the commercial fish oil concentrate and for his assistance with the GC analyses of preparative HPLC fractions of ethyl esters.

REFERENCES

1 W. E. M. Lands, *Fish and Human Health*, Academic Press, New York, 1986, Ch. 1.
2 J. Dyerberg, S. M. Barlow and N. E. Stansby, in S. M. Barlow and N. E. Stansby (Editors), *Nutritional Evaluation of Long Chain Fatty Acids in Fish Oil*, Academic Press, New York, 1982, pp. 245–266.
3 W. S. Harris, W. E. Connor, S. B. Inkeles and D. R. Illingsworth, *Metabolism*, 33 (1978) 1016.
4 T. H. Lee, R. L. Hoover, J. D. Williams, R. I. Sperling, J. Ravalese, III, B. W. Spur, D. R. Robinson, E. J. Corey, R. A. Lewis and K. F. Austen, *N. Engl. J. Med.*, 312 (1985) 1217.
5 J. Dyerberg, E. Stoffersen, H. O. Bang, S. Moncada and J. R. Vane, *Lancet*, i (1978) 117.
6 K. K. Carroll, *Lipids*, 21 (1986) 731.
7 V. E. Kelley, A. Ferrotti, S. Izui and T. B. Strom, *J. Immunol.*, 134 (1985) 1914.
8 D. Kromhaut, E. B. Bosschieler and C. L. Coulander, *N. Engl. J. Med.*, 312 (1985) 1205.
9 B. E. Phillipson, D. W. Rothrock, W. E. Connor, W. S. Harris and D. R. Illingworth, *N. Engl. J. Med.*, 312 (1985) 1210.
10 T. A. B. Sanders and F. Roshanhai, *Clin. Sci.*, 64 (1973) 91.
11 A. Leaf and P. C. Weber, *N. Engl. J. Med.*, 318 (1988) 549.
12 M. S. F. Lie Ken Jie, *Adv. Chromatogr.*, 18(1980) 1.
13 M. S. J. Dallas, L. J. Morris and B. W. Nichols, in E. Heftmann (Editor), *Chromatography*, Van Nostrand Reinhold, New York, 3rd ed., 1975, pp. 527–570.
14 M. J. Cooper and M. W. Anders, *J. Chromatogr. Sci.*, 13 (1975) 407.
15 A. Kuksis and J. J. Myher, *J. Chromatogr.*, 379 (1986) 57.

16 S. Tokiwa, A. Kauazawa and S. Teshma, *Bull. Jpn. Soc. Sci. Fish.*, 47 (1981) 675.
17 J. G. Turcotte, N. N. Sinchuk, W. R. Russo and B. M. Vittimberga, *U.S. SBIR/GM36168 Grant Rep.*, August, 1986; personal communication.
18 J. Grant, *Am. Lab.*, June (1988) 80.
19 J. M. Beebe, *Doct. Diss.* University of Rhode Island, Kingston, RI, 1988.
20 W. W. Christie, *Lipid Analysis*, Pergamon, Oxford, 1985, pp. 53–54.
21 F. D. Gunstone, J. McLaughlan, C. M. Scrimgeour and A. P. Watson, *J. Sci. Food Agric.*, 27 (1976) 675.
22 J. J. Kirkland and L. R. Snyder, *Introduction to Modern Liquid Chromatography*, Wiley, New York, 1979, p. 617.
23 S. W. Wright, E. Y. Kuo and E. J. Corey, *J. Org. Chem.*, 52 (1987) 4399.

Author Index

กำหนดส่ง		
-1. มิ.ค. 2533 13. มิ.ย. 2534		

PUBLICATION SCHEDULE FOR 1988

Journal of Chromatography and Journal of Chromatography, Biomedical Applications

MONTH	J	F	M	A	M	J	J	A	S	O	N	D
Journal of Chromatography	435/1 435/2 435/3 436/1	436/2 436/3	437/1 437/2	438/1 438/2	439/1 439/2 440 441/1	441/2 442 443	444 445/1 445/2 446	447/1 447/2 448/1	448/2 448/3 449/1	449/2 450/1 450/2 450/3 452	453 454 455	456/1 456/2 457 458 459
Bibliography Section		460/1		460/2		460/3		460/4		460/5		460/6
Cumulative Indexes, Vols. 401–450												451
Biomedical Applications	424/1	424/2	425/1 425/2	426/1 426/2	427/1	427/2 428/1	428/2 429	430/1	430/2 431/1	431/2	432	433 434/1 434/2

INFORMATION FOR AUTHORS

(Detailed *Instructions to Authors* were published in Vol. 445, pp. 453–456. A free reprint can be obtained by application to the publisher, Elsevier Science Publishers B.V., P.O. Box 330, 1000 AH Amsterdam, The Netherlands.)

Types of Contributions. The following types of papers are published in the *Journal of Chromatography* and the section on *Biomedical Applications:* Regular research papers (Full-length papers), Notes, Review articles and Letters to the Editor. Notes are usually descriptions of short investigations and reflect the same quality of research as Full-length papers, but should preferably not exceed six printed pages. Letters to the Editor can comment on (parts of) previously published articles, or they can report minor technical improvements of previously published procedures; they should preferably not exceed two printed pages. For review articles, see inside front cover under Submission of Papers.

Submission. Every paper must be accompanied by a letter from the senior author, stating that he is submitting the paper for publication in the *Journal of Chromatography*. Please do not send a letter signed by the director of the institute or the professor unless he is one of the authors.

Manuscripts. Manuscripts should be typed in double spacing on consecutively numbered pages of uniform size. The manuscript should be preceded by a sheet of manuscript paper carrying the title of the paper and the name and full postal address of the person to whom the proofs are to be sent. Authors of papers in French or German are requested to supply an English translation of the title of the paper. As a rule, papers should be divided into sections, headed by a caption (*e.g.*, Summary, Introduction, Experimental, Results, Discussion, etc.). All illustrations, photographs, tables, etc., should be on separate sheets.

Introduction. Every paper must have a concise introduction mentioning what has been done before on the topic described, and stating clearly what is new in the paper now submitted.

Summary. Full-length papers and Review articles should have a summary of 50–100 words which clearly and briefly indicates what is new, different and significant. In the case of French or German articles an additional summary in English, headed by an English translation of the title, should also be provided. (Notes and Letters to the Editor are published without a summary.)

Illustrations. The figures should be submitted in a form suitable for reproduction, drawn in Indian ink on drawing or tracing paper. Each illustration should have a legend, all the *legends* being typed (with double spacing) together on a *separate sheet*. If structures are given in the text, the original drawings should be supplied. Coloured illustrations are reproduced at the author's expense, the cost being determined by the number of pages and by the number of colours needed. The written permission of the author and publisher must be obtained for the use of any figure already published. Its source must be indicated in the legend.

References. References should be numbered in the order in which they are cited in the text, and listed in numerical sequence on a separate sheet at the end of the article. Please check a recent issue for the layout of the reference list. Abbreviations for the titles of journals should follow the system used by *Chemical Abstracts.* Articles not yet published should be given as "in press" (journal should be specified), "submitted for publication" (journal should be specified), "in preparation" or "personal communication".

Dispatch. Before sending the manuscript to the Editor please check that the envelope contains three copies of the paper complete with references, legends and figures. One of the sets of figures must be the originals suitable for direct reproduction. Please also ensure that permission to publish has been obtained from your institute.

Proofs. One set of proofs will be sent to the author to be carefully checked for printer's errors. Corrections must be restricted to instances in which the proof is at variance with the manuscript. "Extra corrections" will be inserted at the author's expense.

Reprints. Fifty reprints of Full-length papers, Notes and Letters to the Editor will be supplied free of charge. Additional reprints can be ordered by the authors. An order form containing price quotations will be sent to the authors together with the proofs of their article.

Advertisements. Advertisement rates are available from the publisher on request. The Editors of the journal accept no responsibility for the contents of the advertisements.

AQUEOUS SIZE-EXCLUSION CHROMATOGRAPHY

edited by **P.L. DUBIN,** *Indiana-Purdue University*

(Journal of Chromatography Library, 40)

The rapid development of new packings for aqueous size-exclusion chromatography has revolutionized this field. High resolution non-adsorptive columns now make possible the efficient separation of proteins and the rapid and precise determination of the molecular weight distribution of synthetic polymers. This technology is also being applied to the separation of small ions, the characterization of associating systems, and the measurement of branching. At the same time, fundamental studies are elucidating the mechanisms of the various chromatographic processes.

These developments in principles and applications are assembled for the first time in this book.

- Fundamental issues are dealt with: the roles of pore structure and macromolecular dimensions, hydrophobic and electrostatic effects, and the determination and control of column efficiency.
- High-performance packings based on derivatized silica are reviewed in detail.
- Special techniques are thoroughly described, including SEC/LALLS, inverse exclusion chromatography, and frontal zone chromatography.
- Attention is focussed on special applications of size-exclusion methods, such as the characterization of micelles, separations of inorganic ions, and Hummel-Dreyer and related methods for equilibrium systems.
- Protein chromatography is dealt with in both dedicated sections and throughou the book as a whole.

This is a particularly comprehensive a authoritative work - all the contributio review broad topics of general signifi ance and the authors are of high repu

The material will be of special value for t characterization of synthetic water-solub polymers, especially polyelectrolytes. B chemists will find fundamental and practi guidance on protein separations. Rese chers confronted with solutes that exhi complex chromatographic behavior, su as humic acids, aggregating proteins, a micelles should find the contents of this v ume illuminating.

Contents: Part I. Separation Mechanism Part II. Characterization of Stationa Phases. Part III. New Packings. Part IV. B polymers. Part V. Associating System Subject Index.

1988 xviii + 454 pages
US$ 144.75 / Dfl. 275.00
ISBN 0-444-42957-3

ELSEVIER SCIENCE PUBLISHERS

P.O. Box 211, 1000 AE Amsterdam, The Netherlands
P.O. Box 1663, Grand Central Station, New York, NY 10163, USA